SLAC-R-502
CONF-970374
UC-414

PROCEEDINGS OF THE WORKSHOP ON NEW KINDS OF POSITRON SOURCES FOR LINEAR COLLIDERS

March 4-7, 1997

Stanford Linear Accelerator Center
Stanford University, Stanford, California 94309

Editors

J. Clendenin
R. Nixon

Prepared for the Department of Energy under contract number DE-AC03-76SF00515. Printed in the United States of America. Available from the National Technical Information Service, U.S. Department of Commerce, 5385 Port Royal Road, Springfield, Virginia 22161.

Proceedings of the Workshop on New Kinds of Positron Sources for Linear Colliders

Table of Contents

Preface

It has been very clear from the beginning of studies for future linear colliders that the conventional positron source approach, as exemplified by the SLC source, is pushing uncomfortably close to the material limits of the conversion target. Nonetheless, since this type of positron source is better understood and relatively inexpensive to build, it has been incorporated into the initial design studies for the JLC/NLC.

New ideas for positron sources for linear colliders have been regularly reported in the literature and at accelerator conferences for at least a decade, and indeed the recirculation scheme associated with the VLEPP design is nearly two decades old.

Considerable attention was given to both conventional and unconventional positron sources at the *International Workshop on e^+e^- Sources and Pre-Accelerators for Linear Colliders* (SOURCES '94) held at Schwerin, Germany, in 1994. By "unconventional" is generally meant any design that utililzes significantly different techniques or physical processes from those already employed for linear colliders such as SLC. The progress with positron sources that was evident at SOURCES '94 has continued, especially in the areas of undulator and crystal sources, and to some extent Compton sources, so that now, nearly three years later, it seemed expedient to organize an international workshop dedicated to new kinds of positron sources for linear colliders. Although workshops dedicated to positron beams have been held before, e.g., *the 1987 Workshop on Intense Positron Beams* held at INEL, ID, USA, this is the first workshop dedicated to positron sources for accelerators.

Nearly all the new types of positron sources discussed in this workshop come under the heading of crystals (or channeling), undulators, and Compton. Storage ring and nuclear reactor sources were not discussed. The positron source designs that were discussed have varying degrees of maturity, but except for the case of crystal sources, where proof of principle experiments have been undertaken, experimental results are missing. It is hoped that these presentations, and especially the recommendations of the working groups, will prove useful to the various linear collider groups in deciding if and when new experimental programs for positron sources should be undertaken.

The majority of Workshop presentations included in these proceedings are in the form of transparencies. To make these more understandable by both the other participants as well as by the general reader, all of the authors have submitted a discursive summary and most have made helpful annotations on the transparencies themselves. Nonetheless, it is admitted that transparencies themselves are a very poor way to create a useable record.

Special thanks are given to the Workshop Secretariat, Robbin Nixon, who along with Jym Clendenin has co-edited the proceedings, and to the various members of the SLAC staff who assisted in the details of the local organization.

The organizing committee:

Robert Chehab
Jym Clendenin
Stan Ecklund

WORKSHOP ON NEW KINDS OF POSITRON SOURCES FOR LINEAR COLLIDERS

	TUESDAY 3/4/97	WEDNESDAY 3/5/97	THURSDAY 3/6/97	FRIDAY 3/7/97
08:30 - 09:00	**REGISTRATION**	**CONTINENTAL BREAKFAST**		
09:00 - 10:30	J. M. Paterson T. Omori J. Clendenin	V. Baier J. Frisch	A. Kulikov G. Silvestrov	Working Group 2B Working Group 3B
10:30 - 11:00		**COFFEE BREAK**		
11:00 - 12:30	S. Ecklund Organization of WGs	T. Omori T. Takahashi	Working Group 1A	Working Group 1B Working Group 4B
12:30 - 14:00		**LUNCH**		**12:30 - 14:30**
14:00 - 15:30	R. Chehab K. Floettmann	Working Group 2A	Working Group 4A	**14:30 - 17:00** Summaries of Working Groups
15:30 - 16:00		**COFFEE BREAK**		
16:00 - 17:30	A. Mikhailichenko V. Baier	Working Group 3A	A. Jejcic T. Kamitani	
		BANQUET **18:30 COCKTAILS** **19:00 DINNER**	**17:30 TOUR (?)**	

Working Group 1: New Approaches to Conventional Sources / R. Miller (SLAC)
Working Group 2: Crystals / R. Chehab (Orsay)
Working Group 3: Undulators/Compton / V. Baier (BINP)
Working Group 4: Collaboration/Parameters / J. Sheppard (SLAC)

Working Group #1: Conventional Sources

Group Leader: Roger Miller (SLAC)

1. General Considerations

We know how to build conventional sources which meet the high frequency collider (NLC, JLC, CLIC, VLEPP) requirements, but ...

A. We should design for easy operation:

1) All limiting apertures after the capture region should have $r \geq 4\sigma_{beam}$.

2) Position monitors should be placed every 90° of β phase advance.

B. For REPAIRABILITY, either redundant or remotely replaceable modules should be used.

C. Liquid Metal Targets:

Rotating solid targets appear to be simpler that liquid metal targets since they can survive single pulse heating and the consequent shock wave.

An interesting proposal for a magnetically driven rotating target cooled by a liquid metal pool was presented. (See Silvestrov, Appendix.)

D. Should check designs to see if deceleration of e^+ in capture region is advantageous.

2. Polarization ???

Not possible with a "conventional" source.

Perhaps "conventional" source should not be built!!! SLAC and KEK should work on the design of polarized sources, compare cost, feasibility, operability, etc. with "conventional" source, and then decide.

The strategies of starting with a conventional positron source and later upgrading to a polarized source should be studied. Do any of these strategies make sense?

Working Group 2: Crystal Sources

Group Leader: R. Chehab (Orsay)

RELEVANT WORKSHOP TALKS

* "A crystal source using a 10 GeV e^- beam"

  The ability of a crystal source to replace a conventional one in a linear collilder was discussed.

* "Positron production into standard phase space by high energies (200-300 GeV) e^- in an oriented crystal"

  Yields provided by crystals submitted to high energy electrons with acceptances defined using the same limits as with intermediate energy electrons was explored.

* "Positron production in single crystals by 1.2 GeV channeled e^-"

  Experiments (Tokyo)with Si<100> and W<100> crystals submitted to 1.2 GeV electrons were described. (Average enhancement: ~2.6)

* "Use of codes and computing for the simulations of e^+ beams"

  Simulation of photon and positron generation in thick crystals was discussed.

MAIN CONCLUSIONS

Simulation and experiments are in satisfactory agreement.

Experiments already completed at Orsay and Tokyo in the 1-2 GeV region provide *proof of principle* that oriented crystals can be used to generate positrons with enhanced yields with respect to amorphous targets of the same thickness.

WORKING GROUP DISCUSSION

* *Yield*: A crystal could give a yield of at least 1 e^+/e^- at the IP.

* *Phase space:* How good could the positron phase space be? Are the available matching systems good enough for crystals? The yield for a complete crystal and matching system that has been optimized together needs to be determined.

* *Energy deposited:* Much less energy deposited in the crystal target than an amorphous target for the same yield.

* *Definition of figure of merit:* Number of positrons in unit phase volume per peak energy density deposited. (This FOM is chosen to be useful for comparing different positron source systems after optimization.)

* *Heating:* A hybrid-crystal source can sustain high intensities.

◐.. *Radiation damage:* Analysis of crystals irradiated using 30 GeV electrons at the SLC are expected to be completed by summer 1997.

* *Incident energy:* Is it possible to lower the incident energy on the target so as to get

$$E_{in}^{-}[Crystal] < E_{in}^{-}[Amorphous]$$

for the same yield? This requires crystal optimization.

* *Orientation:* Proper orientation requires a good goniometer (resolution < 10^{-2} degrees).

◐.. *Crystal quality:* High quality requires mosaic spread < 300 μrad and 10 GeV [W].

Issues of special concern are indicated by ◐

WORK TO BE DONE

* Simulations:	• Figures of merit • Equivalent crystal solution for the various LC projects (such as NLC and CLIC) at moderate energies • Optimizations
* Tests:	• Radiation damage at different fluences [possibly use SLC or LEA beams] • Crystals at Stuttgart now for analysis of effects of radiation (results due by summer 1997)
* Planned experiments:	• Experiment at KEK with a W crystal at 1 GeV in fall 1997 • Experiment at CERN with a W crystal at 10 GeV during 1998-99 Note: Both experiments will produce information on the transverse phase space of the positrons generated
* Theory:	• Investigation of photon and positron generation in crystals

Summary of Working Group 3: Undulators/Compton Sources

Group Leader: V. Baier (BINP)

There are two approaches for organization of radiation of circularly polarized photons with energy 10-80 MeV which then produce longitudinally polarized positrons in a thin target. These are undulator and backwards laser (LB) scattering. In both cases, positrons are produced in the target via Coulomb interaction.

Undulator

The undulator is required to be ~150 m long. The approach that has been the most studied is to use a superconducting undulator. A second possibility, which has recently generated interest, is to construct the undulator from permanent magnets using strong field alloys (with working fields on the order of 5 T).

Undulator Advantages

1. Emittance and spin perturbations are small, so that the undulator-conversion system could be inserted before the IP as well.

2. Some further possibilities (two targets, Ti target) can, in principle reduce the undulator length.

3. When a very high intensity of polarized positrons is required (TESLA/SBLC), the undulator system is the only possibility since LB in this case is not feasible.

Undulator Disadvantages

1. Requires a long 100-150m superconducting undulator.

Laser Backscattering

This type of system can be designed for a variety of different laser wavelengths and accelerator energies, ranging from about 1 micron wavelength and 1.7GeV, to 10 microns and 7GeV. The required laser peak power is approximately constant (for similar positron collection efficiency and electron beam emittance assumptions) at 1-10TW. This wide range in peak powers is due to variations in the above assumptions. Much better modeling is needed to pin down the parameters. The effect of varying wavelength from short to long wavelengths is:

1. Decreases nonlinear effects at the laser/electron IP. Calculations of the final polarization need to be done to see if this is significant.

2. Increases the required accelerator energy and beam power (from about 200kW to about 1MW).

3. Changes the available optical technology: At 1 micron, solid state lasers are available with very high peak power, but limited average power. At 10 microns, CO_2 lasers are available with very high average power, but more limited peak power.

The other design issue is the use of optical cavities to recycle the optical beam. For the short wavelength (1μm) solution, this is probably required - high average power lasers are not available in this range. For the long wavelength (10μm) solution, it is possible to use an array of very high average power lasers.

There are no single technical limits which prevent the use of compton backscattering as a positron source. There are a large number of technical issues which will need to be resolved to make the systems practical.

The comparison of laser backscatter systems vs. undulator systems is:

Laser Backscattering Advantages

1. System does not required a >100GeV electron beam for operation - allows the source to be developed and tested before the main NLC, JLC, CLIC, etc. linac is completed.

2. System operation is independent of the main linac energy - may allow more flexibility in operation. This advantage may be negated if the undulator operates at 100GeV and is installed before the IP.

3. With the laser system deactivated, the system can easily be converted to a conventional un-polarized source. However, for conventional source electron linac, one needs $1x10^{10}$ e^-/bunch, for laser backscattering one needs $(5\text{-}10)x10^{10}$ e^-/bunch.

Laser Backscattering Disadvantages

1. The system requires a very large, complex, and technically challenging laser and optical system - 10-20MW plug power, especially if a dedicated beam of electrons with relatively high energy is used.

2. System requires a large and expensive (200kW ->1MW) drive accelerator.

Recommendations

1. Build a short version of the final undulator design and test it at 50GeV using, e.g., the FFTB beam at SLAC. (Note: this test would not result in positron production.)

2. Make a detailed design of a laser backscattered system.

Working Group #4: Collaboration/Parameters Summary

Group Leader: John Sheppard, (SLAC)

Updated Positron System Parameters

Positron source parameters for various linear collider projects as presented in the TRC (International Linear Collider Technical Review Committee Report 1995; SLAC Report #471) were evaluated. Six of the twelve members of the TRC Injector Systems Group were present at this workshop (Flottmann, Frisch, Mikhailichenko, Miller, Tang, and Yeremian). A seventh group member (Rinolfi) was an organizer of this workshop and was contacted for an update of the CLIC positron system parameters. There were a number changes in the table for the CLIC, DESY, and NLC sources. An editorial correction was made to an entry in the VLEPP table for the rf wavelength in the capture section. No changes were made to the JLC parameter list. An updated positron source parameter list is attached.

Features and Limitations of Positron Schemes

The features and limitations of various positron schemes were discussed. In summary, conventional sources are expected to work but are limited to present design values as far as incident beam power capabilities. It was difficult to compare crystal sources with conventional sources because of the different criteria presented. The promise of greater efficiency in the initial gamma production potentially reduces the power in the drive electron beam. High energy experiments are underway or have been proposed that should clarify the capability of crystals to handle high incident beam power. Undulator and Compton backscatter sources can produce polarized positrons. Direct production of polarized positrons from Compton backscattering requires significant drive beam and laser development. Gamma production from Compton backscattering also requires high power lasers and drive beams but can be done with a drive beam energy of several Gev versus the requirement of drive beam energy in excess of 150 GeV which is required for undulator systems. The undulator scheme has been thoroughly studied, whereas a self-consistent Compton backscattering scheme has yet to be worked out in detail. All schemes have power handling issues associated with the gamma converters but there appears to be some advantage to the thin (0.4 Xo) low Z converters being considered by DESY. Development of liquid metal targets began at BINP in the 1970's. Liquid metal targets are ready for beam tests but nothing is presently scheduled.

Active Developments and Topics of Common Interest

There are significant numbers of computer codes being used and there does not appear to be a need for new code development. A radiation quench test in association with the KEK superconducting capture/matching solenoid development has been proposed using the B-factory/Photon-factory linac; in the fall of 1997; a tungsten crystal target test has also been proposed at KEK B-factory/Photon-factory linac for the fall of 1997. A Compton backscatter test using the KEK/ATF has been outlined. A 10 GeV crystal study at CERN is scheduled in 1999. DESY would like to see titanium converter tests done and undulator/wiggler prototype development begun; BINP suggested that a 50 GeV wiggler test for polarized positrons could be done at the FFTB. No consensus was developed regarding the need to extend the beam power density target tests which were done at SLAC 15 years ago.

Continued Collaboration

The rate of progress in positron system design and development is steady but slow. There did not seem to be a driving need to change the way of doing business in order to advance the state of the art. Continued communication is encouraged. The results of this workshop should be discussed at LC97.

Table W4.1

Positron source parameters for various linear collider projects. SLC parameters are given as a reference.

	Unit	SLC	TESLA	SBLC	JLC-X	NLC	VLEPP	CLIC
Positron Source Type			wiggler/ undulator based	wiggler/ undulator based	SLC-type	SLC-type	wiggler/ undulator based	SLC-type
General Parameters								
Ne^+/pulse at IP	10^{10}	3–5	4120	366	53.6	77	20	16
No. of bunches per pulse		1	1130	333	85	90	1	20
Pulse duration	μ s	$3 \cdot 10^{-6}$	800	2	0.119	0.126	NA	0.006
Bunch spacing	ns	–	708	6	1.4	1.4	–	1
Repetition frequency	Hz	120	5	50	150	180	~ 150	700
Primary Beam								
Energy	GeV	30	≥ 150	≥ 150	10	3.11	150	2.15
Ne^-/pulse	10^{10}	3–5	4100	360	35	135	20	80
Beam power	kW	17–29	4900	4400	84	121	721	193
Linac frequency	MHz	2856	1300	2998	2856	2856	14000	1500
Wiggler length	m	–	$35(\geq 150)$	$35(\geq 150)$	–	–	~ 150	–
Wiggler period	cm	–	$3.6(\sim 1.2)$	$3.6(\sim 1.2)$	–	–	~ 1.0	–
Peak field	T	–	$1.7(\sim 0.9)$	$1.7(\sim 0.9)$	–	–	0.5	–
No. of photons per electron		–	370	~ 350	–	–	100	–
Conversion Target								
Material		$W_{75}Re_{25}$	Ti alloy	Ti alloy	$W_{75}Re_{25}$	$W_{75}Re_{25}$	W, Hg	$W_{75}Re_{25}$
Thickness	χ_0	6.0	0.4	0.4	6.0	4	0.5	4.5
RMS spot size of drive beam	mm	0.8	0.7	0.7	1.2	1.2	1.0	1.0
Temperature rise per pulse	K	200–300	360	760	~ 220	~ 200	~ 200	~ 200
Mean deposited power	kW	4.2–6.0	7	6	~ 30	23	0.2	60
Ne^+/pulse at exit	10^{10}	180–300	48235	4305	750	1000	60	200
Capture System								
Matching device		AMD*	AMD*	AMD*	AMD*	AMD*	Li-Lens	AMD*
Initial field	T	7.0	6	7	8.0	7.0	–	7.0
Taper parameter	m^{-1}	–	30	30	50	–	–	–
End field	T	0.5	0.16	0.7	0.8	0.5	–	0.5
Length	m	0.15	1.2	0.3	0.18	0.2	0.01	0.15
Wavelength of accel. RF	m	0.1	0.23	0.1	0.105	0.21	0.1	0.2
Minimum iris radius	mm	9.0	23	10	13	20	–	18.0
Gradient	MV/m	30	15	30	30	24	–	12
Pre-damping ring required		No	No	No	Yes	Yes	No	Yes
Ne^+/pulse at entrance of pre-damping ring	10^{10}	4.5–7.5	8200	732	108	150	50	9
Efficiency incl. dephasing	%	4	17	17	14	15	–	4.5
γA of pre-damping ring§	πm	0.01	0.048	0.41	0.027	0.09	0.1	0.34
Energy of pre-damping ring	GeV	1.15	3.5	3	1.98	2.0	3.0	2.15
Energy accept. of match. device	MeV	20	± 30	± 30	40	20	–	20
Polarization								
Degree of polarization	%	–	(70)	(70)	–	–	~ 75	–
Power consumption (up to DR)	MW		option	option				25

* adiabatic matching device

§ γA = normalized acceptance

On Use of Oriented Crystals in Positron Source at Different Energies

V. N. Baier, V. M. Katkov and V. M. Strakhovenko
Budker Institute of Nuclear Physics, 630090 Novosibirsk, Russia

Abstract

The development of an electromagnetic cascade at axial alignment of a single crystal is discussed. For the initial electron energies from a few GeV to 300 GeV a special attention is paid to the production of positrons in given phase-space, providing the possibility of further acceleration of them.

1 Introduction

For high energies, the probability of photon emission from charged particles [1] and the probability of pair production by photons [2] in oriented crystals differ essentially from those of the corresponding processes in amorphous media, as a result of the collective interaction of a certain set of ordered atoms of the crystal lattice with the incident particle.

A specific property of electromagnetic processes in single crystals is their energy and orientation dependence. For the moderate energy region the angular width of orientation phenomena concerning an axis or plane is determined by the Lindhard critical angle $\vartheta_c = \sqrt{2V_0/\varepsilon}$, where ε is the particle energy and V_0 is the scale of the average potential of the axis (plane) relative to which the angle of incidence ϑ_0 is determined.

Characteristics of radiation depend essentially on the parameter [1]

$$\rho = 2\gamma^2 < (\mathbf{v}(t) - < \mathbf{v} >)^2 >, \tag{1}$$

where $\gamma = \varepsilon/m$, $\mathbf{v}(t)$ is the particle's velocity and $< \ldots >$ denotes averaging over time. When $\rho \ll 1$ the radiation has a dipole nature and at quasi-periodic (periodic in the frame moving with $< \mathbf{v}(t) >$) is formed during the period of motion T or so. For $\rho \gg 1$ it has a magnetic bremsstrahlung nature (for frequencies contributing to the total intensity) and occurs from a small portion of the trajectory in a time $\sim T/\sqrt{\rho}$. When $\rho \sim 1$ we have an intermediate case of non-dipole radiation.

The parameter ρ depends on the angle of incidence ϑ_0. For angles $\vartheta_0 \leq \vartheta_c$, the incident electrons are captured into channels or into low above-barrier states. In this case the transverse (to the axis or plane) velocity of the particle is $v_\perp \leq \vartheta_c$ and we have from (1) $\rho \leq \rho_c$, where

$$\rho_c = \frac{2V_0\varepsilon}{m^2}. \tag{2}$$

For $\vartheta_0 \gg \vartheta_c$ particles move high above the potential barrier. In this case the straight-line trajectory approximation can be used to obtain the characteristics of motion, and we get from (1) the following estimate:

$$\rho(\vartheta_0) = \left(\frac{2V_0}{m\vartheta_0}\right)^2. \tag{3}$$

Eq (3) means that besides ϑ_c there is another characteristic angle in the problem: $\vartheta_V = V_0/m$, such that we have $\rho \sim 1$ for $\vartheta_0 \sim \vartheta_V$. In the high-energy region when $\rho_c \gg 1$, radiation has a magnetic bremsstrahlung nature for $\vartheta_0 \ll V_0/m$ and is dipole for $\vartheta_0 \gg V_0/m$.

[1] In this paper we put $\hbar = c = 1$.

Thus, in the high-energy region ($\rho \gg 1$) for entry angles $\vartheta_0 \leq \vartheta_c$ when the incident particles are moving in channels or in low above-barrier states the fact that particles are moving along some oscillatory type trajectory become unimportant for the radiation process, since it occurs from a small portion of trajectory, or, in other words, the radiation process becomes *local*. This means that radiation does not depend on the type of the trajectory, what is an important feature of channeling radiation, and becomes *universal* depending on electric field on the trajectory only. In this sense channeling radiation ceases to exist and instead of it we have what it is called magnetic bremsstrahlung.

The theory of the electron radiation and pair creation by a photon in oriented crystals at high energies based on the operator quasiclassical method was developed in [1]-[2], see also review [3]. This method is an adequate formulation of quantum electrodynamics in an external field at high energies. General formulae for probability of radiation and pair creation were obtained which are valid for any entry angle ϑ_0. For small $\vartheta_0 \ll V_0/m$ one obtains from the general formulae probability $\dfrac{dW_\gamma^g(\varepsilon,\omega)}{d\omega}$ of radiation of a photon of energy ω by an electron of energy ε in the form

$$\frac{dW_\gamma^g(\varepsilon,\omega)}{d\omega} = W_\gamma(\varepsilon,\omega) + \left(\frac{m\vartheta_0}{V_0}\right)^2 W_\gamma^{(1)}(\varepsilon,\omega), \tag{4}$$

where the functions W_γ and $W_\gamma^{(1)}$ are independent of ϑ_0. In the r.h.s. of (4),the first term W_γ gives the result of the constant field approximation (CFA) and the second one is a correction to CFA. In accordance with the above discussion, eq.(4) does not contain the Lindhard angle ϑ_c. In probability (4) the important parameter $\chi(\rho)$ appears:

$$\chi(\rho) = \frac{\varepsilon \mid \nabla U(\rho) \mid}{m^3} = \frac{\varepsilon}{m}\frac{E(\rho)}{E_0}, \tag{5}$$

where $E_0 = m^2/e = 1.32 \cdot 10^{16}$ V/cm is the critical quantum field, $E(\rho)$ is the local strength of the electric field of axes on a distance ρ from axis. For the pair production process the corresponding parameter is

$$\kappa(\rho) = \frac{\omega}{m}\frac{E(\rho)}{E_0}.$$

The field strength in crystals may be very high, e.g. $E_{max} \sim 10^{12}$ V/cm in tungsten. A typical magnitude of the parameter χ in crystals can be expressed via V_0 and the screening radius a_s :

$$\chi \sim \chi_s = \frac{V_0\varepsilon}{m^3 a_s}, \tag{6}$$

The parameter χ determines quantum properties of the photon emission process : for $\chi \ll 1$ it is purely classical but when χ increases, very soon quantum

recoil effects become important. Already for $\chi \sim 0.1$ these quantum effects are essential.

For crystals, the role of the conventional radiation length in amorphous media L_{rad} is played by the characteristic length $L_{ch} = \frac{\varepsilon}{I_{ch}(\varepsilon)}$, where $I_{ch}(\varepsilon)$ is the total intensity of radiation. Calculated within CFA, the quantity $L_{ch}^{-1}(\varepsilon)$ (see Fig.1) first rises with increasing energy and then begins to drop, i.e. it has a maximum. The ratio $r_\gamma = L_{rad}/L_{ch}$ is a measure of radiation intensity enhancement in crystals as compared to corresponding amorphous media. The maximal values of this ratio r_γ^{max} are given in the Table. Note, that the smaller is the nuclear charge the larger is the enhancement.

The ratio $r_e = W_e(\omega)/W_{BH}$ plays the same role as r_γ for the photon emission. The maximal values of it r_e^{max} are very close to those of r_γ^{max}. In CFA for small ω, when $\kappa \ll 1$ the probability $W_e(\omega) \propto \exp(-8/3\kappa)$. So, the essential contribution of this mechanism to pair production starts at some threshold value ω_t (given in the Table) which we define more precisely as follows:

$$W_e(\omega_t) = W_{BH}. \tag{7}$$

Here W_{BH} is the probability of the pair production in a corresponding amorphous medium,provided by the Bethe-Heitler mechanism. In Fig.1 the total probabilities of pair production $W_e(\omega)$ and the inverse characteristic lengths of energy losses $L_{ch}^{-1}(\varepsilon)$ for different crystals are shown.

At $\vartheta_0 \gg V_0/m$ one obtains from the general formulae the probabilities of the coherent radiation or pair creation (for the more soft inequality $\vartheta_0 > V_0/m$ the corresponding expressions are modified) and at further increase of the entry angle (to the situation called "random" orientation) the probabilities of the processes smoothly decreasing acquire their amorphous values (BH).

The dramatic change of photon emission and pair production lengths along with that of emitted particles spectra determines the main distinctive features (see [4]) of the specific electron-photon cascade developing along crystal axes as compared to that in amorphous medium.

An evolution of the electromagnetic shower is described by the following set of kinetic equations:

$$\begin{aligned}
\frac{\partial N_\gamma(\omega,t)}{\partial t} &= -W_e(\omega)N_\gamma(\omega,t) + \int_\omega^\infty d\varepsilon W_\gamma(\varepsilon,\omega)N_e(\varepsilon,t), \\
\frac{\partial N_e(\varepsilon,t)}{\partial t} &= -W_\gamma(\varepsilon)N_e(\varepsilon,t) + \int_\varepsilon^\infty d\varepsilon' W_\gamma(\varepsilon',\varepsilon'-\varepsilon)N_e(\varepsilon',t) \\
&\quad +2\int_\varepsilon^\infty d\omega W_e(\omega,\varepsilon)N_\gamma(\omega,t),
\end{aligned} \tag{8}$$

where $N_\gamma(\omega,t)$ and $N_e(\varepsilon,t)$ are energy distribution functions of photons and electrons over ω and ε respectively at a given depth t. For $\vartheta_0 \ll V_0/m$, one can use the probabilities $W_\gamma(\varepsilon,\omega)$ and $W_e(\omega,\varepsilon)$ calculated in CFA; $W_\gamma(\varepsilon) =$

$\int_0^\varepsilon d\omega W_\gamma(\varepsilon,\omega)$ is the total probability of photon emission and $W_e(\omega)$ is the total probability of pair production.

When the energy of initial particles ε_0 (ω_0) $\gg \omega_t$ and the lower boundary for the energy of recorded particles $\varepsilon_f \geq \omega_t$, coherent mechanism dominate in both photon emission and pair production processes during cascade development. We call these *hard cascades*, whose properties were investigated in [4], where under some simplifying assumptions analytical solutions of kinetic equations (8) were obtained. For $\varepsilon_0 < \omega_t$ and $\varepsilon_f \ll \omega_t$ (we call these *soft cascades*), the properties of the arising electromagnetic showers were investigated in [5] by means of a Monte-Carlo simulation (MCS)-procedure. One should realize that the kinetic equations (8) describe the cascade properties in terms of the mean values giving some averaged characteristics and providing no information about fluctuations in the stochastic process under consideration. The MCS-procedure adequately describes all the details of a cascade development, moreover, other processes like multiple scattering and ionization energy loss may be taken into account but, to obtain reliable average characteristics, sufficiently high statistics is needed. The updated MCS-procedure was applied in [6] for the investigation of a *mixed cascade*, when $\varepsilon_0 > \omega_t$ or ($\varepsilon_0 \gg \omega_t$) while $\varepsilon_f \ll \omega_t$ and both coherent and BH mechanisms contribute at different stages of the cascade development. The development of an electromagnetic cascade for various crystal types and different orientations was observed for the first time in [7]. The corresponding results of [6] are in a quite good agreement with experimental data obtained in [7].

2 Positron production at energies from 10 Gev to 300 GeV

For energies of the order of 1 GeV, the intensity of channeling radiation (for main axes) becomes higher than that of bremsstrahlung [8] and consequently starts to dominate the energy loss. The spectral distribution of this radiation is concentrated at low ω and soft ($\omega \ll \varepsilon_0$) photons are numerous. In sufficiently thick crystals these photons may convert into pairs. In other words, for such initial energy we deal with a soft cascade when the pair production is entirely due to the incoherent BH mechanism, while the photon emission is still dominated by the coherent one.

Description of radiation at axial channeling is still a challenge. There is no adequate formula for the spectrum of radiation available in the literature. Because of this, to describe the radiation from channeled and moving not very high above the potential barrier particles, heuristic intensity spectrum was suggested in [5]. For relatively small energies when $\rho_c \ll 1$ the spectrum has a maximum at $\omega = \omega_{max} \simeq 2\varepsilon\sqrt{\rho_c}/(ma_s)$ and coincides with dipole approximation. When $\rho_c \gg 1$ and CFA is valid the spectrum reproduces not only the position of a

maximum but also the shape of spectral distributions like those shown in Fig.2 of [1] obtained within the approximation mentioned . Comparing the shape of the spectrum of [5] with available experimental data, we find a qualitative agreement with known experiments for all energies from 900 MeV up.

The explicit expressions for incoherent contributions to the radiation and pair production probabilities are given in [5] with crystal corrections (as in [9]) and screening effects taken into account. The allowance for multiple scattering was made in the standard small-angle approximation. Mean ionization energy losses were described in [5] by more or less standard expressions too.

To estimate the possibility of utilization of crystal targets in an accelerator positron source, we should know the number of created positrons within a definite phase space accepted by the corresponding matching optical system. We use typical values for the parameters of such system mentioned in [10], assuming that the energies of accepted positrons and their transverse (with respect to the incident beam direction) momenta must satisfy the following relations

$5\,MeV \leq \mathcal{E} \leq 25\,MeV$

$p_\perp \leq 3\,MeV$, $p_\perp \leq 5\,MeV$

$p_\perp \leq 7\,MeV$, $p_\perp \leq 10\,MeV$

The numbers of accepted positrons N_A^+ versus thickness L on $\langle 100 \rangle$ axis of tungsten for indicated energies are presented in Figs 1-5. The normalization per one incident electron is used. Four curves for different boundaries of $p_\perp$ are given to show the distribution of the transverse momentum. The energy deposited in a target by the initial electron and created charged particles is one of the fundamental characteristics of the positron source. The deposited energy Q per one initial electron is shown in all Figures (curve 5), as well as the deposited energy

per unit length (curse 6). In Fig. 1, the energy of the initial electrons is 10 GeV. It is seen that the maximal yield is achieved at thickness $L \sim 5 L_{rad}$. These results may be considered as a reference point for comparison with high energy results (Fig. 2 - Fig. 5). For very high energy electron (spent beam in linear collider in energy interval 200-300 GeV) maximal yield is shifted to the right. However, number of positrons into given phase space N_A^+ become so high, that one can work at relatively low thickness order of one-two standard (amorphous) radiation lengths. For this interval N_A^+ is given in Fig. 5 for energy $\varepsilon = 300$ GeV

It is interesting to compare $(N_A^+)_{cr}$ produced in ~~orientation~~ oriented crystal with $(N_A^+)_{am}$ in amorphous tungsten. For $L = 5 L_{rad}$ and $p_\perp \leq 5$ MeV/c we found $(N_A^+)_{cr} / (N_A^+)_{am} \geq 3$.

3. Conclusion

So, oriented single crystals may be used as a target on the spent beam in linear colliders to serve as positron source. In conditions when no essential multiplication of the number of positrons is needed, one can use very thin target of order of a standard radiation length, where energy deposit is very low.

References

[1] V. N. Baier, V. M. Katkov and V. M. Strakhovenko, Sov. Phys. JETP **65** (1987) 686.

[2] V. N. Baier, V. M. Katkov and V. M. Strakhovenko, Nucl. Instr. Methods **B16** (1986) 5.

[3] V. N. Baier, V. M. Katkov and V. M. Strakhovenko, Sov. Phys. Usp **32** (1989) 972.

[4] V. N. Baier, V. M. Katkov and V. M. Strakhovenko, Nucl. Instr. Methods **B27** (1987) 360.

[5] V. N. Baier, V. M. Katkov and V. M. Strakhovenko, Nucl. Instr. Methods **B103** (1995) 147..

[6] V. N. Baier, V. M. Katkov and V. M. Strakhovenko, Preprint BINP 95-85, Novosibirsk, 1995

[7] R. Medenwaldt, S. P. Moller, S. Tang-Petersen et al. Phys. Lett.**B 227** (1989) 483.

TABLE

Parameters and certain quantities characterizing radiation and pair production processes.

Crystal	Axis	T	$a_s(10^{-8}cm)$	V_0 (eV)	$\chi_s(100GeV)$	$\rho_c(100GeV)$	r_γ^{max}	$\omega_t\ (GeV)$
$C_{(d)}$	$< 111 >$	293	0.326	29	0.13	22.2	168	90
Si	$< 111 >$	293	0.299	54	0.27	41.4	71	150
Si	$< 110 >$	293	0.324	70	0.32	53.6	81	120
Ge	$< 111 >$	293	0.300	91	0.45	59.7	26	100
Ge	$< 110 >$	280	0.337	110	0.48	84.3	30	70
W	$< 111 >$	293	0.215	417	2.87	319	11	22
W	$< 111 >$	77	0.228	348	2.26	267	11	13

Figure captions

- **Fig.1** Number of accepted positrons (positrons with energy $5\ MeV \leq \varepsilon \leq 25\ MeV$ and with transverse momentum $p_\perp \leq 3MeV/c$ (curve 1), $p_\perp \leq 5MeV/c$ (curve 2), $p_\perp \leq 7MeV/c$ (curve 3), $p_\perp \leq 10MeV/c$ (curve 4)) versus thickness traversed by initial electrons with energy $\varepsilon_0 = 10\ GeV$ in single crystal of tungsten, axis $< 100 >$. Energy lost per initial electron in crystal (curve 5) and energy losses per unit length (curve 6).
- **Fig.2** Same as in Fig.1 but for $\varepsilon_0 = 200\ GeV$.
- **Fig.3** Same as in Fig.1 but for $\varepsilon_0 = 250\ GeV$.
- **Fig.4** Same as in Fig.1 but for $\varepsilon_0 = 300\ GeV$.
- **Fig.5** Same as in Fig.4 but for low thickness.

Number of accepted positrons and energy losses
for the initial energy E=10 GeV

Tungsten, axis <100>

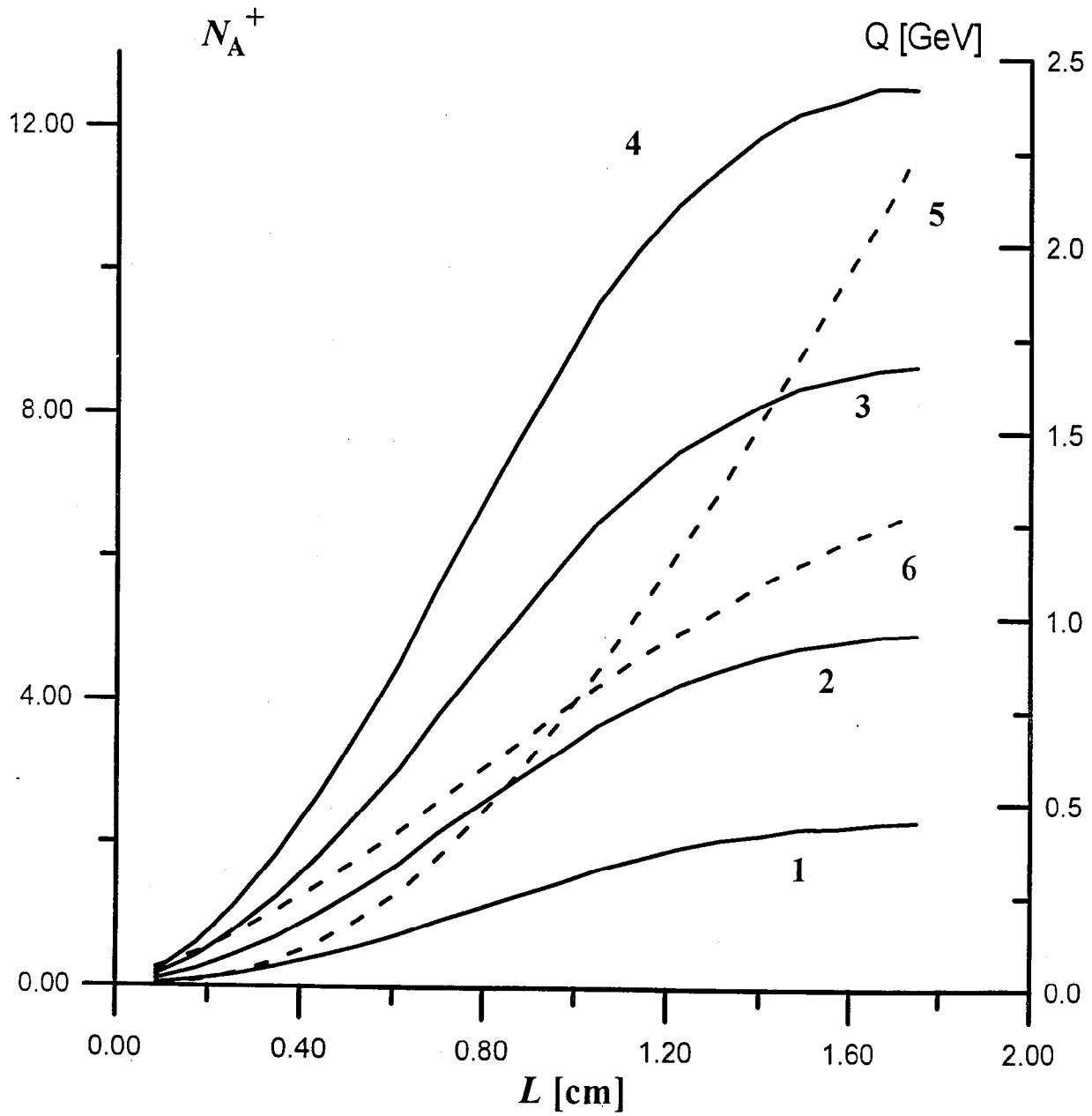

Fig. 1

Number of accepted positrons and energy losses
for the initial energy E=200 GeV

Tungsten, axis <100>

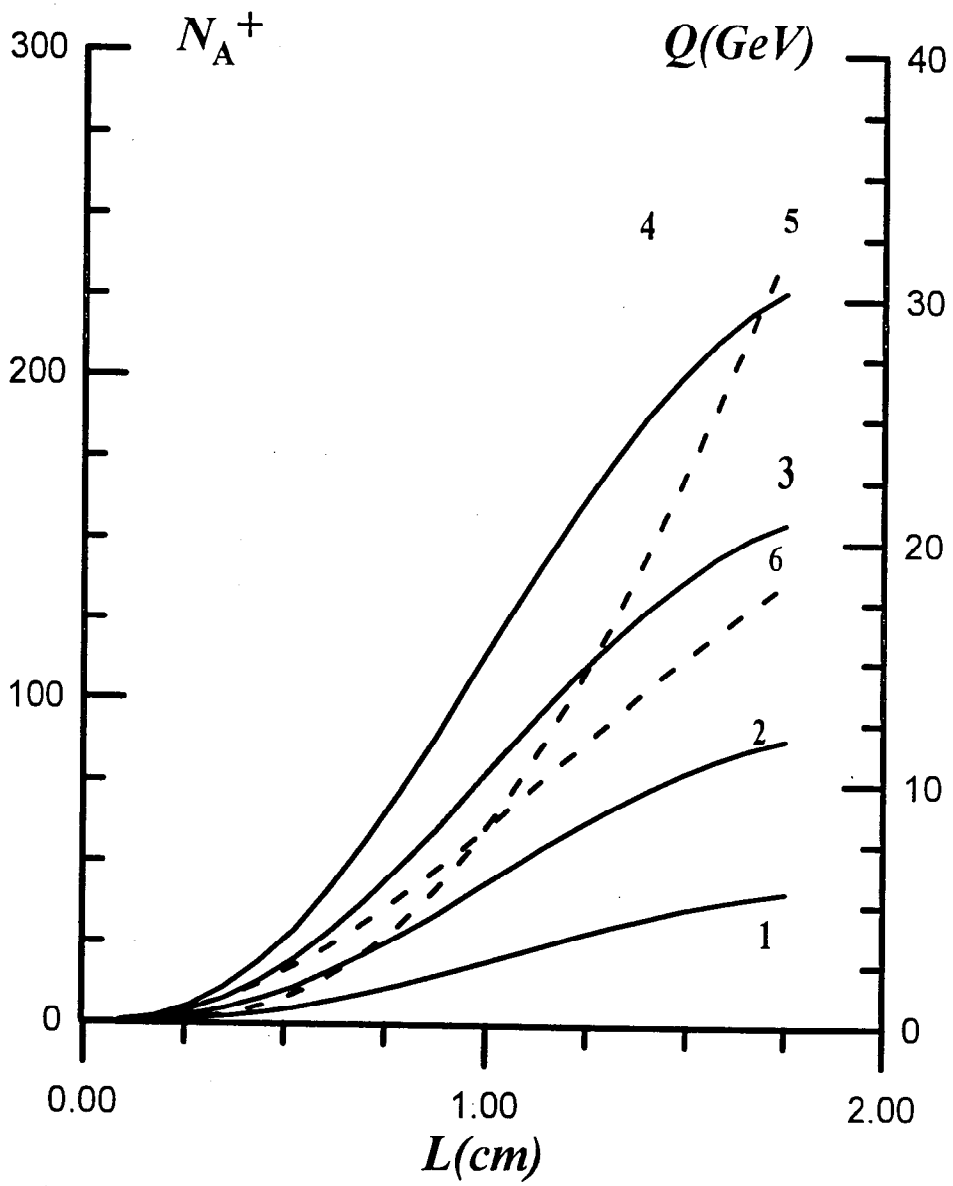

Fig. 2

Number of accepted positrons and energy losses
for the initial energy E=250 GeV

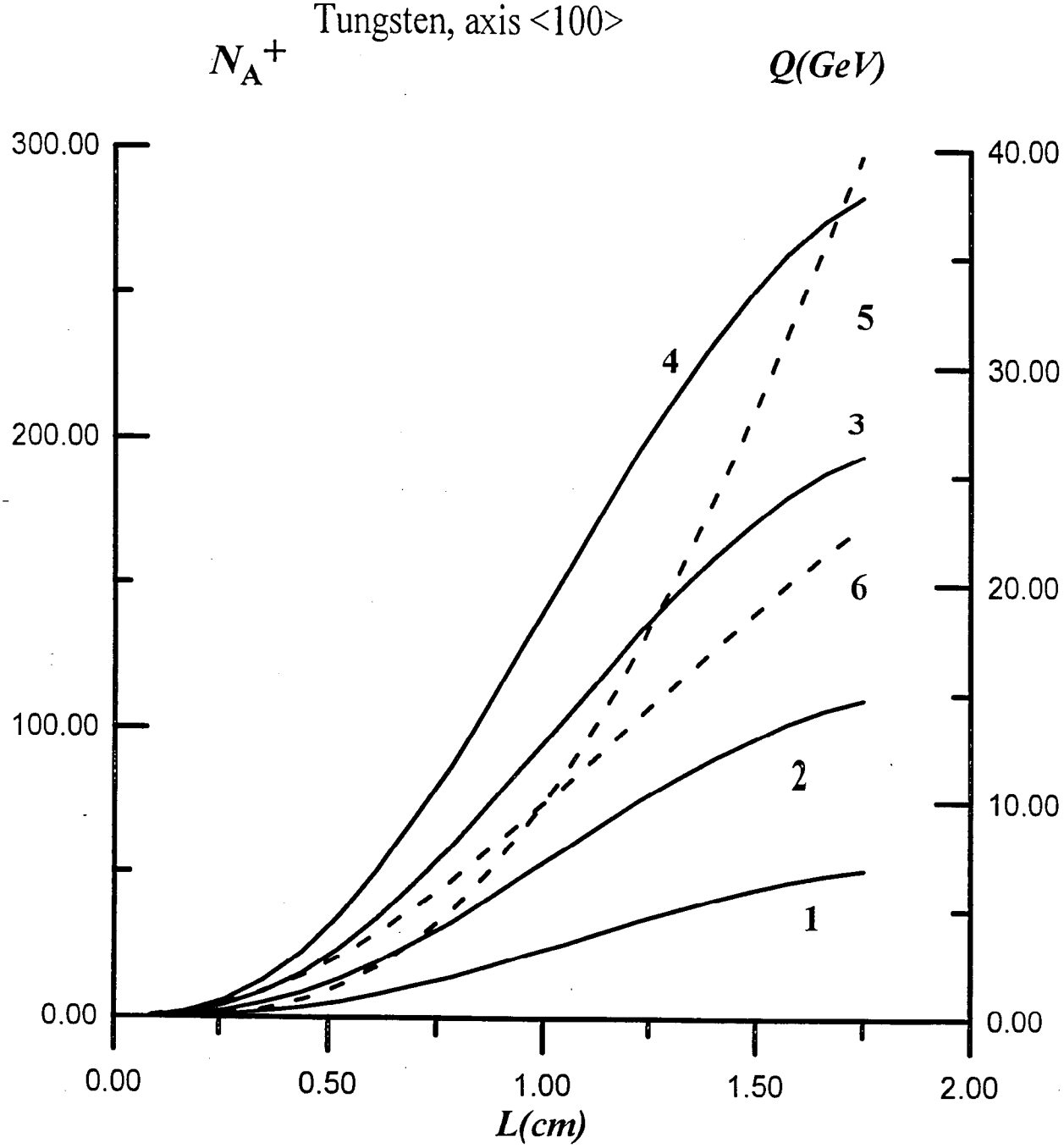

Fig. 3

Number of accepted positrons and energy losses
for the initial energy E=300 GeV

Tungsten axis <100>

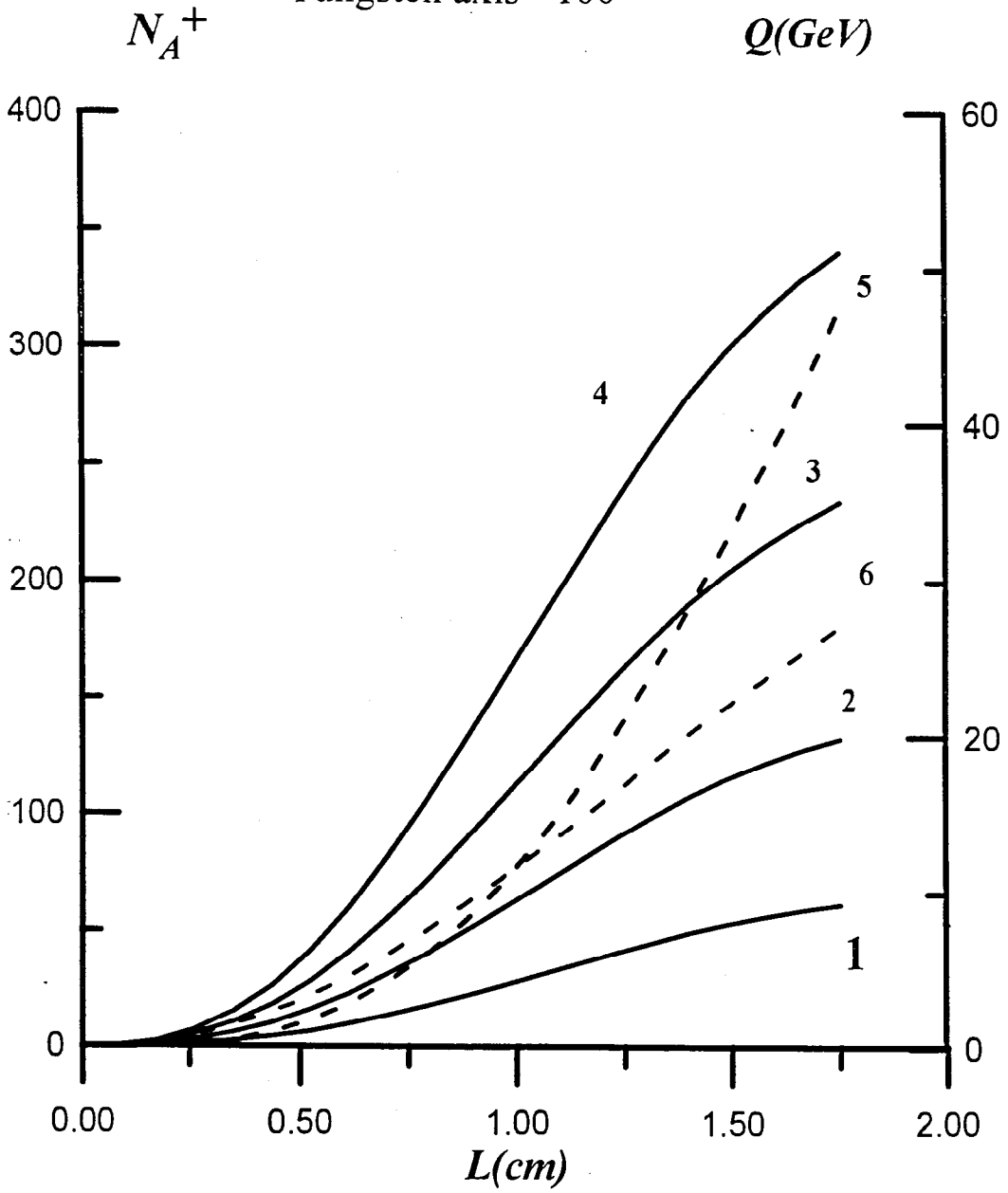

Fig. 4

Number of accepted positrons and energy losses for the initial energy E=300 GeV at low thickness

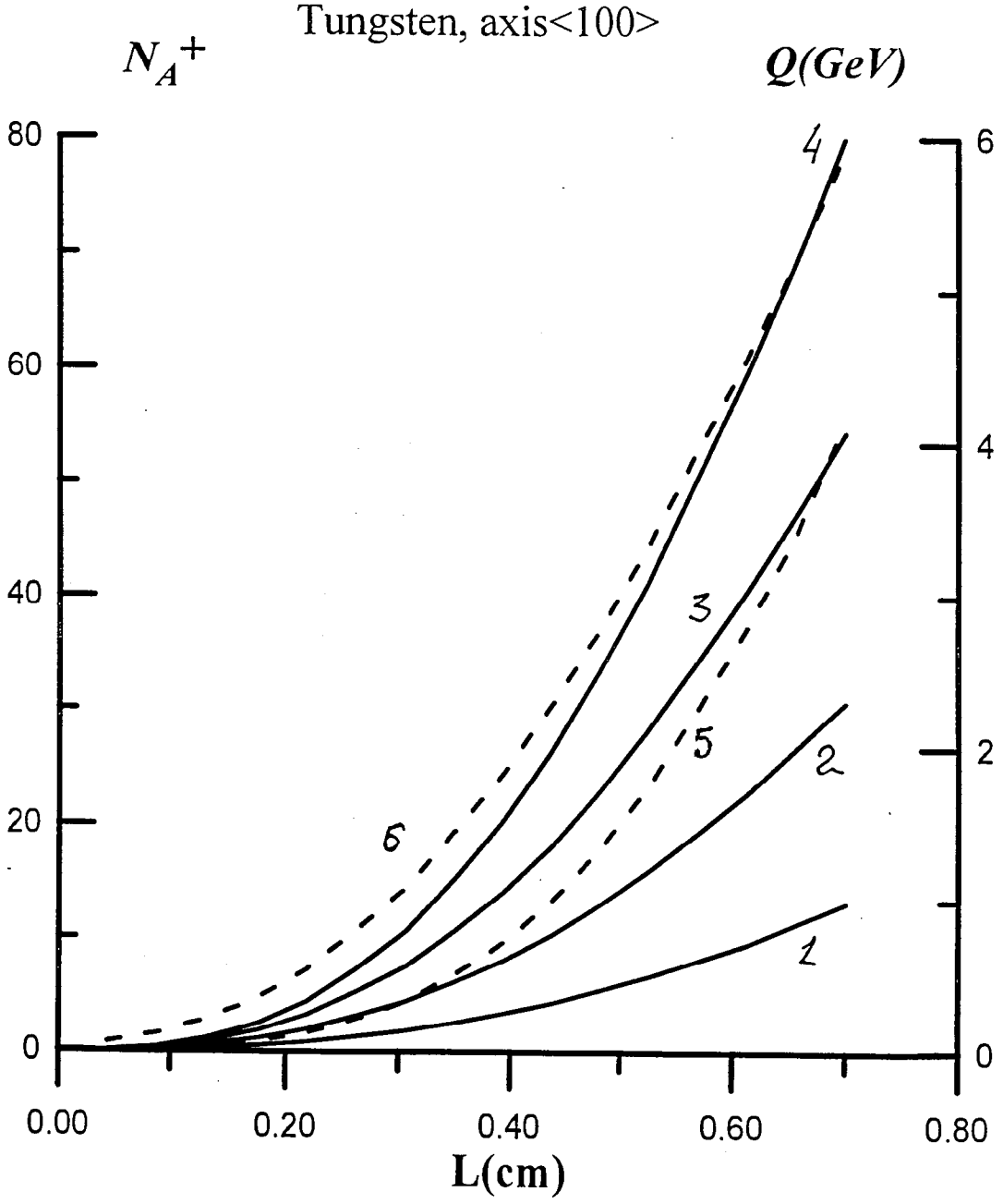

Fig. 5

Production of Polarized Positrons in Interaction of High-Energy Electrons with Laser Wave

V. N. Baier
Budker Institute of Nuclear Physics, 630090 Novosibirsk, Russia

Abstract

Creation of polarized positrons is considered in two-step process of interaction of unpolarized high-energy electrons with circularly polarized soft (laser) photon. The first step is the Compton scattering in which high-energy circularly polarized photon appears. The second step is pair creation in subsequent interaction of this photon with another circularly polarized laser photon. Direct electroproduction of electron-positron pair in interaction of high-energy electron with laser photon (trident production) is considered also. It is shown that high degree of the longitudinal polarization of created positrons can be obtained. An analysis is carried out in the Born approximation.

1 Introduction

Projects of electron-positron linear colliders with the energies of the order of TeV are now being under discussion in several laboratories. For a program of physics research with such collider it will be quite important to have opportunity to work with longitudinally polarized particles.

The are a few proposals to obtain polarized positrons:

1. Longitudinally polarized positrons are created in thin target by circularly polarized photons radiated from high-energy electrons in an appropriate undulator [1], [2].

2. Longitudinally polarized positrons are created at collision of high energy photon with circularly polarized laser photon. A radiation of high-energy electrons in oriented crystals is proposed as a source of high-energy photons [3].

In the present paper creation of longitudinally polarized positrons in interaction of high-energy electrons with photons of circularly polarized laser wave is proposed. We consider two-step process: the first stage is the Compton scattering of circularly polarized soft photon on high-energy unpolarized electron with creation of high-energy partially circularly polarized photon; the second stage is pair creation in interaction of this photon with circularly polarized soft photon from laser wave. Direct electroproduction of electron-positron pair (where a positron is polarized) in interaction of a high-energy electron with a circularly polarized laser photon (trident production) is considered also using the equivalent photon method.

For unpolarized particles such two-step (or cascade) process in an external field [4] and in laser wave [5] was recently considered.

2 Cross sections of basic processes

For convenience, the cross sections of basic processes with polarization under discussion will be presented first. Let for the Compton scattering k and p_c are the initial 4-momenta of a photon and an electron respectively and k' and p'_c are their final momenta, so that $p_c + k = p'_c + k'$.

Let us introduce invariant variables $x_c = s_c/m^2 - 1$, $y_c = 1 - u_c/m^2$;
$s_c = (p_c + k)^2$, $u_c = (p_c - k')^2$. The covariant form of description of photon polarization is given in detail in [6]. Polarization effects in Compton scattering have been analyzed in many papers, see e.g. references in [6]. The complete set of polarization effects, which are written down in covariant form, has been calculated recently in [7], where the method of [6] was used for description of photon polarization.

The cross section of Compton scattering for unpolarized electrons can be written in the form [7] (this cross section can be found also in [6]):

$$\frac{d\sigma_c}{dy_c\,d\phi} = \frac{\alpha^2}{2m^2x_c^4y_c^2}\sum_{jj'} R_{0j}^{0j'}(x_c,y_c)\xi_{cj}\xi'_{cj'},, \tag{1}$$

where ξ_{cj} and $\xi'_{cj'}$ are the Stokes parameters of the initial and the final photons. Note that the Stokes parameters describing linear polarization are defined in [6] and [7] with opposite signs. In (1) summation over final photon polarization is not carried out, so for the unpolarized final photon: $d\sigma = \frac{1}{2}d\sigma_{unpol}$. The right-hand side depends on ϕ because the polarizations are defined relative to the scattering plane, After integration over angle ϕ dependence on linear polarizations vanishes.

The final photon polarization is

$$\xi'_{cj'} = \frac{1}{R}\sum_j R_{0j}^{0j'}(x_c,y_c)\xi_{cj}, \tag{2}$$

where $R = R_{00}^{00}(x_c,y_c)$.

Components $R_{0j}^{0j'}(x_c,y_c)$ depending on photon's polarizations are presented below.

$$\begin{aligned}
R_{00}^{00}(x_c,y_c) &= x_c^3y_c - 4x_c^2y_c + 4x_c^2 + x_cy_c^3 + 4x_cy_c^2 - 8x_cy_c + 4y_c^2,\\
R_{00}^{03}(x_c,y_c) &= -4(x_c-y_c)(x_cy_c - x_c + y_c),\\
R_{01}^{01}(x_c,y_c) &= 2x_cy_c\,(x_cy_c - 2x_c + 2y_c)\,,\\
R_{02}^{02}(x_c,y_c) &= (x_c^2+y_c^2)\,(x_cy_c - 2x_c + 2y_c)\,,\\
R_{03}^{03}(x_c,y_c) &= 2\,(x_c^2y_c^2 - 2x_c^2y_c + 2x_c^2 + 2x_cy_c^2 - 4x_cy_c + 2y_c^2)
\end{aligned} \tag{3}$$

Now the process $\gamma\gamma \to e^+e^-$ will be discussed [8]. The initial photons momenta are k, k' and momenta of created electron and positron are p and p', so that $k + k' = p + p'$. The Mandelstam invariants are $t = (k-p)^2 = m^2(1-x)$, $u = (k-p')^2 = m^2(1-y)$, $s = m^2(x+y)$.

It is convenient to use the basis

$$n_0 = \frac{Q}{v}, \quad n_1 = \frac{K}{v}, \quad n_2 = \frac{v}{2w}P_\perp, \quad n_3^\mu = -\frac{1}{2vw}\varepsilon^\mu{}_{\alpha\beta\gamma}Q^\alpha K^\beta P^\gamma, \tag{4}$$

where $Q = k + k' = p + p'$, $K = k - k'$, $P = p' - p$, $P_\perp = P - \frac{PK}{K^2}K$; $v = \sqrt{x+y}$, $w = \sqrt{xy - x - y}$. Then the particles' momenta are

$$\begin{aligned}
p &= \frac{(x+y)n_0 - (x-y)n_1 - 2wn_2}{2v}, \quad p' = \frac{(x+y)n_0 + (x-y)n_1 + 2wn_2}{2v},\\
k &= \frac{v}{2}(n_0+n_1), \quad k' = \frac{v}{2}(n_0-n_1).
\end{aligned} \tag{5}$$

The vectors $\mathbf{n}_1$, $\mathbf{n}_2$, $\mathbf{n}_3$ form a right–handed system.

The vectors n_2 and n_3 can be used as polarization vectors of both photons. For the photon with momentum k, the vectors $\mathbf{n}_2$, $\mathbf{n}_3$, $\mathbf{k}$ form a right–handed system (in the c. m. frame).

The electron and positron density matrices are $\rho = \frac{1}{2}(\hat{p} - m)(1 - \gamma_5 \hat{a})$ and $\rho' = \frac{1}{2}(\hat{p}' + m)(1 - \gamma_5 \hat{a}')$. Let's introduce two bases

$$e_0 = \frac{p}{m}, \quad e_1 = \frac{(x+y-2)p - 2p'}{muv}, \quad e_2 = \frac{2wn_1 - (x-y)n_2}{uv}, \quad e_3 = n_3;$$
$$\epsilon'_0 = \frac{p'}{m}, \quad e'_1 = \frac{(x+y-2)p' - 2p}{muv}, \quad e'_2 = \frac{2wn_1 + (x-y)n_2}{uv}, \quad e'_3 = n_3 \quad (6)$$

where $u = \sqrt{x+y-4}$. Then $a = \sum_{i=1}^{3} \zeta_i e_i$, where in c. m. frame ζ_1 is the longitudinal polarization, ζ_2 is the transverse polarization in the reaction plane, and ζ_3 is the transverse polarization perpendicular to this plane. Introducing formally $\zeta_0 = 1$, we have $\rho = \frac{1}{2}\sum_{i=0}^{3} \zeta_i \rho_i$, where $\rho_0 = \hat{p} - m$, $\rho_i = -\rho_0 \gamma_5 \hat{e}_i$. Similarly, $\rho' = \frac{1}{2}\sum_{i'=0}^{3} \zeta'_{i'} \rho'_{i'}$, where $\rho'_0 = \hat{p}' + m$, $\rho'_i = -\rho'_0 \gamma_5 \hat{e}'_i$.

The cross section of the process $\gamma\gamma \to e^+e^-$ may be written in the form

$$\frac{d\sigma_p}{dt\, d\varphi} = \frac{\alpha^2}{4s^2x^2y^2} \sum_{ii'jj'} F^{ii'}_{jj'}(x,y) \xi_j \xi'_{j'} \zeta_i \zeta'_{i'}, \quad (7)$$

The right-hand side of (7) depends on φ because the polarizations are defined relative to the reaction plane. The final particles' polarizations ζ_i, $\zeta'_{i'}$ describe probabilities of their registration by the detector; when they are absent, $d\sigma = \frac{1}{4} d\sigma_{\text{unpol}}$ [6]. The cross section summed over the final particles' polarizations is

$$\frac{d\sigma_p}{dt\, d\varphi} = \frac{\alpha^2}{s^2x^2y^2} F, \quad F = \sum_{j'j} F^{00}_{jj'}(x,y) \xi_j \xi'_{j'}. \quad (8)$$

Polarizations of the final particles themselves are

$$\zeta_i^{(f)} = \frac{1}{F} \sum_{jj'} F^{i0}_{jj'}(x,y) \xi_j \xi'_{j'}, \quad \zeta_{i'}^{(f)\prime} = \frac{1}{F} \sum_{jj'} F^{0i'}_{jj'}(x,y) \xi_j \xi'_{j'}. \quad (9)$$

The four-vectors of the final particles' polarization are evidently $a = \sum_{i=1}^{3} \zeta_i e_i$, $a' = \sum_{i'=1}^{3} \zeta'_{i'} e'_{i'}$.

The components $F^{ii'}_{jj'}(x,y)$ needed for our problem are presented below (where the notation $\overline{F}^{ii'}_{jj'}(x,y) = F^{ii'}_{jj'}(y,x)$ is used).

$$\begin{aligned}
F^{00}_{00}(x,y) &= x^3y + 4x^2y - 4x^2 + xy^3 + 4xy^2 - 8xy - 4y^2, \\
F^{00}_{03}(x,y) &= F^{00}_{30}(x,y) = 4v^2w^2, \\
F^{01}_{02}(x,y) &= \overline{F}^{01}_{20}(x,y) = -\left(x^2y - 2x^2 - xy^2 - 2xy + 4x + 4y\right) v^3/u, \\
F^{02}_{02}(x,y) &= -F^{02}_{20}(x,y) = 4v^2w^3/u, \\
F^{00}_{22}(x,y) &= -\left(x^2 + y^2\right)(xy - 2x - 2y), \\
F^{01}_{23}(x,y) &= 4v^3w^2/u, \\
F^{02}_{23}(x,y) &= -2\,(y-2)\, v^4 w/u,
\end{aligned} \quad (10)$$

3 Cascade creation of the longitudinally polarized positrons

Using probabilities given in previous section (probability of a process is dW, $d\sigma = \dfrac{dW}{J}$, J is the flow of the initial particles, in our case $J = 1 + v_z \simeq 2$, v_z is the velocity of the initial electron) as kernels of corresponding kinetic equation one can calculate characteristics of a cascade caused by a initial high-energy electron.

Here the method of successive approximations will be used. This method, generally speaking, is applicable if the total probability of cascade is relatively small. In this case for probability of cascade electroproduction one has

$$\frac{dw_{cas}}{d\omega'} = \frac{dW_c}{d\omega'}\left[L - \frac{1}{W_p(\omega')}\left(1 - \exp(-W_p(\omega')L)\right)\right], \tag{11}$$

where ω' is the energy of the final photon in the Compton effect, $\dfrac{dW_c}{d\omega'}$ is the probability of the Compton scattering, $W_p(\omega')$ is the total probability of pair creation, L is the interaction length, notation is used:$dW = \dfrac{dw}{dL}$. When $W_p(\omega')L \ll 1$ one can expand exponent in (11):

$$\frac{dw_{cas}}{d\omega'} = \frac{1}{2}\frac{dW_c}{d\omega'}LW_p(\omega', \xi_2 = \xi'_{c2})L, \quad \frac{dn_c}{d\omega'} = \frac{dW_c}{d\omega'}L, \tag{12}$$

where n_c is the total number of final photons in Compton effect.

Let us introduce kinematic variables:

- ω is the energy if the initial photon in the Compton scattering;
- ω' is the energy if the final photon in the Compton scattering;
- ε is the energy if the initial electron in the Compton scattering;
- $\varepsilon_p = \epsilon$ is the energy if the created electron in the pair creation process;
- $\varepsilon_{p'} = \epsilon'$ is the energy if the created positron in the pair creation process;
- $x_c = \lambda = \dfrac{2kp}{m^2} = \dfrac{4\varepsilon\omega}{m^2}$ is the energy invariant for Compton scattering;
- $z = \dfrac{\epsilon'}{\varepsilon}$, $z' = \dfrac{\omega'}{\varepsilon}$ are the dimensionless variables.

The differential cross sections written down in previous section present spectral distributions over energy of the final particles. Using these distributions, one

can obtain the spectral distribution of created positrons in the cascade process. In terms of the introduced variables it has the form:

$$\frac{dw_{cas}}{dz} = \frac{L^2}{2}\int\limits_{z_1'}^{z_2'} dz' \frac{dW_c}{dz'}\frac{dW_p(z', \xi_2 = \xi_{c2}')}{dz}, \tag{13}$$

where

$$z_1' = \frac{z^2\lambda}{z\lambda - 1}, \quad z_2' = \frac{\lambda}{1+\lambda}. \tag{14}$$

Value of z varies within limits: $z_1 \leq z \leq z_2$, where

$$z_1 = \frac{\lambda - f(\lambda)}{2(\lambda+1)}, \quad z_2 = \frac{\lambda + f(\lambda)}{2(\lambda+1)}, \quad f(\lambda) = \sqrt{\lambda^2 - 4\lambda - 4}. \tag{15}$$

At the threshold of the cascade process $f(\lambda) = 0$, so that $t_{th} = 2(1+\sqrt{2})$ (compare [5]). The limits in (14), (15) follow from simple kinematic consideration.

Substituting into (13) the explicit expressions for probabilities of Compton scattering (1),(3) and pair creation (7),(10) one obtains for the probability of the cascade production of a positron in interaction of a high-energy electron with a soft (laser) photon

$$\frac{dw_{cas}}{dz} = \frac{(2\pi\alpha^2 L)^2}{2m^2\lambda^2}\left(I_0 + \zeta_1'\xi_{c2}I_\zeta\right), \tag{16}$$

where ζ_1' describes probability of registration of the longitudinal polarization of the positron by detector, ξ_{c2} is the circular polarization of the initial soft photon,

$$\begin{aligned} I_0 &= \int\limits_{z_1'}^{z_2'} \frac{dz'}{z'^2}\left[R_{00}^{00}(x_c, y_c)F_{00}^{00}(x,y) + R_{02}^{02}(x_c, y_c)F_{22}^{00}(x,y)\xi_{c2}^2\right], \\ I_\zeta &= \int\limits_{z_1'}^{z_2'} \frac{dz'}{z'^2}\left[R_{02}^{02}(x_c, y_c)F_{02}^{01}(x,y) + R_{00}^{00}(x_c, y_c)F_{20}^{01}(x,y)\right], \end{aligned} \tag{17}$$

here one has to substitute

$$x_c = \lambda, \quad y_c = \lambda(1-z'), \quad x = \lambda z, \quad y = \lambda(z'-z). \tag{18}$$

We took into account in (16) that $dt = -\lambda dz$.

The longitudinal polarization of the created positron itself is

$$\zeta_1^{(f)'} = \frac{I_\zeta}{I_0}\xi_{c2} \tag{19}$$

The results obtained are illustrated in Fig.1-3 for $\lambda = 5$, $\lambda = 8$ and $\lambda = 50$ respectively. Figures (a) are the spectral distributions of the probability of cascade process for unpolarized particles with correlation term of the circular

polarizations (for $\xi_{c2}^2 = 1$) of photons (I_0 (17)) in units $\frac{(2\pi\alpha^2 L)^2}{2m^2\lambda^2}$. Figures (b) present longitudinal polarization of the created positrons plotted vs z for $\xi_{c2} = 1$. In Fig.1 the situation near threshold of cascade process ($\lambda_{th} = 4.83$) is shown. The maximum of the spectral distribution is near the middle of the available interval of z (15), slightly shifted to the left. There is sizable longitudinal polarization of positrons for high-energy tail of positrons only. In Fig.2 the situation far from threshold of cascade process is shown. The maximum of the spectral distribution is shifted noticeably to the left. There is sizable longitudinal polarization of positrons in the whole interval of z. Especially high degree of polarization is attained both in soft and hard part of the spectrum. In Fig.3 the situation in high-energy region of cascade process is shown. There is pronounced peak in the spectral distribution of created positrons near soft boundary of the spectrum. Here also there is sizable longitudinal polarization of positrons in the whole interval of z. Especially high degree of polarization (up to $\zeta_1^{(f)'} = 1$) is attained both in soft and hard part of the spectrum. Collecting positrons created within the peak one obtains polarized beam of positrons.

4 Direct electroproduction of polarized positron

Another mechanism is a direct electroproduction of electron-positron pair. The main contributions give the diagrams shown in Fig.4. Cross section of this process can be obtained using the method of equivalent photons:

$$\frac{d\sigma_{ep}}{dz} = \frac{\alpha^3 \ln\lambda}{m^2\lambda}\left(J_0 + \zeta_1'\xi_{c2}J_\zeta\right), \tag{20}$$

where ζ_1' describes probability of registration of the longitudinal polarization of the positron by detector, ξ_{c2} is the circular polarization of the initial soft photon.

$$\begin{aligned} J_0 &= \lambda^2 \int_{z_1'}^{z'_{max}} \frac{dz'}{z'}\left(1 - z' + \frac{z'^2}{2}\right)\frac{F_{00}^{00}(x,y)}{s^2x^2y^2}, \\ J_\zeta &= \lambda^2 \int_{z_1'}^{z'_{max}} \frac{dz'}{z'}\left(1 - z' + \frac{z'^2}{2}\right)\frac{F_{01}^{02}(x,y)}{s^2x^2y^2}, \end{aligned} \tag{21}$$

here

$$\lambda = \frac{2kq}{m^2}, \quad s = \lambda z', \quad x = \lambda z, \quad y = \lambda(z' - z), \quad z'_{max} = 1 - \frac{1}{2\lambda}, \tag{22}$$

and z_1' is defined in (14). The longitudinal polarization of the created positron itself for this case is

$$\zeta_1^{(f)'} = \frac{J_\zeta}{J_0}\xi_{c2} \tag{23}$$

Formally, these results are valid when $\ln\lambda \gg 1$. Note, that in (20) summation over final particle polarizations is not carried out.

The results obtained in this section are illustrated in Fig.5-6 for $\lambda = 20$ and $\lambda = 50$ respectively. Figures (a) are the spectral distributions of the probability of direct electroproduction process for unpolarized particles and photons in units $\frac{\alpha^3 \ln\lambda}{m^2\lambda}$ (the term J_0 in eq.(20)). Figures (b) present longitudinal polarization of the created positrons plotted vs z for $\xi_{c2} = 1$. In Fig.5 the situation enough far from threshold ($\lambda_{th} = 8$) of direct electroproduction process is shown. The maximum of the spectral distribution is lying in the soft part of the spectrum. There is sizable longitudinal polarization of positrons in the region of the peak. Especially high degree of polarization (up to $\zeta_1^{(f)'} = 1$) is attained in soft of the spectrum. In Fig.6 the situation in high-energy region of direct electroproduction process is shown. There is pronounced peak in the spectral distribution of created positrons near soft boundary of the spectrum just as in the case of cascade process. Especially high degree of polarization (up to $\zeta_1^{(f)'} = 1$) is attained in the redion of the peak. Collecting positrons created within the peak one obtains polarized beam of positrons. So, independent of mechanism of positron production created positrons are longitudinally polarized especially in soft part of the spectrum.

References

[1] V. E. Balakin and A. A. Mikhailichenko, Preprint INP 79-85, Novosibirsk, 1979.

[2] A. D. Bukin and A. A. Mikhailichenko, Preprint BINP 92-76, Novosibirsk, 1992.

[3] V. N. Baier, R. Chehab and V. M. Katkov, Nucl. Instr. Methods **A 338** (1994) 156.

[4] V. N. Baier, V. M. Katkov and V. M. Strakhovenko, Sov.J.Nucl.Phys **53** (1991) 632.

[5] V. N. Baier and K. Yokoya, Particle Accelerators **44** (1994) 77.

[6] V. B. Berestetskii, E. M. Lifshitz, L. P. Pitaevskii, *Quantum Electrodynamics*. Pergamon Press, Oxford (1982).

[7] A. G. Grozin, in *Proc. VIII Workshop on High Energy Physics and Quantum Field Theory*, Zvenigorod, 1993, ed. B. B. Levtchenko, Moscow University Press (1994), p.60.

[8] V. N. Baier and A. G. Grozin, in *Proc. X Workshop on High Energy Physics and Quantum Field Theory*, Zvenigorod, 1995, ed. B. B. Levtchenko, Moscow University Press (1996), p.344.

Figure captions

- **Fig.1** Characteristics of the cascade process for $\lambda = 5$.
  The spectral distribution of the probability of cascade process for unpolarized particles with correlation term of the circular polarizations (for $\xi_{c2}^2 = 1$) of photons (I_0 in eqs.(16), (17)) in units $\frac{(2\pi\alpha^2 L)^2}{2m^2\lambda^2}$ (a). Longitudinal polarization of the created positrons plotted vs z for $\xi_{c2} = 1$ (b).

- **Fig.2** Same as Fig.1 but for $\lambda = 8$.

- **Fig.3** Same as Fig.1 but for $\lambda = 50$.

- **Fig.4** Diagrams of direct electroproduction of electron-positron pair.

- **Fig.5** Characteristics of the direct electroproduction process for $\lambda = 20$.
  The spectral distributions of the probability of direct electroproduction process for unpolarized particles and photons in units $\frac{\alpha^3 \ln\lambda}{m^2\lambda}$ (the term J_0 in eq.(20)) (a). Longitudinal polarization of the created positrons plotted vs z for $\xi_{c2} = 1$ (b).

- **Fig.6** Same as Fig.5 but for $\lambda = 50$.

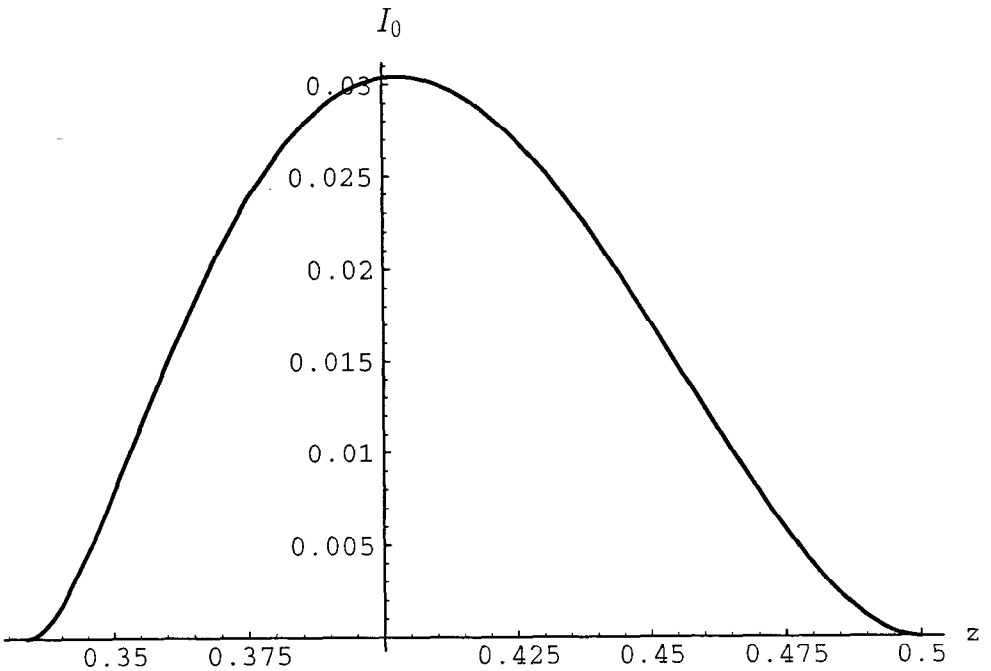
I_0
0.03
0.025
0.02
0.015
0.01
0.005
0.35
0.375
0.425
0.45
0.475
0.5
z

(a)

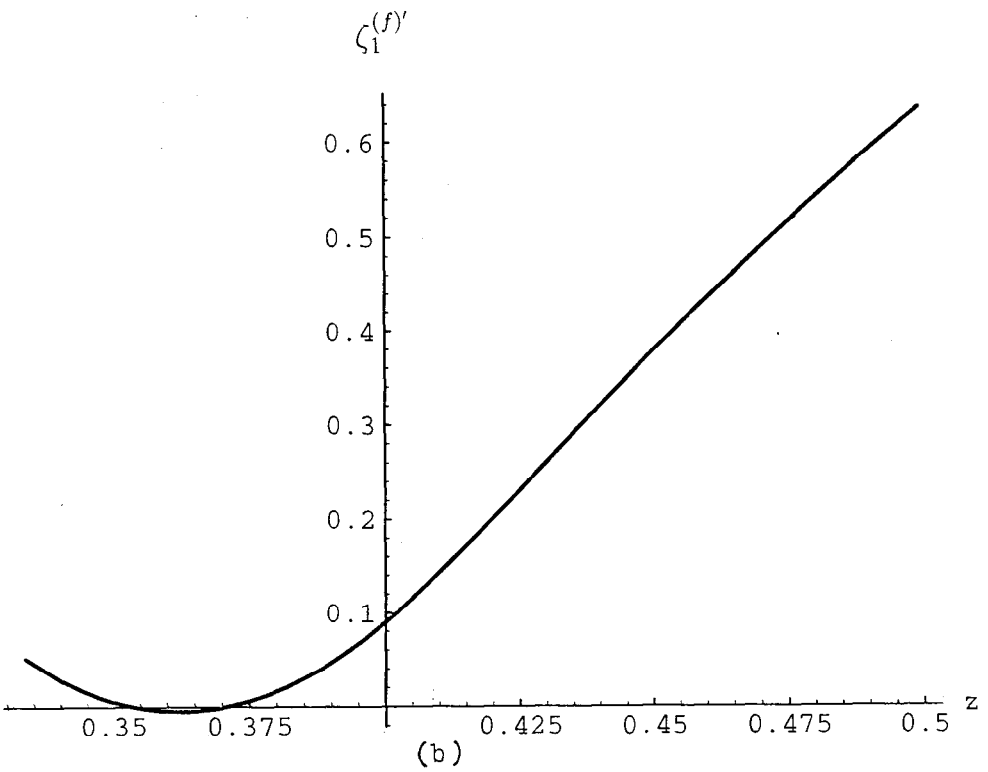
$\zeta_1^{(f)'}$
0.6
0.5
0.4
0.3
0.2
0.1
0.35
0.375
0.425
0.45
0.475
0.5
z

(b)

Fig.1

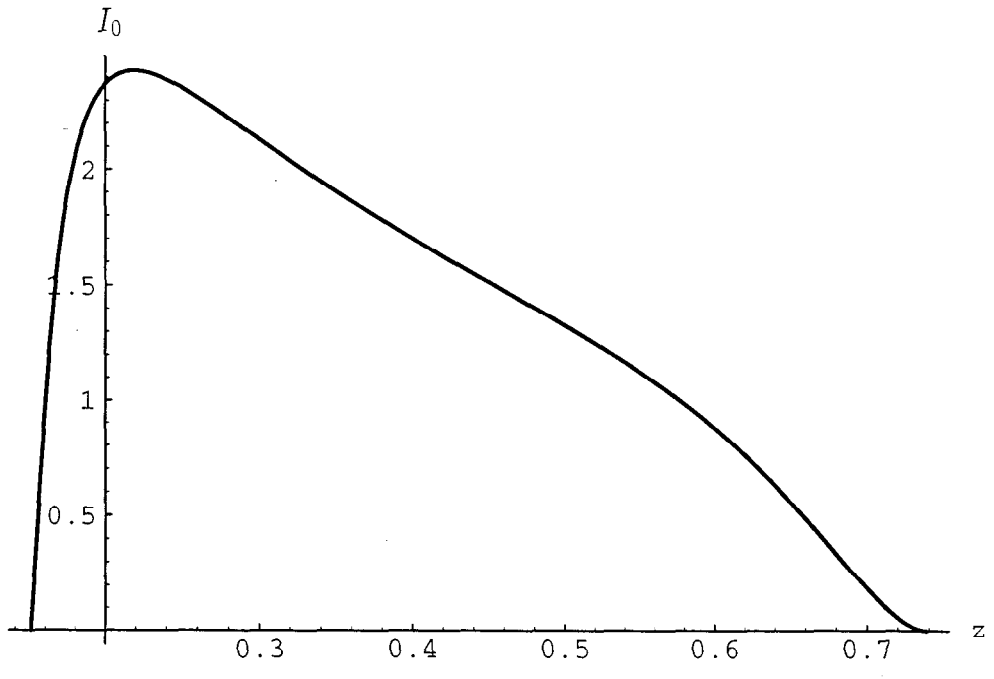

(a)

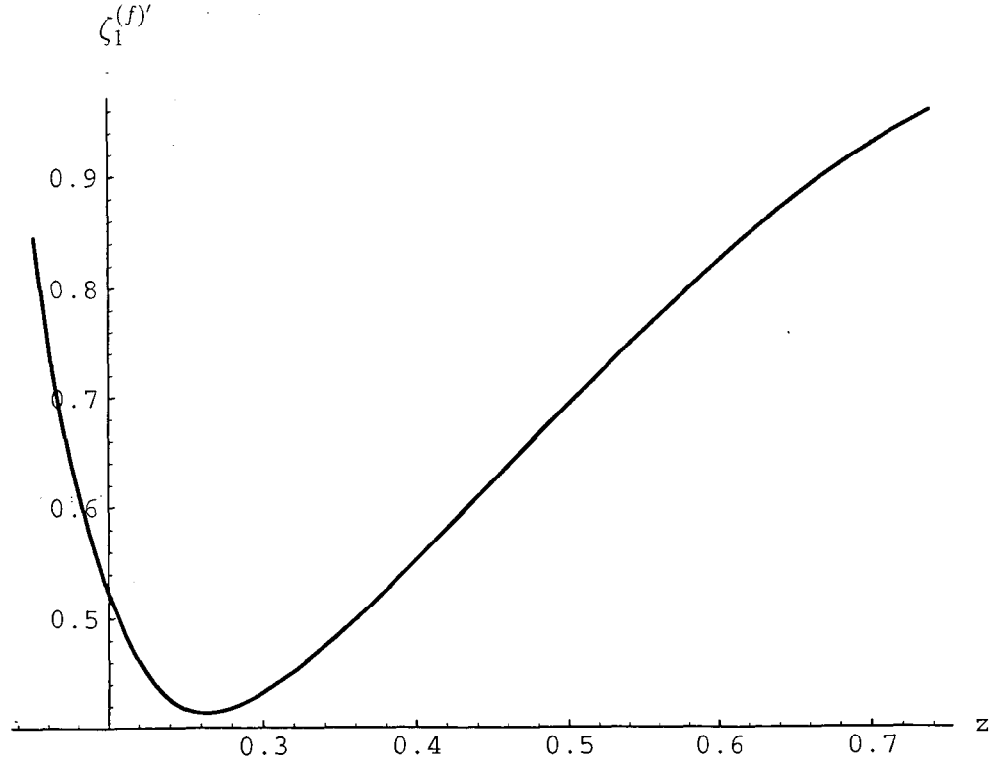

(b)

Fig.2

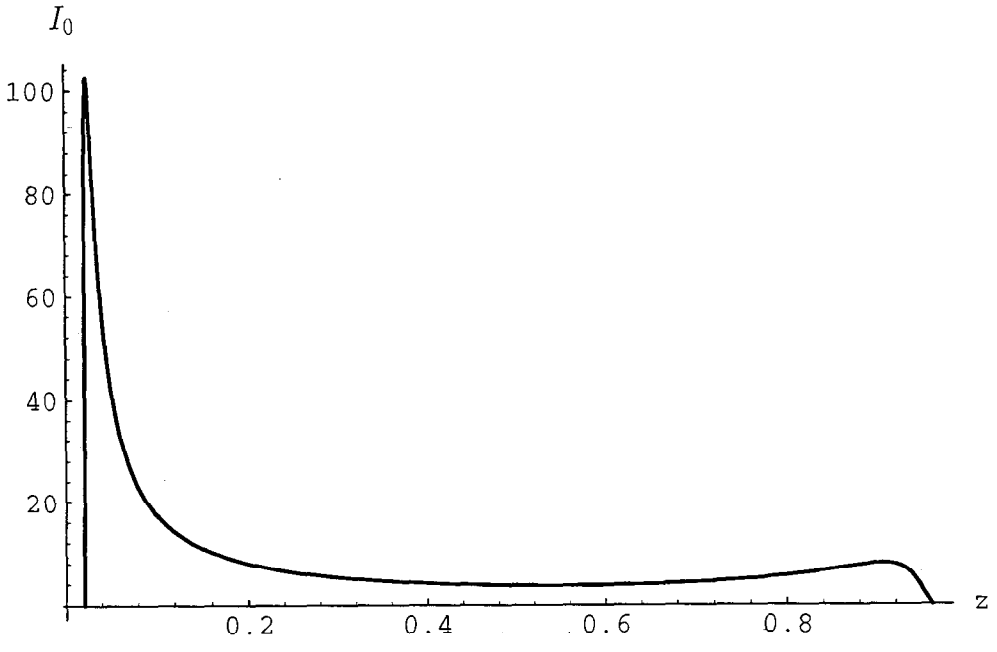

(a)

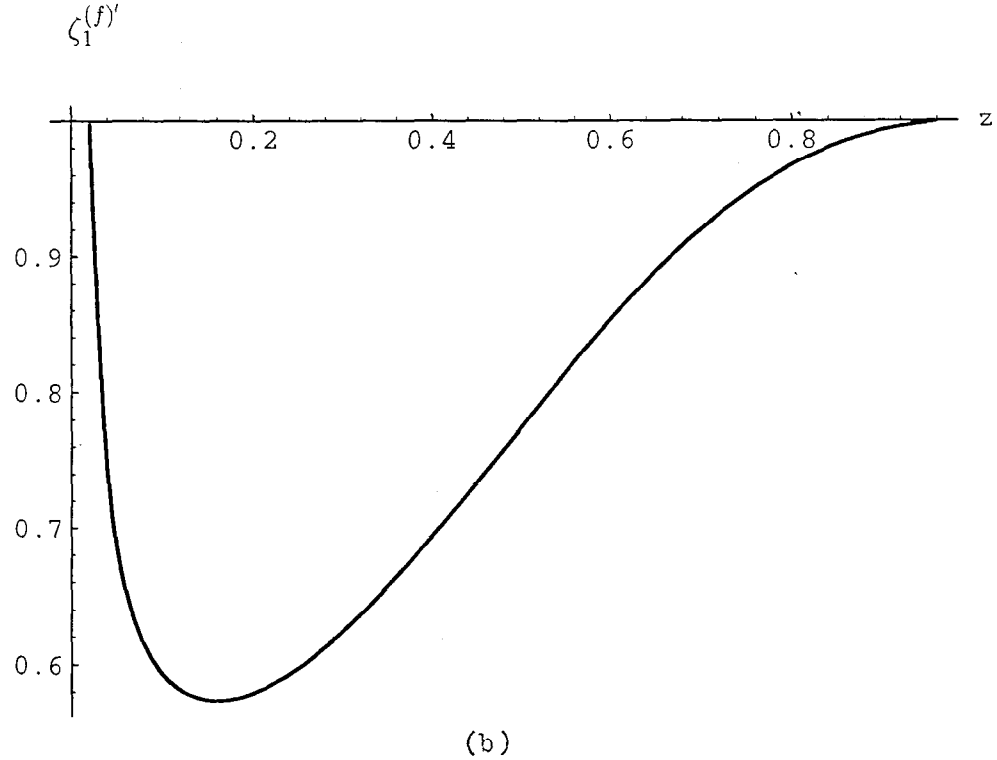

(b)

Fig.3

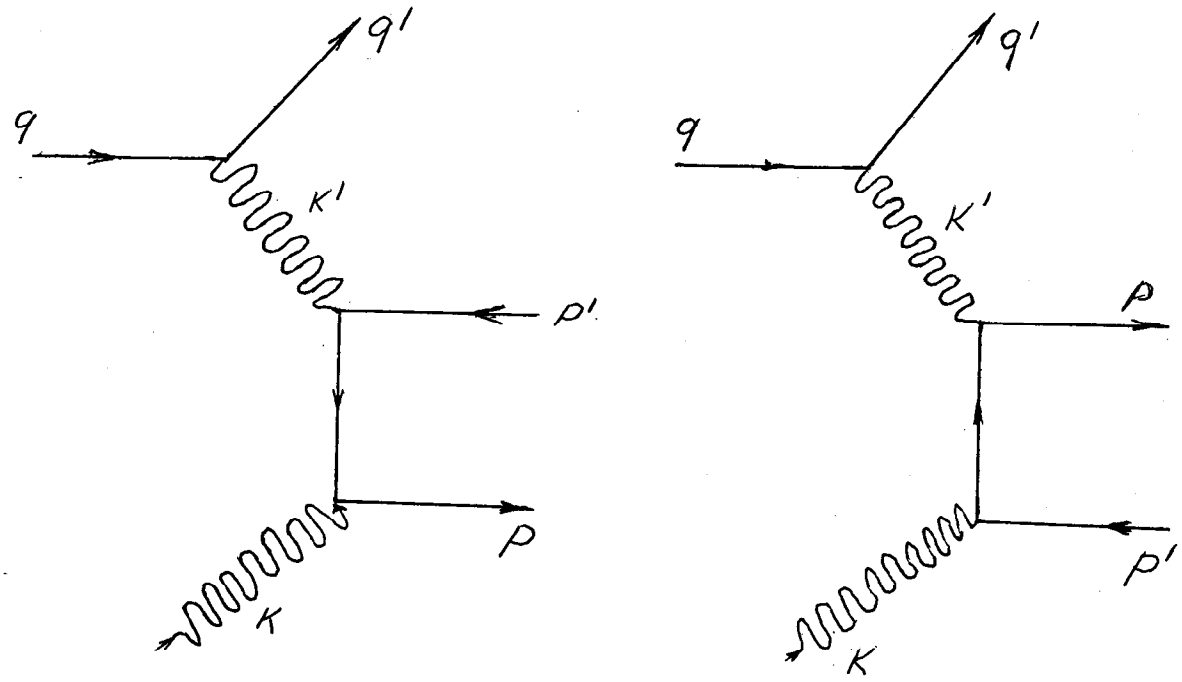

Fig.4

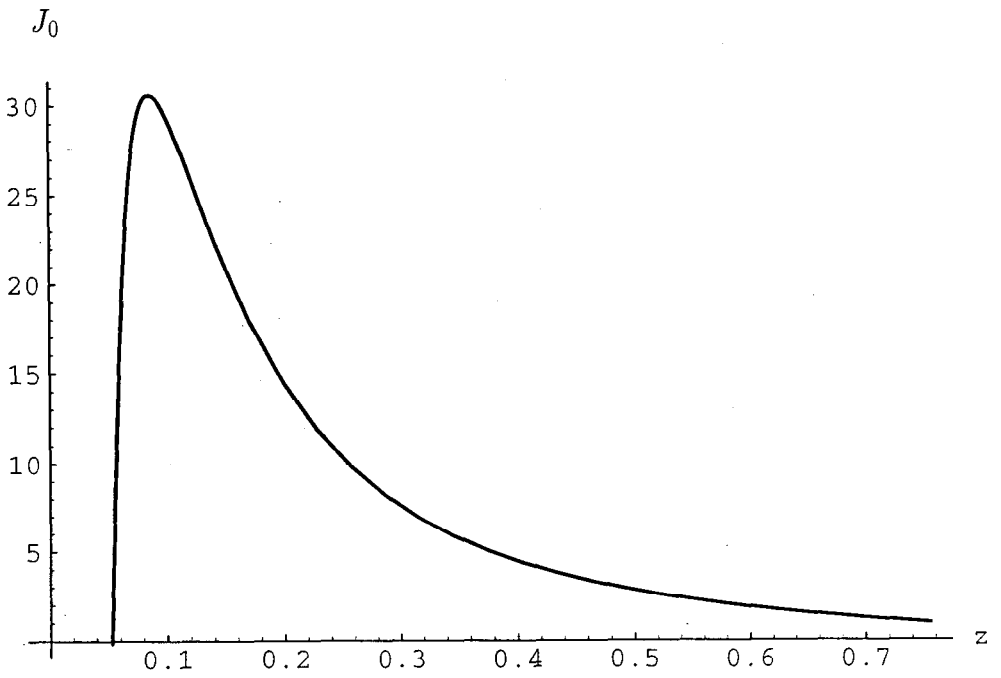
J_0
30
25
20
15
10
5
0.1
0.2
0.3
0.4
0.5
0.6
0.7
z

(a)

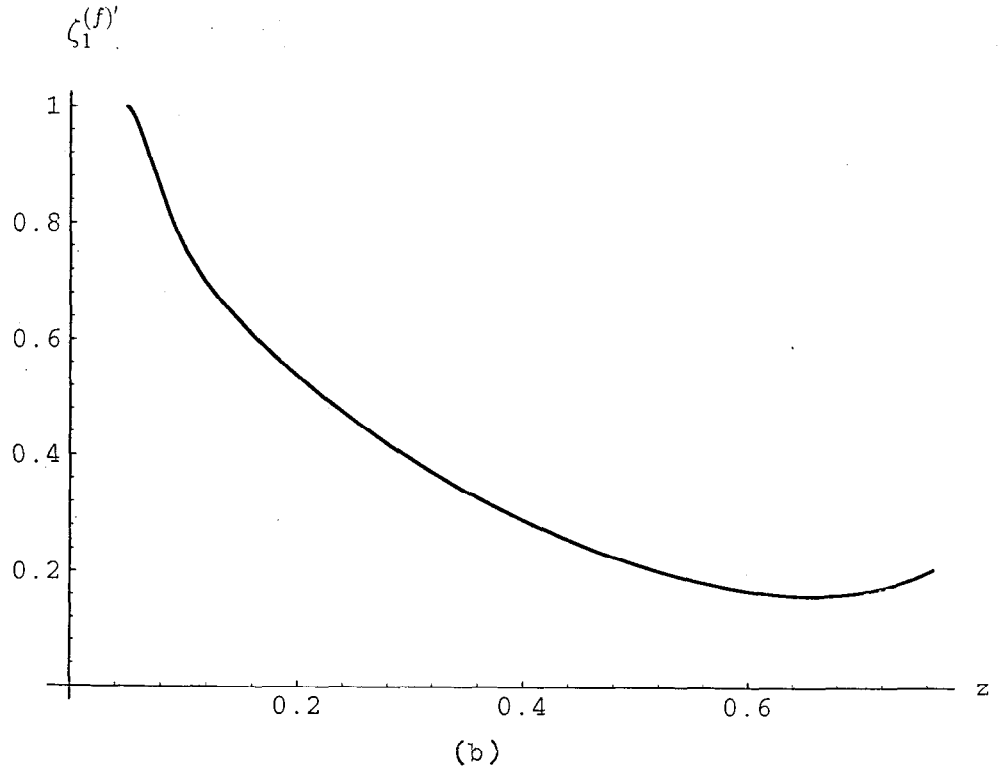
$\zeta_1^{(f)'}$
1
0.8
0.6
0.4
0.2
0.2
0.4
0.6
z

(b)

Fig.5

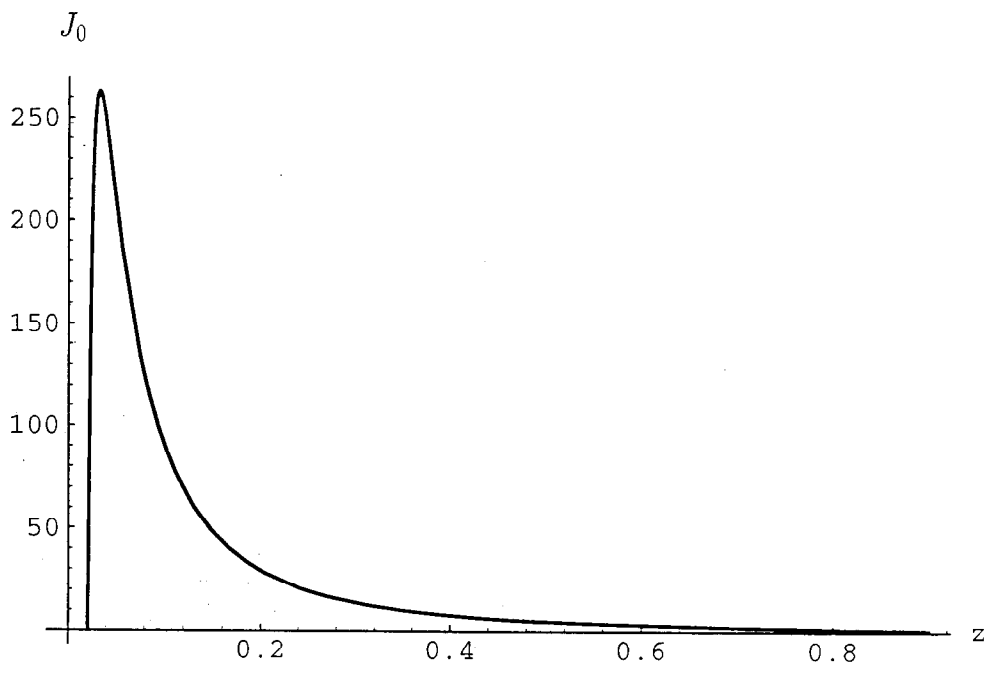

(a)

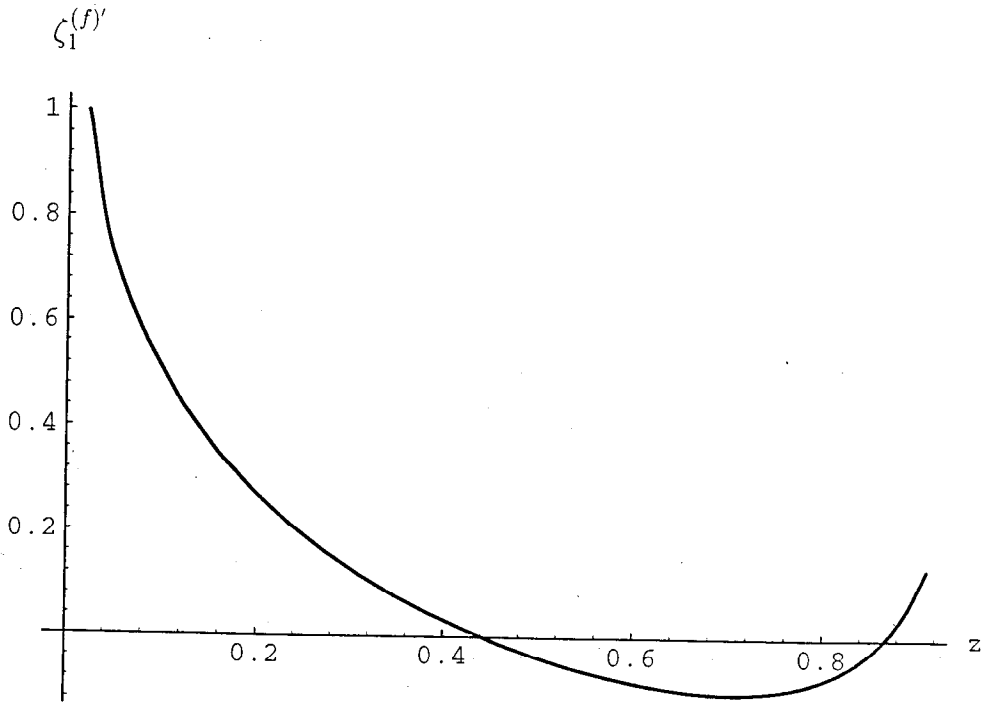

(b)

Fig.6

A CRYSTAL SOURCE USING A 10-GEV ELECTRON BEAM

R. Chehab*

Laboratoire de l'Accélérateur linéaire,
IN2P3-CNRS et Université de Paris-Sud, F-91405 Orsay Cedex

ABSTRACT

A tentative comparison between positron sources using crystal or amorphous targets is presented. Both kinds of sources, dedicated to linear colliders, make use of multi-GeV incident electron beams. After a recall of the peculiarity of the radiation in crystals, acting as atomic undulators, a comparison with a classical source, the JLC one, is worked out. Choosing a typical scheme for the positron accelerator, yields, energy deposited and heating of both targets are examined. Particular attention is put on the effects of the temperature on the crystal characteristics and performances. As the ability of a crystal positron source to sustain high intensities has to be checked, a test of radiation damage has been operated at SLC, which results are expected in the near future.
From this comparison, it appears that a tungsten crystal target, 8 mm thick, using channeling of 10 GeV electrons along its $< 111 >$ axis provides almost the same yield at the Interaction Point of a linear collider as the classical source foreseen for JLC. Moreover, the energy deposited is about six times lower. At least, an hybrid solution made of crystal and amorphous disks of equal thickness is recommended. Its advantage is to preserve mainly the performances of the crystal in a warm regime.

*representing the group:
V.N. Baier[1], A. D. Bukin, T.V. Dimova, V. P. Druzhinin, M.S. Dubrovin, V. B. Golubev, S. I. Serednyakov, V. V. Shary, X. Artru[2] M. Chevallier, R. Kirsch, J-C. Poizat, J. Remillieux, R. Chehab[3], A. Jejcic[4], J. Silva, J. Major[5]

[1]Budker INP, Novosibirsk 630090 Russia
[2]Institut de Physique Nucléaire, IN2P3 - CNRS, F-69622 Villeurbanne Cedex, France
[3]Laboratoire de l'Accélérateur linéaire, IN2P3-CNRS et Université de Paris-Sud, F-91405 Orsay Cedex, France
[4]Collège de France, IN2P3-CNRS, Laboratoire de Physique Corpusculaire, 75231 Paris Cedex 05, France
[5]Stuttgart Max-Planck Institut für Metallforschung

1 Introduction

In the present LC projects we meet two approaches for the e^+ sources:

- Generation of e^+ with the e^- spent beam, after the IP (Long Wiggler for photon generation and thin converter)
  TESLA & SBLC

- Classical sources : high energy e^- beams on thick targets
  E-: 2 to 10 GeV and target thickness:
  4 to 6 Xo
  CLIC, NLC, JLC

In the latter, e^+ obtained by materialization of photons from Bremsstrahlung
To obtain enough e^+, we need thick targets; consequences are:

- Important thermic effects

- Too large emittance

Question:

If we consider moderate incident energies, is there a photon source more powerfull than Bremsstrahlung and generating consequently a large e^+ yield, allowing thinner values for the target ?

$\rightarrow$ CHANNELING = enhancement of radiation in ordered structures

Could a positron source, based on channeling of Multi-GeV electrons in a crystal , present an alternative to the classical sources foreseen for LC ? Clearly: could we reach 1 e^+/e^- at the IP with a crystal sustaining high intensities and having long enough life time ?

2 The Crystal

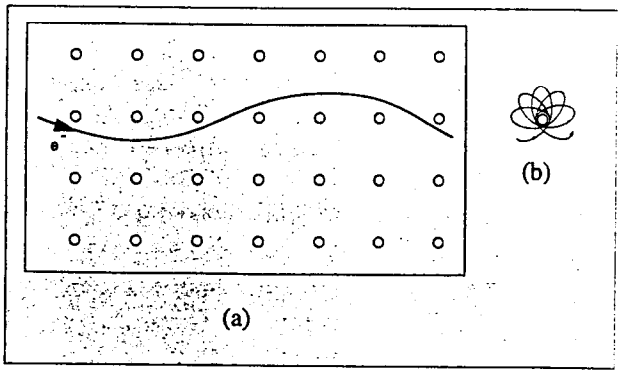

A particle moving rapidly along an axis direction sees N nuclei aligned on its trajectory and the action of this "Super nucleus" is stronger than the individual actions of the N nuclei (Bremsstrahlung) . As a consequence, the particle radiates more than in a random structure. Such a device presents, w.r.t. Bremsstrahlung, interesting properties concerning:

- the yield
- the directivity

Comparison with a magnetic wiggler:

- Fields larger: B, about a thousand Teslas
- Period shorter: about 1 micrometer

Comparison with the Bremsstrahlung:

- Larger photon yields
- Softer photons
  (The curvature radius is larger than with Bremsstrahlung)

Due to the large field value, W crystal with axial orientation on <111> axis is chosen.

2.1 The thick crystal

If we associate a radiation length to the channeling radiation, this length is much shorter than the classical radiation length (amorphous). The channeled e- radiates a much larger amount of photons in the first millimeters of the target. If we consider a rather thick (1 cm) W crystal submitted to a 10 GeV incident electron beam, most of the radiation occurs in the first 4-5 mm. The pair creation concerns mainly the last part of the target.

For instance: an 8 mm thick W crystal is almost equivalent to an hybrid target made of: (4 mm crystal) + (4 mm amorphous) for a 10 GeV incident e- beam. Slight differences could come from:

-e+ energy spectrum
-e+ emittance, due to possible channeling of the emitted e+ in the whole crystal.

Therefore, the calculations presented concern an all-crystal source (8 mm) which should be compared with JLC (same Ei).

3 TYPICAL SCHEME FOR A POSITRON SOURCE FACILITY

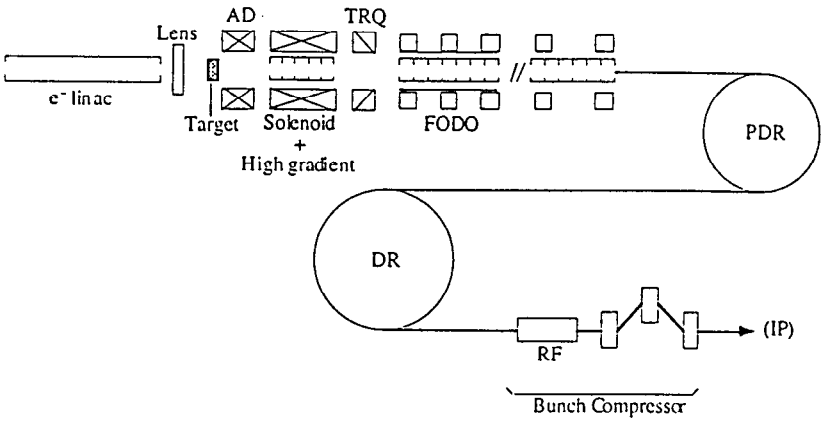

Figure 1: The positron facility
AD: Adiabatic device
TRQ: matching optics

The focusing system is an adiabatic lens followed by a constant field solenoid.

Maximum field: 8 Teslas
Minimum field: 0.8 Teslas
Lens length: 18 cms
Tapering parameter: 50 m^{-1}.

At the end of the adiabatic lens the trajectory lengthening due to spiralization in the focusing channel is:

$$\Delta L = \frac{(\theta_i)^2}{2.\alpha}.\ln(\frac{Bo}{Bs})$$

The yields are calculated on three locations:

-at the exit of the target,
-at the entrance of the first DR
-at the Interaction Point.

3.1 A CONVENTIONAL SOURCE TAKEN AS A REFERENCE: JLC

→ Target, 6Xo amorphous W
Incident beam: 10 GeV
Yields: Total= 21 e^+/e^-
Entrance of first DR: 3.1 e^+/e^-
IP: 1.5 e^+/e^-

The e+ energy spectra, for the three locations, are shown below.

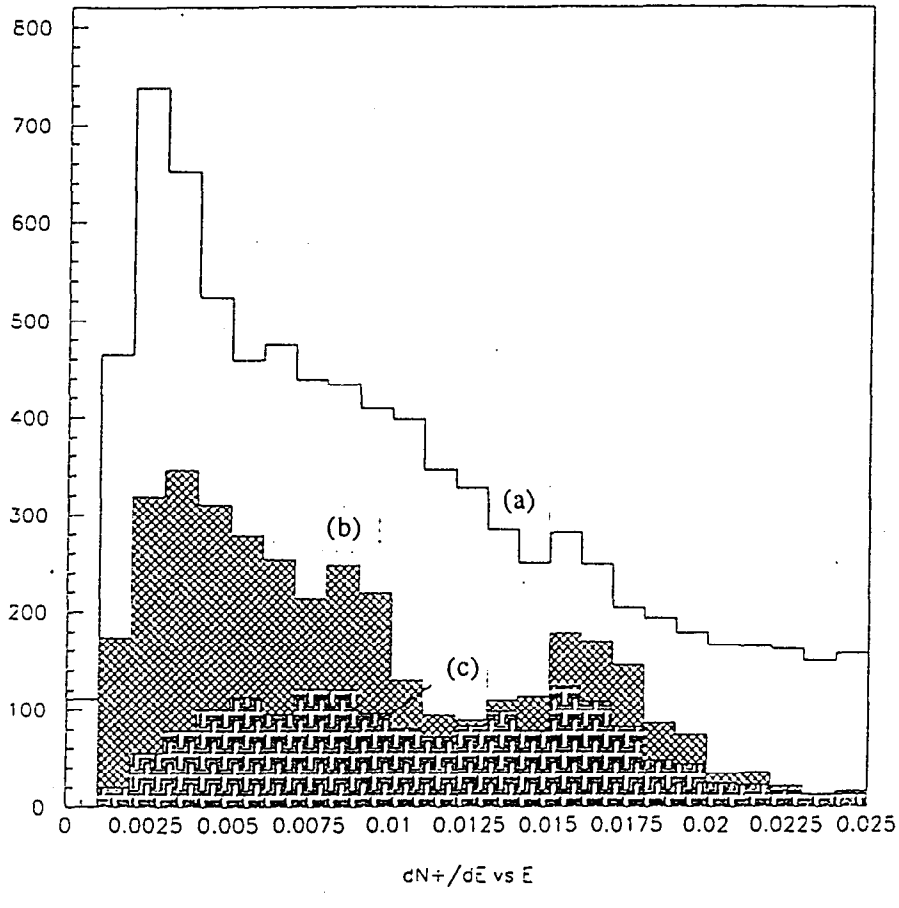

Figure 4 : E^+ Spectra for a $6X_0$ amorphous target, (a) Total yield, (b) Accepted yield in transverse phase space, (c) Accepted yield in transverse and longitudinal phase spaces.

3.2 A CRYSTAL AS A POSITRON SOURCE FOR AN LC

→ Target: 8 mm W crystal
Incident beam: 10 GeV
Yields: Total=19 e^+/e^-
Entrance of first DR: 2.4 e^+/e^-
IP: 1.2 e^+/e^-

The e+ energy spectra, for the three locations, are shown below.

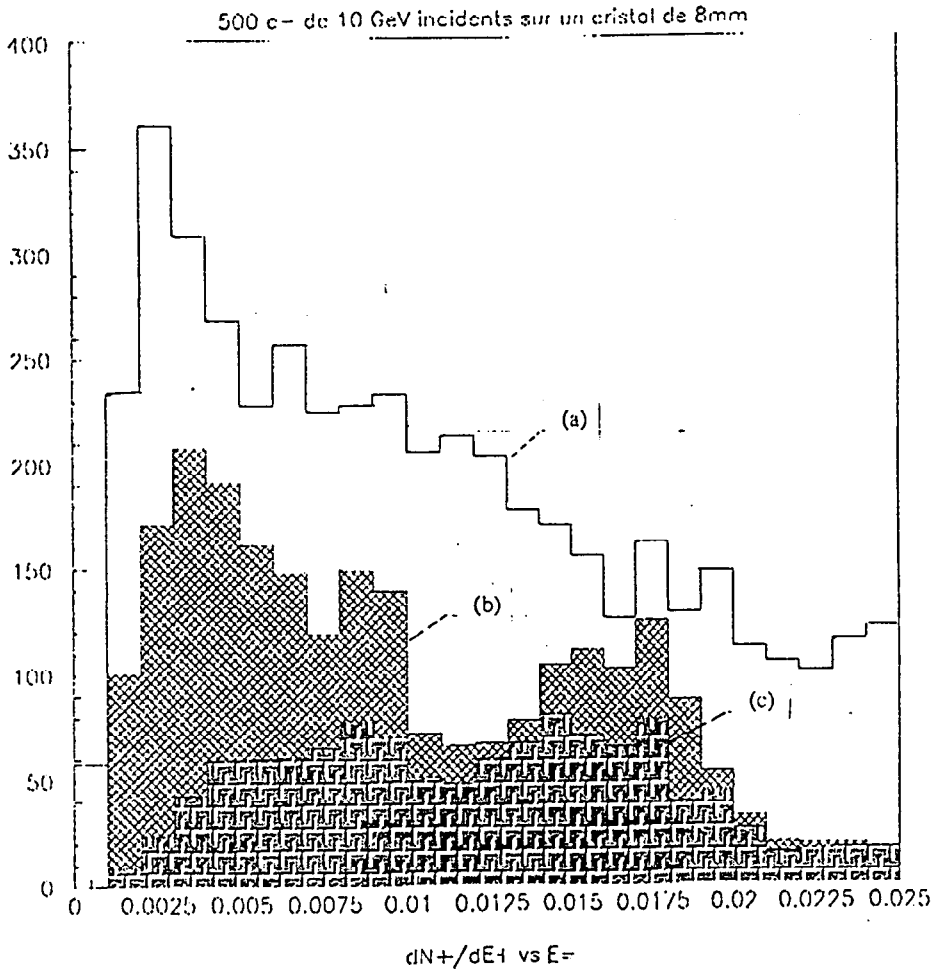

Figure 6 : E^+ Spectra for a 8 mm crystal, (a) Total yield, (b) Accepted yield in transverse phase space, (c) Accepted yield in transverse and longitudinal phase space.

3.3 The Crystal Source: Acceptance condition for LC

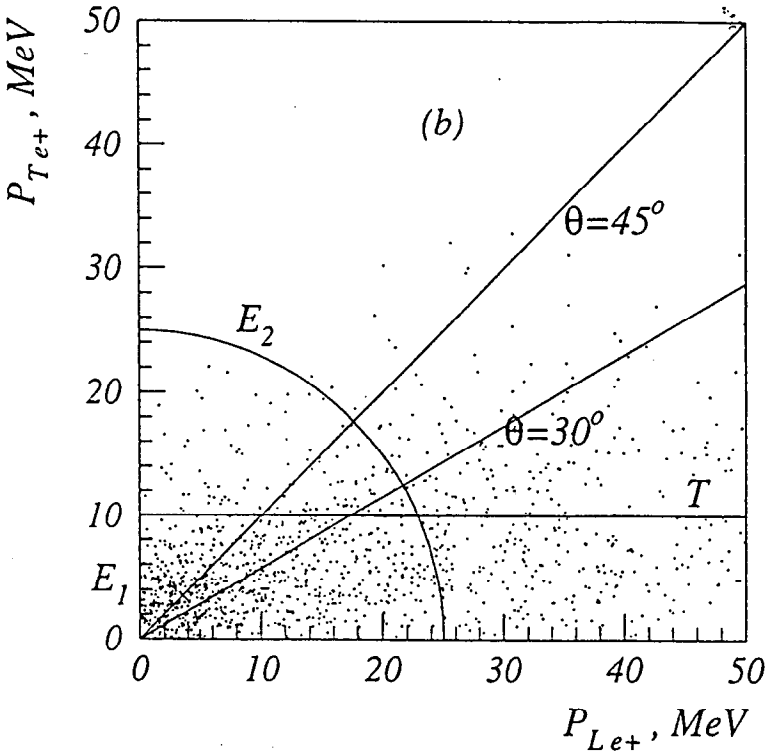

The acceptance limit concerning the energy, transverse momentum and exit angle from the target are shown on the figure above.

Limits : $5.\text{MeV} \leq \text{E} \leq 25.\text{MeV}$

$p_T < 10$ MeV/c

$\theta = 30 \rightarrow$ S-Band

$\theta = 45 \rightarrow$ L-Band

($\theta \rightarrow$ Bunch-lengthening)

4 Heating

- Limit induced by mechanical stresses (SLAC)

$$\rho = N^- E^- / (\pi \sigma^2) < 2.10^{12} GeV/mm^2$$

- Energy deposited in the target
  Comparison for CLIC, NLC, JLC and crystal source

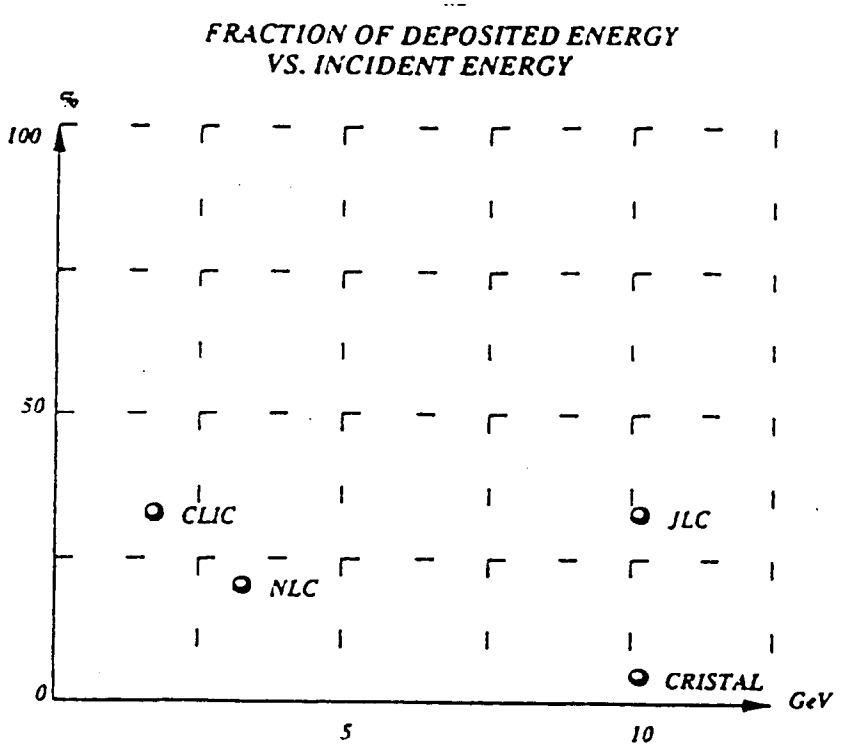

Figure 8 : Energy deposited in the target

4.1 Heating of the target

Local temperature distribution is obtained with Finite Element Programs:

2 programs: SYSTUS
PRIAM/PROMETHEE

As we have almost equivalent solutions (Yield) for:

8 mm all crystal
8 mm hybrid

we consider: the hybrid solution

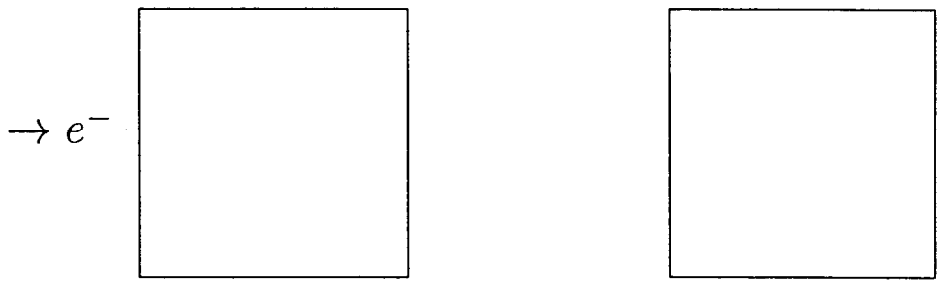

CIBLE AMORPHE DIAM. 10 HAUT. 21

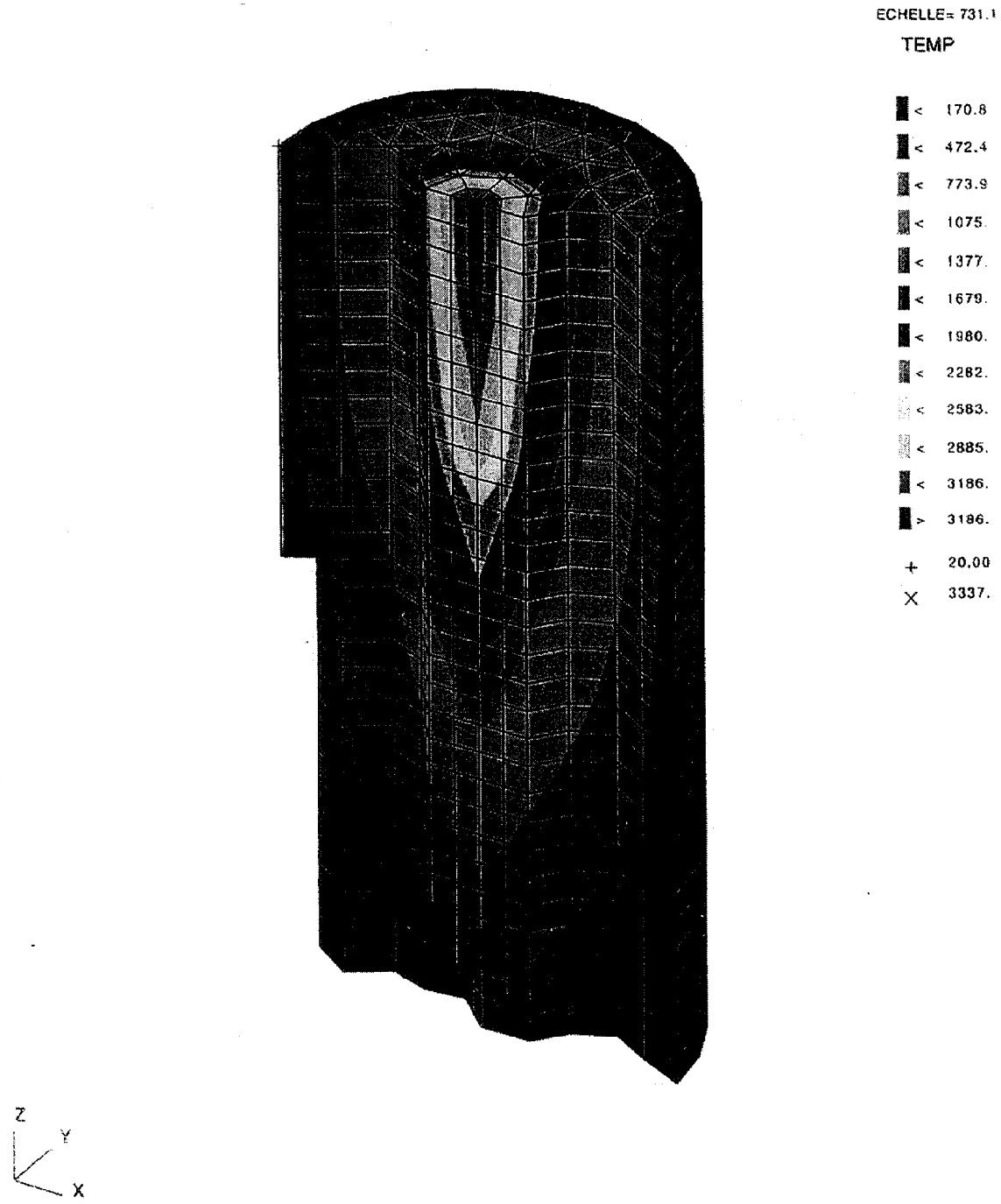

SYSTUS VAX-233 21-11-96

ECHAUFFEMENT CIBLE SOUS FAISCEAU 10 GEV

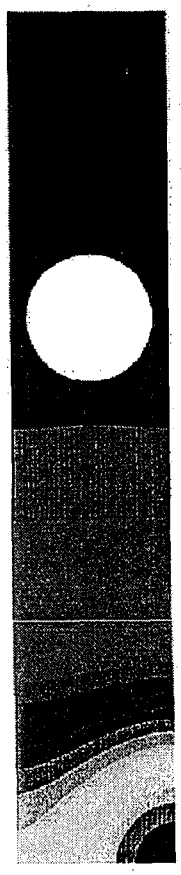

MODULEF : lemeur
ISO-POTEN. 0.00 PS
29/11/96

cristal4.V

2886 POINTS
2886 NOEUDS
5416 ELEMENTS
5416 TRIANGLES

INCONNUE : 1 MNEMO :VN

489.1
489.1
470.2
451.4
432.5
413.6
394.8
375.9
357.1
338.2
319.4
300.5
281.7
262.8
244.0
225.1
206.2
187.4
168.5
149.7
130.8

20 ISOVALEURS

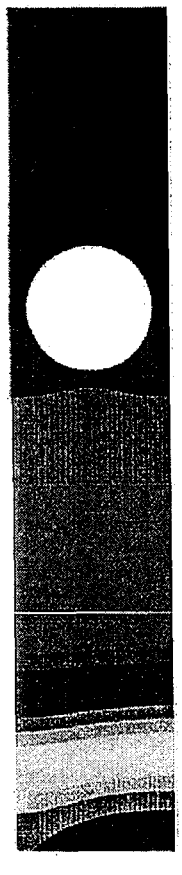

MODULEF : lemeur
ISO-POTEN. 0.00 PS
29/11/96

amor4.V

2886 POINTS
2886 NOEUDS
5416 ELEMENTS
5416 TRIANGLES

INCONNUE : 1 MNEMO :VN

2184.
2184.
2102.
2020.
1938.
1857.
1775.
1693.
1611.
1529.
1447.
1365.
1283.
1201.
1120.
1038.
955.8
873.9
792.1
710.2
628.3

20 ISOVALEURS

4.2 Crystal in the warm regime

$\Delta T \Longrightarrow$ Increase of amplitude of thermal vibration

$\Longrightarrow$ Decrease of amplitude of Potential Wells

$\Longrightarrow$ Decrease of the field in the crystal
(Sensitive effect for particles near the axis)

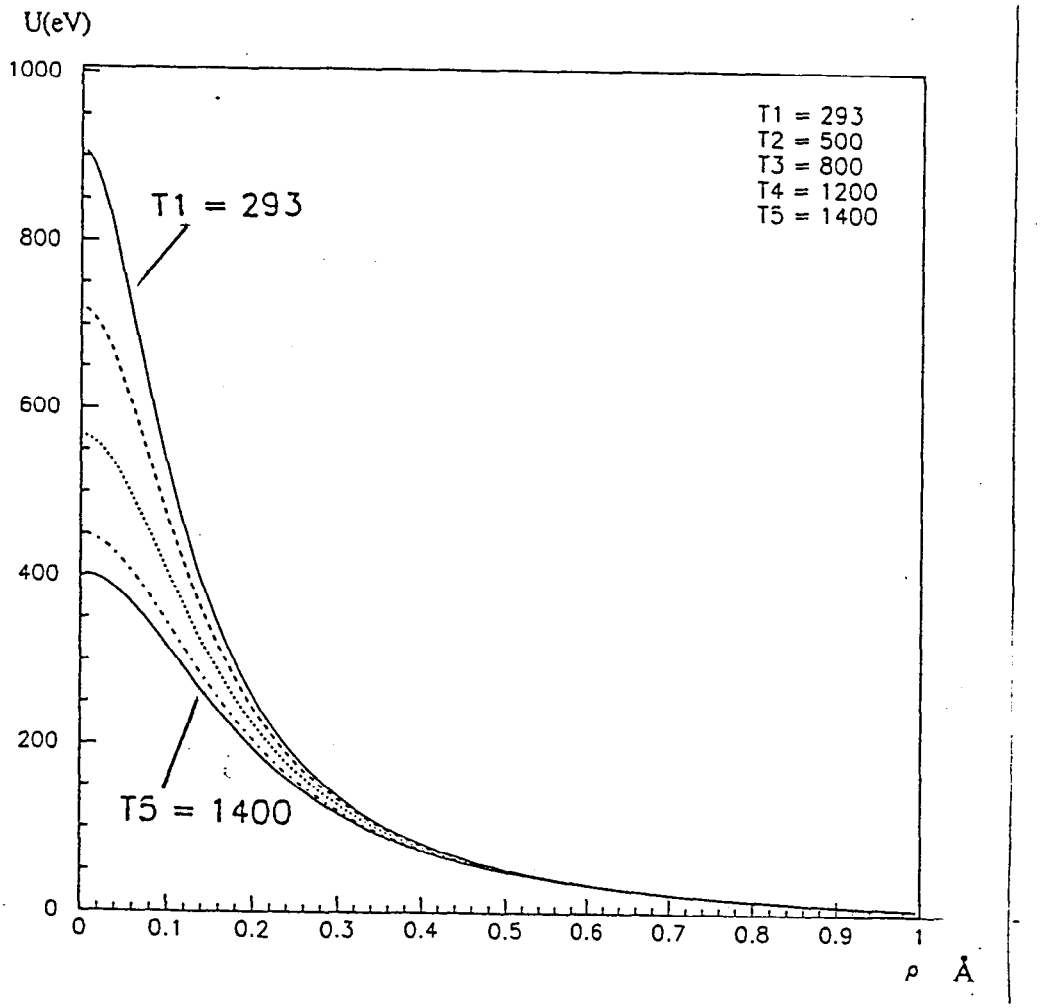

Figure 9 : Continuum potentials for the < 111 > axis of the tungsten crystal. The temperatures are expressed in ° Kelvin

4.3 Effect of the temperature on the yield

On the table are represented the positron yields (total and accepted) for :

- ALL CRYSTAL
- HYBRID

targets.

	Total Yield		Accepted Yield	
	T = 20° C	T = 600° C	T = 20° C	T = 600° C
All crystal	19.1	16.3	2.4	2.
Hybrid	18.3	16.5	2.3	2.1

4.4 Comparison of positron spectra for two temperatures (Ambient and 600°C)

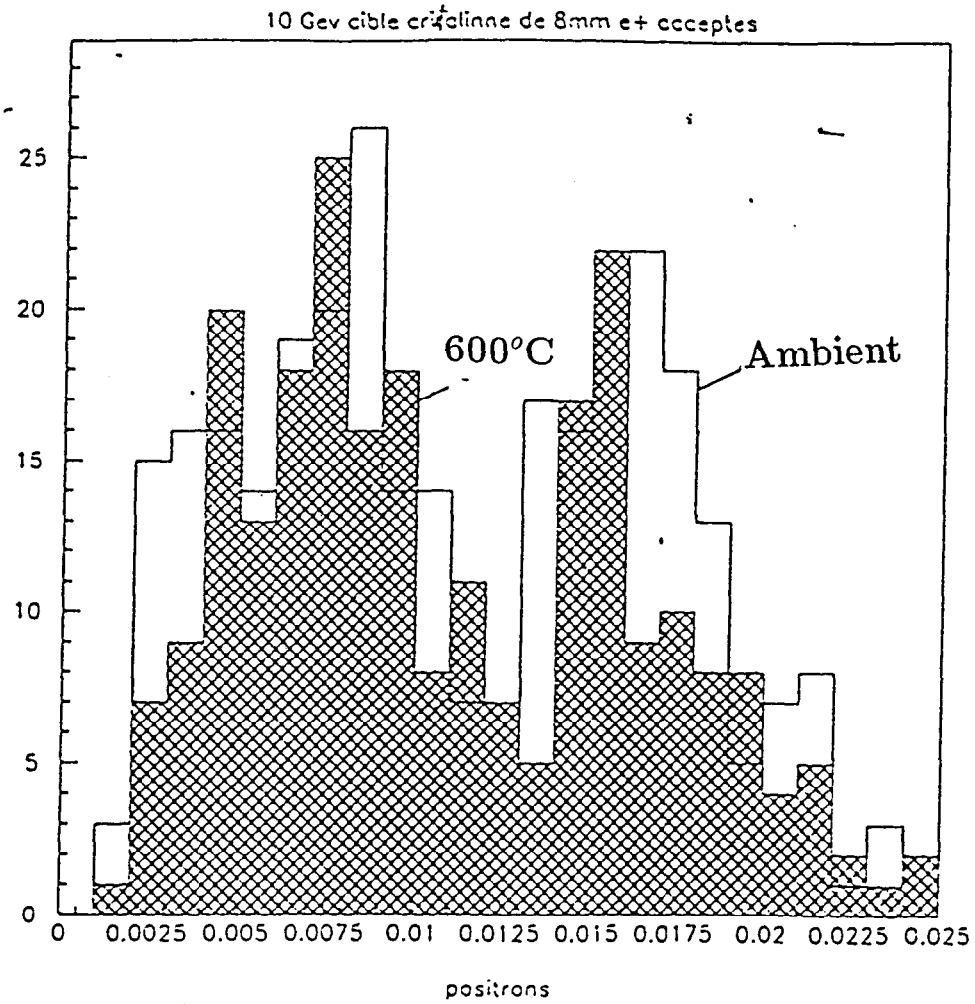

5 Qualities required for the incident electron beam

EMITTANCE:

- Channeling requires:

$$\Psi < (\Psi)_c = [2Vo/Eo]^{1/2}$$

$\Longrightarrow$ Low divergence e- beams
$\Longrightarrow$ Mosaic spread $<<$ $(\Psi)_c$
(Control ensured at Max-Planck Institute-Stuttgart)

- Typical emittance, for a 10-GeV incident electron beam.

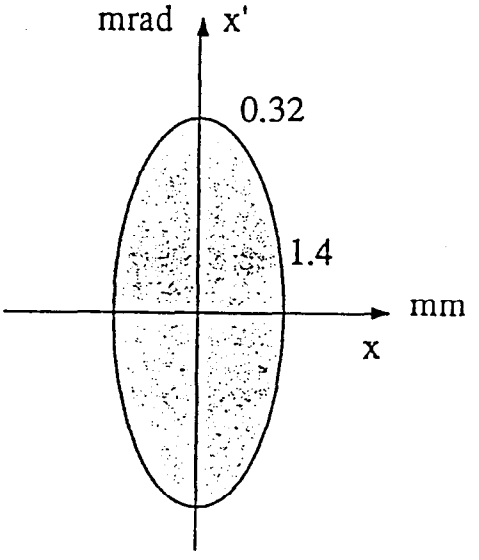

Figure 10 :

$\epsilon_{x,y} \sim 0.5\pi$ mm mrad

5.1 Constraints associated with an intense incident beam

Radiation Damage

Due to Coulomb scattering of the electron beam on the nuclei.
$\Longrightarrow$ dislodgments of the nuclei from the lattice

Experiments with protons:
(28 GeV p) $\rightarrow$ limit $\simeq 4 - 5.10^{20}/cm^2$

Experiments with electrons: SLAC
Fluence reached: $2.10^{18} e^-/mm^2$
(Will be analysed in the near future)

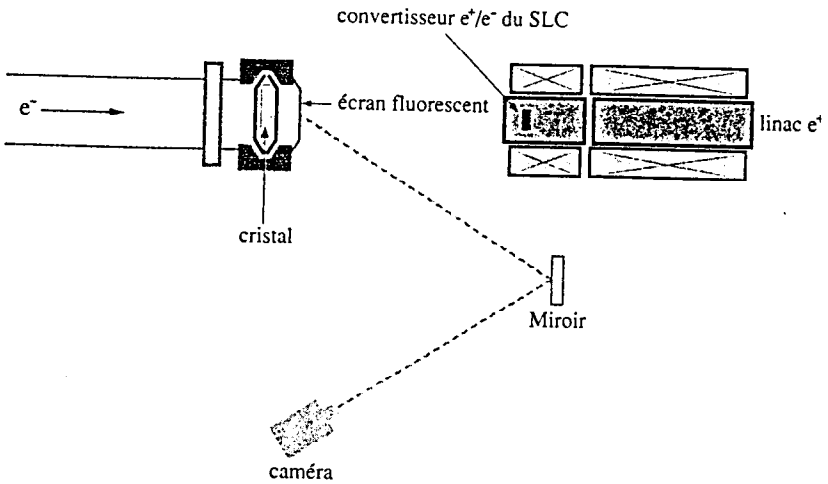

Figure 1

6 Summary & Conclusions

- Similar yields at the IP for a crystal target as for JLC. Adjustment of the final e- intensity on the crystal (so as to equalize exactly JLC yield) $\rightarrow$ Higher intensity (+25 %) larger beam radius (+ 12 %)

- Energy deposited in an all-crystal target: 5 % whereas it is of 32 % for JLC target.

- A crystal target, in usual LC conditions, is heated. An hybrid solution with a 4 mm crystal followed by a 4 mm amorphous disk gives almost the same yield as JLC. Such solution presents reasonable heating values ($< 500°C$) for the crystal part. That corresponds to 1 % of deposited energy. The yields are slightly affected (- 10%).

- Radiation damage in crystal is a serious problem: it is under investigation. With the BNL test, the limit if applied to LC gives $\simeq$ a hundred hours of working time. Test with electrons should give, in the near future, interesting answers.

The SLC Positron Source Design and Performance

Stan Ecklund, Stanford Linear Accelerator Center

Summary

The source is designed to produce up to 7 x 10^{10} positrons at the interaction region with over a factor of two more positrons in the upstream parts of the SLC system. The requirements are listed in the front of the presentation. Typical operation is with about 3 x 10^{10} positrons at the interaction region because of limitations of wake fields in the LINAC, resultant emittance growth and jitter requirements.

Because wake field limitations in the LINAC are approximately the same for the positrons and the electrons producing them, the positron system must have an overall yield of unity. Because of losses and emittance dilution, a factor of 2.5 was built into the design.

A thick target was chosen to use the gain in numbers of positron provided by the cascade shower. While the pair production cross section becomes asymptotic above 1 GeV, a targeting energy of 33 GeV was chosen to provide adequate yield, while maintaining reasonable pulse heating of the target, and using existing facilities in the SLAC LINAC. The graphs show the dependence of positron yield on the phase space parameters. Points to note are the multiplicity or yield obtained from the shower, the dependence on phase space acceptance, and material dependence. Note that high Z materials do give more positrons overall and provide them in a smaller emittance. Note that the transverse momentum of positrons in the shower does not change after the first radiation length, but does correlate strongly with the energy accepted.

Early in the design of the positron target, number of beam tests were run to explore material strengths. These tests established a beam brightness limit, above which failure occurred, at about 1 x 10^{11} incident electrons per square mm. Detailed thermal and stress calculations give a consistent limit.

Optimization of the system was done with a ray tracing program (ETRANS). This allowed tracking a wide energy spread, large

emittance beam through combined RF fields and magnetic solenoid focusing fields. The gradient and magnet field parameters were optimized with this program. Estimates of space charge forces were made using the MASK program.

Because of the large angular spread of positrons emerging from a target, special focusing devices are needed to have efficient collection. We chose a pulsed coil called a flux concentrator to do so, obtaining 6 Tesla peak fields. This device improves the yield by a factor of two.

Performance of the source is consistent with that calculated. Yields of 4 are routinely obtained at 200 MeV before momentum analysis and 2.5 after momentum clipping. Intensity losses in the downstream systems occur in sector 1 where the beam is accelerated to 1.2 GeV, and in the positron damping ring system. The resultant yield obtained is typically unity, meeting the overall requirements. As noted in the lessons learned, it would have been advantageous to design acceptances larger in the downstream parts of the system to avoid sizable losses and to relax tolerances for those components.

The SLC Positron Source Design and Performance

Stan Ecklund

SLAC

Workshop on New Kinds of Positron Sources for Linear Colliders

4-7 Mar. 1997

Requirements for SLC

- **Positron Beam**
  - Ne^+ : 3×10^{10} to 7×10^{10} at IP
  - Rate: 120 Hz
  - $\varepsilon = \gamma \sigma_x \sigma_{x'} = 0.01$ m to D.R.
  - dp/p = 5%
- **Electron Beam**
  - Energy: 33 GeV
  - Ne^- : 3×10^{10} to 7×10^{10}
    - $Y = Ne^+ / Ne^- = 1$ (overall)
    - $Y = Ne^+ / Ne^- = 2.5$ (design)
    - Y/E=0.075 /GeV
  - Pulse Energy: 160 - 370 joules
  - Power: 20 - 45 KW
- **Use of Existing Available Facility**
  - S-Band LINAC
  - Buildings (Tunnels)
- **Reasonable (Minimum) Cost**

Table 9.2.4.1 Luminosity Specifications

	First Year	Nominal	Units
Beam Energy	50	50	E(GeV)
Repetition Rate	120[a]	180	$f(\text{sec}^{-1})$
Interaction Flux	5×10^{10}	7.2×10^{10}	$N^{\pm}(\text{e}^{\pm}/\text{bunch})$
Normalized Emittance (at RTL)	3×10^{-5}	3×10^{-5}	$\gamma\epsilon$(m rad)
Effective Emittance (at FF)	4.2×10^{-10}	4.2×10^{-10}	$\epsilon_{x,y}$(m rad)
Momentum Spread	± 0.2	± 0.2	$\frac{\Delta P}{P}$ (percent)
Bunch length (linac)	1.5	1.5	σ_z(mm)
Bunch length (IP)	1.0[b]	1.0[b]	σ_z(mm)
Final Demagnification	$\times 4$[c]	$\times 5$	
Spot Size (IP)	2.07	1.65	$\sigma_{x,y}$ (μm)
Disruption Parameter	0.34	0.76	D
Pinch Factor	1.14	2.2	H
Luminosity	6.4×10^{29}	6.0×10^{30}	$\text{cm}^{-2}\ \text{sec}^{-1}$

(a) Assumes technical contingency exercised initially.

(b) Assumes σ_z compression in arcs due to p/z correlation.

(c) Assumes conventional iron quadrupoles initially.

Design Considerations

- e+, e- Intensities
  ==> Overall Yield = 1
- Shower Multiplication
- Phase Space of e+ from thick target.
  - Need for Special Collection Devices (focusing)
- Space Charge Considerations
- Capture Accelerator Gradient
- Yield Dependence on Z.
- Material (Pulse) Strength Limit
- Power sets size of moving target
- Beam Transport Optics
  - Achromatic
  - Isochronous
  - Reasonable Second Order

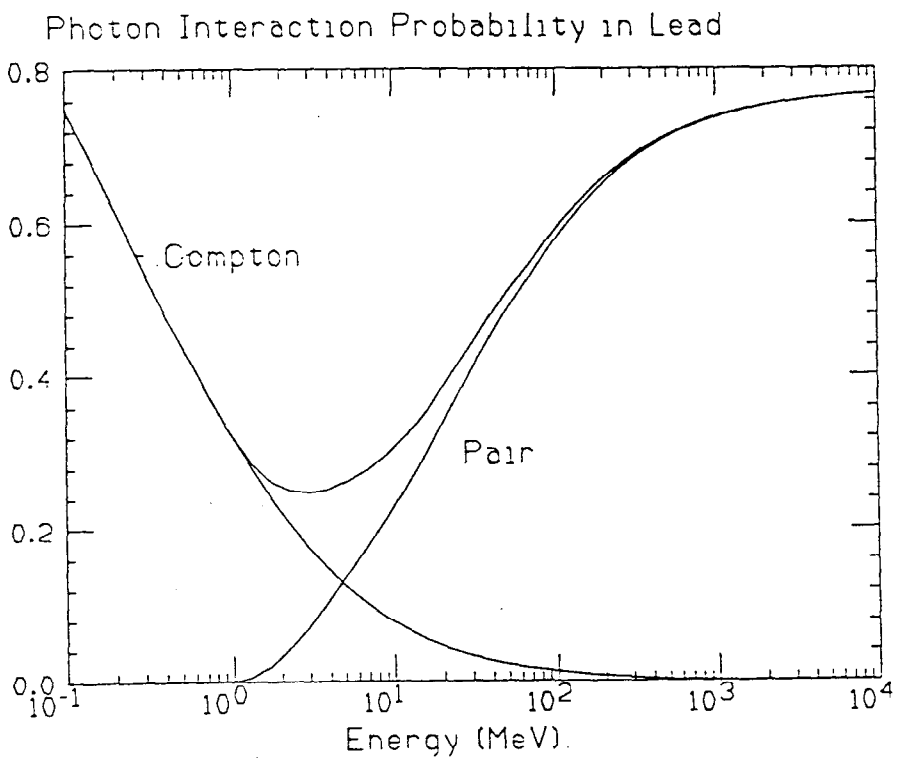

Fig. 1. Probability per radiation length of e^+e^- pair production and Compton scattering as a function of photon energy. These data come from the EGS program.

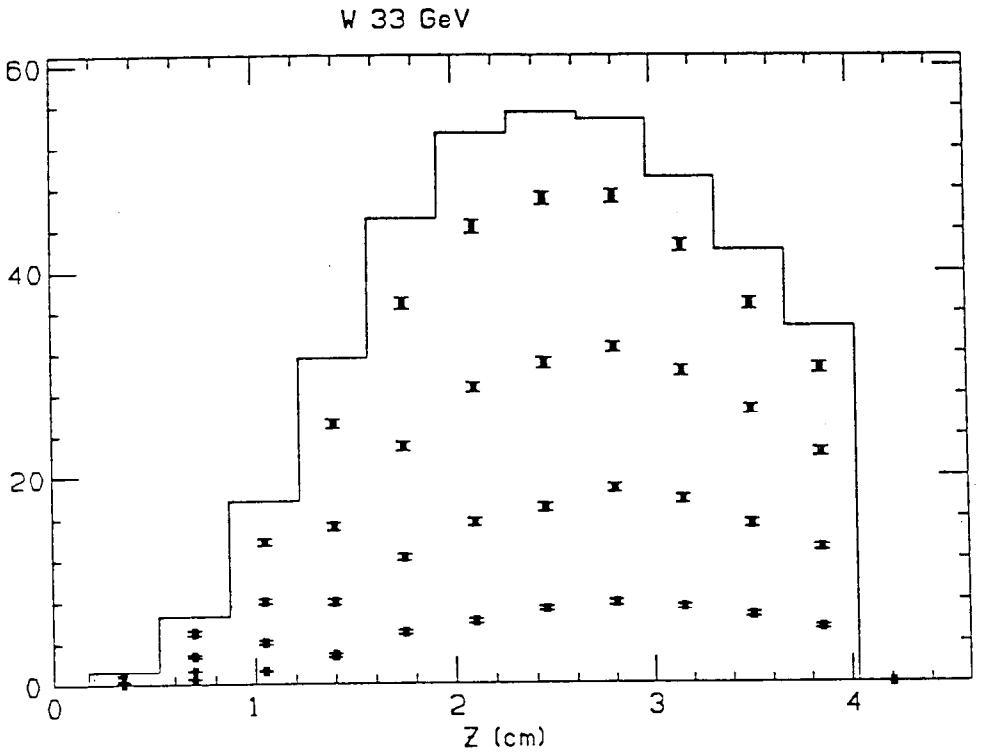

Fig. 2. Positron flux in tungsten per incident electron vs z for incident energy of 33 GeV. The different curves are for successively bigger cutoffs in maximum positron energy of 5, 10, 20, 50, and 100 MeV. The minimum energy cutoff is 2 MeV. The z bins are one radiation length. Note the shower maximum is around seven radiation lengths for this energy. The calculation covers the first eleven radiation lengths.

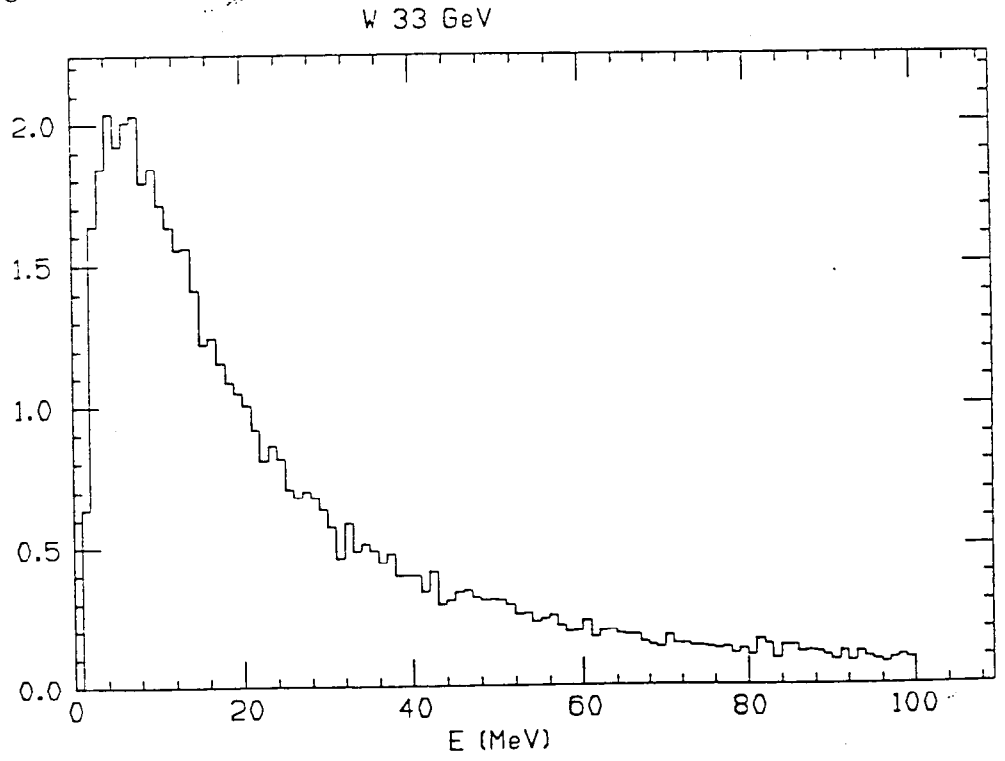

Fig. 3. Yield per 1–MeV energy (E) bin versus E at $z = 6$ radiation lengths.

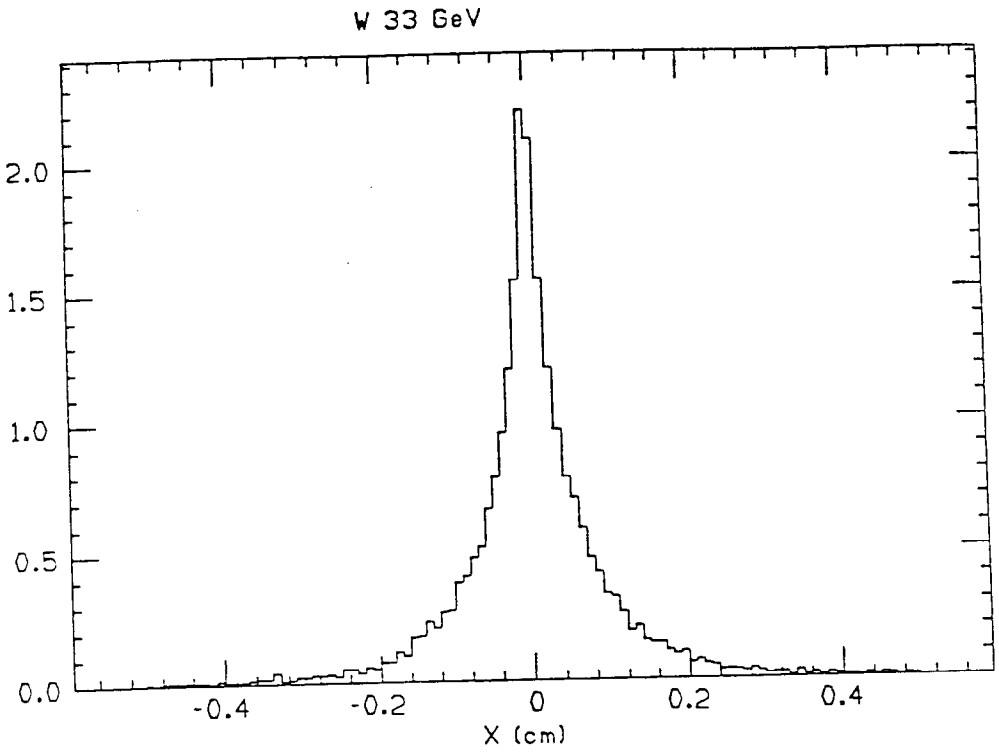

Fig. 4. Yield per 0.01–cm bin versus x at $z = 6$ radiation lengths.

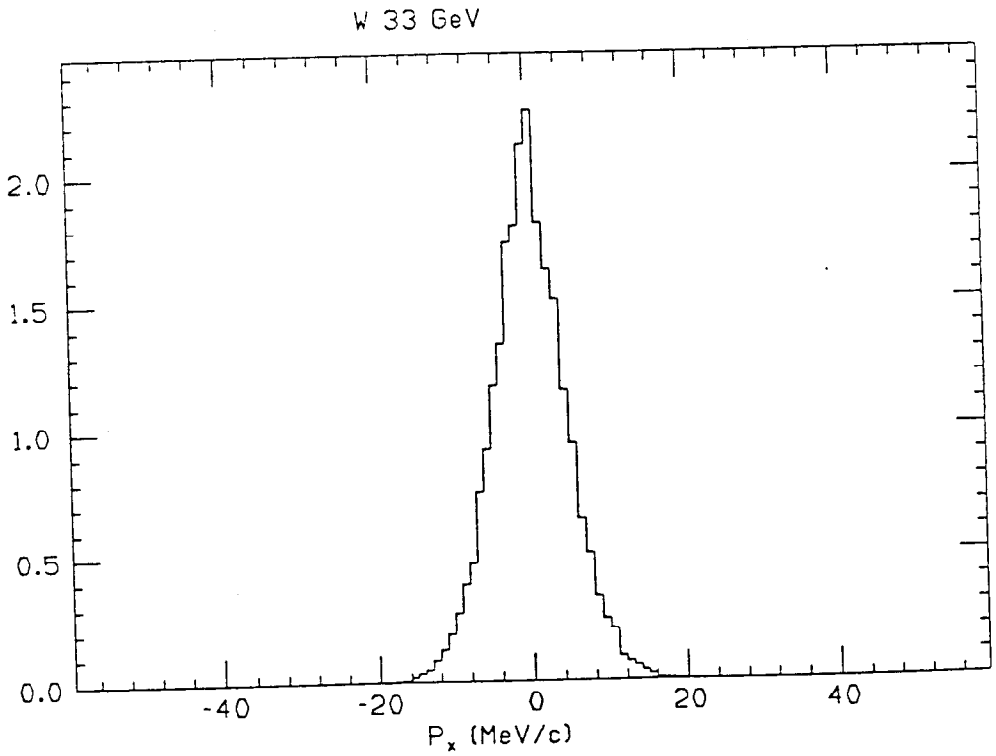

Fig. 5. Yield per 1–MeV bin versus P_x at $z = 6$ radiation lengths.

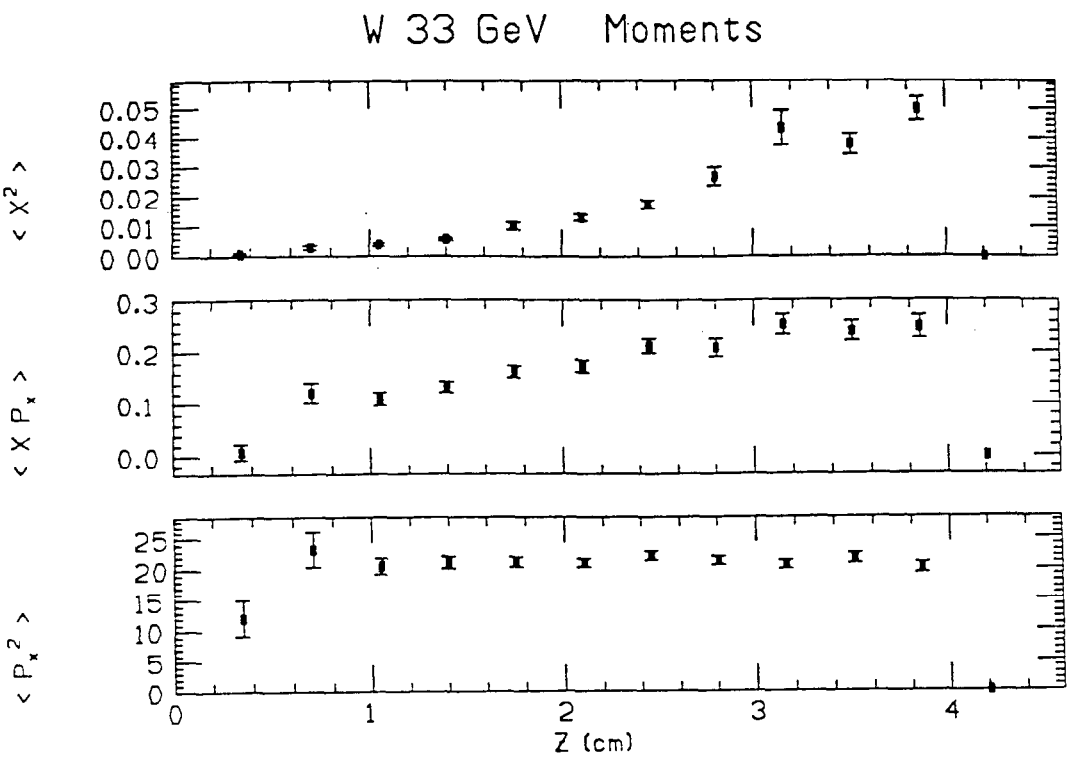

Fig. 6. Moments in x, P_x versus z for $5 \leq E \leq 20$ MeV.

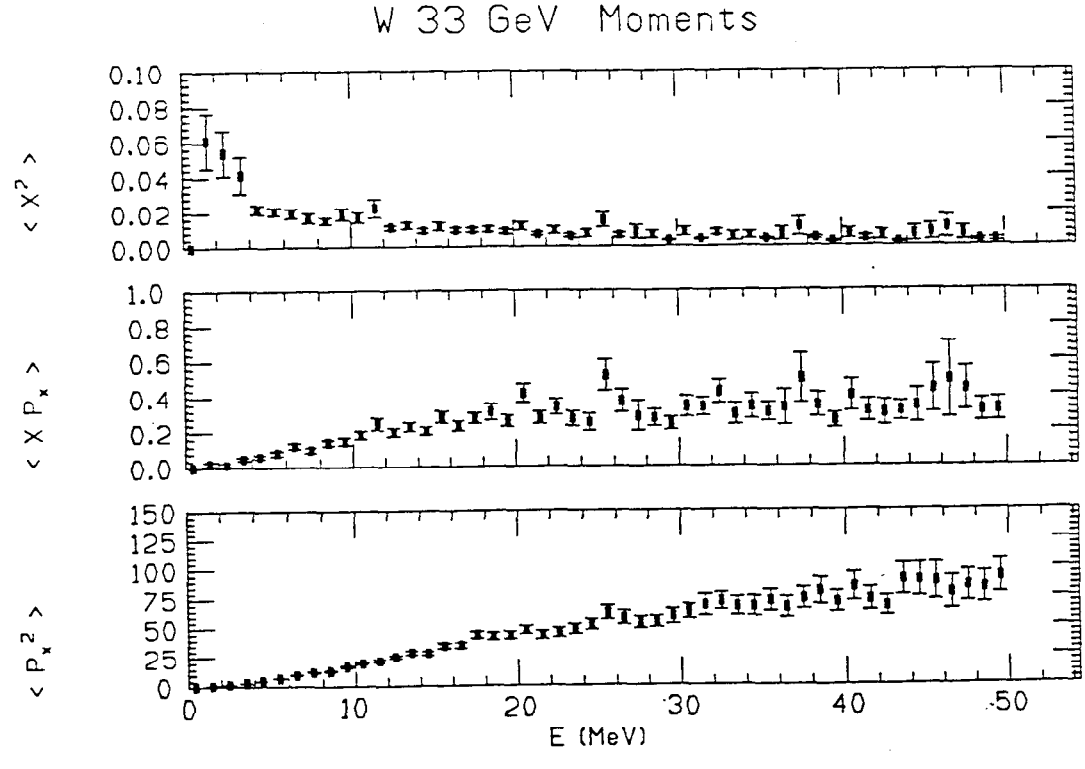

Fig. 7. Moments in x, P_x versus E for $z = 6$ radiation lengths.

Table I. Positron Yield Properties from Copper and Tungsten

Incident Energy:	17 GeV		50 GeV	
Material	Cu	W	Cu	W
Radiation Length	14.3	3.5	14.3	3.5
Yield at $z = 6$ r.l. for $2 < E < 5$	2.8	5.8	7.4	13.4
σ_z (mm)	2.1	1.1	1.8	1.1
σ_{P_z} (MeV/c)	3.0	3.3	3.0	3.5

Material Tests

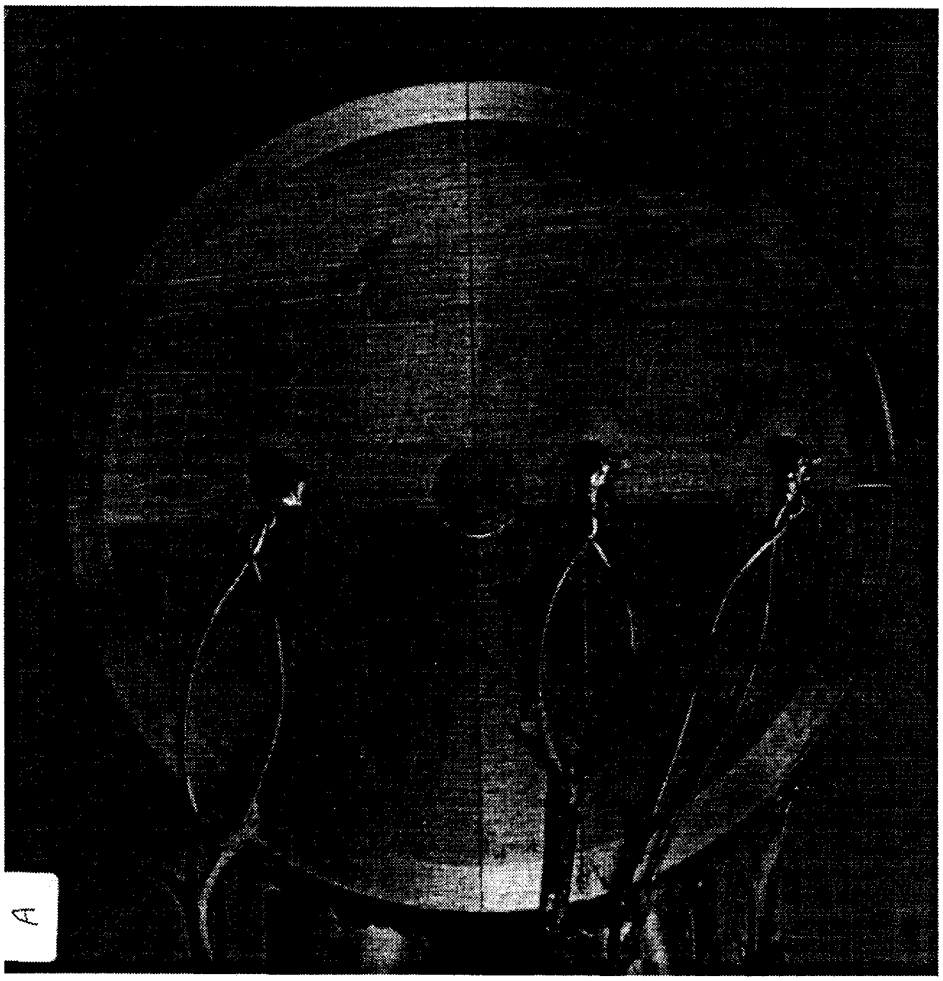

- **Sample A**
  - **W 25% Re**
  - **1/4 inch diameter**
  - **23.5 mm long (6.8 r.l.)**

After

A B

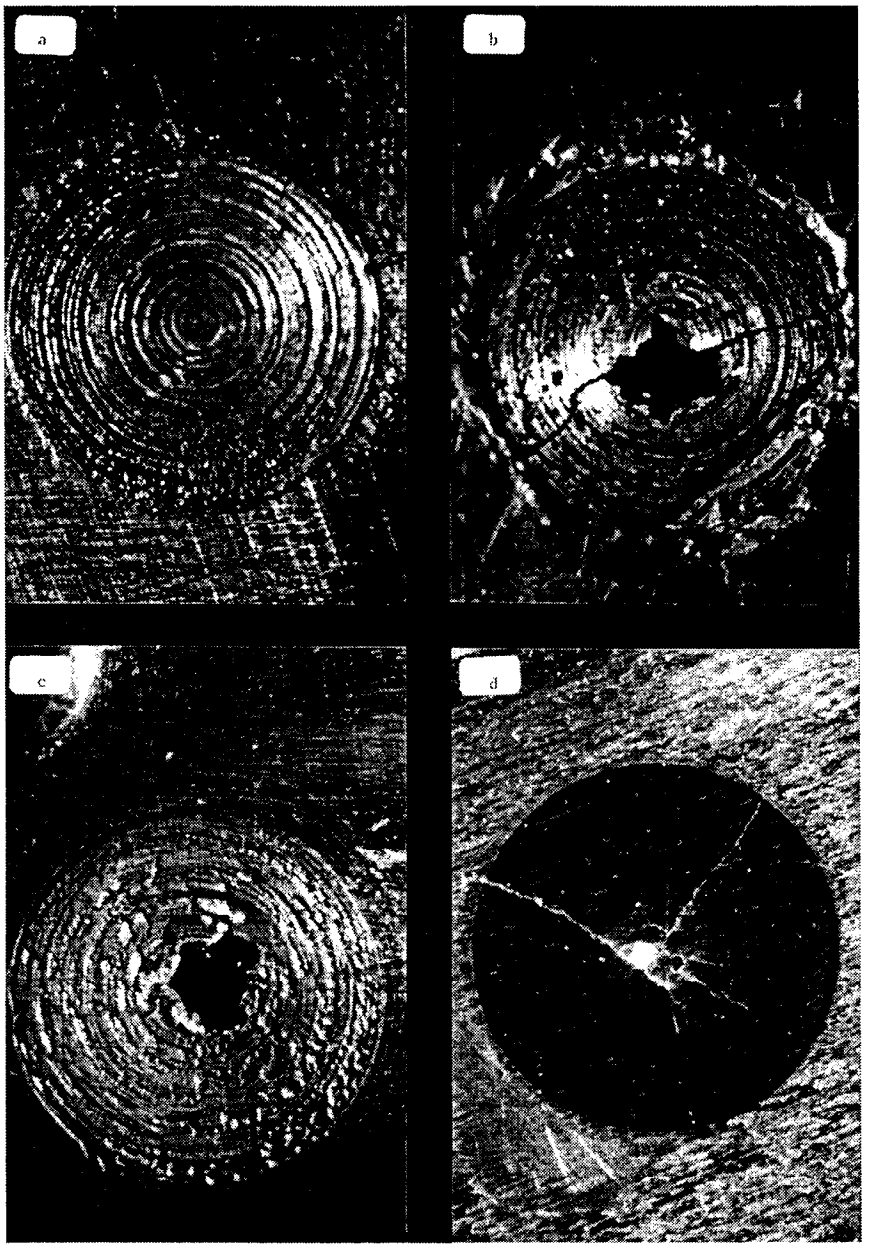

C D

TABLE 5.2.6.1 SLC e^+ Target Tests

	Units	SLC	A_1	A_2	B_1	B_2	C	D_1	D_2	E	F_1	F_2	G
Material			W-Re		W-Re		Ta	W-Re		W-Re	Ta		Ta-W
Length	mm		23.5		18.6		27.6	18.7		18.6	21.9		20.6
L/Lr	r.l.	6	6.8		5.4		6.7	5.4		5.4	5.3		5.1
Exposure Date			6/21/80	6/7/81	7/16/80		7/31/80	12/18/80	12/22/80	6/17/81	6/16/81		6/12/81
Beam Energy	GeV	33	20.5	21.0	24.4		20.5	25.1	20.4	21	21		21
Rep. Rate	Hz	180	10 – 39	20	40		30	10	10 – 30	20	20		30
Pulse Width	ns	0.003	120	200	150		200	110	150	200	220		200
Beam Power	KW	35	1.8 – 7.2	4.7	12	20	11	2.6	1.6 – 7.8	5.3	4.8		4.7
Beam Pulse Energy	Joules	195	187	235	312	492	374	261	163 – 261	262	259	242	235
Number Pulses	10^6		1.0	0.75	0.74	0.22	0.37	0.38	0.27	0.78	0.17	0.3	1.0
Electrons/Pulse	10^{10}	3.7	5.7	7.0	8.0	12.6	11.4	6.5	5.0 – 8.0	7.8	7.7	7.2	7.0
Total Electrons	10^{16}		5.7	5.2	6.3	2.8	4.2	2.5	2.2	6.1	1.2	2.2	7.0
σ_x	mm	0.4 – 1.0	.7	.83	.91	.70	.27	.73	.6	.72	.70	.60	.63
σ_y	mm	0.4 – 1.0	.5	.56	.35	.40	.20	.48	.4	.48	.47	.20	.50
Area	mm^2	0.5 – 3.1	1.1	1.46	1.00	0.88	0.17	1.10	0.75	1.1	1.03	.38	0.99
e/Area	$10^{10}/mm^2$	7.4 – 1.2	5.2	4.8	8.0	14.3	67.0	5.9	10.6	7.2	7.4	19.1	7.1
Damage			None	None	None Observed	Cracked & Hole	Hole	None Observed	Cracked	None	None	Cracked & Hole	None

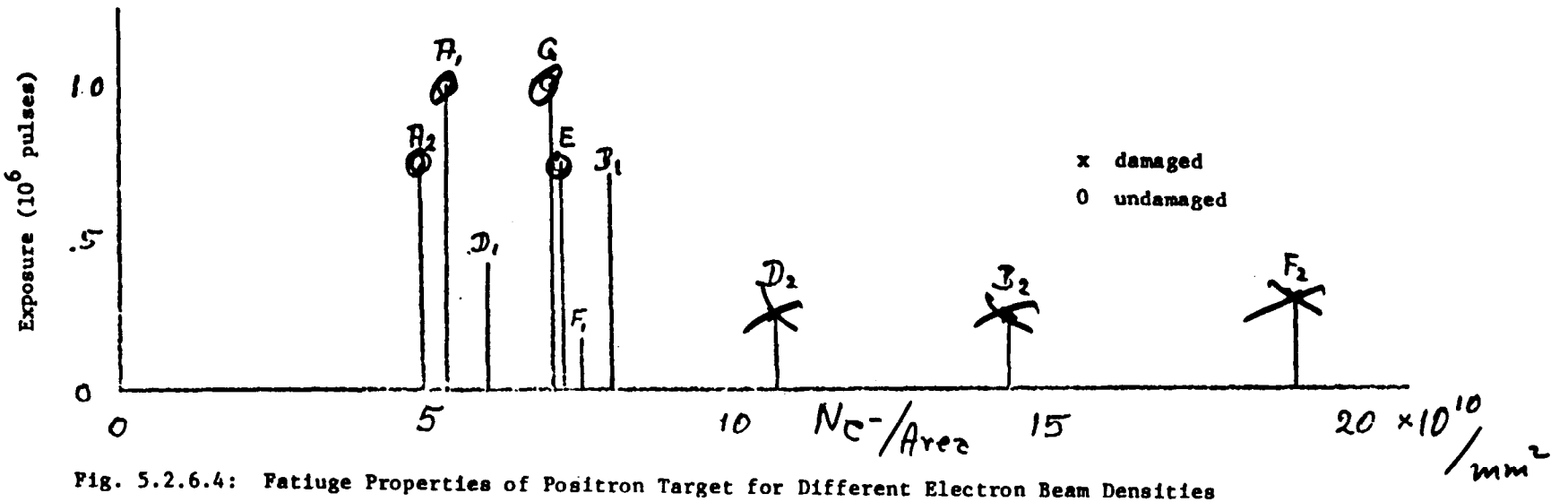

Fig. 5.2.6.4: Fatiuge Properties of Positron Target for Different Electron Beam Densities

Alternatives Considered

- **Conventional Shower Cascade target**
  - **Solid Target**
  - **Liquid Target**
    - + Easy to move (pump)
    - - Containment
    - - Radioactivity - Chemistry
    - Beam window or Liquid in Vacuum
    - - Shock wave splash if in Vacuum
    - - Window Power Limit if not
- **Wiggler Photon Generator with Thin target**
  - **Generator Beam Energy: 50 GeV available**
  - **Reuse of collider spent beam - jitter**
- **Channeling Enhancements**
  - **Radiation Damage**
  - **Material Strength**

POSITRON SUBSYSTEMS

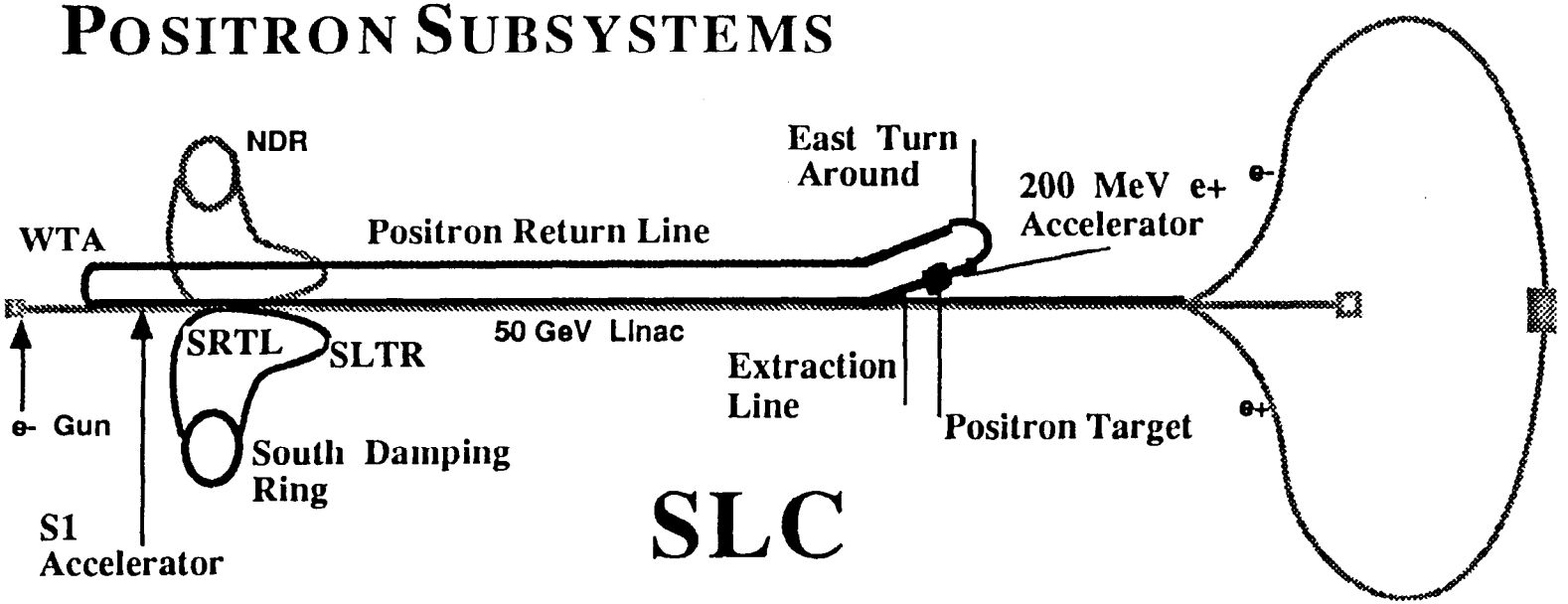

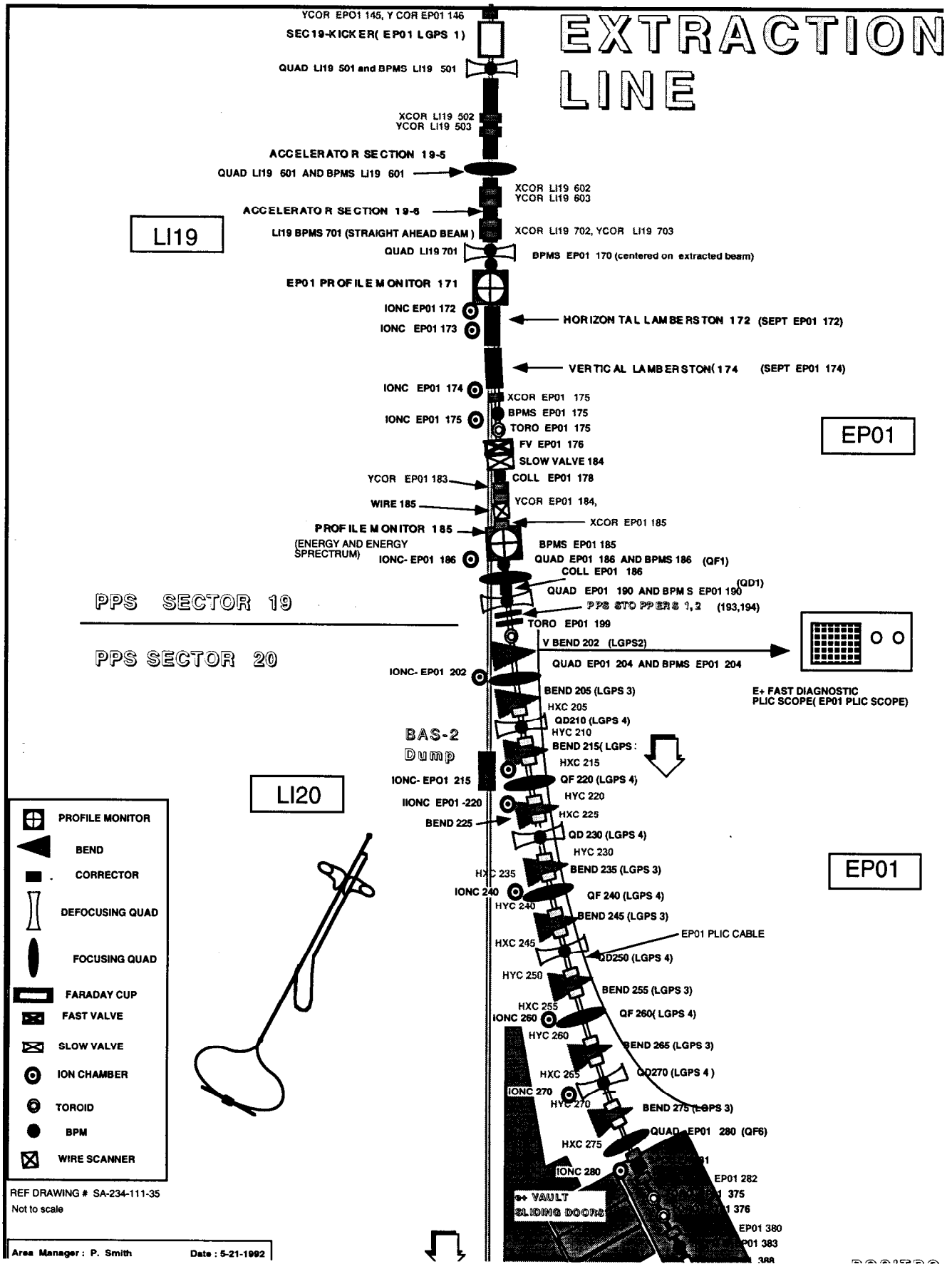
EXTRACTION LINE
YCOR EP01 145, Y COR EP01 146
SEC19-KICKER(EP01 LGPS 1)
QUAD LI19 501 and BPMS LI19 501
XCOR LI19 502
YCOR LI19 503
ACCELERATOR SECTION 19-5
QUAD LI19 601 AND BPMS LI19 601
XCOR LI19 602
YCOR LI19 603
ACCELERATOR SECTION 19-6
LI19
LI19 BPMS 701 (STRAIGHT AHEAD BEAM)
XCOR LI19 702, YCOR LI19 703
QUAD LI19 701
BPMS EP01 170 (centered on extracted beam)
EP01 PROFILE MONITOR 171
IONC EP01 172
HORIZONTAL LAMBERSTON 172 (SEPT EP01 172)
IONC EP01 173
VERTICAL LAMBERSTON(174 (SEPT EP01 174)
IONC EP01 174
XCOR EP01 175
IONC EP01 175
BPMS EP01 175
TORO EP01 175
EP01
FV EP01 176
SLOW VALVE 184
YCOR EP01 183
COLL EP01 178
WIRE 185
YCOR EP01 184,
XCOR EP01 185
PROFILE MONITOR 185
(ENERGY AND ENERGY SPRECTRUM)
BPMS EP01 185
IONC- EP01 186
QUAD EP01 186 AND BPMS 186 (QF1)
COLL EP01 186
QUAD EP01 190 AND BPMS EP01 190 (QD1)
PPS SECTOR 19
PPS STOPPERS 1,2 (193,194)
PPS SECTOR 20
TORO EP01 199
V BEND 202 (LGPS2)
QUAD EP01 204 AND BPMS EP01 204
IONC- EP01 202
E+ FAST DIAGNOSTIC
PLIC SCOPE(EP01 PLIC SCOPE)
BEND 205 (LGPS 3)
HXC 205
QD210 (LGPS 4)
HYC 210
BEND 215(LGPS:
BAS-2
Dump
HXC 215
IONC- EP01 215
QF 220 (LGPS 4)
LI20
HYC 220
IIONC EP01 -220
HXC 225
BEND 225
QD 230 (LGPS 4)
HYC 230
EP01
HXC 235
BEND 235 (LGPS 3)
IONC 240
QF 240 (LGPS 4)
HYC 240
BEND 245 (LGPS 3)
EP01 PLIC CABLE
HXC 245
QD250 (LGPS 4)
HYC 250
BEND 255 (LGPS 3)
HXC 255
IONC 260
QF 260(LGPS 4)
HYC 260
BEND 265 (LGPS 3)
HXC 265
QD270 (LGPS 4)
IONC 270
HYC 270
BEND 275 (LGPS 3)
QUAD EP01 280 (QF6)
HXC 275
IONC 280
EP01 282
E+ VAULT
SLIDING DOORS
EP01 380
EP01 383
PROFILE MONITOR
BEND
CORRECTOR
DEFOCUSING QUAD
FOCUSING QUAD
FARADAY CUP
FAST VALVE
SLOW VALVE
ION CHAMBER
TOROID
BPM
WIRE SCANNER
REF DRAWING # SA-234-111-35
Not to scale
Area Manager : P. Smith
Date : 5-21-1992

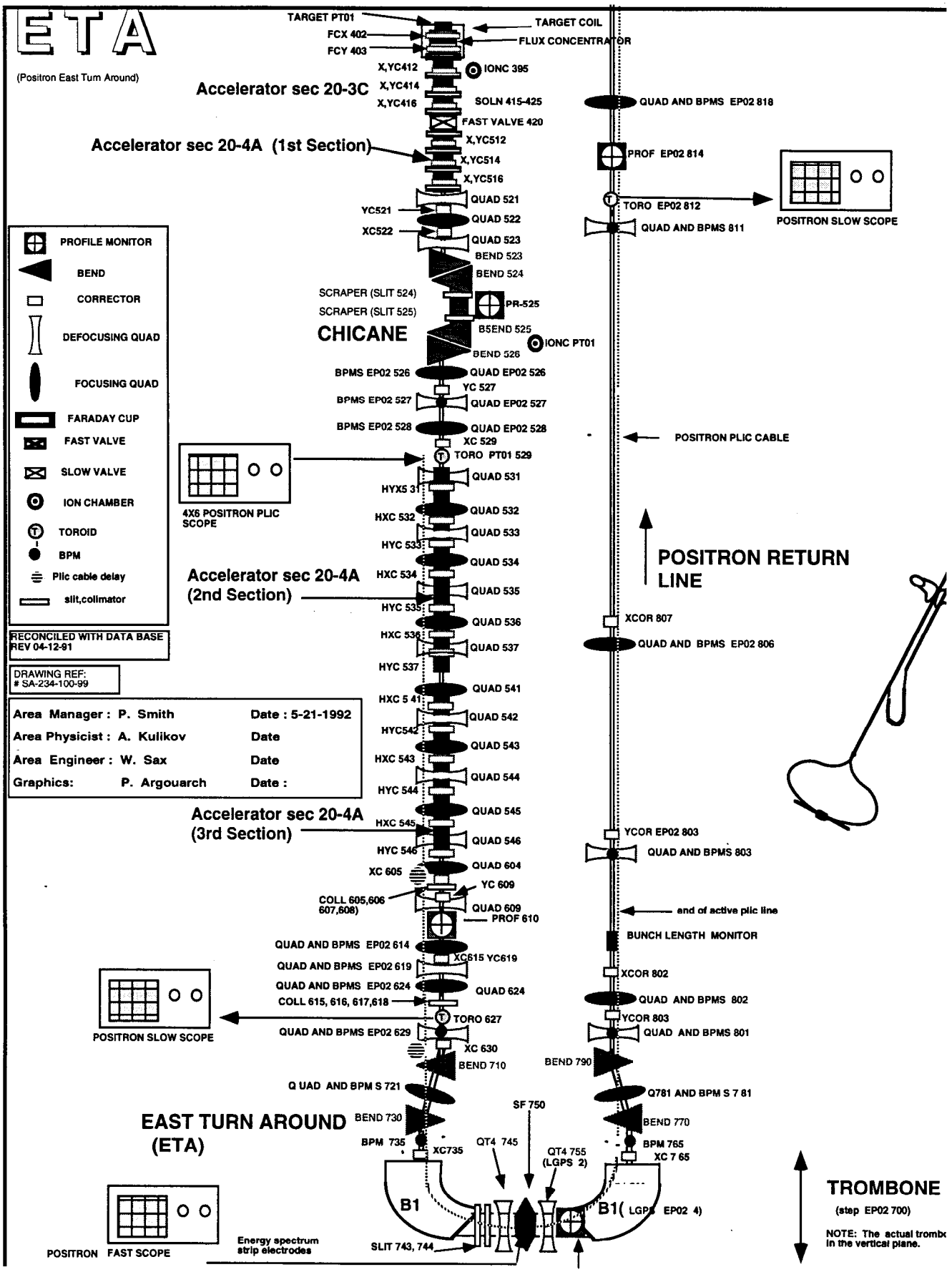
ETA
(Positron East Turn Around)
TARGET PT01
TARGET COIL
FCX 402
FCY 403
FLUX CONCENTRATOR
X,YC412
IONC 395
Accelerator sec 20-3C
X,YC414
X,YC416
SOLN 415-425
FAST VALVE 420
Accelerator sec 20-4A (1st Section)
X,YC512
X,YC514
X,YC516
QUAD 521
YC521
QUAD 522
XC522
QUAD 523
BEND 523
BEND 524
SCRAPER (SLIT 524)
SCRAPER (SLIT 525)
PR-525
CHICANE
B5END 525
IONC PT01
BEND 526
BPMS EP02 526
QUAD EP02 526
YC 527
BPMS EP02 527
QUAD EP02 527
BPMS EP02 528
QUAD EP02 528
XC 529
TORO PT01 529
QUAD 531
HYX5 31
QUAD 532
HXC 532
QUAD 533
HYC 533
QUAD 534
Accelerator sec 20-4A (2nd Section)
HXC 534
QUAD 535
HYC 535
QUAD 536
HXC 536
QUAD 537
HYC 537
QUAD 541
HXC 5 41
QUAD 542
HYC542
QUAD 543
HXC 543
QUAD 544
HYC 544
QUAD 545
Accelerator sec 20-4A (3rd Section)
HXC 545
QUAD 546
HYC 546
QUAD 604
XC 605
YC 609
COLL 605,606 607,608)
QUAD 609
PROF 610
QUAD AND BPMS EP02 614
XC615 YC619
QUAD AND BPMS EP02 619
QUAD AND BPMS EP02 624
QUAD 624
COLL 615, 616, 617,618
TORO 627
QUAD AND BPMS EP02 629
XC 630
BEND 710
Q UAD AND BPM S 721
EAST TURN AROUND (ETA)
BEND 730
BPM 735
XC735
SF 750
QT4 745
QT4 755 (LGPS 2)
B1
B1(LGPS EP02 4)
SLIT 743, 744
Energy spectrum strip electrodes
POSITRON FAST SCOPE
4X6 POSITRON PLIC SCOPE
POSITRON SLOW SCOPE
QUAD AND BPMS EP02 818
PROF EP02 814
TORO EP02 812
QUAD AND BPMS 811
POSITRON SLOW SCOPE
POSITRON PLIC CABLE
POSITRON RETURN LINE
XCOR 807
QUAD AND BPMS EP02 806
YCOR EP02 803
QUAD AND BPMS 803
end of active plic line
BUNCH LENGTH MONITOR
XCOR 802
QUAD AND BPMS 802
YCOR 803
QUAD AND BPMS 801
BEND 790
Q781 AND BPM S 7 81
BEND 770
BPM 765
XC 7 65
TROMBONE
(step EP02 700)
NOTE: The actual trombo in the vertical plane.
PROFILE MONITOR
BEND
CORRECTOR
DEFOCUSING QUAD
FOCUSING QUAD
FARADAY CUP
FAST VALVE
SLOW VALVE
ION CHAMBER
TOROID
BPM
Plic cable delay
slit,collimator
RECONCILED WITH DATA BASE REV 04-12-91
DRAWING REF: # SA-234-100-99
Area Manager : P. Smith Date : 5-21-1992
Area Physicist : A. Kulikov Date
Area Engineer : W. Sax Date
Graphics: P. Argouarch Date :

Table 5.2.0.1 Positron Source Specifications	
EXTRACTION	
Electron Scavenger Pulse	
Energy	33 GeV
Intensity	5.0×10^{10} e^-/pulse
Size (1 σ)	0.6 mm
Pulse energy	264 Joules/pulse
Pulse rate	180 Hz
Power	47 kW
Target	
Material	90% Ta – 10% W
Length	6 radiation lengths = 24 mm
Energy deposited in target	53 J/pulse
Pulse temperature rise	380°C
Max. pulse temp.	580°C
Max. compressive stress	32,000 psi
Power deposition	9 kW
Steady-state temp.	200°C
Positron Beam at Target	
Energy range	2 – 20 MeV
Transverse emittance (Invariant)	2 mm × 2.5 MeV/c = 0.01 m-radians
Yield (e^+/e^- in.)	2.5
Beam Properties at End of Sector 1	
Energy	1.21 GeV
Energy spread	2% full
Transverse emittance	4.2×10^{-6} m-radians

Computer Simulations

- Shower Generation (EGS)
- Ray Tracing, No Space Charge ETRANS, TURTLE
- Ray Tracing, With Space Charge - MASK
- Target Heating and Stress

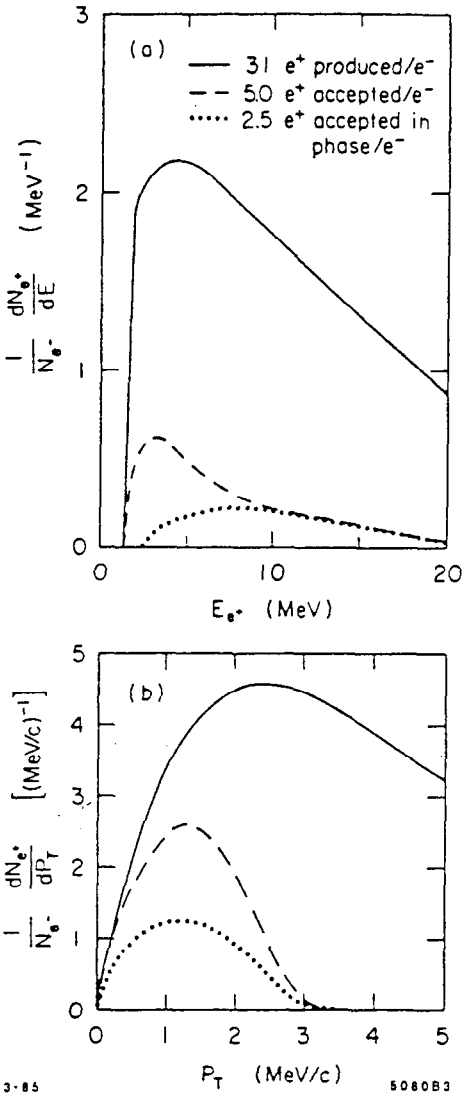

Fig. 6. Energy and transverse momentum of the positrons as they leave the target. Full curve shows all positrons produced, dashed curve gives the yield for positrons reaching the end of the accelerating system and the dotted curve shows those positrons in phase that would be accepted by the damping ring.

3D Numerical Thermal Stress Analysis of the High Power Target for the SLC Positron Source*

Eric M. Reuter and John A. Hodgson
Stanford Linear Accelerator Center Stanford University, Stanford, CA 94309 USA

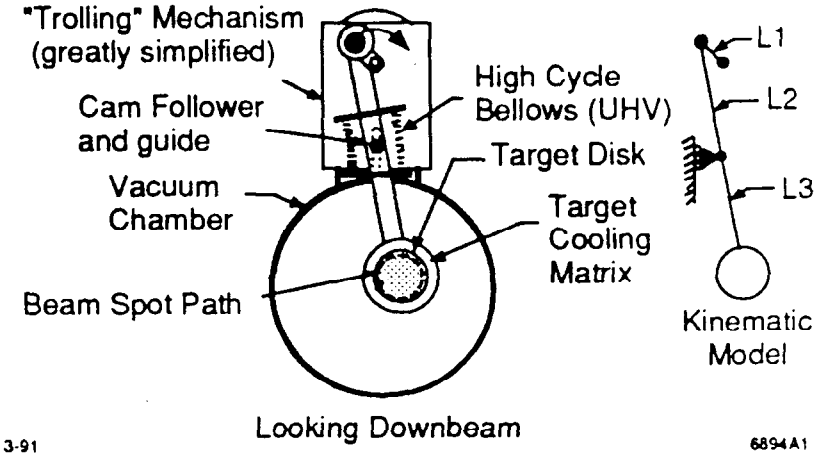

Figure 1. "Trolling" target mechanism.

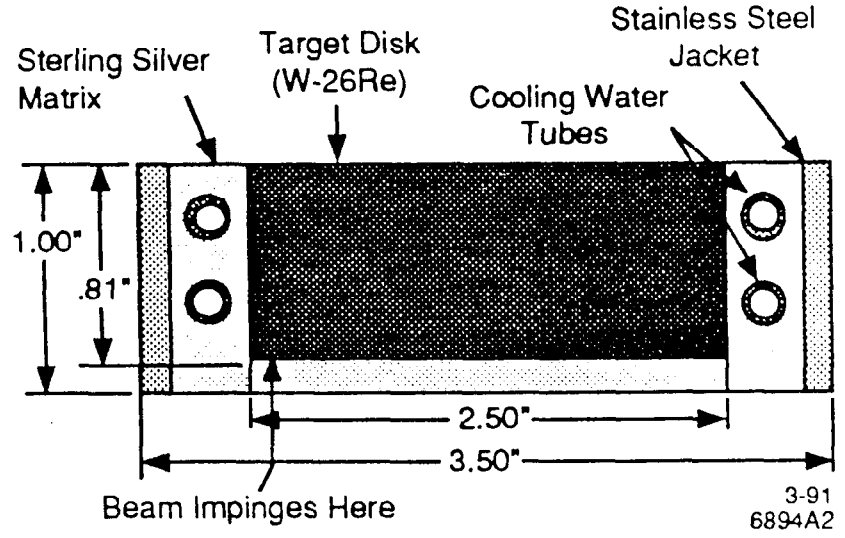

Figure 2. Target disk cross section.

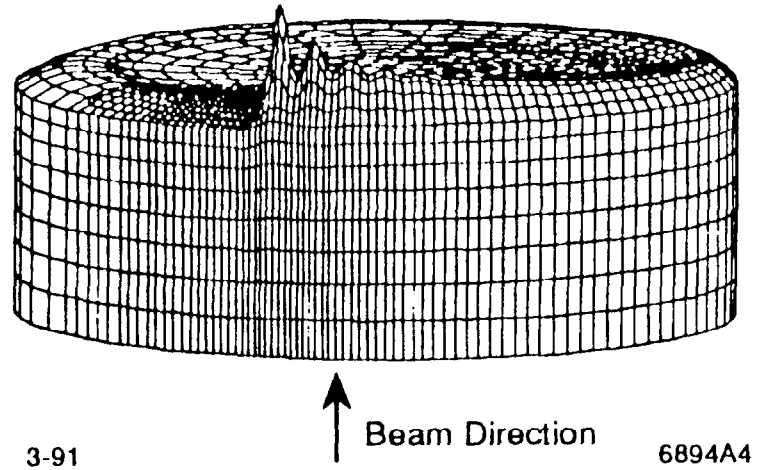

Figure 3. Raised contour temperature map of High Power Target in "steady state," just after a pulse.

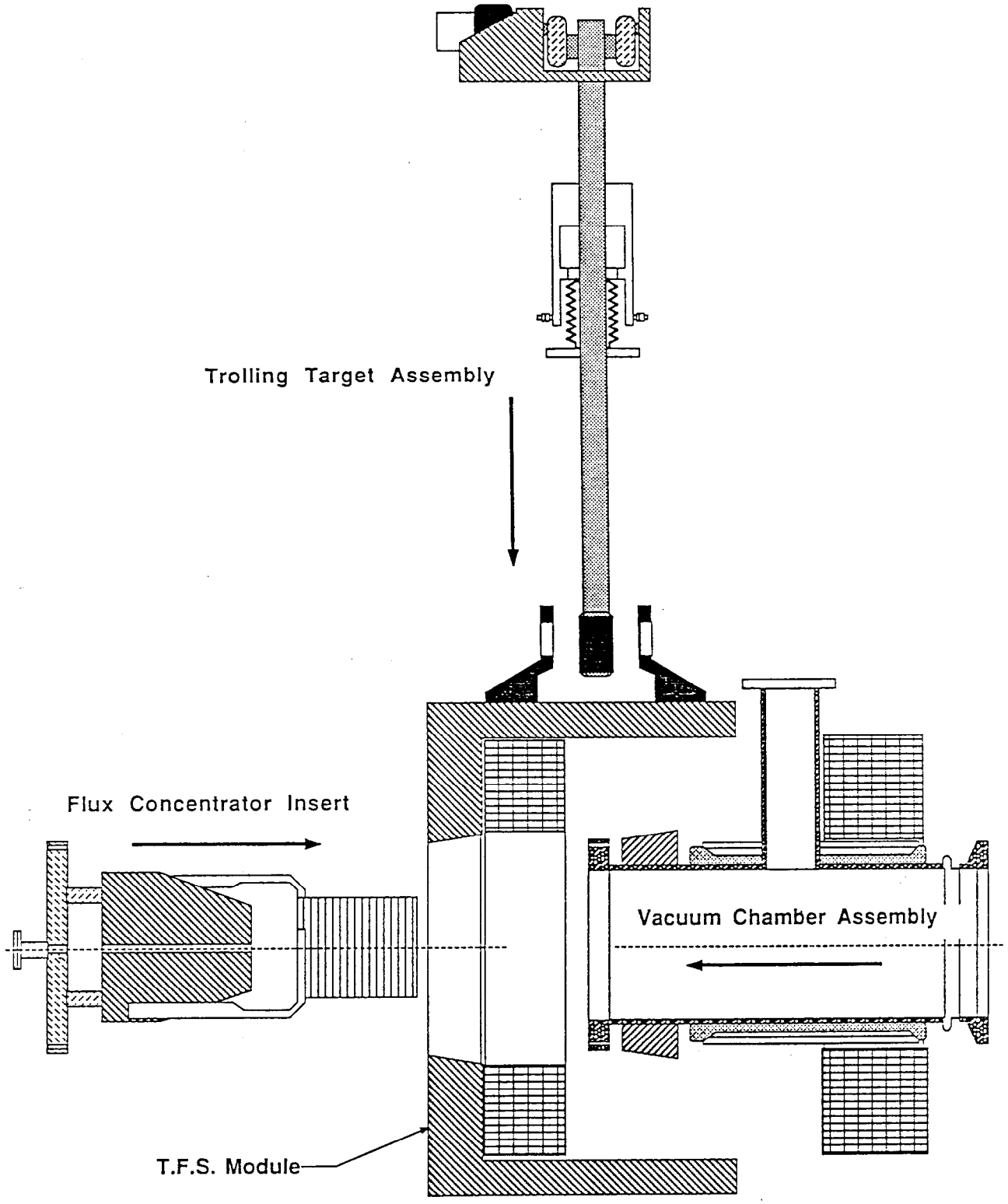

Target/Flux Concentrator/Tapered Field Solenoid
Expanded View

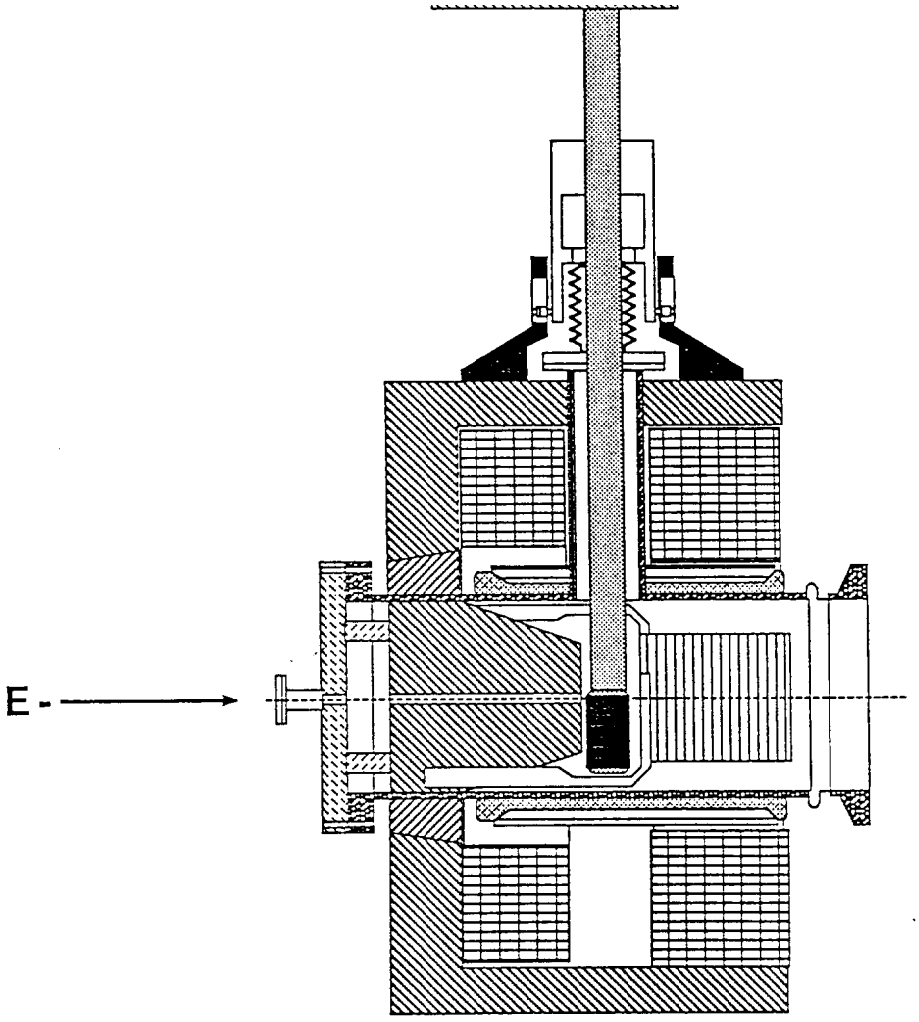

Complete Module Assembly

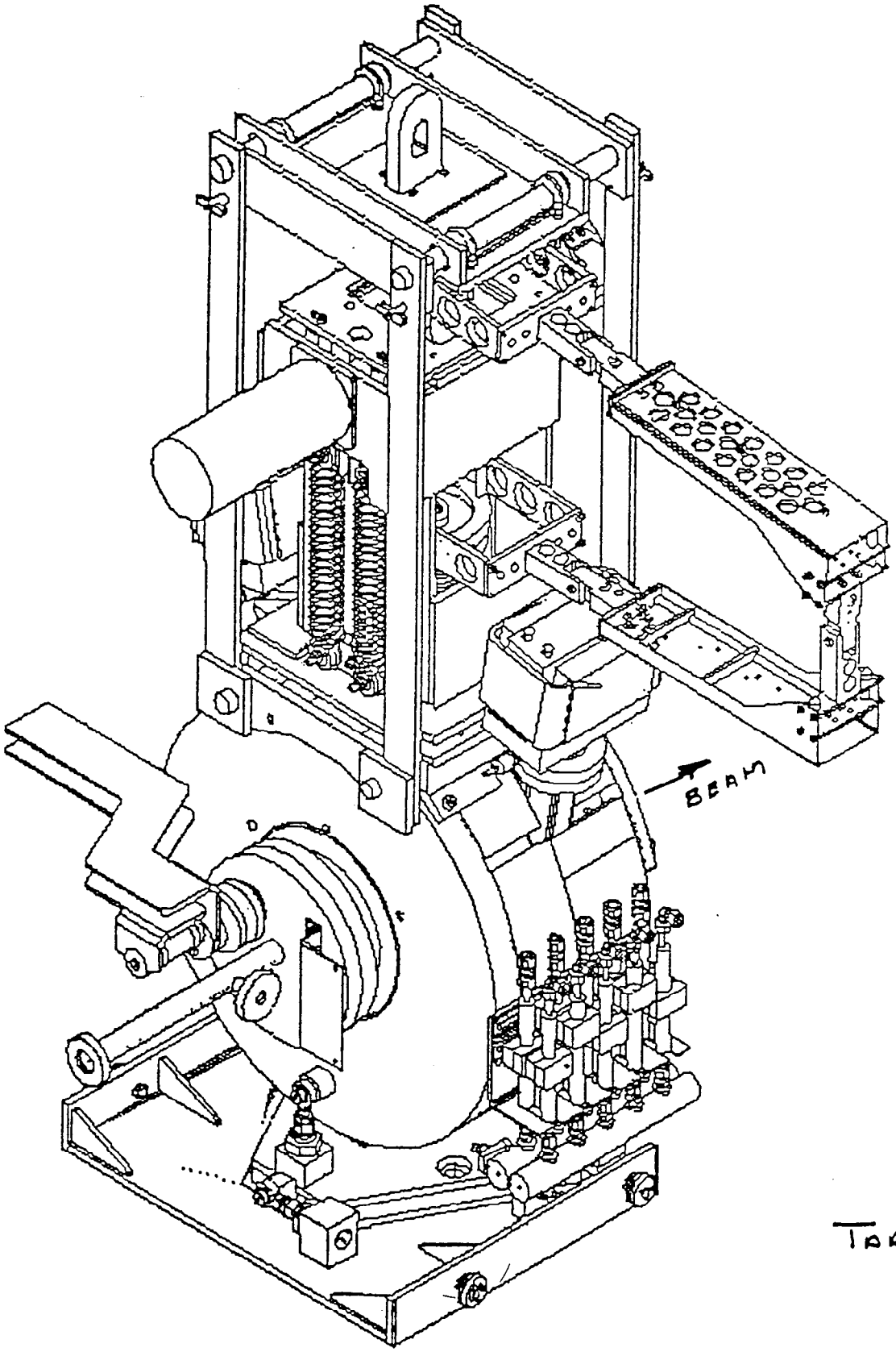
BEAM
TARGET

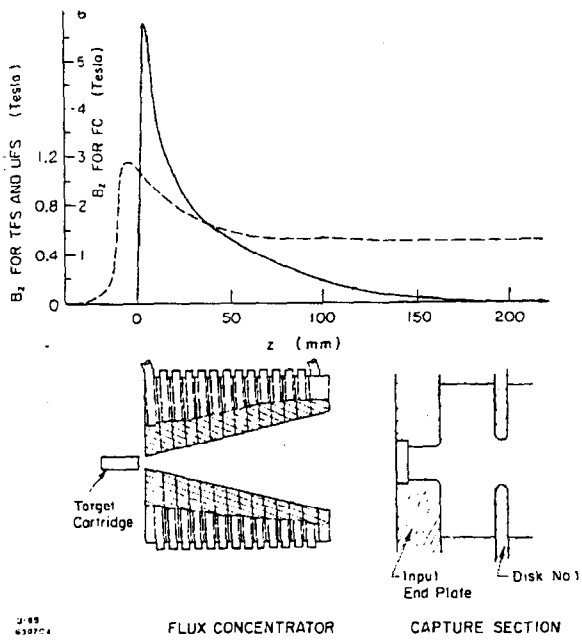

Figure 1. The positron source adiabatic system. The devices shown in cross section at bottom are to scale. The computed solenoidal fields and measured FC pulsed field are shown above with the same z-scale as for the devices.

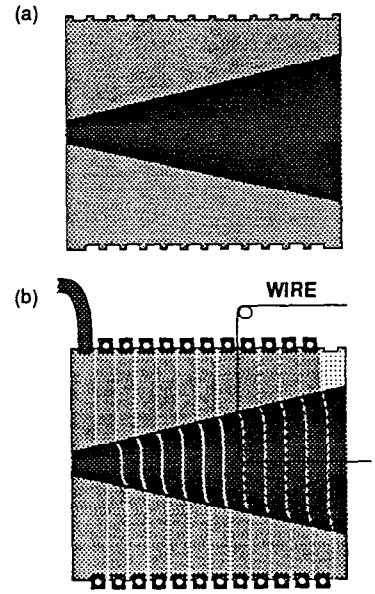

Figure 2. FC body cross section: (a) Showing internal cone and grooves fro rectangular conductor; (b) Showing EDM wire cuts after conductor is brazed into grooves.

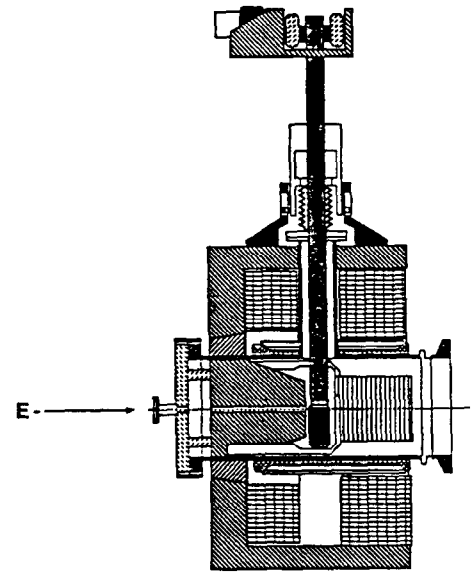

Figure 3. Complete target module assembly showing trolling target driven from above, TFS surrounding both the target (solid black) and FC, and the FC itself supported by the TFS yoke (hashed) on the upstream end.

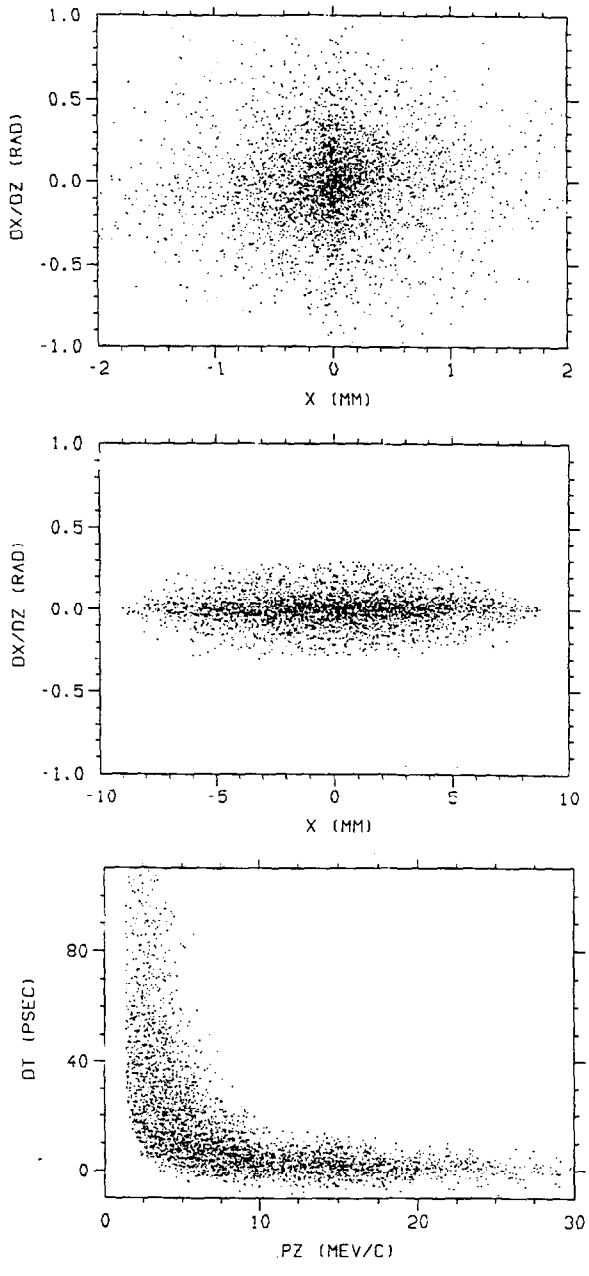

Figure 4. Phase space transformations. (a) EGS simulated phase space at target exit; (b) Transverse phase space at exit of FC (z = 140 mm) as simulated by ETRANS; (c) Longitudinal phase space at exit of FC, also ETRANS.

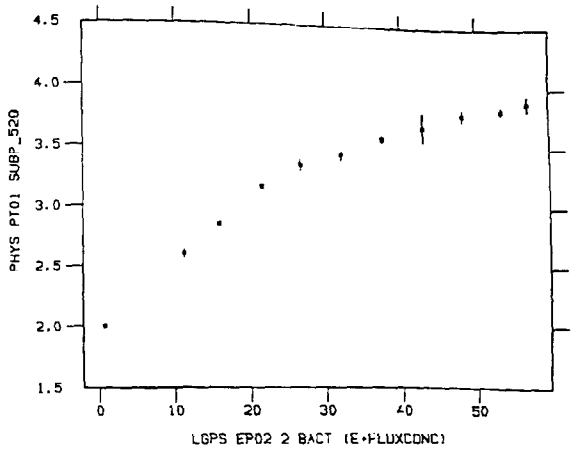

Figure 5. Positron yield at first intensity monitor (at 120 MeV location) as function of peak FC field in kG.

Performance

- At 200 MeV
- After ETA (dP/P cut)
- To Sector 1
- To SDR 1.2 GeV
- From SDR 1

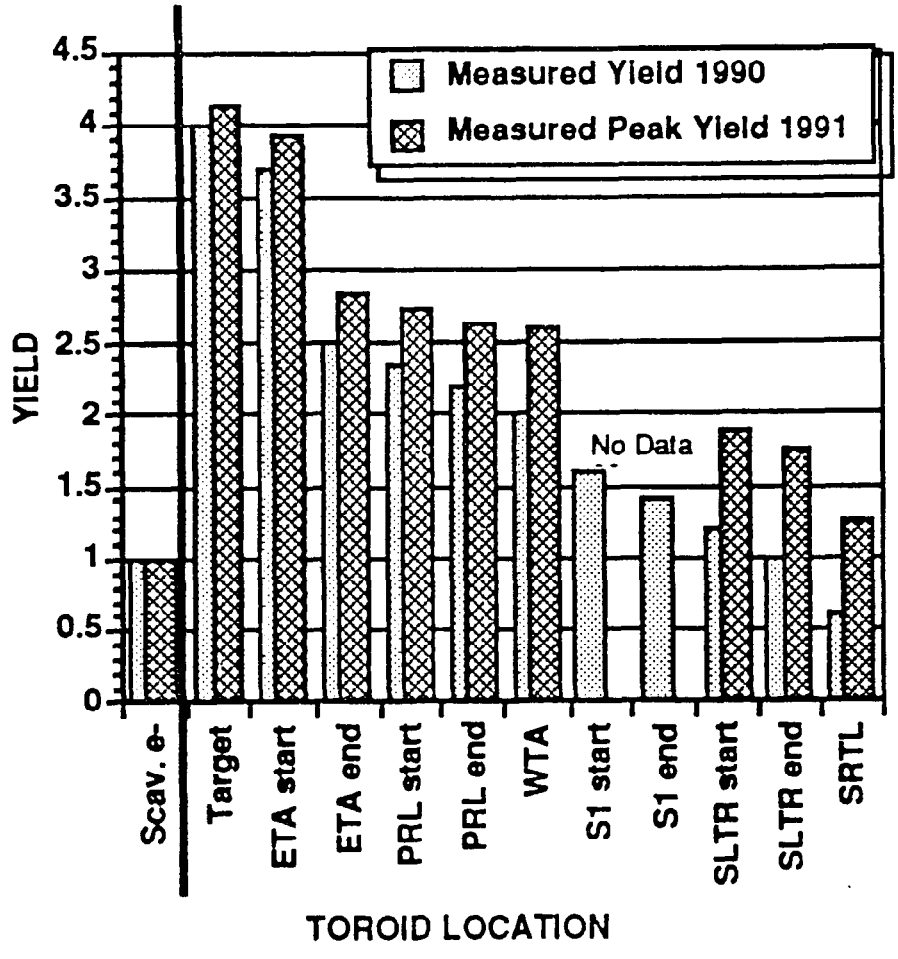
Measured Yield 1990
Measured Peak Yield 1991
No Data
YIELD
4.5
4
3.5
3
2.5
2
1.5
1
0.5
0
Scav. e-
Target
ETA start
ETA end
PRL start
PRL end
WTA
S1 start
S1 end
SLTR start
SLTR end
SRTL
TOROID LOCATION

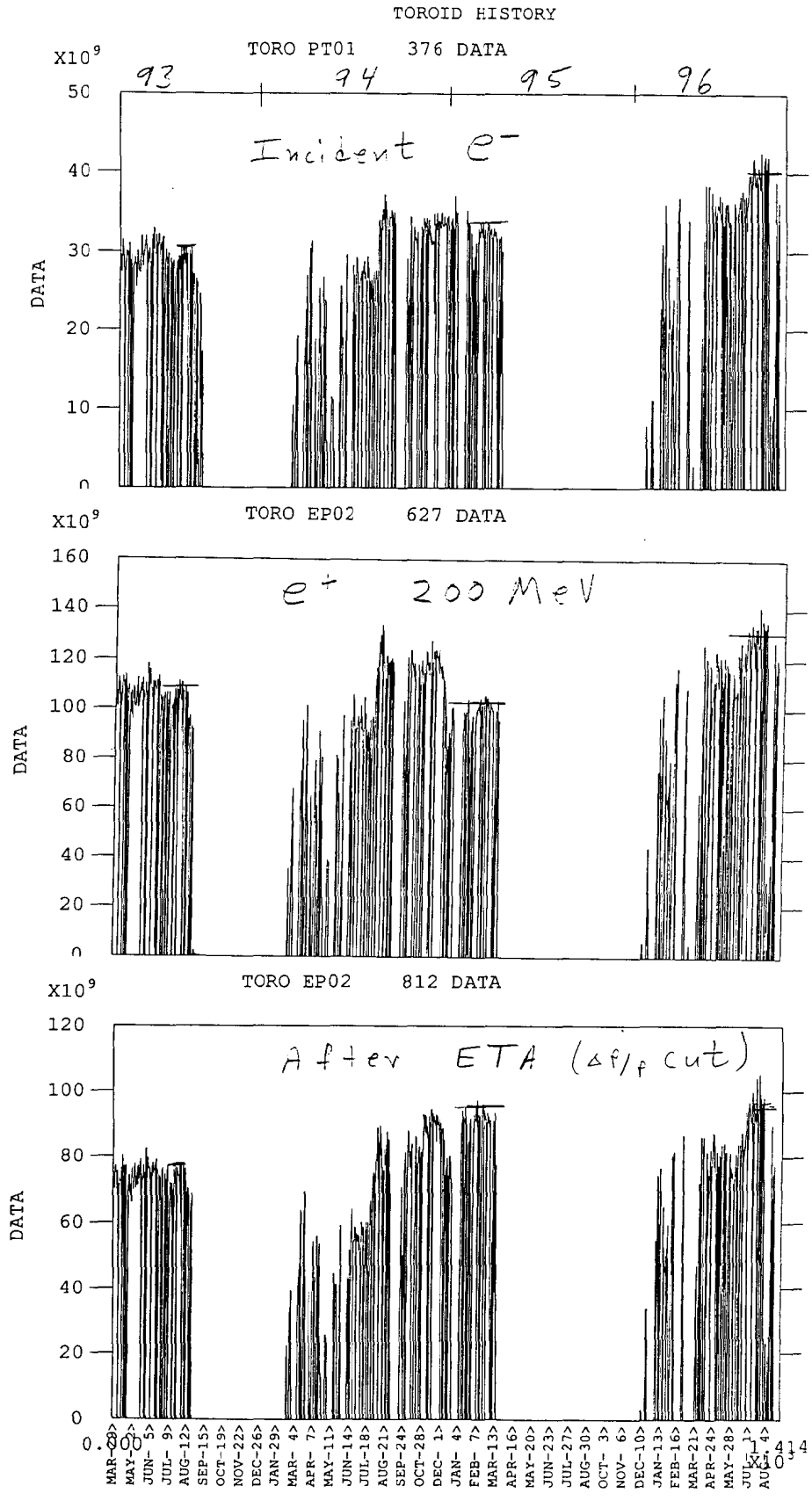
TOROID HISTORY
TORO PT01 376 DATA
X10⁹
93
94
95
96
Incident e⁻
DATA
TORO EP02 627 DATA
e⁺ 200 MeV
TORO EP02 812 DATA
After ETA (Δf/f cut)
MAR-20>
MAY-22>
JUN- 5>
JUL- 9>
AUG-12>
SEP-15>
OCT-19>
NOV-22>
DEC-26>
JAN-29>
MAR- 4>
APR- 7>
MAY-11>
JUN-14>
JUL-18>
AUG-21>
SEP-24>
OCT-28>
DEC- 1>
JAN- 4>
FEB- 7>
MAR-13>
APR-16>
MAY-20>
JUN-23>
JUL-27>
AUG-30>
OCT- 3>
NOV- 6>
DEC-10>
JAN-13>
FEB-16>
MAR-21>
APR-24>
MAY-28>
JUL- 1>
AUG- 4>

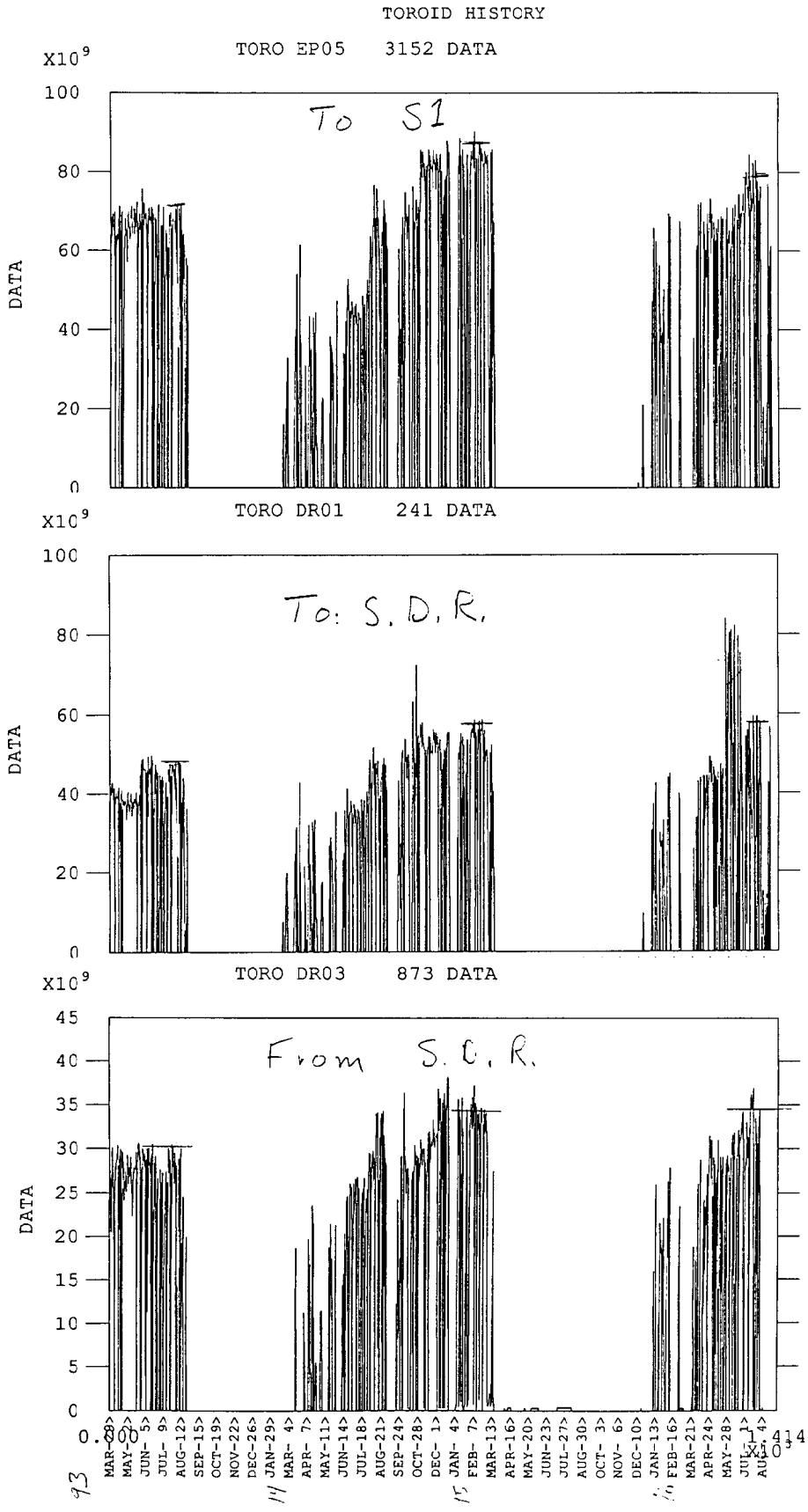
TOROID HISTORY
TORO EP05 3152 DATA
X10⁹
100
80
60
40
20
0
DATA
To S1
TORO DR01 241 DATA
X10⁹
To: S.D.R.
TORO DR03 873 DATA
From S.C.R.
45
40
35
30
25
20
15
10
5
0
0.000
1.414
MAR-09>
MAY-22>
JUN- 5>
JUL- 9>
AUG-12>
SEP-15>
OCT-19>
NOV-22>
DEC-26>
JAN-29>
MAR- 4>
APR- 7>
MAY-11>
JUN-14>
JUL-18>
AUG-21>
SEP-24>
OCT-28>
DEC- 1>
JAN- 4>
FEB- 7>
MAR-13>
APR-16>
MAY-20>
JUN-23>
JUL-27>
AUG-30>
OCT- 3>
NOV- 6>
DEC-10>
JAN-13>
FEB-16>
MAR-21>
APR-24>
MAY-28>
JUL- 1>
AUG- 4>

Typical Positron Yields

	Intensity (1E10)		
	Aug-93	Feb-95	Jul-96
Incident e-	3.0	3.3	4.0
at 200 MeV	10.8	10.0	13.0
after ETA	7.7	9.5	9.5
To S1	7.0	8.7	8.0
To SDR	4.8	5.7	6.0
From SDR	3.0	3.5	3.4

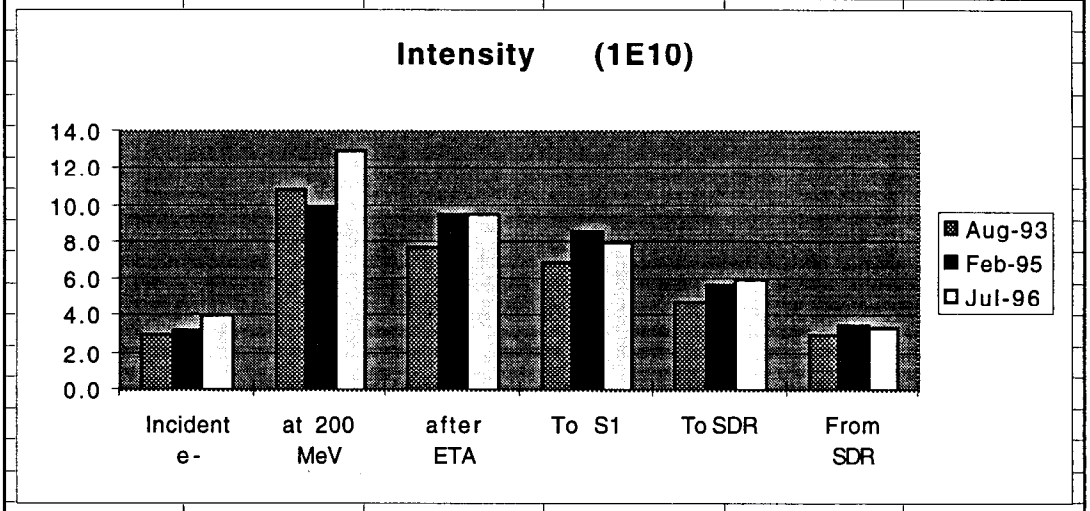

	Yield		
	Aug-93	Feb-95	Jul-96
Incident e-	1.0	1.0	1.0
at 200 MeV	3.6	3.0	3.3
after ETA	2.6	2.9	2.4
To S1	2.3	2.6	2.0
To SDR	1.6	1.7	1.5
From SDR	1.0	1.1	0.9

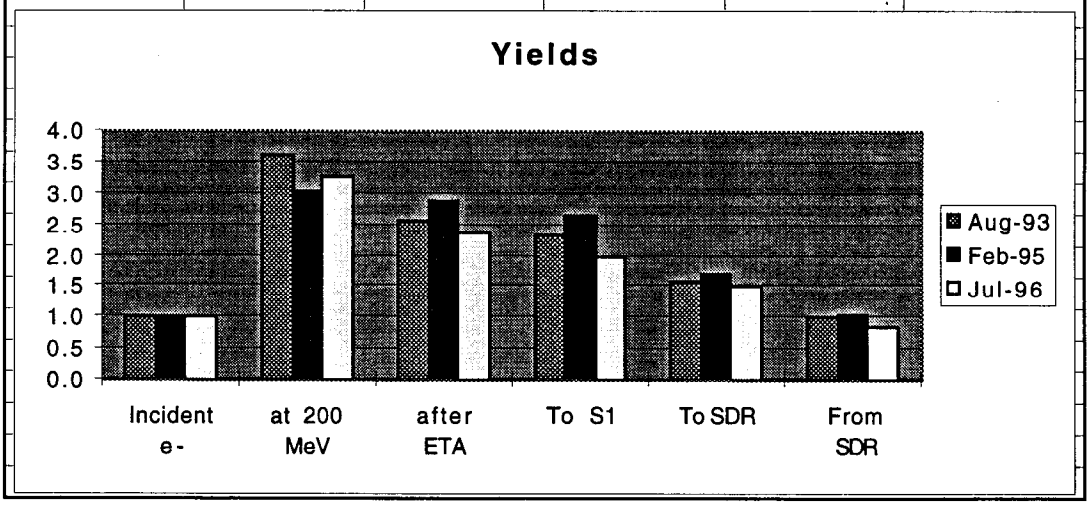

Lessons Learned

- **Calculations agree with Measurements**
  - **Include Error Tolerances !**
- **Increase Optics Acceptance vs. S or accept losses**
- **Consider Stability due to Beam - Beam coupling**
  - **2/3 LINAC**
    - positron intensity loads accelerator
    - which affects scavenger electron intensity
    - which affects positron production
  - **Sector 1**
    - Three beam pulses
    - Orbit
    - Loading
- **Damping Ring allows use of Feed forward**
  - **Down stream LINAC Phase**
  - **Intensity**

References

POSITRON JITTER AND WAKE FIELD EFFECTS IN THE SLC INJECTOR LINAC.
By F. Tian, D. McCormick, M. Ross (SLAC). SLAC-PUB-6556, Jun 1994. 3pp.
Presented at 4th European Particle Accelerator Conference (EPAC 94), London, England, 27 Jun - 1 Jul 1994.
In *London 1994, Proceedings, EPAC 94, vol. 2* 1312-1314, and SLAC Stanford - SLAC-PUB-6556 (94/06,rec.Aug.) 3 p.

A SIMPLE MODEL FOR SLC POSITRON STABILITY ISSUES.
By P. Krejcik, V. Ziemann (SLAC). SLAC-PUB-5725, Jun 1992. 18pp. Presented at the General Meeting of the American Physical Society, Washington, DC, Apr 20-23, 1992.

RECENT IMPROVEMENTS IN THE SLC POSITRON SYSTEM PERFORMANCE.
By P. Krejcik, W.J. Corbett, Stanley D. Ecklund, P. Emma, T.H. Fieguth, Richard H. Helm, A.V. Kulikov, T. Limberg, H. Moshammer, M.C. Ross, R. Siemann, W.L. Spence, M.D. Woodley (SLAC). SLAC-PUB-5786, Mar 1992. 3pp.
Contributed to 3rd European Particle Accelerator Conf., Berlin, Germany, Mar 24-28, 1992.

MECHANICAL DESIGN AND DEVELOPMENT OF A HIGH POWER TARGET SYSTEM FOR THE SLC POSITRON SOURCE.
By Eric M. Reuter, D. Mansour, T.G. Porter, Werner Sax, Anthony Szumillo (SLAC). SLAC-PUB-5369, Dec 1991. 3pp. Contributed to IEEE Particle Accelerator Conf., San Francisco, CA, May 6-9, 1991.
Published in Particle Accel.Conf: IEEE 1991:1999-2001 (QCD183:P3:1991)

SLC POSITRON SOURCE FLUX CONCENTRATOR MODULATOR.
By J. de Lamare, A.V. Kulikov, R. Cassel, V. Nesterov (SLAC). SLAC-PUB-5472, Jun 1991. 3pp. Presented at IEEE Particle Accelerator Conf., San Francisco, CA, May 6-9, 1991.
Published in Particle Accel.Conf: IEEE 1991:3138-3140 (QCD183:P3:1991)

SLC POSITRON SOURCE: SIMULATION AND PERFORMANCE.
By R. Pitthan, H. Braun, J.E. Clendenin, Stanley D. Ecklund, Richard H. Helm, A.V. Kulikov, A. Odian, G.X. Pei, M.C. Ross, M.D. Woodley (SLAC). SLAC-PUB-5547, Jun 1991. 3pp. Presented at IEEE Particle Accelerator Conf., San Francisco, CA, May 6-9, 1991.
Published in Particle Accel.Conf: IEEE 1991:2098-2100 (QCD183:P3:1991)

SLC POSITRON SOURCE PULSED FLUX CONCENTRATOR.
By A.V. Kulikov, Stanley D. Ecklund, E.M. Reuter (SLAC). SLAC-PUB-5473, Jun 1991. 3pp. Presented at Particle Accelerator Conf., San Francisco, CA, May 6-9, 1991.
Published in Particle Accel.Conf: IEEE 1991:2005-2007 (QCD183:P3:1991)

ISOCHRONOUS 180-DEGREE TURNS FOR THE SLC POSITRON SYSTEM.
By Richard H. Helm, J.E. Clendenin, Stanley D. Ecklund, A.V. Kulikov, R. Pitthan (SLAC). SLAC-PUB-5500, May 1991. 3pp. Contributed to IEEE Particle Accelerator Conf., San Francisco, CA, May 6-9, 1991.
Published in Particle Accel.Conf: IEEE 1991:500-502 (QCD183:P3:1991)

3-D NUMERICAL THERMAL STRESS ANALYSIS OF THE HIGH POWER TARGET FOR THE SLC POSITRON SOURCE.
By John A. Hodgson, Eric M. Reuter (SLAC). SLAC-PUB-5370, May 1991. 3pp. Contributed to IEEE Particle Accelerator Conf., San Francisco, CA, May 6-9, 1991.
Published in Particle Accel.Conf: IEEE 1991:1996-1998 Also in Reuter first author in proceedings (QCD183:P3:1991)

HIGH-YIELD POSITRON SYSTEMS FOR LINEAR COLLIDERS.
By J.E. Clendenin (SLAC), SLAC-PUB-4743, April 1989. Published in Proceedings of the 1989 Particle Accelerator Conference, March 23 - 27, 1989, Chicago, IL. p. 1107.

ENERGY MATCHING OF 1.2-GEV POSITRON BEAM TO THE SLC DAMPING RING.
By J.E. Clendenin, Richard H. Helm, R.Keith Jobe, A.V. Kulikov, J.C. Sheppard (SLAC). SLAC-PUB-5050, Aug 1989. 9pp. Presented at 14th Int. Conf. on High Energy Particle Accelerators, Tsukuba, Japan, Aug 22-26, 1989.
Published in Part.Accel.30:105-114,1990. Also in Tsukuba Accel.Conf.1989:1063-1072 (JOURNAL)

THE HIGH GRADIENT S BAND LINAC FOR INITIAL ACCELERATION OF THE SLC INTENSE POSITRON BUNCH.
By J.E. Clendenin, Stanley D. Ecklund, H.A. Hoag (SLAC). SLAC-PUB-5049, Aug 1989. 6pp. Contributed to 14th Int. Conf. on High Energy Accelerators, Tsukuba, Japan, Aug 22-26, 1989.

SLC POSITRON SOURCE STARTUP.
By J.E. Clendenin, G. Bartha, H.C. DeStaebler, Stanley D. Ecklund, Richard H. Helm, L.P. Keller, A.V. Kulikov, A. Odian, M.C. Ross, J.B. Truher, C.G. Yao (SLAC), B.A. Barnett (Johns Hopkins U.), Alan Breakstone (Hawaii U.). SLAC-PUB-4704, Sep 1988. 3pp. Contributed to Linear Accelerator Conf., Williamsburg, Va., Oct 3-7, 1988.

POSITRONS FOR LINEAR COLLIDERS.
By S. Ecklund (SLAC). SLAC-PUB-4484, 1987
Presented at the U.S. Summer School on High Energy Particle Accelerators, Batavia, IL, August 13-24, 1984.

THE STANFORD LINEAR COLLIDER POSITRON SOURCE.
By S. Ecklund (SLAC) E.H. Ottewitte and W. Kells, eds., SLAC-PUB-4437, 1987.
Presented at the Workshop on Intense Positron Beams, June 18-19, 1987, Idaho Falls, ID.
Singapore: World Scientific (1988), p. 42.

POSITION, ANGLE AND ENERGY STABILIZATION FOR THE SLC POSITRON TARGET AND ARCS.
By R.Keith Jobe, K. Thompson, I. Almog, N. Phinney, J. Seeman, J.C. Sheppard, Hamid Shoaee (SLAC). SLAC-PUB-4232, Feb 1987. 3pp. Presented at Particle Accelerator Conf., Wash., D.C., Mar 16-19, 1987.
Published in Washington PAC 1987:713 (QCD183:P3:1987)

CALCULATIONS AND MEASUREMENTS FOR THE SLAC SLC POSITRON RETURN QUADRUPOLE MAGNET.
By Richard A. Early, Joseph K. Cobb (SLAC). SLAC-PUB-4093, Sep 1986. 3pp. Presented at 12th Particle Accelerator Conf., Wash., D.C., Mar 16-19, 1987.
Published in Washington PAC 1987:1428 (QCD183:P3:1987)

HIGH FIELD CAPTURE SECTION FOR SLC POSITRON SOURCE.
By H.A. Hoag, H. Deruyter, James F. Kramer, C.G. Yao (SLAC). SLAC-PUB-3971, May 1986. 4pp. Contributed to 1986 Linear Accelerator Conf., Stanford, CA, Jun 2-6, 1986.
Published in Stanford LINAC86:437 (QCD191:C62:1986)

PI DECAY MUONS FROM THE SLC POSITRON SOURCE.
By W.Ralph Nelson, R.A. Shore (SLAC). SLAC-CN-300, May 1985. 5pp.

SLC POSITRON DAMPING RING OPTICS DESIGN.
By Jean Pierre Delahaye (CERN), L.Z. Rivkin (Cal Tech). SLAC-PUB-3649, Apr 1985. 3pp. Poster paper presented at Particle Accelerator Conf., Vancouver, Canada, May 13-16, 1985.
Published in Particle Accel.Conf.IEEE 1985:1695 (QCD183:P3:1985)

ADDITIONAL MUON CALCULATIONS FOR THE SLC POSITRON SOURCE.
By W.Ralph Nelson, Richard C. McCall (SLAC). SLAC-CN-295, Apr 1985. 8pp.

TEMPERATURE RISE AND GRADIENT OF SLC POSITRON ACCELERATING SECTION AND WAY TO REDUCE THEIR EFFECTS ON POSITRON DYNAMICS.
By C.G. Yao (SLAC). SLAC-CN-288, Feb 1985. 9pp.

DESIGN OF A HIGH YIELD POSITRON SOURCE.
By F. Bulos, *et al.* (SLAC). SLAC-PUB-3635, 1985.
Published in IEEE Trans. Nucl. Sci. NS-32 (1985) 1832.

SLC POSITRON DAMPING RING OPTICS DESIGN.
By Jean Pierre Delahaye, L.Z. Rivkin (SLAC). SLAC-CN-283, Dec 1984. 29pp.

NOTES ON THE RF SYSTEM FOR THE SLC POSITRON SOURCE.
By H.A. Hoag (SLAC). SLAC-CN-282, Oct 1984. 6pp.

THE SNAKE RING: A FEASIBILITY STUDY OF A SMALL PREDAMPING RING FOR THE POSITRON SOURCE OF SLC.
By K. Wille (SLAC). SLAC-PUB-3417, Aug 1984. 29pp.
Published in Nucl.Instrum.Meth.A238:5,1985.

A NOTE ON SHIELDING THE SLC POSITRON SOURCE.
By Theodore M. Jenkins (SLAC). SLAC-CN-221, Apr 1983. 7pp.

Positron sources for TESLA and SBLC

K. Flöttmann
DESY

Workshop on New Kinds of Positron Sources for Linear Colliders
SLAC, March 4-7

Positron sources for TESLA and SBLC

SBLC and TESLA require 10^2-10^3 more positrons per pulse as SLC (1). A major problem for any high intensity source is the thermal stress induced in the target by ionization losses of the electrons and positrons. For SBLC and TESLA a wiggler based source is considered which utilizes the 250GeV electron beam after interaction (2). The beam is captured in a special optics section and passed through a wiggler of ~35m length. The high energy photons are used to generate e^+e^- pairs in a thin target .

The heat load problem is reduced by two factors:

-since only a thin target ($0.4X_0$) is required it is possible to use a low Z material with a high heat capacity (3).

- the effect of multiple scattering is reduced in the thin target (4). The lower emittance of the positrons leads to a higher capture efficiency in the subsequent optics.

TESLA runs with a very long bunch spacing, thus it is possible to distribute the bunch impacts within on pulse on a fast rotating target (5). Temperature distributions in the target for a single shot are shown in (6).

A conventional capture optics is used behind the target. Due to recent improvements in the design of the Damping Rings it was possible to increase the acceptance of the capture optics and reduce the peak field of the adiabatic matching device (7). (8) shows the energy distribution of the positrons and (9) shows the longitudinal beam profile.

After presentation of the general layout the preparation of the 250GeV electron beam after interaction is discussed in some detail. This work has been performed by R. Glantz (DESY).

After interaction the phase space of the disrupted beam is distorted and the emittance is increased (10). A long tail of low energy particles has been developed due to beamstrahlung losses which leads to further emittance growth in the subsequent optics via chromatic effects. While TESLA works with head-on collisions a small crossing angle is required for SBLC. The outgoing electron beam has to pass through a nonlinear field region of the final focus quadrupole (11). Additional constrains for the optics design are:

-the beam line has to fit into a common tunnel with the final focus system.

- bending magnets have to be weak in order to reduce emittance growth due to synchrotron radiation.

Beam line geometry's and optics are shown in (12, 13, 14, 15) for TESLA and SBLC. The dispersion is zero at the entrance of the wiggler. The horizontal chromaticity is corrected in a correction section similar to the CCS section in final focus system. Various collimators are distributed along the beam line. 15-20% of the electrons have to be to scraped off in order to fulfill the emittance requirements (16). The transfer efficiency of the optics depends on the strength of the interaction, i.e. if no interaction occurs 100% of the electrons are transmitted through the optics. (17) shows the development of the e^+ bunch charge after a 'missing interaction'. The distortion is damped within a few shots. Even though not all effects that may occur in the main linac are taken into account, the simulation shows that the source is not instable in itself.

(18) shows the dependence of the transfer efficiency on the horizontal β-function at the IP. The efficiency can be increased on the expense of some luminosity. In case of a

polarized e^+ source the emittance requirements are much higher and an optimization of the horizontal β-function is necessary in order to improve the source performance.
For the polarized source a long helical undulator is required (19). (20) compiles some important aspects of the source design. From the technical point of view the helical undulator is the most critical component. (21) shows an artist view of a simple helical undulator without iron. MAFIA calculations were performed in order to study the effect of an iron yoke and iron between the conductors. After optimization of all parameters the field amplitude was raised by a factor of 2. The required undulator length is reduced by ~33% (22).

Overview

1) general layout of the source

2) preparation of the 250GeV electron beam

(work by R. Glantz)

3) optional upgrade to a polarized positron source

Comparison of parameters of SBLC and TESLA with SLC parameters

Parameter	SLC	TESLA	SBLC
number of positrons per pulse at IP	$3\text{-}5 \cdot 10^{10}$	$4102 \cdot 10^{10}$	$366 \cdot 10^{10}$
number of bunches per pulse	1	1130	333
pulse duration	3ps	0.8ms	2μs
bunch spacing	8.3ms	708ns	6ns
repetition frequency	120Hz	5Hz	50Hz

The main problem for high intensity positron sources is the heating of the target:

* dominated by the ionization losses of electrons and positrons given by:

E_{dep} ~2MeV cm^2/g per charged particle

* the temperature rise of the target ΔT can be estimated as:

$$\Delta T[K] = 3.2 \cdot 10^{-13} J \cdot \frac{2N}{c \cdot A \cdot \eta}$$

c = heat capacity $\left[\frac{J}{g \cdot K}\right]$

A = source area $[cm^2]$

η = capture efficiency

Wiggler based positron source

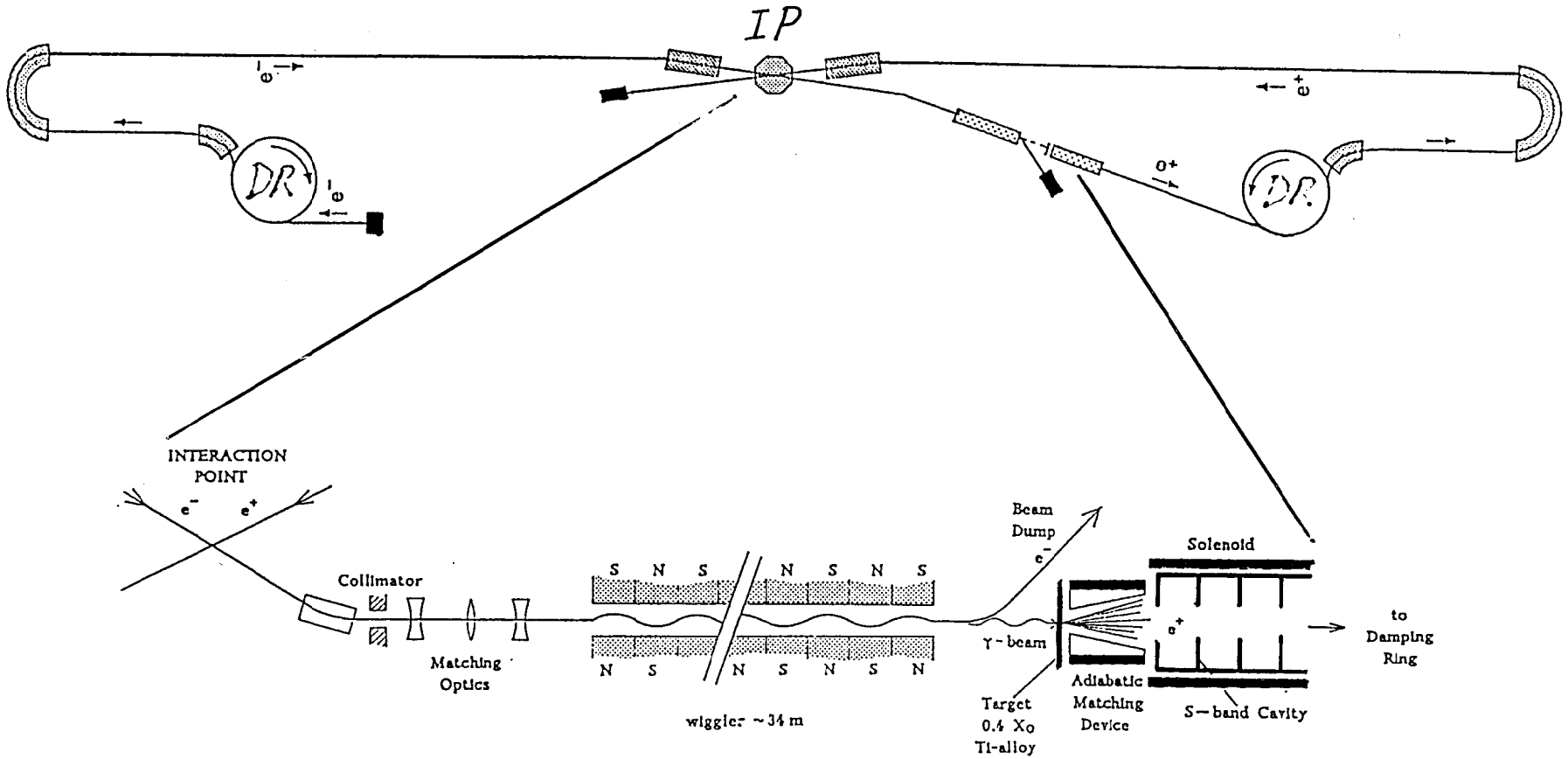

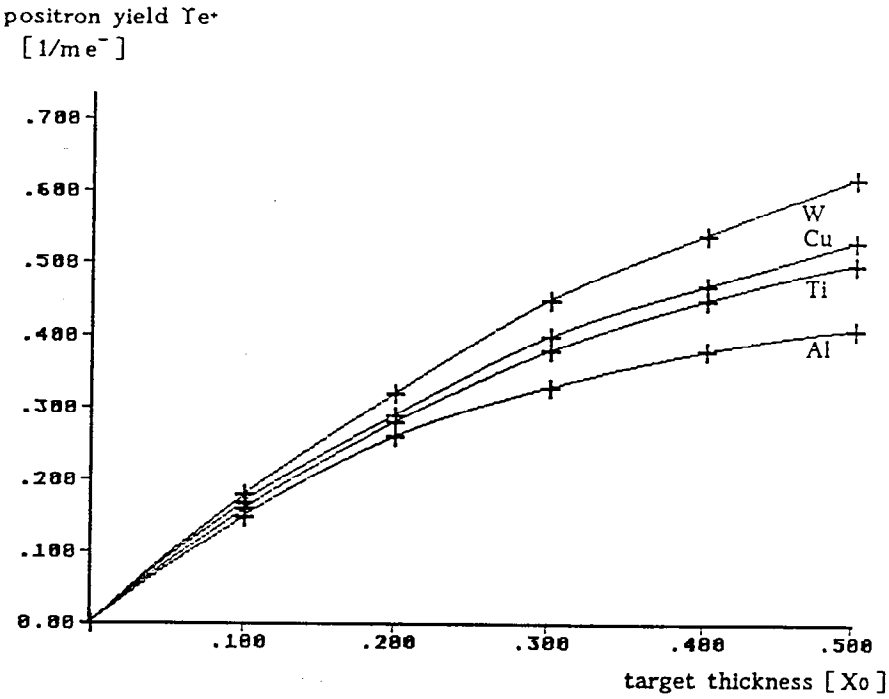

Fig. 1.11 Positron yield for various materials obtained with wiggler photons (B = 1.7 T, S = 1 m) versus target thickness in units of radiation length; E = 250 GeV

thermal stress in the target

$\sigma \sim \Delta T \cdot \alpha \cdot E$

α = coeff. of linear expansion

E = elastic modulus

$\Delta T \sim \frac{1}{c}$

σ_{max} = tensile strength

Material	σ_{max}/σ
W-26 Re	60
Ti-13V-11Cr-3AL	690

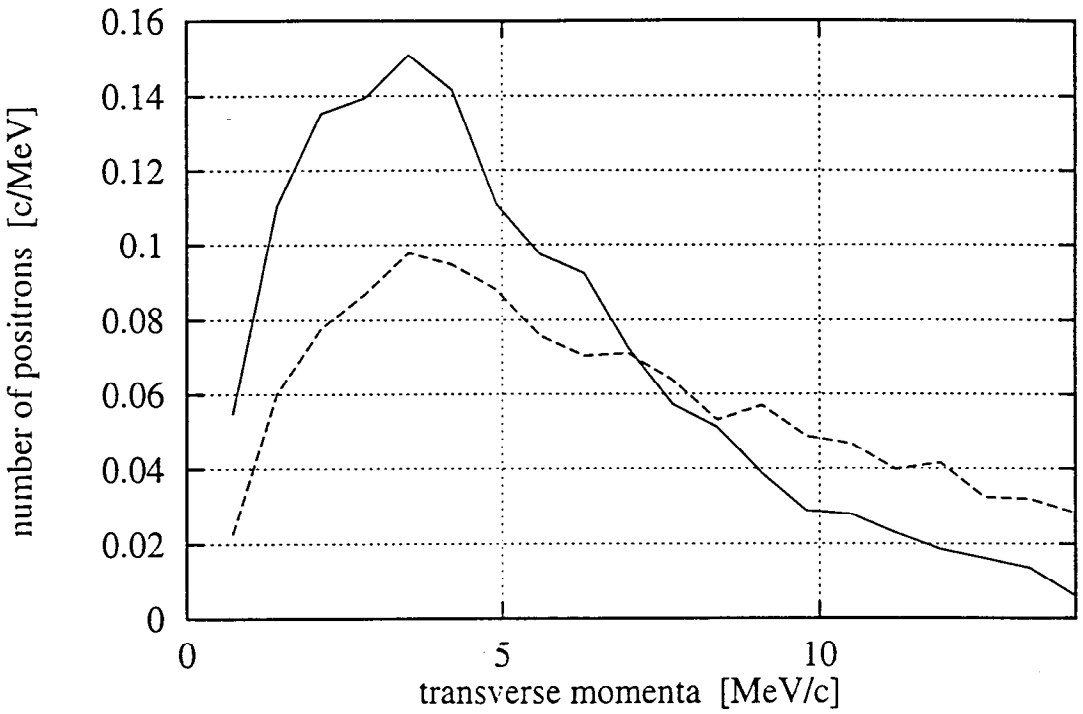

Comparison of transverse momenta for a SLC like source ($6X_0$, W, dotted line) and a thin target driven by wiggler photons ($0.4\ X_0$, Ti, solid line).

For a given acceptance of the capture optics the capture efficiency is increased by a factor of ~ 5 in case of the wiggler based source.

TESLA - Target

velocity on circumference: 50 $\frac{m}{s}$

$\Rightarrow$ ~ 60 bunches overlap

$\Delta s = 0,04\ m$

rep. rate 5 Hz

$\Delta T \sim 360°$

$P = 7\ kW$

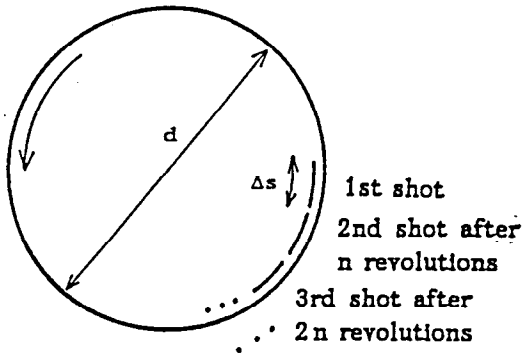

Fig. 1. 24 The rotating target disk

n	N	d [m]	τ_{cool} [s]	revolutions per minute
1	124	1.58	12.4	605
2	62	0.79	6.2	1210
3	41.3	0.53	4.1	1815
4	31	0.39	3.1	2419

Tab. 7 Comparison of target parameters.

Temperature distribution in the target

SBLC

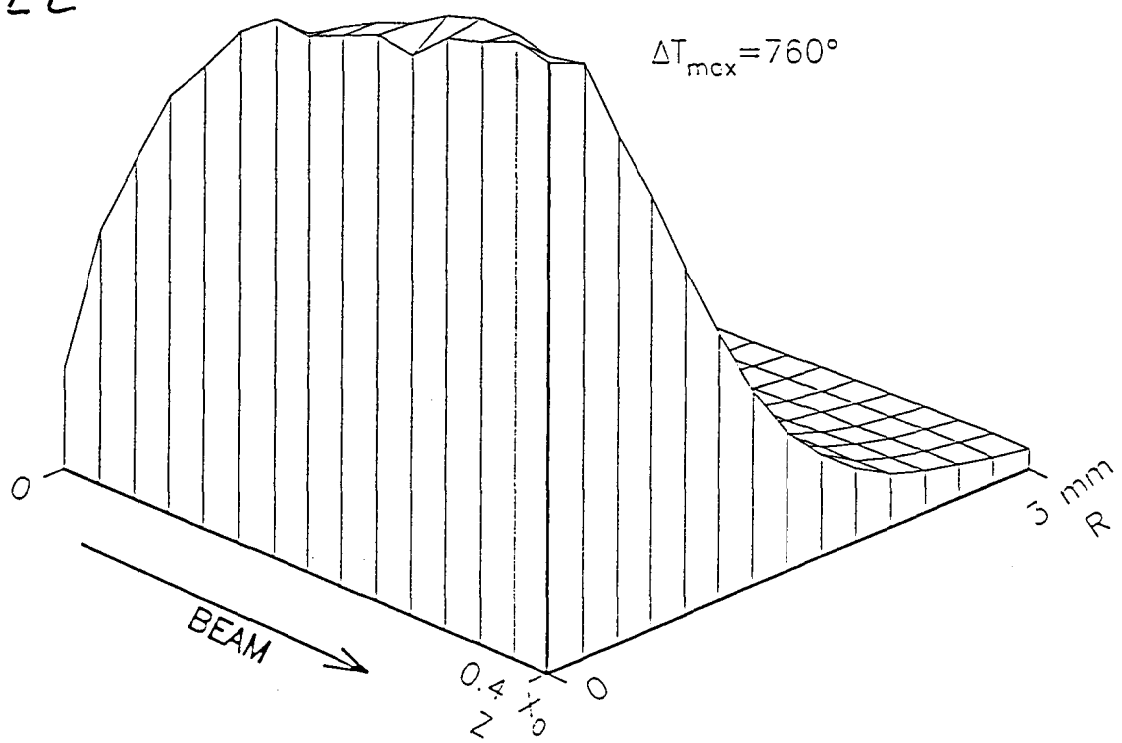

TESLA

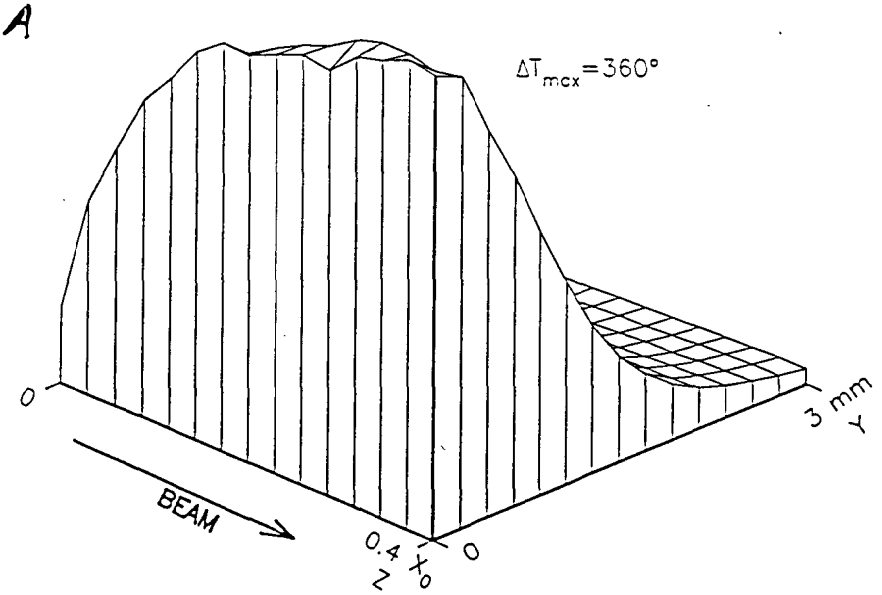

Wiggler	SBLC	TESLA
field on axis	~1.7T	~1.7T
period length	≤31mm	≤31mm
gap height	5mm	5mm
total length	35m	35m
beam size in the wiggler:		
σy at $\varepsilon y=1\cdot10^{-9}$m	0.33mm	0.33mm
σx at $\varepsilon x=1\cdot10^{-8}$m	1.0mm	1.0mm
spot size of radiation on the target $\sigma_{x,y}$	0.7mm	0.7mm
number of photons per electron	367.5	367.5
mean photon energy	22MeV	22MeV
power of photon beam	~230kW	~250kW
Target		
material	Titanium alloy	Titanium alloy
target thickness	$0.4X_0$ = 1.42cm	$0.4X_0$ = 1.42cm
pulse temperature rise	760K	360K
mean deposited power	6kW	7kW
Adiabatic matching device		
initial field	7.0T	6.0T
taper parameter g	$30m^{-1}$	$30m^{-1}$
end field	0.7T	0.16T
wavelength of accel. structure	0.1m	0.23m
radius of cavity iris	10.0mm	23.0mm
Damping ring		
required norm. acceptance $\gamma\varepsilon x+\gamma\varepsilon y$	0.041πm	0.048πm
capture efficiency	17%	17%
estimated overall efficiency	8.5%	8.5%
norm. rms emittance of positron beam $\gamma\varepsilon x=\gamma\varepsilon y$	$7.0\cdot10^{-3}\pi$m	$1.1\cdot10^{-2}\pi$m
energy width	±30MeV	±30MeV

Parameters for the wiggler based positron source for SBLC and TESLA

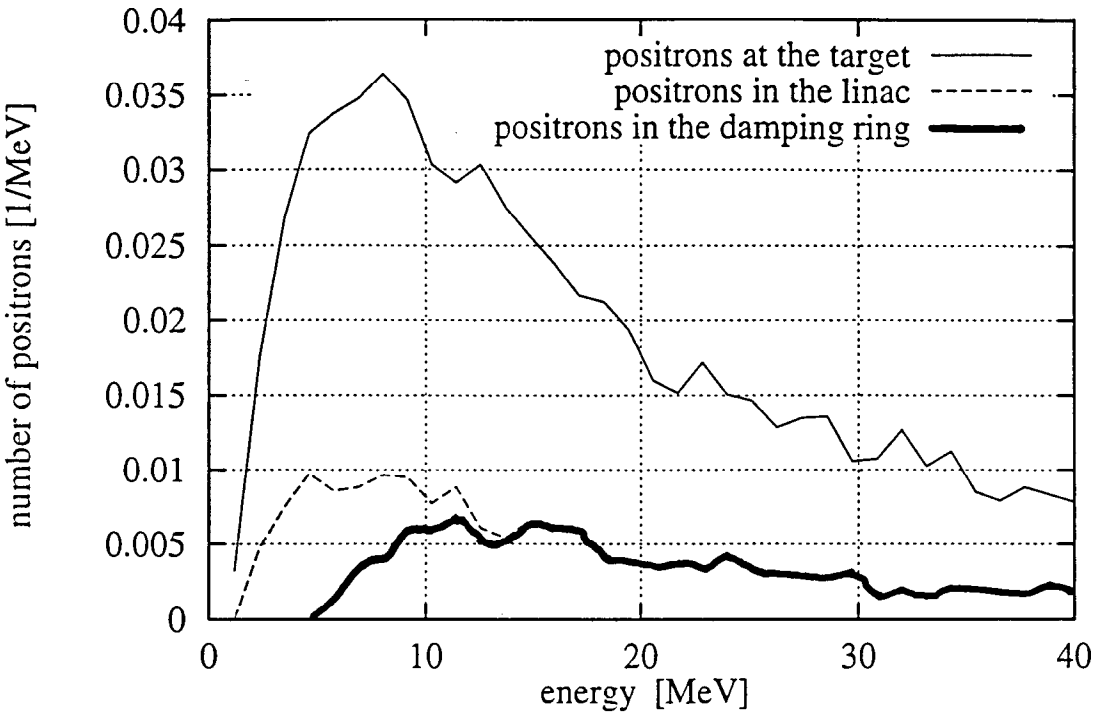

Energy distribution of the positrons emerging from the target (solid line) and the fraction of captured positrons (dashed lines).

SBLC

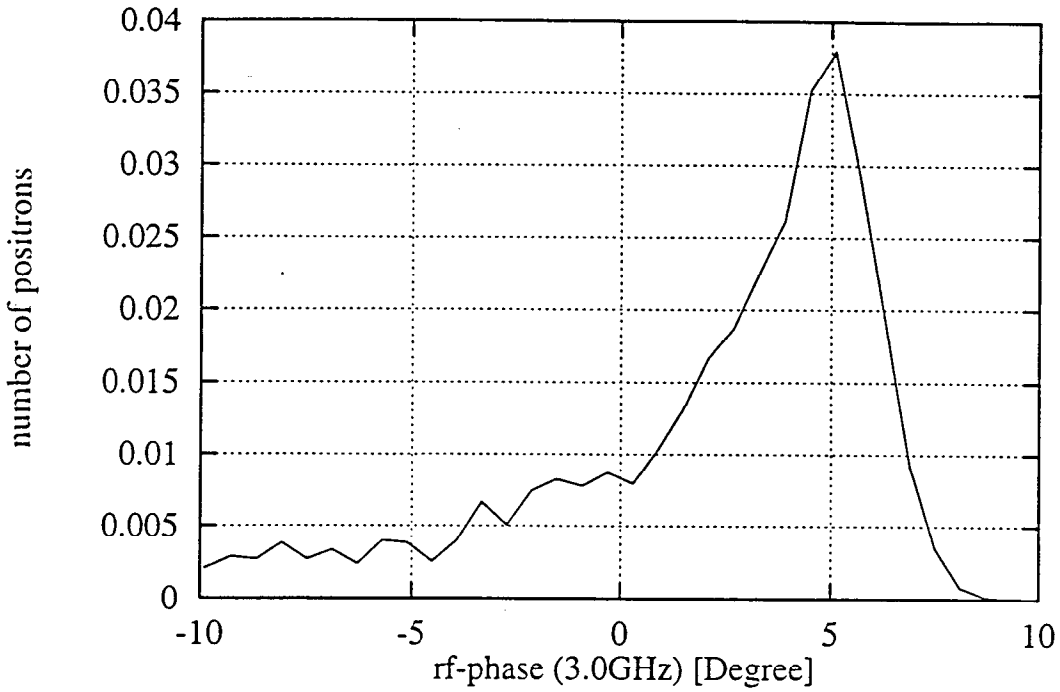

Longitudinal beam profile of the positrons behind the matching device. Only the fraction of positrons within ±7.5° is accepted in the simulations.

TESLA

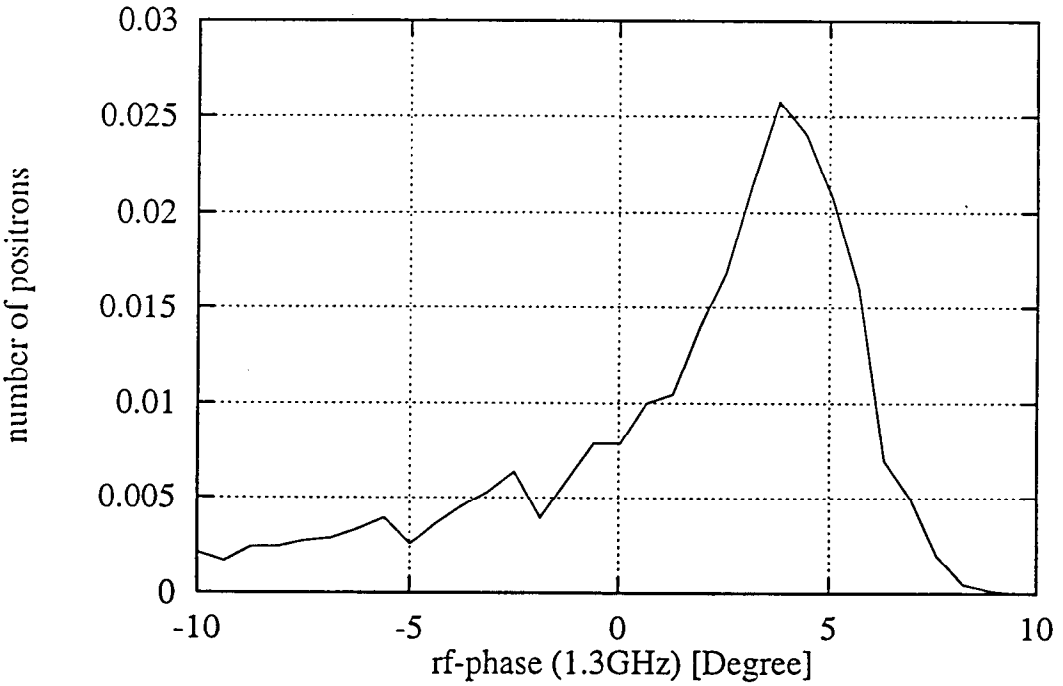

Longitudinal beam profile of the positrons behind the matching device. Only the fraction of positrons within ±7.5° is accepted in the simulations.

Preparation of the 250 GeV Beam after Interaction

R. Glantz

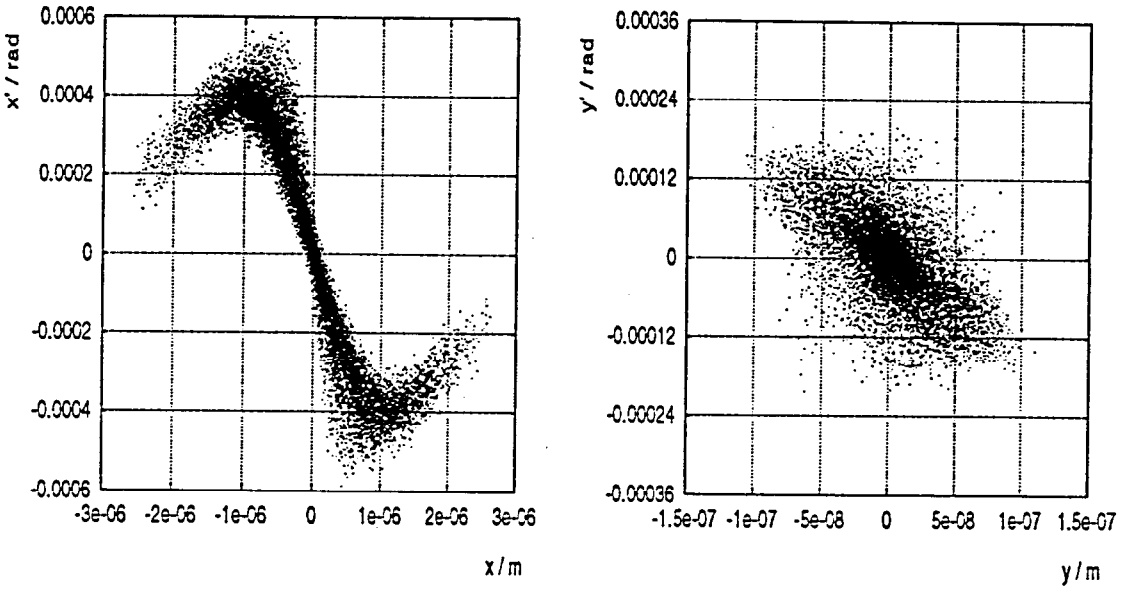

Horizontal and vertical phase space distribution after interaction

		Tesla	SBLC
electron beam after interaction:			
emittance εx / εy	10^{-12} m	113.0 / 1.2	34.5 / 0.88
energy width	%	3.15	2.76
emittance requirements:			
unpolarized source εx / εy	10^{-8} m	1.0 / 0.5	1.0 / 0.5
polarized source εx / εy	10^{-10} m	5.0 / 1.0	5.0 / 1.0

Comparison of beam parameters after interaction and emittance requirements. The large energy spread leads to further emittance growth in the transfer optics.

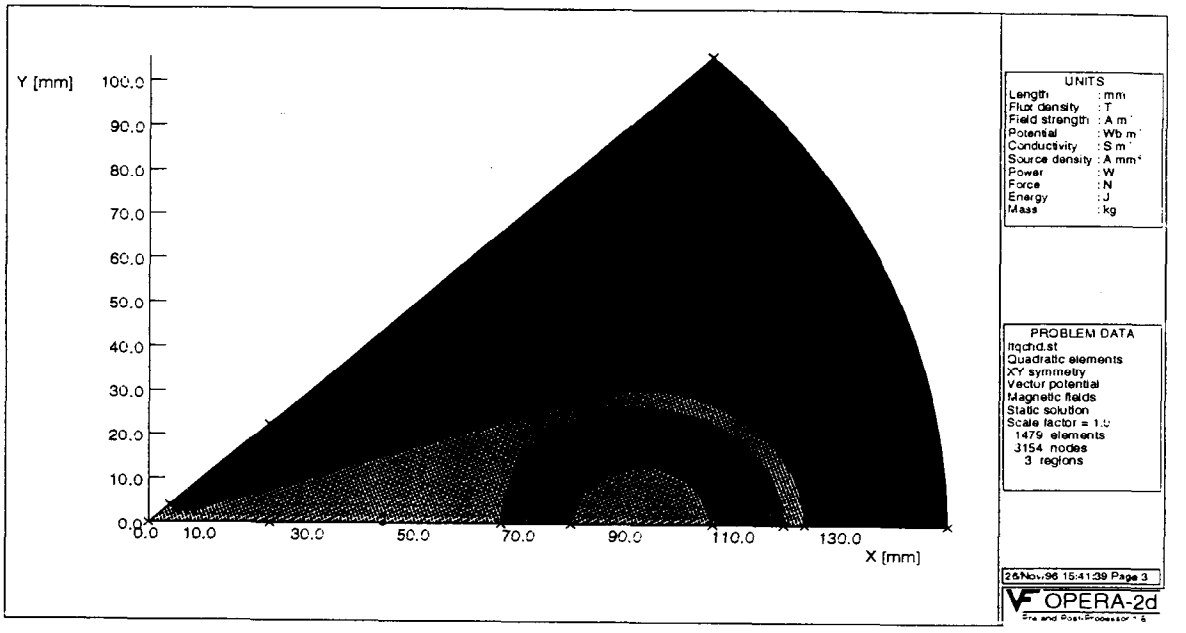

Figure 5.4: *Cross section of 1/8 of the FFQ.* of SBLC

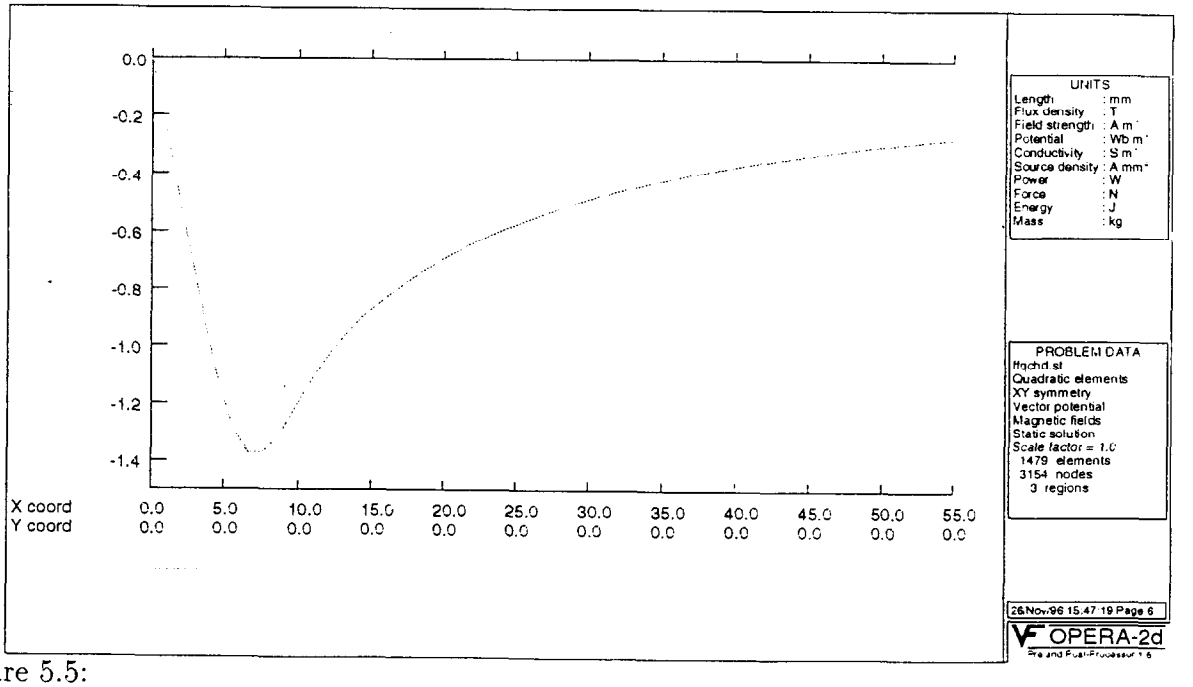

Figure 5.5:
Vertical magnetic field as a function of distance from the longitudinal symmetry axis. The spent beam enters the first FFQ with a horizontal offset of x=12mm.

SBLC

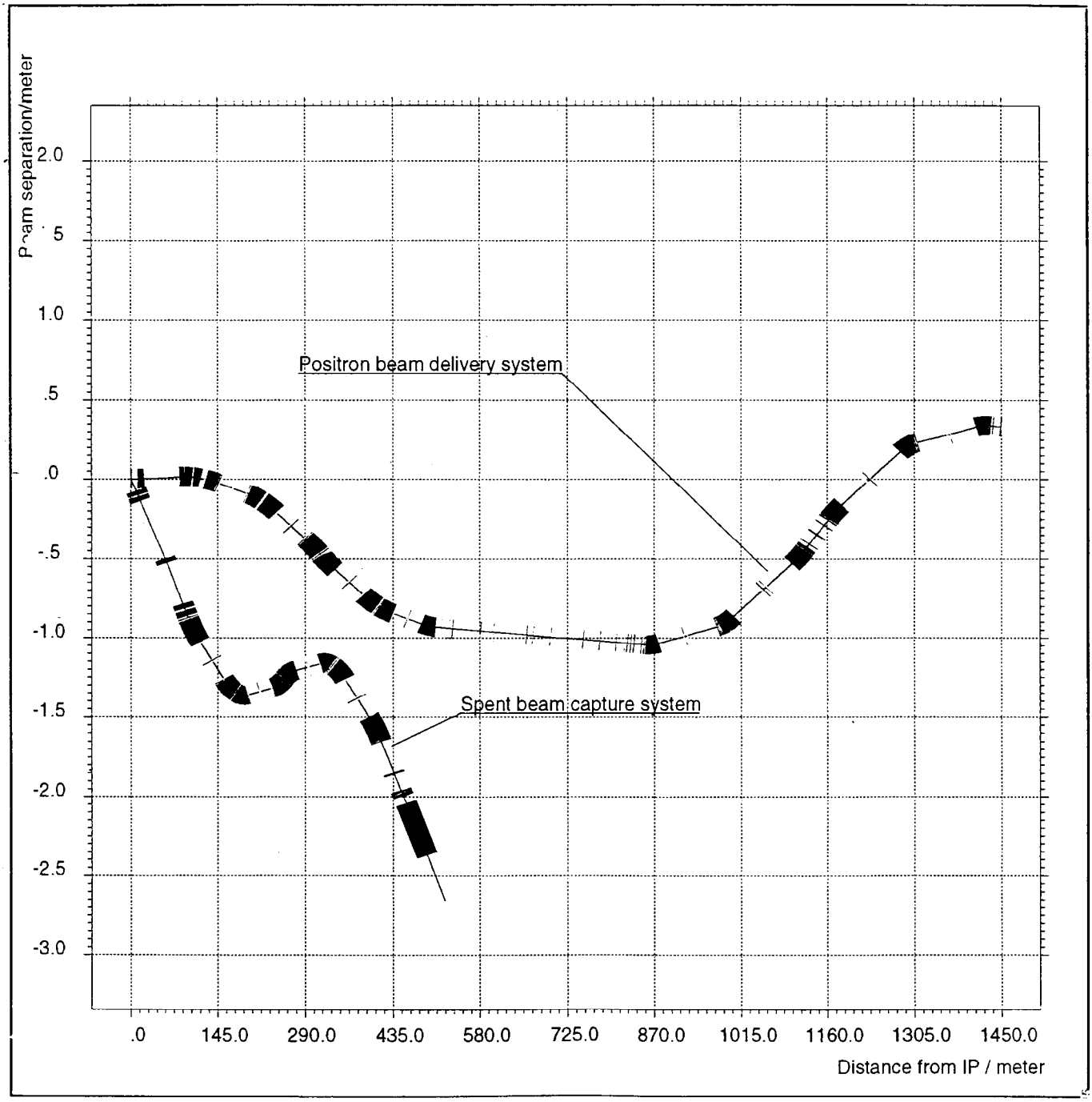
Beam separation/meter
2.0
.5
1.0
.5
.0
-.5
-1.0
-1.5
-2.0
-2.5
-3.0
Positron beam delivery system
Spent beam capture system
.0
145.0
290.0
435.0
580.0
725.0
870.0
1015.0
1160.0
1305.0
1450.0
Distance from IP / meter

SBLC

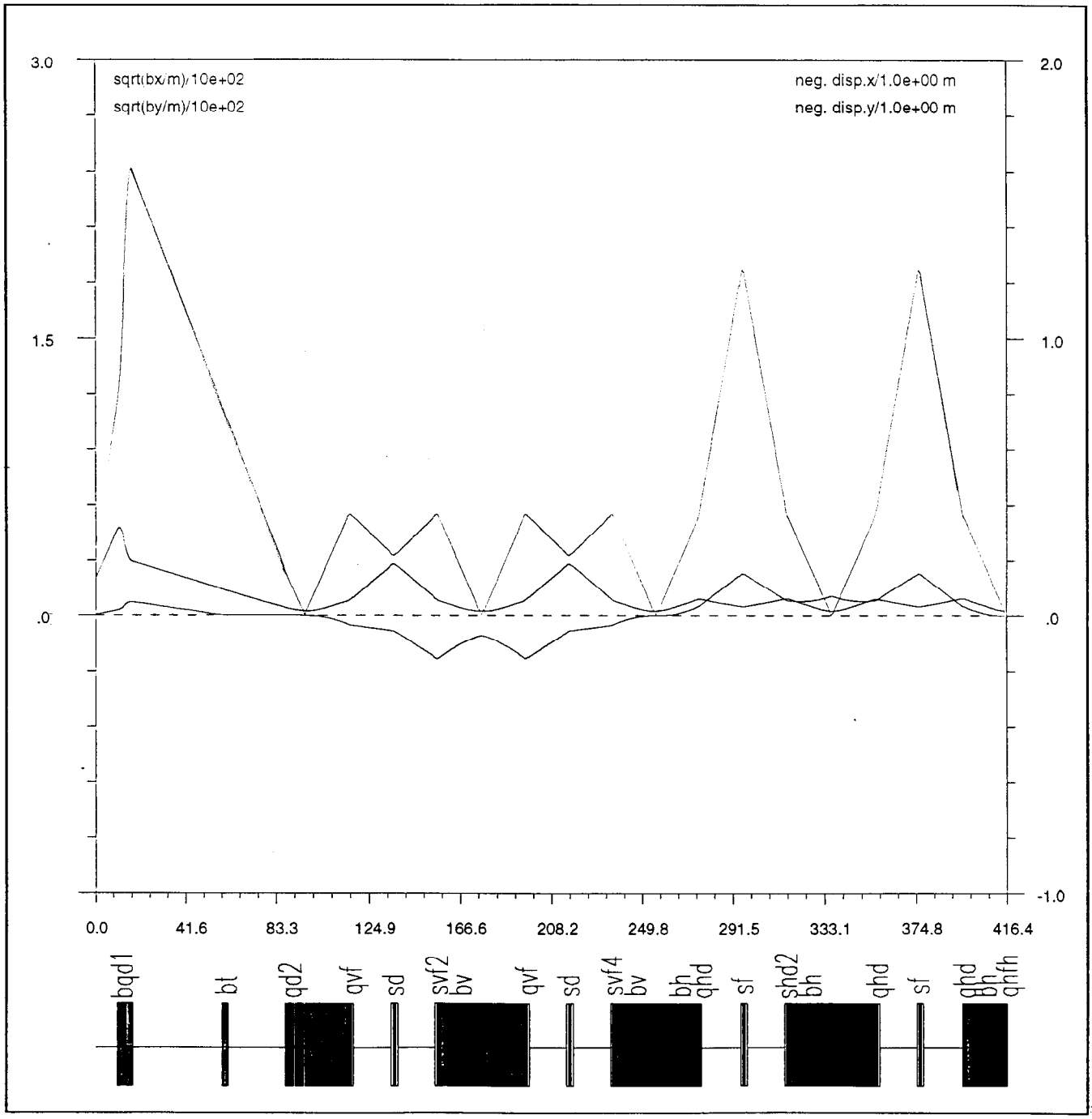
sqrt(bx/m)/10e+02
sqrt(by/m)/10e+02
neg. disp.x/1.0e+00 m
neg. disp.y/1.0e+00 m
3.0
1.5
.0
2.0
1.0
.0
-1.0
0.0
41.6
83.3
124.9
166.6
208.2
249.8
291.5
333.1
374.8
416.4
bqd1
bt
qd2
qvf
sd
svf2
bv
qvf
sd
svf4
bv
bh
qhd
sf
shd2
bh
qhd
sf
qhd
bh
qhfh

TESLA

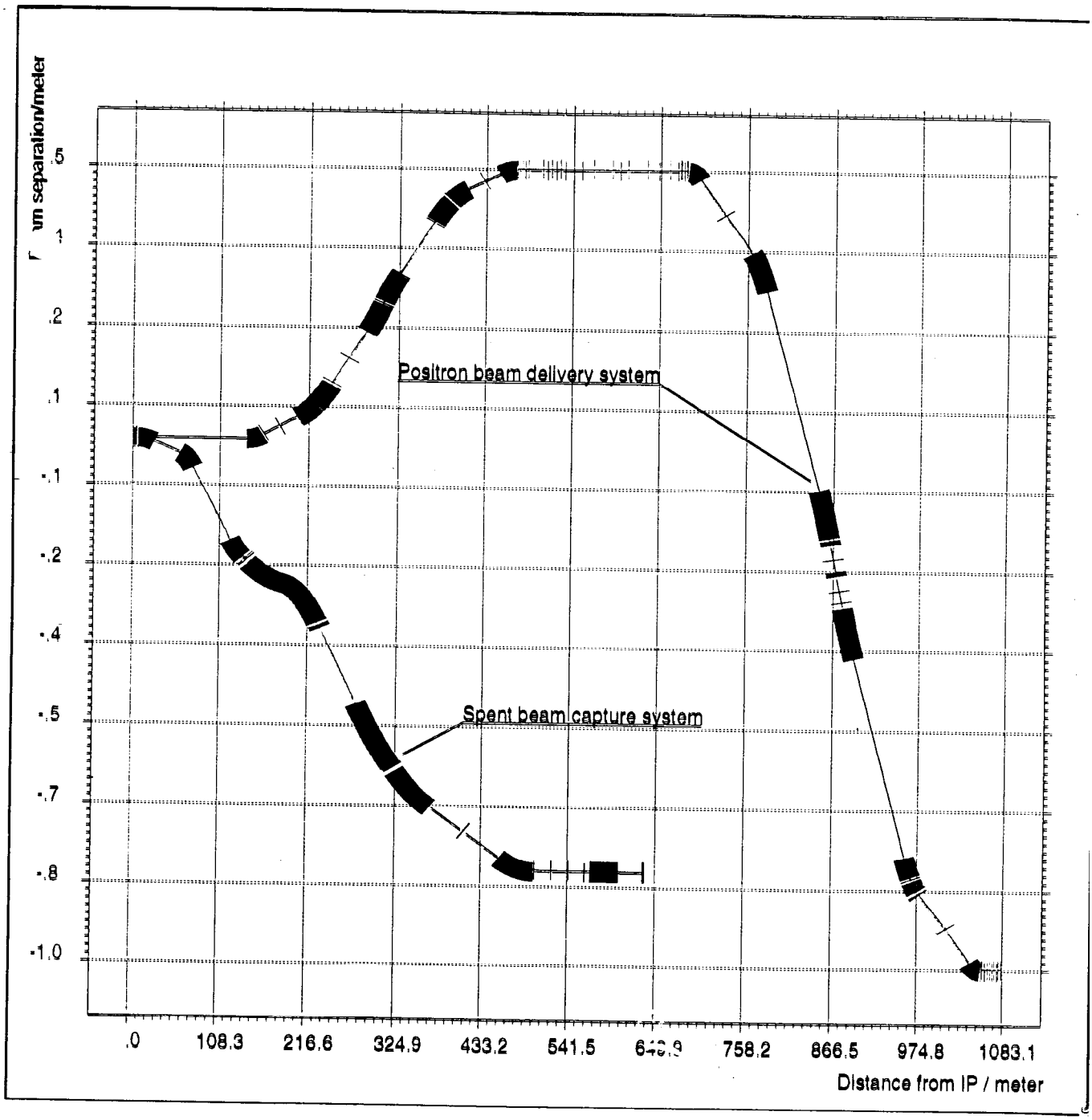
um separation/meter
.5
.1
.2
.1
-.1
-.2
-.4
-.5
-.7
-.8
-1.0
Positron beam delivery system
Spent beam capture system
.0
108.3
216.6
324.9
433.2
541.5
758.2
866.5
974.8
1083.1
Distance from IP / meter

TESLA

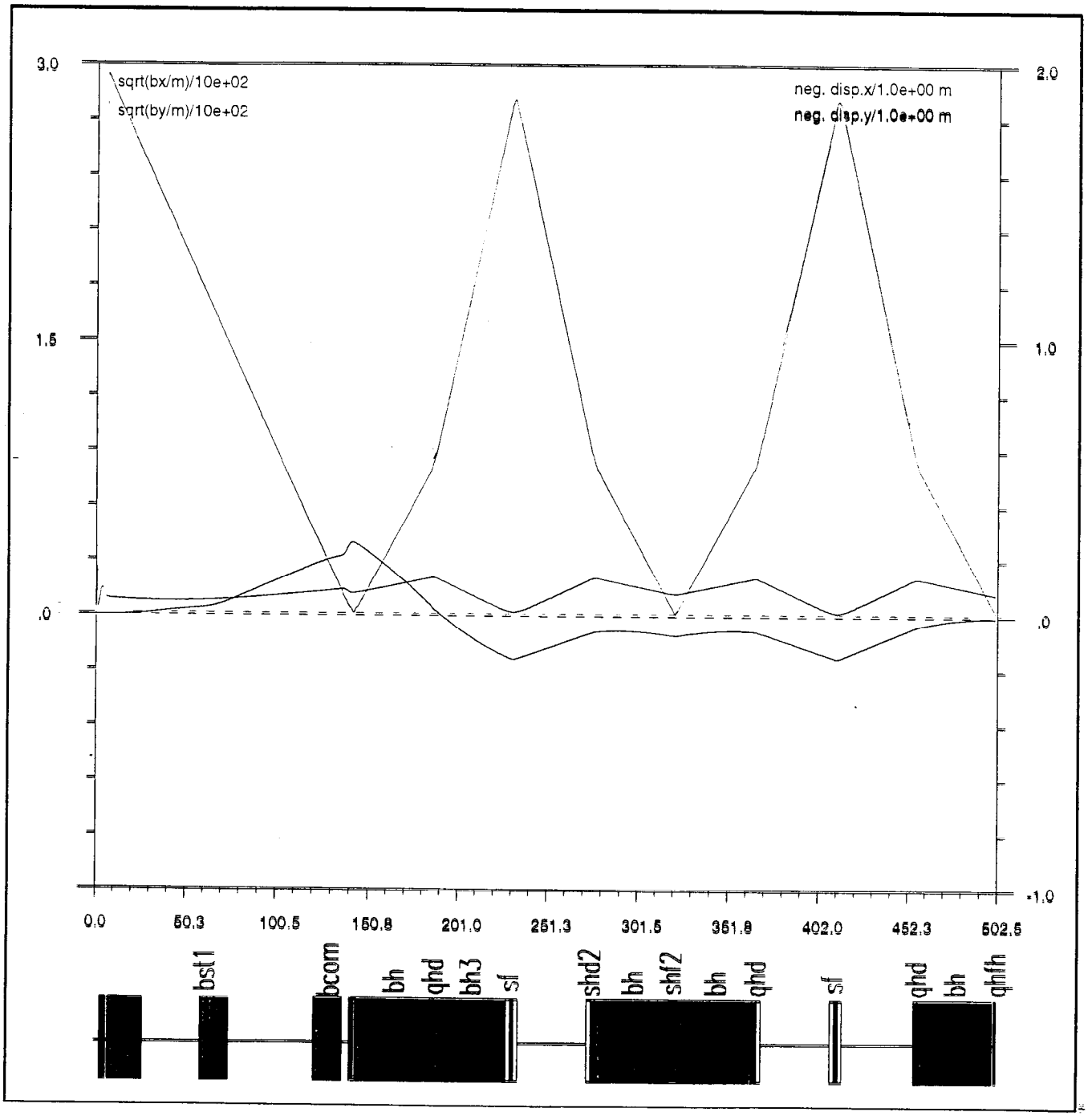
sqrt(bx/m)/10e+02
sqrt(by/m)/10e+02
neg. disp.x/1.0e+00 m
neg. disp.y/1.0e+00 m
3.0
1.5
.0
2.0
1.0
.0
-1.0
0.0
50.3
100.5
150.8
201.0
251.3
301.5
351.8
402.0
452.3
502.5
bst1
bcom
bh
qhd
bh3
sf
shd2
bh
shf2
bh
qhd
sf
qhd
bh
qhfh

Collimator	Position behind IP [m]	Collimated beam power [KW]	Remarks
COL1	27.51-59.51	[illegible]	between the separator and the septa
COL2	75.51-122.12	[illegible]	between the septa and the first bend
COL3	188.64-229.14	74.6	inside the second bend in the 1st FODO cell
COL4	235.89-274.14	144.48	inside the CCS
COL5	502.52-522.52	212.33	after the CCS
COL6	547.74-552.74	1.88	5m before the wiggler to avoid vertical amplitudes > 2mm

Collimator positions and collimated beam power for TESLA

Collimator	Position behind FFQ's [m]	Collimated beam power [KW]	Remarks
COL0	0.00-10.00	67.57	between the last FFQ and the 1st mirror quadrupole
COL1	38.23-58.23	70.08	between the last mirror quadrupole and the first bending magnet
COL2	61.23-87.40	[illegible]	behind the first bending magnet and the following quadrupole doublet
COL3	137.90-154.90	214.56	along 17m drift inside the CCS
COL4	197.90-214.90	27.99	along 17m drift inside the CCS
COL5	217.90-234.90	128.50	along 17m drift inside the CCS
COL6	377.90-394.90	75.37	along 17m drift inside the CCS
COL7	416.40-436.40	41.63	along 20m drift behind the CCS
COL8	445.40-450.40	8.17	5m before the wiggler to avoid vertical amplitudes > 2mm

Collimator positions and collimated beam power for SBLC

Transfer efficiency as function of the hor. beta function at the IP for SBLC (top) and TESLA (bottom)

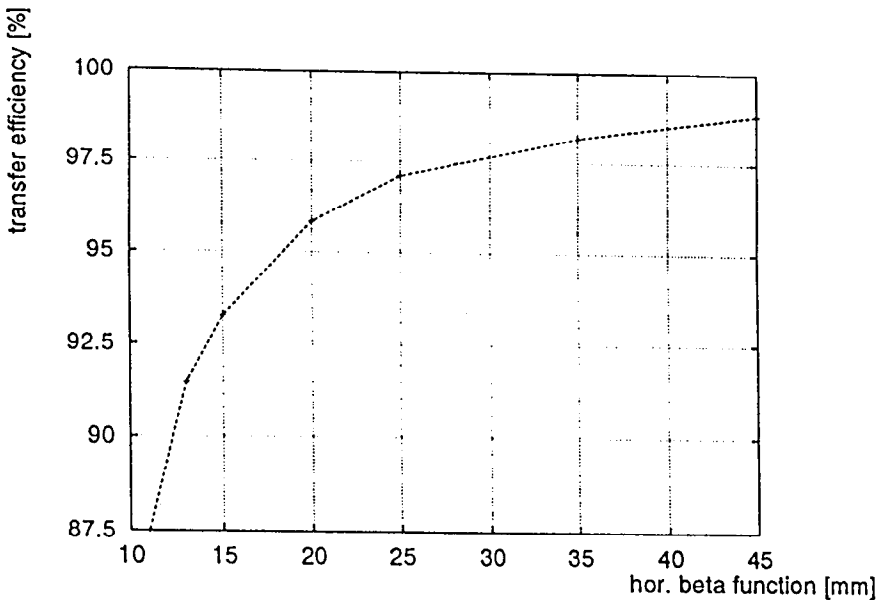

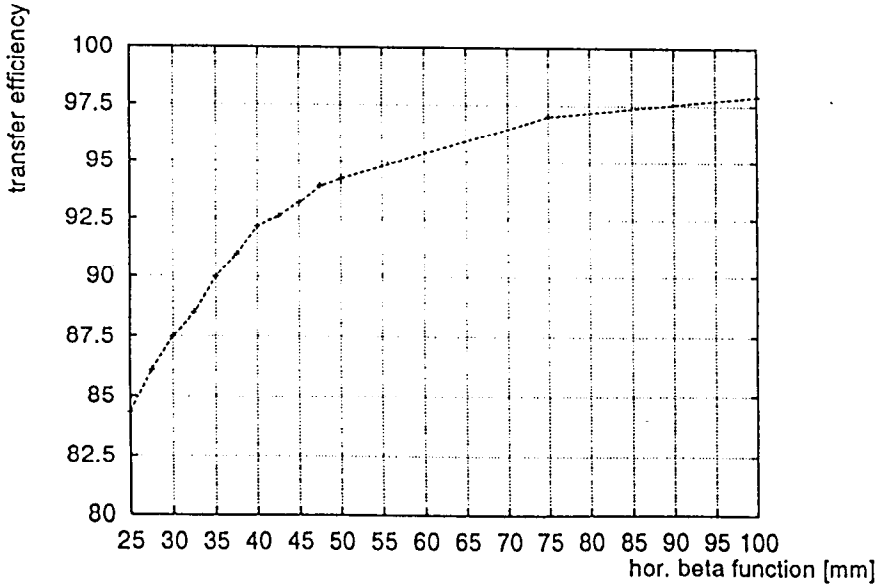

Charge oscillation after a 'missing interaction' for SBLC (top) and TESLA (bottom)

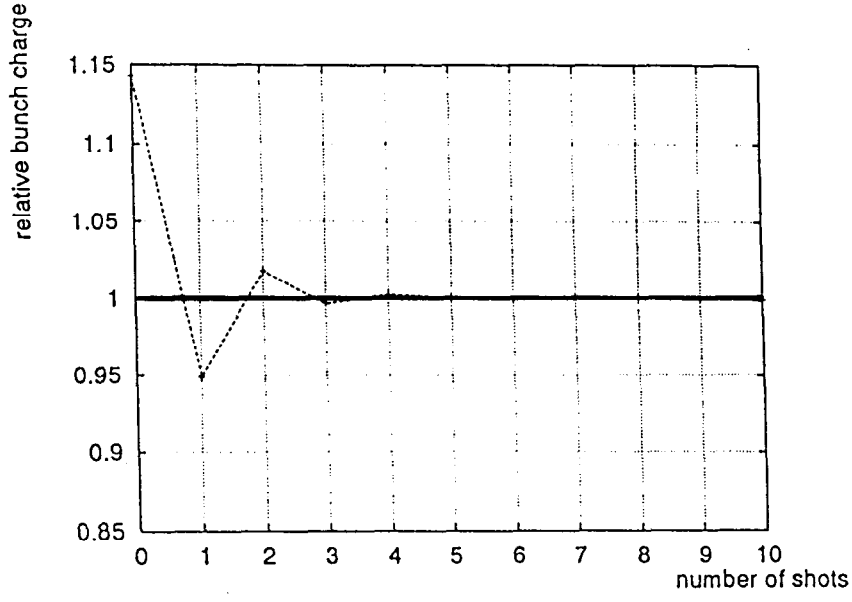

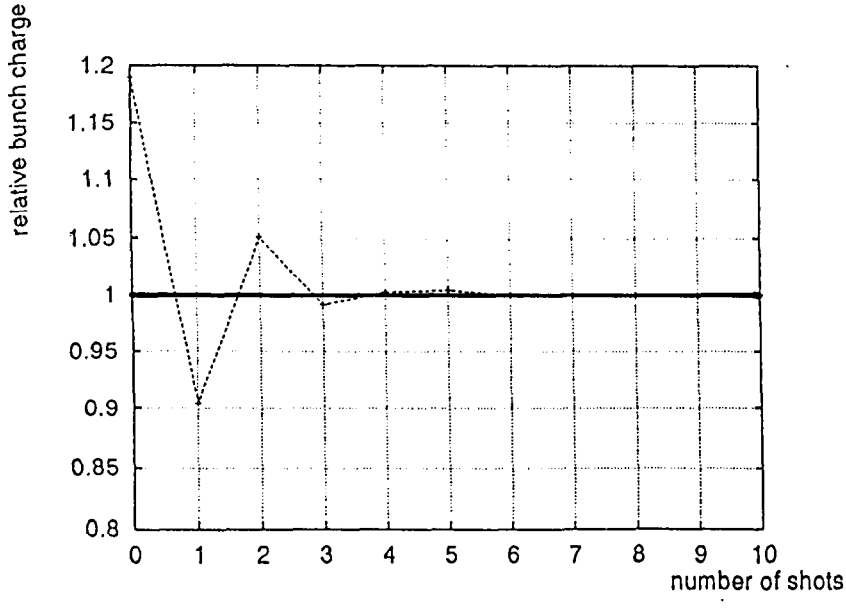

Polarized Positron Sources

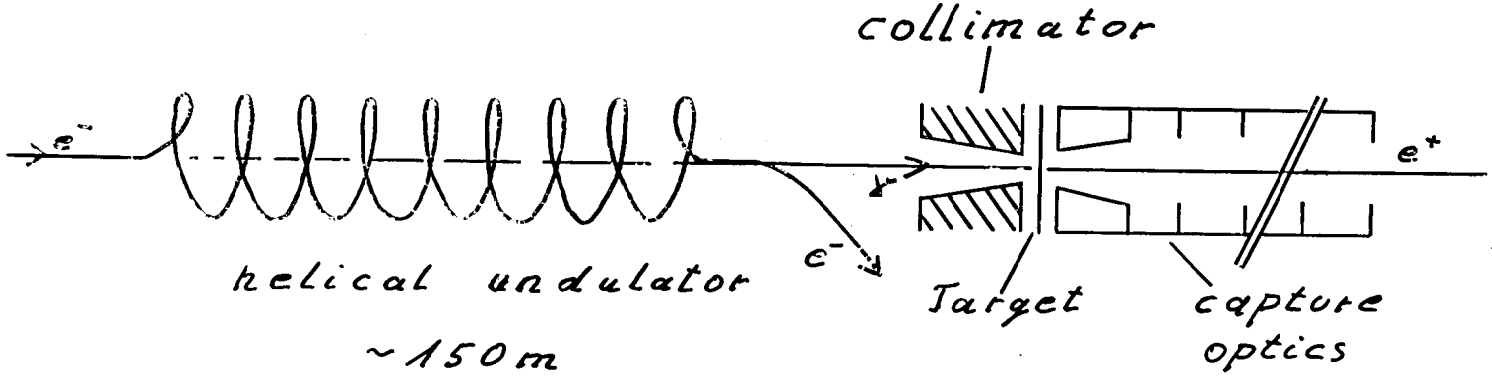

V. E. Balakin, A. A. Mikhailichenko 1979

Potential Upgrade to a polarized Source

For the design optimization the EGS code has been extended to polarized electromagnetic cascades.

Compilation of important results:

- besides pair-creation bremsstrahlung has been found to contribute significantly to the distribution of the polarization of the outgoing positrons.
- the polarization can be increased by scraping off-axis photons off the undulator radiation.
- scraping is only efficient if the emittance of the electron beam is small enough.

  $\varepsilon x, \varepsilon y < 5 \cdot 10^{-10}$ m
- a drift of about 150m is required between the undulator exit and the target .
- depending on the design of the helical undulator an undulator length of 100 -150 m is required.
- . the estimated polarization of the source is ~60%.

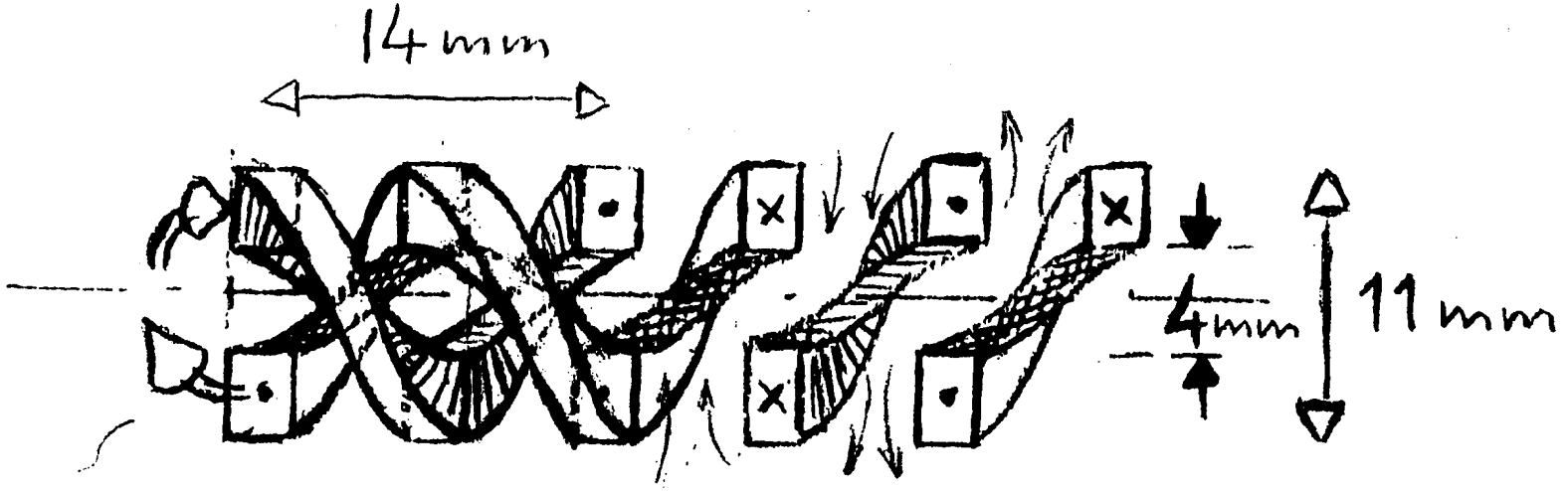

~10 kA

S.L. Wipf

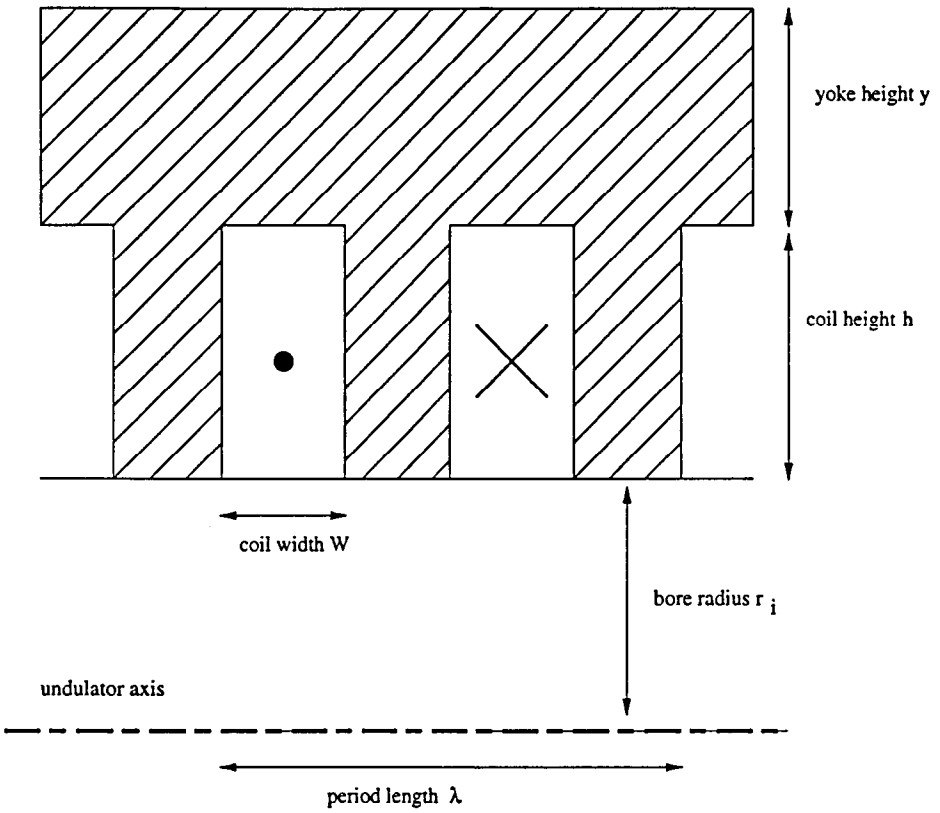

Cross-section of an undulator with iron between the conductors and return yoke (shaded area).

	undulator with iron	undulator without iron
undulator period λ	10.0 mm	10.0 mm
inner radius r_i	2.0 mm	2.0 mm
coil width w	2.8 mm	3.3 mm
coil height h	5.5 mm	4.0* mm
yoke height y	5.0 mm	–
on-axis field B_r	1.3 T	0.62 T
required undulator length	100m	150m

* At this coil height the on axis magnetic field reaches 90 % of the field of a coil of infinite height.

Optimized parameters for an undulator with iron in comparison with an iron free undulator. The current density is 900 A/mm^2.

Design Considerations for a Compton Backscattering Positron Source

Josef Frisch, Synaptics, San Jose, CA

The laser backscatter positron source uses Compton scattering of a medium energy (~2GeV) electron beam from a polarized laser beam to produce polarized gamma which are converted to polarized positrons in a thin target. This system is similar to helical undulator polarized positron source. The primary advantages / disadvantages are:

Does not require a >200GeV electron beam: simplifies development and testing.
Does not required a >100M long superconducting helical undulator.

Produces a higher emittance positron beam: requires a more complex collection and damping system
Does require a very large and complex laser system

A straightforward system would require excessive laser power (>500KW average, >10TW peak) to produce the required number of positrons. In order to reduce the laser requirements, this system uses an optical resonant cavity to "recycle" the optical power, by allowing the same optical pulse to interact with may electron bunches. The requirement for a reasonable length optical cavity to minimize optical damage, determines the pulse timing structure of the drive electron beam. The standard NLC beam structure will be reconstructed by the pre-damping and damping rings. The required drive accelerator parameters are:

Frequency	L-Band
Beam energy	1.7GeV
Micropulse charge	$5x10^{10}$
Micropulses / macropulse	100
Micropulse spacing	67nsec
Average beam power	200KW
Beam emittance	15pmm-mr (RMS)

The power recycling optical cavity requirements are:	
Cavity length	10M
Cavity optical mode waist	6.9mM s
Cavity optical Q	~100
Cavity alignment and surface figure tolerances	~1nM

The laser requirements are:	
Laser material	Nd:Glass (APG-1)
Operating wavelength	1.05mM
Peak power	85GW
Pulse length	3psec
Average power	9KW

The drive accelerator and positron optics are fairly conventional, and do not appear to pose any severe technical challenges.

The primary technical challenge for the optical cavity is the alignment tolerances, coupled with the high peak and average operating powers. Thermal, and photo-mechanical effects from the optical beam may significantly disturb the cavity stability. It is believed that with appropriate use of feedbacks, and adaptive optics, the it should be possible to construct cavity system.

The primary technical challenge of the laser system is the very high average power (9KW) for a solid state laser. This system is designed to use 180 main amplifier modules, each operating at 1Hz, to provide the required average beam power and repetition rate.

Design considerations for a Compton Backscattering Positron Source

Josef Frisch

The laser backscatter positron source uses Compton scattering of a medium energy (~2GeV) electron beam from a polarized laser beam to produce polarized gammas.

The polarized gammas are converted to polarized positrons in a thin target.

This system is similar to helical undulator polarized positron source. The primary advantages / disadvantages are:

- Does not require a >200GeV electron beam: simplifies development and testing.
- Does not required a >100M long superconducting helical undulator.

BUT

- Produces a higher emittance positron beam: requires a more complex collection and damping system
- Does require a very large and complex laser system

This talk will focus on the laser and optical system, the electron and positron beam systems are similar to those for conventional sources.

General block diagram of the positron source:

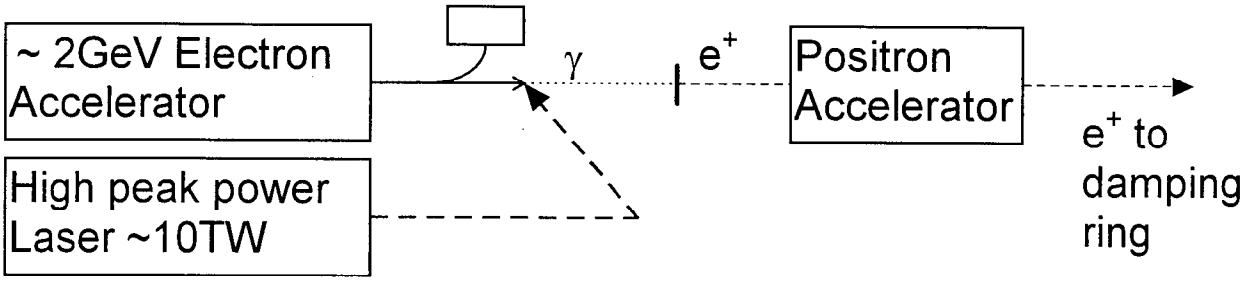

Positron beam requirements (typical NLC):

Positrons per microbunch	$1X10^{10}$
microbunches per macrobunch	100
microbunch spacing	1.4ns
Macrobunch rate	180Hz

For Compton backscattering, if the laser focus spot diameter is the same as the electron spot, diameter, and if the laser bunch length is >3X the electron beam length, one backscattered gamma will be produced for each incident electron for a peak laser power of approximately 450GW.

Approximately 100 gammas incident on the target are required for each positron delivered to the IP. (The γ beam size at the target is large, reducing the capture efficiency).

Positron production requires polarized gammas at approximately 10MeV. For laser wavelengths of approximately 1μm, this requires electron energies of approximately 1.5GeV.

If we use an electron beam energy of approximately 1.7Gev, we can extract about 20 gammas from each incident electron.

If the production e^- beam has 5X the current of the main NLC beam, we can extract the required $100\gamma/e^+$.

For a straightforward laser backscatter system, assuming a 1ps long production electron bunch, and a diffraction limited laser beam, the laser requirements would be:

Laser Peak power	9TW
Laser pulse length	3ps
Laser micropulse energy	27J
Laser macropulse energy	2700J (!!!)
Laser average power	500KW (!!!!!!!)

This is far beyond the current state of the art for high power lasers. Instead an optical resonant cavity to recycle the laser power.

A classic optical resonator allows the intra-cavity power to be much larger than the incident power for a monochromatic beam, if the cavity length is an exact number of wavelengths. This scheme works for any repetitive waveform if the cavity length is equal to the repetition rate.

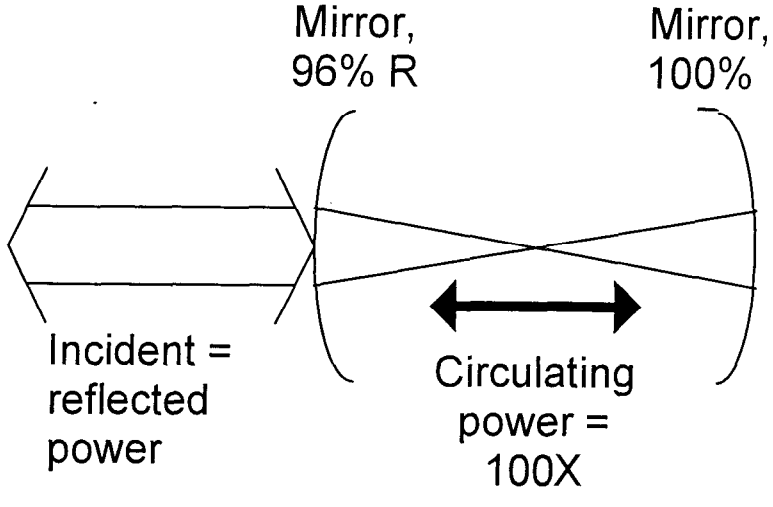

System Design:

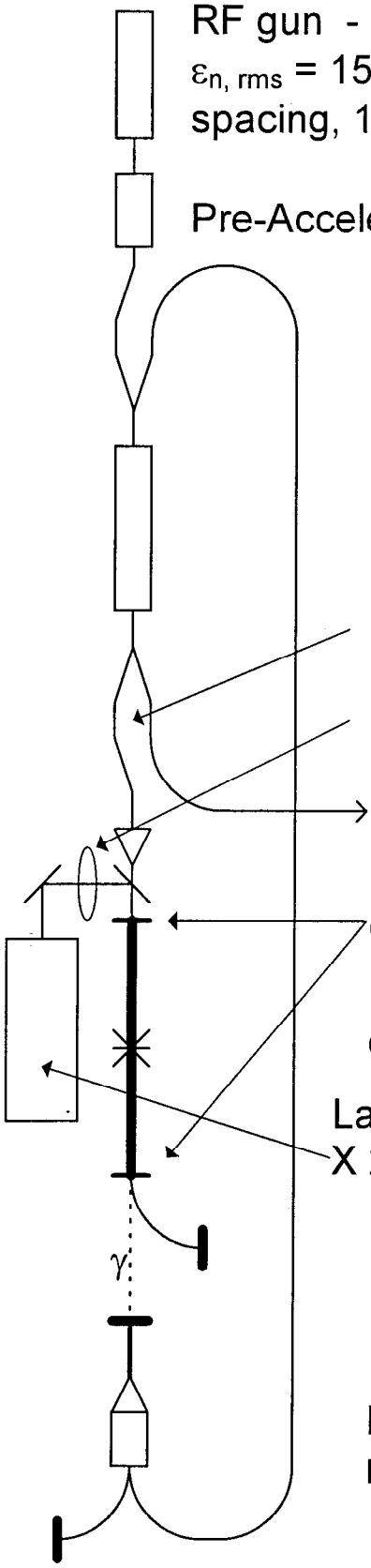

RF gun - L band, ~3MeV, 30psec,
$\varepsilon_{n,\,rms}$ = 15πmm-mr, 5X10^{10} e$^-$, 67nsec bunch spacing, 100 bunches, 7μs train length.

Pre-Accelerator, L-Band, 200MeV, 30ps

Bunch compressor / combiner 5ps

L-Band Linac, 1.7GeV, ~200Kw beam power.

Bunch compressor / separator

Laser focus optics F/# = 11

e^+ to pre and main damping rings

Electron focus optics θ=720μr

Cavity mirror (with beam aperture)

e^-/γ IP 6.9μm σ (both beams)

Laser system, 1μm, 3ps, 85GW, 250mJ
X 200 pulses at 180Hz (9KW average)

Spent e^- beam dump (200KW)

Positron production target

Flux concentrator and 200MeV e^+ pre-accelerator

There are a variety of solutions for various electron currents, energies, and emittances. The following represents just one point in the design phase space - and may not be optimal.

The required electron beam current ($5x10^{10}$) should be obtainable in a L- band RF gun. Based on RF gun scaling estimates, the emittance should be $\varepsilon_{n,\,rms} = 15\pi$mm-mr.

For good overlap, the optical Ralegh length should be equal to about ½ the electron beam (1ps assumed) pulse length ($R_l = 150\mu m$).

This results in an optical beam waist σ=6.9μm. Intracavity power is 9TW, (Peak power density is 10^{22}W/cm^2.)

The maximum allowable peak power density on the cavity mirrors is 10^{10} W/cm^2, requiring a optical beam at the mirrors with σ=23cm. With the above Ralegh length, this gives an optical cavity length of 10M.

If we match the electron and optical beam sizes, we obtain an electron spot size (calculated from emittance) at the exit mirror (near the target) σ=3mm. Note that an aperture in the mirrors of this size will not significantly affect the optical cavity losses.

The optical cavity input mirror transmission is set to 4%. This will result in a buildup time of approximately 100 pulses to an intra-cavity power 100X the incident power.

The technical challenges of the optical system divide into the Laser and the Optical Cavity.

The Optical Cavity

The optical cavity must have a length that is an exact number of wavelengths - to an accuracy of approximately λ/Q, or about 10^{-9}M. Interferometric feedback techniques can be used to stabilize optical cavities to this resolution.

The cavity must produce an optical mode with σ=6.9μm, in a 10M long cavity. This puts a severe constraint on the radius accuracy of the cavity mirrors.

Mirror radius = $5 + 5\times10^{-9} +/- 2\times10^{-9}$ M.

Mirrors can normally only be fabricated to a radius accuracy of approximately 10^{-4}. It is possible to mount piezoelectric actuators on the back of the mirror. By observing the mode shape in the cavity, it should be possible to use feedback to stabilize the mirror radius.

The mirror phase front accuracy must be approximately $\lambda/100$ in order to not significantly distort the mode shape. This corresponds to a surface accuracy of about 10^{-8}M.

The mirror angular alignment must be controlled to within about 0.1μrad, corresponding to an edge motion of 10^{-8}M.

- The light will bounce off the mirror surfaces approximately 200 times (total). If the mirror surfaces are within $\lambda/1600$ (0.6nm) of ideal, the beam mode will be nearly ideal.

- Feedback systems will be needed to control the mirror positions and shapes.

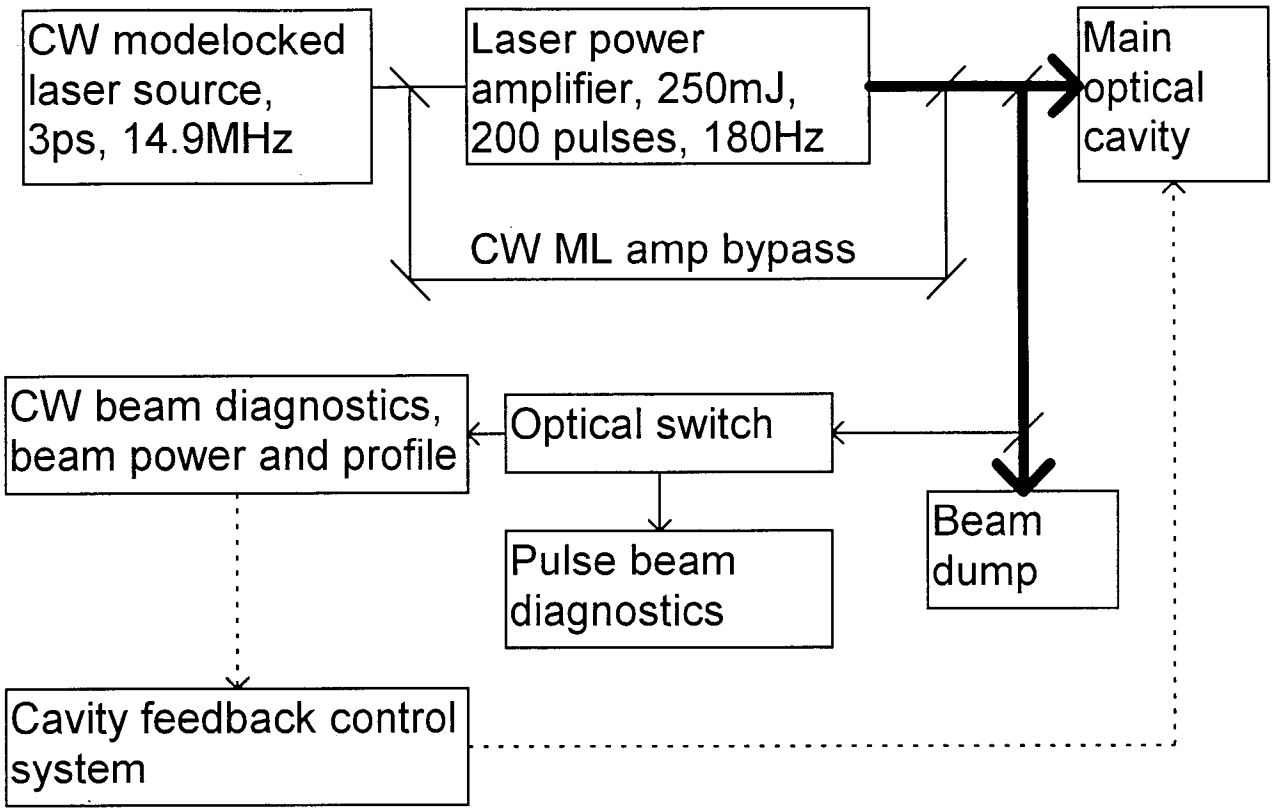

The cavity mirrors will be located in the accelerator vacuum system (transmitting optics is not possible at the intra-cavity power levels), so they should be immune to most external effects. Interferometric gravity wave detectors have used optical cavities with mirrors stabilized against external (eg seismic) effects many orders of magnitude better than our requirements.

High power beam induced effects are probably the most significant.

Power absorption:

Good quality laser mirrors absorb approximately 10^{-4} of the incident laser energy.

The micropulse energy density on the mirrors is 30mJ/cm^2. This energy will be absorbed over several microns of depth. In fused silica, thermal time constants are a few microseconds for a few microns. The macropulse energy density will be more significant.

The macropulse energy density on the mirrors is 6J/cm^2 (about 1KW/cm^2 average), which will produce a temperature rise of about 100^0C (in a 3μm depth). This produces a change in thickness of ~10^{-10}M. (OK)

Single macropulse heating does not cause unacceptable mirror distortion

Average power heating, (assuming a 10cm path to thermal ground) is approximately 100^0C. This can result in a 5μm average thermal distortion, and must be fixed with feedback.

Alternately, at 200^0K, fused silica has near zero thermal expansion. The 100^0C temperature rise would produce $8x10^{-8}$M distortion, greatly reducing the reliance on feedback.

Mirrors have been constructed with energy absorption as low as $3x10^{-6}$. If this technology can be applied to high power mirrors, the thermal problem would be greatly reduced.

Photon Pressure:

Photons carry momentum p = E/c, the 10^{10}W/cm^2 peak power density incident on the mirrors corresponds to $6x10^6$N/m^2 pressure (about 800psi).

During a micropulse, the mirror surface will be deflected by $5x10^{-12}$M.

During a 7μs macropulse, the acoustic wave will travel 4mm, with a total deflection of about 10^{-9}M. This may be sufficient to be of concern.

Additionally, the acoustic attenuation at 70KHz (the approximate macropulse acoustic frequency), is only about 40dB/second. Acoustic waves from previous macropulses will not have decayed away, and may build up in an unpredictable fashion.

The average pressure during operation on each mirror is 6mN. The mounting system (with the addition of feedback) must have a stiffness of > 10^7 N/M. This is approximately the stiffness in compression of a 1cm area, 1M long bar of aluminum - should be fairly easy to obtain.

Radiation damage:

The cavity optics must be protected from ionizing radiation. Fortunately, the techniques for shielding systems near an electron beam focus are well understood from detector research. Note that It is probably impossible to put an electron beam bend inside the optical cavity due to synchrotron radiation.

The laser system

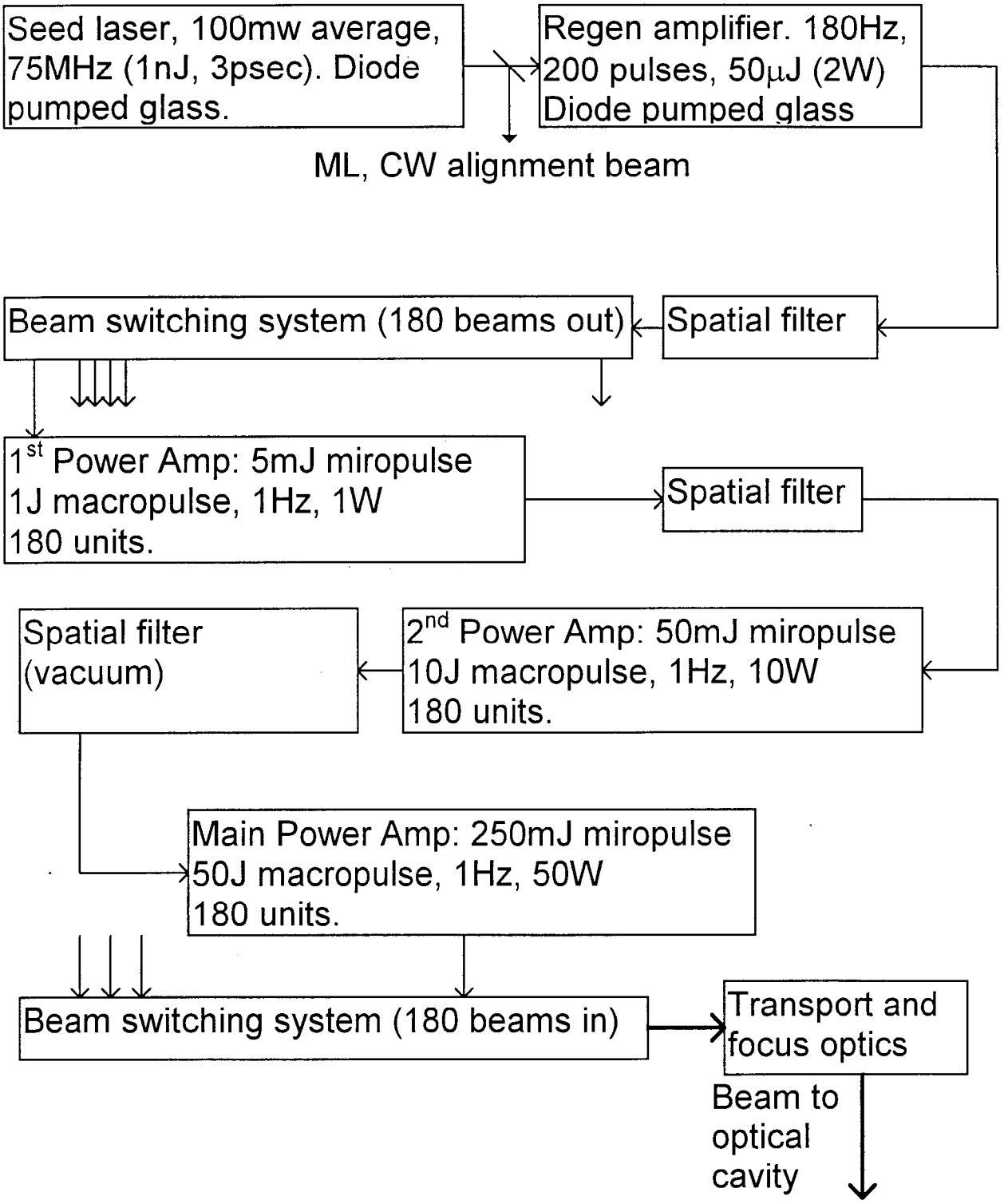

The following properties are important for laser material selection:

Bandwidth: The laser material must have sufficient bandwidth to amplify 3psec long pulses. This unfortunately eliminates several gaseous lasers, but does not substantially restrict solid state lasers.

Saturation Fluence: This is the amount of energy which can be extracted from a laser material when it has been pumped to have a gain of e. Lasers will operate at energy densities near their saturation fluence. Values less than about 1 J/cm^2 will result in excessively large optics. Values greater than about $10J/cm^2$ will need to be operated at dangerously high power densities. (Eliminates Alexandrite, and Erbium based glass systems).

Ease of Pumping: The material must have broad absorption features (for use with flashlamps), and a long excited state lifetime. Laser diode pumping is not feasible for these powers and duty factors. Direct laser pumped systems (like Ti:Sapphire) will require excessively high pump powers (~100KW pump beam).

Thermal lensing and thermal fracture: The average power limit in solid state lasers is either beam degradation due to temperature induced index changes, or mechanical fracture of the laser material due to thermal gradients.

For this study we use Nd:Glass (APG-1 phosphate glass), a material commonly used in high peak power lasers.

Wavelength	1.055μm
Bandwidth	206 cm^{-1}
Saturation fluence	5.4J/cm^2
Excited state lifetime	390μs
Index change (net) with temperature	4x10^{-6}/^{0}C
Thermal conductivity	0.83 W/(M K)
Thermal fracture strength (theory)	0.72 W/$M^{1/2}$
Estimated thermal fracture strength	700W/M

Brewster plate geometry laser:

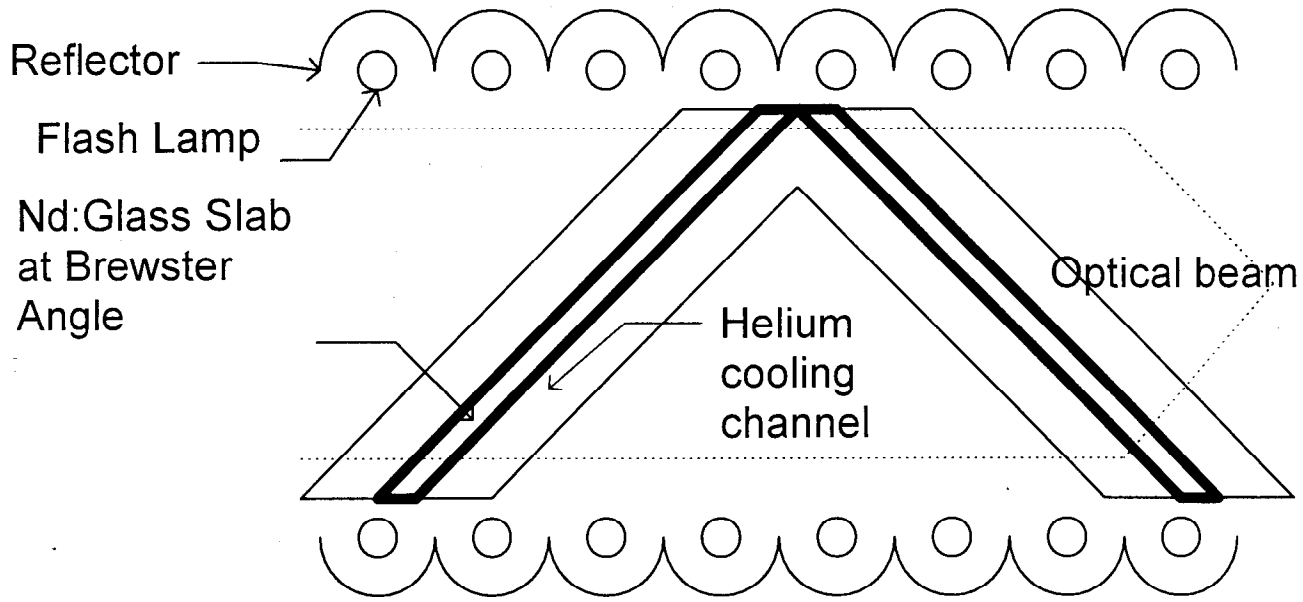

We can calculate the required mode area from the required macropulse energy (50J) and the saturation fluence (5.4J/cm^2) to get an approximate mode area of 10cm^2. Allowing for mode clearance, this is probably a 6cm X 12cm plate.

This gives a peak power density during a micropulse of about 10^{10} W/cm^2.

Nonlinear Effects:

High peak optical powers produce a change in refractive index in materials.. At 10^{10}W/cm^2 the nonlinear index change in APG-1 is $5x10^{-6}$. If we allow a maximum path length change corresponding to $\lambda/4$ in the final amplifier, we get a maximum path length of 5cm. This will turn out to be reasonable for thermal effects as well.

Thermal effects - Single pulse:

With flashlamp pumping, the laser material absorbs approximately 4X as much energy as heat, as results in excited state energy. When reasonable optical losses are taken into account, a factor of 10X relative to the output energy is more reasonable. This gives an absorbed energy of about 60J/cm^2 of beam area.

If we use a total thickness of 5cm (the non-linear effect limit) we get a temperature rise of 10^0C in a single pulse. This produces a stress on the order of 5MPa, (about 700psi), well below the fracture strength of the material (50-500MPa depending on condition).

The thermal distortion of the wave front is 2μM. This implies that the illumination uniformity across the amplifier plates will need to be <10%.

Thermal effects - average power:

Most Brewster plate lasers are operated at very low repetition rates - Several minutes between shots is common.

The limitation is plate cooling. If the heat is transported to the edge of the slab (about 3cm), the time constant is about 4 minutes.

Unfortunately we need a macropulse rate of 180Hz, and constructing 40,000 amplifiers is pretty unreasonable.

Face Cooling:

If heat could be removed from the face, rather than the sides, of the Brewster laser plates, the time constant for a 4mm thick plate would be about 1 second. This system would use a total of 12 plates in each amplifier.

The required surface heat removal rate is about $2W/cm^2$.

D_2O (normal water absorbs at 1μM) cooling could be used. Relatively slow flow rates (10cm/sec for 2°C rise) would proabably allow laminar flow, but the wavefront distortions are unknown.

Helium gas at 100M/sec, 2^0C rise flow rate at atmospheric pressure would also provide sufficient cooling. The expected pressure fluctuations scale as approximately V^2/V_s^2 or about 0.01.

The index of refraction of helium is $1+3x10^{-5}$. The change in index due to pressure changes would be about $3x10^{-7}$. The effect of the temperature change in the helium is similar. This results in a path length change of $\lambda/6$ (sum for all 12 slabs). Might work.

There may be optical damage issues for components operating in helium.

- If face cooling works, the system could be built with a total of 180 1Hz amplifiers. Still a lot, but might not be impossible.

Key Technical Issues:

- Alignment and stabilization of the main optical cavity.
- High power damage to cavity mirrors
- High power effects on cavity stability (thermal, photomechanical)
- High average power laser system (1Hz, 50J module using face cooling).

Possible Development plan:

- Optimize system design: there are many free parameters
- Test a low power, near concentric cavity.
- Test feedback systems on a near concentric cavity
- Test seed laser
- Test (low power) cavity resonant power enhancement with seed laser.
- Test single high power amplifier system
- Test Full array (180) of high power amplifiers and beam combiners
- Construct high power cavity (probably operate at 200^0C in vacuum.
- Start constructing electron beam system

Crystalline Positron Sources: Simulation, Codes and Computing

A. Jejcic
LPC College de France.IN2P3
11, Place Marcelin Berthelot
F-72531 Paris Cedex 05, France

Abstract

An overview on software tools used for simulating crystalline positron sources is presented. After a brief description of the basical principles underlying the codes used, three groups of results are presented. The first outlines some spectral characteristics resulting from electron propagation through aligned crystal lattice. The second provides some insight on the question of comparison of simulated date with those obtained experimentally. The third concerns some problems under investigation in the framework of a planned experiment at CERN SPS. Code implementation and the resulting performances are discussed. Finally some tentative remarks are made in order to draw conclusions for further work.

Crystalline Positron Sources : Simulation, Codes and Computing

A.Jejcic

Laboratoire de Physique Corpusculaire

Collège de France

75231 PARIS CEDEX 05

1. Simulation : principles and description of a code

2. Code operation : some results

3. Implementation and performances

4. Conclusions

The work on crystallinne e+ sources was initiated within a collaboration including X.Artru (IPN-Lyon) and R.Chehab (LAL-Orsay).

Parralel code implementation was done with J.Maillard and J.Silva (LPC-Paris).

Particular applications and futher developments were achieved by T.Baier, M.Dubrovin (BINP-Novosibirsk) V.Lapko and I.Mondrus (KFTI-Kharkov).

All of them are associated to the contribution I am presenting hereafter.

1. SIMULATION :

principles and description of a code

Investigation of crystalline e+ sources represents a tentative to take advantage on the radiation enhancement provided by the channeling phenomenon.

The e+ production results from :

1. channelling (Khumakov) radiation,

2. shower formation according to Bethe-Heitler process.

The simulation of this new type of device requires the addition to the usual shower simulation code (GEANT) of a specific software providing the capability of simulating the radiation induced by e- and e+ propagation through the crystalline lattice under channeling conditions.

Thus one has :

GEANT ('amorphous Monte-Carlo')

+

FOT ('crystalline Monte-Carlo')

GEANT : physical processes contributing to shower formation are computed using Bethe-Heitler formulas.

FOT : channeling radiation is generated on the basis of more general description provided by the Baier-Katkov formula.

GEANT ensures the simulation of the propagation in above barrier regime and physical proceses induced in theese conditions.

Following relevant physical processes are mainly simulated :

1. multiple scattering,
2. continuous energy loss,
3. Compton scattering,
4. pair creation,
5. bremstrahlung,
6. positron annihilation.

Electromagnetic showers are simulated in satisfactory conditions for the considered energy domain from both physical point of view (large number of experimental tests) and processing time.

see : GEANT Users Guide CERN 1995

FOT ('cristaline Monte-Carlo') simulates the e-/e+ propagation through the crystalline lattice and generates photons under these specific conditions.

Particles trajectories X^{μ} are obtained by integrating an equation of movement within a crystalline cell where the potential is described on the basis of the formula :

$$U(r) = V_o \, ln(1 + \frac{1}{r + \beta}) -$$

$$V_o \, ln(1 + \frac{1}{r_o + \beta})$$

with $r = \rho^2 / a_s^2$ where a_s is the screening radius. β proportional to squared amplitude of thermal vibrations.

Cf. V. N. BAIER et al. - Phys. St. Solidi b. 133 (1986) 583

The photons are generated according to the Baier-Katkov formula :

$$dP = \alpha \frac{d^3k}{8\pi^2\omega}[(1/\gamma - 1/\gamma')^2 |a_o|^2 +]$$

$$[(1+\gamma^2/\gamma'^2)a_\perp \bullet a_\perp^*]$$

$$a^\mu = i\int exp(i\omega'\tau)d(\frac{dX^\mu}{d\tau})$$

where $X^\mu(t)$ is the classical trajectory and

$$\tau = \frac{1}{2}\int_o^t dt'(\gamma^{-2} + v_\perp^{-2})$$

the retarded time

cf. V. N. BAIER, V. M. KATKOV
Sov. Phys. JETP 26 (1968) 854
28 (1969) 807

The Baier-Katkov formula is evaluated on the basis of a truncated radiating particle trajectory.

This method has two disadvatages :

1. an infrared divergence is introduced

2. interference effects are not taken into account.

But presents two essential advantages for the application discussed here :

3. the emission point could be established,

4. the energy losses are taken into account in building up the trajectory.

cf. X. ARTRU NIM B48 (1990) 278-282

An interplay between two codes is worked out ; two different modes of propagation through the crystalline lattice are taken into account.

The discrimination of the two regimes is done according to the well known criterion based on the so-called Lindhard angle :

$$\Psi_{lindh} = \sqrt{2V_o / E}$$

$\Psi > \Psi_{lindh}$ above barrier motion (amorphous propagation)

$\Psi < \Psi_{lindh}$ channeling

cf. X. ARTRU et al. Proc. of the IEEE 91 PAC Chicago, Ill.

2. CODE OPERATION :

SOME RESULTS

Three types of results could be quoted according to the particular aim considered :

1. results concerning characteristic features of radiative effects in an aligned cristal,

2. results concerning the comparison of experimental and simulated data

   a) Tomsk and Kharkov experiments

   b) Orsay experiment,

3. results connected to thefuture 10 GeV experiment

1. Results concerning characteristic features of radiative effects in an aligned crystal.

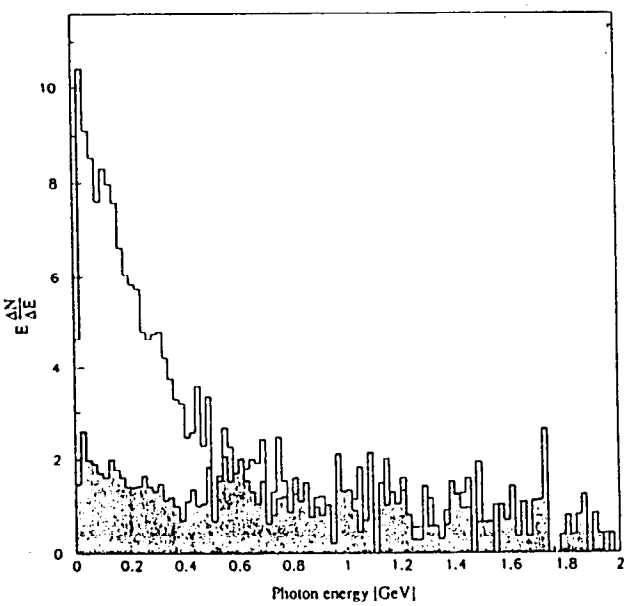

Photon spectra for an amorphous target (darkened area) and for a crystal both of 1 mm thickness $E^- = 2$ GeV. Cut-off energy 10 MeV

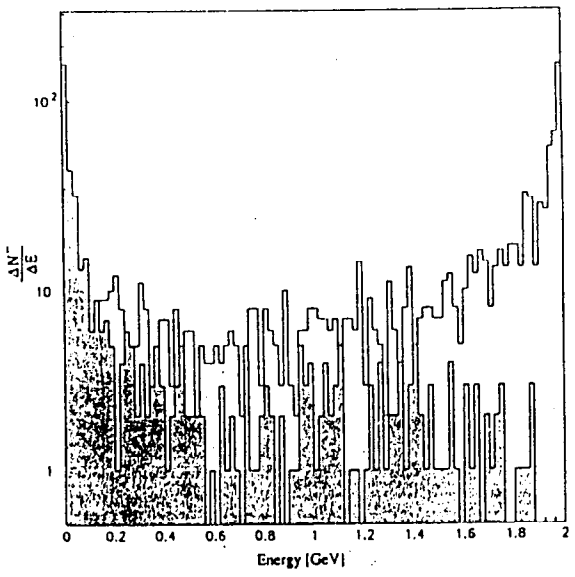

Energy spectrum of outcoming electrons for 1-mm [redacted] (darkened area for crystal). Incident electron beam energy : 2 GeV

cf. X. ARTRU et al. NIM B 344(1994) 443-454

2. Experimental results vs simulated data.

a) Tomsk and Kharkov experiments

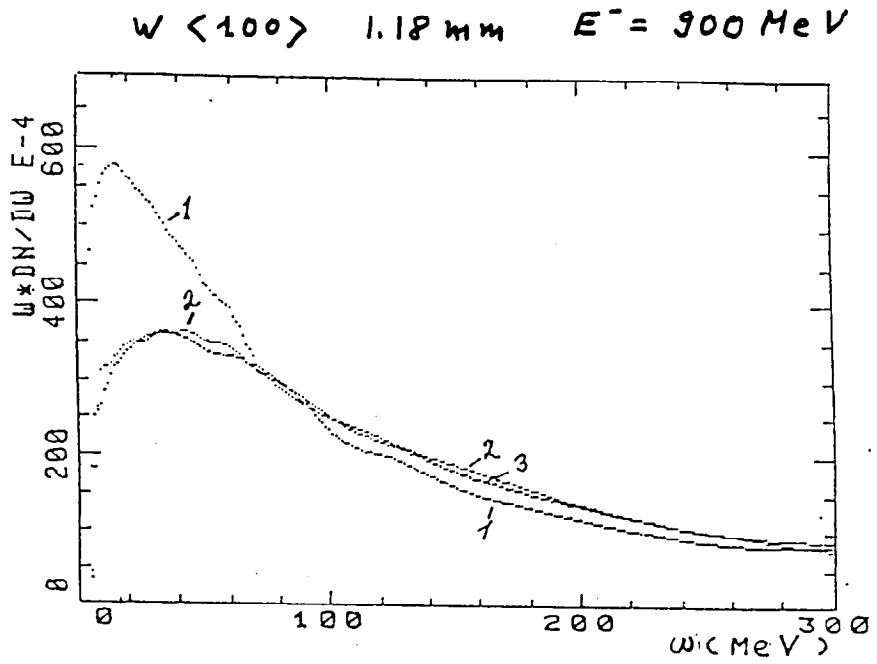

Figure 1: Experimental spectra from [8]:
1 - spectrum of real photons from Kharkov experiment,
2 - spectrum of total radiation intensity from Tomsk experiment,
[redacted]

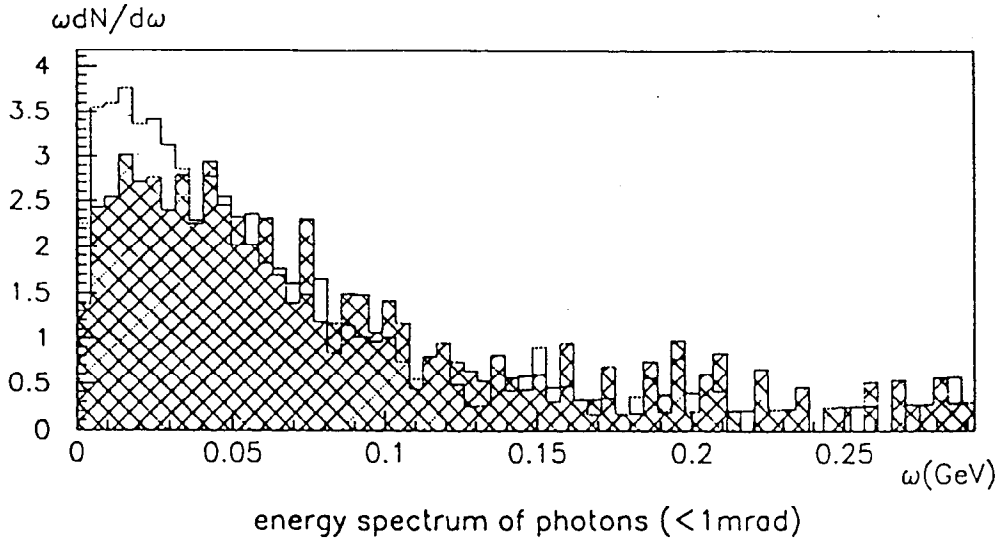

energy spectrum of photons (<1mrad)

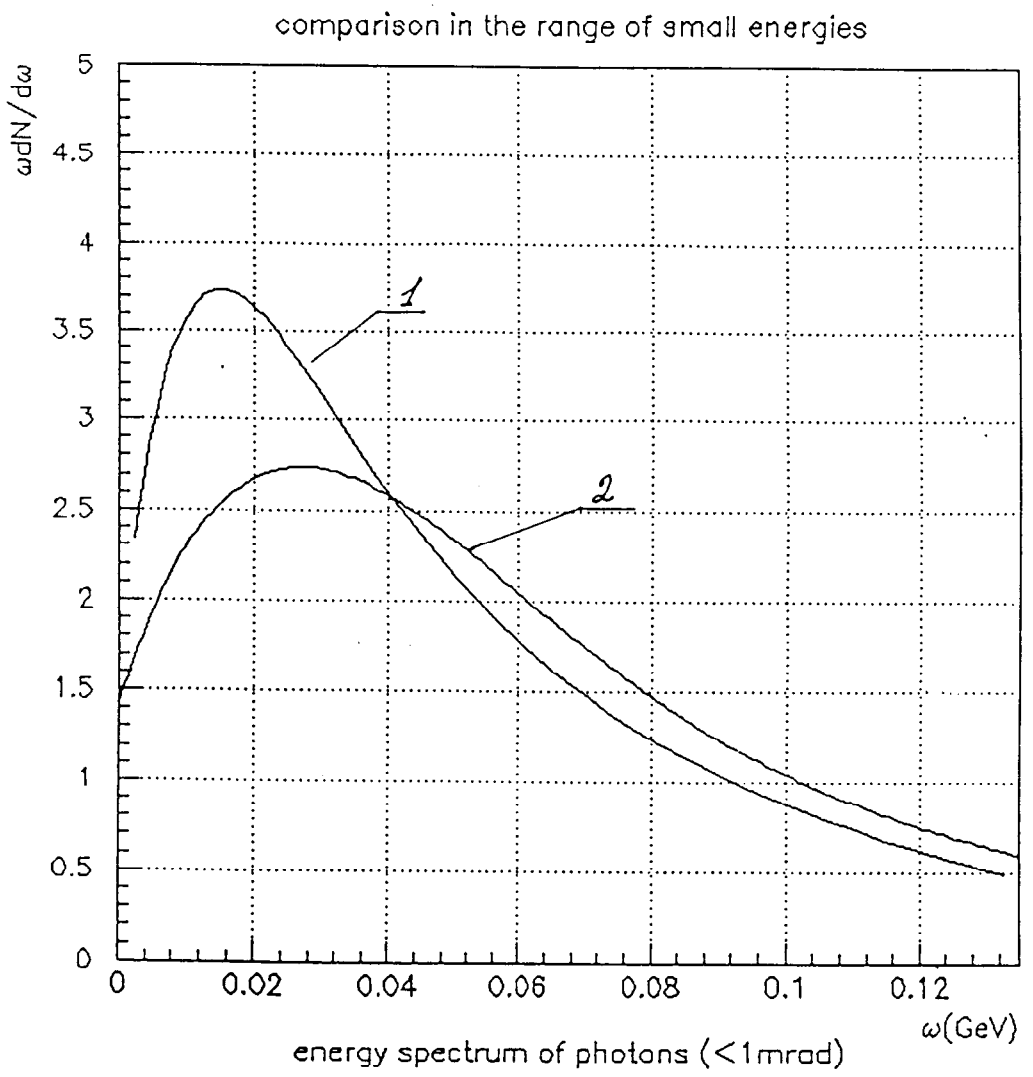

(c) Comparison of fitted spectra.
1 – real photon's spectrum
2 – spectrum of total intensity

cf. T. BAIER LAL/RT 93-04

b) Orsay experiment

W <111> 1 mm

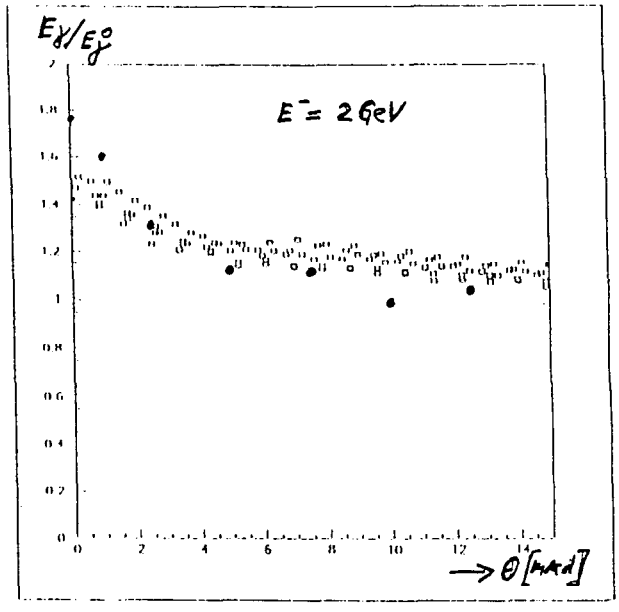

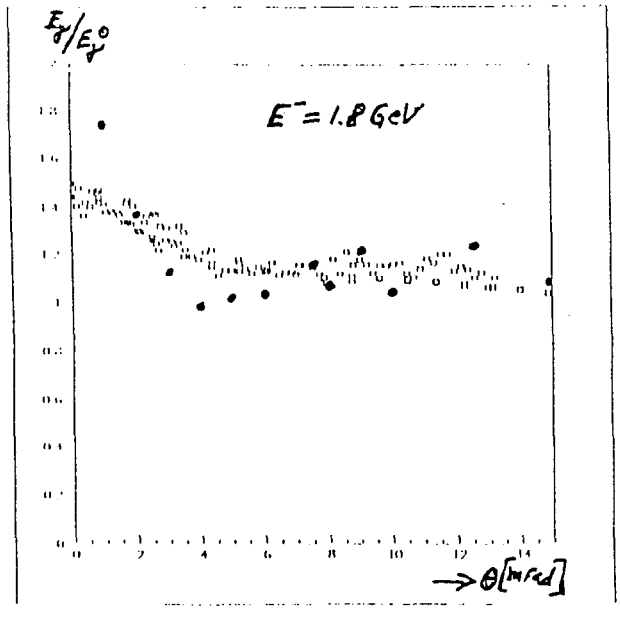

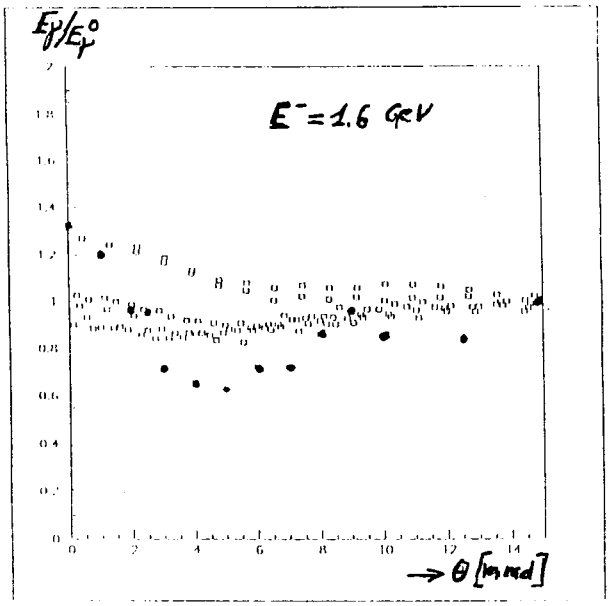
E_γ/E_γ^0
$E^- = 1.6$ GeV
0
0.2
0.4
0.6
0.8
1
1.2
1.4
1.6
1.8
2
0
2
4
6
8
10
12
14
$\rightarrow \theta$ [mrad]

3. Results concerning future 10 GeV experiment

W <111> 4 mm + 4 mm amorphous

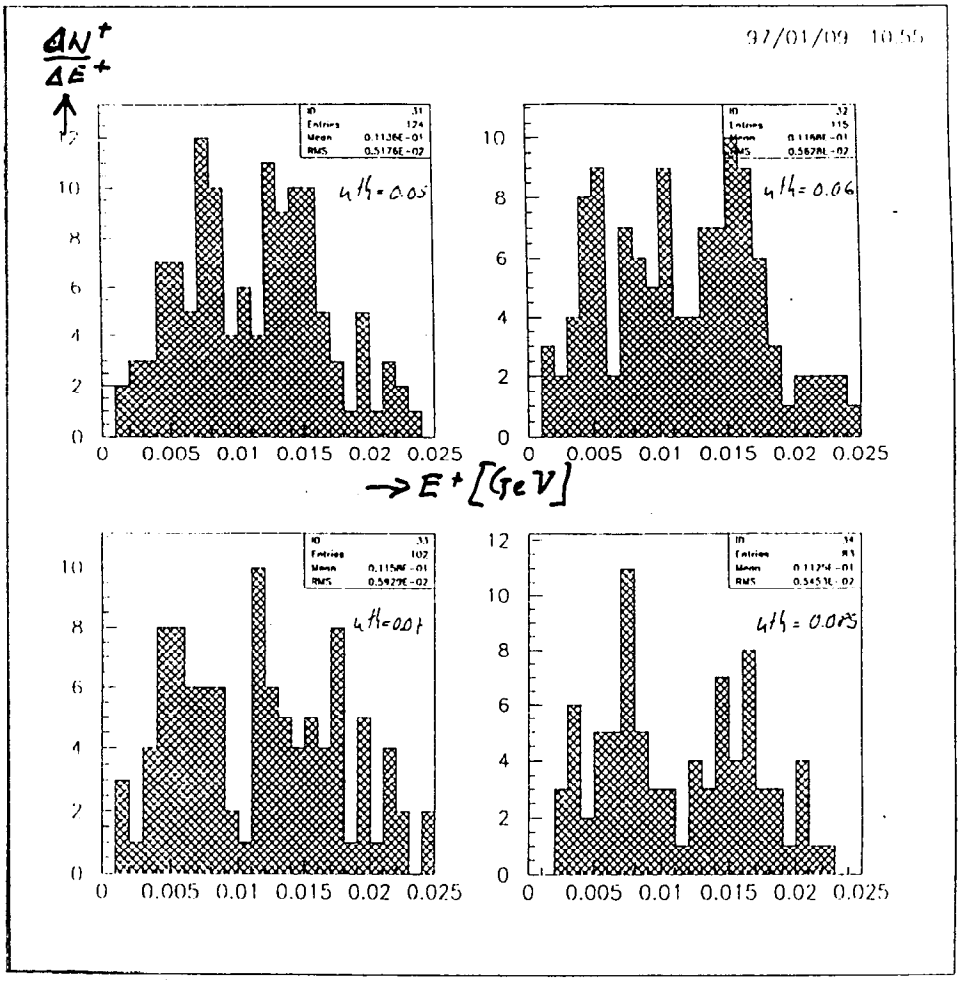

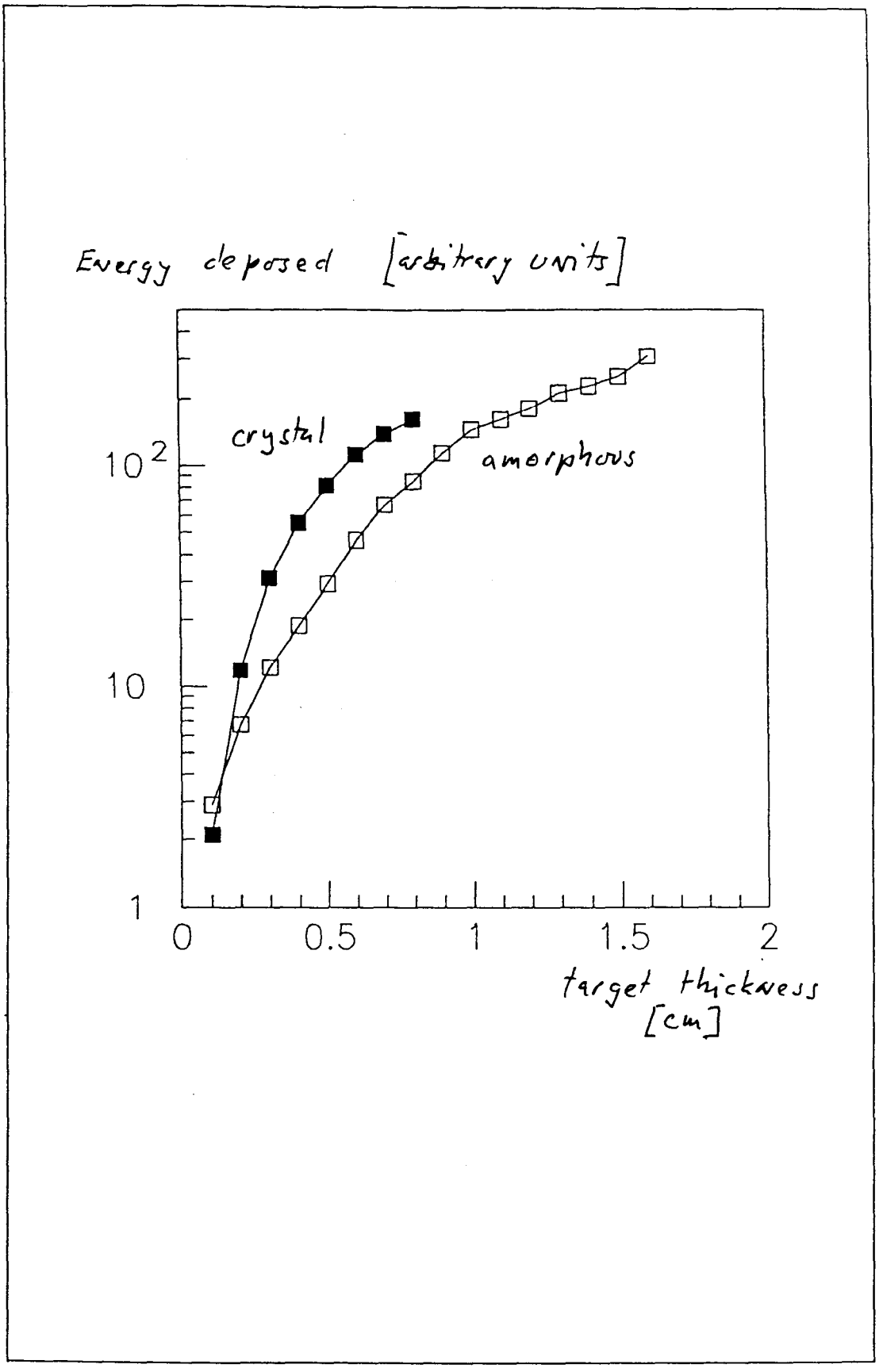
Energy deposed [arbitrary units]
crystal
amorphous
10 2
10
1
0
0.5
1
1.5
2
target thickness
[cm]

3. IMPLEMENTATION and PERFORMANCES

GEANT is world wide distributed code, thus it is submitted to continuous verifications.

It provides mainly two possible applications :

- tracking of particles through an experimental set-up,

- graphical representation of the set-up and trajectories

It represents a valuable environment for FOT implementation.

Two types of performances could be quoted :

1) processing time for a shower induced by high energy photons in an electromagnetic calorimeter

2) processsing time for 10 Gev e- impinging on W crystal of variable thicknesses.

in order to put forward the question of the processing potential needed.

Electromagnetic shower processing time vs impinging photon energy and cut-off

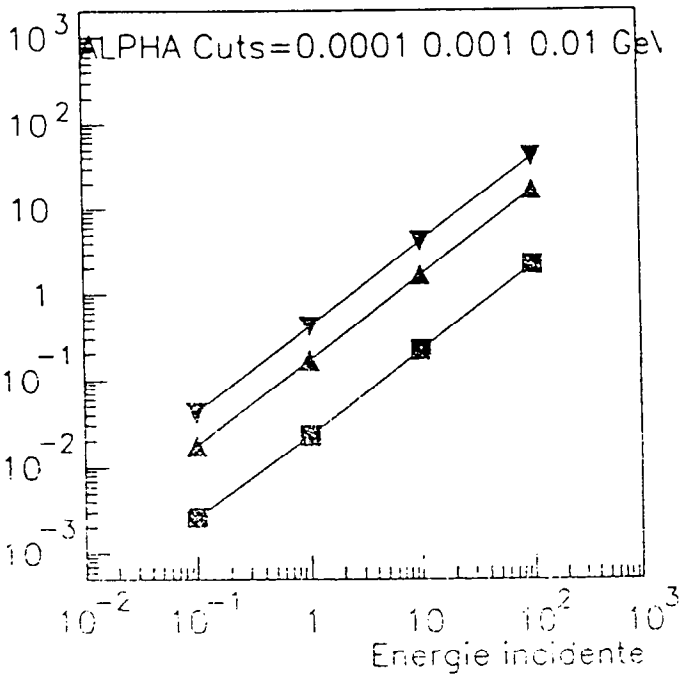

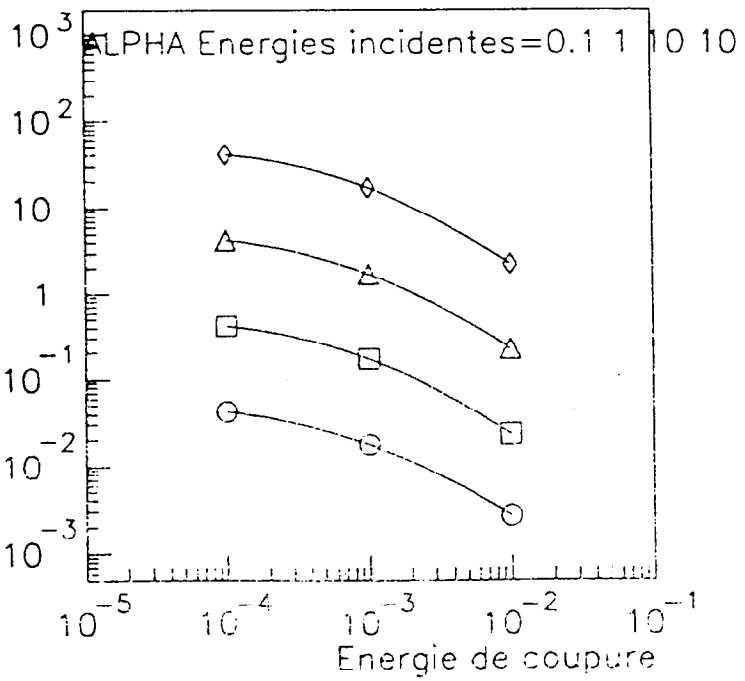

Processing time, photon total number and Khumakov photons vs crystal thickness

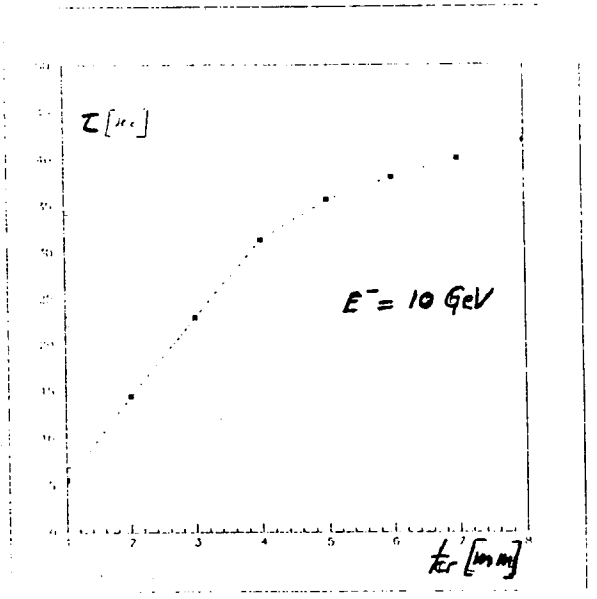

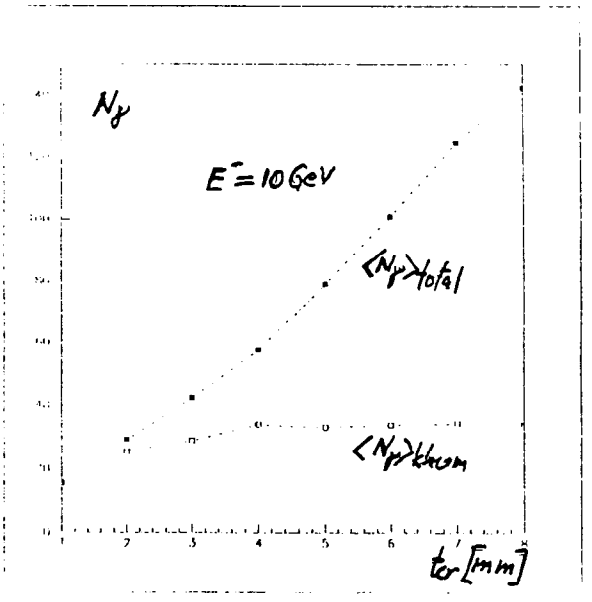

PARALLEL
IMPLENTATION
is NEEDED (OR WELCOME)

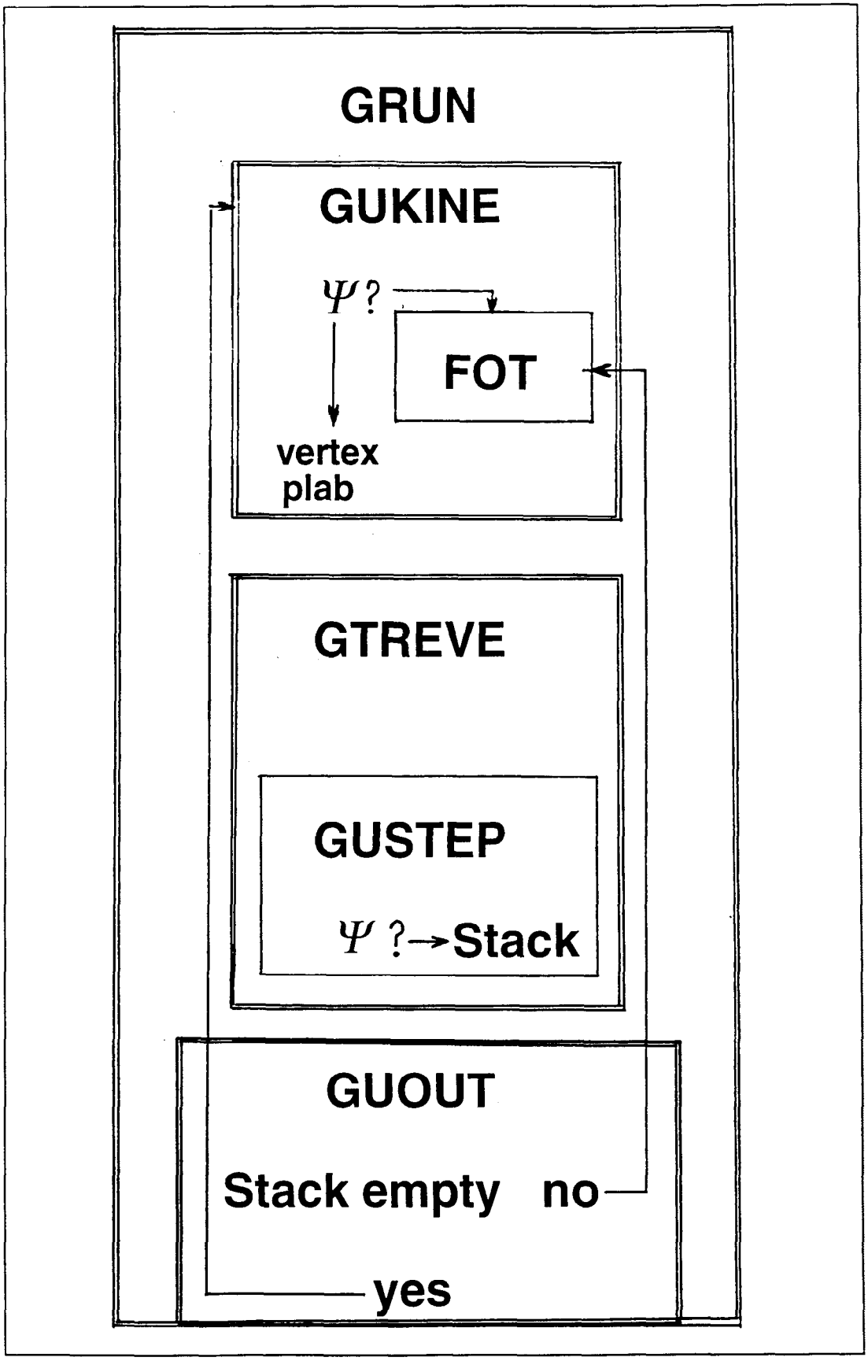
GRUN
GUKINE
Ψ ?
FOT
vertex
plab
GTREVE
GUSTEP
Ψ ?→Stack
GUOUT
Stack empty
no
yes

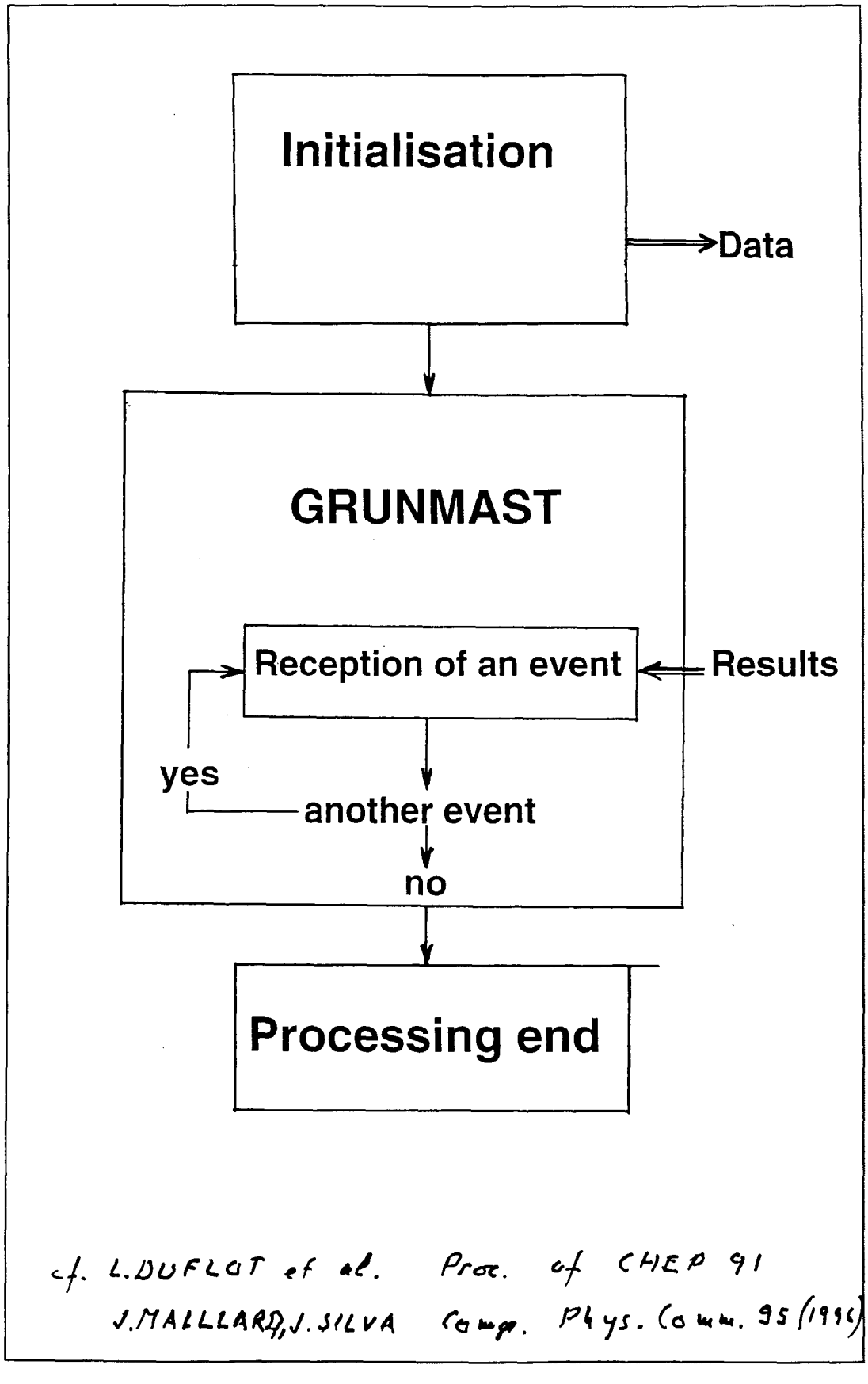

cf. L. DUFLOT et al. Proc. of CHEP 91
J. MALLARD, J. SILVA Comp. Phys. Comm. 95 (1996)

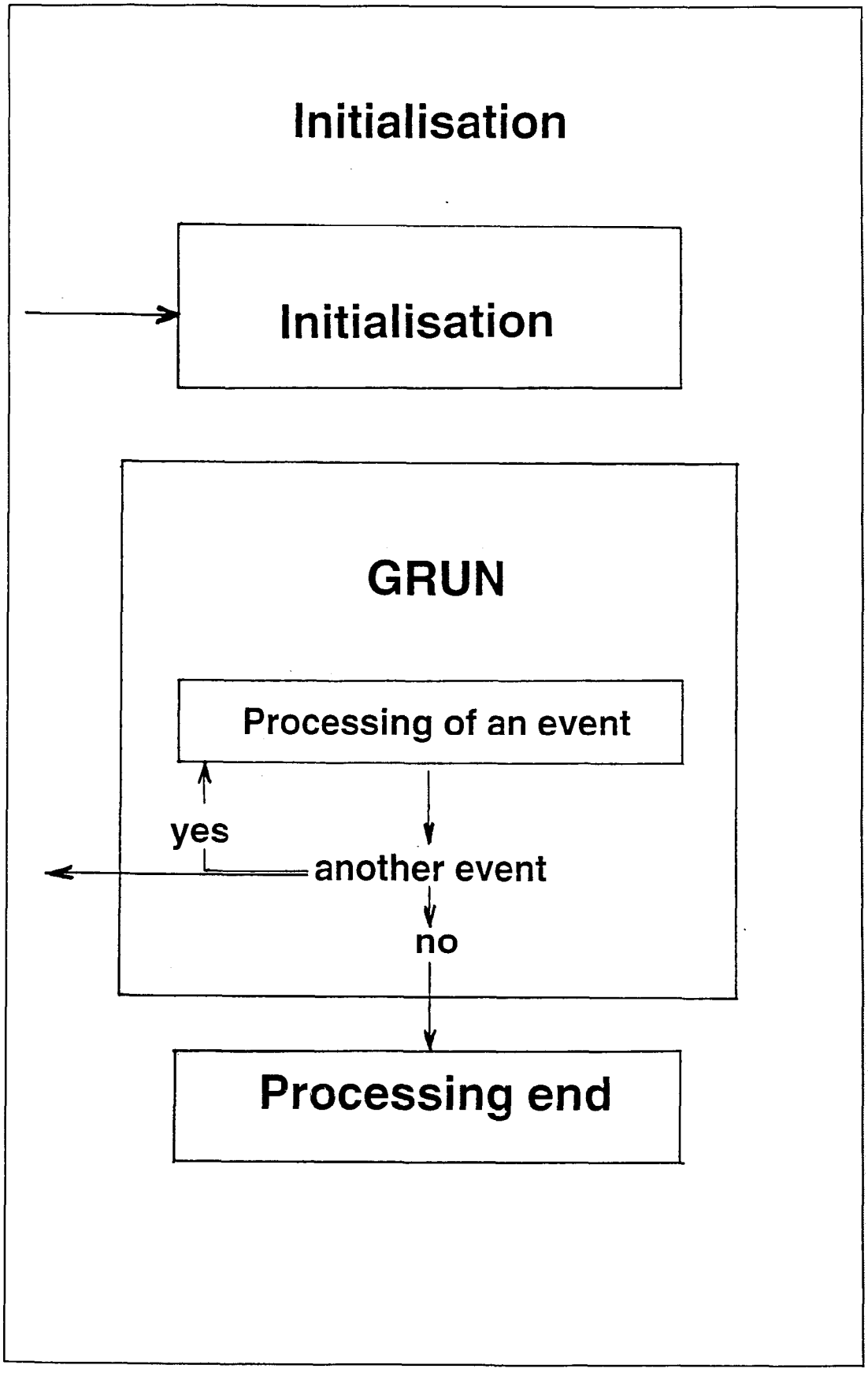
Initialisation
Initialisation
GRUN
Processing of an event
yes
another event
no
Processing end

GEANT+FOT farm on the College de France T_Node

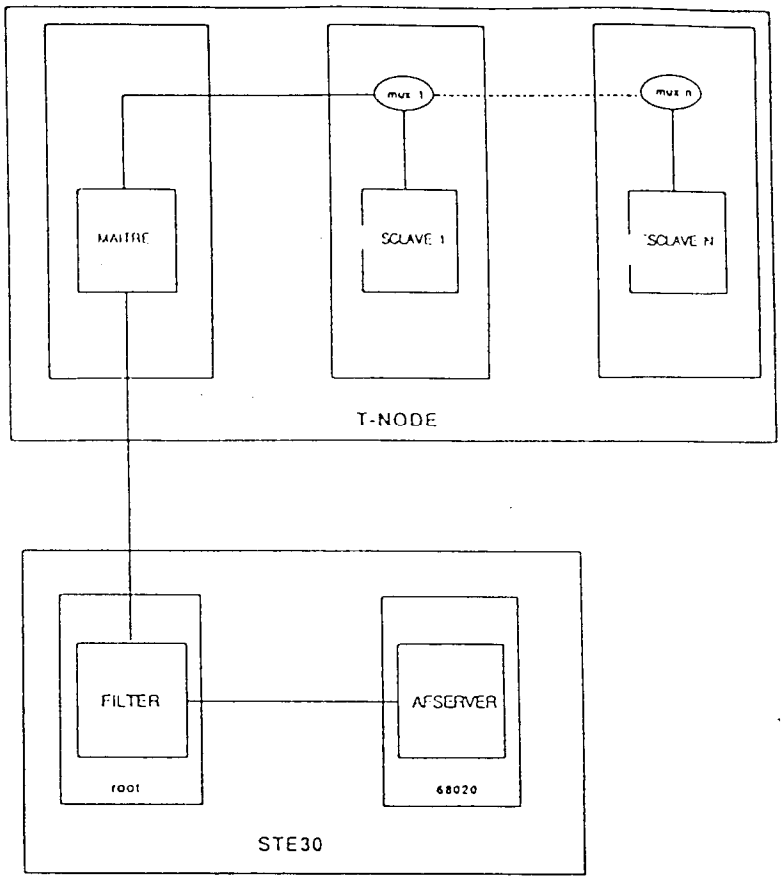

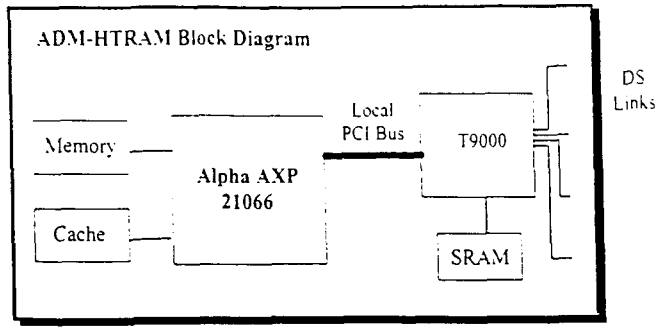

Specifications

Processor	DEC Alpha 21066 fully-pipelined 64-bit RISC architecture 233MHz (466 mips, 233MFLOPS) using dual instruction issue IEEE and VAX-compatible floating point High bandwidth 64-bit memory controller Memory management 8k on-chip data and instruction caches Secondary cache controller Asynchronous PCI I/O controller Intel compatible PCI bus INMOS T9000 Running at 25MHz Supporting Virtual Channel Routing (VCR) Includes 4 DS links based on the IEEE P1355 standard
Memory	DEC Alpha 8MB to 32MB of 60ns DRAM 256K to 1MB 15ns external cache SRAM INMOS T9000 128KB of local SRAM
Host interface	Connected to an HTRAM carrier board
Software	3L Parallel C/AXP compiler with parallel network support (including DEC GEM compiler). IPLib and fast maths libraries INMOS T9000 toolset for the T9000
Warranty	12 months from date of invoice

Ordering Information

ADM-HTRAM HTRAM Module
Please state the main memory and cache requirements.

4. CONCLUSIONS

1. Within the energy domain 2 to 10 GeV FOT + GEANT provide a valuable simulation tool for crystalline e+ sources.

2. The experimental results are reproduced within a precision of about 30 per cent.

3. The operated computing potential has to able to deliver about 500 Mflops if posible.

4. Improvements are needed for higher energy operation.

5. A broad community of physicists take interest in shower calculation, it could be an occasion for collaboration.

Present status of KEK positron generator and Study of Positron focusing with superconducting solenoid

Takuya Kamitani
KEK

Summary

The KEK positron generator is under the upgrade for the KEKB-factory project. The positron intensity is required to increase in about one order of magnitude higher than the present value. To achieve it, the positron generator is moved downstream to increase the primary electron energy from 0.25 GeV to 3.7 GeV. A new conversion target which can deal with its higher heat deposition is installed. The functionally graded material of copper and tungsten is used to release the difference of the thermal expansion coefficients. In the preliminary beam test, two thirds of the designed positron conversion ratio was obtained, though its energy spread is large. To make the positron energy spread smaller, the bunch compression system for the primary electrons and the energy compression system at the end of the linac will be used. A simulation study shows these systems will work well to reduce the positron energy spread which fits to the injection acceptance.

In general, to increase positron intensity, the higher solenoidal field just after the target is desirable. We try an superconducting solenoid approach for it. By replacing the present pulsed coil of the KEK positron generator to the superconducting solenoid, about two times enhancement in positron yield is expected from the simulation study. The first prototype coil was fabricated for checking the wire winding technique and for the cooling test. The result of the cooling test was successful to achieve the current density which is close to the intrinsic limit of the wire material. We are going to design the second prototype coil and its cryostat for the beam test. The tolerance of the superconducting state against the radiations will be clarified with it.

WORKSHOP ON NEW KINDS OF POSITRON SOURCES FOR LINEAR COLLIDERS
March 4-7, 1997, Stanford Linear Accelerator Center, Stanford, CA, USA

Present status of KEKB positron generator and Study of positron focusing with Superconducting solenoid

Takuya Kamitani, Atsushi Enomoto,
Satoshi Ohsawa, Yujiro Ogawa, Kenji Hosoyama
KEK

Contents

TRISTAN

PF / AR Injector Linac

Klystron 20 MW (max 30 MW)

2m-ACC struc. * 4 * 8 MeV/m = 64 MeV/unit

* Pre-Injector unit + 40 Acceleration units for 2.5 GeV e–

* e+ Generator Linac : 0.25 GeV e– –> target –> e+ 0.25 GeV

Main Linac for 2.5 GeV e+

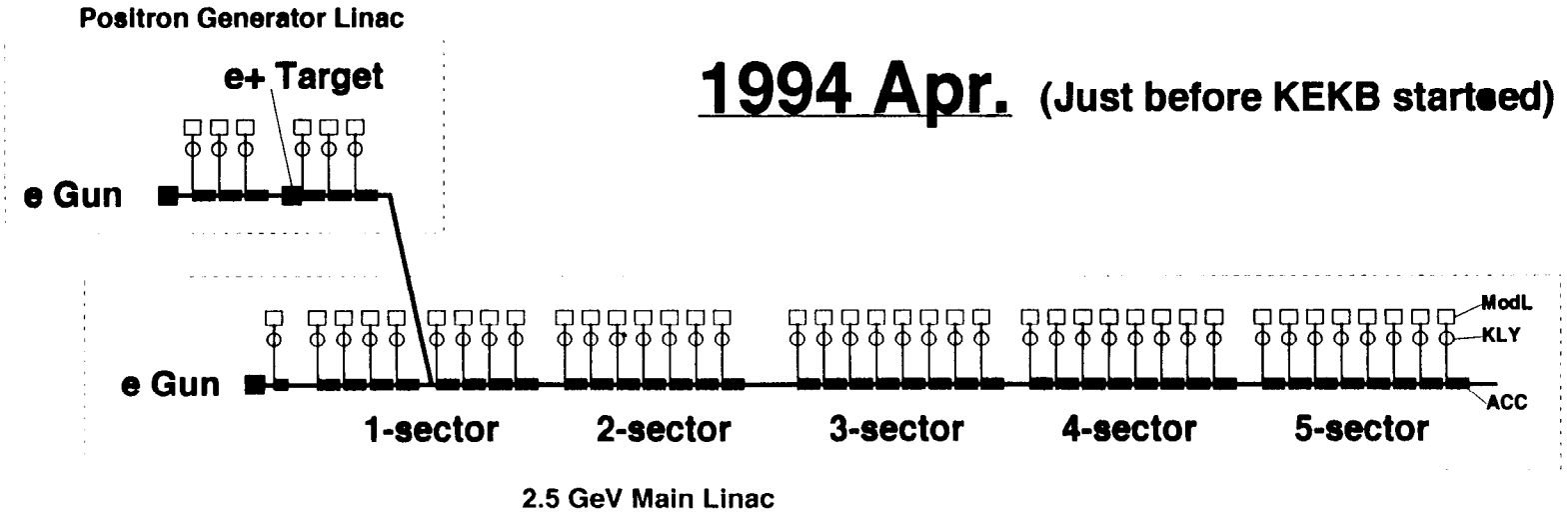

1994 Apr. (Just before KEKB started)

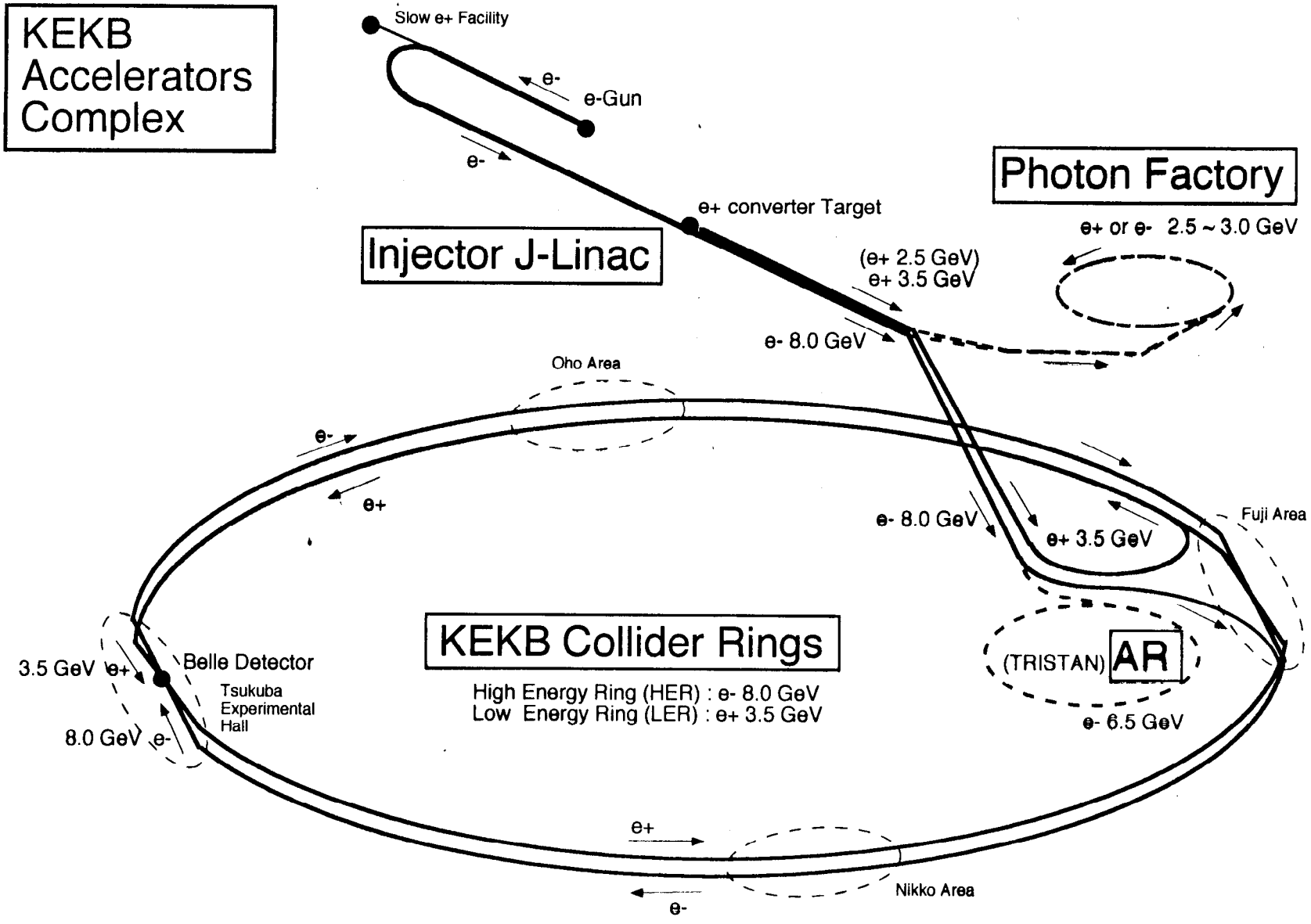
KEKB
Accelerators
Complex
Slow e+ Facility
e-
e-Gun
e-
e+ converter Target
Photon Factory
e+ or e- 2.5 ~ 3.0 GeV
Injector J-Linac
(e+ 2.5 GeV)
e+ 3.5 GeV
e- 8.0 GeV
Oho Area
e-
e+
e- 8.0 GeV
e+ 3.5 GeV
Fuji Area
KEKB Collider Rings
High Energy Ring (HER) : e- 8.0 GeV
Low Energy Ring (LER) : e+ 3.5 GeV
3.5 GeV e+
Belle Detector
Tsukuba
Experimental
Hall
8.0 GeV e-
(TRISTAN) AR
e- 6.5 GeV
e+
e-
Nikko Area

Linac Upgrade

TRISTAN
PF / AR injector --> KEKB injector

(1) Energy Upgrade

E(e–) : 2.5 GeV —> 8.0 GeV
E(e+) : 2.5 GeV —> 3.5 GeV

(Full-energy injection to KEKB rings)

(2) Beam Intensity Upgrade

Q(e–) : 0.320 nC —> 1.280 nC
Q(e+) : 0.070 nC —> 0.640 nC

$I_{HER}(e–) = 1.1$ A, $T_{100\%Fill}(e–) \sim 3$ min
$I_{LER}(e+) = 2.6$ A, $T_{100\%Fill}(e+) \sim 14$ min

KEKB Injector Linac (Completed)

Klystron 41 MW (max 50 MW)

2m-ACC struc. * 4 * 20 MeV/m = 160 MeV/unit

* Pre-injector (A-1) unit + 57 Acceleration units for 8.0 GeV e–

* A-1 + 26 Accel. units for 3.7 GeV e– –> target –> 31 Accel. units for e+ 3.5 GeV

No SLED in A-1 unit ; e- pre-injector
In 2-1 unit ; e+ focusing solenoid

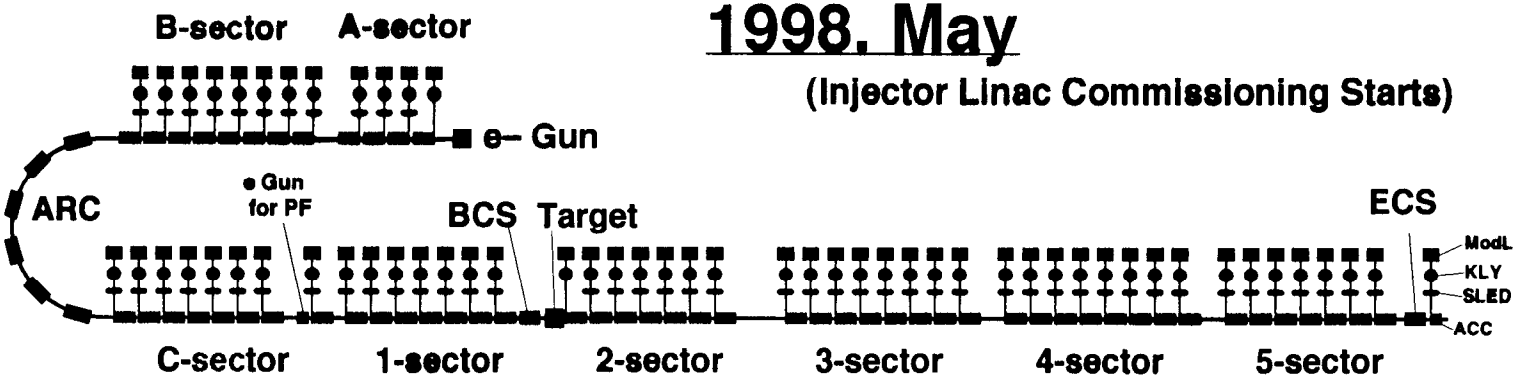

1998. May

(Injector Linac Commissioning Starts)

e+ Intensity Upgrade

Q(e+) : 0.070 nC —> 0.640 nC

Primary e– energy
0.25 GeV –> 3.7 GeV

Needs thicker conversion Target

QWT e+ focusing system

Pulsed coil + DC solenoid available
Shorter Acc. structure
Higher Acc. gradient

e+ Energy-spread
has to be improved.

(Smaller injection acceptance)

Positron Generator Parameters

	TRISTAN/PF	KEKB	
Primary Electron			
Energy	0.25	3.7	GeV
Particles (Charge)	1×10^{11} (16)	6×10^{10} (10)	(nC)
# of bunches	5	1	
Target			
Material	Ta	W	
Thickness	8.0 ($2\ X_0$)	14.0 ($4\ X_0$)	mm
e+ Focusing system			
Type	QWT		
High Field (Bi)	2.3 T × 45 mm (Pulsed coil)		
Low Field (Bf)	0.4 T × 8 m (DC coil)		
Final Positron			
Energy	2.5	3.5	GeV
Particles (Charge)	4.4×10^{8} (0.070)	4×10^{9} (0.640)	(nC)
Emittance (Normalized)	5.7×10^{-3}	5.7×10^{-3}	rad.m
Ring Acceptance			
Transverse emittance	6×10^{-3}	6×10^{-3}	rad.m
Energy	0.22	0.125	(1σ) %
Longitudinal position	−1 ~ +1 ns	−30 ~ +30 ps	
Efficiency			
Conversion Ratio	1.8 %	≥ 1.8 %	e+/e-/GeV

New e+ conversion target

Primary e– beam

5 bunches

16 nC * 0.25 GeV * 25 pps = 0.1 kW

(PF/ AR)

Single bunch

10 nC * 3.70 GeV * 50 pps = 1.9 kW

(KEKB)

1. Target thickness optimization

0.25 GeV 3.7 GeV

Ta; $2\,X_0$ —> W; $4\,X_0$

2. Cooling problem

Tantalum —> Tungsten

(Advantages)

Easy processing

Melting point
Thermal conductivity
Tensile strength

Cu/W FGM

(Functionally Graded Material)

Grading the difference of the thermal expansion coefficients of Cu and W

Positron Converter Target

KEKB

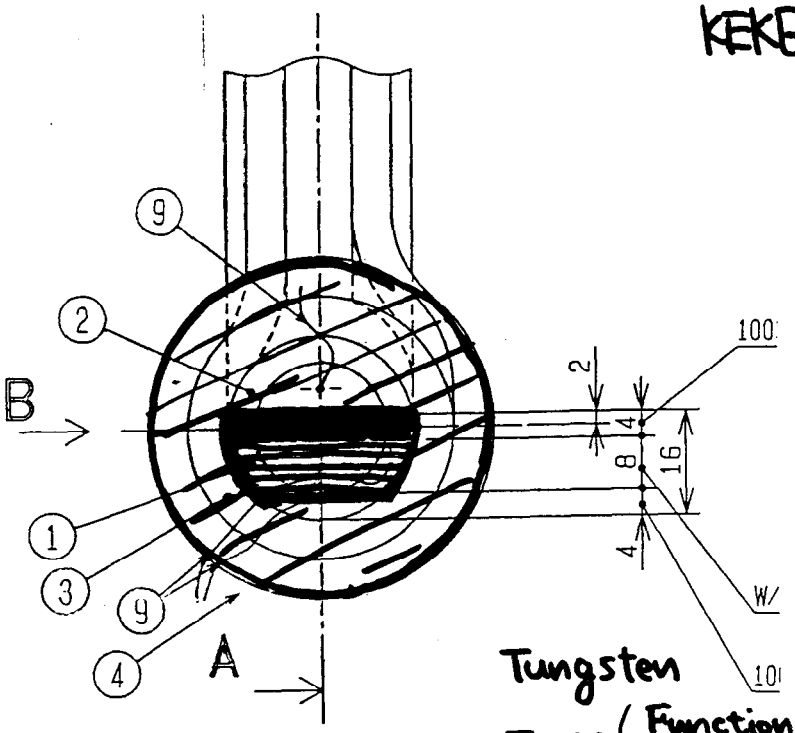

Tungsten

FGM { Functionally Graded Material

Cupper

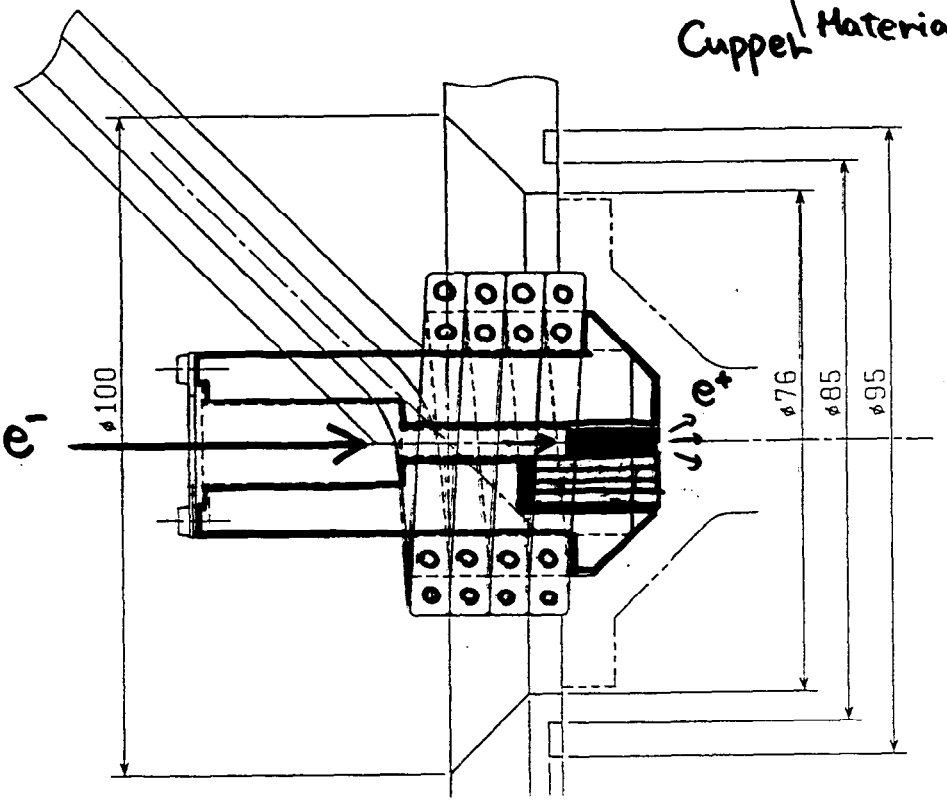

Cupper / Tungusten

銅/タングステン傾斜機能材料

Functionally ~~Gradient~~ Material ; FGM

Graded

宇宙航空機用として日本で考案された傾斜機能材料は熱応力の緩和を目的としております。

銅／タングステン傾斜機能材料は熱伝導性に優れた銅と耐熱性に優れたタングステンを段階的に組成を変化させたもので、耐熱部にはタングステンを多く、冷却部には銅を多く含んだ組成で使用されます。核融合炉など耐熱、放熱性両方の特性を必要とする構造材に適しています。

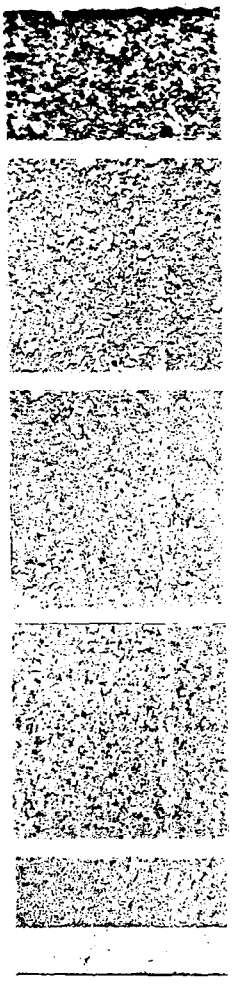

100%銅 Cu

30%銅 Cu
70%タングステン W

25%銅 Cu
75%タングステン W

20%銅 Cu
80%タングステン W

15%銅 Cu
85%タングステン W

銅（接合層）Cu

100%タングステン W

日本タングステン株式会社

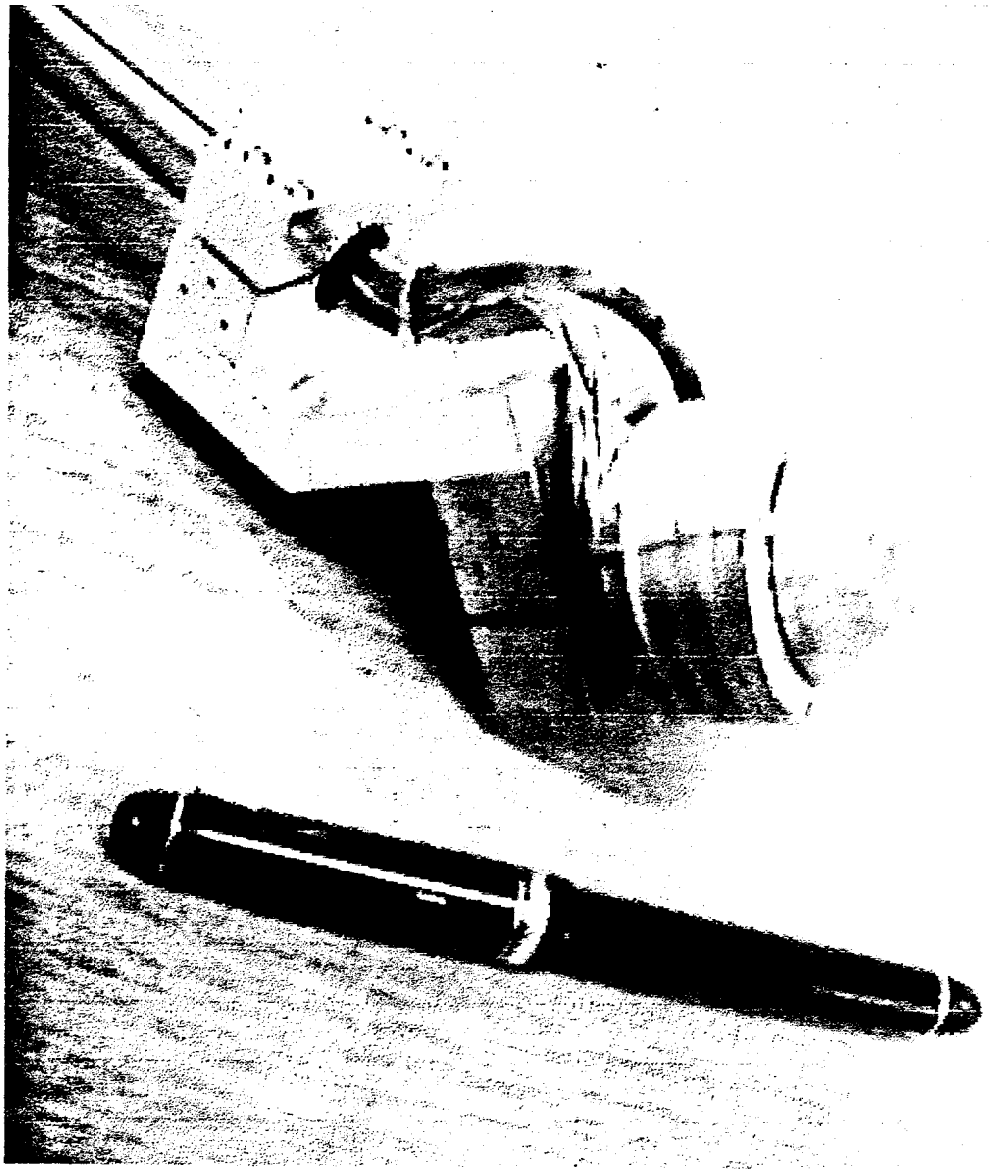

Thermal Analysis

図2：標的の温度分布

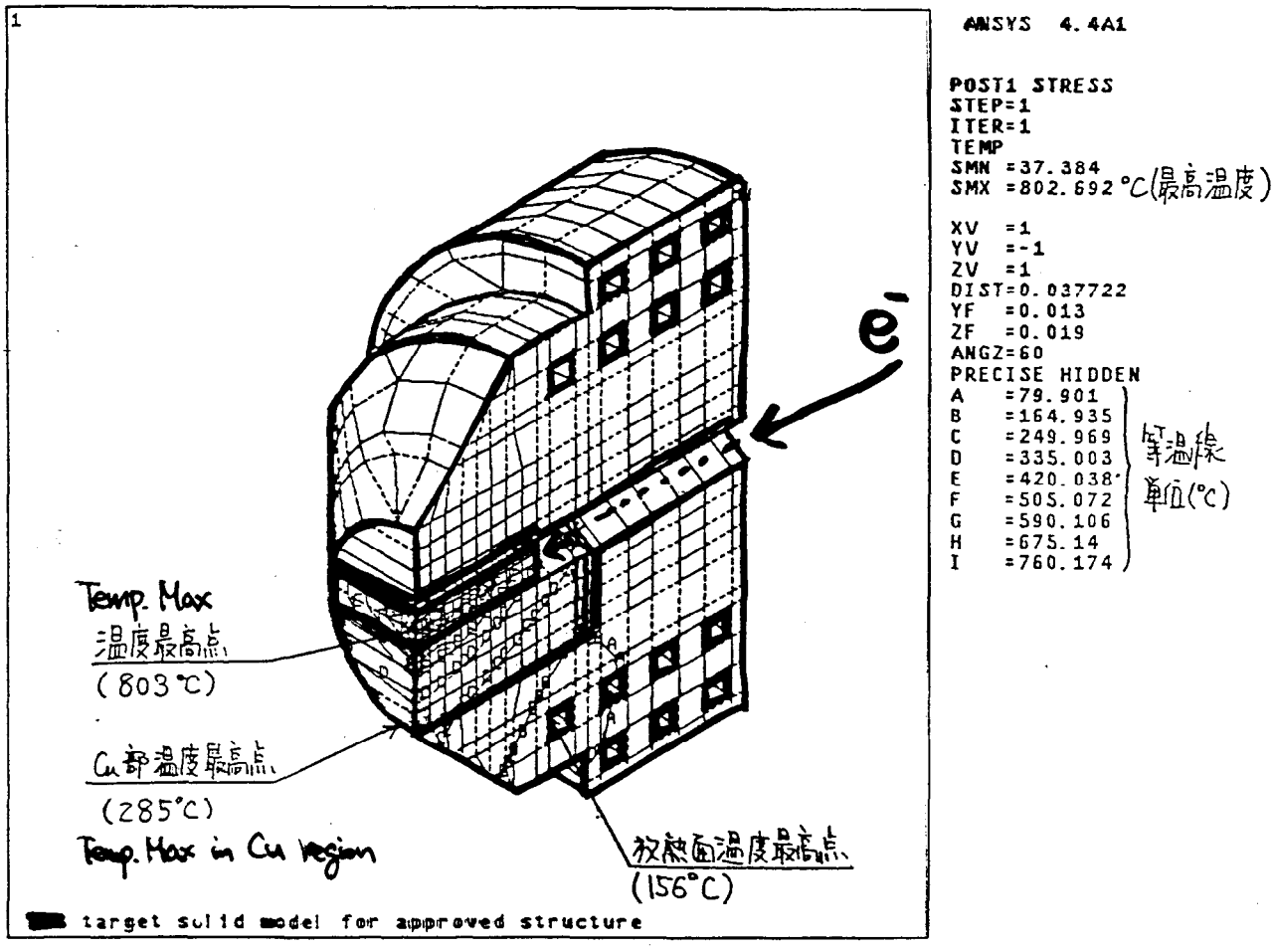

(3/4)

e^+ focusing coils

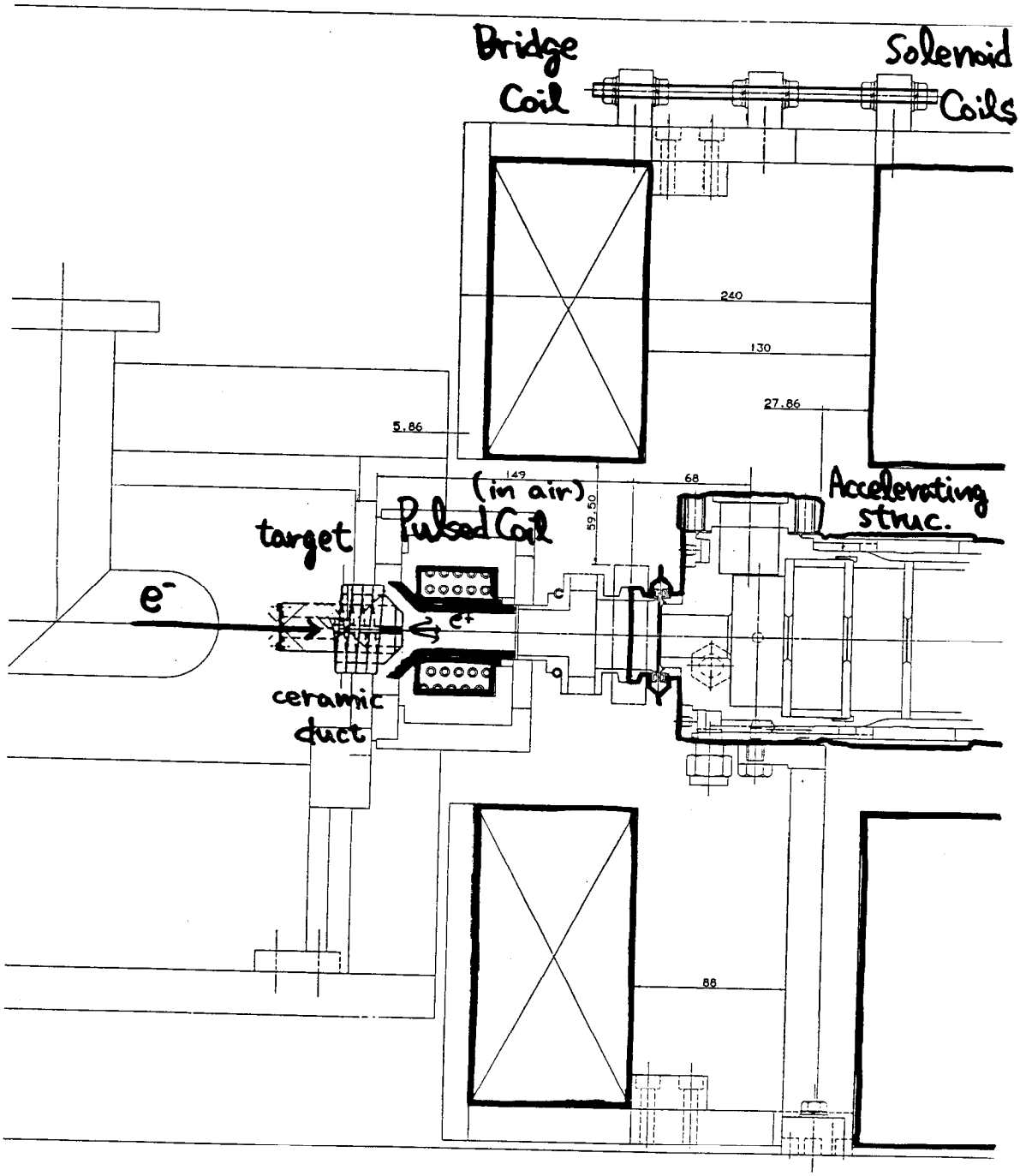

KEKB e+ generator Solenoidal field profile

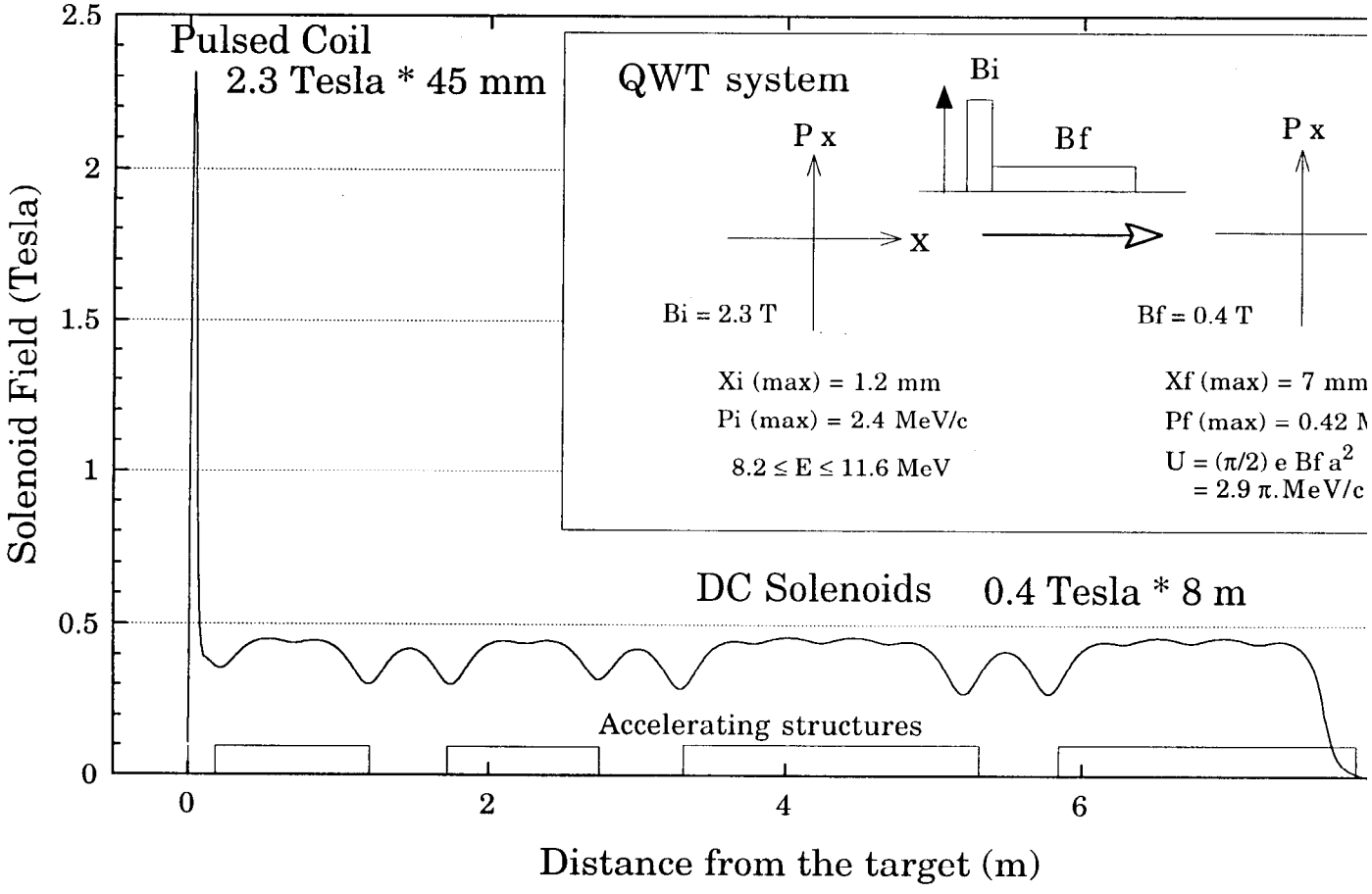

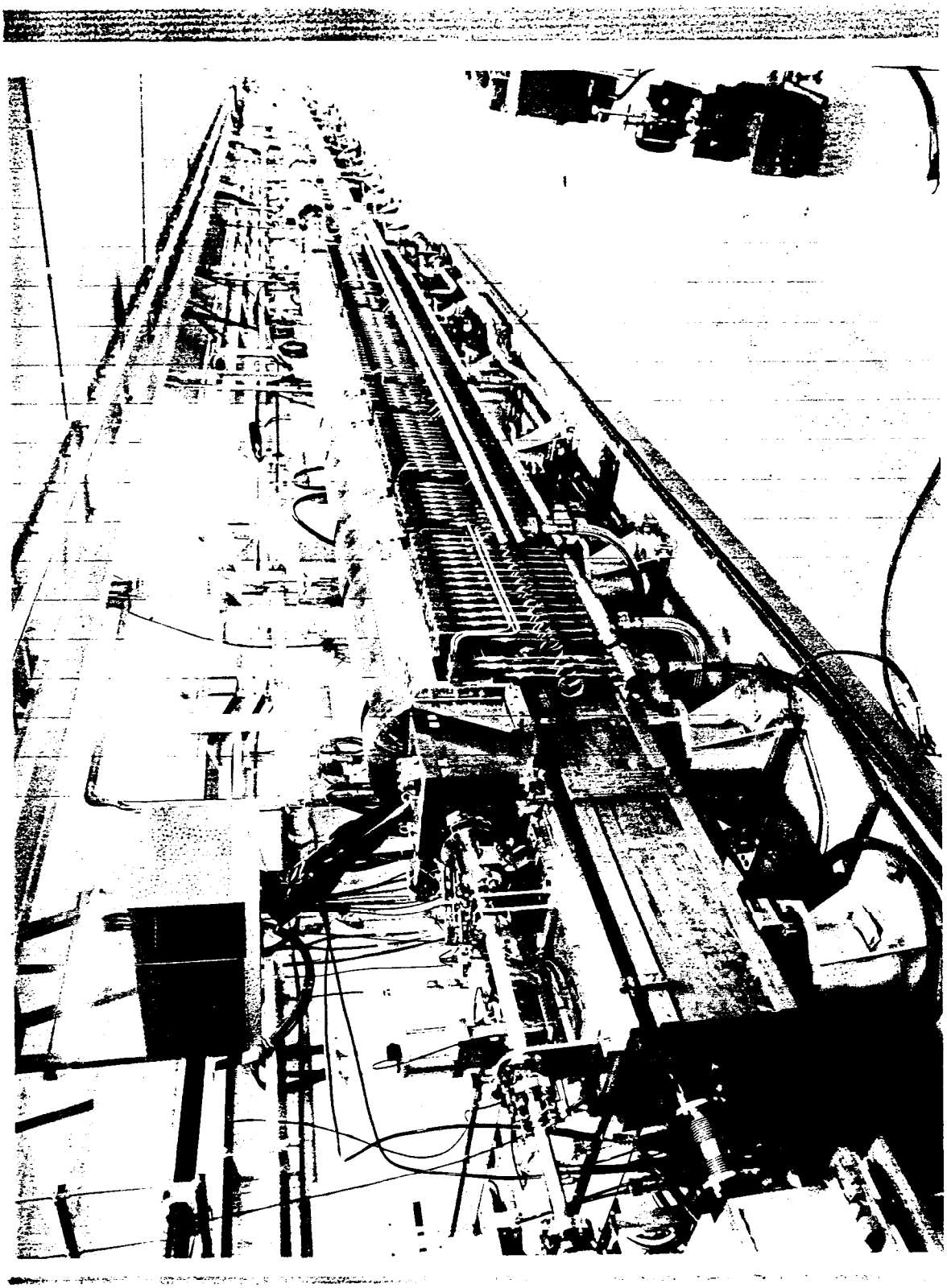

Present Layout (97 Jan.)

Some RF Modulators and Klystrons upgraded
Some SLED installed

Positron Generator Linac has Decomposed
e+ focusing pulsed coil & DC solenoids have Moved
New e+ conversion target has installed
QM focusing system layout for e+ has renewed

- High Power RF Modulator
- Ordinary RF Modulator
- High Power Klystron
- Ordinary Klystron
- Accelerating Unit
- SLED

1997 Jan. (At Present)

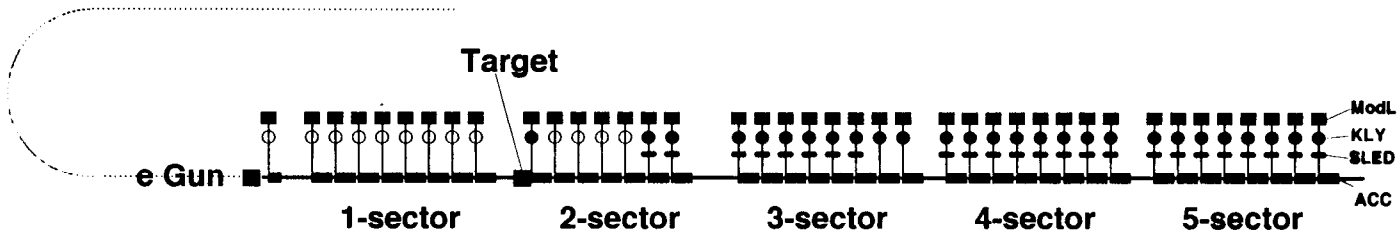

Positron Charge (Generated & Transmitted)

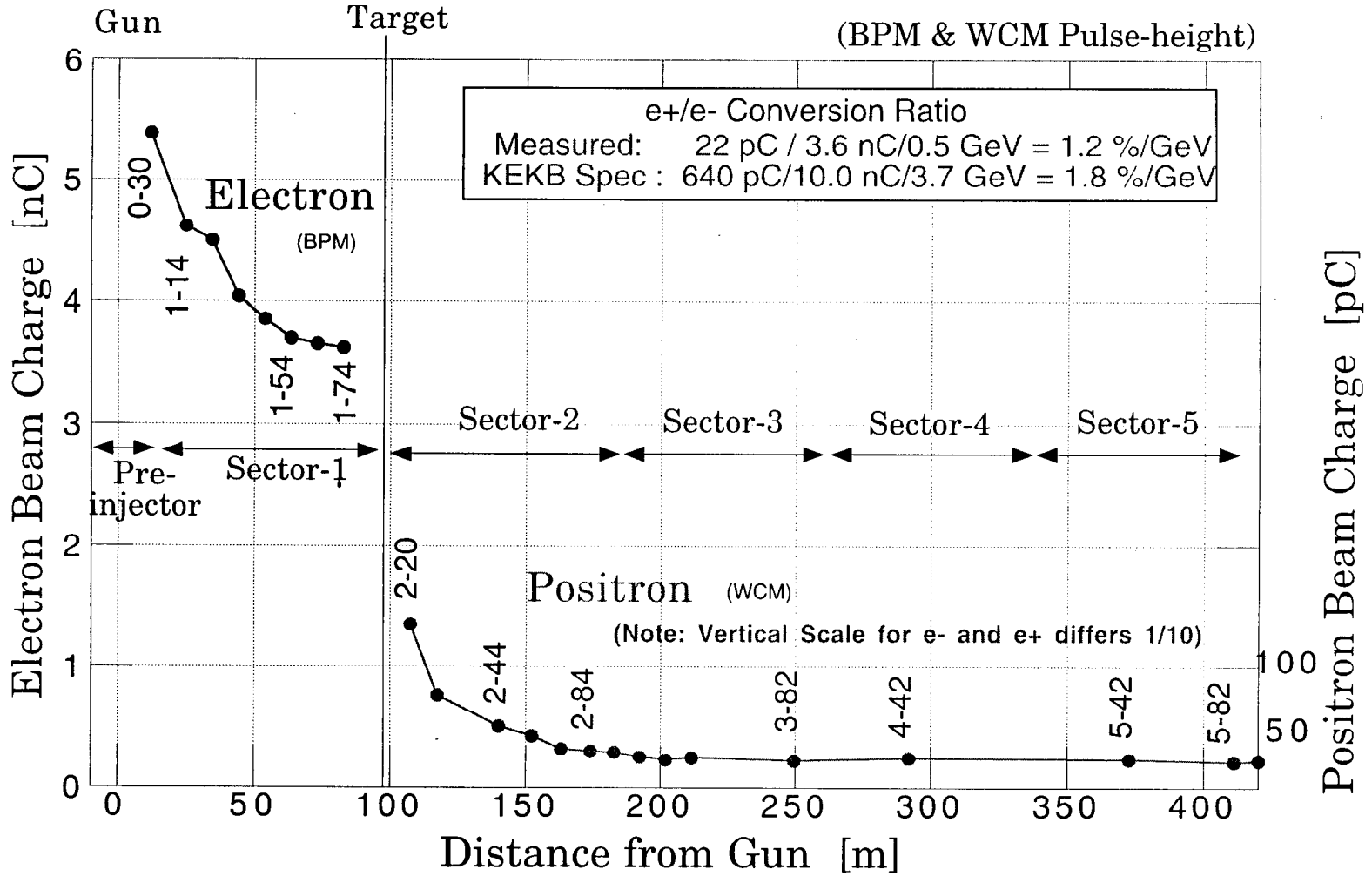

Energy-spread issue

Energy acceptance narrowed

for Beam transfer line & LER injection

PF/AR KEKB

0.22 % —> 0.125 % (1σ)

(+/– 2σ spread is acceptable at maximum)

Needs improvement

on linac e^+ energy-spread

To be Considered

(1) Primary e^- bunch is Long

(Space charge effect in rf Bunching)

(2) De-bunching in Solenoids

(Path difference for various P_T)

(3) Initial e^+ energy-spread

(QWT characteristics)

e+ Energy-spread Compression Scheme

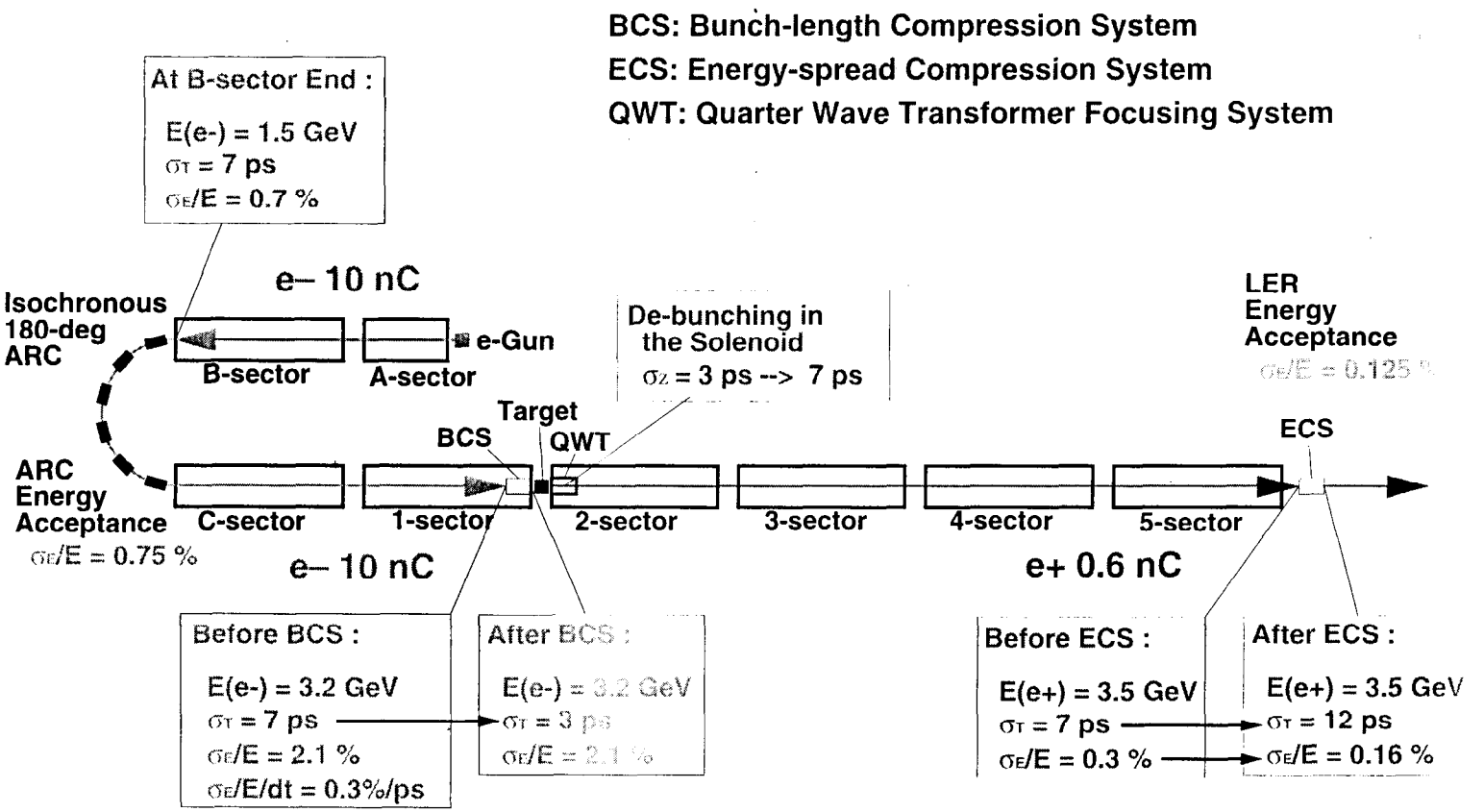

(1) Bunch Compression System

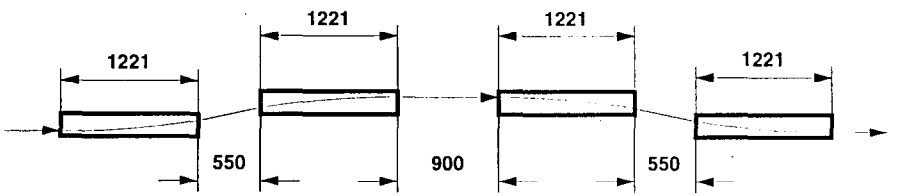

BCS Specs

- Beam Energy = 3.5 [GeV]
- Acceleration = 2.0 [GeV] with θ_{RF} = 30 [deg]
- Magnetic Field = 1.46 [Tesla]
- R_{56} = ds/(dp/p) = –0.78 [mm/%]
- Trajectory shift = 297 [mm]

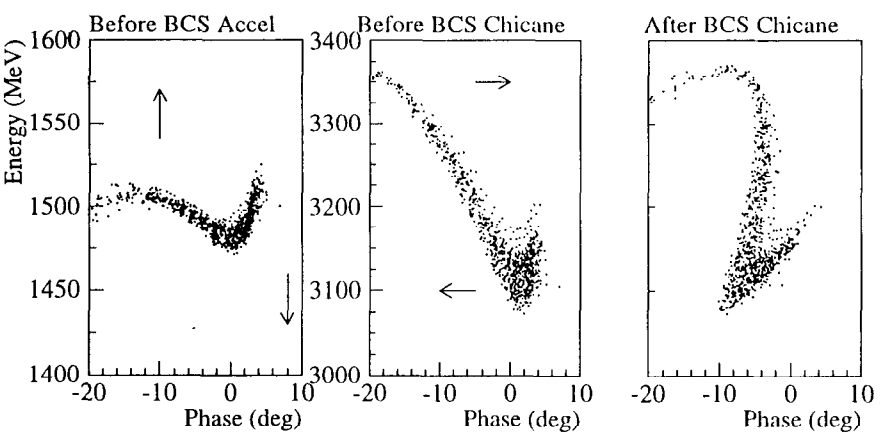

(2) Energy-spread compression system

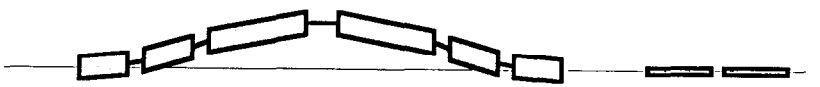

ECS specs

- Beam Energy = 3.5 [GeV]
- Magnetic Field = 1.40 [Tesla]
- R_{56} = ds/(dp/p) = –9.2 [mm/%]
- Trajectory shift = 1422 [mm]
- Acceleration = 80 [MeV]

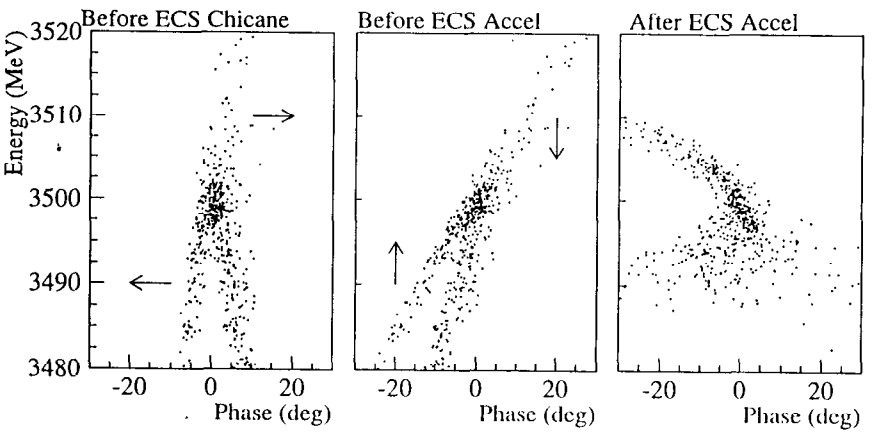

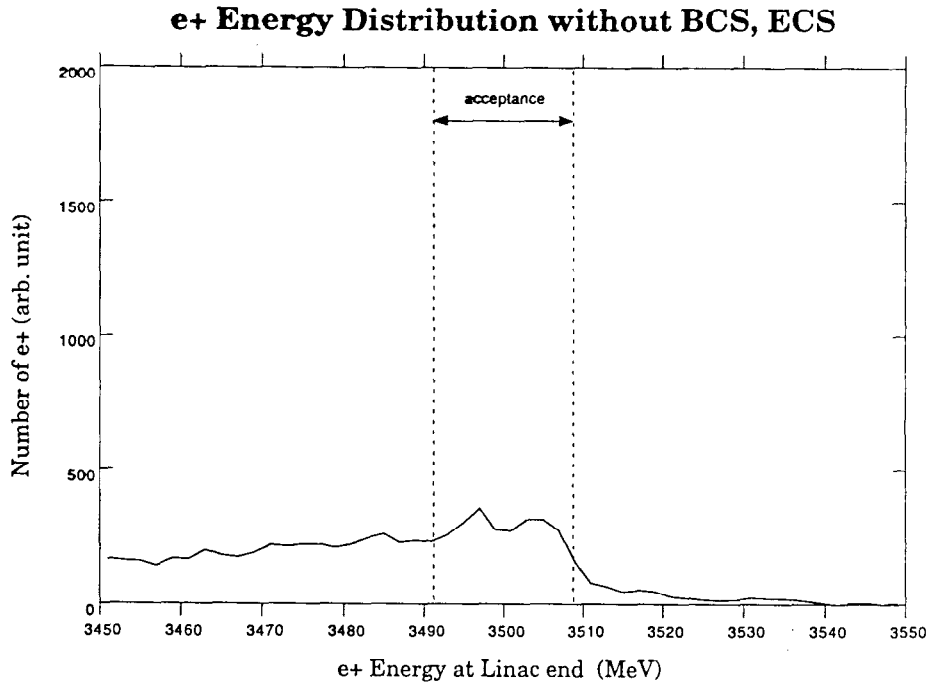
e+ Energy Distribution without BCS, ECS
acceptance
Number of e+ (arb. unit)
2000
1500
1000
500
0
3450
3460
3470
3480
3490
3500
3510
3520
3530
3540
3550
e+ Energy at Linac end (MeV)

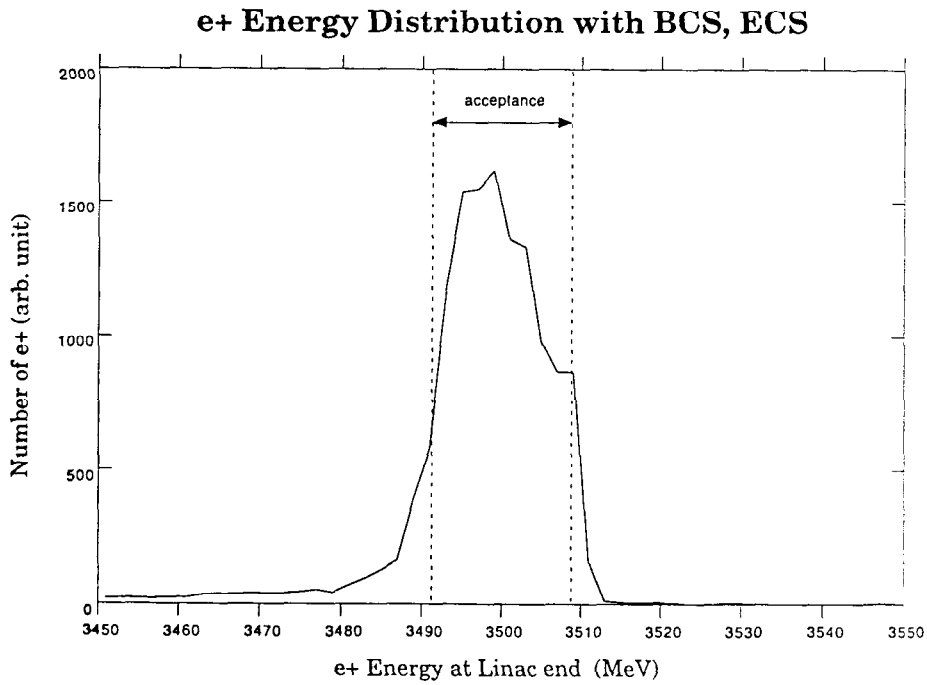
e+ Energy Distribution with BCS, ECS
acceptance
Number of e+ (arb. unit)
2000
1500
1000
500
0
3450
3460
3470
3480
3490
3500
3510
3520
3530
3540
3550
e+ Energy at Linac end (MeV)

Positron Focusing with SC solenoid

To increase e^+ intensity

→ Higher Focusing field

- Flux concentrator (SLC)
- ⊙Super conducting coil

Advantages

1. High current density (~500 A/mm²)
   [Pc : 160 A/mm²]

   High Solenoidal field with small power supply (~ 120→150 A)
   [pc : 10 kA]

2. DC operation

   Free from eddy current effects

3. Cryogenic experience at KEK

   Liq He facility
   capac. 8kW → 3kW (KEKB SC Acc Cavity)
   → 1kW (Crab Cavity)
   → extra 4kW

   Experts
   SSC SC magnet

Conceptual Design of SC coil

for simulation

Goal Field strength ~ 6 Tesla

Coil Specification

Wire : 0.76 mmϕ, Nb-Ti, Cu ratio 4.5

Inner diameter : $2a_1$ = 250 mm

Outer diamter : $2a_2$ = 400 mm

Length : L = 100 mm

Number of turns : N = $1.33*10^4$ turn

Current : I = 121 Ampere

N*I : N*I = $1.61*10^6$ Ampere.turn

Current Density : i = 325 A/mm^2

Effective Field length : L_{eff} ~ 260 mm

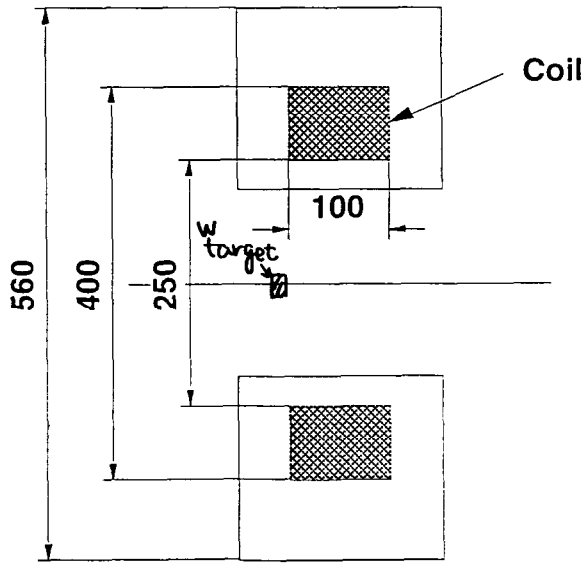

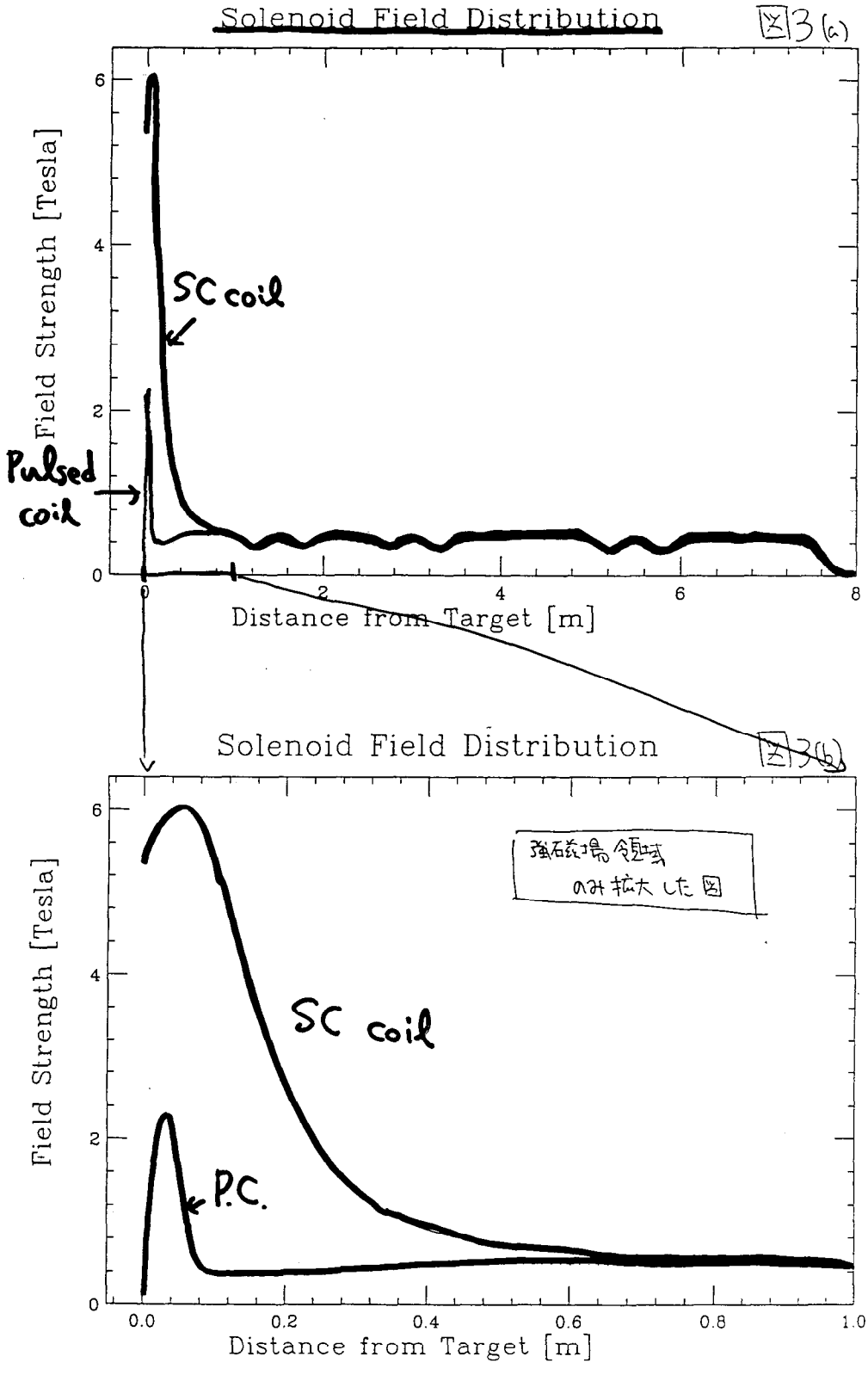
Solenoid Field Distribution
図3(a)
Field Strength [Tesla]
SC coil
Pulsed coil
Distance from Target [m]
Solenoid Field Distribution
図3(b)
強磁場領域のみ拡大した図
Field Strength [Tesla]
SC coil
P.C.
Distance from Target [m]

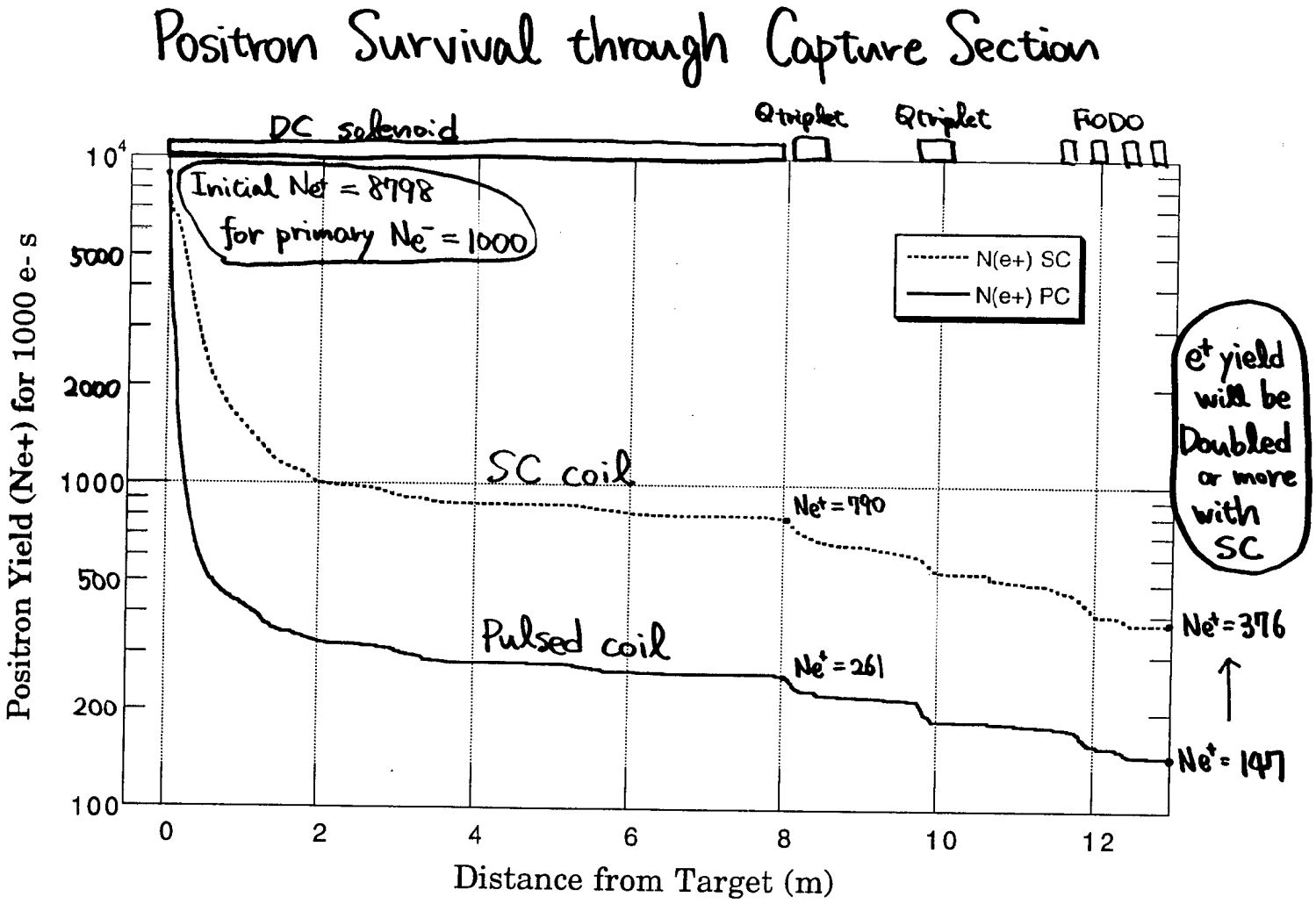
Positron Survival through Capture Section
DC solenoid
Q triplet
Q triplet
FODO
Initial Ne+ = 8798
for primary Ne- = 1000
N(e+) SC
N(e+) PC
e+ yield will be Doubled or more with SC
SC coil
Pulsed coil
Ne+ = 790
Ne+ = 376
Ne+ = 261
Ne+ = 147
Positron Yield (Ne+) for 1000 e- s
Distance from Target (m)
10^4
5000
2000
1000
500
200
100
0
2
4
6
8
10
12

[at the end of capture section. (same for all plots)]

x distribution for PC vs SC

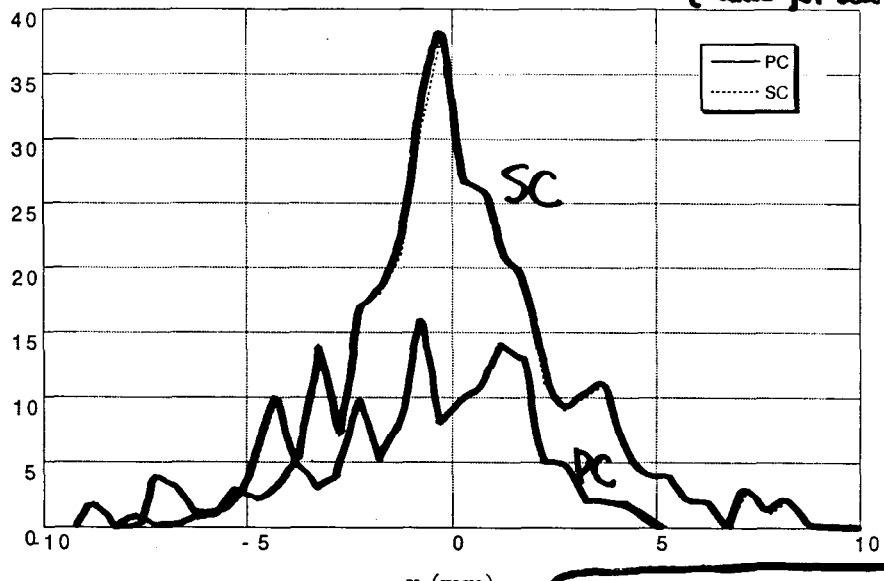

Transverse Phasespaces are not so different for SC and PC

x' distribution for PC vs SC

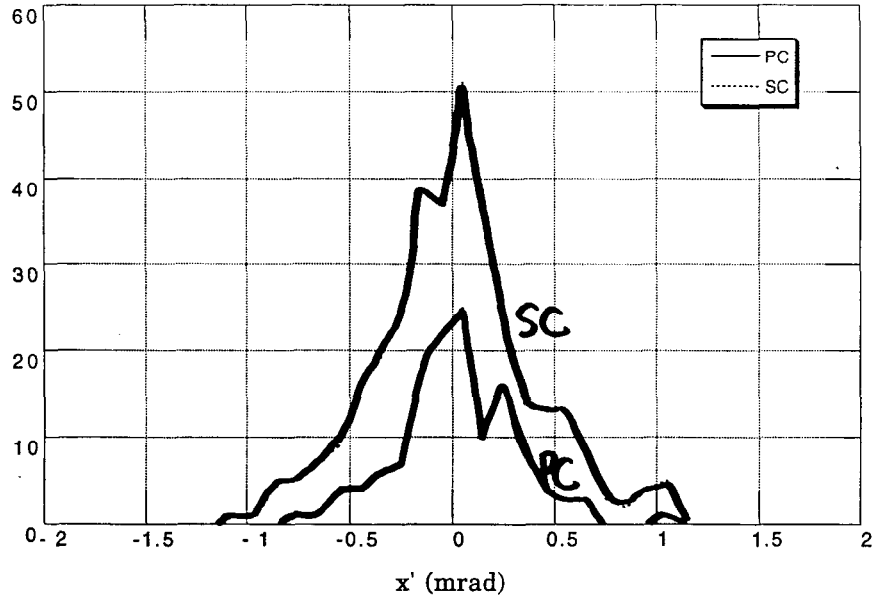

Bunch lengths are almost same for PC and SC

Bunch Length for PC vs SC

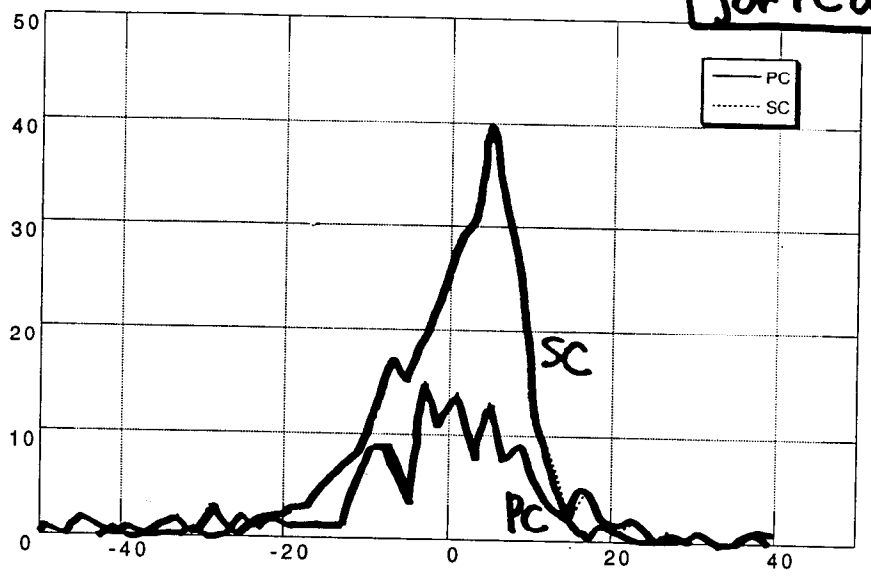

longitudinal position (psec)

Energy acceptance is much broader for SC

Positron Energy Distribution for PC vs SC

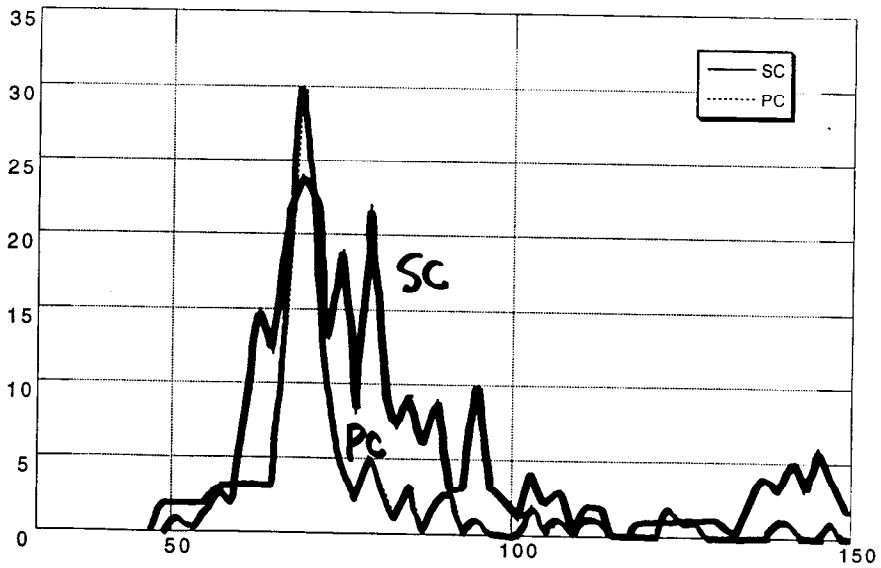

e+ Energy (MeV)

For more realistic design

① Current limit on wires

Wires have material dependent limits

on temperature (T_c)

magnetic field (B_c)

current density (I_c)

for superconducting state to be realized.

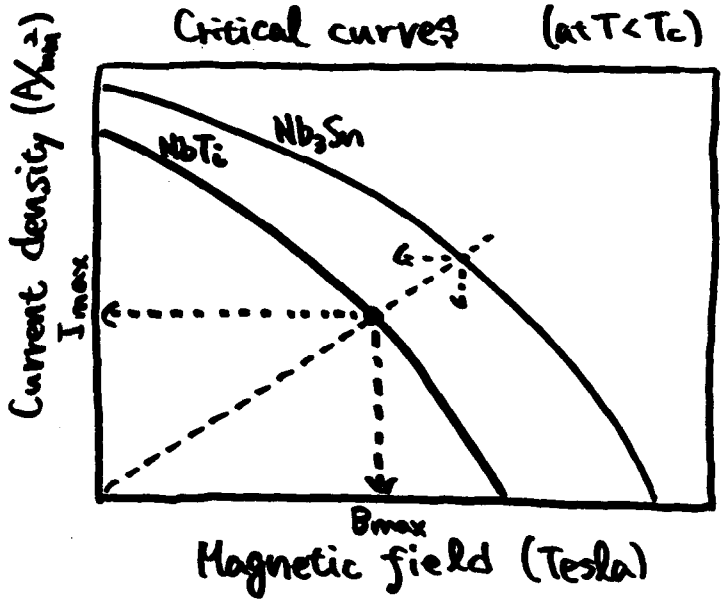

We use NbTi/Cu (Cu ratio 1.8)

ϕ 0.648mm wire (SSC legacy)

Why not high-T_c material? → WAIT a few years!

② Coil Geometry effects

Highest field is generated not in the center (B_o) but inside the coil. (B_w)

(Not B_o)

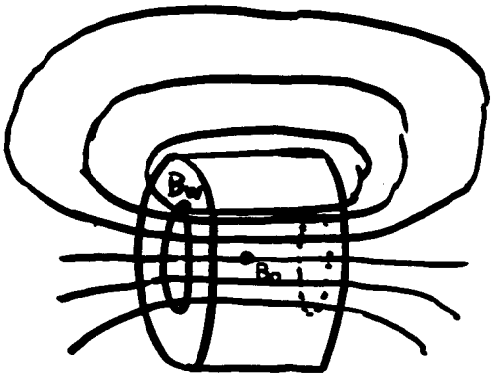

Bw limits the highest attainable field.

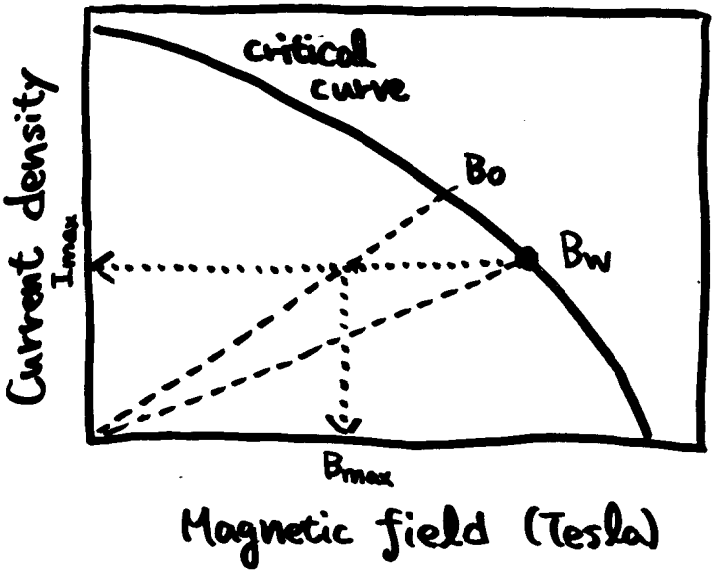

B_w/B_o ratio is determined by the coil geometry.

③ Coil Fabrication Quality

- Winding tension control
- Wire arrangement
  to minimize extra space
  for the wires to move
- Epoxy

First prototype coil

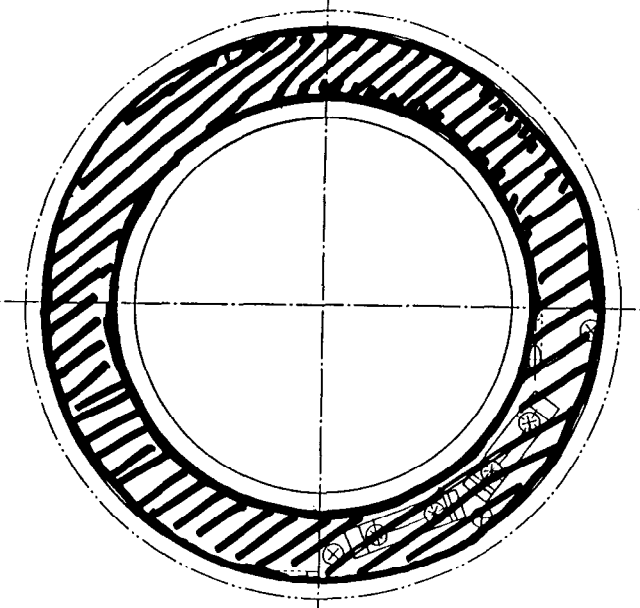

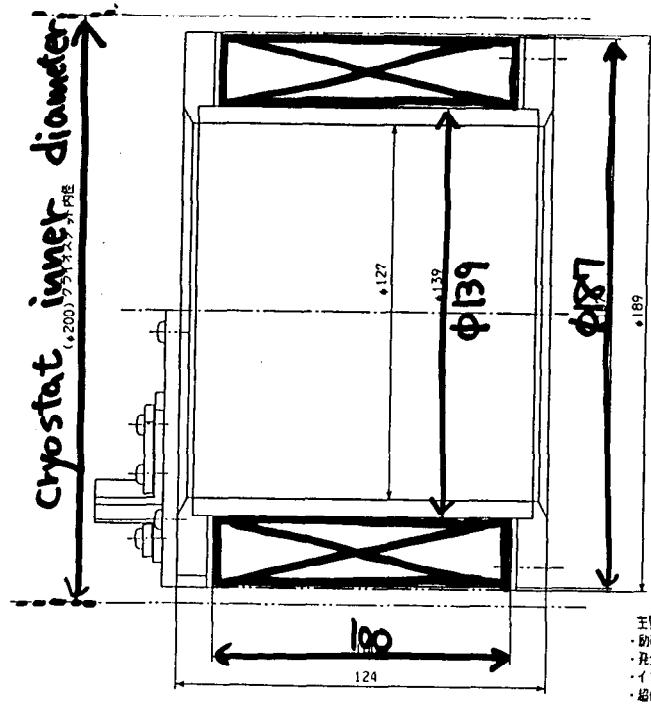

主要諸元
- 励磁電流 約180A
- 発生磁場 6T以上
- インダクタンス 約3.4H
- 超伝導線 φ0.648×3.0km

- Winding technique
- Epoxy effect
- Cooling test with existing cryostat

REVISIONS				
NO.	DESCRIPTION	(DATE)	APPROVED	CHECKED

PLAN RECORD

ISO METRIC SCREW THRE

PREVIOUS DRAWING NO.

SURFACE ROUGHNESS (MAXIMUM HEIGHT)	Rmax (μm)	UNDER 0.8	UNDER 6.3	UNDER 25	UNDER 100	NOT MACHINED SURFACE	COMMON VARIATION OF TOLERANCE (MACHINING) (mm)	RATING OF NOMINAL DIMENSION	OVER 0.5TO 6	OVER 6 TO 30	OVER 30TO 120	OVER 120TO 315	OVER 315TO 1000
	SYMBOL	▽▽▽▽	▽▽▽	▽▽	▽	～		TOLERANCE	±0.1	±0.2	±0.3	±0.5	±0.8

IND. TEST PRESS.	特殊機械部本中機器設計課	超伝導電力貯蔵装置
STOP kgf/cm	APPROVED	
AT SITE kgf/cm	CHECKED 浅野	ポジトロンコンバータ用 超伝導マグネット計画
CERTIFIED	ITAWN	
	SCALE 1:1	
	ORDER / ITEM	3rd ANGLE PROJECTION (三角法) DRAWING NO. N9Z-210-P004 REV.NO

MITSUBISHI HEAVY INDUSTRIES,LTD.
NAGASAKI SHIPYARD & MACHINERY WORKS

DRAWN 96.09.18 ISSUED

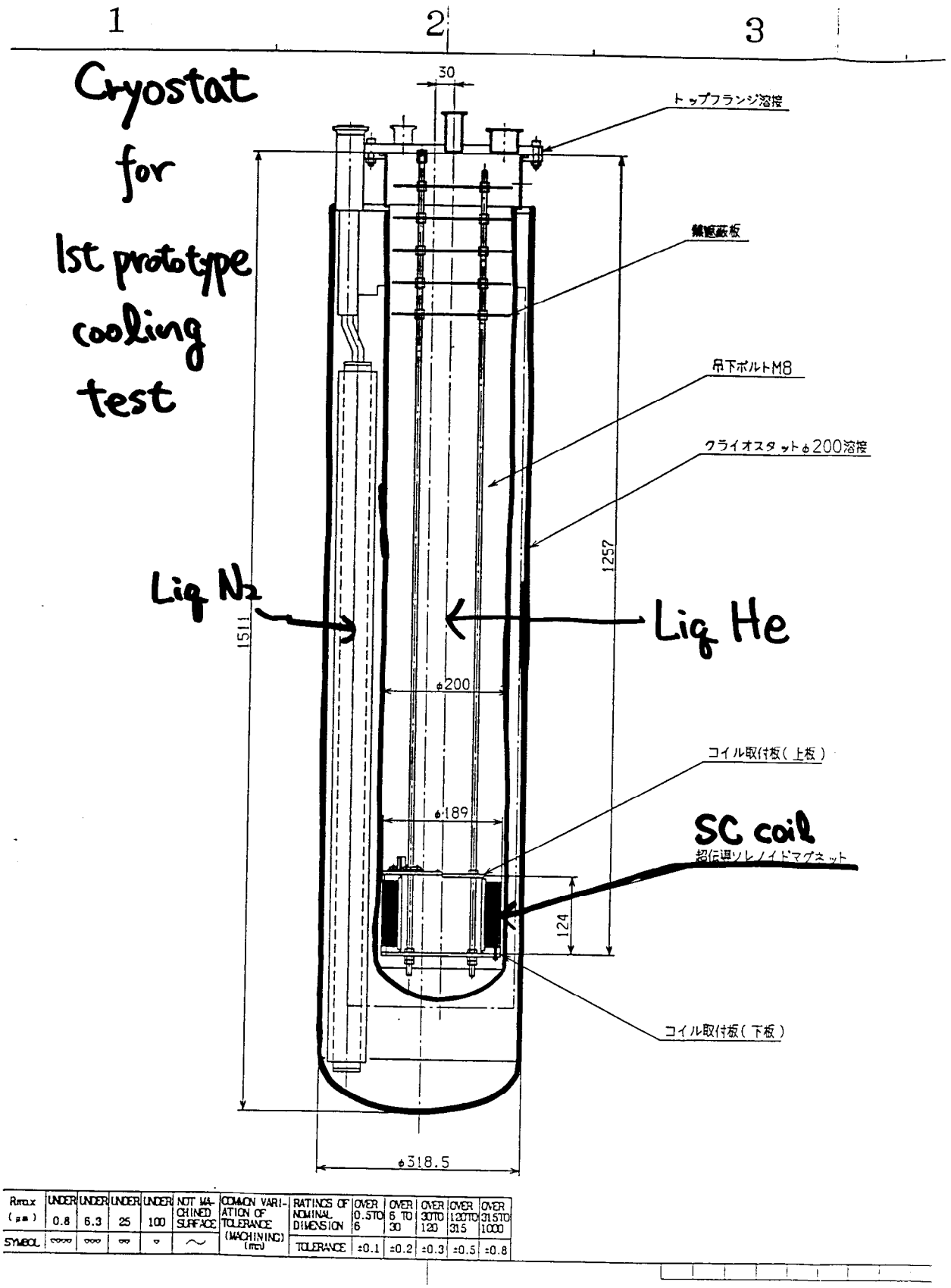

Rmax (μm)	UNDER 0.8	UNDER 6.3	UNDER 25	UNDER 100	NOT MACHINED SURFACE
SYMBOL	▽▽▽	▽▽	▽	▽	～

COMMON VARIATION OF TOLERANCE (MACHINING) (mm)	RATINGS OF NOMINAL DIMENSION	OVER 0.5 TO 6	OVER 6 TO 30	OVER 30 TO 120	OVER 120 TO 315	OVER 315 TO 1000
	TOLERANCE	±0.1	±0.2	±0.3	±0.5	±0.8

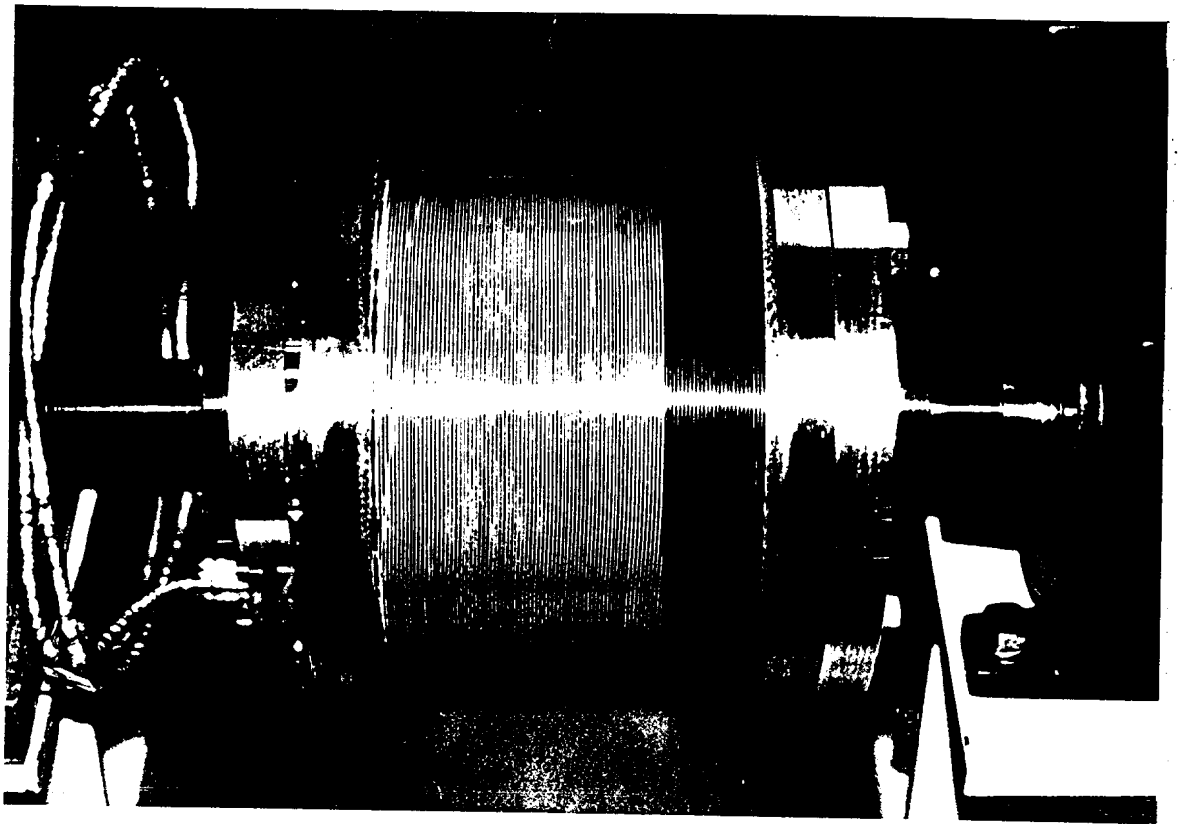

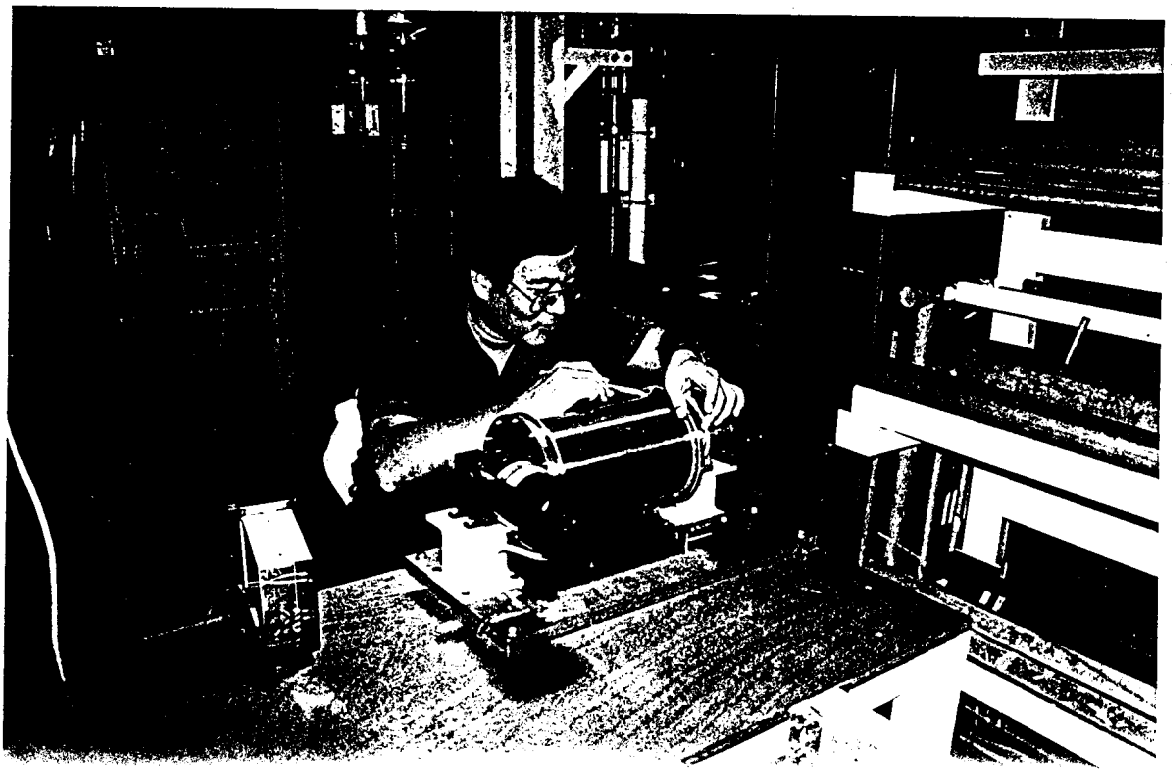

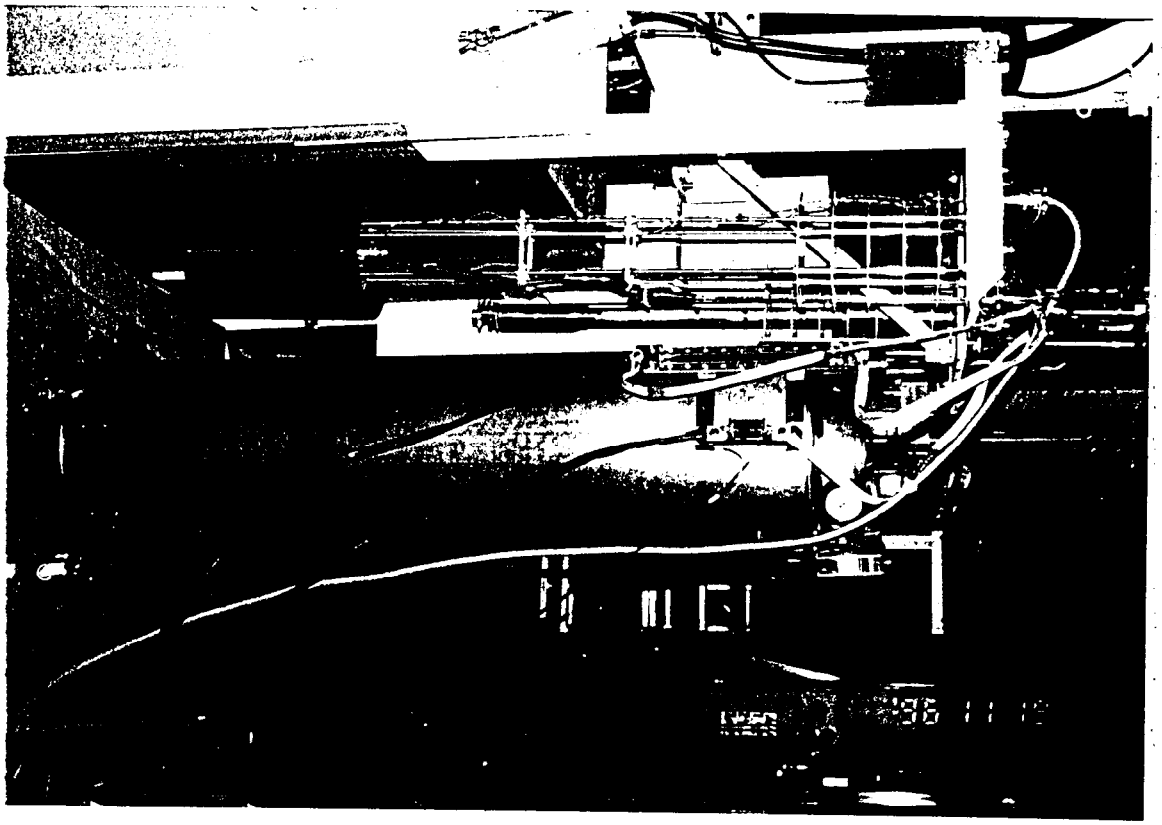

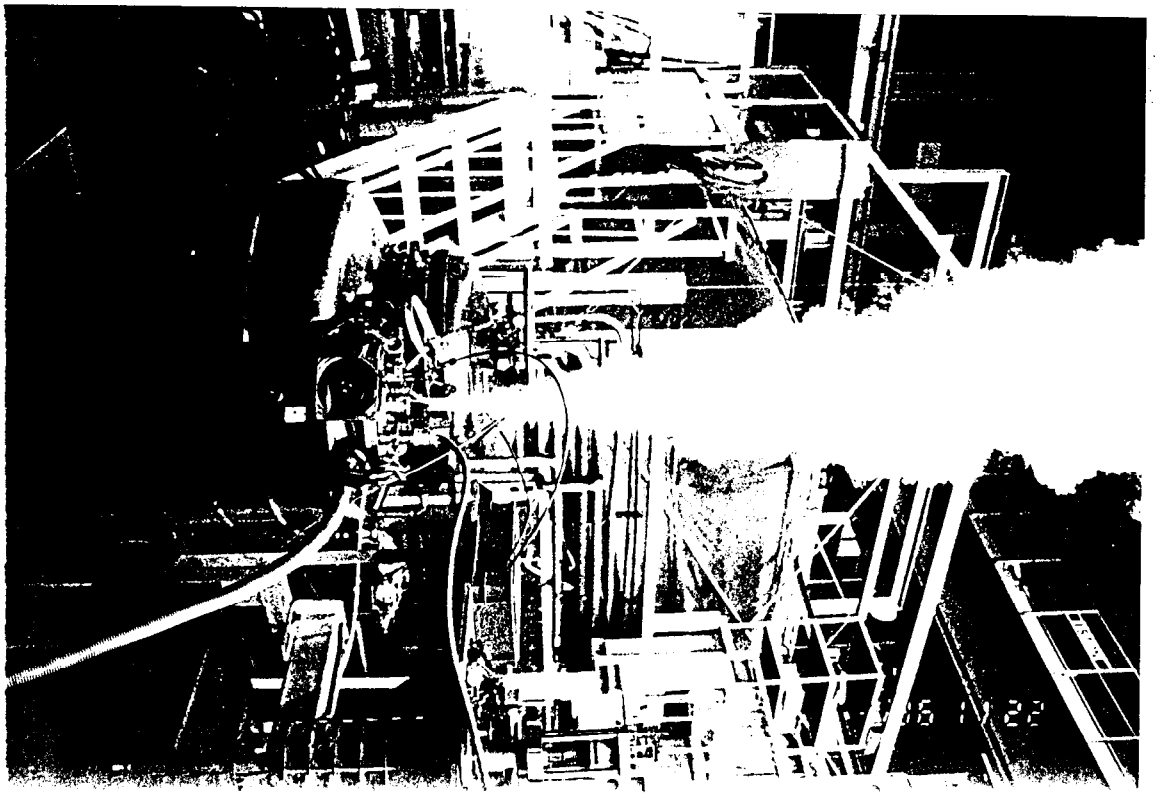

Angular and Energy distribution of γ from Target

図1 γ線の散乱角とエネルギーの関係

$E_\gamma - \theta_\gamma$ plot

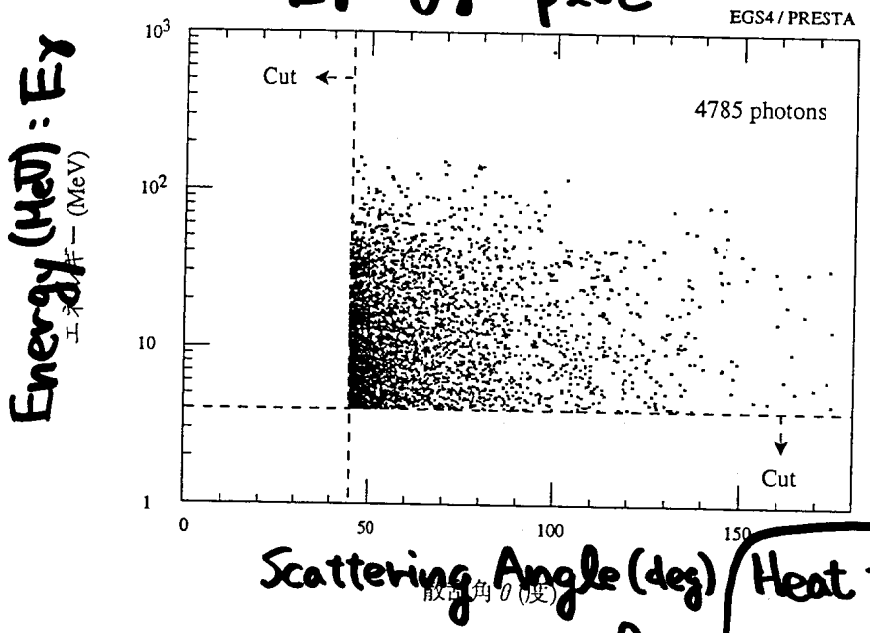

Heat by γ

2.0W $(45° \leq \theta \leq 90°)$

0.19W $(90° \leq \theta \leq 135°)$

0.028W $(135° \leq \theta \leq 180°)$

Heat from radiation γ is at most 3W.

図2 γ線のエネルギー分布

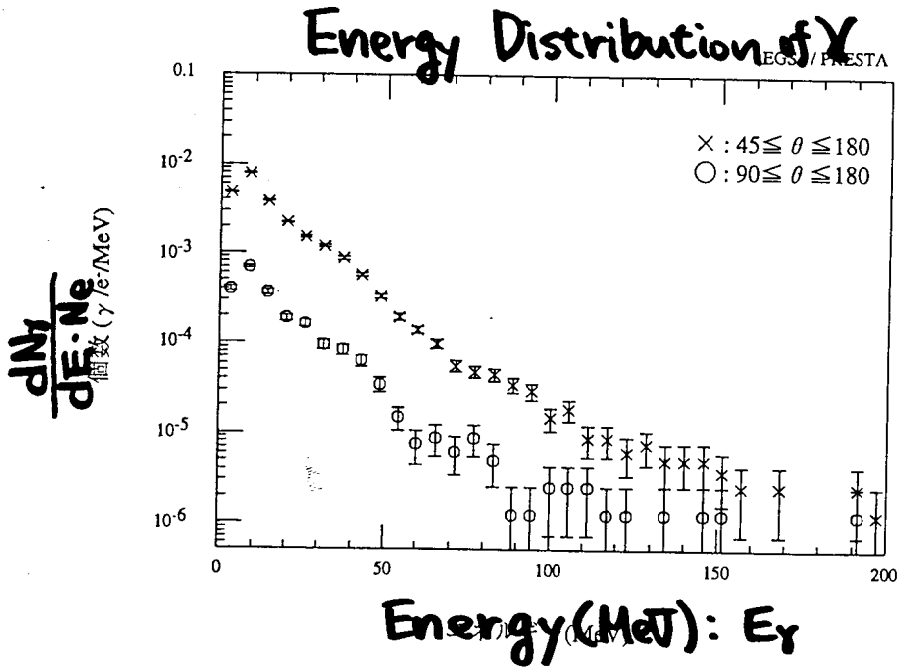

[contribution of $e^\pm$ will be negligible due to spiral orbit

unsuccessful coil (for comparison)

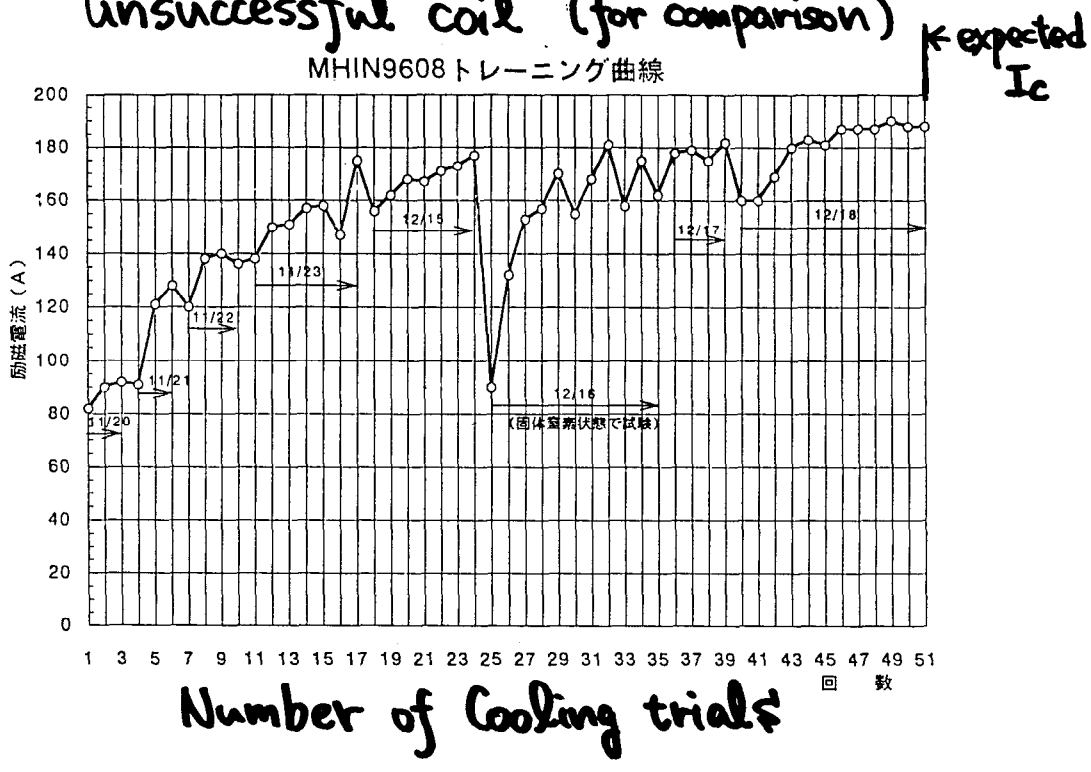

2

First prototype cooling test (Successful!)

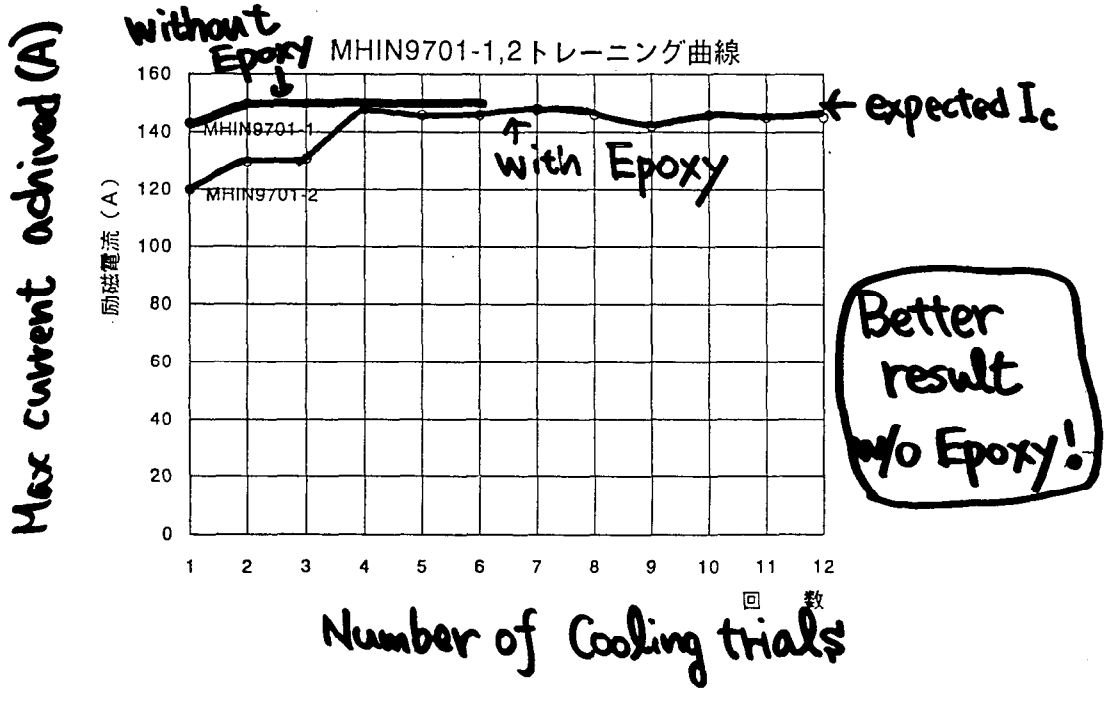

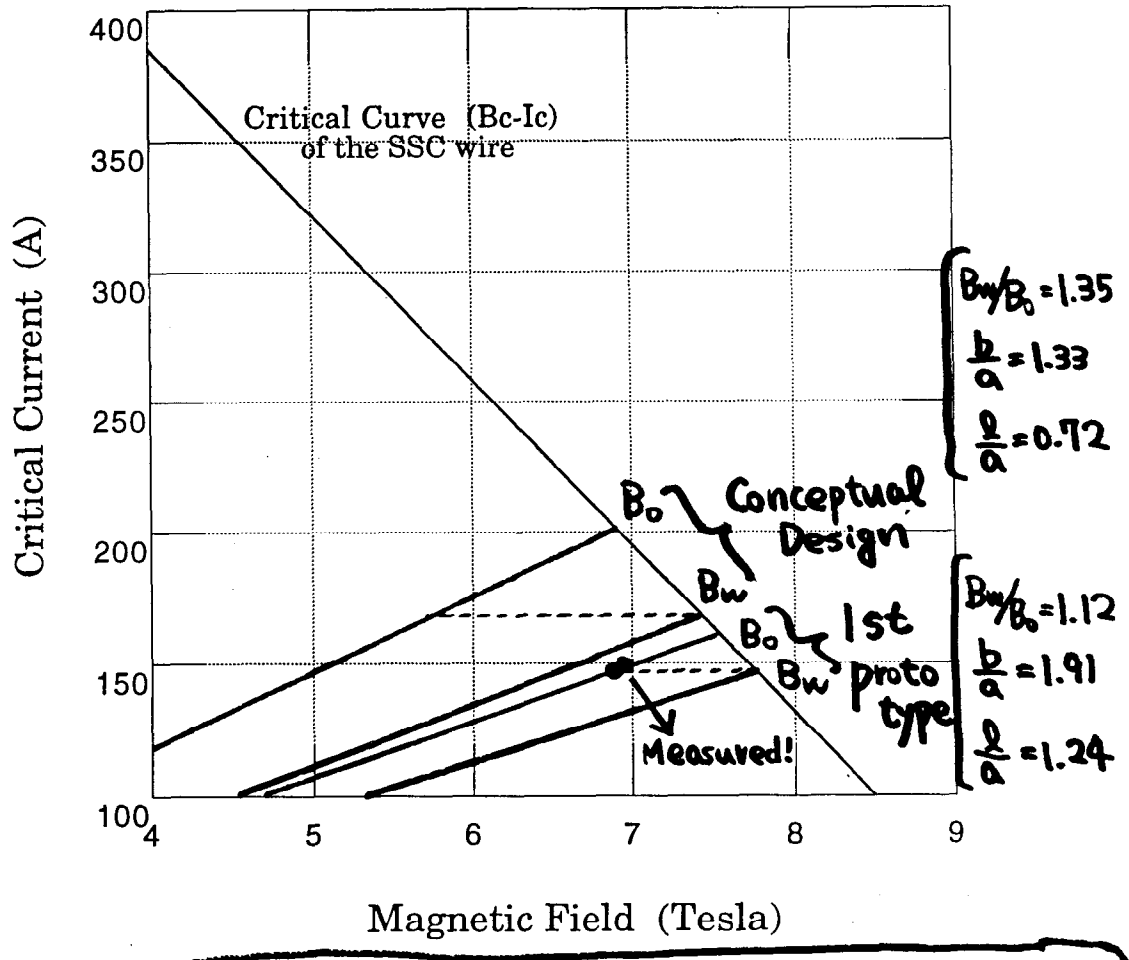

Achieved the performance which is close to the limit of wire material with 1st prototype !

Cooling Capacity Requirement

- Heat leak through Current lead (0.5W obsvd. 1st prototype) $\leq 5W$
- Heat from radiation $\leq 3W$

at most $\underline{8W}$

- Conduction Cooling? → Not enough capacity ($\leq 1W$)

⊙Liq He Transfer

$(8W)/(0.8\ W\text{-}h/\ell) = 10\ \ell/h \rightarrow 240\ \ell/day$ (Liq He)

OK!

- Stand-alone compact refrigerator

8W for HAGLEV (Magnetically Levitated Train)

Even though, total heat amount from radiation is OK,

local heating may cause quenching!

→ Need Beam test

→ Radiation Shield

Things Established with 1st prototype

① Achieved almost wire intrinsic highest magnetic field !

② Wire winding technique → OK!

③ Not use Epoxy

④ Coil current switching ~ 20sec
0A ⇄ Max current

Next to be done

① Design of 2nd prototype

Coil dimension should be determined considering,

- geometry effect on B_w/B_0
- radiation shield space
- radiation heating simulation
- e^+ yield simulation

② Fabrication of 2nd prototype coil and cryostat for beamline

③ Beam test for radiation heating (local heating)

Summary

1. Present Status on KEK e+ generator

Under the upgrade for KEKB

- e^+ intensity increase (≈20)
- primary e^- energy 0.25 -> 3.7 GeV
- New Tungusten target installed
- Better Cooling of target

Energy-spread compression

- Bunch compression for primary e^-
- Energy compression at Linac end
  - —> Can be Reduced to fit injection acceptance

2. Superconducting Solenoid

Pulsed coil (2.3 T) —> SC coil (6 T)

- e+ yield will be doubled

Prototype Cooling Test started

NLC Positron Source

Artem Kulikov
Stanford Linear Accelerator Center

Summary

A conventional source of non-polarized positrons for the NLC is presented. The source is designed to produce 1.1×10^{12} positrons per pulse at the interaction point -- more that 20 times higher than the existing SLC source was designed to produce.

The major improvement compared with the SLC source came from the use of the large aperture L-band capture and booster positron accelerators. The large transverse and longitudinal acceptances of the system improved the positron capture efficiency compared with the SLC source by approximately 3 times, and at the same time permitted a significantly increased transverse size of the drive beam at the target. The large size of the drive beam allowed more energy to be deposited in the target per accelerator pulse, producing more positrons and keeping the deposited energy density in the target at a safe level. The rotating W-Re target was designed to handle an average drive-beam power of up to 161 kW.

Transparencies

Figure 1. SLC and NLC positron sources: table of parameters.

Figure 2. Geometrical acceptance at the entrance of the capture accelerator as a function of the accelerator aperture and the drive beam size.

Figure 3. Positron collection efficiency as a function of the system transverse acceptance for the S- and L-band accelerators.

Figure 4. Main parameters of the NLC positron collection system.

Figure 5. Conceptual design of the NLC positron target.

Figure 6. 'Twin' design of the NLC positron source layout.

Figure 7. Phase space distribution of the positron beam at E=250 MeV.

Figure 8. Phase space distribution of the positron beam at E=2 GeV.

Parameter	SLC 93	SLC max design	NLC 500 GeV	NLC 1 TeV	
Scavenger Beam					
Energy Ee- (GeV)	30.00	30.00	3.11	6.22	
Intensity Ne- / bunch	3.00E+10	7.00E+10	1.50E+10	1.50E+10	
coul / bunch	4.80E-09	1.12E-08	2.40E-09	2.40E-09	
bunch length (psec)	3	3	5	5	
n bunches / pulse	1	1	90	67	
Intensity Ne- / pulse	3.00E+10	7.00E+10	1.35E+12	1.01E+12	
coul / pulse	4.80E-09	1.12E-08	2.16E-07	1.61E-07	
Beam Pulse Energy (Joules)	144	336	672	1001	
rep. rate (Hz)	120	120	180	120	
Beam Power (Watts)	1.73E+04	4.03E+04	1.21E+05	1.20E+05	x 7
Beam size , sigma (mm)	0.6	0.8	1.6	1.6	
Power Density=Ee-*Ne-/pulse/(pi*sigma^2) (GeV/mm^2)	7.96E+11	1.04E+12	5.22E+11	7.78E+11	x 0.75
Positron Collection					
Wall emittance (m)	0.01	0.01	0.06	0.06	x 6
Energy Cut at 200 MeV (MeV)	20	20	20	20	
Long. Cut at 200 MeV/c (psec	15	15	30	30	x 2
Yield/Ee- (1/GeV)	0.083	0.083	0.300	0.300	
Yield	2.50	2.50	0.93	1.87	
Intensity Ne+ / bunch	7.5E+10	1.75E+11	1.4E+10	2.8E+10	
coul / bunch	1.20E-08	2.80E-08	2.24E-09	4.48E-09	
Intensity Ne+ / pulse	7.50E+10	1.75E+11	1.26E+12	1.88E+12	x 10.7
coul / pulse	1.20E-08	2.80E-08	2.02E-07	3.00E-07	
Global					
Efficiency	0.4	0.4	0.5	0.5	
N e+ / bunch at IP	3.00E+10	7.00E+10	7.00E+09	1.40E+10	

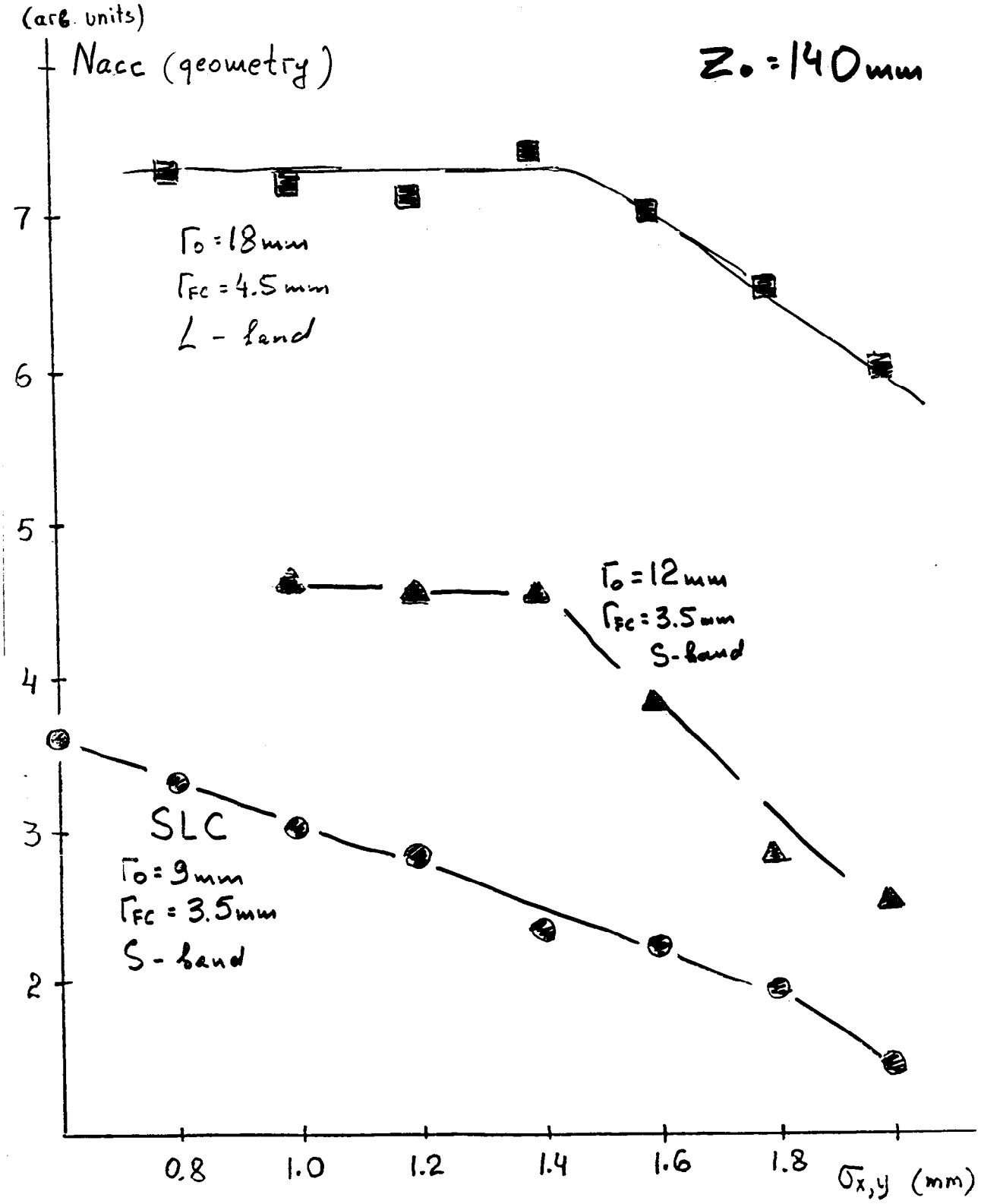
(arb. units)
Nacc (geometry)
Z₀ = 140mm
7
6
5
4
3
2
r₀ = 18mm
r_FC = 4.5mm
L - band
r₀ = 12mm
r_FC = 3.5mm
S-band
SLC
r₀ = 9mm
r_FC = 3.5mm
S - band
0.8
1.0
1.2
1.4
1.6
1.8
σx,y (mm)

$E_{e^-} = 33$ GeV ; $\sigma_x = \sigma_y = 1.6$ mm

$\sigma_t = 5$ psec

$r_{Fc} = 4.5$ mm

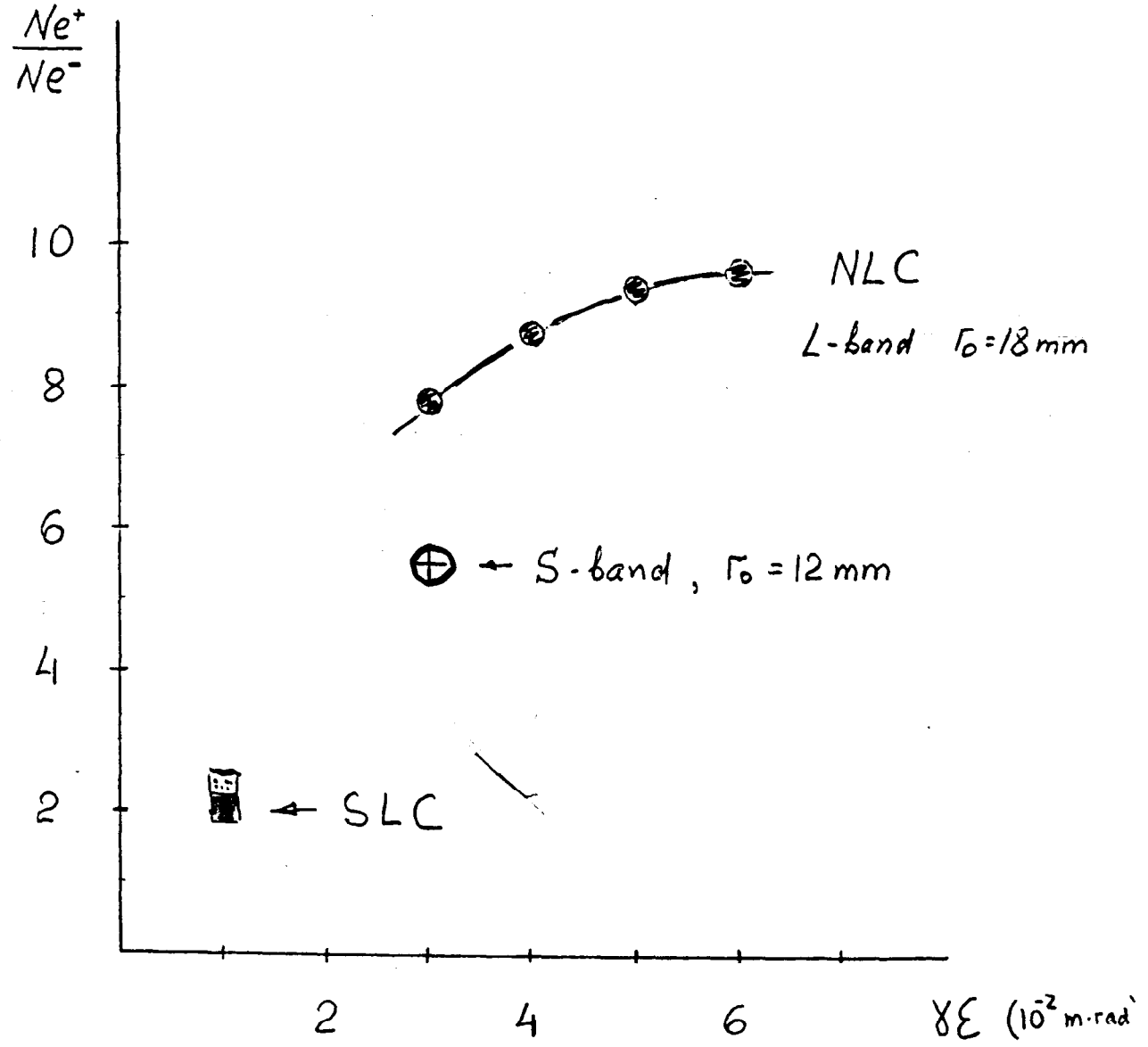

Positron Collection System

- Flux concentrator

Minimum radius:	4.5 mm
Maximum field:	5.8 T

- Tapered-field and uniform-field solenoids

Maximum field:	1.2 T
Uniform field:	0.5 T
Inner radius:	11.5 cm
Total length:	~17 m

- 2×5-meter and 2×3-meter L-band sections

Gradient:	24 MV/m (loaded)
Minimum iris radius:	20 mm (>2× SLC)

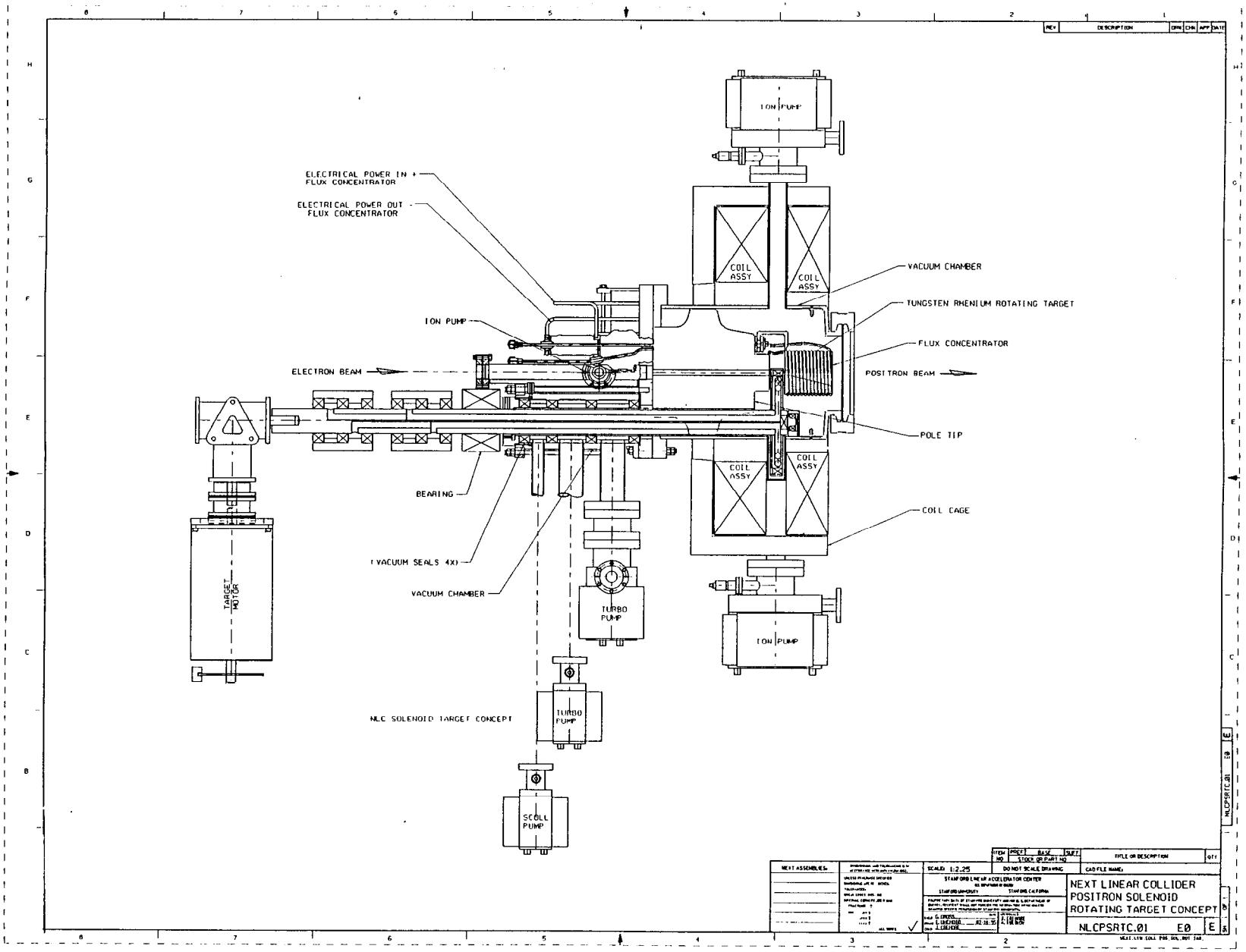
ELECTRICAL POWER IN + FLUX CONCENTRATOR
ELECTRICAL POWER OUT - FLUX CONCENTRATOR
ION PUMP
ELECTRON BEAM
BEARING
(VACUUM SEALS 4X)
VACUUM CHAMBER
TARGET MOTOR
TURBO PUMP
SCOLL PUMP
NLC SOLENOID TARGET CONCEPT
COIL ASSY
COIL ASSY
COIL ASSY
COIL ASSY
VACUUM CHAMBER
TUNGSTEN RHENIUM ROTATING TARGET
FLUX CONCENTRATOR
POSITRON BEAM
POLE TIP
COIL CAGE
ION PUMP
TURBO PUMP
ION PUMP
NEXT ASSEMBLIES
SCALED 1:2.25
DO NOT SCALE DRAWING
CAD FILE NAME:
STANFORD LINEAR ACCELERATOR CENTER
STANFORD UNIVERSITY
STANFORD CALIFORNIA
NEXT LINEAR COLLIDER
POSITRON SOLENOID
ROTATING TARGET CONCEPT
NLCPSRTC.01
E0
E

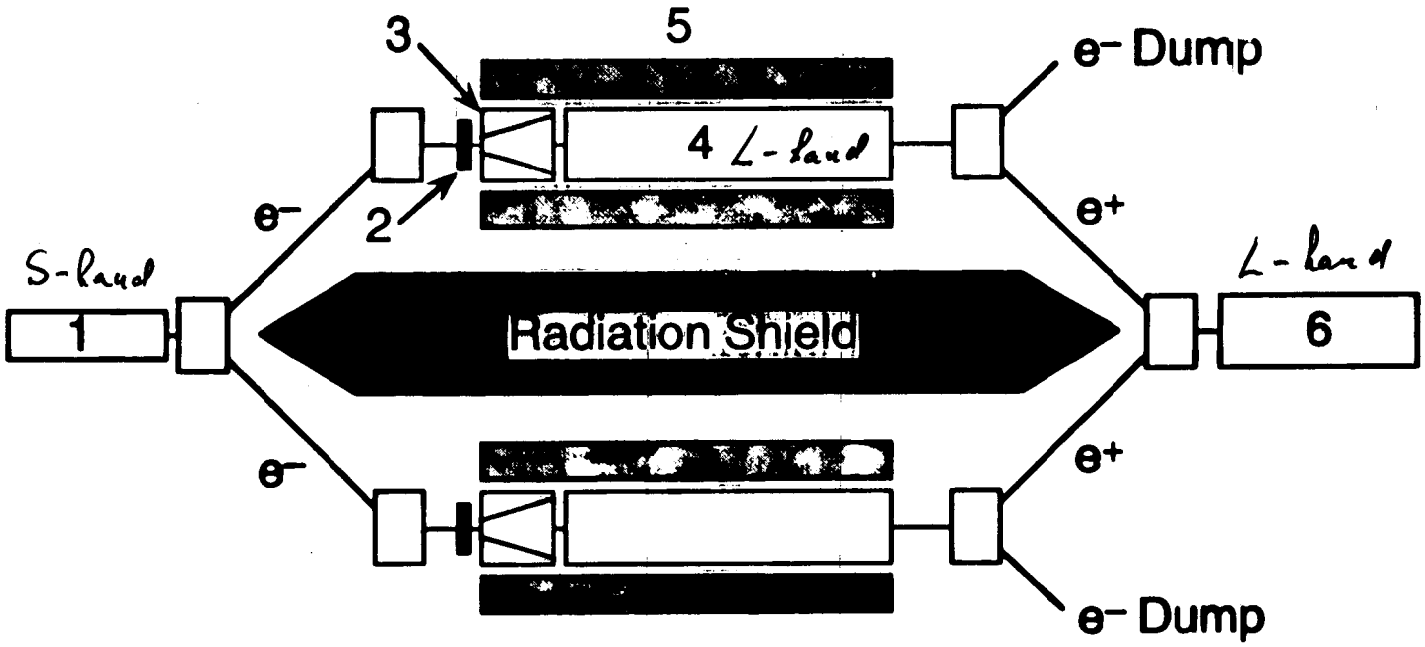
3
5
e⁻ Dump
4 L-band
e⁻
2
e⁺
S-band
L-band
1
Radiation Shield
6
e⁻
e⁺
e⁻ Dump

Phase Space Distributions of Positron Beam after Capture Accelerator (E = 250 MeV)

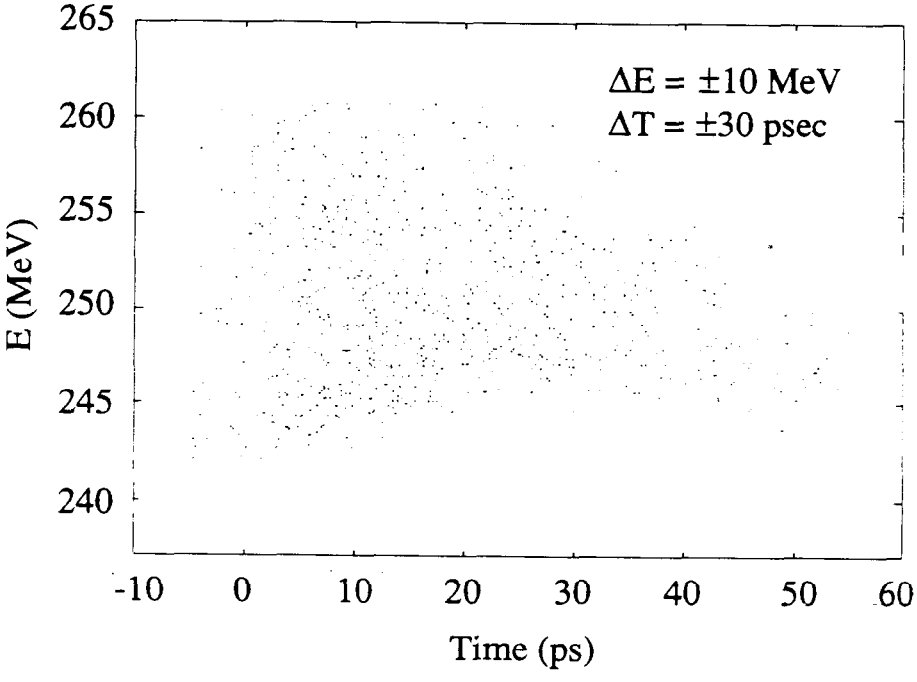

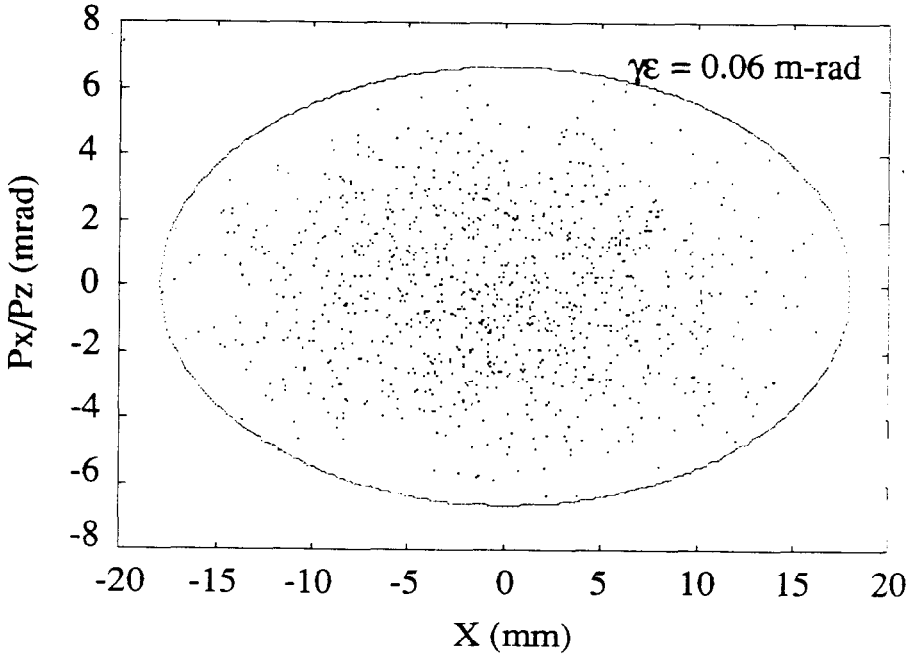

Phase Space Distributions of Positron Beam at End of Booster Linac (E = 2 GeV)

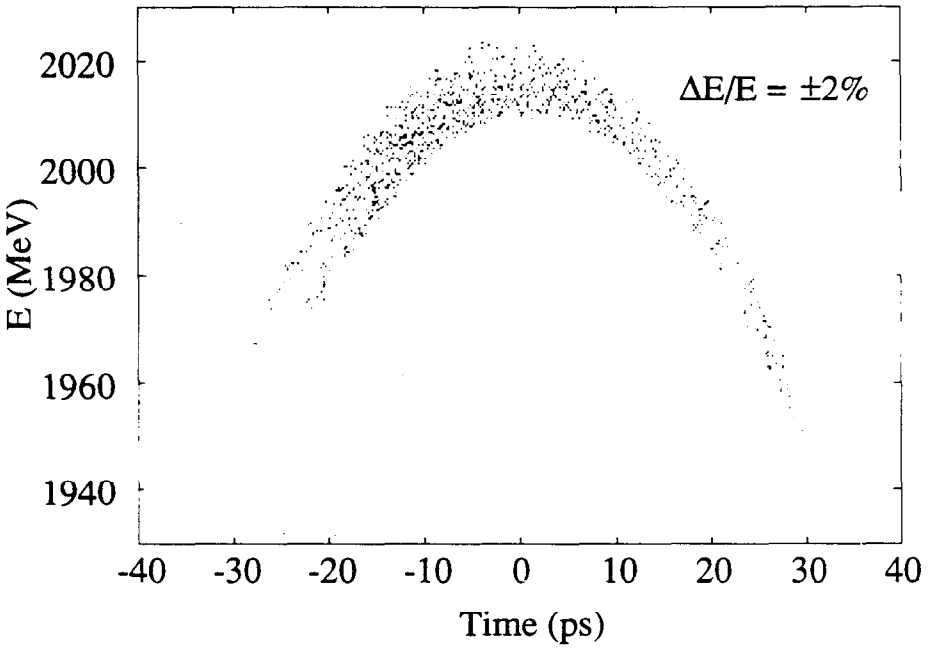

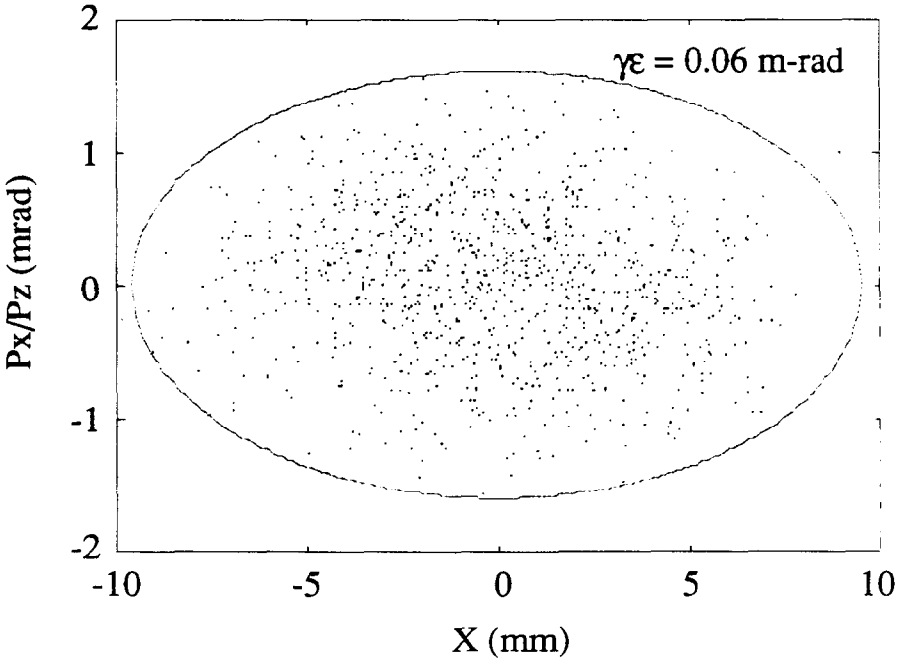

Use of Undulators at High Energy to Produce Polarized Positrons and Electrons

Alexandre A. Mikhailichenko
Cornell University

Polarized positrons, in addition to polarized electrons, can drastically increase the yield/background ratio for planned experiments with future linear colliders.

The undulator conversion system uses a ~150m undulator of ~1cm period and ~5kG field to produce circularly polarized gammas from a primary electron (or positron) beam of ~150GeV. After that, these gammas, having an energy ~20MeV with a narrow spectrum, are converted into longitudinally polarized positrons if the positron energy is restricted to the maximal one.

Here we considered the undulator conversion system properties, efficiency calculations and some possible perturbations. The conclusion is that all the desired characteristics are within present-day technological possibilities. A proposal is made to test the method using a short undulator (~4m) in the SLAC 50GeV beam.

USE OF UNDULATORS AT HIGH ENERGY TO PRODUCE POLARIZED POSITRONS AND ELECTRONS

Alexander A. Mikhailichenko
Cornell University, Ithaca, NY 14850

- **Importance of polarization**
- **A concept of conversion system for polarized e^+, e^- production**
- **Undulator radiation**
  Number of quants on harmonics
  Polarization for different harmonics as a function of angle and fractional energy

- **Undulator design**
  Codes for the field calculations
  Tested wigglers with the shortest period 7 and 10 *mm*

- **Interaction of the gammas with the matter**
  Polarization
  Cross-section

- **Calculations done for efficiency**
  Analytical calculations
  Numerical codes for gamma-positron production

- **Technical aspects of the collection system**
  Energy deposition in a target
  Dulongue-Petit law. Titanium target
  Lithium and solenoidal lenses
- **Perturbations**
  Emittance perturbation in an undulator
  Spin perturbation in an undulator
  Spin perturbation in the interaction point
  Resistive instability in an undulator chamber
  Wall irradiation

- **How to baffle the length of the undulator**
  Few targets in series
  Form-factor for Ti target

- **Proposal for SLAC accelerator**
  Undulator Converter Test Facility -**UCTF**

- **Conclusion**

• IMPORTANCE OF POLARIZATION

• High energy statement is a polarized one, so each particle of the beam looks only for an appropriate polarized one from incoming beam

So each particle can see only half of the particles from the incoming beam

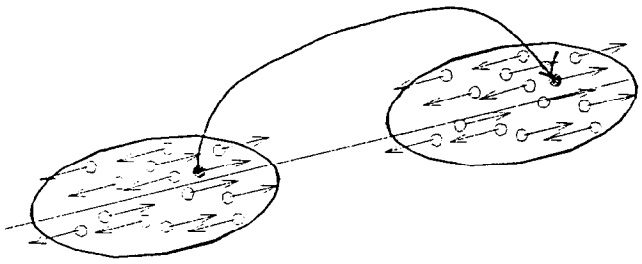

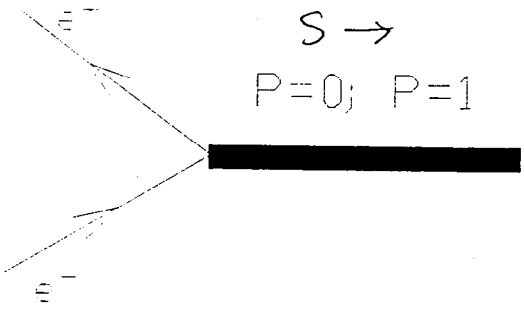

A. Likhoded, M. Shevlagin
O. Yashenko, J Mod Ph. A.
Vol 8 N 28 (1993) pp 5063

• Cross section

$$\sigma(P_z^-, P_z^-) = \frac{4\pi\alpha^2}{3s} \cdot (A_1 S_1 + A_2 S_2)$$

$$S_1 = 1 + P_z^+ P_z^- \qquad S_2 = P_z^+ + P_z^-$$

• For $\sqrt{s} = 500GeV$

$$e^- e^- \to \mu^+ \mu^- \;\rightarrow\; A_1 = 1.13 \qquad A_2 = 0.08$$

$$e^- e^- \to hadrons \;\rightarrow\; A_1 = 6.45 \qquad A_2 = 3.03$$

• Importance of polarization for seeking new bosons beyond the Standard Model discussed

The output made there, is that at the energy range $\sqrt{s} \cong 500GeV$ for the settings the Z' boson mass, the polarized beams gives the luminosity gain by ~ 5 times, or with unpolarized beams the total energy need to be 2-3 times higher.

• A CONCEPT OF CONVERSION SYSTEM FOR POLARIZED e^+, e^- PRODUCTION

- Average flux is about $10^{13} \div 10^{14}$ positrons (and electrons) per second.
- Power carried by the beams is of the order of few Megawatts

The method includes the following procedure

- Irradiate a thin (in terms of radiation length) target with circularly polarized photons of sufficient energy.
  The source of radiation might be a helical undulator.
- Collect the positrons at the top of its energy
  The positrons at the top of energy spectra has a longitudinal polarization.

This method solves the problem of the target overheating also (*by the way*)

V. Balakin, A. Mikhailichenko
1978-1979

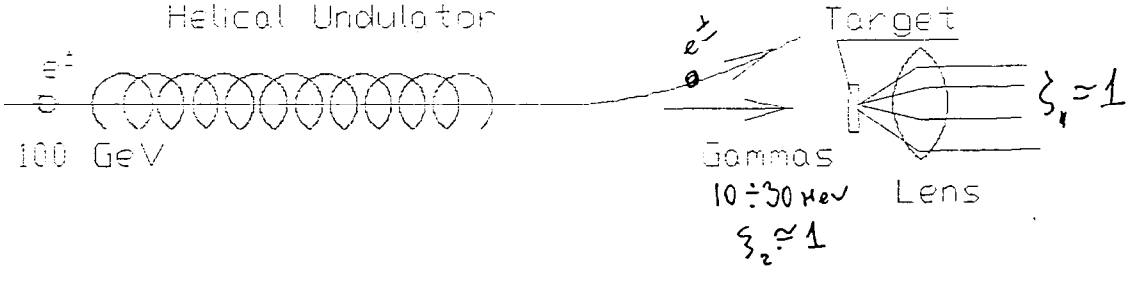

The helical undulator converter insertion

• UNDULATOR RADIATION

- The main requirements for the photon beam is the *monochomaticity, sufficient flux, polarization*
- ***Undulator*** radiation satisfy these requirements

Evgeny Bessonov

Field

$$\vec{H}_{\perp}(z) = \vec{e}_x H_{xm} Cos\frac{2\pi z}{\lambda_u} + \vec{e}_y H_{ym} Sin\frac{2\pi z}{\lambda_u},$$

x, y -- are the transverse coordinates, z is the longitudinal one,
λ_u --is the period of the undulator,
H_{xm}, H_{ym} -- are the magnetic field amplitudes in corresponding directions
Motion:

$$\bar{\beta}(t') = \{\beta_{xm} Cos\Omega t', -\bar{\beta}_{ym} Sin\Omega t', \bar{\beta} - (\delta\beta_z)_m Cos2\Omega t'\}$$

$$\vec{r}(t') = \{x_m Sin\Omega t', y_m Cos\Omega t', \bar{\beta}ct' - (\delta z_m) Sin2\Omega t'\},$$

$\Omega = 2\pi\bar{\beta}c/\lambda_u$, $\beta_{xm} = H_{ym}/H_c$, $\beta_{ym} = H_{xm}/H_c$, $(\delta\beta_z)_m = (\beta_{xm}^2 - \beta_{ym}^2)/4$,
$x_m = c\beta_{xm}/\Omega$, $y_m = c\beta_{ym}/\Omega$, $\delta z_m = c(\delta\beta_z)_m/2\Omega$, $\bar{\beta} = \beta(1 - \beta_m^2/4)$,
$\beta_m = (\beta_{xm}^2 + \beta_{ym}^2)^{1/2}$, $H_c = 2\pi mc^2/e\lambda_u \cong 10700[G \cdot cm]/\lambda_u[cm]$,
$t' = t - R(t')/c$ is the time in the moment of radiation

Helical undulator (or wiggler) has $H_{xm} = H_{ym} = H$

- Motion is circular in transverse plane
- Helix in 3D
- Circular polarization

Deflection parameter or the undulatority factor defined

$$K = \beta_{\perp}\gamma = H_{\perp}/H_c = eH_{\perp}\lambda_u/2\pi mc^2 \cong 93.4 \cdot H_{\perp}[Tesla]\lambda_u[m].$$

Induced ↔ Spontaneous

Frequency of radiation ω

$$\omega_n = \frac{n\Omega}{1-\vec{\beta}\vec{n}} \cong \frac{n\Omega}{1-\beta_{\parallel} Cos\vartheta} \cong \frac{n\Omega}{1-\beta_{\parallel}\cdot(1-\frac{\vartheta^2}{2})} \cong \frac{n\Omega}{1-\beta\sqrt{1-\frac{\beta_{\perp}}{\beta^2}}\cdot(1-\frac{\vartheta^2}{2})}$$

$$\cong \frac{n\Omega}{1-\beta\cdot\left[1-\frac{\vartheta^2}{2}-\frac{\beta_{\perp}^2}{2}\right]} \cong \frac{2n\Omega\gamma^2}{1+K^2+\gamma^2\vartheta^2} = \frac{\omega_{n\max}}{1+\frac{\gamma^2\vartheta^2}{1+K^2}}$$

n --is the number of the harmonic
ϑ -- is the angle of observation calculated from the forward direction
$\omega_{n\max} = 2n\Omega\gamma^2/(1+K^2)$ corresponding *forward* direction

That was a frequency of ***spontaneous*** radiation
For ***induced*** radiation

$$\Delta E = \int_0^{\tau} Pdt = e\int(\vec{v}_{\perp}\vec{E}_{\perp})dt = e\beta_{\perp}cE_{\perp}\int Cos\Omega t\cdot Cos\left(\omega t \mp kv_{\parallel}t+\varphi\right)dt =$$

$$= \frac{eP_{\perp}cE_{\perp}}{\gamma}\int Cos\Omega t\cdot Cos\left(\omega t\left(1\mp\frac{v}{v_p}\left(1-\frac{\beta_{\perp x}^2}{2}-\frac{\beta_{\perp y}^2}{2}\right)\right)+\varphi\right)dt = \frac{eP_{\perp}LE_{\perp}}{2\gamma}Cos\varphi$$

where $v_{\parallel} \cong \sqrt{v^2-v_{\perp}^2} \cong v\left(1-\frac{v_{\perp}^2}{2v^2}\right) \cong v\left(1-\frac{\beta_{\perp x}^2+\beta_{\perp y}^2}{2}\right)$, and it was used the resonance condition

$$\Omega \cong \omega\left(1\mp\frac{v}{v_p}\left(1-\frac{\beta_{\perp x}^2+\beta_{\perp y}^2}{2}\right)\right),$$

In case of ***co-directional*** movement of the wave and the particles

$$\Omega \cong \omega\left(1-\frac{v}{v_p}\left(1-\frac{\beta_{\perp x}^2+\beta_{\perp y}^2}{2}\right)\right) = \omega\left(1-\frac{v}{v_p}+\frac{v}{v_p}\frac{\beta_{\perp x}^2+\beta_{\perp y}^2}{2}\right) \cong$$

$$\cong \omega\left(\frac{(1-v/v_p)(1+v/v_p)}{2}+\frac{\beta_{\perp x}^2+\beta_{\perp y}^2}{2}\right) = \omega\left(\frac{1}{2\gamma^2}+\frac{\beta_{\perp x}^2+\beta_{\perp y}^2}{2}\right) = \frac{\omega}{2\gamma^2}\left(1+K^2\right)$$

$\lambda \cong \lambda_u\cdot(1+P_{\perp}^2)/(2\gamma^2)$ i.e. the **same**

• *Electromagnetic field*

$$\vec{E}(t) = \frac{e(\vec{n} \times ((\vec{n} - \vec{\beta}) \times \dot{\vec{\beta}}))}{cR(1 - \vec{n}\vec{\beta})}\Big|_{t'=t-R(t')/c}$$

$\vec{n}$ -- is the unit vector in the direction of observation

• ***Spectral angular distribution*** on the area $dS = Rdo$

$$\frac{\partial^2 \varepsilon}{\partial \omega \partial S} = c\left|\vec{E}_\omega\right|^2,$$

$\vec{E}_\omega = \frac{1}{2\pi}\int_{-\infty}^{+\infty} \vec{E}(t)\, exp(i\omega t)dt$ --is a Fourier image. t --is a time of observation.

Parameter s

$$s = \frac{\omega_n}{\omega_{n\max}} = \frac{1}{1 + \frac{\gamma^2 \vartheta^2}{1 + K^2}} \qquad \gamma\vartheta = \sqrt{(1 + K^2)(1 - s)/s}$$

Solid angle $do = 2\pi \cdot Sin\vartheta \cdot d\vartheta \cong \pi d\vartheta^2 = -\frac{\pi(1 + K^2)}{s^2\gamma^2} ds$

This angle *does not* depend on the harmonic number

• ***Spectral distribution***

$$\frac{dN_{;n}}{ds} = \frac{\pi(1 + K^2)}{s^2\gamma^2}\frac{dN_{;n}}{do} = 4\pi\alpha n M \frac{K^2}{1 + K^2} F_n(K, s),$$

$$\xi_{2n} = \frac{\sqrt{1 + K^2}}{K}\frac{2s - 1}{\sqrt{s(1 - s)}}\frac{J_n(n\kappa)J_n'(n\kappa)}{F_n(K, s)},$$

where $\kappa = 2K\sqrt{s(1 - s)/(1 + K^2)}$, $F_n(K, s) = J_n'^2(n\kappa) + \frac{1 + K^2}{4K^2}\frac{(2s - 1)^2}{s(1 - s)} J_n^2(n\kappa)$,

J_n and J_n' are the Bessel function and its derivative,

M --is the number of the wiggler periods,

$\alpha = e^2/\hbar c = 1/137$ is a fine structure constant.

• **In dipole approximation** $K \le 1$

$$F_n(K,s) =$$

$$\frac{(nK)^{2(n-1)}}{2(n-1)!(n-1)!}\left(\frac{s(1-s)}{1+K^2}\right)^{n-1}\left(1-2s+2s^2-\frac{2n}{n+1}\cdot\frac{K^2}{1+K^2}s(1-s)[1+n(1-2s+2s^2)]\right)$$

$$\xi_{2n}(K,s) = \frac{(2s-1)\left(1-\frac{2n^2+1}{n+1}\cdot\frac{K^2}{1+K^2}s(1-s)\right)}{\left(1-2s+2s^2-\frac{2n}{n+1}\cdot\frac{K^2}{1+K^2}s(1-s)[1+n(1-2s+2s^2)]\right)}$$

$$\frac{dN_\gamma}{ds} = \sum_n \frac{dN_{\gamma n}}{ds} = 4\pi\alpha M\frac{K^2}{1+K^2}\sum_n nF_n(K,s)$$

$$s = \frac{\hbar\omega_n}{\hbar\omega_{n\max}} = \frac{1}{1+\frac{\gamma^2\vartheta^2}{1+K^2}}$$

Play with "MATHEMATICA"

• ***Angular spread in the beam***

$$\vartheta_m \cong \sqrt{\gamma\varepsilon / \gamma\beta_u}$$

$\gamma\varepsilon$ -- is a normalized emittance

β_u -- is an envelope function value in the wiggler

Example :

$\beta_u \approx \lambda_u \cdot M \approx 100\ m$

$\gamma\varepsilon \approx 10^{-4}\ cm \cdot rad$

$\gamma \approx 4 \cdot 10^5$ $(200\ GeV)$

$1/\gamma \cong 2.5 \cdot 10^{-6}$

$$\vartheta_m \cong \sqrt{10^{-4} / 4 \cdot 10^9} \approx 1.6 \cdot 10^{-7}, \text{ so } \gamma\vartheta_m \cong 0.06$$

• ***Angular spread does not affect the angular distribution***

• The beam dimensions in the wiggler

$$r_\perp \cong \sqrt{\gamma\varepsilon\beta_u / \gamma} \approx \sqrt{10^{-4} \cdot 10^4 / 4 \cdot 10^5} \approx 1.6 \cdot 10^{-3} cm$$

• The 10σ criteria gives $10 \cdot r_\perp \approx 0.016 cm$ or $0.16\ mm$

what gives the idea about possible aperture of the wiggler and also an influence of the field inhomogeneties across the aperture.

$$\frac{dN_{\gamma n}}{ds} = \frac{\pi(1+K^2)}{s^2\gamma^2}\frac{dN_{\gamma n}}{do} = 4\pi\alpha n M \frac{K^2}{1+K^2} F_n(K,s)$$

• For harmonics n = 1,2 in approximation $K \le 1$

$$F_1(K,s) \cong \frac{1}{2}(1-2s+2s^2), \quad F_2(K,s) \cong 2s(1-s)(1-s+2s^2)K^2$$

$$\xi_{21} = \xi_{22} = \frac{2s-1}{1-2s+2s^2}$$

As a function of the angle

$$F_1(\vartheta) = \frac{1+\gamma^2\vartheta^2}{2(1+\gamma^2\vartheta^2)^2}, \quad F_2(\vartheta) = 2(K\gamma\vartheta)^2\frac{1+\gamma^4\vartheta^4}{(1+\gamma^2\vartheta^2)^4}$$

$$\xi_{21} = \xi_{22} = \frac{1-\gamma^4\vartheta^4}{1+\gamma^4\vartheta^4}$$

Polarization becomes linear ($\xi_{21} = \xi_{22} \cong 0$), when the angle of observation $\vartheta \cong 1/\gamma$.

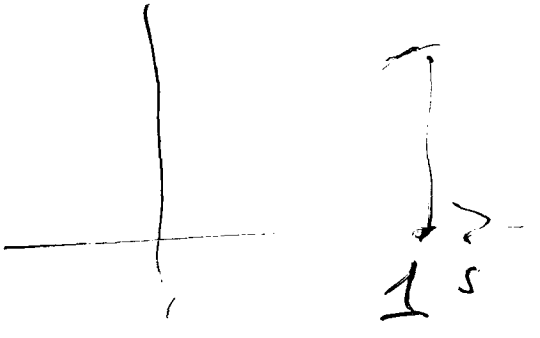

Play with "MATHEMATICA"

• **Total number of the photons** from $s = 1$ (straight forward direction), to the threshold value $s = s_t$ defined by the maximal possible angle of incoming radiation, selected by the diaphragm

$$\gamma\vartheta_t = \sqrt{(1+K^2)(1-s_t)/s_t}\,.$$

The number of the photons

$$N_{\gamma n}(K,s_t) = \int_{s_t}^{1} \frac{dN_{\gamma n}}{ds} ds = 4\pi\alpha n M \frac{K^2}{1+K^2} \int_{s_t}^{1} F_n(K,s_t) = 4\pi\alpha n M \frac{K^2}{1+K^2} \Phi_n(K,s_t)\,,$$

In approximation $\kappa = 2K\sqrt{s(1-s)/(1+K^2)} \le 1$ ($K \le 1$ or/and $\gamma\vartheta \le 1$) for harmonics with the numbers $n = 1,2$

$$\Phi_1(K,s) = \frac{1}{6}(1-s_t)(2-s_t+2s_t^2) - \frac{K^2}{2(1+K^2)}(1-s_t)^2\left(\frac{4}{15}+\frac{8}{15}s_t-\frac{1}{5}s_t^2+\frac{2}{5}s_t^3\right)$$

$$\Phi_2(K,s) =$$

$$= \frac{K^2}{10(1+K^2)}(1-s_t)^2\left[(1+2s_t-2s_t^2+4s_t^3) - \frac{20K^2(1-s_t)}{21(1+K^2)}\left(\frac{2}{15}+\frac{2}{5}s_t+\frac{4}{5}s_t^2-s_t^3+2s_t^4\right)\right]$$

Play with "MATHEMATICA"

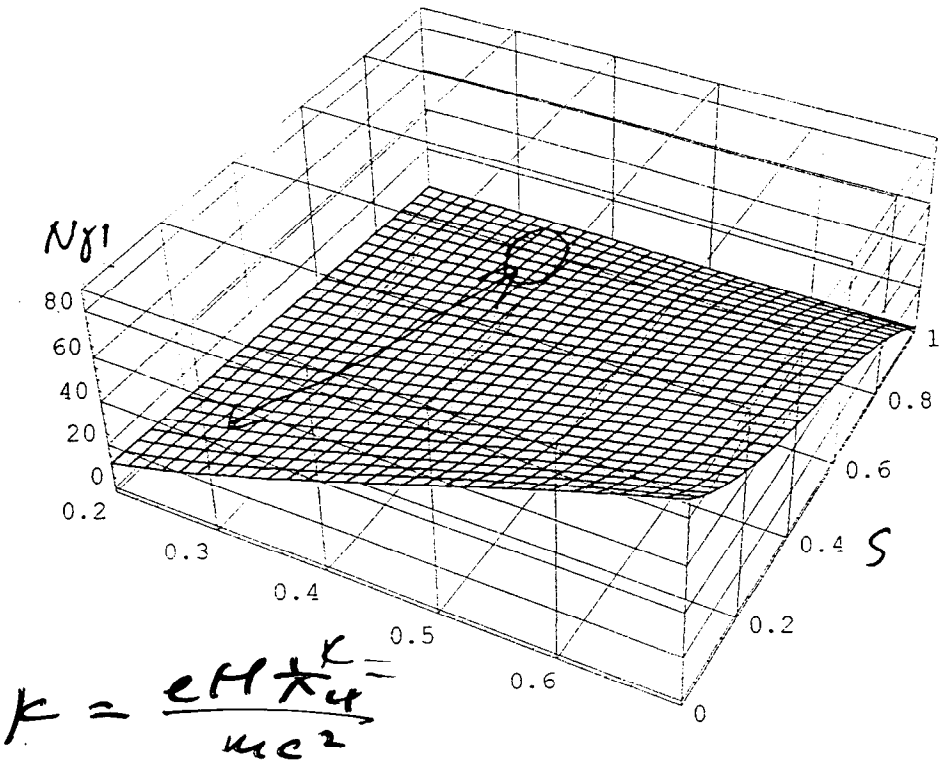

Number of the quants as a function of K and $s = \omega_n / \omega_{nmax}$. $M=10^4$.
First harmonic

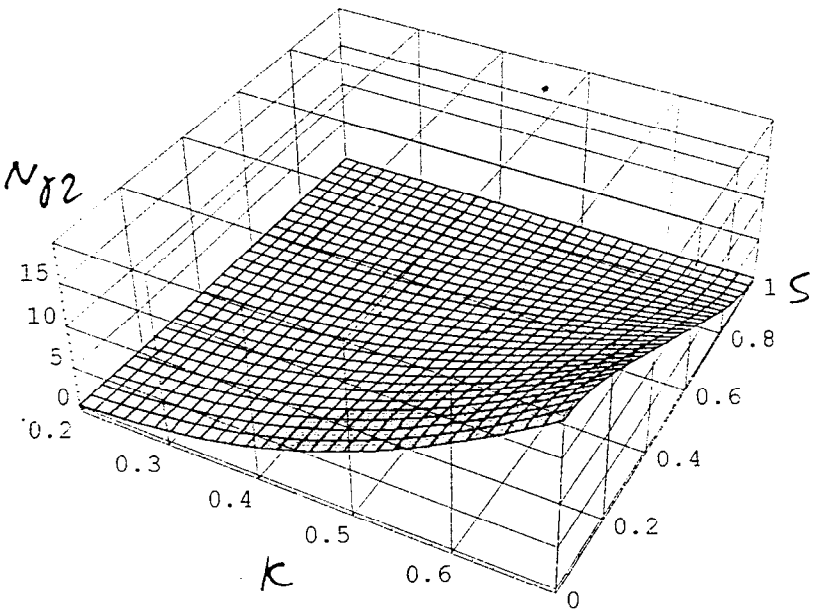

The same as above for the second harmonic.

Number of the photons on the first and the second harmonics. Number of periods $M = 10^4$

K =		0.7	0.5	0.35	0.2	0.1
s=0.9	ΔN_1	13.	8.2	4.4	1.59	0.41
	ΔN_2	1.6	0.59	0.18	0.02	.0014
s=0.8	ΔN_1	23.4	14.6	8.1	2.89	0.75
	ΔN_2	5.2	1.98	0.58	0.073	0.005
s=0.7	ΔN_1	31.3	19.8	11.1	3.98	1.032
	ΔN_2	9.6	3.6	1.1	0.13	.009
s=0.6	ΔN_1	37.8	24.1	13.6	4.9	1.27
	ΔN_2	14.3	5.37	1.6	0.2	0.013
s=0.5	ΔN_1	43.	28.1	15.9	5.79	1.5
	ΔN_2	19.	7.15	2.15	0.27	0.018
s=0.	ΔN_1	87.	56.2	31.9	11.6	3.0
	ΔN_2	38.	14.6	4.3	0.54	0.036

• ***About angular separation***

If system collects only 20% of maximal possible energy down from the maximum, i.e. $s_t \cong 0.8$

$$< \xi_{21} > \cong 0.96 , < \xi_{22} > \cong 0.95 .$$

For $s_t \cong 0.7$ (30% interval) $< \xi_{21} > \cong 0.92 , < \xi_{22} > \cong 0.89$

Level of polarization is rather high

The corresponding maximal values of the angles for selection (minimal value is zero for the forward direction) are

$$\vartheta(s_t = 0.7) = \sqrt{(1+K^2)(1-s)/s} \cong \frac{0.65\sqrt{1+K^2}}{\gamma} \text{ and } \vartheta(s_t = 0.8) \cong \frac{0.5\sqrt{1+K^2}}{\gamma} .$$

$L \approx 200\ m$ (distance between the end of helical wiggler and the target)

$\gamma \approx 4 \cdot 10^5$ (200 GeV), $1/\gamma \cong 2.5 \cdot 10^{-6}$

$K^2 \approx 0.25$,

$s_t \cong 0.8$

Corresponding radius of the diaphragm at the face of target will be

$$r_D \cong L \cdot \vartheta_s \cong 2.8 \cdot 10^{-2} cm$$

what gives the diaphragm diameter 0.56 mm

• **Not to overheat the target**

• Polarization for different harmonics as a function of angle and fractional energy. Averaged polarization.

We have

$$\xi_{21} = \xi_{22} = \frac{2s-1}{1-2s+2s^2}$$

An ***averaged*** value of circularly polarization of the photons concentrated in the solid angle between 0 and $\gamma\vartheta_t = \sqrt{(1+K^2)(1-s_t)/s_t}$ can be evaluated as

$$<\xi_{2n}>=\frac{\int_{s_t}^{1}\xi_{2n}(s)\frac{dN_{\gamma n}}{ds}ds}{\int_{s_t}^{1}\frac{dN_{\gamma n}}{ds}ds}=\frac{\int_{s_t}^{1}\xi_{2n}(s)\frac{dN_{\gamma n}}{ds}ds}{N_{\gamma n}}.$$

Substitute here the expressions for ξ_{2n}, one can obtain in approximation $K^2 \le 1$

$$<\xi_{21}>=\frac{3s_t}{2-s_t+2s_t},\quad <\xi_{22}>=\frac{5s_t}{1+2s_t-2s_t^2+4s_t^3}.$$

Play with "MATHEMATICA"

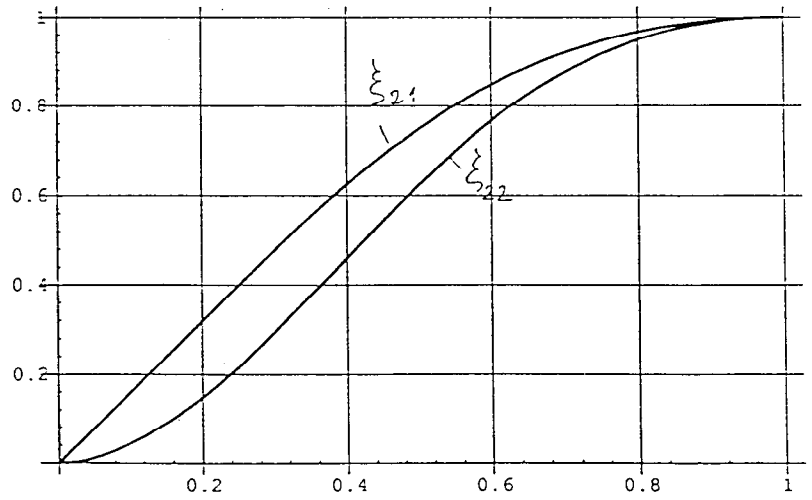

$s_t = 0$ -- absence of any selection

$s_t = 1$ -- straight forward direction

$s_t = 0.8$ -- selection in 20% down from the maximal possible energy of the quanta

• UNDULATOR DESIGN

- Helical undulator is a bifilar helix with currents opposed
- Corkscrew

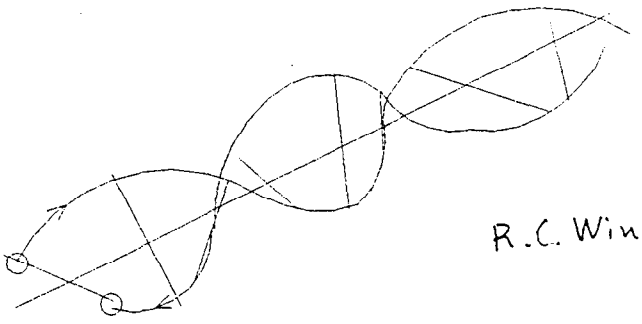

• Codes for the field calculations

Two dimensional fields with substitution of longitudinal coordinate dependence as

$$\xi = x + iy \rightarrow \xi e^{-i\varphi} = \xi \cdot exp(-i2\pi \frac{z}{\lambda_u})$$

• ONDI

Analytical formulas E. Perevedentsev

• MERMAID

Numerical code A.N. Dubrovin, E.A. Simonov

Xmin= .000000 Ymin= .000000
Xmax= 1.25000 Ymax= 1.25000

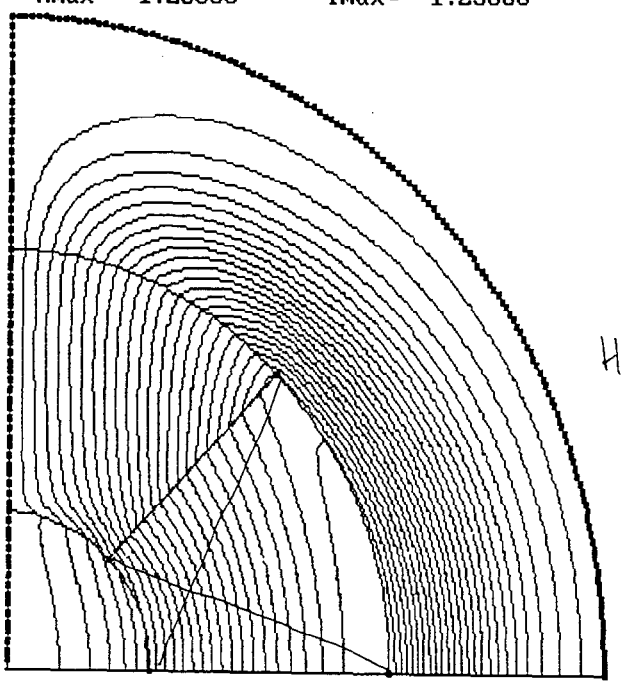

Mermaid

Helical

Flux from: -6.76484 To:-8.858999E-87 Step: .338242
Xmin= .000000 Ymin= .000000
Xmax= 1.25000 Ymax= 1.25000

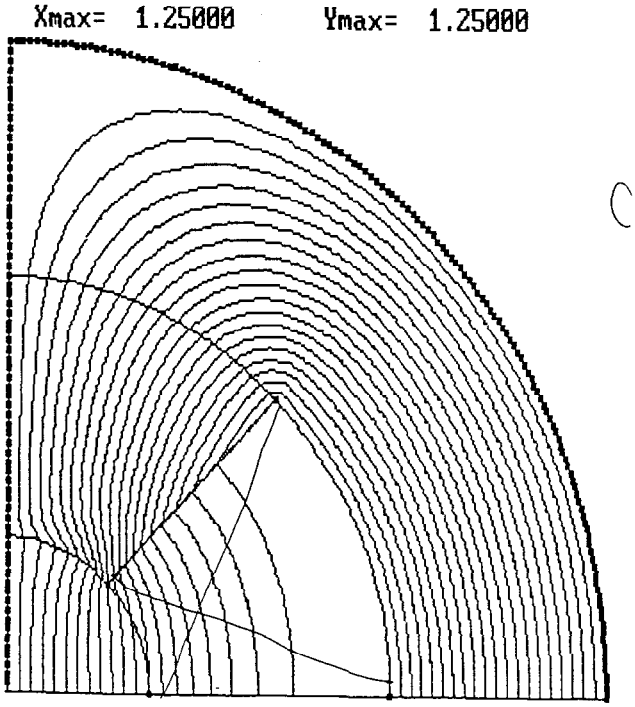

Cartesian

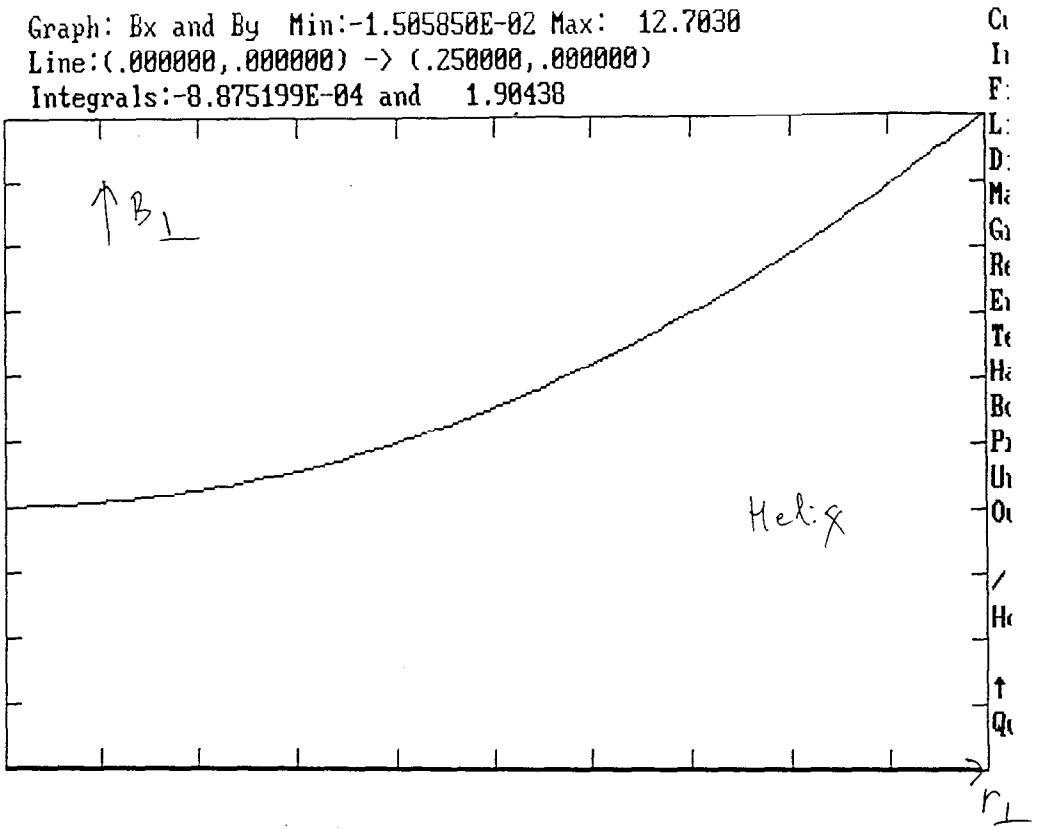
Graph: Bx and By Min:-1.505850E-02 Max: 12.7030
Line:(.000000,.000000) -> (.250000,.000000)
Integrals:-8.875199E-04 and 1.90438
$B_\perp$
Helix
$r_\perp$

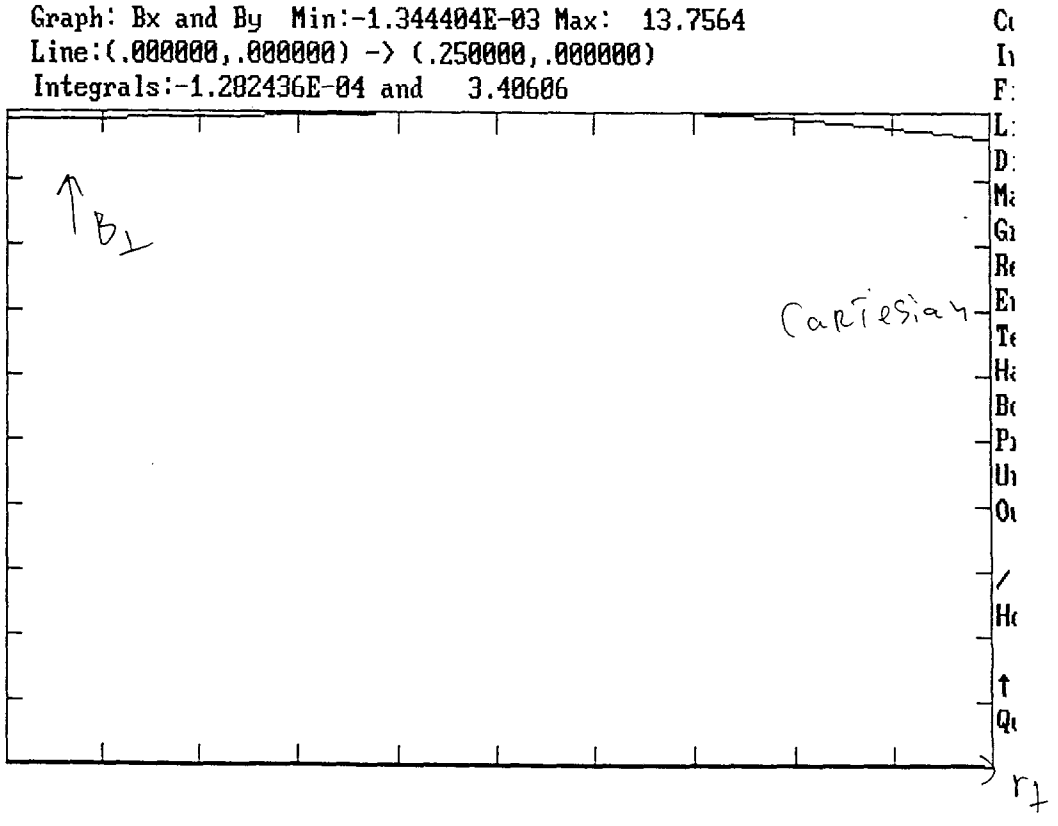
Graph: Bx and By Min:-1.344404E-03 Max: 13.7564
Line:(.000000,.000000) -> (.250000,.000000)
Integrals:-1.282436E-04 and 3.40606
$B_\perp$
Cartesian
$r_\perp$

- **Tested wigglers with the shortest period 6 and 10 *mm***

- ***Superconducting undulator***
- The current in each of 22/turn coil was around 200 A
  Period-- 1.0*cm*
  Axis field ~ 5 *kG*
  Length ~ 30 *cm*

  This undulator was supplied with the ***captured flux*** also
  That was made with the help of superconducting transformer

- ***The impulse undulator***
  Period -- 0.6 *cm* (!)
  Axis field ~ 6*kG*
  $K \cong 0.35$
  Current ~10 *kA*
  Pulse duration ~50 μsec
  Voltage ~ 1.19 *kV*
  Inductance --1.3 μH
  Repetition rate --25*Hz*

A. Cherniakin, A. Mikhailichenko
E. Perevedentsev, G. Silvestrov
T. Vsevolojskaja

S/C
30 cm
$\lambda_u = 1$ cm
$B_\perp = 5$ kG
1986

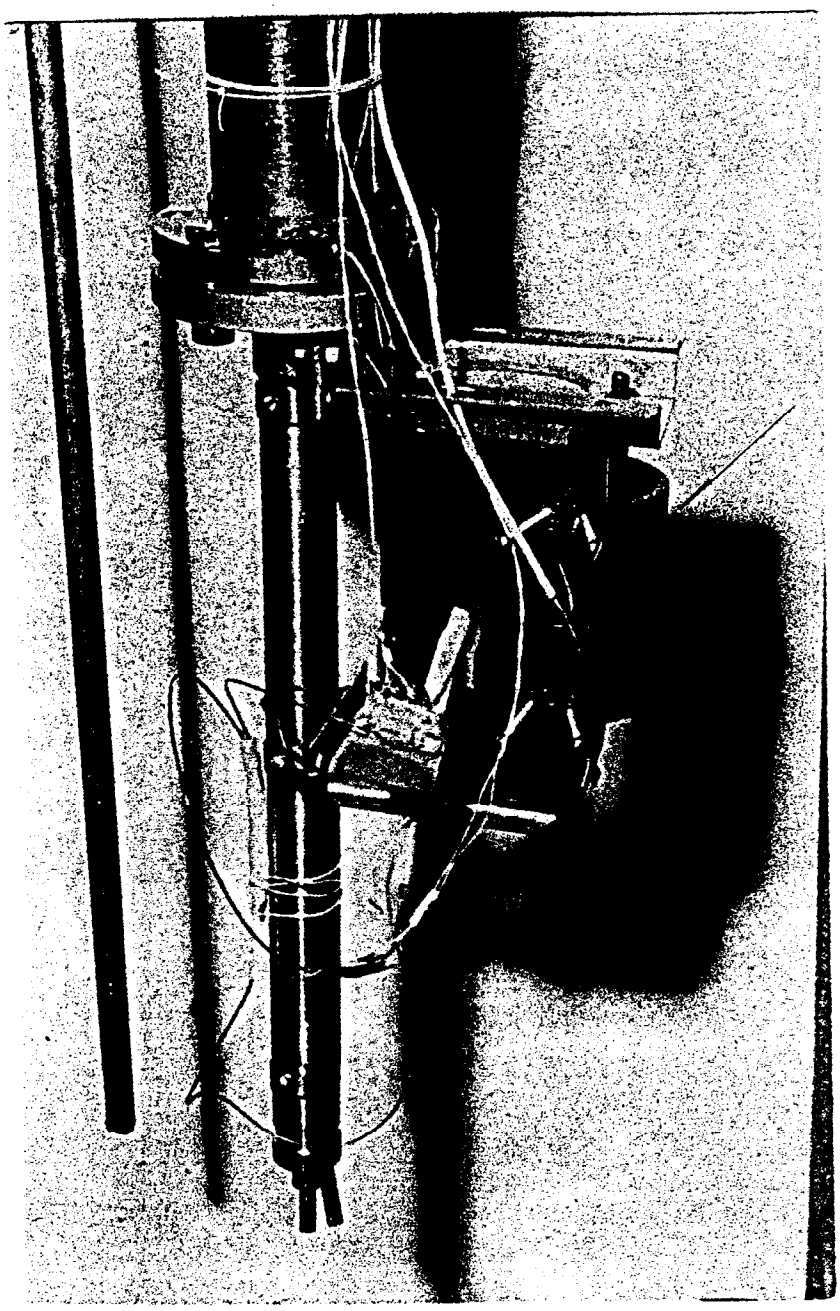

SC Transformer

Captured flux.

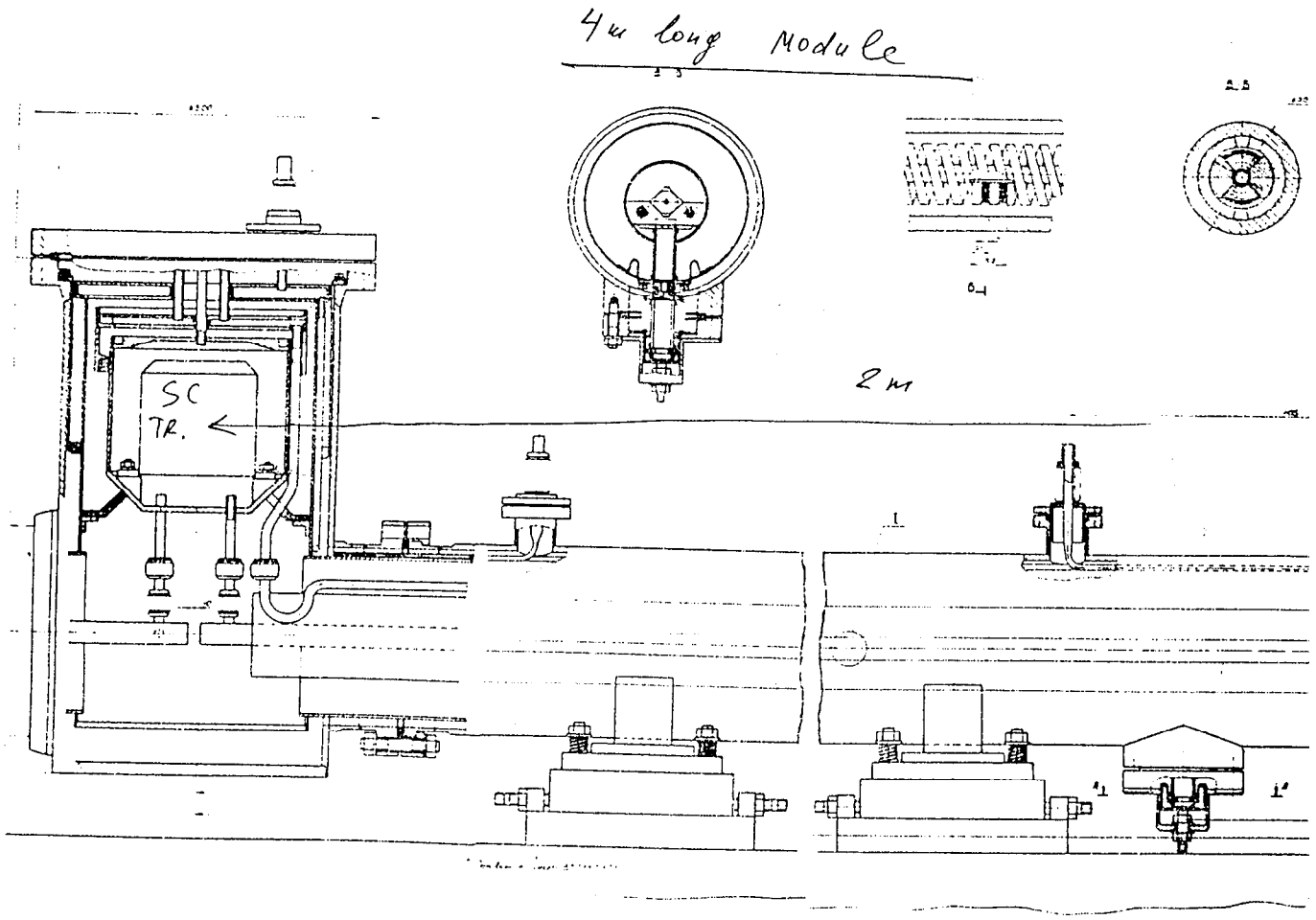
4m long Module
SC
TR.
2m

• INTERACTION OF THE GAMMAS WITH THE MATTER

• Polarization

- The transferring the polarization from the gamma to the positron and/or electron
- The longitudinal polarization of the particle created is a function of its energy, E_+, E_- and the polarization ξ_2 of the incoming gamma

V.N. Baier, V. Katkov, V. Fadin

$$\vec{\varsigma} = \xi_2 \cdot \left[f(E_+, E_-) \cdot \vec{n}_{\parallel} + g(E_+, E_-) \cdot \vec{n}_{\perp} \right] = \vec{\varsigma}_{\parallel} + \vec{\varsigma}_{\perp},$$

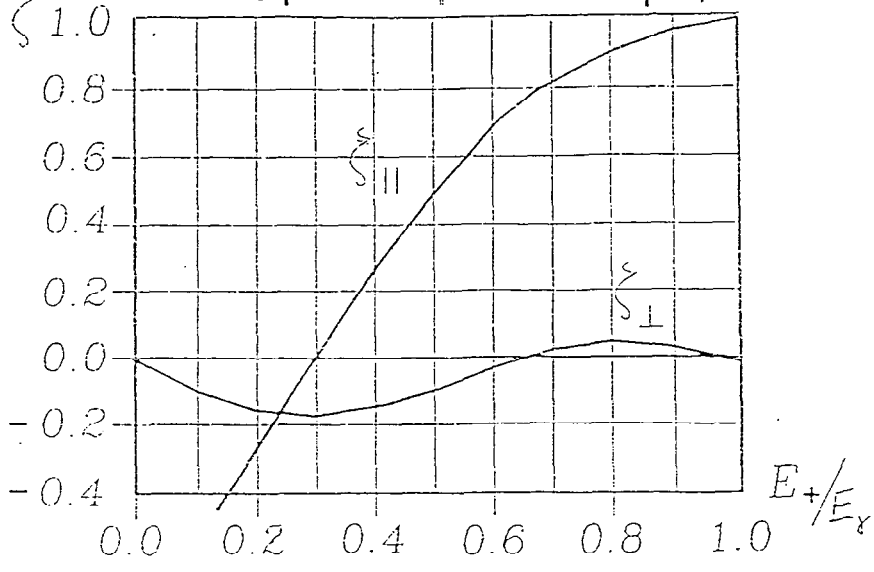

The longitudinal polarization of the positron created as a function of its fractional energy

$\vec{n}_{\parallel}$ -- is along the initial direction of the gamma radiation

$\vec{n}_{\perp}$ -- is rectangular to it

$$f = E_\gamma \frac{E_+\psi_1 - E_-(\psi_1 - 2\psi_2/3)}{(E_+^2 + E_-^2)\psi_1 + 2E_+E_-/3} = \frac{x\psi_1 - (1-x)(\psi_1 - 2\psi_2/3)}{(x^2 + (1-x)^2)\psi_1 + 2x(1-x)/3},$$

where $\psi_1 = ln183Z^{-1/3} - F(\alpha Z)$, $\quad F(\sigma) = \sigma^2 \sum_{n=1}^{\infty} \frac{1}{n(n^2+\sigma^2)}$, $\quad \psi_2 = \psi_1 - \frac{1}{6}$,

$x = E_+ / E_\gamma$.

The function f is weakly dependent of Z.

- The source of gammas must generate them with highest possible value ξ_2
- With the amount what necessary for one to one (at IP) conversion

• So, in the *first approximation*, the level of polarization of the *positrons* created, can be estimated by averaging the function $f(E_+, E_-)$, describing the longitudinal polarization of the positron

$$< \vec{\varsigma}_1 > \cong < \xi_2 > \cdot < f(E_+, E_-) > \cdot \vec{n}_1 .$$

For $E_+, E_- > E_{+max}/2$, where $E_{+max} = E_{+max}(s) = s\hbar\omega_{nmax} - 2mc^2$, the function $f(E_+, E_-)$ can be approximated

$$f(E_+, E_{+\max}) \cong 1 - 2\left(\frac{E_{+\max} - E_+}{E_{+\max}}\right)^2 = 1 - 2\left(\frac{s\hbar\omega_{n\max} - 2mc^2 - E_+}{s\hbar\omega_{n\max} - 2mc^2}\right)^2 = 1 - 2(1-x)^2,$$

where $x = \frac{E_+}{E_{+\max}}$. By averaging this expression one can obtain

$$< f(E_+, E_{+\max}) > = \frac{\int_{\Delta}^{1} [1 - 2(1-x)^2] dx}{\int_{\Delta}^{1} dx} = 1 - \frac{2}{3}(1-\Delta)^2,$$

where $\Delta = \frac{E_{+cap}}{E_{+\max}}$, E_{+cap} is the minimal energy of the positron, captured by the focusing system after the target. For $E_{+cap} \cong 0.5E_{+\max}$ (the positrons in the energy interval 50% down to the maximal possible energy) $< f(E_+, E_{+\max}) > = 1 - \frac{2}{3}(1-0.5)^2 = 0.83$, so

$$\left| < \vec{\varsigma}_1 > \right| \cong < \xi_2 > \cdot < f(E_+, E_-) > \cong 0.96 \cdot 0.83 = 0.8 .$$

i.e. rather high level of polarization. In next approximation we need to take into account that there are few of particles with maximum energy according to the $G(E_+, E_\gamma)$ dependence

$$\left| < \vec{\varsigma}_1 > \right| \cong \frac{\int_{E+cap}^{E_{+\max}} \xi_2(E_\gamma) f(E_+, E_-) \frac{d\sigma(E_\gamma, E_-)}{dE_+} dE_+}{\int \frac{d\sigma(E_\gamma, E_+)}{dE_+} dE_+},$$

where N_+ is the number of positrons in the energy interval from the maximal possible $E_{+\max} = sE_{\gamma\max} - 2mc^2$ to E_{+cap}. Notice here that the energy distribution must be taken in the moment of pair production without recalculation with the probability W.

• **Cross-section**

• ***Interaction of the photons with the nuclei***

The screening becomes important when the minimal wavelength, connected with the momentum q_{min}, transferred to the nuclei, becomes bigger, than the size of the nuclei, i.e. $\hbar / q_{min} \geq a_0 Z^{-1/3} \cong \hbar^2 / e^2 m \cdot 1 / Z^{1/3}$, where Z is the atomic number of the conversion target and it was substituted the Bohr radius value $a_0 = \hbar^2 / e^2 m$. This gives $q_{min} \leq mc\alpha Z^{1/3}$.

$E_+ \approx E_\gamma \approx 20MeV$, $Z \approx 80$, $\alpha Z^{1/3} \cong 0.03$, so $\chi \approx 32mc^2 / E_- >> 1$ no screening.

Born approximation

$$\frac{d\sigma(E_\gamma, E_-)}{d(E_- / E_\gamma)} =$$ W. Heitler

$$4\alpha Z^2 r_0^2 G(E_-, E_-^{\max}) = \alpha Z^2 r_0^2 \frac{p_- p_-}{E_\gamma^2}\left\{-\frac{4}{3} - 2E_+E_- \frac{p_+^2 + p_-^2}{p_+^2 p_-^2} + m^2c^4\left(\frac{E_+ l_-}{p_-^3} + \frac{E_- l_+}{p_+^3} - \frac{l_+ l_-}{p_+ p_-}\right) + \right.$$

$$\left. + L\left[\frac{E_\gamma^2(E_+^2 E_-^2 + p_+^2 p_-^2}{p_+^3 p_-^3} - \frac{8}{3}\frac{E_+E_-}{p_+p_-} - \frac{m^2c^4 E_\gamma}{2p_+p_-}\left(\frac{E_+E_- - p_+^2}{p_-^3} l_- + \frac{E_-E_- - p_-^2}{p_+^3} l_+ + \frac{2E_\gamma E_+E_-}{p_+^2 p_-^2}\right)\right]\right\},$$

$\alpha = e^2 / \hbar c = 1/137 \quad r_0 = e^2 / mc^2$

$l_\pm = ln\frac{E_\pm + p_\pm}{mc^2}$, $L = ln\frac{E_+E_- + p_+p_- + m^2c^4}{mc^2 E_\gamma}$ and the relation between the energy and momentum is the following $p_\pm^2 = E_\pm^2 - m^2c^4$ (c included in p, definition of [16a]).

When $E_\gamma, E_+, E_- >> 2mc^2$

$$\frac{d\sigma(E_\gamma, E_+)}{d(E_+ / E_\gamma)} \cong 4\alpha Z^2 r_0^2 \ln(183 / Z^{1/3})\hat{G}(E_+/E_\gamma) \cong \frac{A}{N_0 X_0}\hat{G}(E_+/E_\gamma),$$

A --is its atomic weight

$N_0 \cong 6.022 \cdot 10^{23}$ is the Avohadro number

X_0 --is a radiation length

$$X_0^{-1} \cong 4r_0^2 \alpha \frac{N_0}{A} Z^2 ln(\frac{183}{Z^{1/3}})[cm^2 / gramm],$$

$G(x)$ in this case

$$\hat{G}(x) = x^2 + (1-x)^2 + \frac{2}{3}x(1-x) - \frac{x(1-x)}{9\ln(183Z^{-1/3})}$$

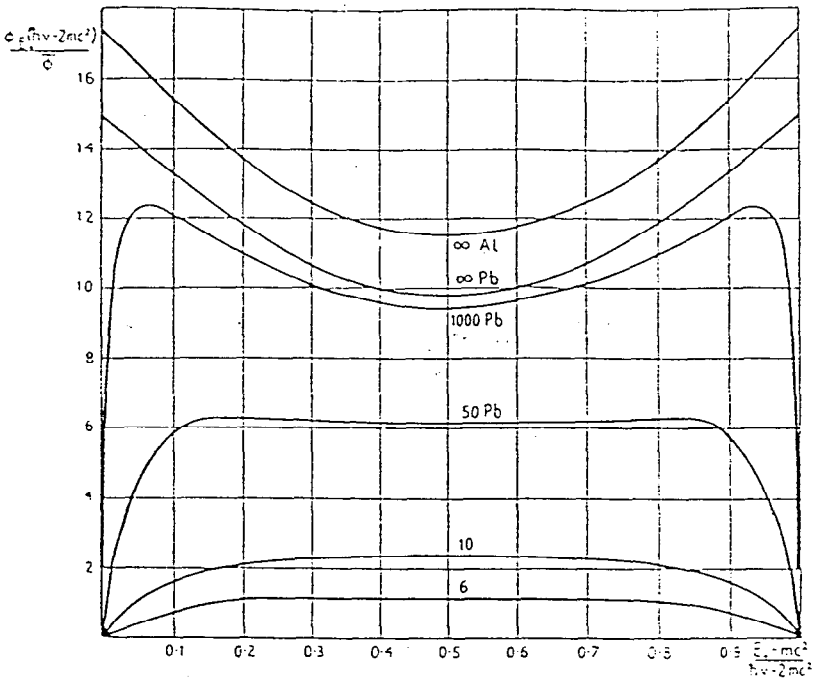

The differential cross-section of the pair production $\frac{E_\gamma - 2mc^2}{\alpha Z^2 r_0^2}\frac{d\sigma(E_\gamma, E_+)}{dE_+}$ as the function of the positron partition energy $y = \frac{E_+ - mc^2}{E_\gamma - 2mc^2}$ The numbers at the top of each curve indicates the energy of incoming quanta in units mc^2. The curves for $E_\gamma = 6, 10mc^2$ are valid for any element.

- The value at the boundary condition, when $E_+, E_- \approx E_\gamma$, is so that the function $G \to 0$

- Increasing the energy of incoming photos from 5 to 25 MeV yields increasing the efficiency about 6 times

• CALCULATIONS MADE FOR EFFICIENCY

• Analytical calculations

• ***Preliminary estimations***

Total cross-section per one atom

$$\sigma_{tot} \cong \int_0^1 \frac{A}{N_0 X_0} G(x) dx \cong \frac{7}{9} \frac{A}{N_0 X_0}.$$

The number of the atoms N in the volume $d \times 1cm^2$

$$N = N_0 \frac{g[g/cm^3] \cdot 1cm^2 \cdot d[cm]}{A[g]}$$

g -- is the specific weight of the target material

The number of the positrons at the exit of the target

$$N_+ \cong N_\gamma \sigma_{tot} N \cong \frac{7}{9} N_\gamma \frac{gd}{X_0} = \frac{7}{9} N_\gamma \delta$$

$\delta = \frac{gd}{X_0}$ --is the target thickness (length), measured as a fraction of the radiation length

d -- is the thickness of the target

Let 1/5 of all positrons only carrying the necessary level of polarization, $\delta \leq 0.5$

$$N_+ / N_\gamma \approx \frac{7}{9} \cdot \frac{1}{5} \cdot 0.5 = 0.077, \text{ or } 7.7\%$$

This estimation looks very close to that obtained from numerical calculation

We supposed also, that the phase volume of the positrons created, corresponds mostly to multiscattering in a target, and the particles could be accepted by appropriate collecting system

• For obtaining the formula, describing the spectrum of the positrons created, we can write

$$\frac{d^2N_+}{dE_+d\tau}=\frac{1}{\sigma_{tot}}\iint\frac{d\sigma(E_\gamma,E_+)}{dE_+}\frac{d^2N_\gamma}{dE_\gamma dS}dE_\gamma dS,$$

where $\frac{d^2N_\gamma}{dE_\gamma dS}=\frac{d^2N_\gamma}{dE_\gamma R^2do}$ is the spectral density of the photon source, illuminating the target, $dS=R^2do$, do is the solid angle, R is the distance from the source to the target.

• The probability WdE_+ that the positron, created by the photon at the depth τ with initial energy E_+, will have the energy in the interval from E_+^{out} to $E_+^{out}+dE_+^{out}$ at the output of the target, is described by the formula B. Rossi

$$W(E_+,E_+^{out},\delta-\tau)dE_+^{out}=\frac{dE_+^{out}}{E_+}\cdot\left(ln\frac{E_+}{E_+^{out}}\right)^{(\delta-\tau)/ln2-1}\Big/\Gamma\left(\frac{\delta-\tau}{ln2}\right),$$

where $\Gamma(x)=\int_0^\infty t^{x-1}e^{-t}dt$ is the Gamma function

The number of the positrons, generated by the photon flux, having spectral-angular density $d^2N_\gamma/dE_\gamma dS$, and with the initial energy in the interval from E_+ to E_++dE_+ and leaving the converter at the energy interval from E_+^{out} to $E_+^{out}+dE_+^{out}$ is

$$\frac{d^2N_+}{dE_+dE_+^{out}}=\int\frac{d^2N_+}{dE_+d\tau}\cdot exp(-\frac{7}{9}\tau)\cdot W(E_+,E_+^{out},\delta-\tau)d\tau\ ,$$

• The energy spectrum at the output of the target

$$\frac{d^2N_+}{dE_+^{out}}=\int\frac{d^2N_+}{dE_-dE_+^{out}}dE_+=$$

$$=\frac{1}{\sigma_{tot}}\int\frac{d\sigma(E_\gamma,E_-)}{dE_-}\frac{d^2N_\gamma}{dE_\gamma dS}\cdot\exp(-\frac{7}{9}\tau)W(E_+,E_+^{out},\delta-\tau)d\tau dE_+dE_\gamma dS$$

where the factor $exp(-\frac{7}{9}\tau)$ reflects the photon flux attenuation by the target

• The spectral angular distribution of the gammas from undulator has a form

$$\frac{d^2N_\gamma}{dE_\gamma dS}=\sum_n\frac{d^2N_{\gamma n}}{dE_\gamma dS}=\sum_n\frac{1}{E_{\gamma n}}\frac{d^2\varepsilon_n}{dE_\gamma dS}=\sum_n\frac{1}{E_{\gamma n}R^2}\frac{d^2\varepsilon_n}{dE_\gamma do}=\sum_n\frac{1}{E_{\gamma n}R^2(\gamma\vartheta)}\frac{M}{E_{\gamma 1}}\frac{\partial\varepsilon_n}{\partial o}Sinc^2\sigma_n,$$

where $Sinc(x)=Sin(x)/x$, $\sigma_n=\pi nM\frac{(\omega-\omega_n)}{\omega_n}$, M is the number of periods in the undulator. When $M>>1$, $Sinc^2\sigma_n\cong\frac{E_{\gamma 1}}{M}\delta(\omega-\omega_n(\gamma\vartheta))$, so

$$\frac{d^2N_{\gamma n}}{dE_\gamma dS}=\frac{1}{E_{\gamma n}}\frac{d^2\varepsilon_n}{dE_\gamma dS}=\frac{1}{\hbar\omega_n(\gamma\vartheta)}\frac{1}{R^2(\gamma\vartheta)}\frac{\partial\varepsilon_n}{\partial o}\delta(\omega-\omega_n(\gamma\vartheta)).$$

For positrons

$$\frac{d^2N_+}{dE_+^{out}}=\frac{1}{\sigma_{tot}}\int\frac{d\sigma(E_\gamma,E_+)}{dE_+}\frac{d^2N_\gamma}{dE_\gamma dS}\cdot\exp(-\frac{7}{9}\tau)W(E_+,E_+^{out},\delta-\tau)d\tau dE_+dE_\gamma dS$$

$L_u=M\lambda_u<<L$

for finite distances

• We need to average the flux

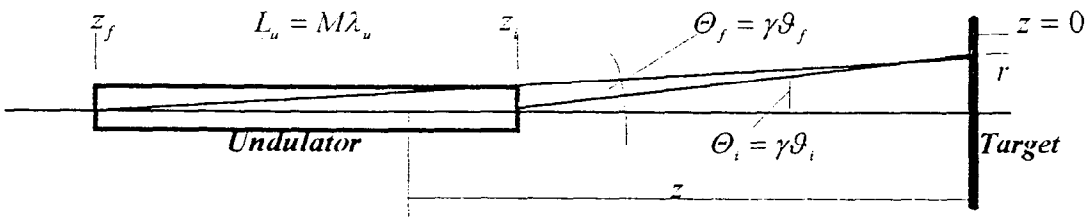

So the spectral density of the energy falling onto the converter 's area dS becomes

$$\frac{d^2N_m}{dE_\gamma dS} \rightarrow$$

E. Bessonov

$$\frac{1}{L_u}\int_{z_i}^{z_f}\frac{d^2N_m}{dE_\gamma dS}dz = \frac{1}{M\lambda_u}\int_{z_i}^{z_f}\frac{1}{R^2(\vartheta)}\frac{\partial N_m}{\partial o}\delta(\omega-\omega_n(\vartheta))dz = \frac{1}{M\lambda_u r}\int_{\vartheta_i}^{\vartheta_f}\frac{\partial N_m}{\partial o}\delta(\vartheta-\vartheta(\omega_n))\frac{\partial\vartheta}{\partial\omega}d\vartheta$$

$$\vartheta = -\tan^{-1}(\frac{r}{z}) \cong -\frac{r}{z}$$

$$R(\vartheta)\cong z,\ \frac{dz}{z^2} = -\frac{d\vartheta}{r}\ ,\qquad \delta(\omega-\omega_n(\vartheta)) = \delta(\vartheta-\vartheta(\omega_n))\cdot\frac{\partial\vartheta}{\partial\omega}.$$

$$\frac{\partial N_m}{\partial o} = 4\alpha nM\frac{s^2\gamma^2K^2}{(1+K^2)^2}F_n(K,s)$$

• Finally, the number of photons on n-th harmonic

$$N_m = 2\pi\iint\frac{dN_m}{dSdE_\gamma}dSdE_\gamma = \frac{4\pi\alpha\gamma K^2}{\lambda_u(1+K^2)^{3/2}}\int_0^{r_m}rq_n(K,r_m)dr = \frac{4\pi\alpha\gamma K^2}{\lambda_u(1+K^2)^{3/2}}Q_n(K,r_m),$$

$$q_n(K,s) = \frac{n}{r}\int_{s_i}^{s_f}\sqrt{\frac{s}{1-s}}F_n(K,s)ds,$$

$$s_i = \frac{1}{1+\frac{\gamma^2(r/z_i)^2}{1+K^2}},\quad s_f = \frac{1}{1+\frac{\gamma^2(r/z_f)^2}{1+K^2}}$$

r_m is the radius of the target (the radius of the diaphragm installed before the target).

• For the first harmonic

$$N_{\gamma 1} = \frac{4\pi\alpha\gamma K^2}{\lambda_u(1+K^2)^{3/2}}\left[\frac{1}{2}\frac{\gamma r_m^2}{\sqrt{1+K^2}}\left(\frac{1}{z_f}-\frac{1}{z_i}\right)-\frac{5\gamma^3r_m^4}{24(1+K^2)^{3/2}}\left(1+\frac{4}{5}\frac{K^2}{1+K^2}\right)\left(\frac{1}{z_f^3}-\frac{1}{z_i^3}\right)\right]$$

- The ***number of the positrons*** in the energy interval $\Delta E_{+cup} = E_{yn}^{\max} - 2mc^2 - E_{+cup}$ created by the undulator radiation on the n-th harmonic

$$\Delta N_{+n}(E_+^{out}, E_+^{\max}) \cong \frac{\alpha K^2 \delta}{c\gamma \log(183 Z^{-1/3})} \Gamma_n ,$$

where

$$\Gamma_n = \int_0^{r_w} dr \int_{s_f}^{s_i} \frac{F_n ds}{\sqrt{s(1-s)}} \int_{E_{+cup}}^{E_+^{\max}} G(E_+, E_+^{\max}) \hat{Y}(E_+, E_+^{out}) dE_+ ,$$

$$\hat{Y} = \frac{1}{\delta} \int_{E_+^{cup}}^{E_+} dE_+^{out} \int_0^{\delta} I(E_+, E_+^{out}) d\tau = \frac{1}{\delta} \int_{E_+^{cup}}^{E_+} dE_+^{out} \int_0^{\delta} \exp(-\frac{7}{9}\tau) W(E_+, E_+^{out}, \delta - \tau) d\tau ,$$

and function $\hat{Y}$ defines the share of the positrons produced with the energy E_+, that have the out energy in the interval $\{E_+, E_+^{out}\}$. One can evaluate

$$\hat{Y}\left(\frac{E_+}{E_+^{out}}\right) \cong \frac{\ln 2}{\delta \ln \Delta} (1 - \Delta^{\delta/\ln 2}) ,$$

where $\Delta \cong \frac{E_+ - E_+^{out}}{E_+}$. For thin target $I(E_+, E_+^{out}) \cong \delta(E_+ - E_+^{out})$ and hence $\hat{Y} \approx 1$.

• Finally

$$\Delta N_{+n}(E_+^{out}, E_+^{\max}) \cong \frac{\alpha K^2 E_+^{\max} \delta Q_n}{c\gamma m \log(183 Z^{-1/3})} \int_{\zeta_{cap}}^{1} G(\zeta) d\zeta ,$$

$$\zeta_{cap} = \frac{E_+^{cap} - 2mc^2}{s_t E_\gamma^{\max} - 2mc^2}$$

$$\int_{\zeta}^{1} G(x)dx \cong -0.773 + \zeta - 0.681\zeta^2 + 0.454\zeta^3$$

For n=1 , $r_m = \kappa r^* = \kappa z_f \frac{\sqrt{1+K^2}}{\gamma}$

$$\Delta N_{+1} \cong 3 \cdot 10^{-2} \kappa^2 M \delta \frac{K^2}{1+K^2} \frac{z_f}{z_i} (1 - \zeta_{cap})$$

For $\kappa = 1/2$, $M = 10^4$, $\delta = 0.2$, $K = 1$, $z_f = M\lambda_u = 2z_i$, $\zeta_{cap} = 0.7$

$$\Delta N_{+1} \cong 5$$

• ***The changing*** of the $\varsigma_{\parallel}$, when the particle goes from the point of creation τ to the output surface of the target is described by the length of depolarization $l_{dep} \cong 3X_0$ so

$$\varsigma_{\parallel out} = \varsigma_{\parallel} \cdot \exp(-\frac{\delta - \tau}{3X_0})$$

V.N. Baier, V. Katkov
V. Fadin

Thickness of the target $\delta \le X_0 / 2$

Radiativ depolarization in the target after creation in less than

$$\exp(-\frac{1}{2 \cdot 2 \cdot 3}) \cong 1 - \frac{1}{12} \cong 0.917$$

additional factor 1/2 reflects the mean path length of the individual positron in the target

• Numerical calculations shows that the mean path length even less than 1/2 reflecting the total tendency that the particles created at the out side of the target have more probability to come out of the target

• The expression for polarization

$$\left| < \vec{\varsigma}_{\parallel} > \right| \cong$$

$$\frac{1}{\delta} \frac{\iiint \int_{E-cap}^{E_{+max}} \xi_2(E_\gamma) f(E_-, E_-) \frac{d\sigma(E_\gamma, E_+)}{dE_-} \frac{d^2 N_\gamma}{dE_\gamma dS} \exp(-\frac{7}{9}\tau) \exp(-\frac{\delta - \tau}{3X_0}) dE_+ d\tau dE_\gamma dS}{\int \frac{d\sigma(E_\gamma, E_-)}{dE_+} \frac{d^2 N_\gamma}{dE_\gamma dS} \exp(-\frac{7}{9}\tau) dE_+ d\tau dE_\gamma dS}$$

Play with "MATHEMATICA"

• **Numerical codes for gamma-positron production**

• **LPI (KONN)** T.A. Vsevolojskaia

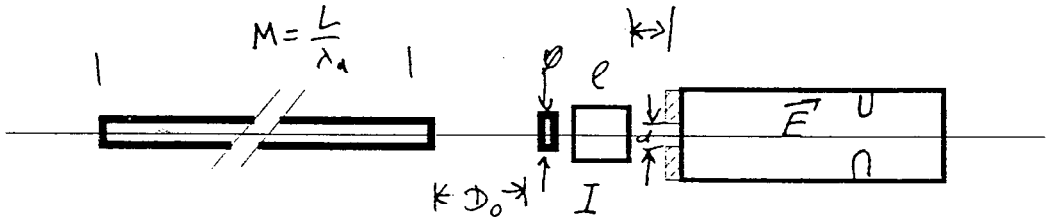

$$\frac{dE_n}{do} = E_{tot}\underbrace{\frac{6\gamma^2}{\pi}\frac{n^2F_n(K,\gamma)}{1+K^2+\gamma^2\vartheta^2}}_{PROBABILITY} = E_{tot}\cdot W_n(K,\vartheta),$$

F_n--the same as above;

$$E_{tot} = \frac{4\pi}{3}\frac{\Omega}{c}M\,e^2K^2\gamma^2 = \frac{4\pi}{3}mc^2\frac{r_o}{\lambda_u}K^2\gamma^2$$

$$\int_o \frac{dE}{do}do = \sum_n \int_o \frac{dE_n}{do}do = E_{tot}\sum_n \int W_n(K,\vartheta)do \cong E_{tot}\sum_n \underbrace{\int W_n(K,\vartheta)\pi\, d\vartheta^2}_{=1} = E_{tot}$$

$$W_n = W_n^+ + W_n^-$$

Probability to have a certain polarization

$$\xi_{2n} = \frac{W_n^+ - W_n^-}{W_n}$$

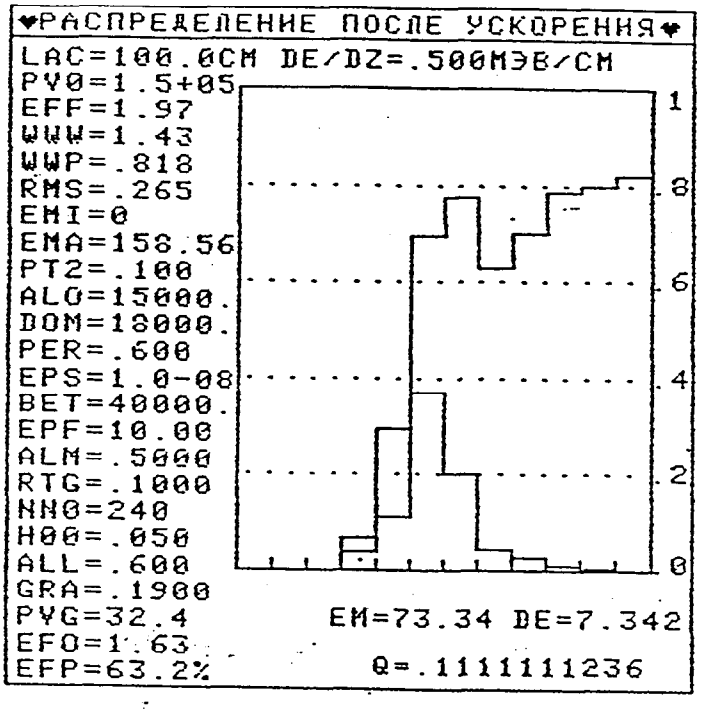
♥РАСПРЕДЕЛЕНИЕ ПОСЛЕ УСКОРЕНИЯ♥
LAC=100.0СМ DE/DZ=.500МЭВ/СМ
PV0=1.5+05
EFF=1.97
WWW=1.43
WWP=.818
RMS=.265
EMI=0
EMA=158.56
PT2=.100
ALO=15000.
DOM=18000.
PER=.600
EPS=1.0-08
BET=40000.
EPF=10.00
ALM=.5000
RTG=.1000
NN0=240
H00=.050
ALL=.600
GRA=.1900
PVG=32.4
EFO=1.63
EFP=63.2%
EM=73.34 DE=7.342
Q=.1111111236
1
.8
.6
.4
.2
0

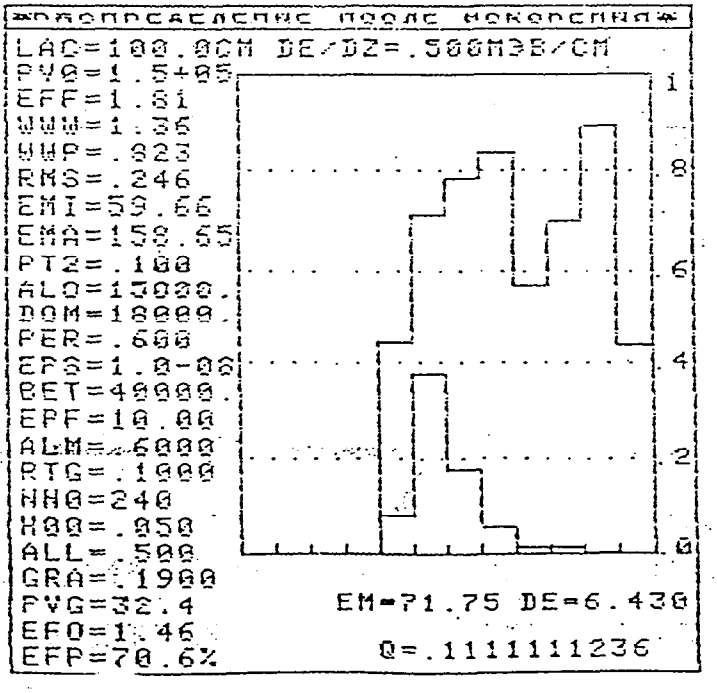
LAC=100.0СМ DE/DZ=.500МЭВ/СМ
PV0=1.5+05
EFF=1.81
WWW=1.36
WWP=.823
RMS=.246
EMI=59.66
EMA=159.65
PT2=.100
ALO=13000.
DOM=18000.
PER=.600
EPS=1.0-08
BET=40000.
EPF=10.00
ALM=.6000
RTG=.1000
NN0=240
H00=.050
ALL=.500
GRA=.1900
PVG=32.4
EFO=1.46
EFP=70.6%
EM=71.75 DE=6.430
Q=.1111111236
1
.8
.6
.4
.2
0

• **UNIMOD2** (an analog of EGS) A.D. Bukin, N.A. Grozina, M.S. Dubrovin
• **CONVER**

Individual history of about 6000-10000 incoming photons (depending of the accuracy required)

A.D. Bukin

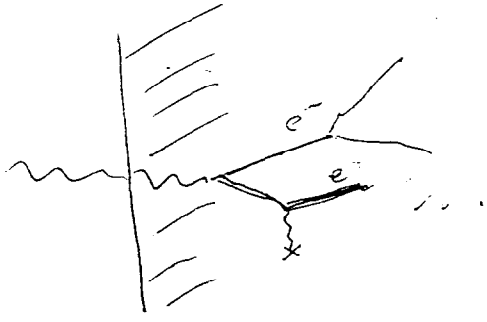

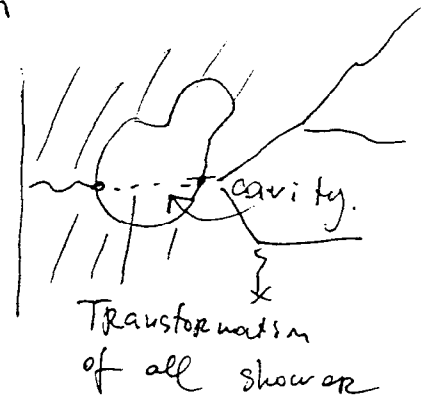

in progress

• **OBRA** → **PARMELA** for further transport A.M.

The main output of these considerations that the efficiency of the particle production could be made around 6% for each initial photon. The mean polarization can reach 70% total

The transverse space distribution of the positrons at the output surface of the target

Efficiency of the pair production as a function of the angle captured.

The energy distribution and polarization. The energy distribution is shown at the moment of positron creation.

EFFICIENCY, %
Angle of capture = 0.5rad
Wide Titanium target
LX_c= 3.5cm
Acc.= +-5%

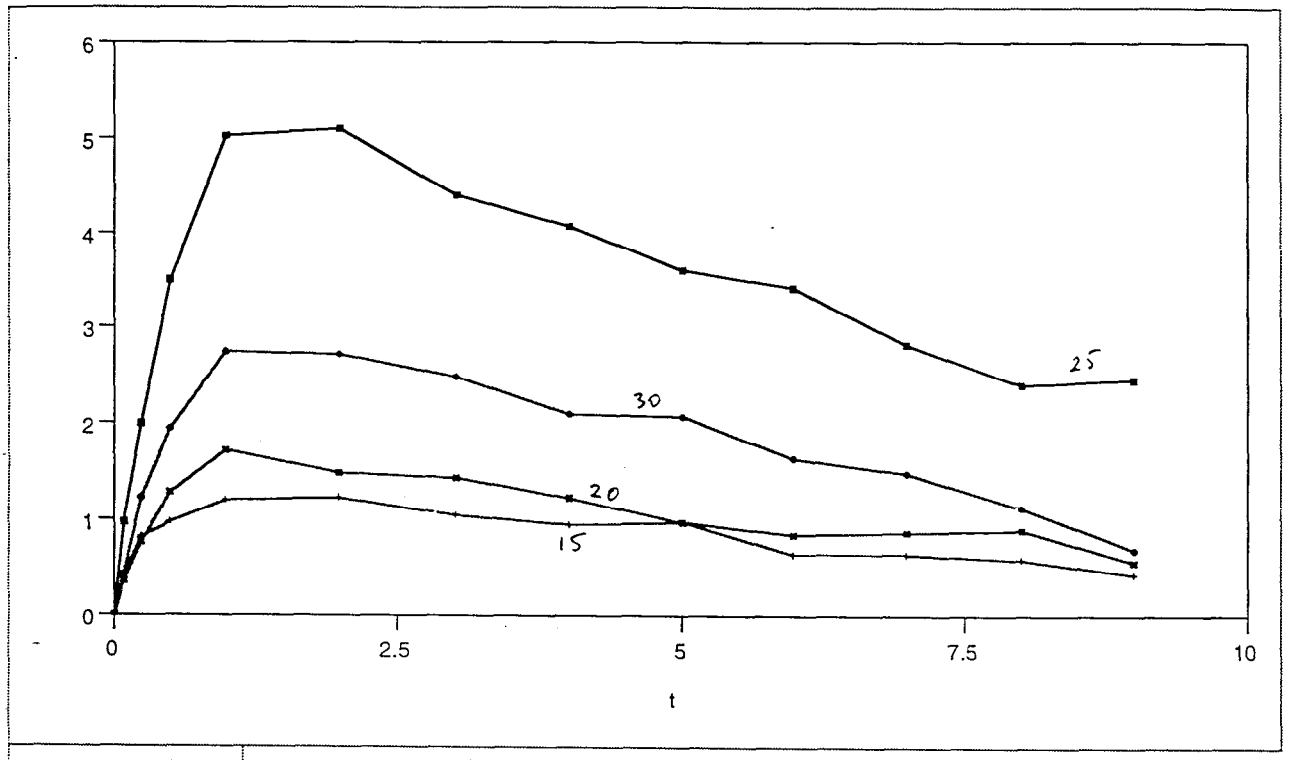

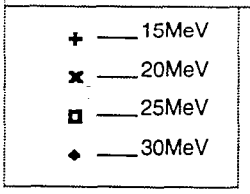

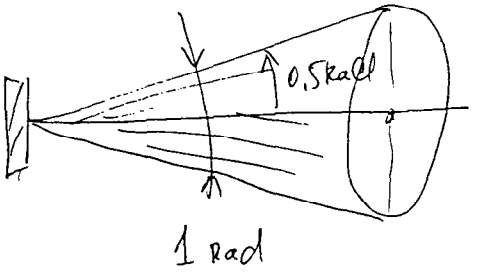

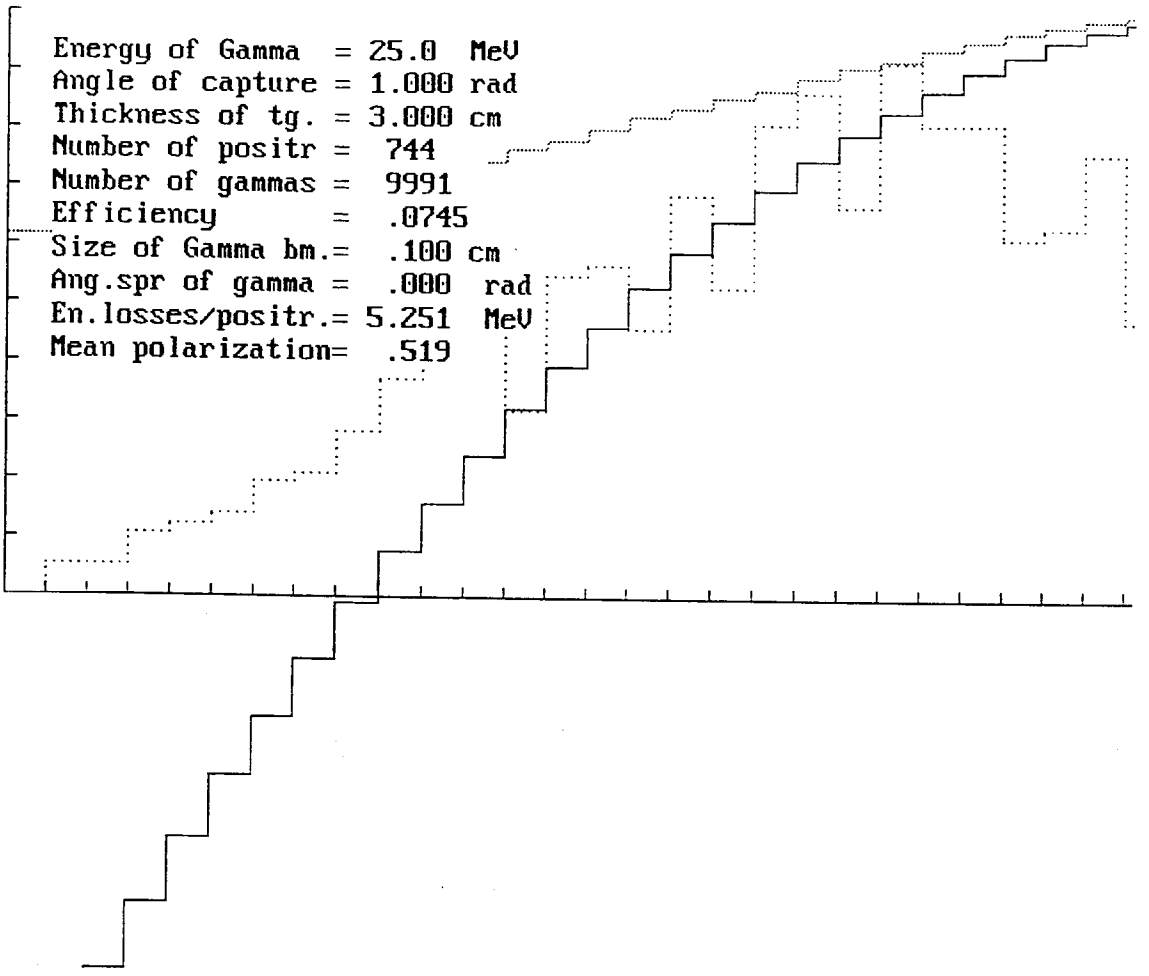
Energy of Gamma = 25.0 MeV
Angle of capture = 1.000 rad
Thickness of tg. = 3.000 cm
Number of positr = 744
Number of gammas = 9991
Efficiency = .0745
Size of Gamma bm.= .100 cm
Ang.spr of gamma = .000 rad
En.losses/positr.= 5.251 MeV
Mean polarization= .519

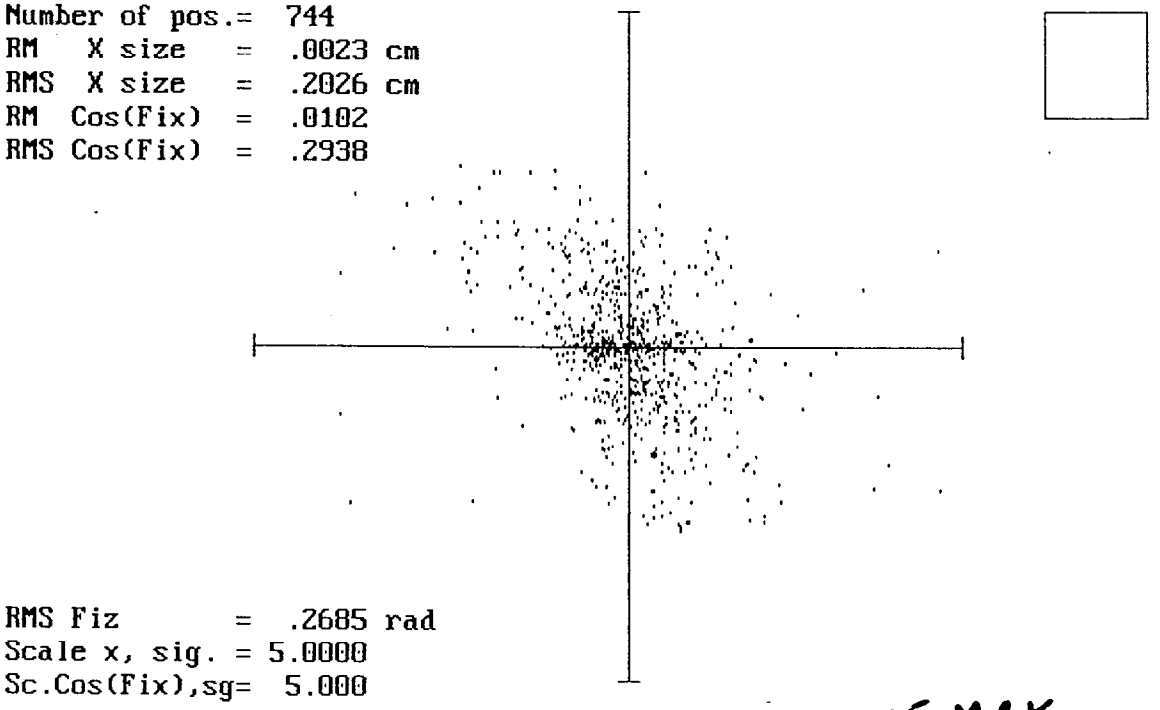
Number of pos.= 744
RM X size = .0023 cm
RMS X size = .2026 cm
RM Cos(Fix) = .0102
RMS Cos(Fix) = .2938
RMS Fiz = .2685 rad
Scale x, sig. = 5.0000
Sc.Cos(Fix),sg= 5.000

25 MeV

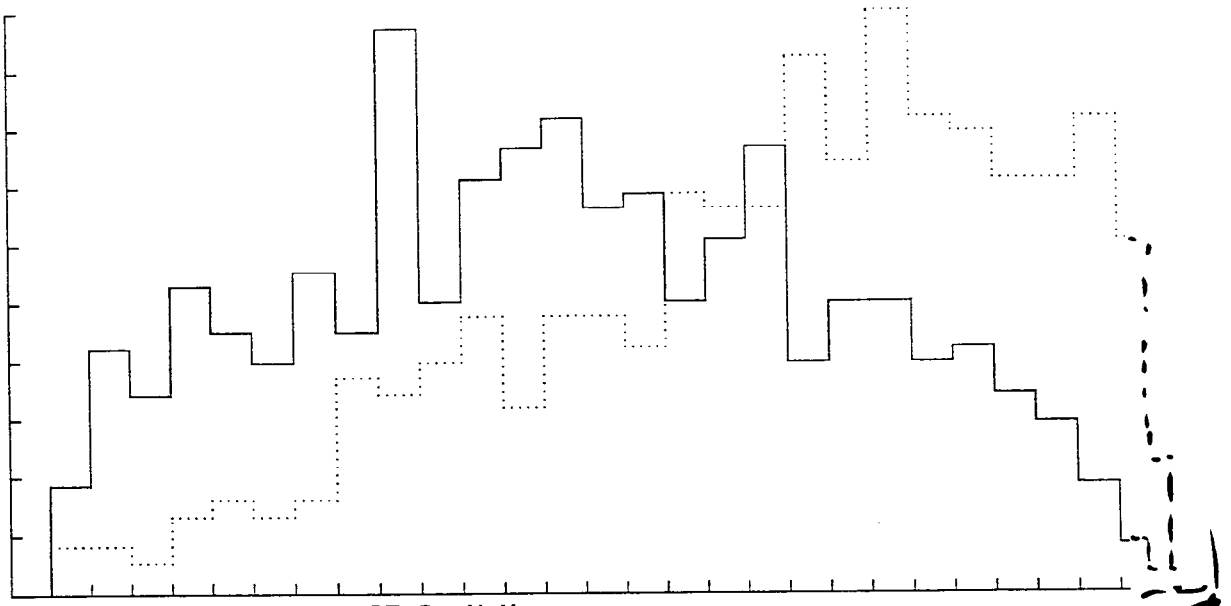

Energy of Gamma = 25.0 MeV
Angle of capture = .500 rad
Thickness of tg. = 3.000 cm
Number of positr = 510
Number of gammas = 9991
Efficiency = .0510
Size of Gamma bm.= .100 cm
Ang.spr of gamma = .000 rad
En.losses/positr.= 4.114 MeV
Max. num. on sc. = 38

Number of pos.= 510
RMean square X = .1620 cm
RMean square Y = .1673 cm
Mean size X = -.0048 cm
Mean size Y = .0052 cm
Scale, sigmas = 5.000

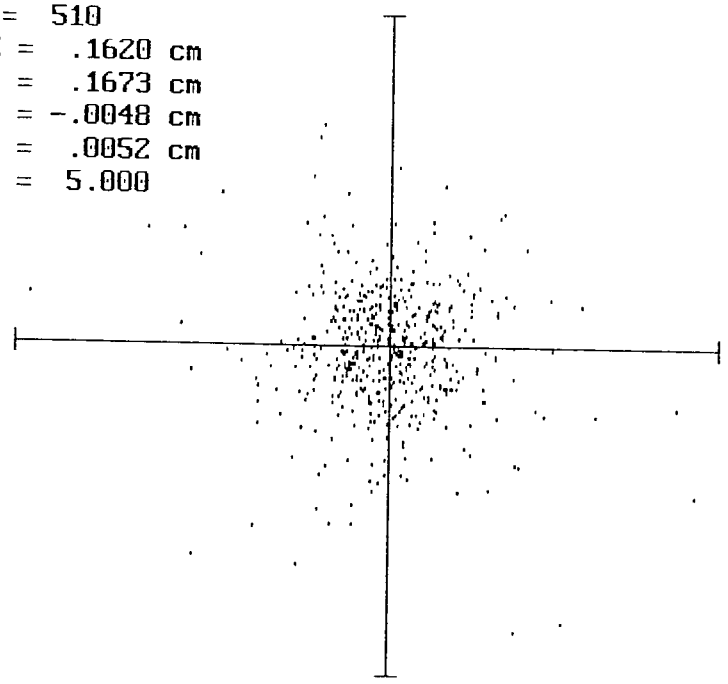

• TECHNICAL ASPECTS OF THE COLLECTION SYSTEM

• Energy deposition in a target

Some special considerations was made to estimate the energy deposition in the material of the target. It was found that this value is around 250 MeV/gram at the end of the target. The thickness of the target was about 0.2 *cm*. This yield the temperature gain of the order 116 deg for the beam with 10^{10} positrons in the bunch.

• **Dulongue-Petit law. Titanium target**

$$Q \cong \frac{3}{2} kNT + rotation \approx 3k_B N_A T \qquad k_B \cong 1.38 \times 10^{-23} Joules/^{o}K$$

Heat capacity $c_p \cong \frac{\partial Q}{\partial T} \approx 25 Joule/moll/\deg$

K. Flottman, J. Rossbach

• ***Lithium lens***

E.G. Silvestrov

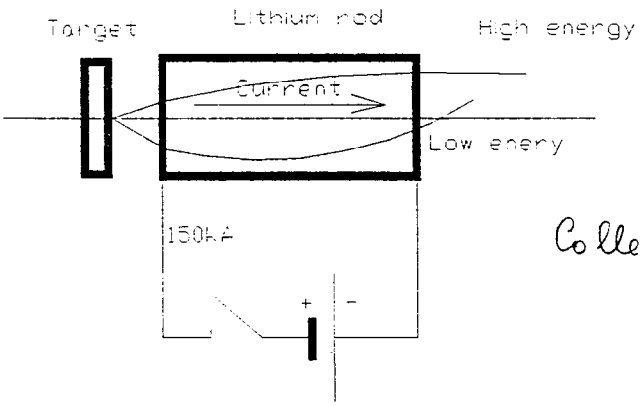

Collects only e^+ (or e^-)

The first selection system described used a lithium lens and a diaphragm as energy separator: the particles with the lower energy was over focused.

• ***Solenoidal lens***

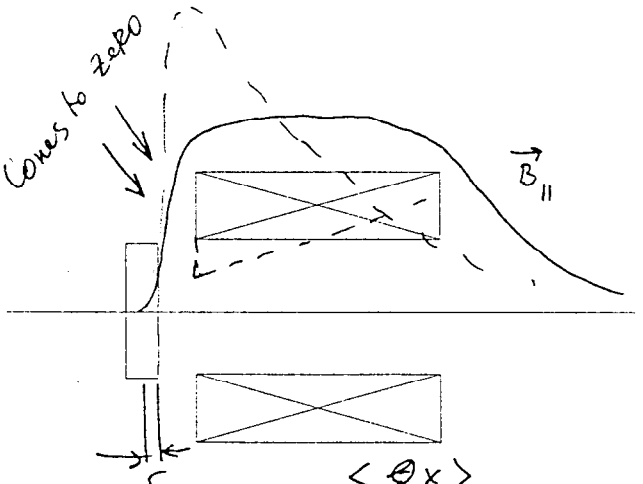

Collects e^+ and e^-

$e \simeq \frac{\langle \theta x \rangle}{\langle \theta^2 \rangle}$ - depth of creation

• PERTURBATIONS

for inseption

• Emittance perturbation in a undulator

Before IP

$$\frac{d\varepsilon_{x,y}}{dz} \cong \left\langle \left(H_{x,y} + \frac{\beta_{x,y}}{\gamma^2} \right) \overline{\frac{d(E_\gamma / E)}{dz}} \right\rangle$$

$$H(z) = \frac{1}{\beta(z)} \left(\eta^2(z) + (\beta\eta' - \frac{1}{2}\beta'\eta)^2 \right), \quad \text{z-- is a longitudinal coordinate}$$

$\langle A \rangle$ -averaging over period of the undulator

$\overline{A}$ - averaging over spectrum of radiation

Combake

$$\eta = \frac{K\lambda_u}{\gamma} Sin\frac{z}{\lambda_u} = \frac{\lambda^2}{\rho} Sin\frac{z}{\lambda_u}, \qquad \eta'(z) = \frac{\lambda}{\rho} Cos\frac{z}{\lambda_u}, \qquad \rho = \frac{\lambda\gamma}{K},$$

$$l_{formation} \approx \frac{\rho}{\gamma} = \frac{\lambda}{K}, \qquad l_{formation} \to \infty, \; K \to 0$$

$$H \cong \beta\eta'^2 = \frac{\lambda_u^2 \beta}{\rho^2} Cos^2\frac{z}{\lambda_u}, = \frac{\lambda_u^2 \beta}{\lambda^2 \gamma^2} K^2 = \frac{\beta K^2}{\gamma^2}$$

$$\overline{\left(\frac{E_\gamma}{E}\right)^2} = \int \left(\frac{E_\gamma}{E}\right)^2 \frac{dN_\gamma}{dE_\gamma} dE_\gamma = \left(\frac{\hbar\omega_{\max}}{E}\right)^2 \int s^2 \frac{dN_\gamma}{ds} ds, \qquad s = \frac{E_\gamma}{E_{\gamma\max}} = \frac{1}{1 + \frac{\gamma^2\vartheta^2}{1+K^2}}$$

We have

$$\frac{dN_\gamma}{ds} = \sum_n \frac{dN_{\gamma n}}{ds} = 4\pi\alpha M \frac{K^2}{1+K^2} \sum_n n F_n(K,s)$$

M-- is the number of periods

$$F_1(K,s) \cong \frac{1}{2}(1 - 2s + 2s^2), \quad F_2(K,s) \cong 2s(1-s)(1-s+2s^2)K^2,$$

$$\int_0^1 s^2(1-2s+2s^2) = \frac{7}{30}, \qquad \int_0^1 s^3(1-s)(1-2s+2s^2) = \frac{13}{420}$$

$$\Delta\varepsilon \cong \frac{\overline{\beta}K^2}{2\gamma^2} \left(\frac{2\Omega\gamma^2\hbar}{(1+K^2)E} \right)^2 \cdot 2\alpha M \frac{K^2}{1+K^2} \cdot \frac{7}{30} = \frac{\overline{\beta}}{2} \frac{K^4}{(1+K^2)^3} \left(\frac{r_0}{\lambda_u}\right)^2 \cdot 2\pi M \cdot \frac{7}{30}$$

$$r_0 = e^2 / mc^2$$

• Emittance perturbation in undulator is negligible

- **Spin perturbation in an undulator** E. Perevedentsev, V. Ptitsin, Y.M. Shatunov
- Vector $\vec{P}$ (spin vector) is defined in the **rest frame** of the positron or electron
- The fields are defined in the **laboratory** system.

$$\frac{d\vec{P}}{dt} = \frac{e}{m\gamma}\left[\left\{1+\gamma\frac{g-2}{2}\right\}\right](\vec{P}\times\vec{B}) + (\gamma-1)\cdot\frac{g-2}{2}\cdot\frac{(\vec{\beta}\vec{B})(\vec{\beta}\times\vec{P})}{\beta^2} + \gamma\left\{\frac{g-2}{2}+\frac{1}{\gamma+1}\right\}\frac{\vec{P}\cdot(\vec{E}\times\vec{\beta})}{c}$$

$$\frac{d\vec{P}}{dt} = \vec{P}\times\vec{\Omega}_s$$

$\vec{\beta} = \vec{v}/c$; $\vec{E}$, $\vec{B}$ -- electric and magnetic fields in the *laboratory* frame

$$\frac{g-2}{2} \cong 1.159652\times10^{-3} \approx \frac{\alpha}{2\pi}$$

- Coming to ***rotating*** system of reference $\vec{\Omega} = \frac{c}{\lambda_u}$

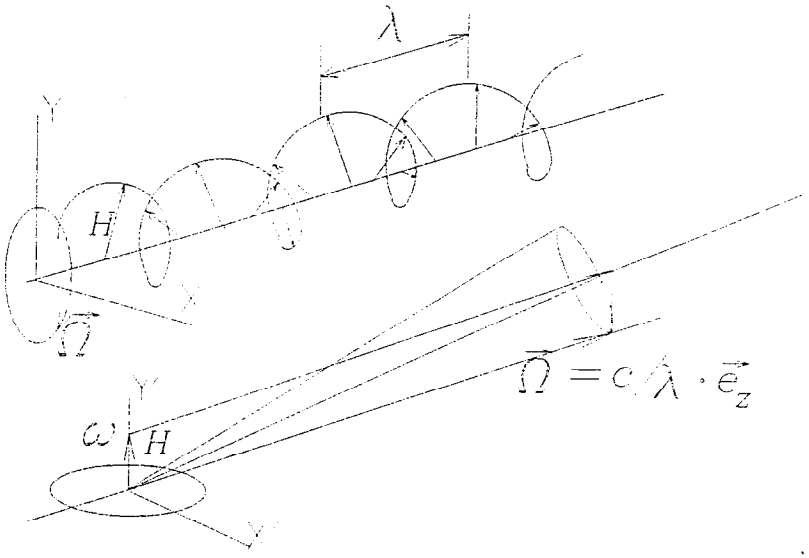

$$\frac{d\vec{P}}{dt} = \vec{P}\times(\vec{\Omega}_s - \vec{\Omega})$$

Components of the vector $\Omega_{eff} = \vec{\Omega}_s - \vec{\Omega}$:

$$\vec{\Omega}_{eff} = \left\{\frac{e}{mc\gamma}\left[1+\gamma\frac{g-2}{2}\right]H_\perp;\ \ 0;\ \ \frac{c}{\lambda_u}\right\} ==>$$

$$\vec{\Omega}_{eff} = \vec{\Omega}_\perp + \vec{\Omega}_\parallel = \left\{\left[1+\gamma\frac{g-2}{2}\right]\cdot\frac{eH_\perp\lambda_u}{mc\cdot\gamma}\cdot\frac{c}{\lambda_u};\ \ 0;\ \ \frac{c}{\lambda_u}\right\} \equiv \left\{\left[1+\gamma\frac{g-2}{2}\right]\frac{K}{\gamma}\cdot\frac{c}{\lambda_u}\vec{e}_\perp;\ \ 0;\ \ \frac{c}{\lambda_u}\vec{e}_\parallel\right\}$$

$\Omega_\perp$ depend on energy $\sim \frac{K}{\gamma}$

Spin frequency is

$$\left|\vec{\Omega}_s\right| = \frac{c}{\lambda_u}\sqrt{\left[1+\gamma\frac{g-2}{2}\right]^2\frac{K^2}{\gamma^2}+1} = \nu_s\cdot\Omega \cong (1+\frac{1}{2}\left[1+\gamma\frac{g-2}{2}\right]^2\frac{K^2}{\gamma^2})\cdot\Omega \cong$$

$$\cong \Omega\cdot(1+\left[\frac{g-2}{2}\right]^2\frac{K^2}{2}) \cong \Omega$$

- Direction of rotation

$$\vec{n} = \frac{\vec{\Omega}_\perp + \vec{\Omega}_\parallel}{\left|\vec{\Omega}_s\right|} \cong \left\{\left[1+\gamma\frac{g-2}{2}\right]\frac{K}{\gamma}\cdot\vec{e}_\perp;\ \ 0;\ \ \vec{e}_\parallel\right\}$$

- Possible depolarization $\quad \delta P \cong \left[1+\gamma\frac{g-2}{2}\right]^2\frac{K^2}{\gamma^2} \approx 10^{-6}K^2$

- **Spin perturbation in the interaction point**

Due to huge magnetic field of incoming beam the vector of spin rotates at the angle $\varphi \cong 2\pi \cdot E[GeV] / 0.4406$ with respect to the vector of momenta.

These effects yield a lost of a few percentages of polarization and need to be taken into account.

Lost E. Kushnirenko, A. Likhoded, M. Shevlyagin
1993

• Resistive instability in a undulator chamber

- The resistive wall instability if the beam, moving in the vacuum chamber of the wiggler considered.
- Heating

$$\omega \approx \frac{c}{\sigma_l} \rightarrow mm \text{ waves !} \quad \sigma_l \text{ is the bunch length}$$

$$\text{Skin depth } \delta \approx \sqrt{\frac{2}{\mu_0 \sigma \omega}}$$

$\sigma \cong \dfrac{1}{1.7 \cdot 10^{-8} Ohm \cdot m}$ for room temperature Cu; $\mu_0 = 4\pi \cdot 10^{-7} H/m$

Area $\Sigma = 2\pi a \cdot \delta$, a is a radius of the vacuum chamber
Resistance for all 100 meters, $\sigma_l \cong 1mm$

$$R \cong \frac{L}{\sigma \cdot \Sigma} = \frac{L}{2\pi a \sigma \cdot} \sqrt{\frac{\mu_0 \sigma \omega}{2}} = \frac{L}{2\pi a \sigma \cdot} \sqrt{\frac{\mu_0 \sigma c}{2\sigma_l}} \cong \frac{100 \cdot 1.7 \cdot 10^{-8}}{2\pi 3 \cdot 10^{-3}} \sqrt{\frac{4\pi \cdot 10^{-7} 3 \cdot 10^{8}}{2 \cdot 1.7 \cdot 10^{-8} \cdot 10^{-3}}} \cong 300[\Omega]$$

Number of the particles $N \cong 10^{10}$, peak current for $\sigma_l \cong 1mm$

$$\hat{I} \cong \frac{eN}{(\sigma_l / c)} \cong \frac{1.6 \cdot 10^{-19} \cdot 10^{10}}{0.001/3 \cdot 10^{8}} \approx 480A$$

Pulsed power for single bunch per second for all 100 meters for $\sigma_l \approx 1mm$

$$P \cong \int \hat{I}^2 R dt \approx \frac{(eN)^2}{(\sigma_l / c)^2} \cdot R \cdot (\sigma_l / c) = 480^2 \cdot 300 \cdot \frac{0.001}{3 \cdot 10^{8}} = 2.3 \cdot 10^{-4} [Watt]$$

One can easily scale this number to the necessary repetition rate and to the number of the bunches per train and for other σ_l and N. (For $\sigma_l \cong 0.1mm$ the losses will be 30 times higher, $P \cong 7 \cdot 10^{-3} W$). Magnetic field on the inner surface is

$$H \cong \frac{0.4 \cdot \pi \hat{I}}{2\pi a} \cong 300G.$$

Liquid helium temperature → drastic reduction of resistance

• This looks as a weak requirement

• **The wall illumination**

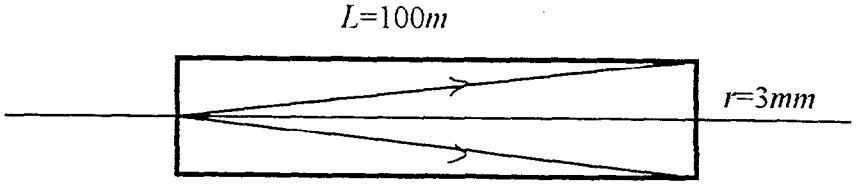

• Angle

$$\vartheta \cong \frac{r}{L} \cong \frac{3\cdot 10^{-3}}{100} = 3\cdot 10^{-5}, \qquad \gamma\vartheta \cong 4\cdot 10^{5} \times 3\cdot 10^{-5} = 12$$

$$E_{\gamma\,\max} = \frac{n2\gamma^2\hbar\Omega}{1+K^2+\gamma^2\vartheta^2} \cong \frac{2.48\cdot(\gamma/10^5)^2}{(1+K^2+\gamma^2\vartheta^2)\lambda[cm]}[MeV] \cong \frac{2.48\cdot 16}{144\cdot 1} = 0.27MeV$$

For beam with E=200GeV

• Quadratic dependence of inner diameter

Req. some screening

• HOW TO BAFFLE THE LENGTH OF THE UNDULATOR

• Few targets in series

The attenuation coefficient $k \approx \exp(-7/9\tau)$ for $\tau \approx 0.25$ is around 0.82

The second target can be used as well

- Further utilization of the gamma -beam, passed through a thin converter
- Possible reduction of the heating of individual target. Use the target thinner, than optimal >
- The combining schemes based on the possibility to stack the bunches in the longitudinal energy space. Energy is slightly different

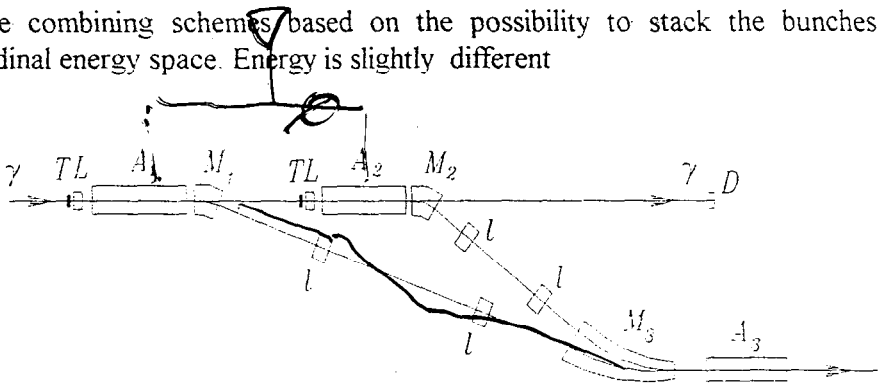

- The difference in the path lengths of these two lines in an integer of the wavelength and a half of the section A_3

This section *eliminates* the energy difference

- At the end of the magnet $M_{1,2}$

$$\eta \cong \rho \cdot (1 - Cos\varphi), \quad \eta'(s) = Sin\varphi, \quad \varphi = \frac{z}{\rho}$$

In the middle of the lens *l*

$$\eta|_l = \rho \cdot (1 - Cos\varphi) + L \cdot Sin\varphi$$

Let $\varphi = \pi/6$, L=300cm, $\rho = 100cm$

$$\eta|_l = 100 \cdot 0.134 + 150 \cong 163cm$$

If energy E_{10}= 200MeV, $E_{\gamma\,\max} \cong 20MeV$ and we collect half of this i.e. $15 \pm 5MeV$

E=215 ± 5

then radial displacement will be $\Delta r = \eta|_l \cdot \frac{10}{200} \cong 8cm$ $(\pm 4cm)$

Focal distance of the lens is $L = \frac{(HR)}{Gl}$

Supposing that the length of the lens is *l*=20cm

Gradient $G = \frac{(HR)}{lL} = \frac{667kGs \cdot cm}{200cm \cdot 20cm} = 0.17kGs/cm$ only

E_2 =225 ± 5MeV

- **Optics could be realized easily.** **Reduction of the length ~ 1/2.**

A. Bukin A. Mikhailichenko

- **Form-factor for Ti target**

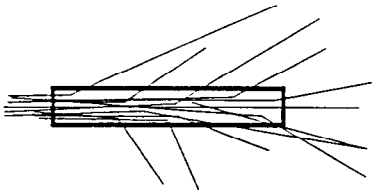

Length/diameter ≈ 10

- For $E_\gamma = 20MeV$ efficiecy ≈ 2.67% for target $4cm$ (compare 1.7%) 50% of energy interval
$\sigma_\gamma - 0.1cm$ Diameter of the target $0.4cm$

- Not possible for Tungsten target
neither for electrons no for gammas //

- **THE SAME MUST WORK FOR ELECTRON CONVERSION**

$$E_{cr} = \frac{600}{Z}[\,MeV\,]$$

Z_{Ti}=22

Number of pos.= 538
RMean square X = .1023 cm
RMean square Y = .0993 cm
Mean size X = -.0046 cm
Mean size Y = -.0012 cm
Scale, sigmas = 5.000

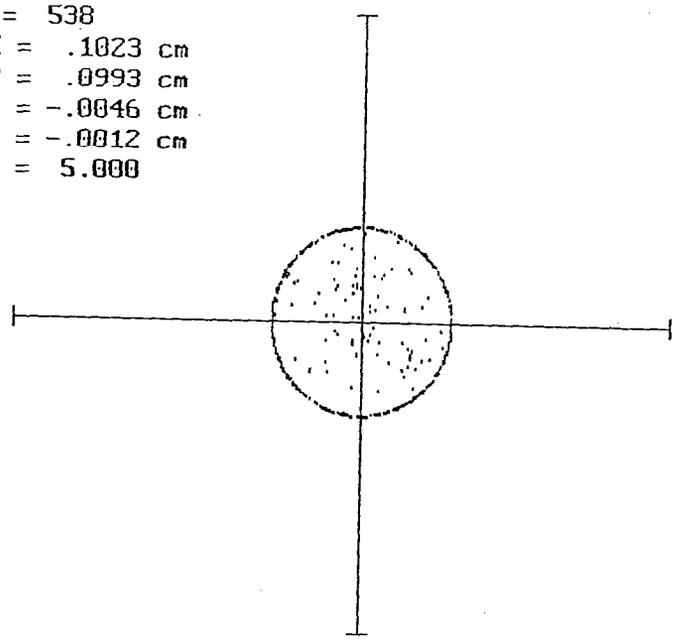

Number of pos.= 538
RM X size = -.0046 cm
RMS X size = .1023 cm
RM Cos(Fix) = -.0160
RMS Cos(Fix) = .2000

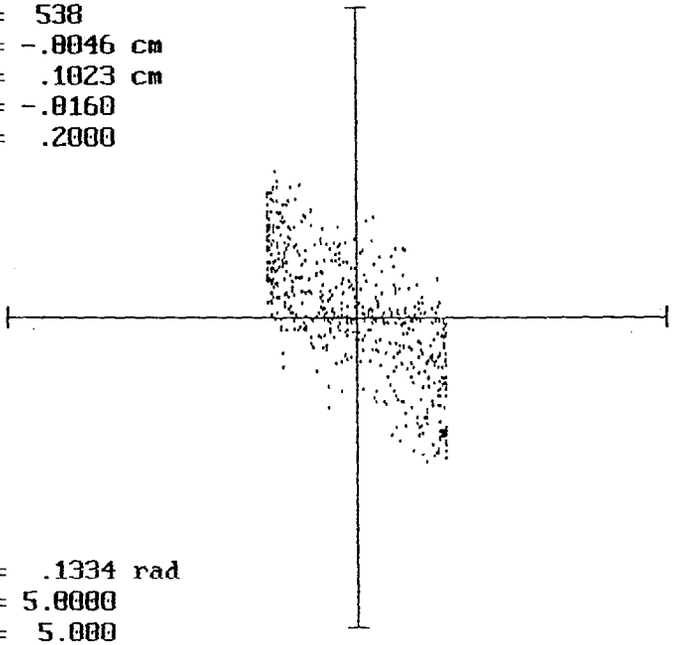

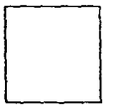

RMS Fiz = .1334 rad
Scale x, sig. = 5.0000
Sc.Cos(Fix),sg= 5.000

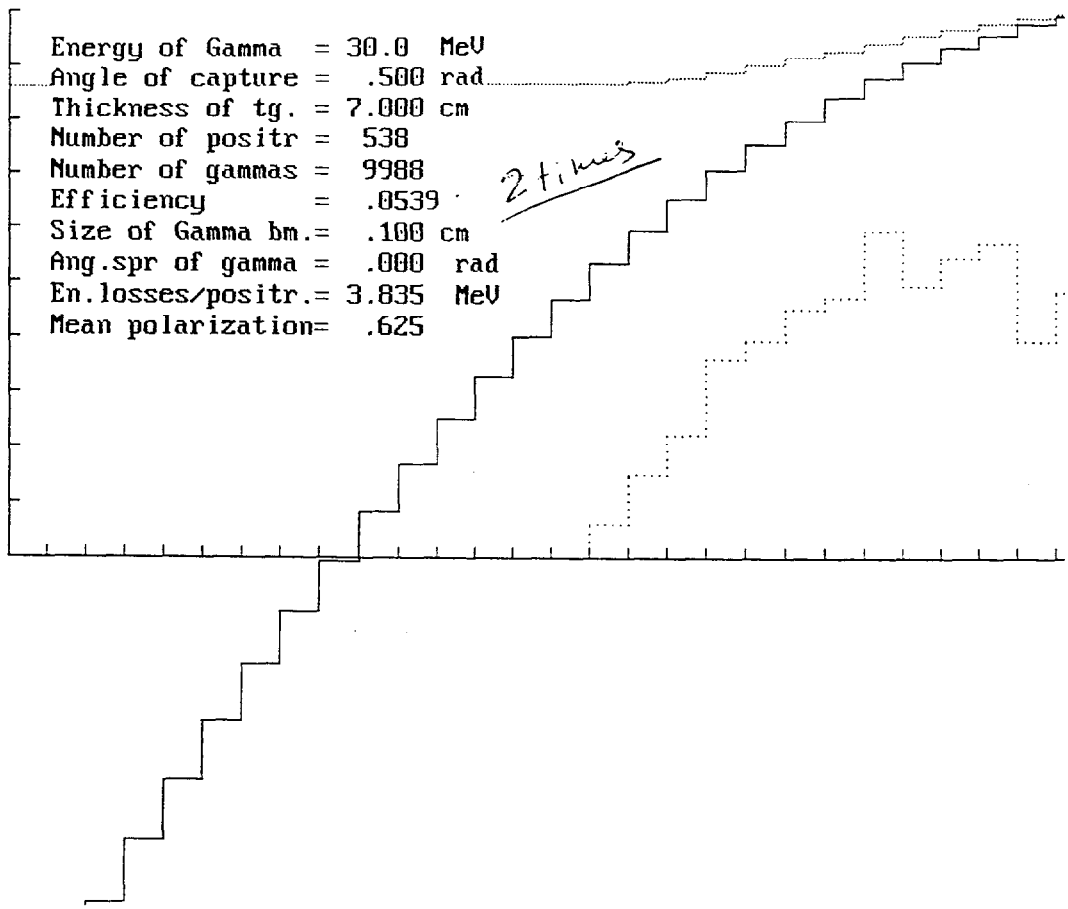
Energy of Gamma = 30.0 MeV
Angle of capture = .500 rad
Thickness of tg. = 7.000 cm
Number of positr = 538
Number of gammas = 9988
Efficiency = .0539
Size of Gamma bm.= .100 cm
Ang.spr of gamma = .000 rad
En.losses/positr.= 3.835 MeV
Mean polarization= .625
2 times

• PROPOSAL FOR SLAC ACCELERATOR

- E~$50GeV$
- $N \cong 5 \times 10^{10}$
- $\gamma\varepsilon \cong 3 \times 10^{-3} cm \cdot rad$

Wiggler installed in crossover with β^*

$$\beta(z) = \beta^* + \frac{z^2}{\beta^*} = \beta^* (1 + \frac{z^2}{\beta^{*2}})$$

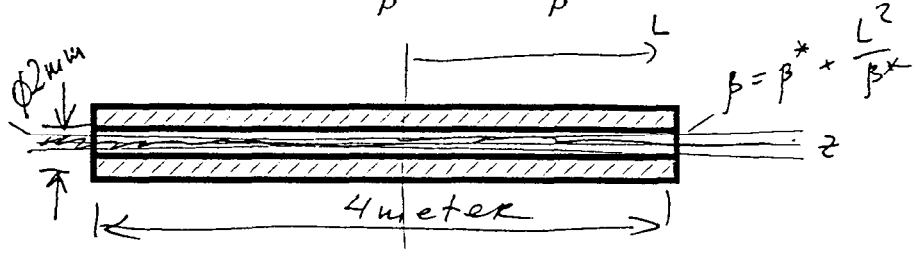

Beam size at the out of the undulator changes only 10% $\rightarrow$ $\frac{L^2}{\beta^{*2}} \approx 0.2$

- L=2m $\rightarrow \beta^* \cong 450cm$

The beam size $\sigma \cong \sqrt{\frac{\gamma\varepsilon\beta^*}{\gamma}} = 3.67 \times 10^{-3} cm$ • Aperture $\cong 10\sigma \cong 0.37mm$ only

- ***Undulator*** calculations made
- K=0.2
- $\lambda_u = 2mm$
- Inner diameter = $2mm$

$$E_{\gamma\,\max} = \frac{n2\gamma^2\hbar\Omega}{1+K^2} \cong \frac{2.48 \cdot (\gamma / 10^5)^2}{(1+K^2)\lambda[cm]}[MeV] \cong 12.4MeV$$

Analytical

$$N_{\gamma 1} = N_{e-} \frac{4\pi\alpha K}{1+K^2}\left(1 - \frac{2}{5} \cdot \frac{K^2}{1+K^2}\right) \quad \rightarrow \quad \frac{N_{\gamma 1}}{N_{e-}} \cong 2.3$$

- ***Numerical calculation*** with **CONVER&OBRA**

$E_\gamma = 10MeV$ A.M.

Tungsten

$E_+ = 7.5 \pm 2.5MeV$; Thickness $\delta = 0.15$

Angle of capture $0.5rad$ $\rightarrow$ Efficiency $\frac{N_+}{N} \cong \frac{N_+}{N_\gamma}\frac{N_\gamma}{N} \cong 0.014 \times 2.3 = 0.025$

What gives $N_+ \cong 0.025 \times 5 \cdot 10^{10} = 1.25 \cdot 10^9$

• ***Analytical estimation***

$$\Delta N_{-} \cong 3 \cdot 10^{-2} \theta_s^{\,2} \delta M \frac{K^2}{1+K^2} \cdot \frac{z_f}{z_i} \cdot (1-\xi_1)$$

z_f -- z- coordinate of the end of the undulator

z_i -- z- coordinate of the beginning of the undulator $(z_i > z_f)$

ξ_1 --energy range of collected positrons (ξ_1 =0 ==> *full* energy interval)

θ_s -- fraction of $\gamma\vartheta$ (1/3 for s=0.9)

δ -- thickness of the target

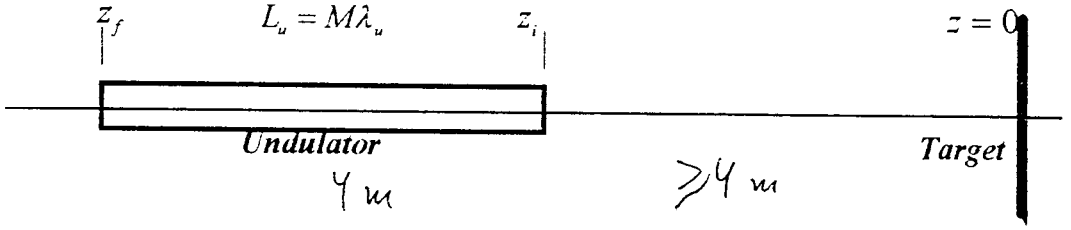

For

• θ_s =1/3 • $\delta = 0.15$ • K=0.2 • $\xi_1 = 0.9$ • $z_f / z_i \cong 1$ • $M = 400 / 0.2 = 2 \cdot 10^3$ •

$$\Delta N_{-} \cong 3 \cdot 10^{-2} \theta_s^{\,2} \delta \frac{K^2}{1+K^2} \cdot \frac{z_f}{z_i} \cdot (1-\xi_1) = 0.034 \text{ (compare with 0.025)}$$

$\theta_s \to 1 \quad \Delta N_+ \to \times 10$

For B-Factory?

• Undulator Converter Test Facility

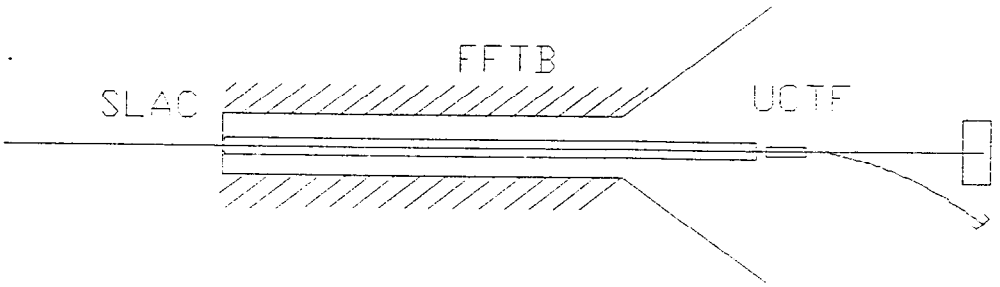

• CONCLUSION

Polarization is a powerful tool for high energy physics (beyond 100 GeV especially)

- High positron (end electron) flow required
- High polarization required
  - Not overheat the target required

All these requirements could be satisfied with the help of undulator/conversion

- Length could be reduced

  Few targets Form-factor

  • Length == 100*m* → 50*m* → 25*m*

- The method could be tested at 50 GeV
  - Undulator Converter Test Facility (UCTF) is a good way forward

Even **100 *m* insertion for polarized positrons and electrons production looks as acceptable price for this**

ADDENDUM

• About optimal energy for conversion

Photon spectrum density, ***normalized*** to the maximal photon energy $s = \omega_n / \omega_n^{max}$

• For harmonics n = 1,2,... in approximation $K \le 1$ or/and $\gamma\vartheta \le 1$

$$\frac{dN_{n\gamma}}{ds} \cong 4\pi\alpha n M \frac{K^2}{1+K^2} \times \begin{cases} \frac{1}{2}(1-2s+2s^2), & n=1 \\ 2s(1-s)(1-s+2s^2), & n=2 \\ \dots \\ F_n(K,s) \end{cases}$$

It is ***not a function of energy*** of a primary electron beam

• The phonon flux as a function of absolute (not normalized) energy is

$$\frac{dN_{n\gamma}}{d(\omega_n / \omega_n^{\max})} \to \frac{dN_{n\gamma}}{d\omega_n} \cong \frac{4\pi\alpha n M}{\omega_n^{\max}} \frac{K^2}{1+K^2} F_n(K,s) = \frac{4\pi\alpha n M}{2\gamma^2\Omega} K^2 F_n(K,s) \quad (1A)$$

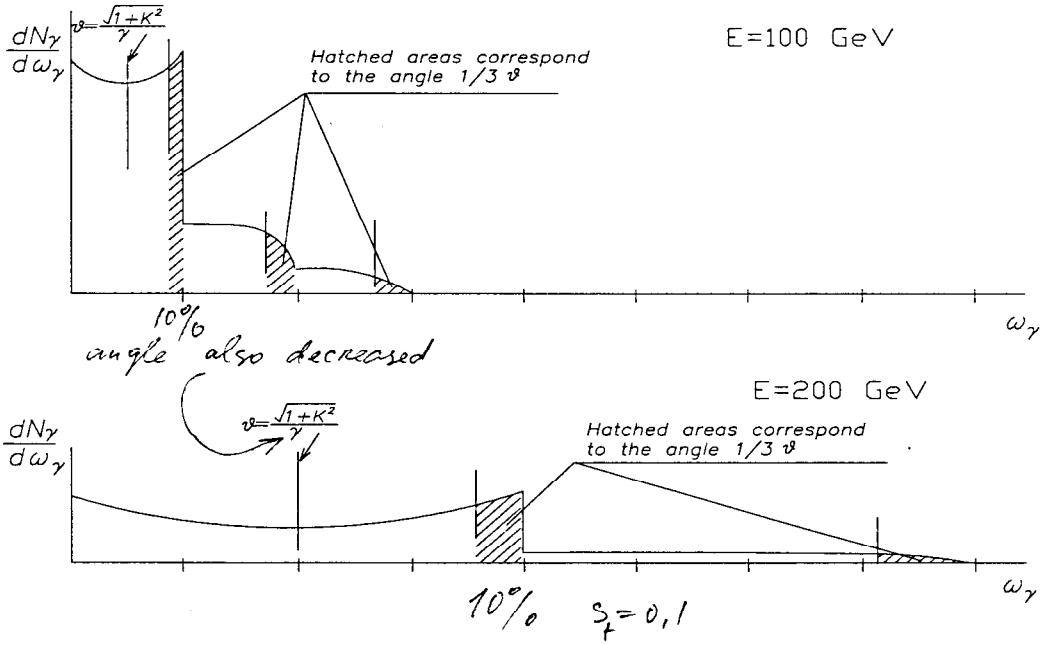

• The number of the photons

$$N_{n\gamma}(K,s_t) = \int_{s_t}^{1} \frac{dN_{n\gamma}}{ds} ds \cong 4\pi\alpha n M \frac{K^2}{1+K^2} \times \begin{cases} \frac{1}{6}(1-s_t)(2-s_t+2s_t^2), & n=1 \\ \frac{K^2}{10\cdot(1+K^2)}(1-s_t)(1+2s_t-2s_t^2+4s_t^3), & n=2 \\ \dots \end{cases}$$

is a function of the ***fractional*** energy only.

The ***fractional*** energy in its turn defined by the diameter d of the diaphragm hole:

$$s_t \cong \frac{1}{1+\frac{\gamma^2 d^2}{R^2(1+K^2)}},$$

R is the distance to the target

- If the diaphragm is large ($\gamma d \geq R$), then the number of the photons in not a function of the beam energy at all
- One can see, that for keeping the same fractional energy, it is necessary to keep the ratio $\gamma d/R$ constant
- So, reduction of the photon density $dN_{n\gamma}/d\omega_n \cong 1/\gamma^2$ (1A) is ***not*** a limitation.

Positives :

With increasing the photon energy the cross-section of the pair creation also increased (not proportionally, however)

Restrictions :

- Lowering the energy of the primary beam $\cong N_{n\gamma} \times \hbar\omega_n^{\max} \cong N_{n\gamma} \times \frac{\hbar 2\gamma^2 \Omega}{1+K^2}$ -

  -not a serious limitation

  Increasing the energy spread in the primary beam $\cong \sqrt{N_{n\gamma}} \times \hbar\omega_n^{\max}$ -

  -probably also not a serious limitation

- The beam optics (for delivery of the primary beam) becomes more complicated for the beam with higher energy.

- With increasing the energy of the primary beam, the maximal possible energy of the *created positrons* also increased, proportionally to the energy of the photons.

- ***Here*** may occur *the first* real problem caused by the primary collection system: it must collect now more wide *absolute* energy interval, increasing as a square of the energy.

  .So utilization of the ***flux concentrator*** is desirable here.

- Energy acceptance of the damping ring available is limited.

  This may become *the second* restriction for the movement to the high energy.

  Energy compressor utilization (combination of the energy dependent path length and correspondingly phased acceleration structure) can help to avoid this restriction

- In general, however, there is no *fundamental* limitation for the motion to the high energy of the primary beam

  This is a question of optimization for the collection system possibilities, damping ring acceptance, space available.

Physics Requirements

Tsunehiko OMORI (KEK)

Physics requirements are summarized from the view point of the usage of beam polarization. Comparison between single beam polarization (only e^- beam is polarized) and double beam polarization (both e^- and e^+ beams are polarized) is discussed.

Polarized beam is very powerful tool in wide range of physics study in lepton colliders. Using longitudinal polarized beam, we can suppress background (most case W^+W^-), can select certain kind of events, and can solve particle components of weak igenstate.

Single beam polarization is already useful for those purpose. This is because that when we choose helicity of electrons, helicity of positrons, which can interact through s-channel vector boson annihilation and through t-cannel ν/W exchange, are automatically selected.

Double beam polarization is more powerful. As an interesting example, we consider suppression of W^+W^- events. Although polarized cross section to create the W^+W^- final state from the $e^-_R e^+_L$ initial state is twice larger than that from the $e^-_R e^+_U$ initial state, in actual colliders, in which beam polarization is less than 100%, number of W^+W^- events created in collision of $e^-_{R:beam} \times e^+_{L:beam}$ is much smaller than that created in $e^-_{R:beam} \times e^+_{U:beam}$. The reason of this interesting inversion is non negrigible population of e^-_L's in the $e^-_{R:beam}$ (when we assume realistic degree of polarization). Therefore double beam polarization suppress W^+W^- background much better. In addition number of signal events in many kinds, for example $f\bar{f}$, created in collision of $e^-_{R:beam} \times e^+_{L:beam}$ is larger than that created in $e^-_{R:beam} \times e^+_{U:beam}$. Then double beam polarization will give us much better signal/noise ratio with larger number of signal. Since W^+W^- events will be most serious background for many studies, this feature is very important.

Define combined (effective) polarization is useful to discuss RL and LR combination of longitudinal polarized beam. Error propagation coefficient from polarization measurement of each beam to the combined polarization is less than unity. Therefore combined polarization can be determined with very high accuracy. This is very useful to reduce systematic error coming from polarization measurement. For example $\sin^2\theta_W$ can be determined with very small uncertainty by double beam polarized collision on Z-pole.

Some of interesting events are good target to search/study with RR and LL combination of double beam polarization. For example we discuss $\tilde{e}^{\mp}\tilde{\chi}^{\pm(-)}\nu$, $\tilde{e}^{-}\tilde{e}^{+}q\bar{q}$, $e^{\mp}W^{\pm(-)}\nu$ events. On the other hand, when $e^{\mp}W^{\pm(-)}\nu$ events are background, only RL combination (e^- beam has R-polarization) of double beam polarization can kill it.

Usage of transverse polarization is briefly discussed. To get effect of transverse polarization, both beams should be polarized. Since a transverse polarization state is a linear combination of longitudinal polarization states, there is possibility to observe effects of new physics through an interference between amplitudes of initial states which have different longitudinal polarization. Therefore usage of transverse polarization should be considered both physics point of view and technical point of view (accelerator, polarimeter, etc.).

High intensity of a positron beam is important. If positron intensity decrease to get polarization, many of advantages of a polarized positron beam will largely decrease or vanish.

Physics Requirments

4-Mar-1997 @SLAC
WS on New Kinds of
Positron Sources for LSs.

Tsunehiko OMORI (KEK)

with Thanks to
Y. Kurihara
K. Fujii
A. Miyamoto
K. Hagiwara

Contents

Define Question

(I) There is NO question,
We need Positrons.

(II) Do we need polarization?

(a) Single Beam Polarization

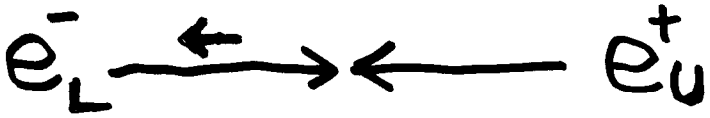

(b) Double Beam Polarization

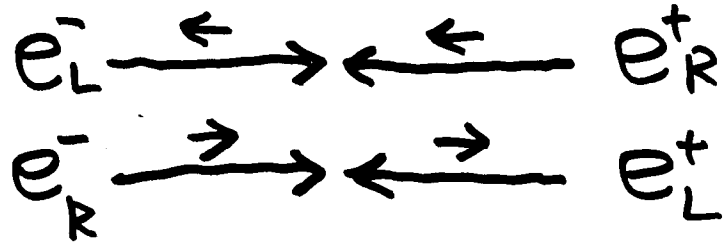

(1) TESLA/DESY-S-Band/VLEPP

Both e^+_s & e^-_s are created by an undulator.

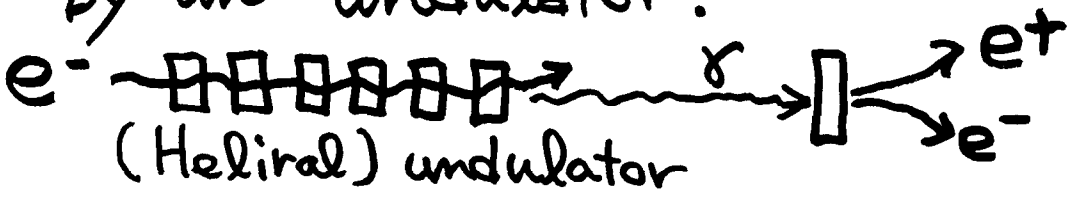

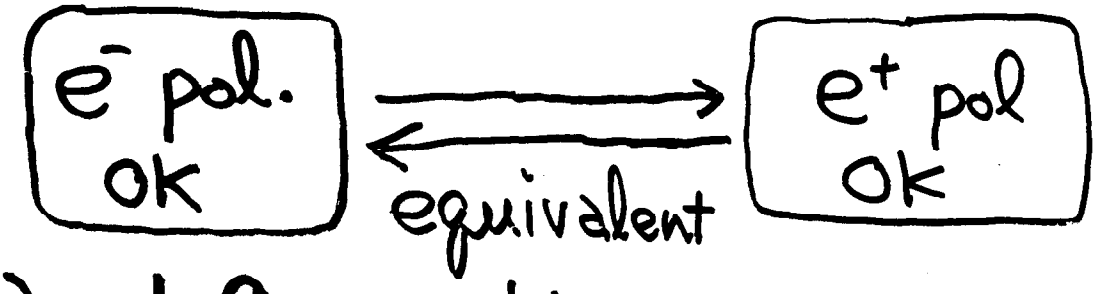

(2) xLC machines

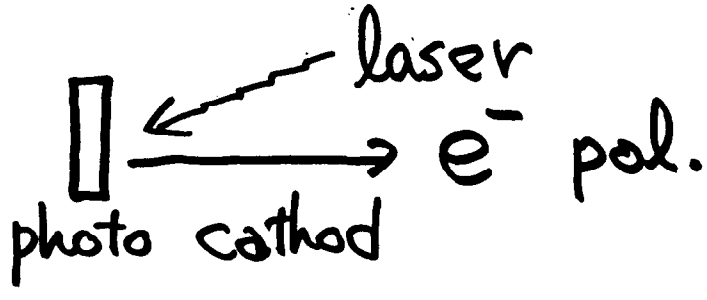

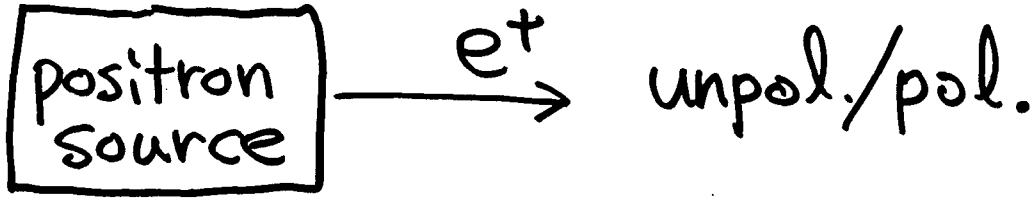

(3) Any Way, e^- beam will be (hopefuly?) polarized.

Question

Polarization of Positron
is Useful ?

↓

How
Double Beam Polarization
is Useful
than
Single Beam Polarization?

Remember Basics

Left-Hand electron (e_L) are different particles in High Energy.

e_R^-

NO Weak Interaction

$\begin{pmatrix} \nu_{eL} \\ e_L^- \end{pmatrix}$

Weak Interaction

Also Positrons: e_R^+ different e_L^+

e_L^+

NO Weak Int.

$\begin{pmatrix} \bar{\nu}_{eR} \\ e_R^+ \end{pmatrix}$

Weak Int.

a Famous Experiment, Wu, et al.

~~Parity~~

Exist

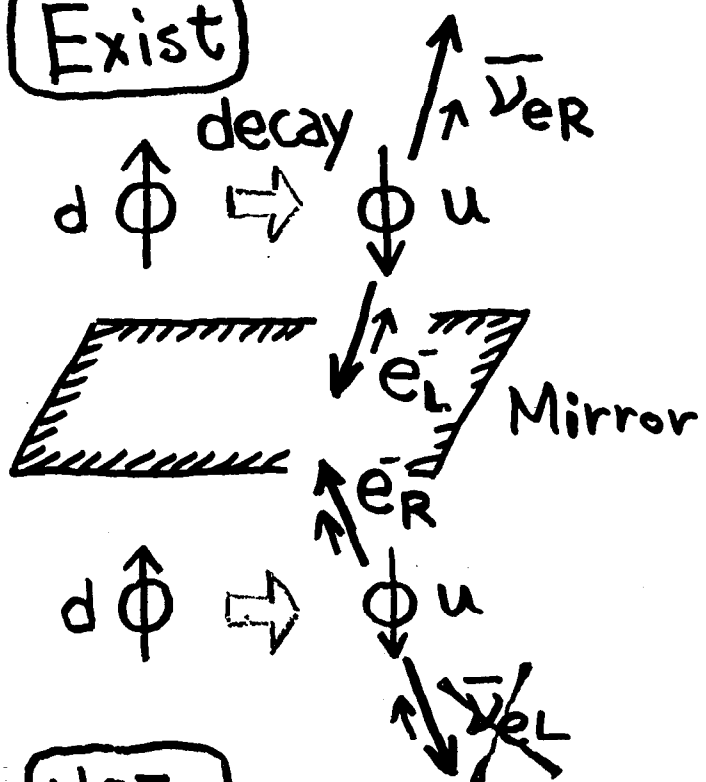

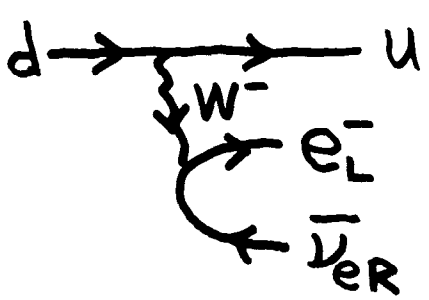

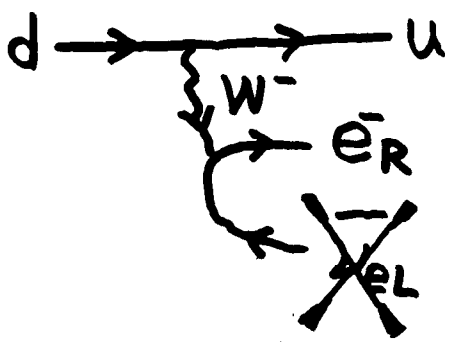

NOT Exist

$$\begin{pmatrix} \nu_{eL} \\ e_L^- \end{pmatrix} \xleftrightarrow{CP} \begin{pmatrix} \bar{\nu}_{eR} \\ e_R^+ \end{pmatrix}$$

$$e_R^- \xleftrightarrow{CP} e_L^+$$

Single Beam Polarization

- Annihilation; Vector Boson

Only Combinations of $e^-_L e^+_R$ and $e^-_R e^+_L$ can interact.

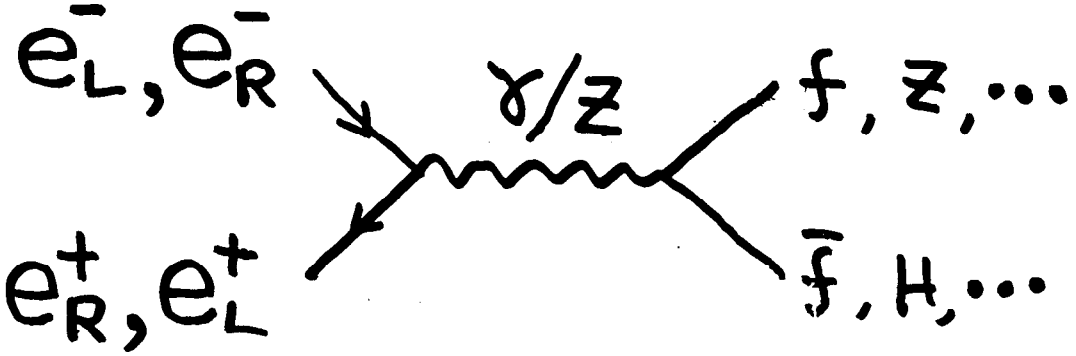

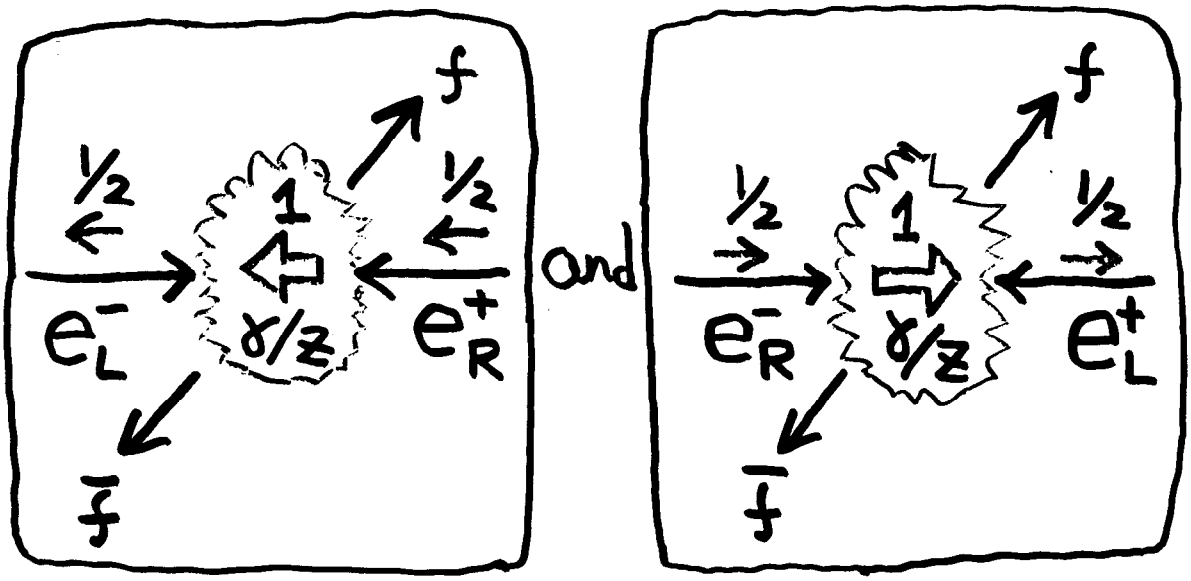

- t-channel exchange; neutrino, W-boson

Only $e_L^- e_R^+$ can interact.

(ν_{eR} dose NOT exist)

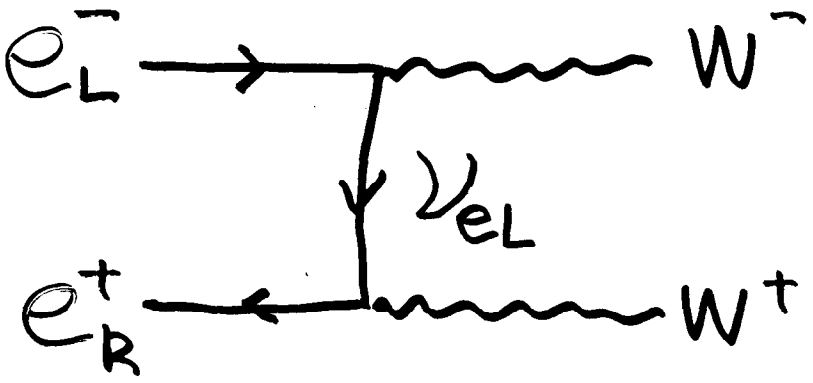

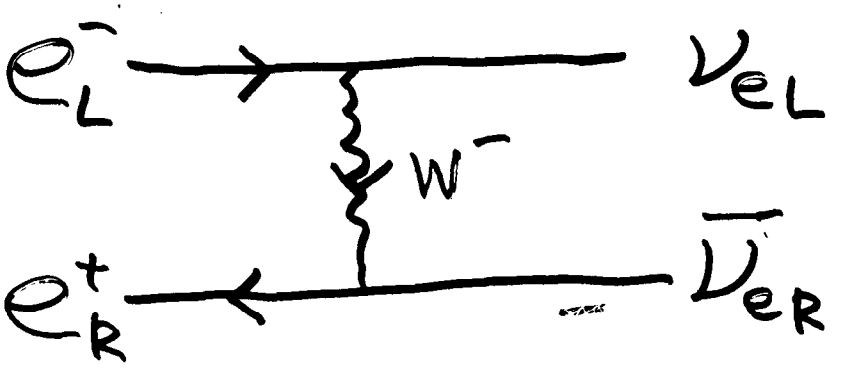

- two photon interaction. All combination can interact.

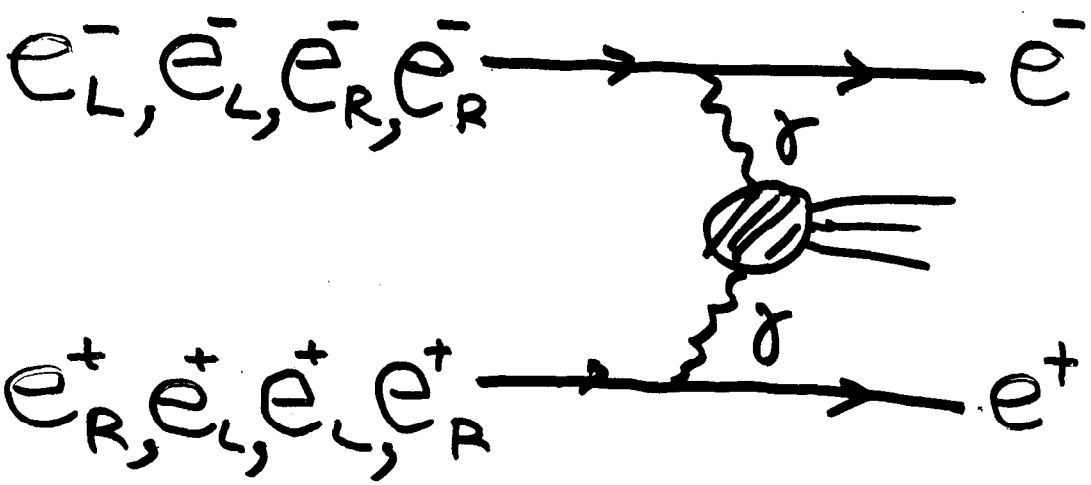

When we choose helicity of e^- beam, helicity of e^+s (can interact) are automatically chosen.

- Annihilation : Vector Boson.

$e_L^- \xrightarrow{\leftarrow}$ { $\xleftarrow{\leftarrow} e_R^+$ chosen ; $\xleftarrow{\rightarrow} e_L^+$ thrown away }

$e_R^- \xrightarrow{\rightarrow}$ { $\xleftarrow{\leftarrow} e_R^+$ thrown away ; $\xleftarrow{\rightarrow} e_L^+$ chosen }

- t-channel, ν, W exchange

$e_L^- \xrightarrow{\leftarrow}$ { $\xleftarrow{\leftarrow} e_R^+$ chosen ; $\xleftarrow{\rightarrow} e_L^+$ thrown away }

$e_R^- \xrightarrow{\rightarrow}$ { $\xleftarrow{\leftarrow} e_R^+$; $\xleftarrow{\rightarrow} e_L^+$ } Both are thrown away

Scalar μ-on Search (Min SUST $\tilde{\mu}_R$)

We will use e^-_R beam

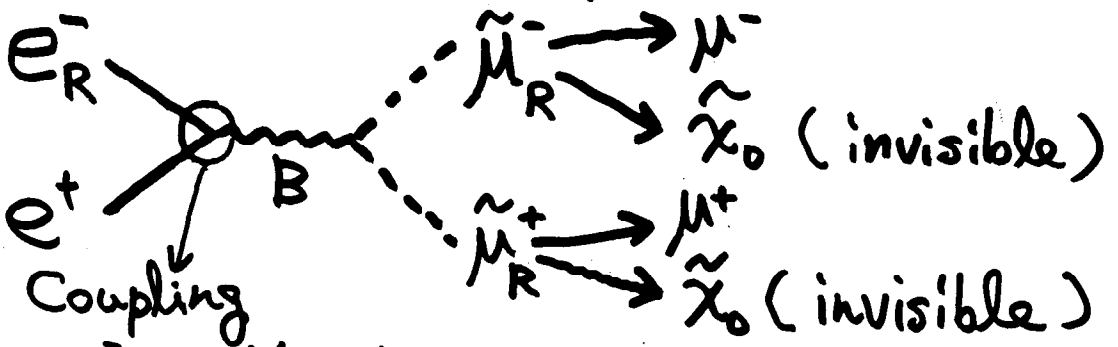

$e^-_L \quad Y = -1/2 \to \sigma_L \equiv 1$

$e_R \quad Y = -1 \to \sigma_R = 4$

Background: W-pair

$e^+e^- \to W^+W^- \to \mu^-\bar{\nu}$
$\to \mu^+\nu$

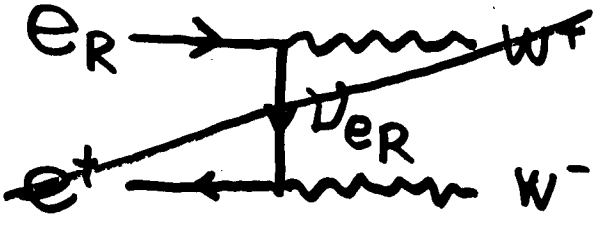

No

No

Cross Sections

$e^+e^- \to \bar{X}X$

NO beam polarization

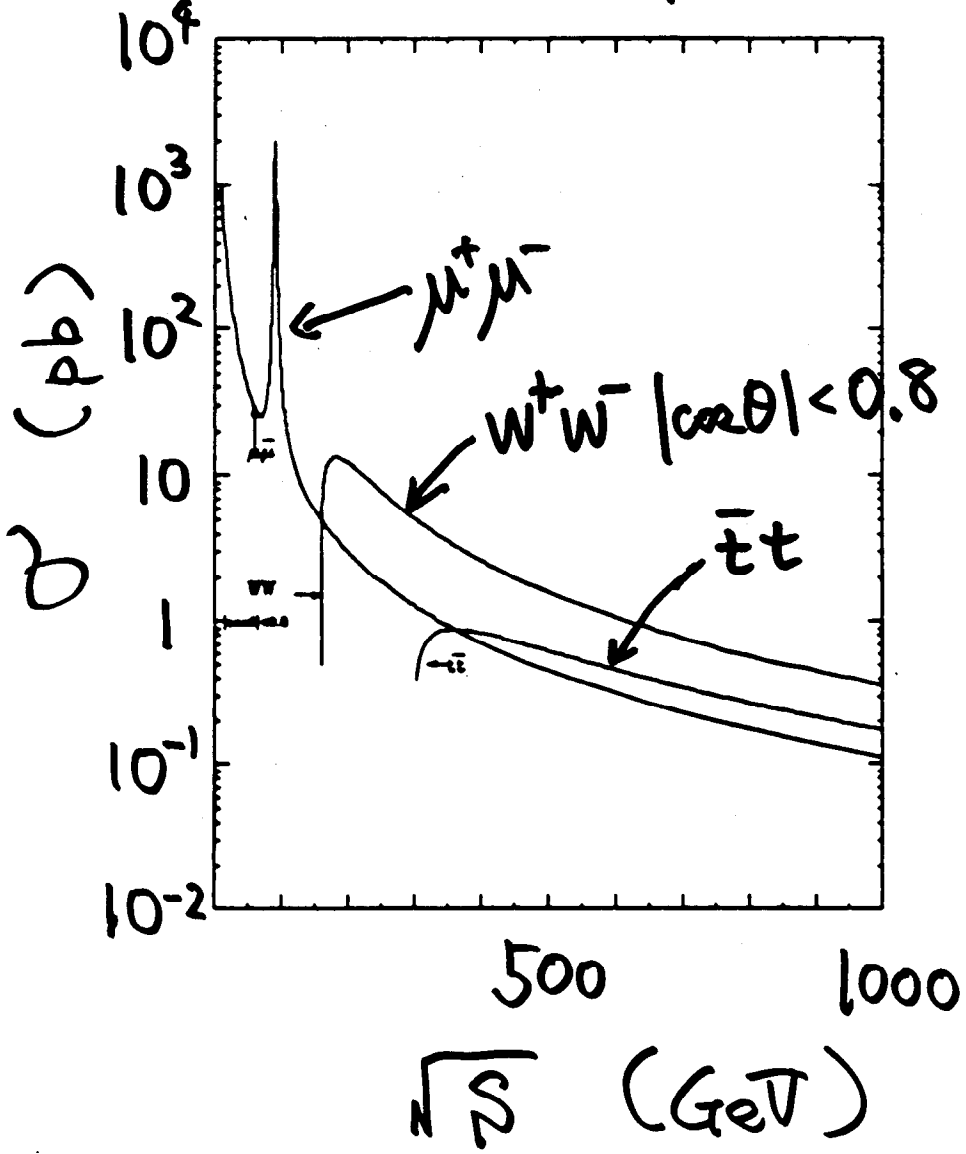

Scalar μ production $\tilde{\mu}_R^- \tilde{\mu}_R^+$ & $\tilde{\mu}_L^- \tilde{\mu}_L^+$

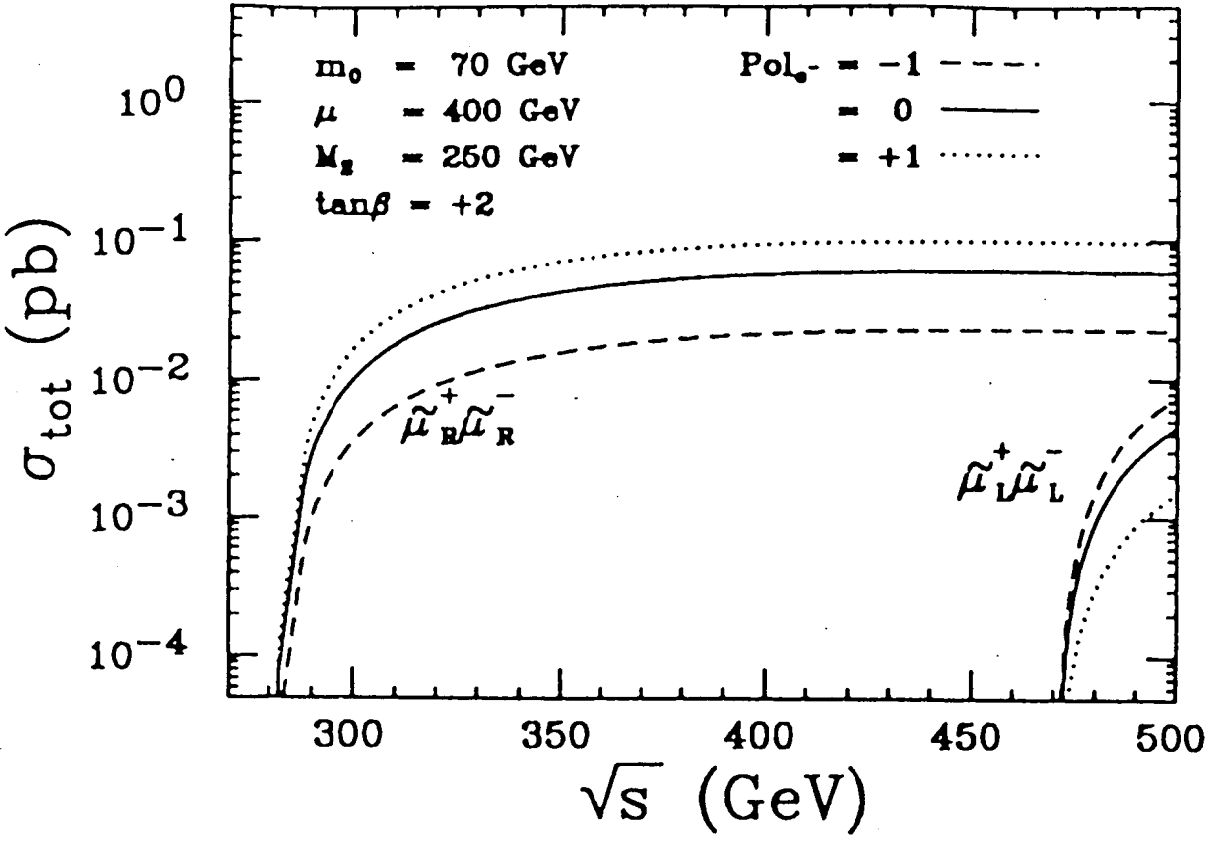

JLC-I KEK-Report 92-16

Scalar-μ $(e^+e^- \to \tilde{\mu}^+_R \tilde{\mu}^-_R)$

$\sqrt{s} = 350$ GeV

non-pol e^--beam e^-_R beam (95%) → optimistic if P=80% BG ~ ×4

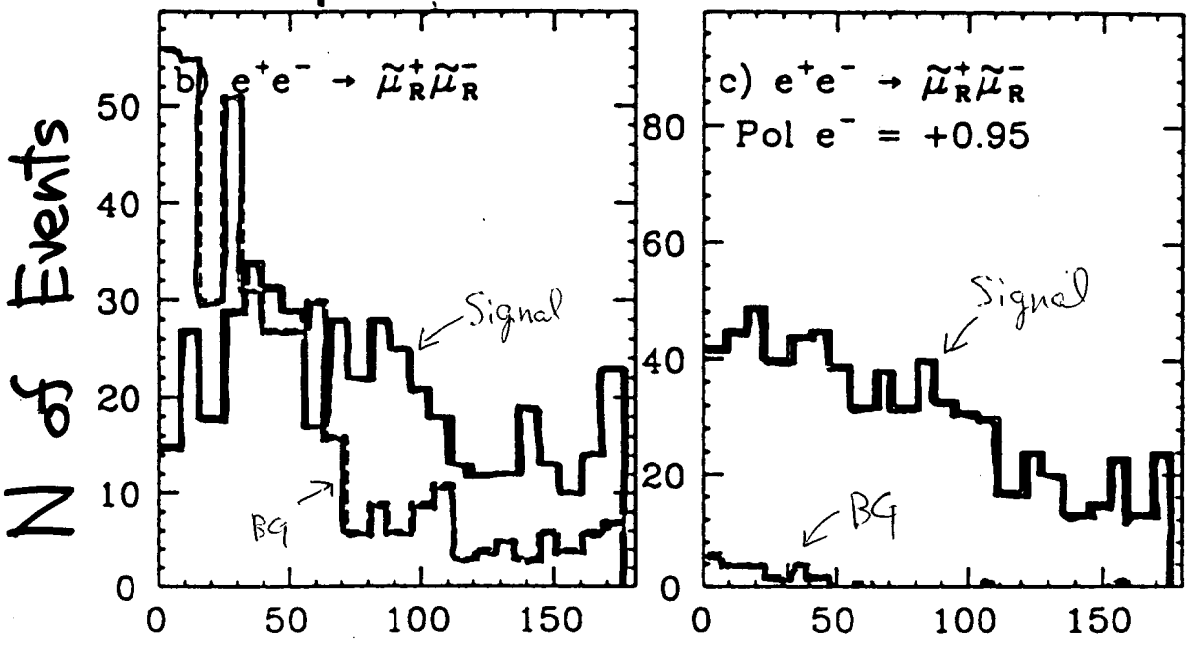

θ_{acop}(deg.) θ_{acop}(deg)

Signal

$e^+e^- \to \tilde{\mu}^+_R\tilde{\mu}^-_R$

$\to \mu^+\mu^-\tilde{\chi}^0_1\tilde{\chi}^0_1$

Background

$e^+e^- \to W^+W^-$

$\to \mu^+\mu^-\nu\bar{\nu}$

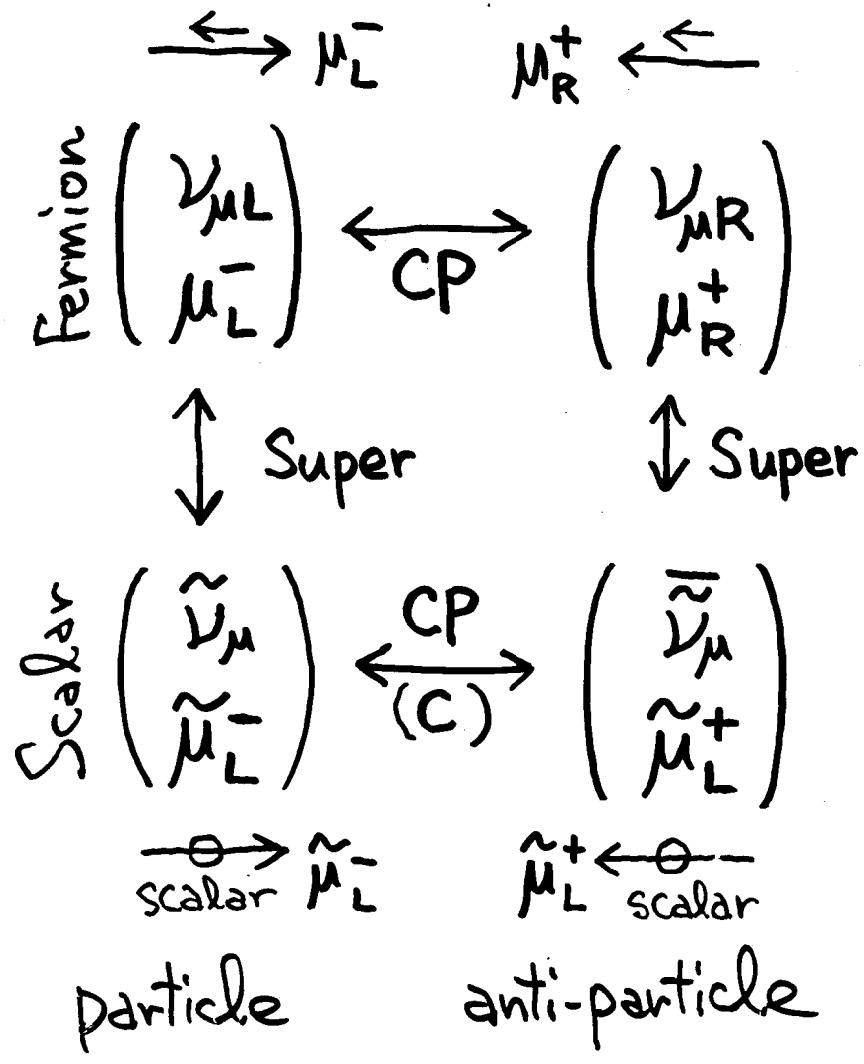
μ_L^-
μ_R^+
Fermion
$\begin{pmatrix} \nu_{\mu L} \\ \mu_L^- \end{pmatrix}$
CP
$\begin{pmatrix} \nu_{\mu R} \\ \mu_R^+ \end{pmatrix}$
Super
Super
Scalar
$\begin{pmatrix} \tilde{\nu}_\mu \\ \tilde{\mu}_L^- \end{pmatrix}$
CP
(C)
$\begin{pmatrix} \tilde{\nu}_\mu \\ \tilde{\mu}_L^+ \end{pmatrix}$
scalar $\tilde{\mu}_L^-$
$\tilde{\mu}_L^+$ scalar
particle
anti-particle

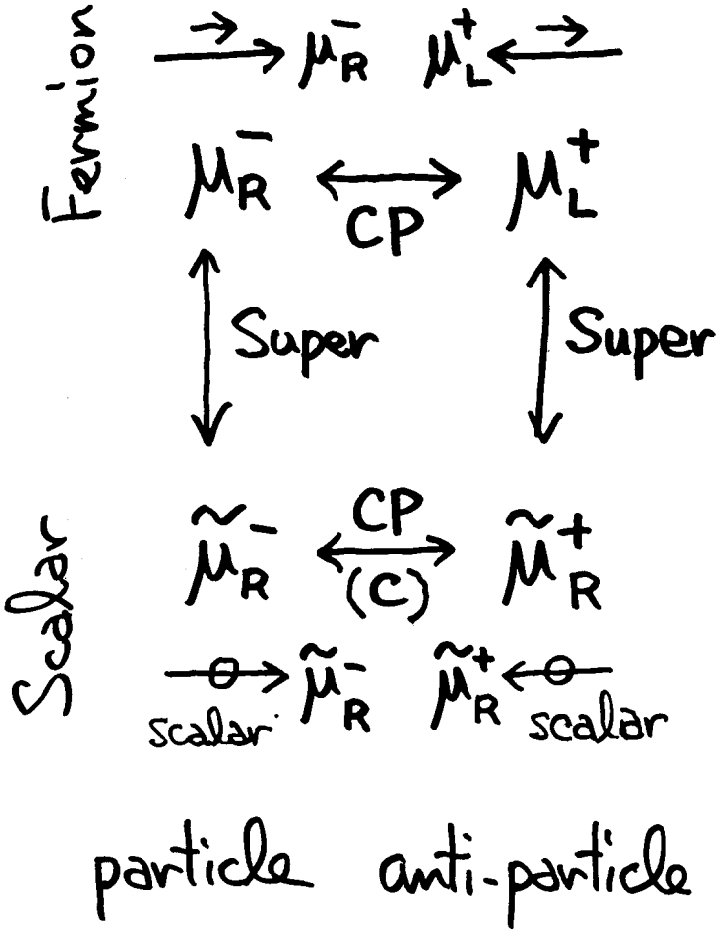
Fermion
μ_R^-
μ_L^+
μ_R^-
CP
μ_L^+
Super
Super
Scalar
$\tilde{\mu}_R^-$
CP
(C)
$\tilde{\mu}_R^+$
scalar $\tilde{\mu}_R^-$
$\tilde{\mu}_R^+$ scalar
particle
anti-particle

Only Electron Polarization
(Single Beam Polarization)
is already Useful.

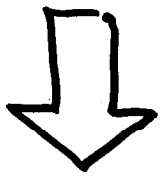

Positron Polarization
(Double Beam Polarization)
is Necessary ?

Double Beam Polarization

Cross Section ↔ Comb. of Pol.

- Non Polarized Beams

(1) $e^-_U \times e^+_U \longrightarrow \bar{f}f$, W^+W^-

	$\bar{f}f$	W^+W^-
$e^-_L \leftarrow\!\!\rightarrow\!\!\leftarrow e^+_R$	$\equiv \sigma_A$ (def)	$\equiv \sigma_B$ (def)
$e^-_L \leftarrow\!\!\rightarrow\!\!\rightarrow e^+_L$	0	0
$e^-_R \rightarrow\!\!\leftarrow\!\!\leftarrow e^+_R$	0	0
$e^-_R \rightarrow\!\!\rightarrow\!\!\leftarrow e^+_L$	$\sigma'_A \simeq \sigma_A$	$\sim \frac{1}{100}\sigma_B$
	~~1/2 of comb.~~	~~3/4 of comb.~~

- Single Beam Pol.

(2) $e^-_L(100\%) \times e^+_U \rightarrow \bar{f}f$, W^+W^-

	$\bar{f}f$	W^+W^-
$e^-_L \leftarrow\!\!\rightarrow\!\!\leftarrow e^+_R$	σ_A	σ_B
$e^-_L \leftarrow\!\!\rightarrow\!\!\rightarrow e^+_L$	0	0
	~~1/2 of Comb.~~	~~1/2 of Comb.~~

(3) $e^-_R(100\%) \times e^+_U \rightarrow \bar{f}f$, W^+W^-

	$\bar{f}f$	W^+W^-
$e^-_R \rightarrow\!\!\leftarrow\!\!\leftarrow e^+_R$	0	0
$e^-_R \rightarrow\!\!\rightarrow\!\!\leftarrow e^+_L$	$\sigma'_A \simeq \sigma_A$	$\sim \frac{1}{100}\sigma_B$
	~~1/2 of Comb.~~	suppressed

Cross Section ↔ Comb. of Pol.

- Double Beam Pol.

(4) $e^-_L(100\%) \times e^+_R(100\%) \to \bar{f}f$, W^+W^-

$e^-_L \xleftarrow{\leftarrow} \xrightarrow{\leftarrow} e^+_R$ σ_A σ_B

(5) $e^-_R(100\%) \times e^+_L(100\%) \to \bar{f}f$, W^+W^-

$e^-_R \xrightarrow{\rightarrow} \xleftarrow{\rightarrow} e^+_L$ $\sigma_A' \simeq \sigma_A$ $\sim \frac{1}{100}\sigma_B$

suppressed

here, $\frac{1}{100}$ means Oder of $\frac{1}{100}$.

actual value depends on CM energy.

σ control for $\bar{f}f$, W^+W^-
100 % pol. is assumed.

	$\bar{f}f$	W^+W^-
Non Pol.		
(1) $e^-_U \times e^+_U$	$\overset{\text{def}}{\equiv} 1$	$\overset{\text{def}}{\equiv} 1$
Single Beam Pol.		
(2) $e^-_L \times e^+_U$	~ 1	~ 2
(3) $e^-_R \times e^+_U$	~ 1	$\sim 2/100$
Double Beam Pol.		
(4) $e^-_L \times e^+_R$	~ 2	~ 4
(5) $e^-_R \times e^+_L$	~ 2	$4/100$

Not eq.

$\sigma(W^+W^-)$
When pol. < 100%,
(5) is much smaller than (3).

$\sigma_{tot}(e^+e^- \to W^+W^-)$

assume $\begin{cases} |\text{Pol. } e^-| = 90\% & \text{for } e^-_L, e^-_R \\ |\text{Pol. } e^+| = 80\% & \text{for } e^+_L, e^+_R \end{cases}$

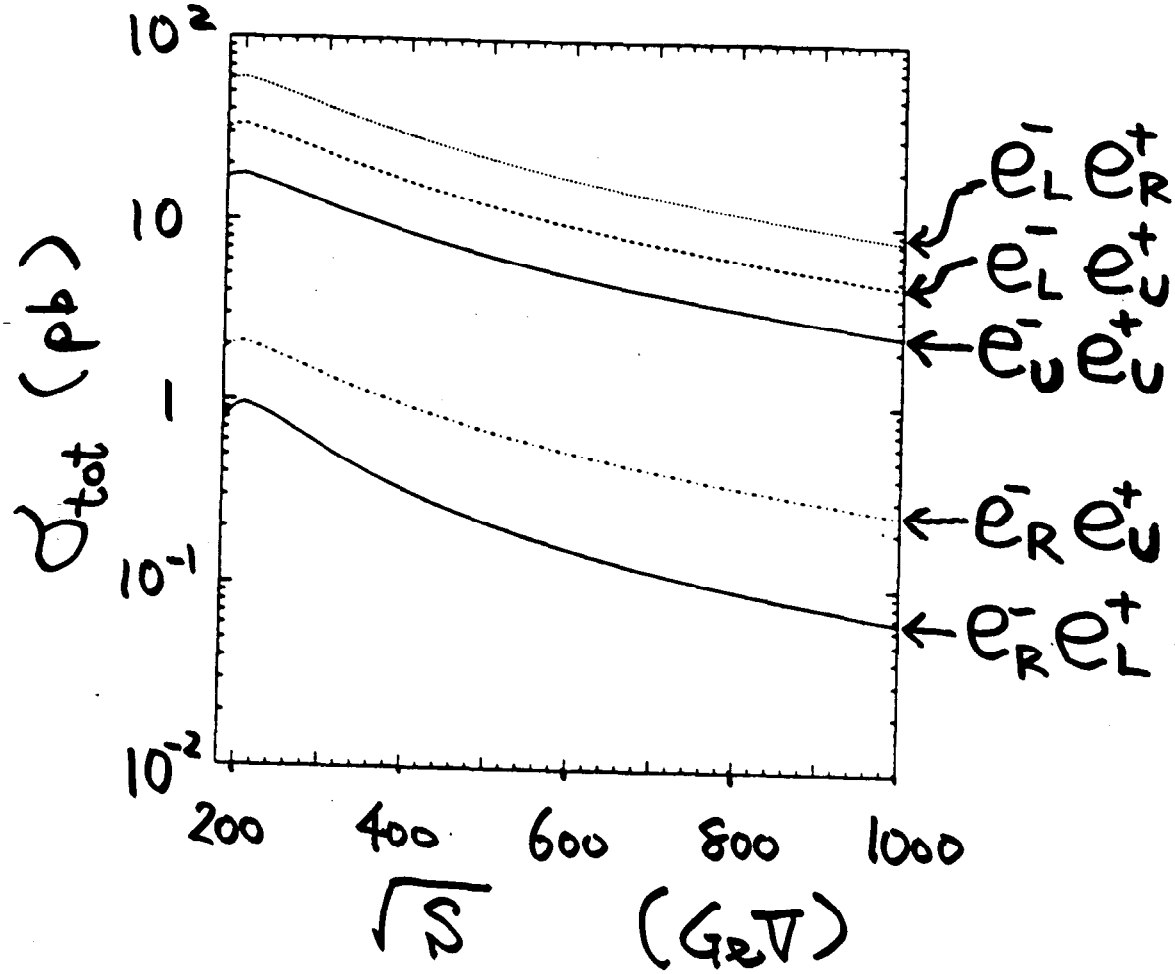

Y. Kurihara with GRACE

Sequential Heavy Lepton

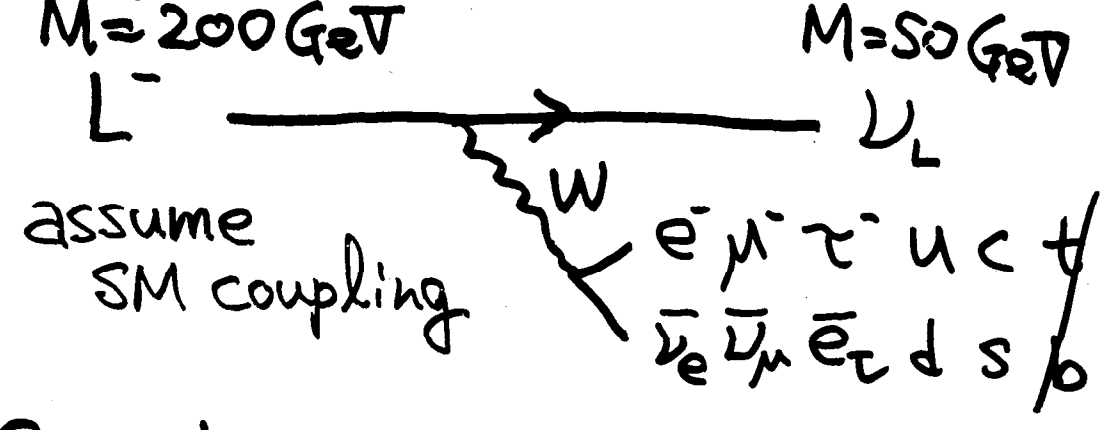

Search

$e^+e^- \to L^+ L^-$

$L^+ \to \mu^+ \bar{\nu}_\mu \nu_L$ & $e^+ \nu_e \bar{\nu}_L$

$L^- \to e^- \bar{\nu}_e \nu_L$ & $\mu^- \nu_\mu \bar{\nu}_L$

determine M_{ν_L} & M_L

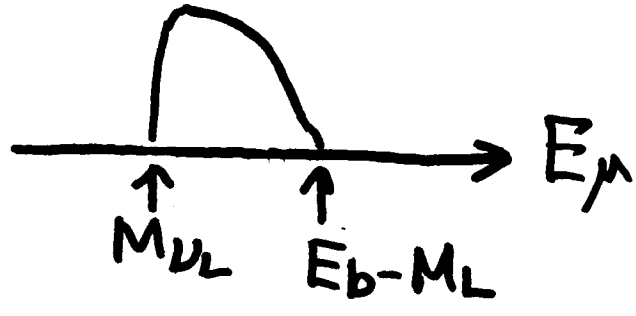

BackGraund

$e^+e^- \to W^+W^-$

$W^+ \to \mu^+ \nu_\mu$ & $e^+ \nu_e$

$W^- \to e^- \bar{\nu}_e$ & $\mu^- \bar{\nu}_\mu$

$e^+e^- \to L^+L^-$ $\sqrt{s} = 500$ GeV

search μ^+e^-, $e^+\mu^-$ $|\cos\theta_{\mu,e}| < 0.8$

No Polarized Beam

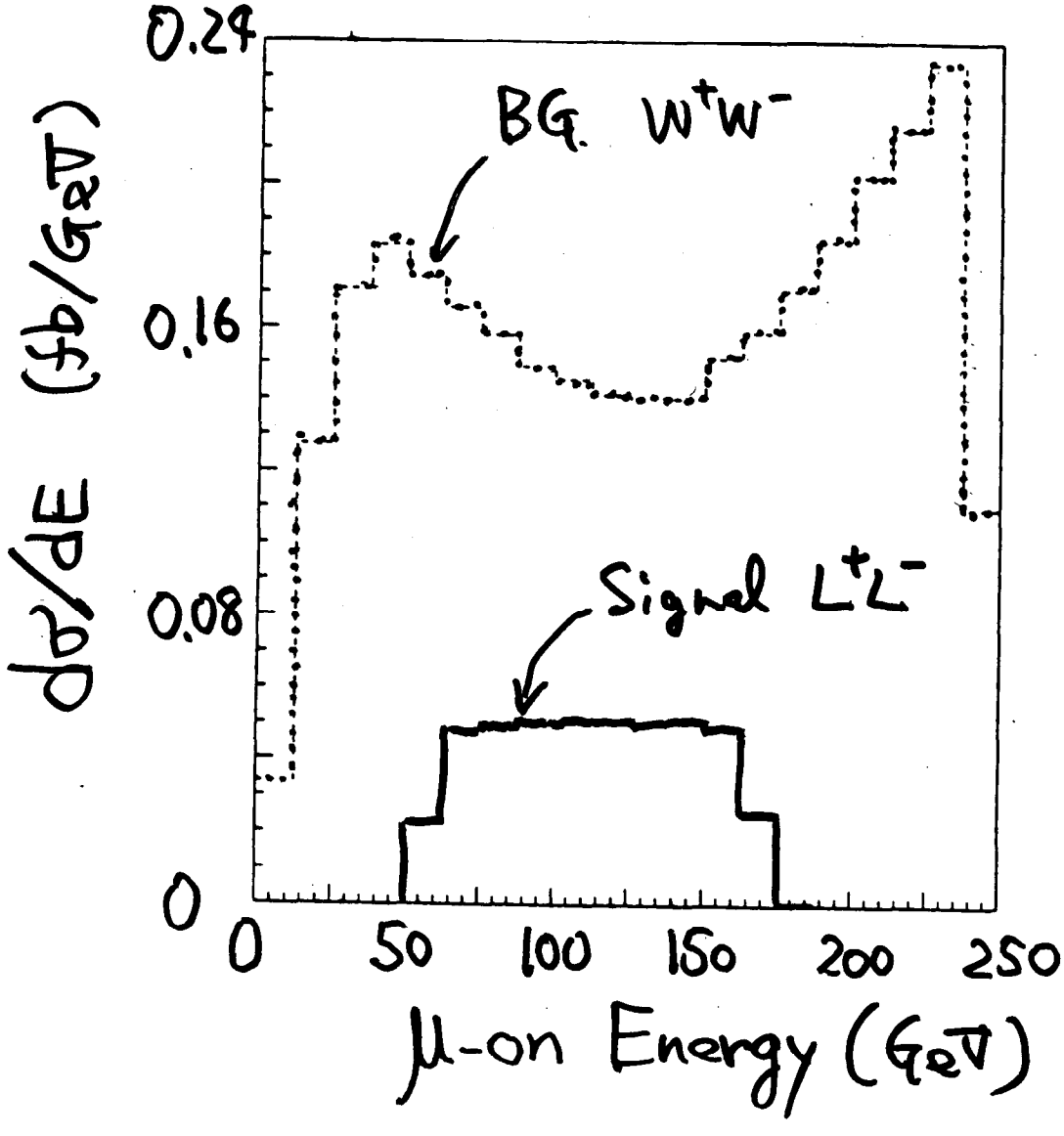

Y. Kurihara with GRACE

$e^+e^- \to L^+L^-$ $\sqrt{s} = 500$ GeV

Search μ^+e^-, μ^-e^+ $|\cos\theta_{\mu,e}| < 0.8$

Single Beam Pol. e^- P=90%R
e^+ Unpol.

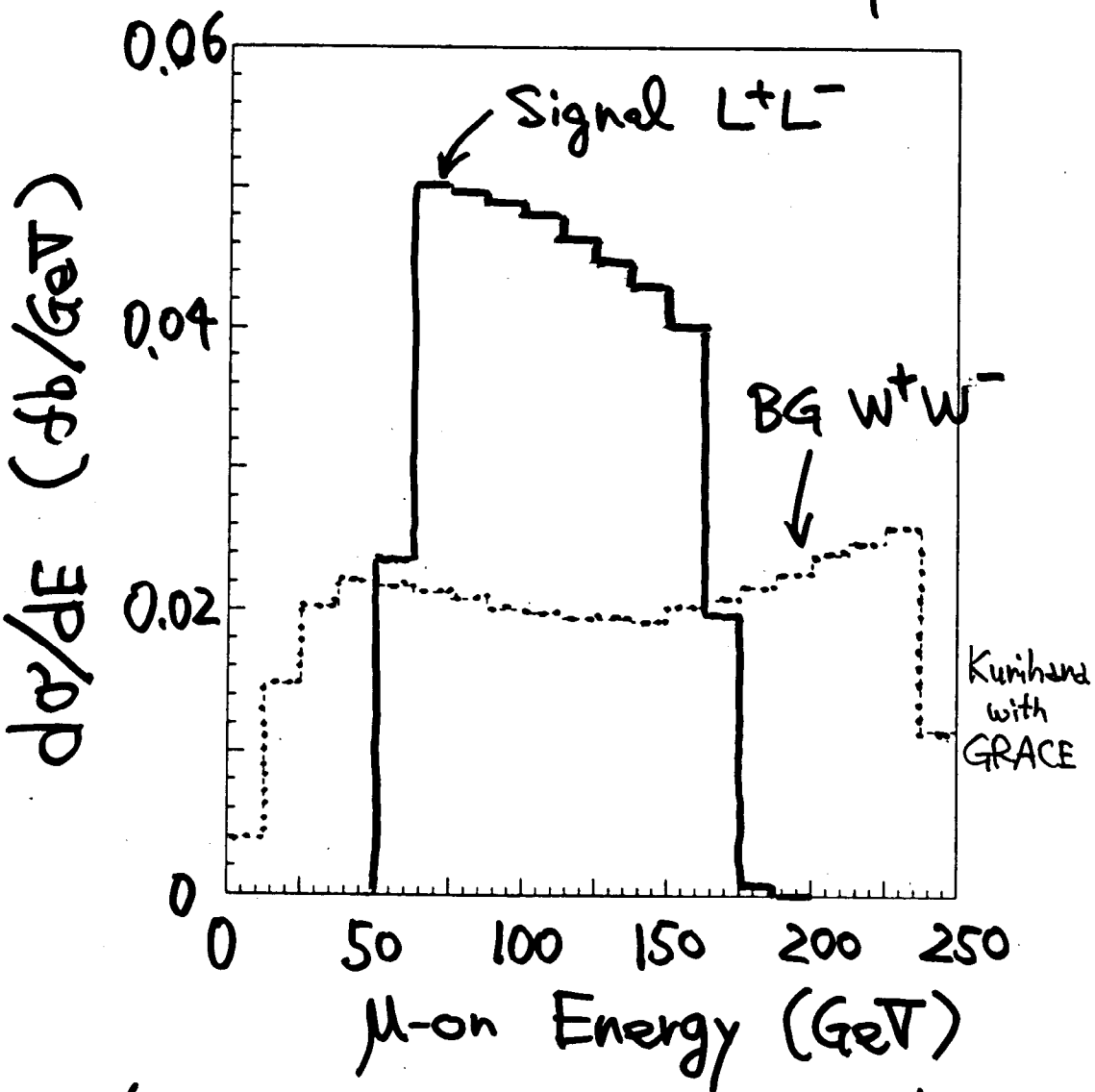

S/BG $\simeq 1$. We see something.
But hard to determine mass.

$e^+e^- \to L^+L^-$ $\sqrt{s} = 500$ GeV

search μ^+e^-, μ^-e^+ $|\cos\theta_{\mu,e}| < 0.8$

Double Beam Pol. e^- P=90%R e^+ P=80%L

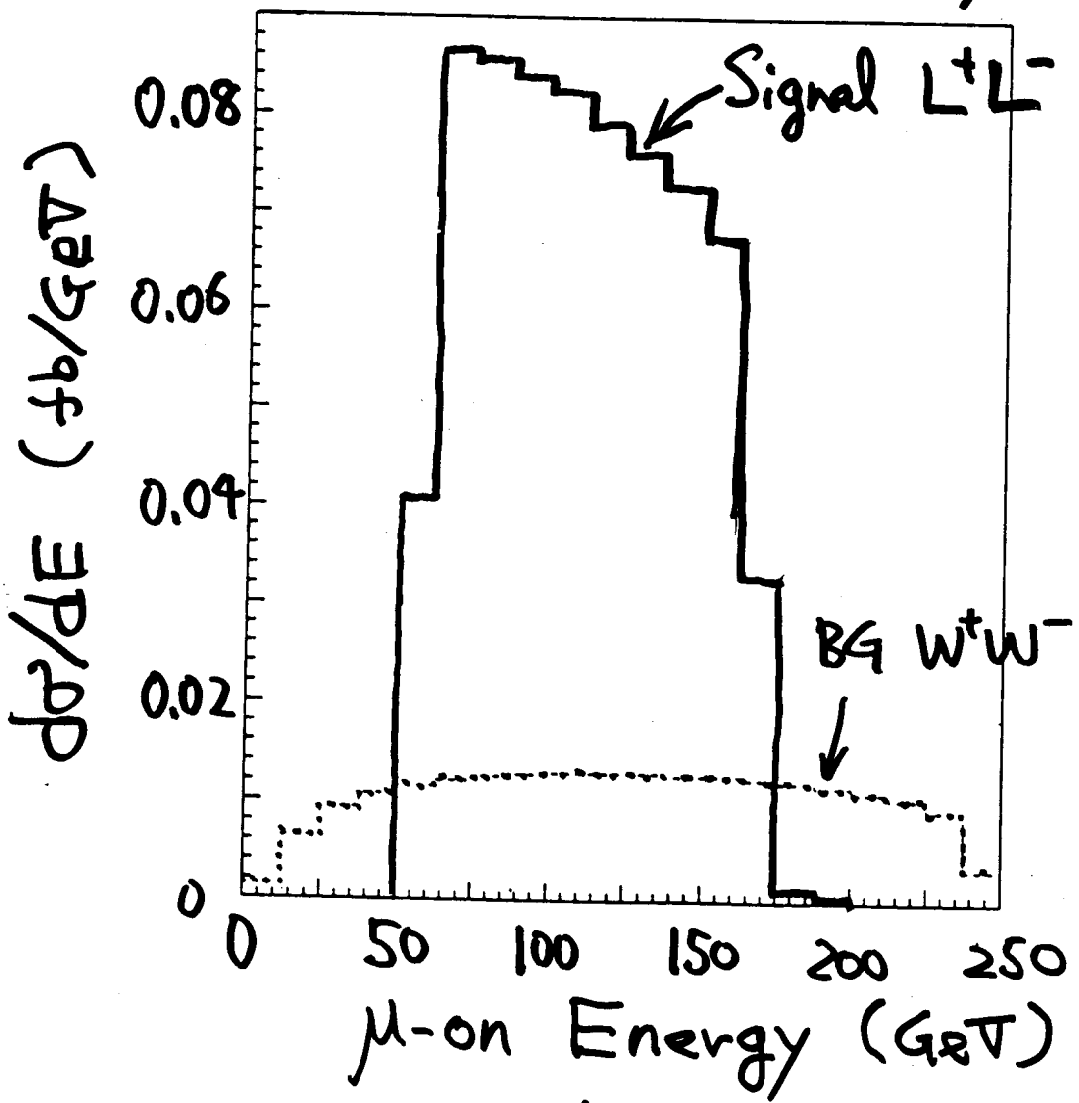

Clean Signal/BG

Y. Kurihara/GRACE

Combined Polarization

$$P_{comb} \overset{def}{\equiv} \frac{N_L^- N_R^+ - N_R^- N_L^+}{N_L^- N_R^+ + N_R^- N_L^+}$$

$$= \frac{P_- - P_+}{1 - P_- P_+}$$

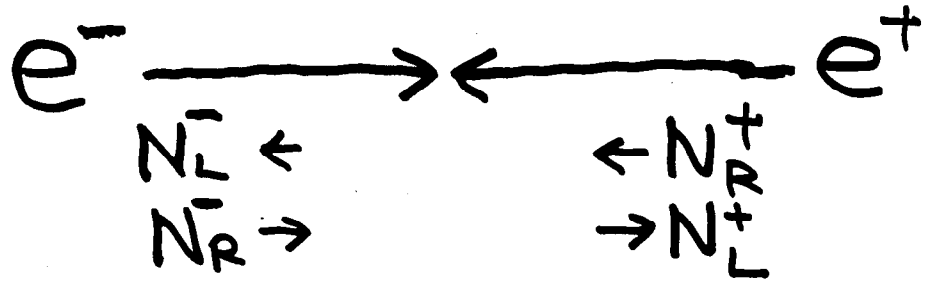

$$P_{\mp} \overset{def}{\equiv} \frac{N_R^{\mp} - N_L^{\mp}}{N_R^{\mp} + N_L^{\mp}}$$

$P_{comb} < 0 \rightarrow e_L^- \text{ beam} \times e_R^+ \text{ beam}$

P_{comb} is NOT useful when

You choose $e_R^- \text{ beam} \times e_R^+ \text{ beam}$

$e_L^- \text{ beam} \times e_L^+ \text{ beam}$

Examples of P_{comb}

(1) $\begin{cases} P_- = 0.90 & e^- \text{ R : Pol=90\%} \\ P_+ = 0.0 & e^+ \text{ unpol} \end{cases}$

$\Rightarrow P_{comb} = 0.90$

(2) $\begin{cases} P_- = 0.90 & e^- \text{ R: Pol= 90\%} \\ P_+ = -0.80 & e^+ \text{ L: Pol=80\%} \end{cases}$

$\Rightarrow P_{comb} = 0.99$

(3) $\begin{cases} P_- = 0.80 & e^- \text{ R: Pol=80\%} \\ P_+ = -0.60 & e^+ \text{ L: Pol=60\%} \end{cases}$

$\Rightarrow P_{comb} = 0.95$

If only $\tilde{\chi}_1^0$ is Available

(LSP: invisible)

Search $e^+e^- \to \tilde{\chi}_1^0 \tilde{\chi}_1^0 \gamma$

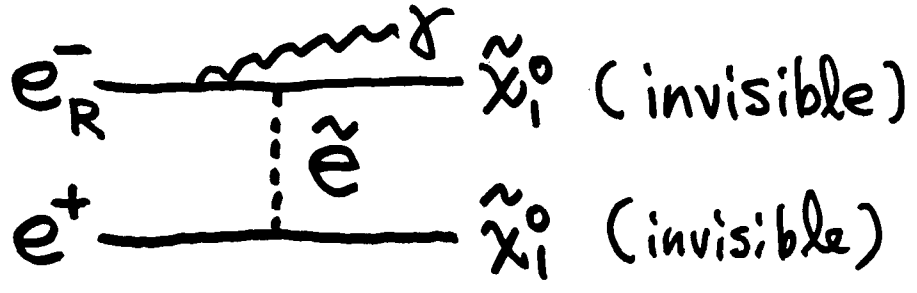

Backgrounds

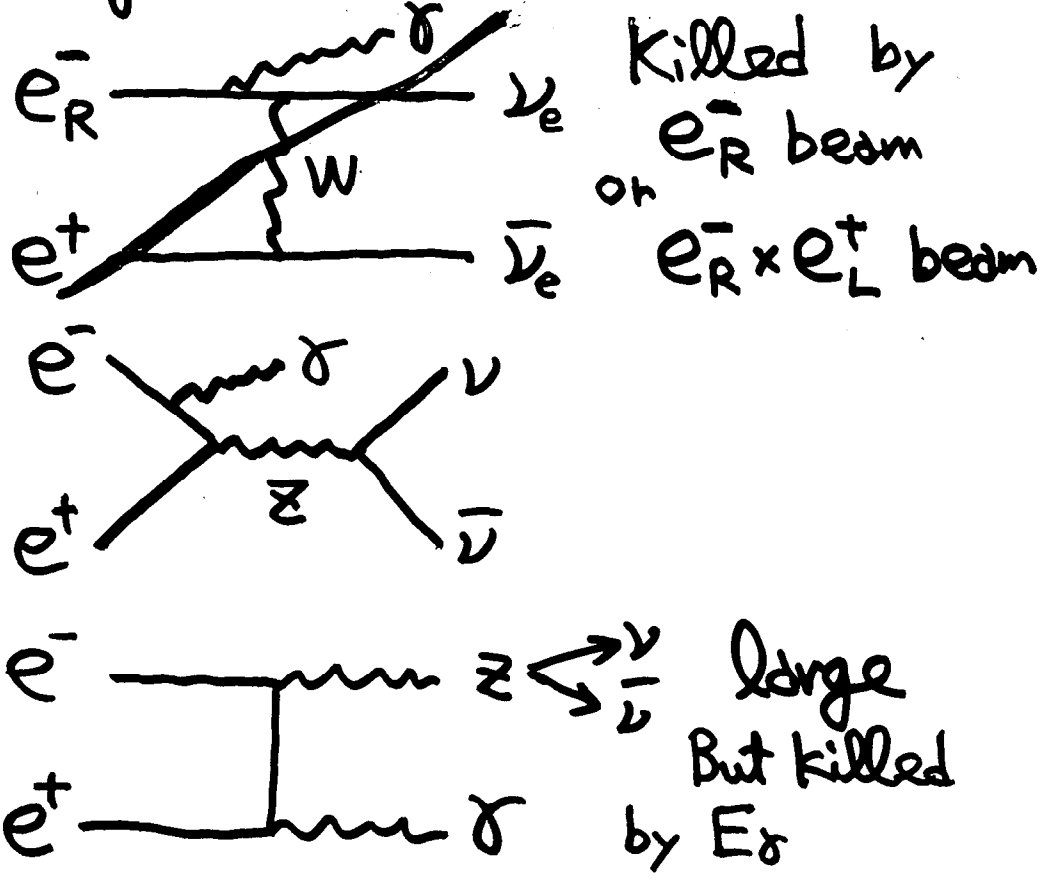

If Only LSP Is Available

Is single photon experiment possible ?

General Belief

Abe-Kon-KF
with GRACE

BG Mask and Final Quads

Huge SM BG

Hard to get θ_{veto} small !

$$e^+e^- \rightarrow \nu\bar{\nu}\gamma$$

⟶ Very difficult if not impossible !

Possible Way Out

Polarized Beam to kill BG, which mainly comes from t-channel W exchange.

Pol. = 100% assumed

e^-_R

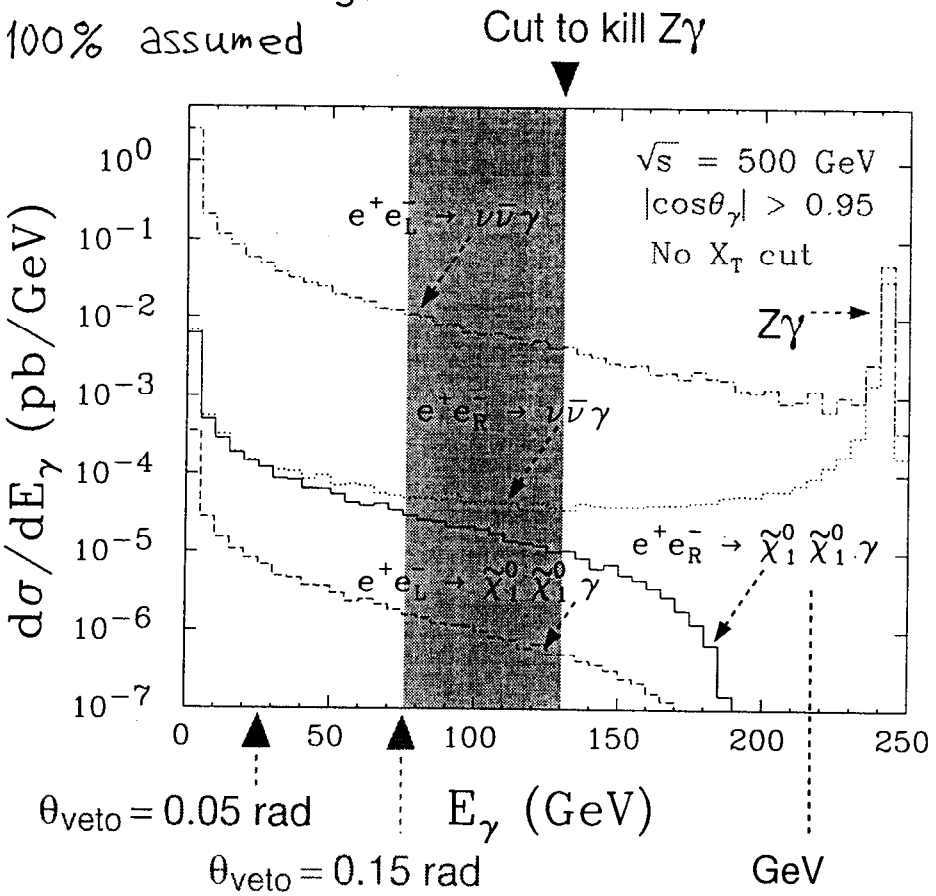

GeV

$(m_0, M_2, \mu, \tan\beta) = (250, 245, 588, -2)$

$(m_{\tilde{e}^\pm_R}, m_{\tilde{\chi}^0_1}) = (278, 124)$ GeV

K. Fujii Morioka-Appi LCWS 95

Search $e^+e^- \to \tilde{\chi}_1^0 \tilde{\chi}_1^0 \gamma$

Physicists Require 100% pol. ??

→ NO! 99.5% is OK.

P_{e^-} = 95% R
P_{e^+} = 80% L
} 99.5%

P_{e^-} = 90% R
P_{e^+} = 90% L
} 99.4%

Error of P_{comb}

$$\Delta P_{comb} = \left(\frac{\partial P_{comb}}{\partial P_-}\right)\left(\frac{\Delta P_-}{P_-}\right)P_- + \left(\frac{\partial P_{comb}}{\partial P_+}\right)\left(\frac{\Delta P_+}{P_+}\right)P_+$$

error of pol. measurements

$$\frac{\partial P_{comb}}{\partial P_\mp} = \frac{1 - P_\pm^2}{(1 - P_-^+ P_+^-)^2}$$

assume $\Delta P_-/P_- = \Delta P_+/P_+ \equiv \Delta P/P$

$$\frac{\Delta P_{comb}}{P_{comb}} = \underbrace{\frac{1 + P_- P_+}{1 - P_- P_+}}_{<1}\left(\frac{\Delta P}{P}\right)$$

We improve accuracy of polrarizatin determination.

K. Flöttman DESY 95-064

P_{comb} & $\Delta P_{comb}/P_{comb}$

$|P_{e^-}| = 0.9$ assemed

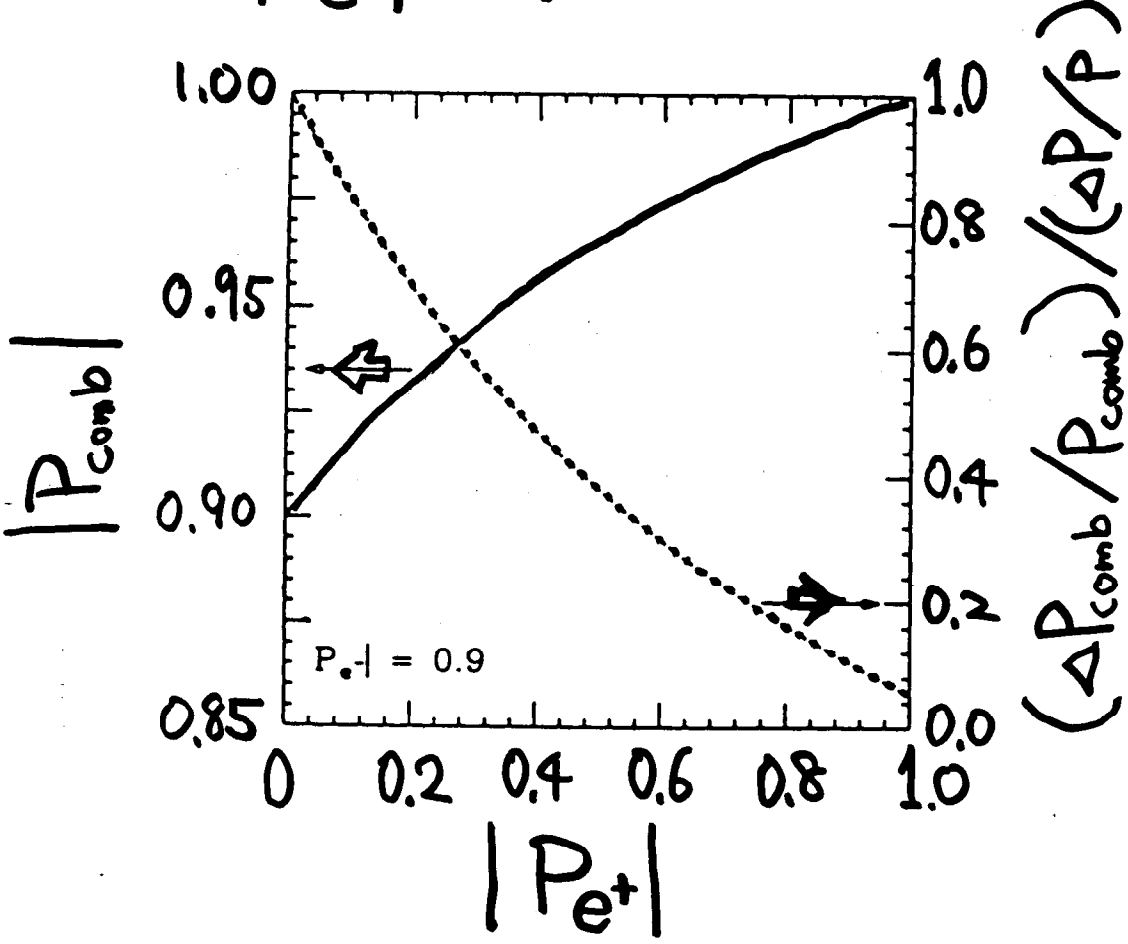

if $\left\{\begin{array}{l} |P_{e^-}| = 0.9 \\ |P_{e^+}| = 0.8 \\ \Delta P/P = 0.01 \end{array}\right\} \Rightarrow \Delta P_{comb}/P_{comb} \simeq 0.0016$

Measure $\sin^2\theta_W$ on Z-pole

assume $\begin{cases} |P_{e^-}| = 0.9 \\ \Delta P/P = 0.01 \end{cases}$

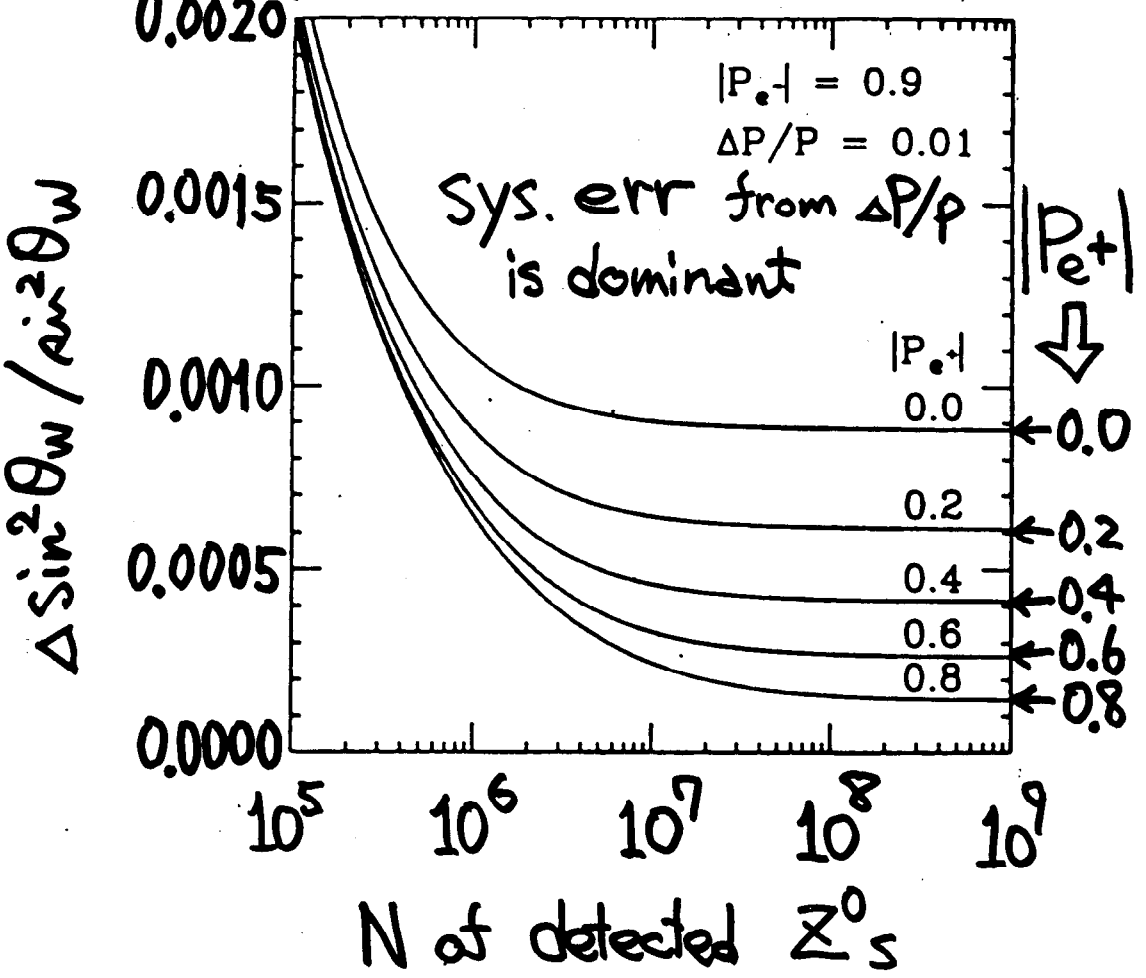

3 weeks

$|P_{e^-}| = 0.9$
$|P_{e^+}| = 0.8$

$L = 1 \times 10^{33}\,cm^{-2}s^{-1}$

Zoo of Interesting Interactions

Indirect Study of $\tilde{q}$

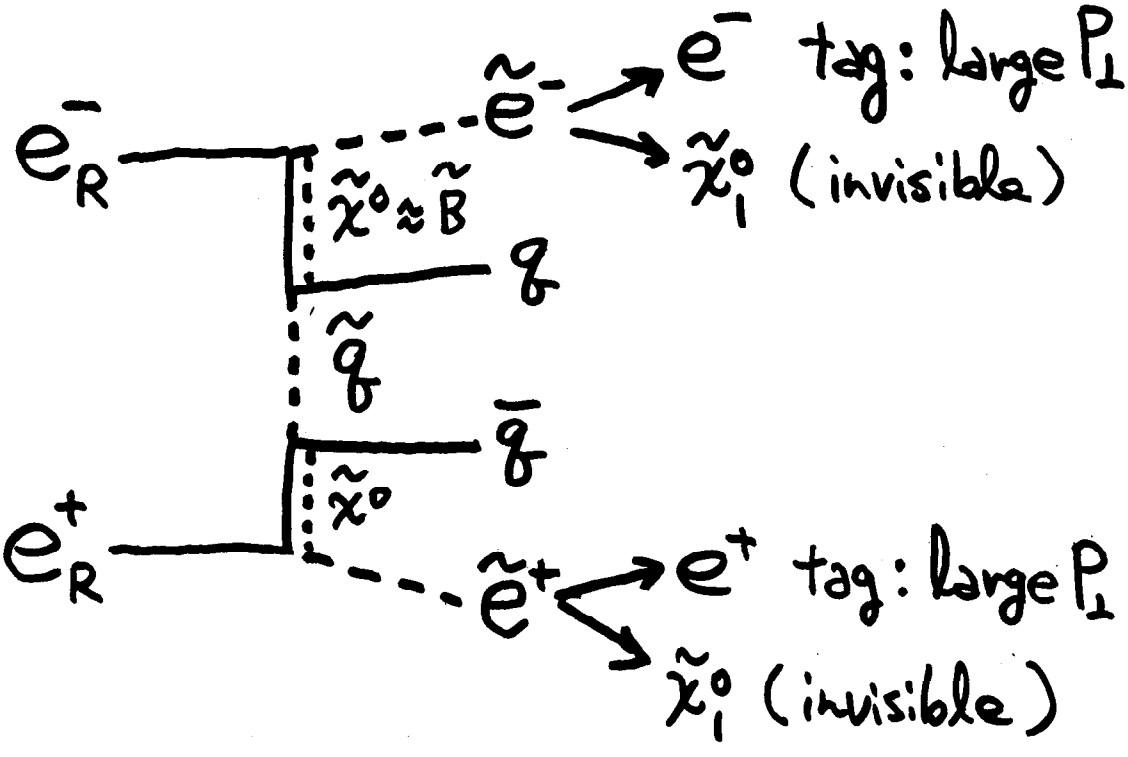

SUSY version of two photon physics

Use $e^-_R \times e^+_R$ beam

$e^-_R \rightarrow \quad \leftarrow e^+_R$

to suppress Backgrounds

Seach $e^+_R e^-_R \to \tilde{e}^-_R \tilde{\chi}^+ \bar{\nu}_e$

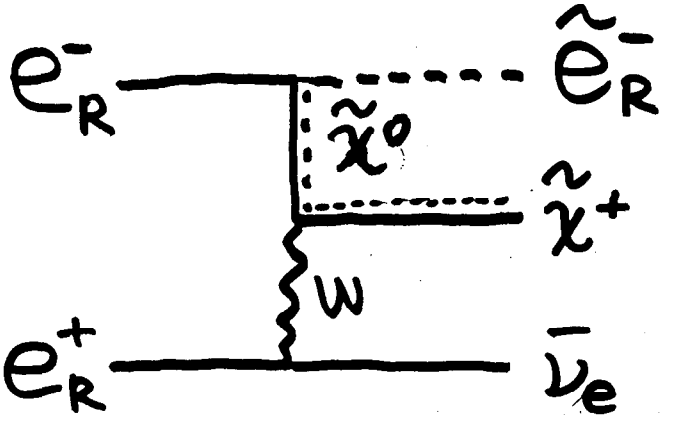

Use $e^-_R \times e^+_R$ beam

(1) No Background

(2) threshold is Lower than

either $e^+_L e^-_R \to \tilde{e}^+_R \tilde{e}^-_R$

or $e^+ e^- \to \tilde{\chi}^+ \tilde{\chi}^-$

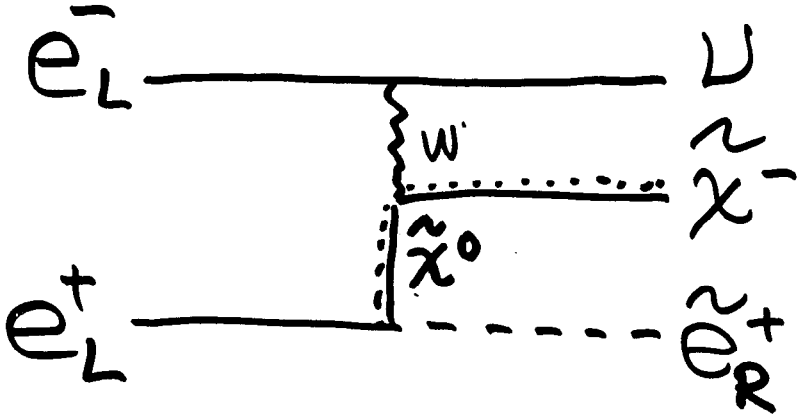
e_L^-
ν
W
$\tilde{\chi}^-$
$\tilde{\chi}^0$
e_L^+
$\tilde{e}_R^+$

$e^+e^- \to e^{\mp} W^{\pm} \overset{(-)}{\nu}_e$ events

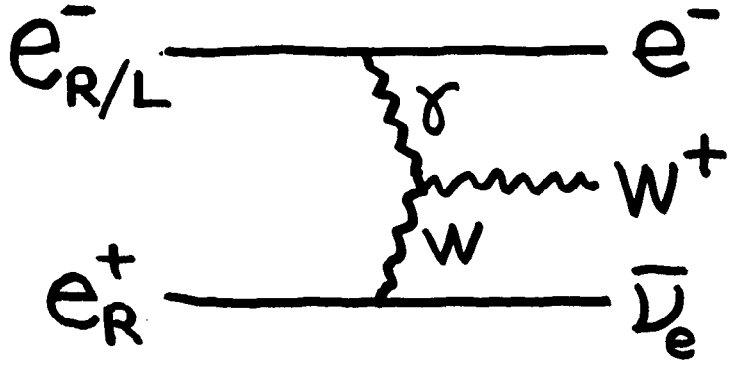

Study WWγ coupling

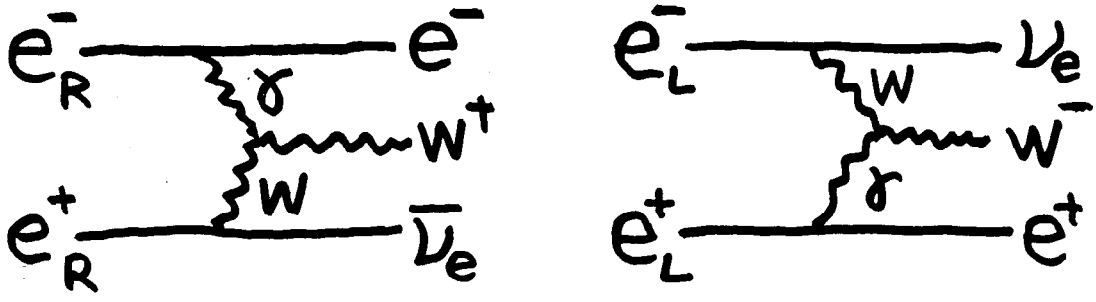

Kill $e^{\mp} W^{\pm} \overset{(-)}{\nu}$ ← if this is Background

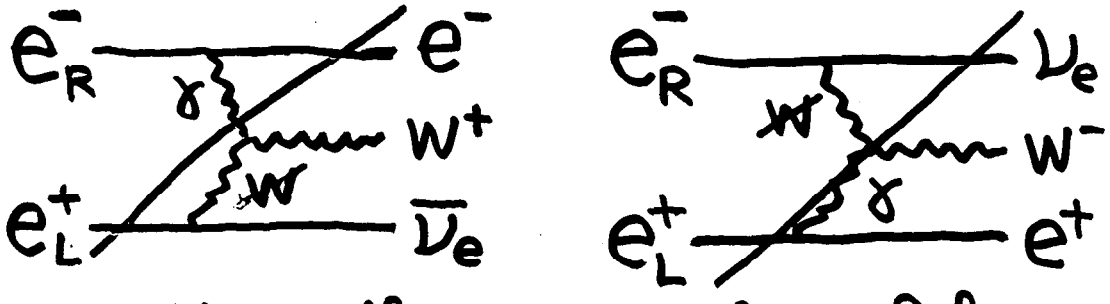

Can NOT kill by Single Beam Pol.

Transeverse Polarization

Transeverse Polarization

- Single Beam Polarization.

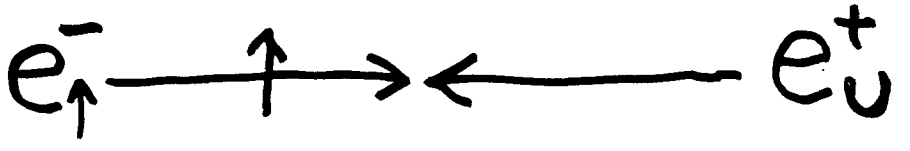

⇨ No effect is observed.

- Double Beam Polarization

⇨ We see effect.

Double Beam Polarization is Essential to use Transeverse Polarization.

transeverse polarization
is
linear combination of
longitudinal polarization.

$$e^-_\uparrow = \frac{1}{\sqrt{2}}\{|e^-_R\rangle + i|e^-_L\rangle\}$$
$$e^+_\downarrow = \frac{1}{\sqrt{2}}\{-i|e^+_R\rangle + |e^+_L\rangle\}$$

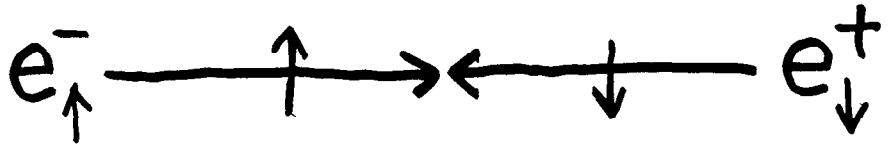

$$|e^-_\uparrow e^+_\downarrow\rangle$$
$$= \frac{1}{2}\{|e^-_R e^+_L\rangle - i|e^-_R e^+_R\rangle + i|e^-_L e^+_L\rangle + |e^-_L e^+_R\rangle\}$$

final state

$$|\langle f|T|e^-_\uparrow e^+_\downarrow\rangle|^2$$

$$\propto \cdots + \underbrace{\langle e^-_R e^+_L|T|f\rangle}_{\text{Standard}\ \text{large}} \underbrace{\langle f|T|e^-_R e^+_R\rangle}_{\text{New Physics}\ \text{may be small}} + \cdots$$

interference

Even if effect of New Physics is small, we may SEE it through interference.

⇨ transeverse polarization may be useful

K. Hikasa Phys. Rev. D33, 3203 (1986)

Summary

Summary

(1) Polarized Beams are Useful.

- ⊙ Suppress Backgrounds.
- ⊙ Select { interactions / final states
- ⊙ Resolve Components of Particles.
  (Weak Eigen State)

(2) Single Beam Polarization is already Useful.

(3) Double Beam Polarization is more Powerful.

- ⊙ Increase Signal (compare to $e^-_U \times e^+_U$) → { $f\bar{f}$ ×2 max. / W^+W^- ×4 max.

- ⊙ Suppress Background Much.
  Especially $e^+e^- \to W^+W^-$
  Get Much Better S/N
  ↑ compare to $e^-_R \times e^+_U$

<u>Important</u>

Because $e^+e^- \to W^+W^-$ is most searious BG to Many of Studies.

(3) continue: Double Beam Pol.

⊙ Select Some Interesting Events by $e^-_R e^+_R$ and/or $e^-_L e^+_L$

$$e^+e^- \to \tilde{e}^+\tilde{e}^- q\bar{q}$$
$$e^+e^- \to \tilde{e}^-\tilde{\chi}^+\bar{\nu}_e$$
$$e^+e^- \to e^\pm W^\mp(^-)\nu_e$$

⊙ Some of Background can be killed only by Double Beam Pol.

$$e^+_R e^-_L \to e^\pm W^\mp(^-)\nu_e$$

(4) Transeverse Polarization.

- Need Double Beam Polarization
- Possibility to Search New Physics through interferense.

$$\langle e^-_R e^+_L | T | f \rangle \langle f | T | e^-_R e^-_R \rangle$$

(5) Intensity of e^+ beam.

Keep Intensity of Pol. e^+ beam as same as Non Pol. e^+ beam.

Even S/N gose Up, by Pol.,
If Number of Events gose Down many of advantages are lost.

References

- GRACE
  Minami-Tateya-Group KEK-Report 92-19
- JLC-I
  JLC-Group KEK-Report 92-16
- 研究成果報告書
  R.Kajikawa et al.
  平成5年度科研費(総合A) 03302016
- 研究成果報告書
  T. Kobayashi et al.
  平成8年度科研費(総合A) 06302019
- Talk by T. Kurihara
  to be published
  Proceedings of the 6-th WS on JLC
  KEK-Proceedings
- Transverse-Polarization ....
  K. Hikasa
  Phys. Rev. D33, 3203 (1986)

- $\Delta P/P$: combined
  K. Flöttmann, DESY 95-064
- $\sin^2\theta_W$ measurement
  K. Fujii & T. Omori KEK-Preprint 95-127
- $\tilde{\chi}^0_1 \tilde{\chi}^0_1 \gamma$
  K. Fujii
  Proc. of WS on Phys. and Exp. with LCs
  Morioka-Appi pp 283-309

Polarized Positron Source for Linear Colliders

Tsunehiko OMORI (KEK)

The KST Collaboration
KEK-Sumitomo_Heavy_Industry-Tokyo_Metroporitan_Univ.

A possible design of polarized positron source for future linear colliders is proposed.

Our goal is to produce a polarized positron beam witch has intensity and time structure described as follows; 0.7×10^{10} positrons/bunch, 85 bunches/train (bunch spacing 1.4 n sec), and 150 Hz repetition rate. Those parameters meet the latest X-band JLC design. However, our design can be applicable to C-band JLC, to NLC, and maybe to CLIC.

Main part of the positron source consists of a 6.7 GeV electron linac and 85 CO_2 lasers. An electron beam of the linac is very high current, which is 1×10^{11} electrons/bunch. The time structure (bunch/train structure) of the electron beam is as same as those of positron beam to be created (see above). Energy of laser pulse from each CO_2 laser is 10 joule. Each laser operate 150 Hz. 85 lasers fire sequentially with 1.4 n sec interval. A laser plus from the first (i-th) laser collide on the first (i-th) bunch of a train of the 6.7 GeV electron beam. Timing and pulse width of those 85 CO_2 lasers are controlled by one Nd:YAG laser.

Collisions of a laser pulse and an electron beam generate γ rays which maximum energy is 80 MeV. Number of γ's per collision (bunch) is 2×10^{11}. Thus we have multiplication of factor of two in this stage. This comes from multiple scattering; an electron kick more than one laser photon. Pulse shape of laser, both in time and in space, are carefully chosen to get multiple scattering in linear QED regime, but avoid non-linear QED effect as much as possible. Those γ's go to the tungsten target which thickness is 3.5 mm. When we collect positrons which energy is greater than 20 MeV, polarization of 50% (include dilution from non-linear QED) and conversion rate of 8 % will be achieved.

Up to here we will get 1.6×10^{10} positrons/bunch. Then if we achieve good capture efficiency (>0.44), we will get $>0.7 \times 10^{10}$ positrons/bunch, which meets our goal. Further optimization of parameters is under way to get margin of intensity against positron losses from the source to IP. Detailed design and experimental R/D are also under way.

Trial to Design

Polarized Positron Source for Linear Colliders

5-Mar-1997 @SLAC
WS on Positron Source

Tsunehiko OMORI (KEK)

by KST Collabaration

[KEK
Sumitomo Heavy Industry
Tokyo Metropolitan Univ.]

KEK
Y. Kurihara
T. Omori
Y. Takeuchi

Sumitomo Heavy Industry
A. Endo
A. Tsunemi

Tokyo Metropolitan Univ.
T. Hirose
T. Kumita
T. Okugi
M. Chiba
R. Hamatsu
H. Ishiyama

Our Goal

an Example
X-band JLC

0.7×10^{10} positrons/bunch

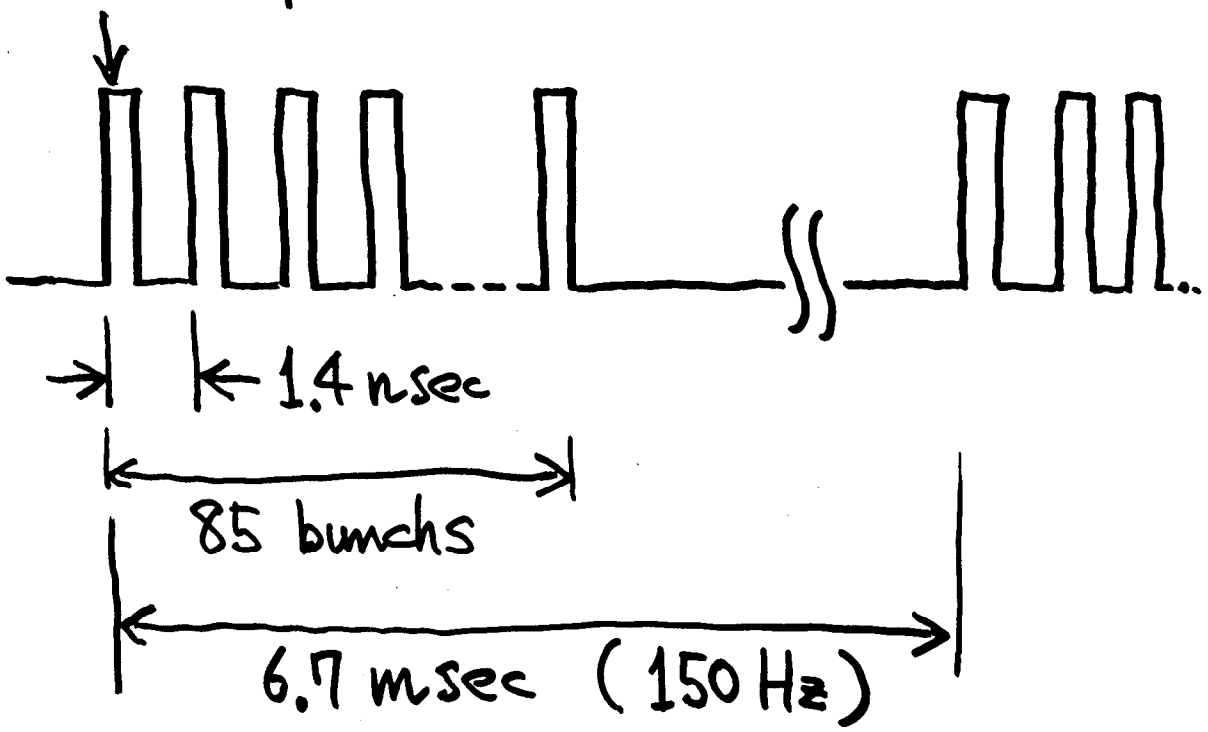

with Polarization

Where is Difficulty?

(1) Huge Number of e^+

(2) Time Structure

Our Choice
conventinal !

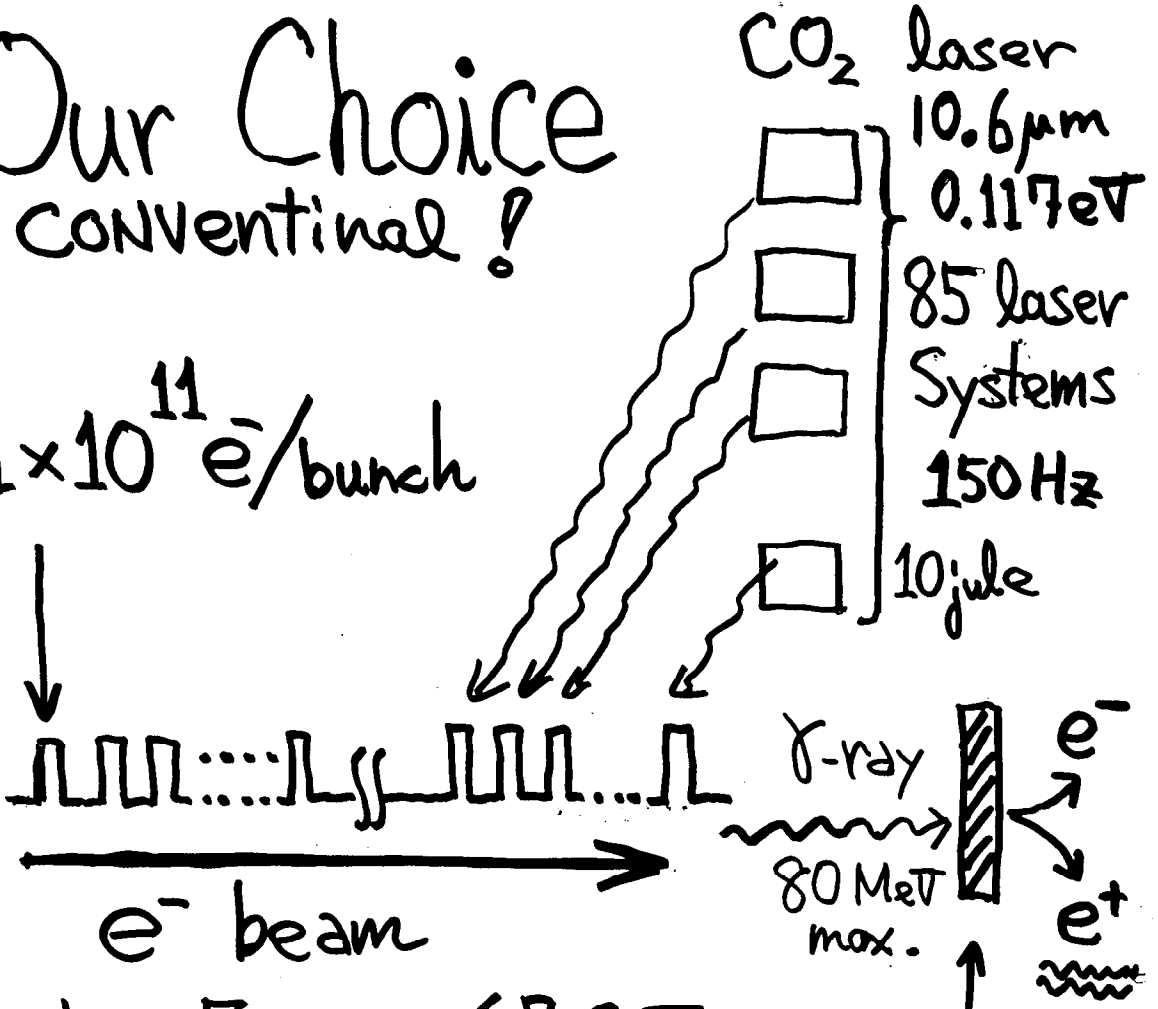

Low Energy 6.7 GeV

High Current

$(1\times10^{11}\ e^-/\text{bunch})$

$\times$ (85 bunch/train)

$\times$ (150 Hz)

time structure is the same as the main linac.

I. Why CO_2 laser? 0.117eV

(1) High Efficiency, High Power

(2) can operate 150 Hz

(3) but can NOT operate
1.4 nsec interval → 85 lasers

II. Why $E_{e^-} = 6.7$ GeV ?

(1) $(E_{e^-} = 6.7\,\text{GeV}) \times (E_{laser} = 0.117\,\text{eV})$
→ $\sigma_{compton} = 657\,\text{mb}$ large!

(2) $E_\gamma\,max = 80$ MeV
→ $\sigma_{pair}(w) \doteqdot 23000$ mb large!

(3) Since 80 MeV ≪ 6.7 GeV

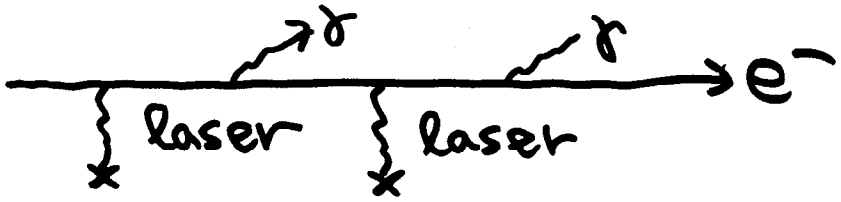

(4) keep Wall Plug Power < Huge

III Why Tangsten(W) Target

$Z = 74$

$\sigma_{pair} \propto Z^2$

$\sigma_{ionization} \underset{\text{Roughly}}{\propto} Z$

large Z is preferable

Basic Study

with Linear QED

w/o ~~NON-Linear QED~~

w/o ~~Beam Shape~~

w/o ~~time structure~~

tools

HELAS

BASES/Spring

EGS (with spin flip by HELAS)

Cross Section : Compton γ

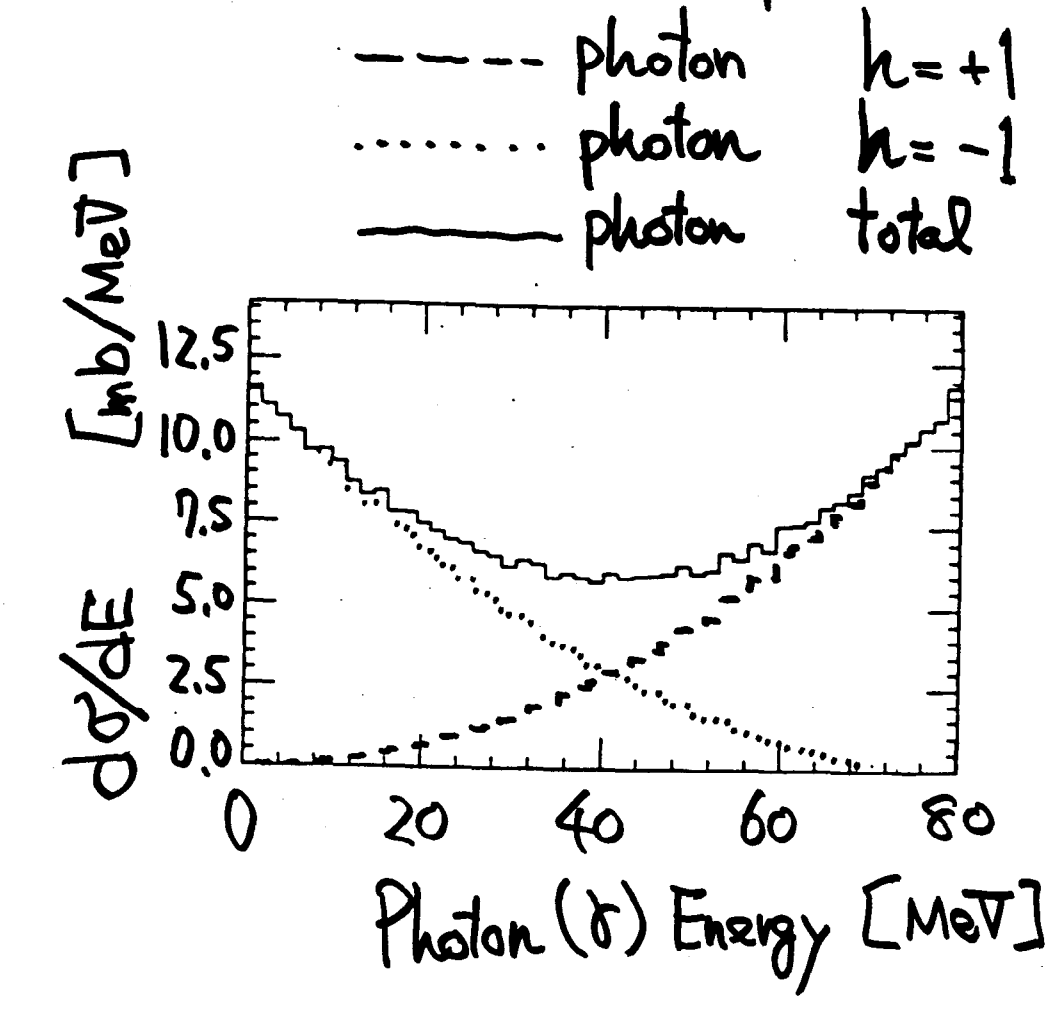

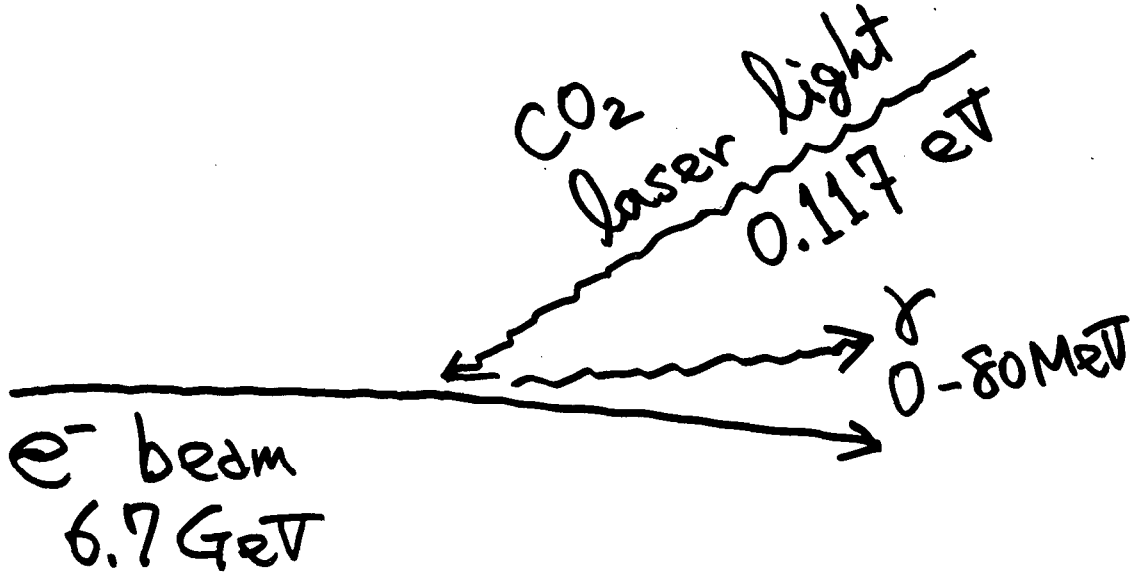

e^+ Production Cross Section

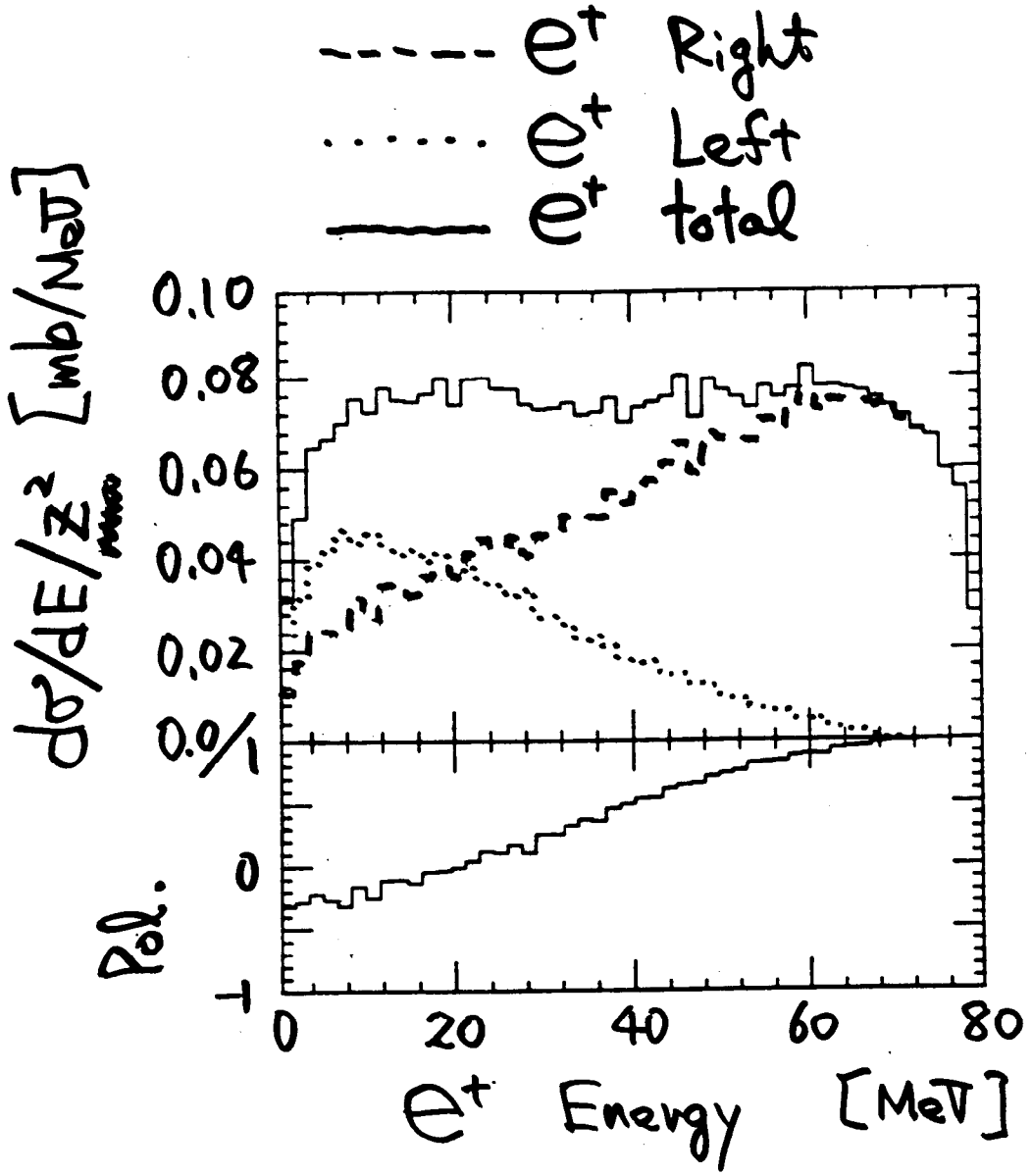

Energy of γ = 80 MeV
helicity of γ = +1
FIXED

e^+ Production Cross Section

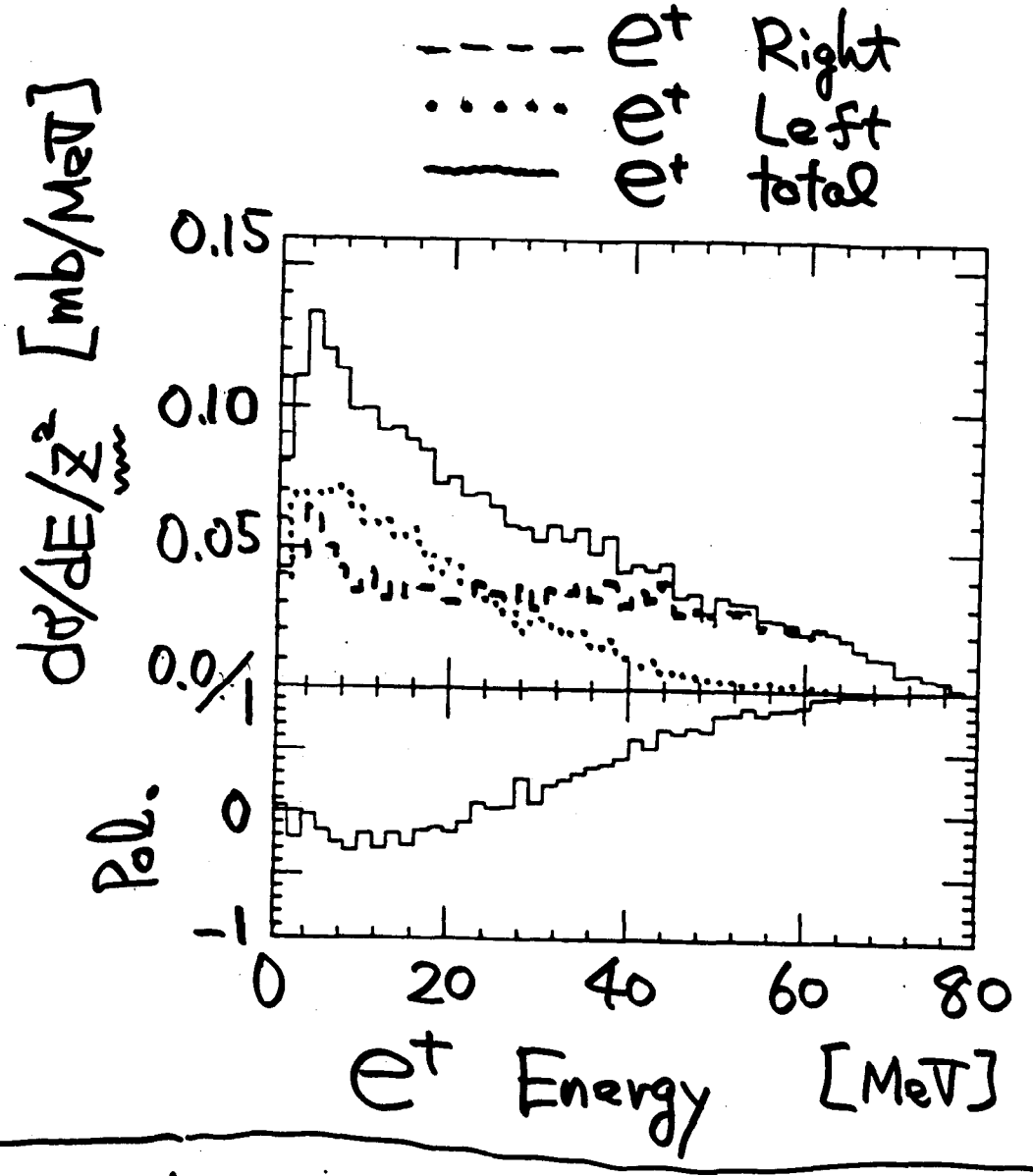

Weighted by Energy/helicity distribution of Compton γ

Production Rate N_{e^+}/N_γ

× P_{e^+} = 40%
□ P_{e^+} = 60%
○ P_{e^+} = 80%
} Required Polarization

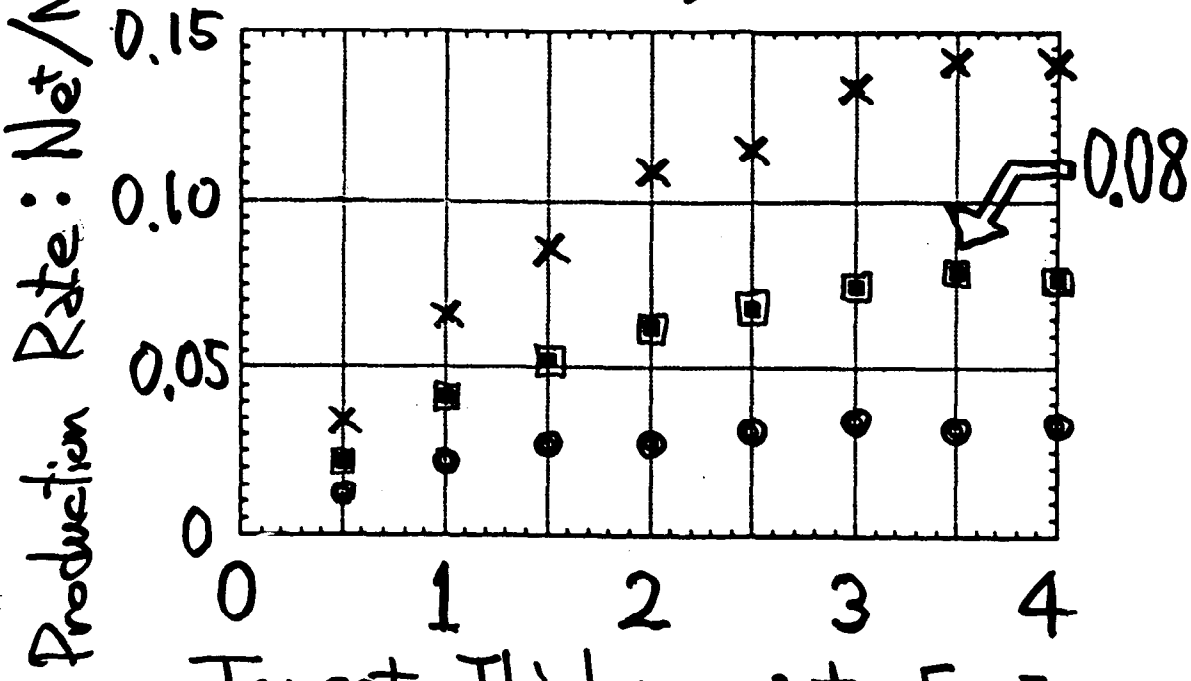

(tongsten Z=74)

e^+ Energy Cut @ t = 3mm

for 40% pol. $E_{e^+} > 10$ MeV
for 60% pol. > 20 MeV
for 80% pol. > 35 MeV

More Study

with Non-Linear QED

with Beam Shape

with Time Structure

tool

CAIN

e^- bunch → ← laser pulse: head-on

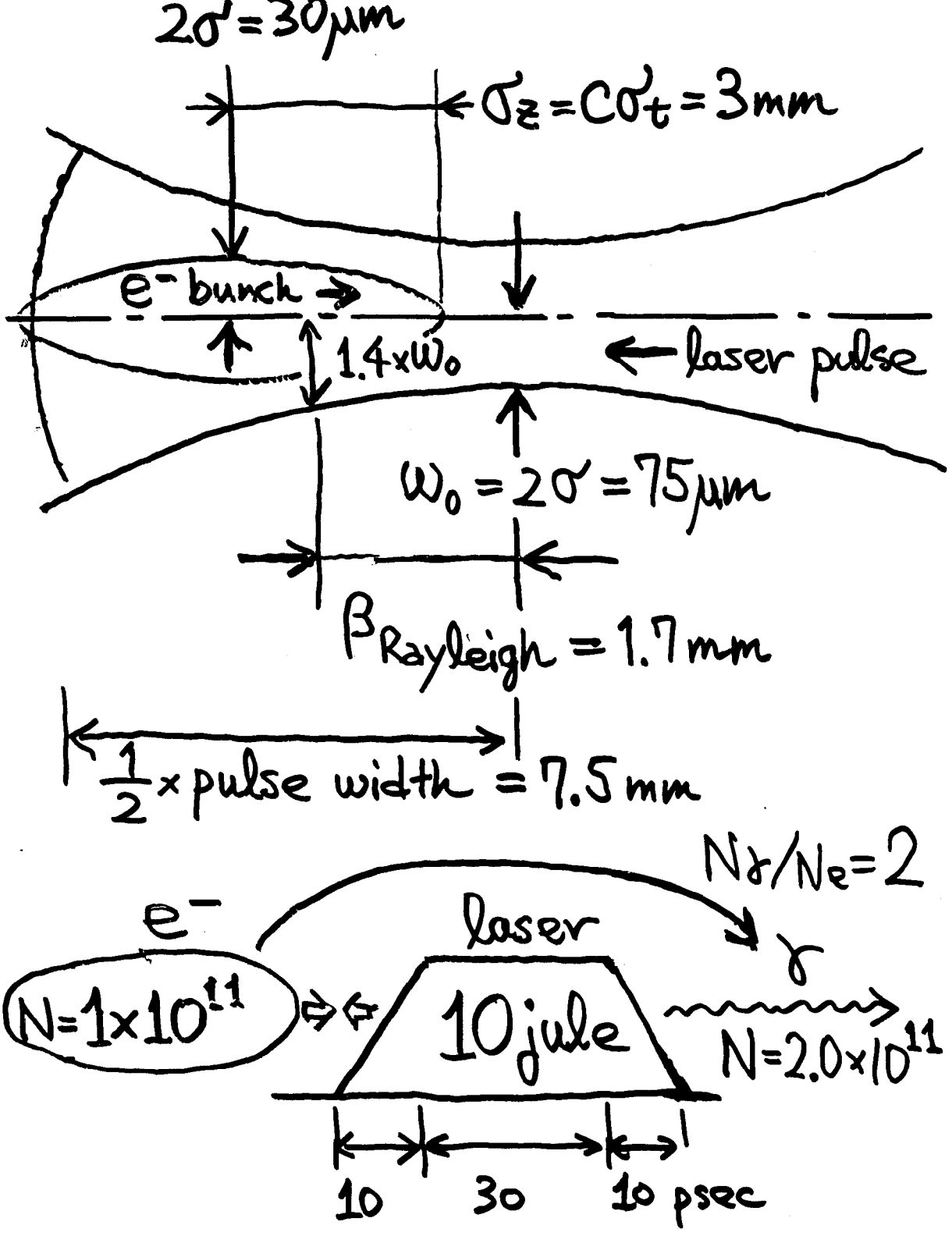

Laser Strength

$$P_{peak}\,(\text{Peak Power}) = 0.28 \times 10^{20}\ W/m^2$$

$$\xi_{max} \equiv \frac{\chi_{laser}}{m_e}\sqrt{\mu_0 c P_{peak}} = 0.34$$

$\mu_0 = 4\pi \times 10^{-7}$

m_e: electron rest mass

laser 10 jule

$\omega_0 = 75\mu m$, $\beta = 1.7 mm$

$C \cdot T_{tot} = 15 mm$, $C \cdot T_{edge} = 3 mm$

50psec 10psec

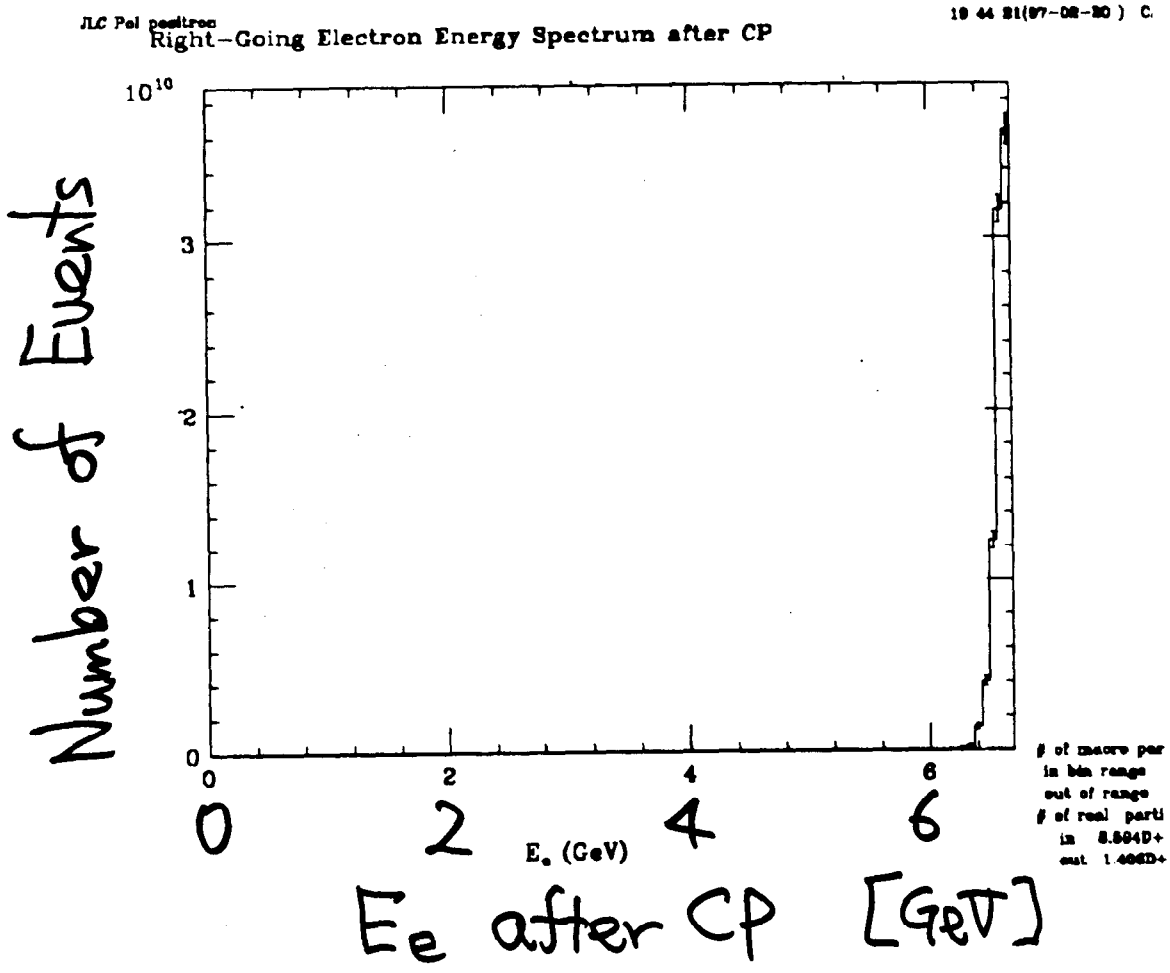

Number of Events

E_e after CP [GeV]

electron 1×10^{11}

$\sigma_z = 3 mm$

$2\sigma_x = 2\sigma_y = 30\mu m$

laser 10 jule

$\omega_0 = 75\mu m$, $\beta = 1.7$ mm

$C \cdot T_{tot} = 15$mm, $C \cdot T_{edge} = 3$mm

(50psec) (10psec)

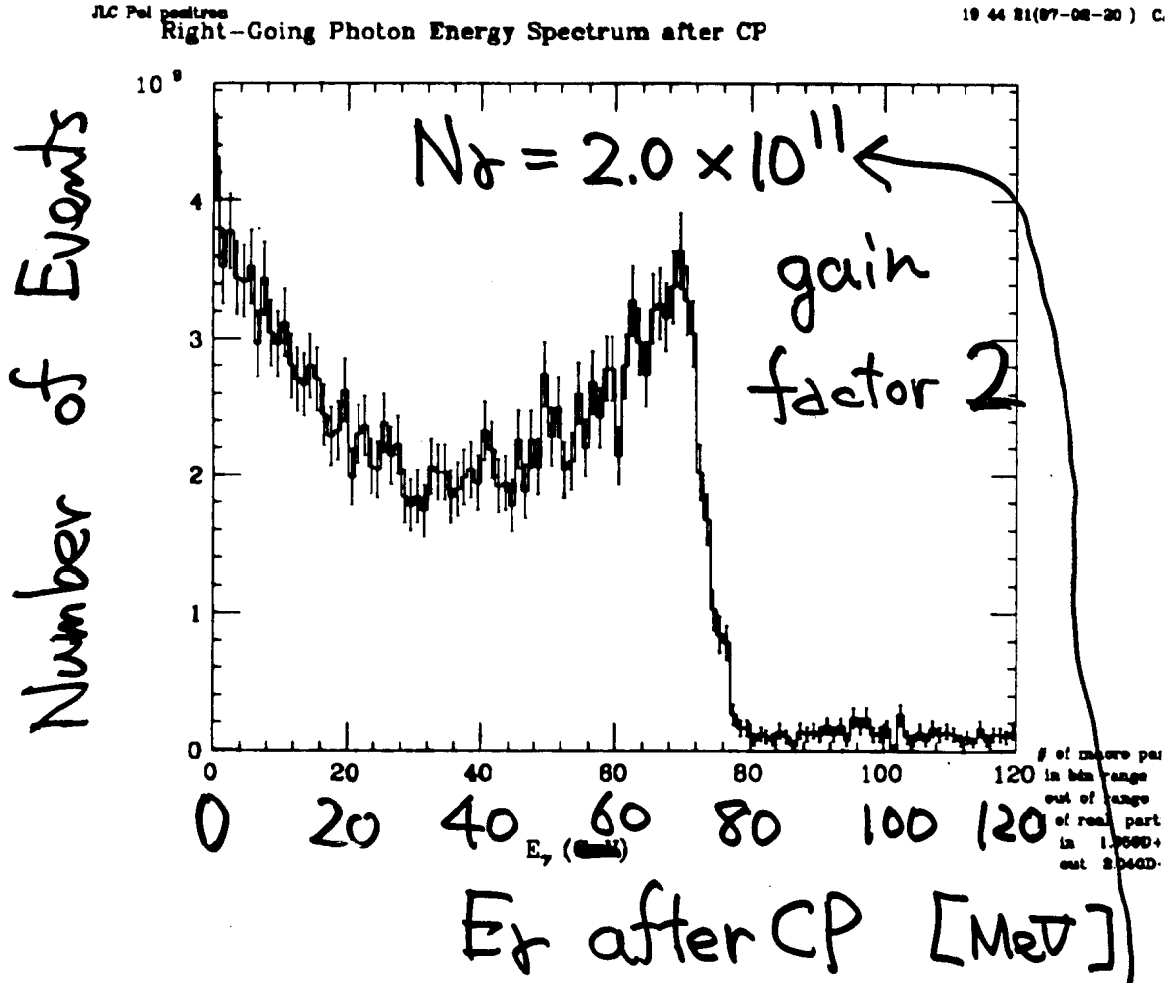

electron $N = 1 \times 10^{11}$

$\sigma_z = 3$mm

$2\sigma_x = 2\sigma_y = 30\mu m$

laser 10 joule, $\omega_0 = 75\mu m$, $\beta = 1.7mm$

$C \cdot T_{tot} = 15mm$, $C \cdot T_{edge} = 3mm$

electron $N = 1 \times 10^{11}$

$\sigma_z = 3mm$, $2\sigma_x = 2\sigma_y = 30\mu m$

Polarization (defined for MACRO particle of Scattered photons)

+1

0

-1

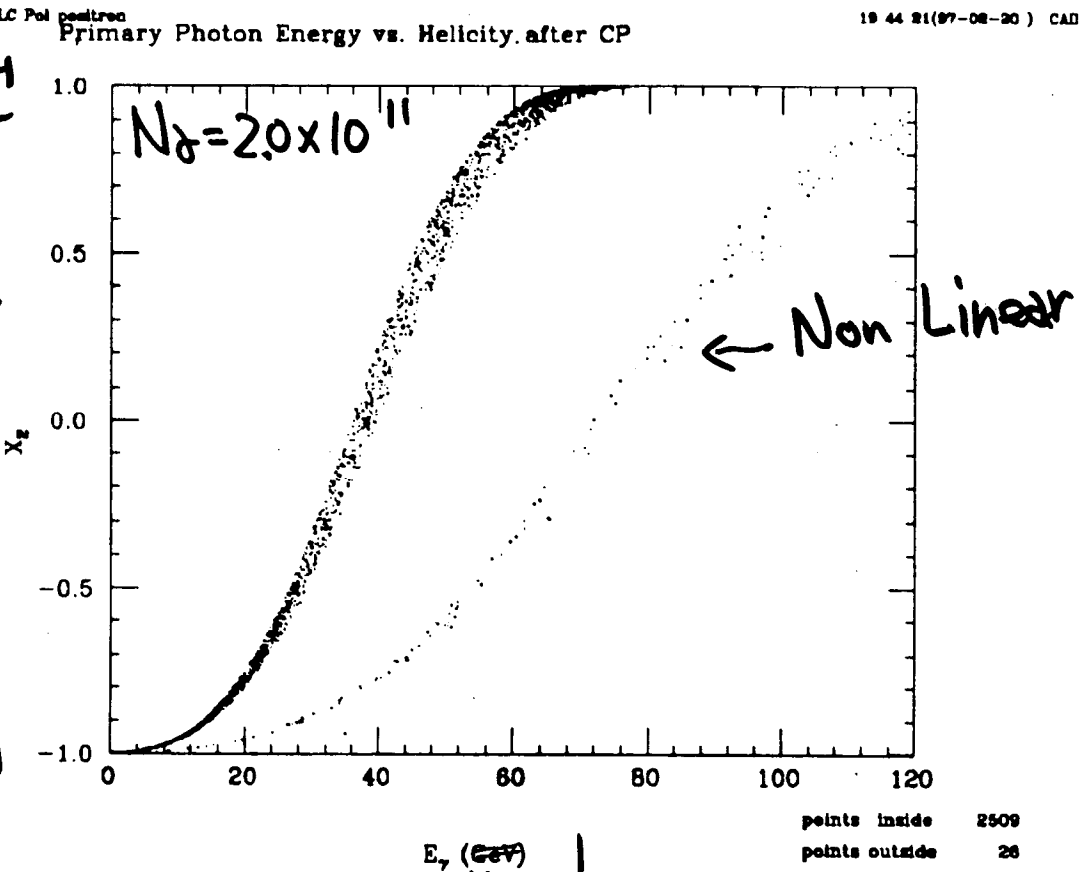

← Non Linear

↳ $E_\gamma > 70$ MeV

Pol. = 81%

if Linear QED

$E_\gamma > 70$ MeV

Pol = 98%

Polarization dilution by Non Linear Effect

$\simeq 0.83$

Linear Compton

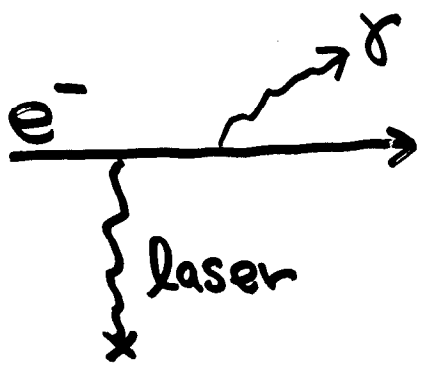

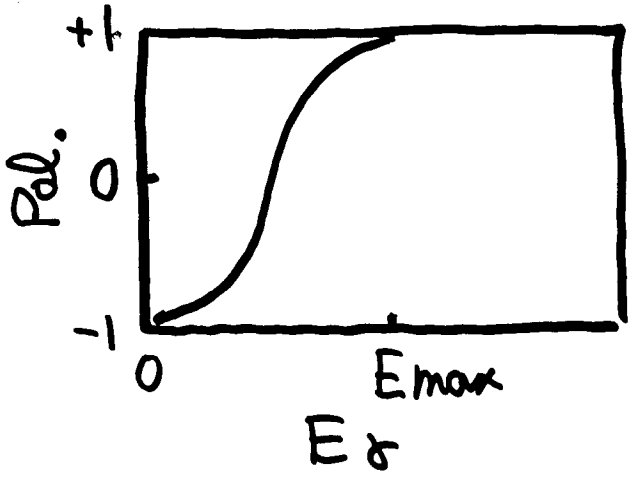

Linear, but multiple

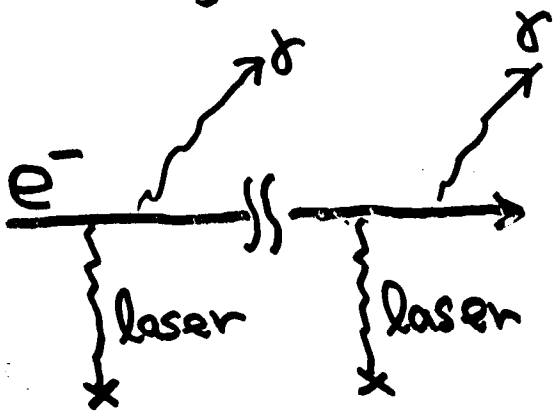

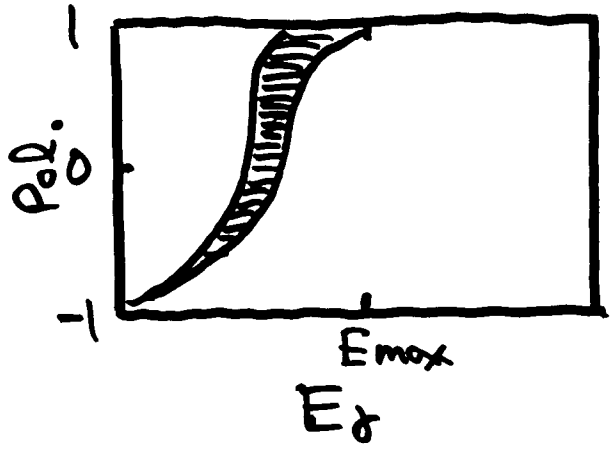

Non Linear

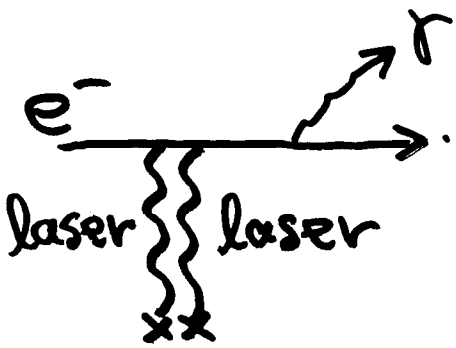

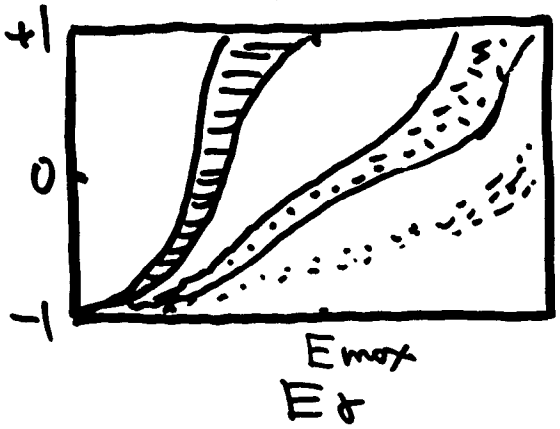

Guideline to Choose Laser Parameters

(1) Use Linear Multiple Scatterings

(2) avoide NON Linear Scatterings

Count Number of e^+s

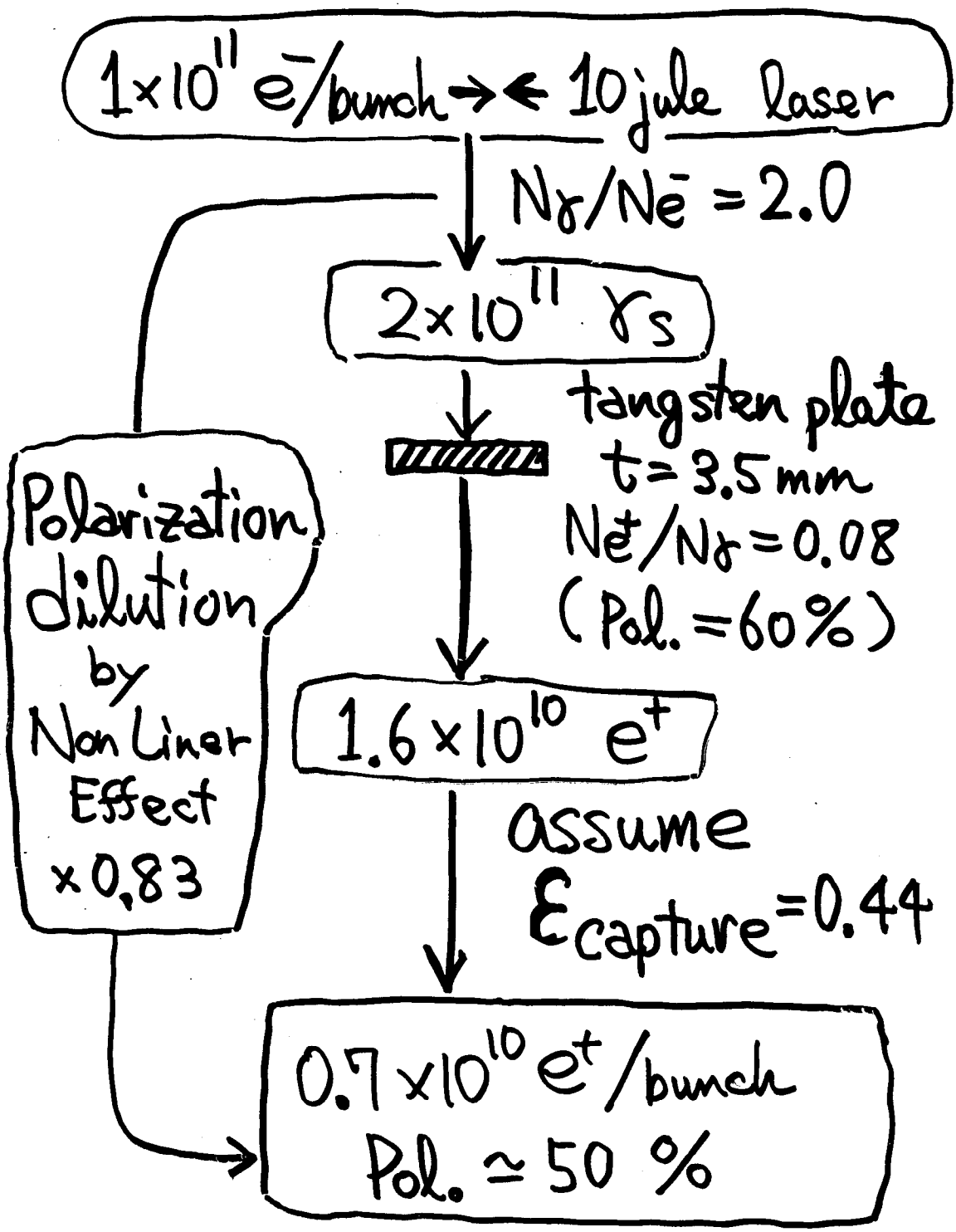

Engineering Issues

e⁻-laser CP

laser system

Wall Plug Power

Head-on Collision

e^- beam → ← laser beam

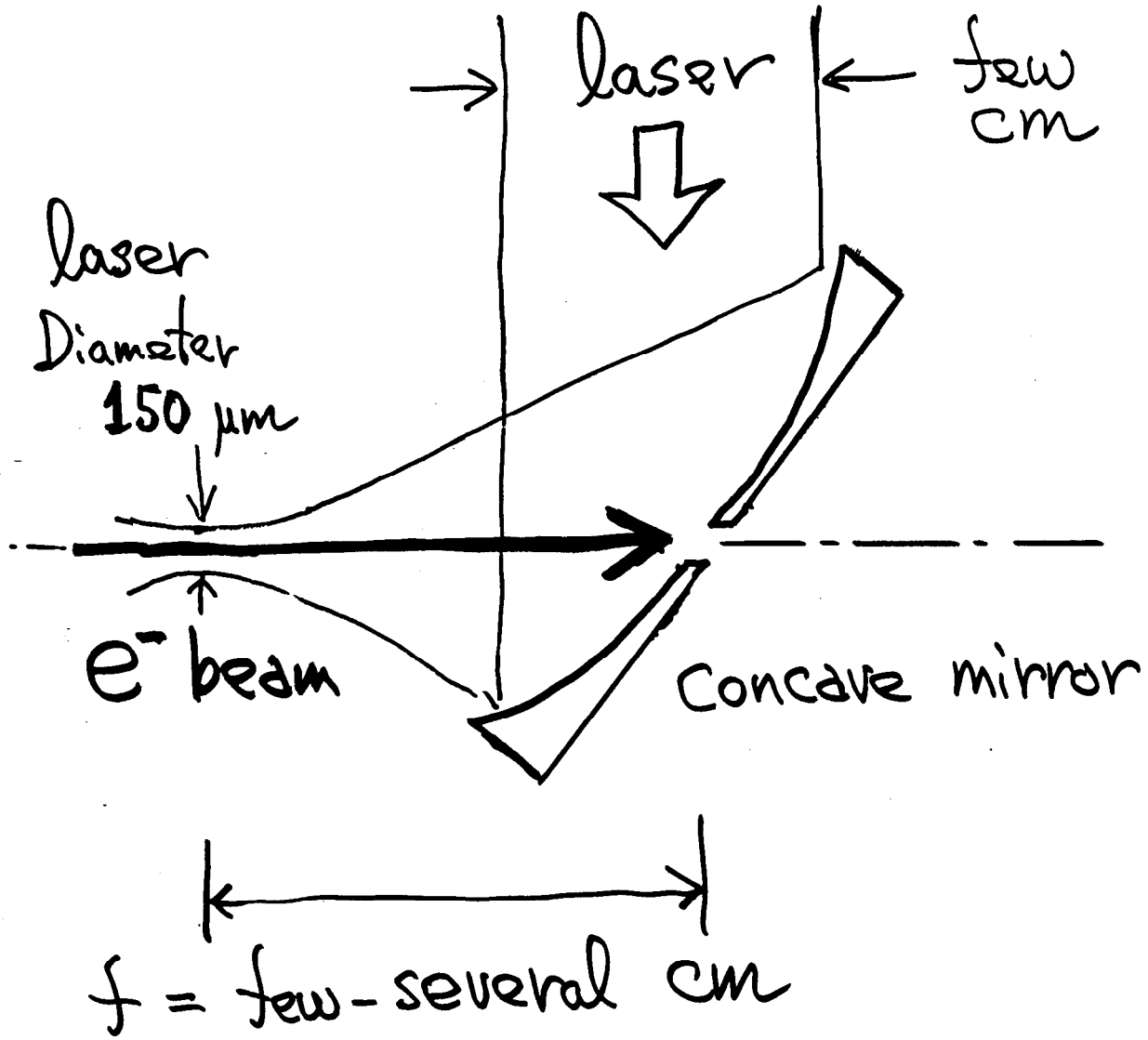

Head-on Collision

an e^- beam →← 85 laser beams

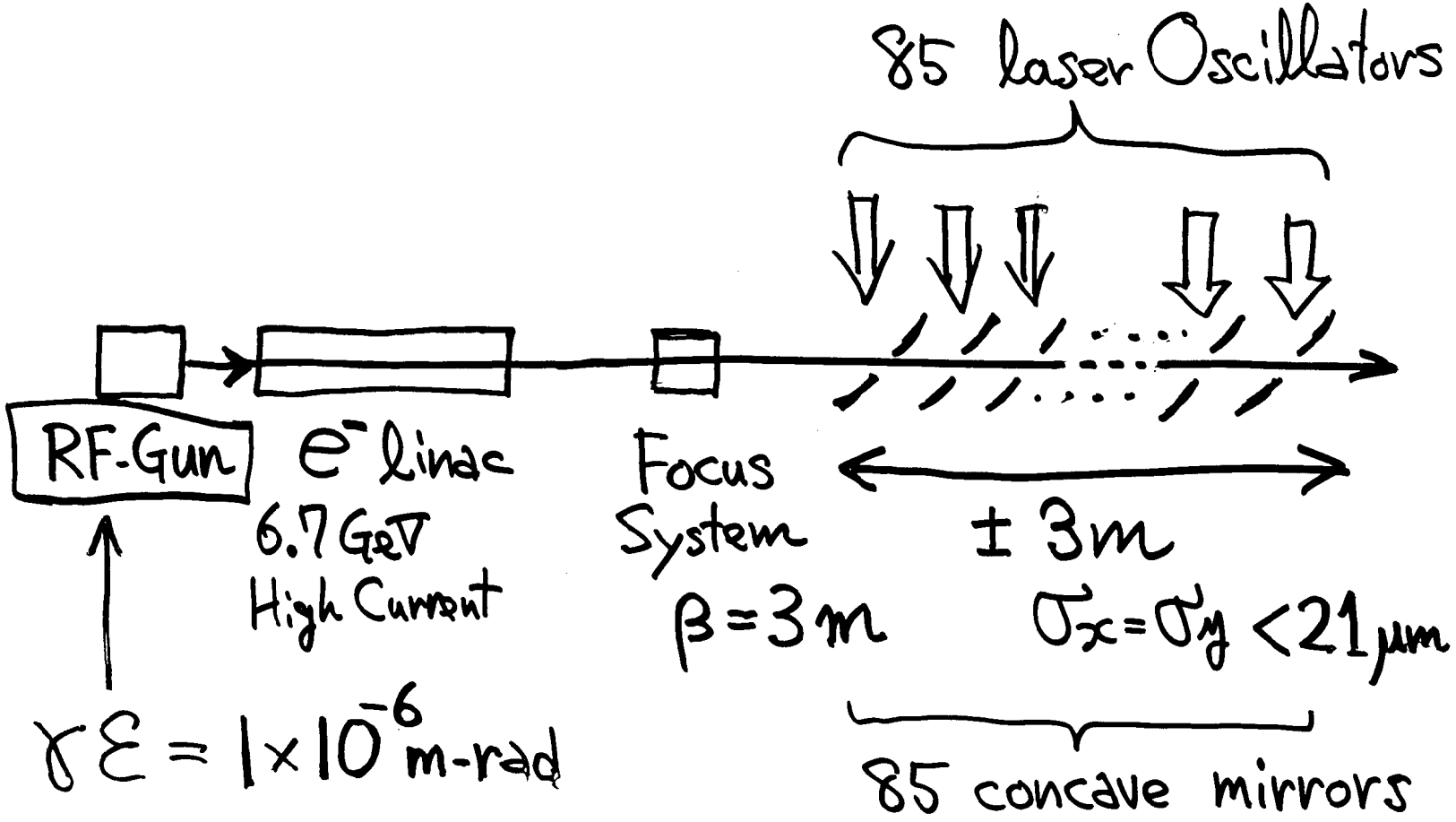

Laser System

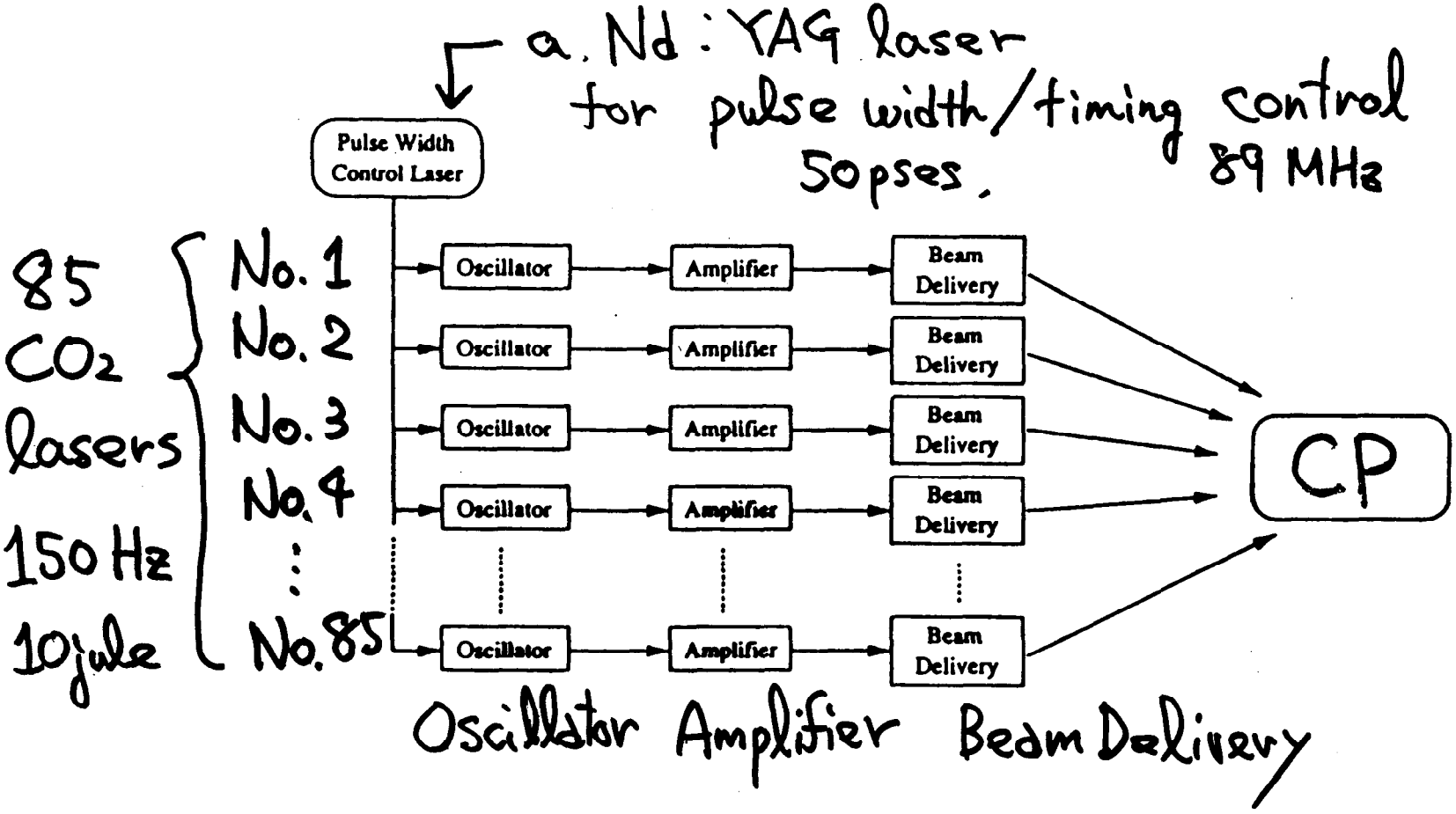

Positron Capture Section

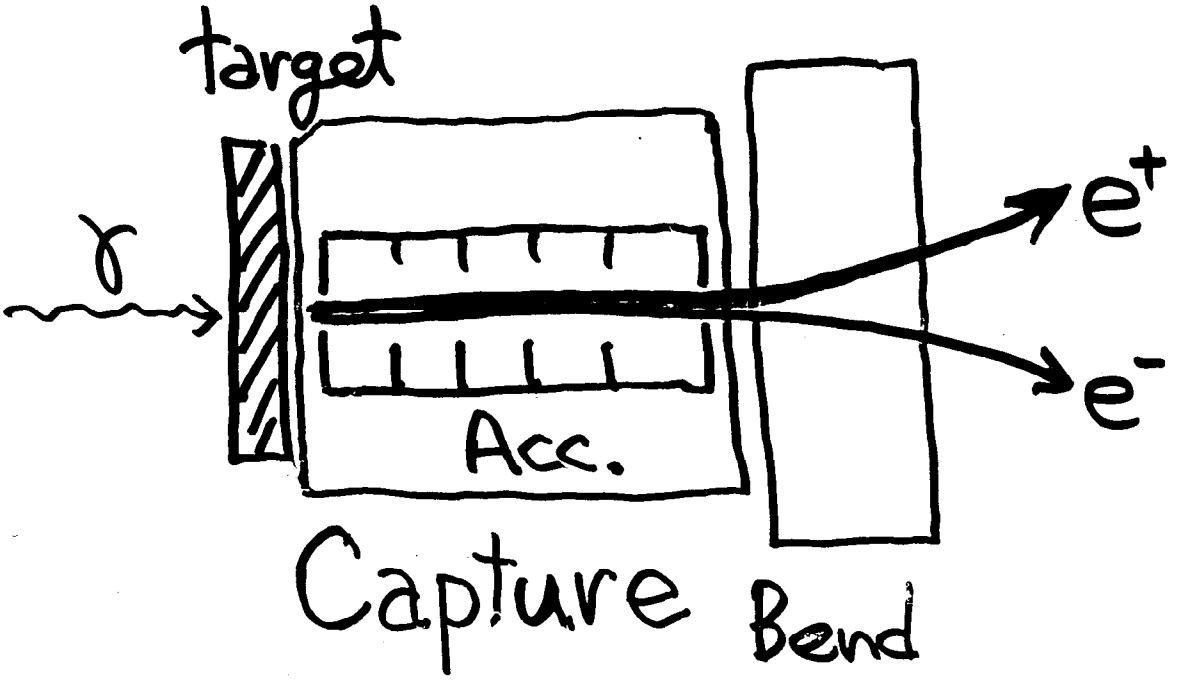

Not Designed yet.

ε : Not Calculated yet.

Wall Plug Power

e^- - linac

6.7 GeV/electron
× 1×10^{11} e^-/bunch
× 85 bunch/train
× 150 Hz
→ 1.36 MW
ε = 8% assume
→ 17 MW W.P.P.

laser System

10 jule/pulse
× 85 laser Oscillators
× 150 Hz
→ 0.128 MW
ε = 4% assume
→ 3.2 MW W.P.P.

total 20 MW

Experimental R/D

Experiment at ATF@KEK

Accelerator Test Facility for LCs

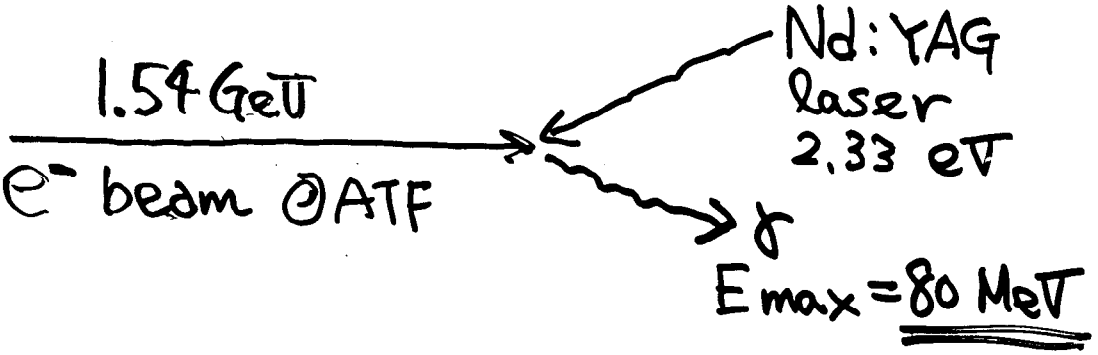

e⁻-beam	2×10^{10} e⁻/bunch	
laser	550 mjule	10 Hz
γ	6×10^{5} /collision	

1996 Warming Up Exp.] Done

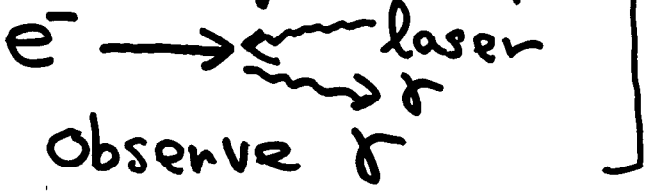

Observe γ

1997 Install Target] Will be done This year.

Observe e⁺

1998 } Measure Pol.
1999 } Study Target

Summary & What's Next.

Summary

(1) 85 CO_2 lasers
10 Jule, 150 Hz
6.7 GeV e^--linac, 150 Hz
1×10^{11} e^-/bunch, 85 bunch/train
→ positrons
0.7×10^{10} e^+/bunch,
85 bunch/train, 150 Hz
Pol. = 50 %

(2) Wall Plug Power ≃ 20 MW

(3) Still Need R/D to get Conclusion.

(i) design : Capture Section

(ii) Simulation:
CAIN → Pair Creation on Target

(iii) detailed design

RF Gun

Linac

laser system

Mirrors

⋮

(4) Experimental R/D at ATF is now under way.

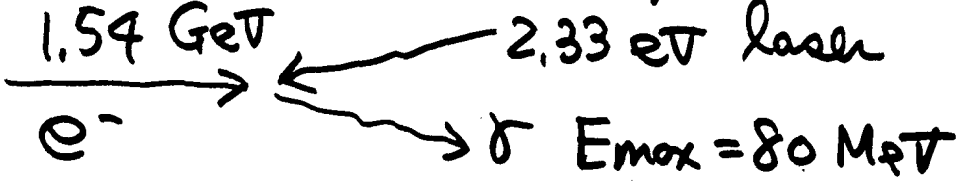

What's Next

Larger Polarization
and
Smaller Wall Plug Power

Multi-Target ?

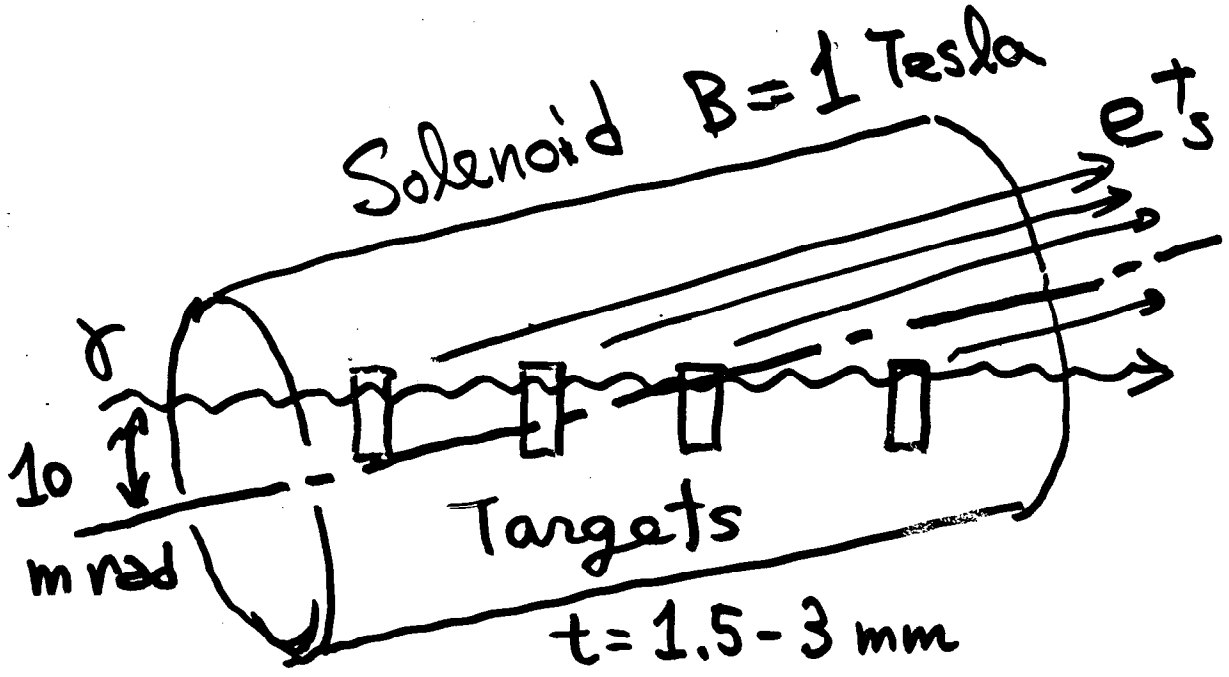

References

- **HELAS**
  HELicity Amplitude Subroutines
  K. Hagiwara, H. Maruyama, I. Watanabe
  KEK-Report 91-11 (1992)

- **BASES/SPRING**
  Numerical Integration and Event Generation
  S. Kawabata, Comp. Phys. Commun. 41 (1986)
  page 127.

- **EGS**
  Electron Gamma Shower
  W.R. Nelson, H. Hirayama, D.W.O. Rogers.
  SLAC-Report-265 (1985)

- **CAIN** Ver 2.1β
  beam-beam interaction Simulator
  K. Yokoya etal. Yokoya@kekvax.kek.jp
  http://130.87.74.156/members/yokoya.html

- **Our Paper**
  of Pol e^+ beam by Laser-Compton
  T. Okugi et al, Jpn. J. Appl. Phys.
  KEK Preprint 95-161 Accepted.

LIQUID METAL TARGETS FOR INTENSIVE HIGH-ENERGY PHYSICS BEAMS

G. Silvestrov

Budker Institute of Nuclear Physics

NOVOSIBIRSK 1997

LIQUID METAL TARGETS FOR INTENSIVE HIGH-ENERGY PHYSICS BEAMS

Gregory I. Silvestrov

Budker Institute for Nuclear Physics
630090 Novosibirsk, Russia

Abstract

The possibility is discussed for creation of liquid metal targets to solve the problems of target survival and removal of energy released. From analyses of hydrodynamic processes in target material under an energy release of 1 kJ/g or more the conclusion is made that the optimum decision consists in use of targets in a form of free plain jet of liquid metal flowing out of narrow nozzle. Described are design and experience in creation of stationary jet targets of liquid gallium-indium alloy and lead, pumped through the target device, as well as of targets for cyclic operation with frequency $\sim 0.5Hz$ made of lead or gold, which can be used for production of pions and antiprotons. The design is presented of mega-watt centrifugal target for projects of Neutron Spallation Sources.

Considered in more details are the positron production systems based on the liquid lithium lenses or adiabatic solenoids made as the magnetic field concentrator. Several kinds of targets are considered for these systems:

– solid tungsten target with liquid metal cooling;

– liquid lead target in a form of small diameter coaxial titanium tubes with liquid metal pumped trough;

– liquid lead target in a form of free jet flowing out of narrow nozzle.

Fig. 1. Schematic view of experiments for the investigation of hydrodynamic processes in target material under the condition of a high density of energy release (1 kJ/g), fulfilled using a special target stand at IHEP Protvino. The proton beam was focused onto the target by a lithium lens of 0.5-cm radius and focal distance f< 1 m. I. A target in the form of a cylinder of aluminum filled with mercury. As the proton beam size was decreased below 1 mm, the destruction of the aluminum cylinder was observed to be caused by a cylindrical wave of compression propagating from the beam axis. (See photos Figs. 3 and 4.) II. A target in the form of a series of lead cylinders of 3-cm length separated by thin titanium foils. As the proton beam size was decreased below 1 mm, there was observed a flow out of the target matter in the form of a sharp cone making a deep crimp in the titanium foil at the outlet of the section where the maximum of the nuclear-electromagnetic shower took place. These experiments lead to the conclusion that the optimum solution to the target destruction problems would be a wall-less target in the form of a plain liquid-metal jet, free-flowing out of a narrow nozzle.

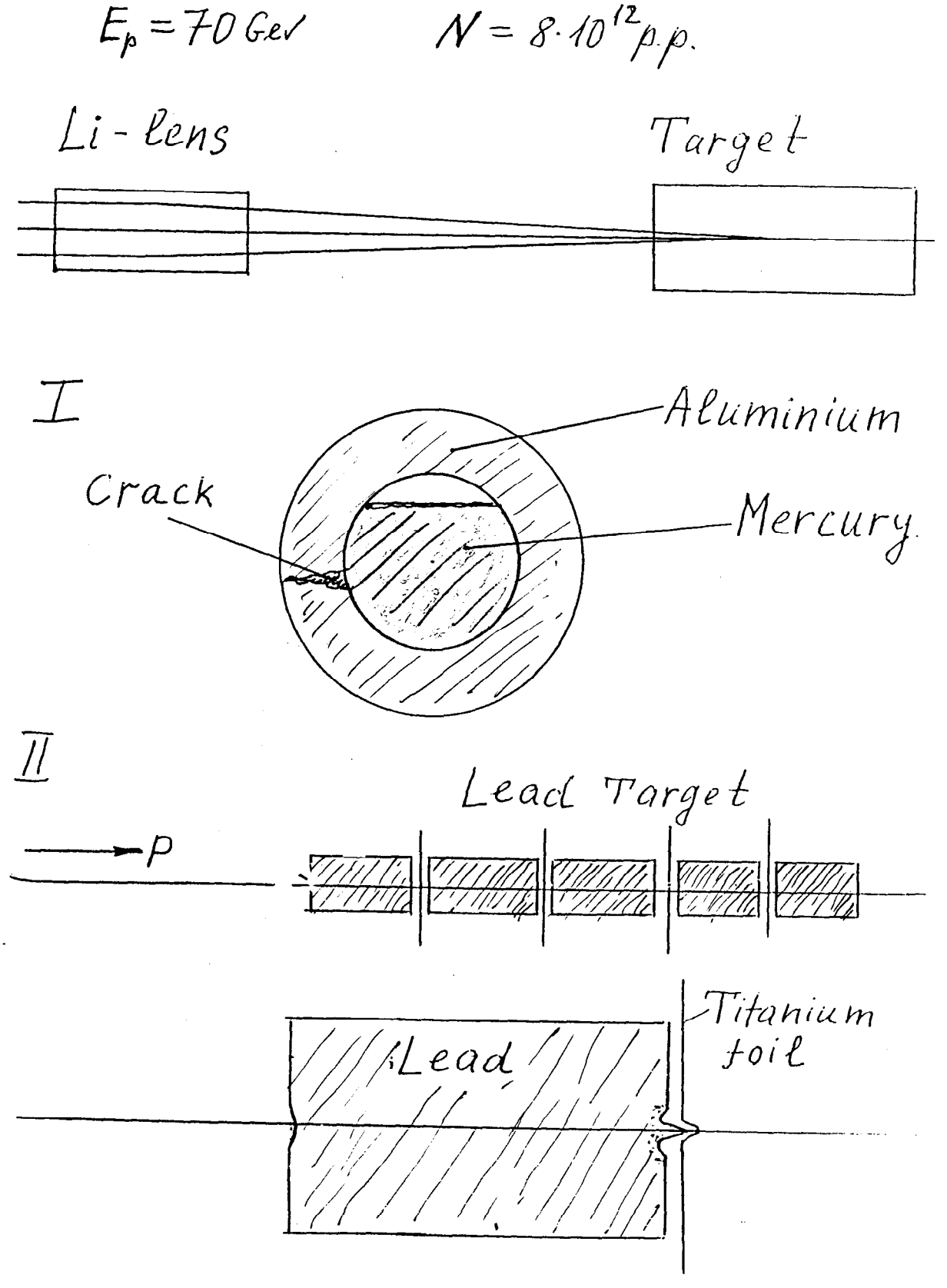
$E_p = 70$ Gev
$N = 8 \cdot 10^{12}$ p.p.
Li - lens
Target
I
Aluminium
Crack
Mercury
II
Lead Target
p
Titanium foil
Lead

FIGURE 1

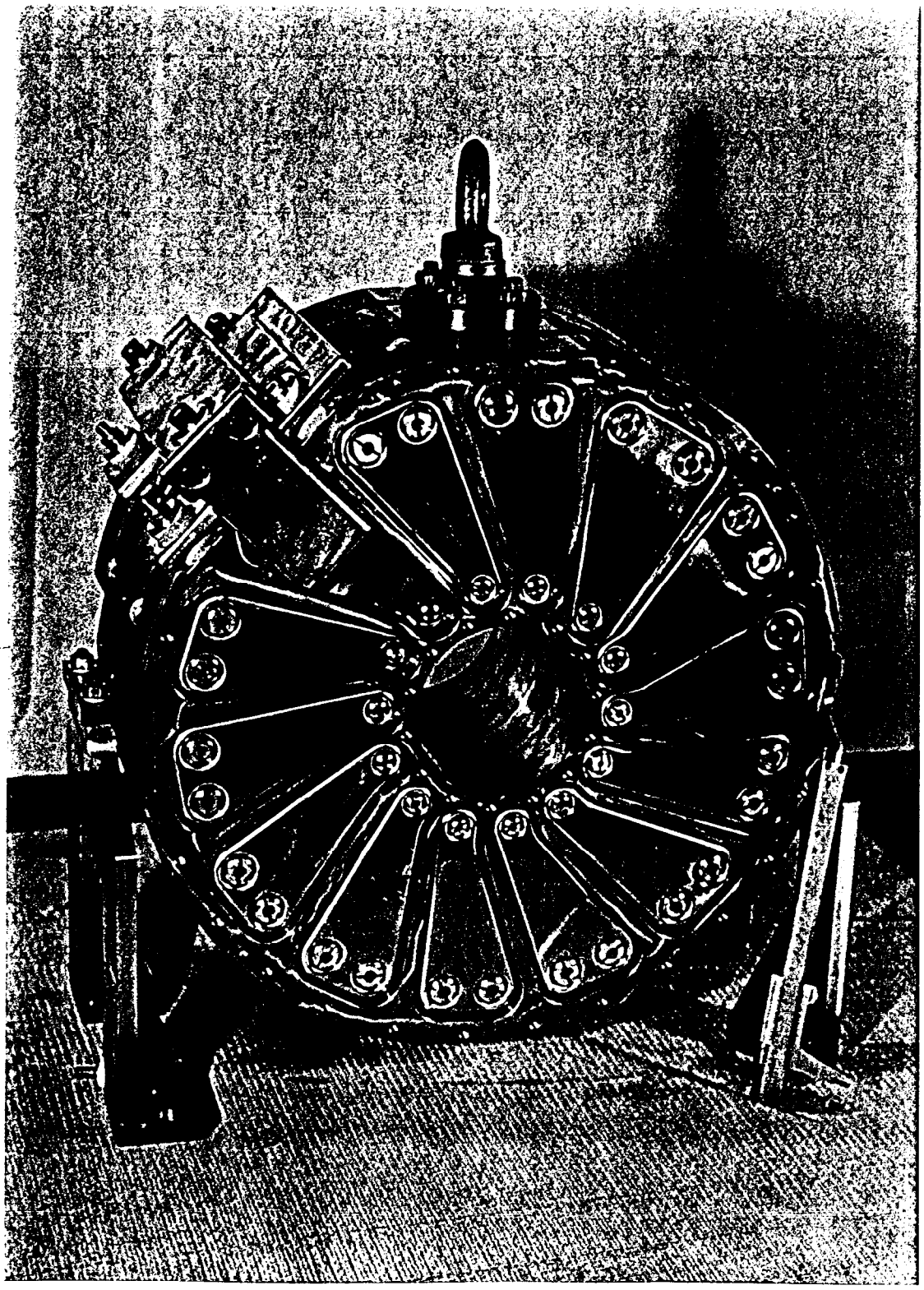

Fig. 2- Photo of the toroidal transformer for the lens supply of Fig. 1 with current up to 0.3 mA

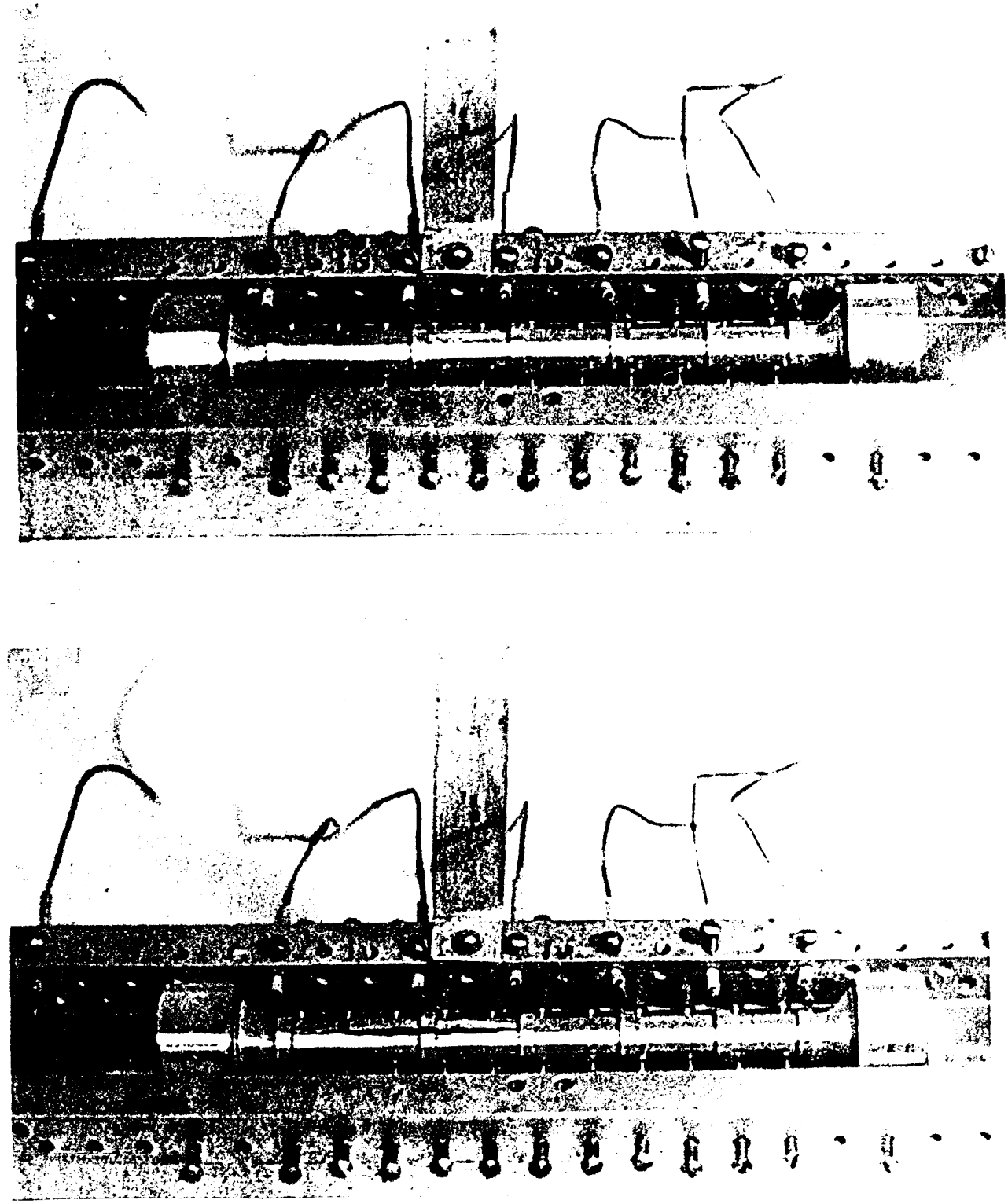

Fig. 3- Photo of the aluminum cylinder of Fig. 1 cracked by the experiments.

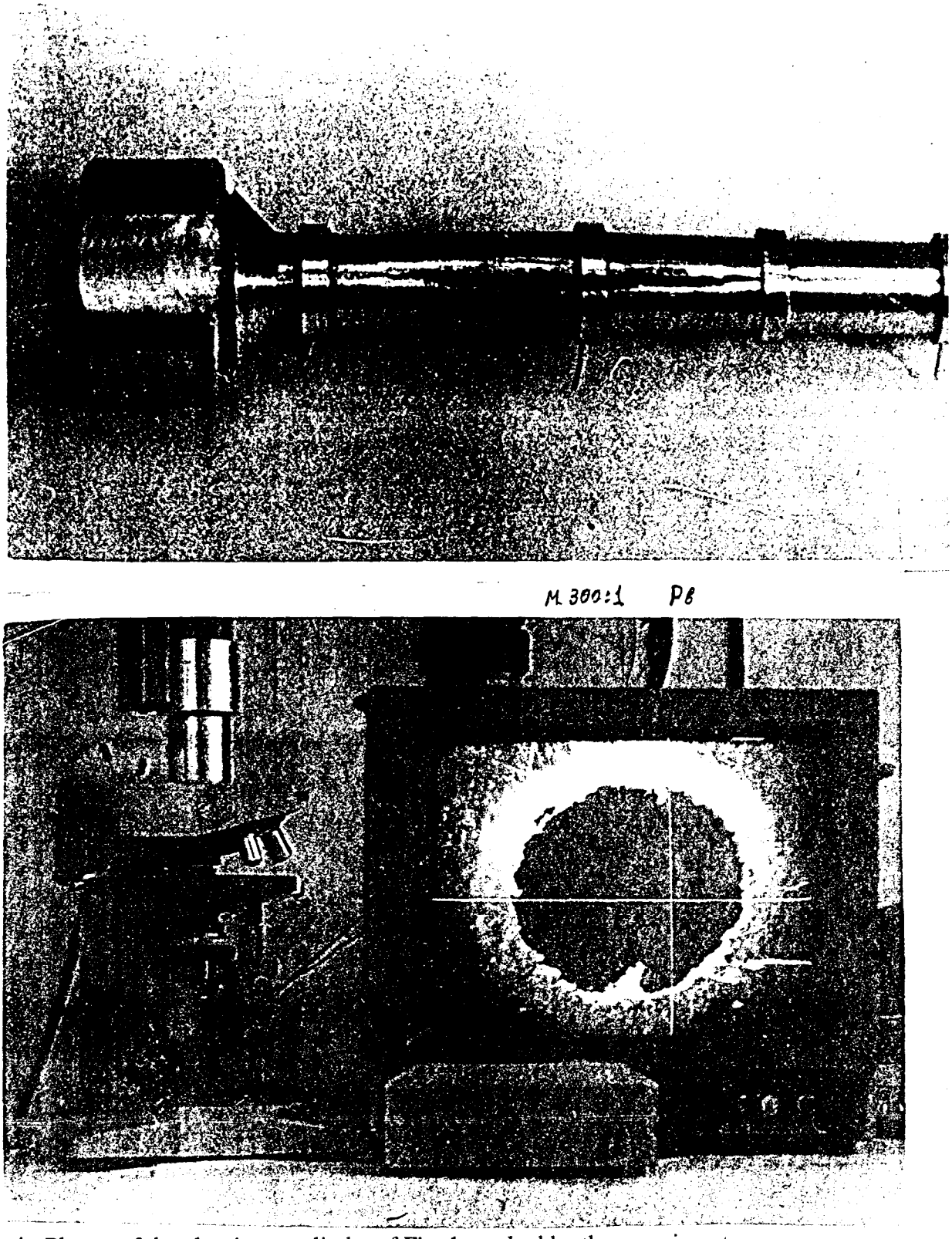

Fig. 4- Photos of the aluminum cylinder of Fig. 1 cracked by the experiments.

Main Reasons to Develop Liquid Metal Jet Target Technology:

1. Decision of heat removal problem.

2. Decision of target destruction problem.

3. Reduction of beam energy deposition in target due to side exit of secondary.

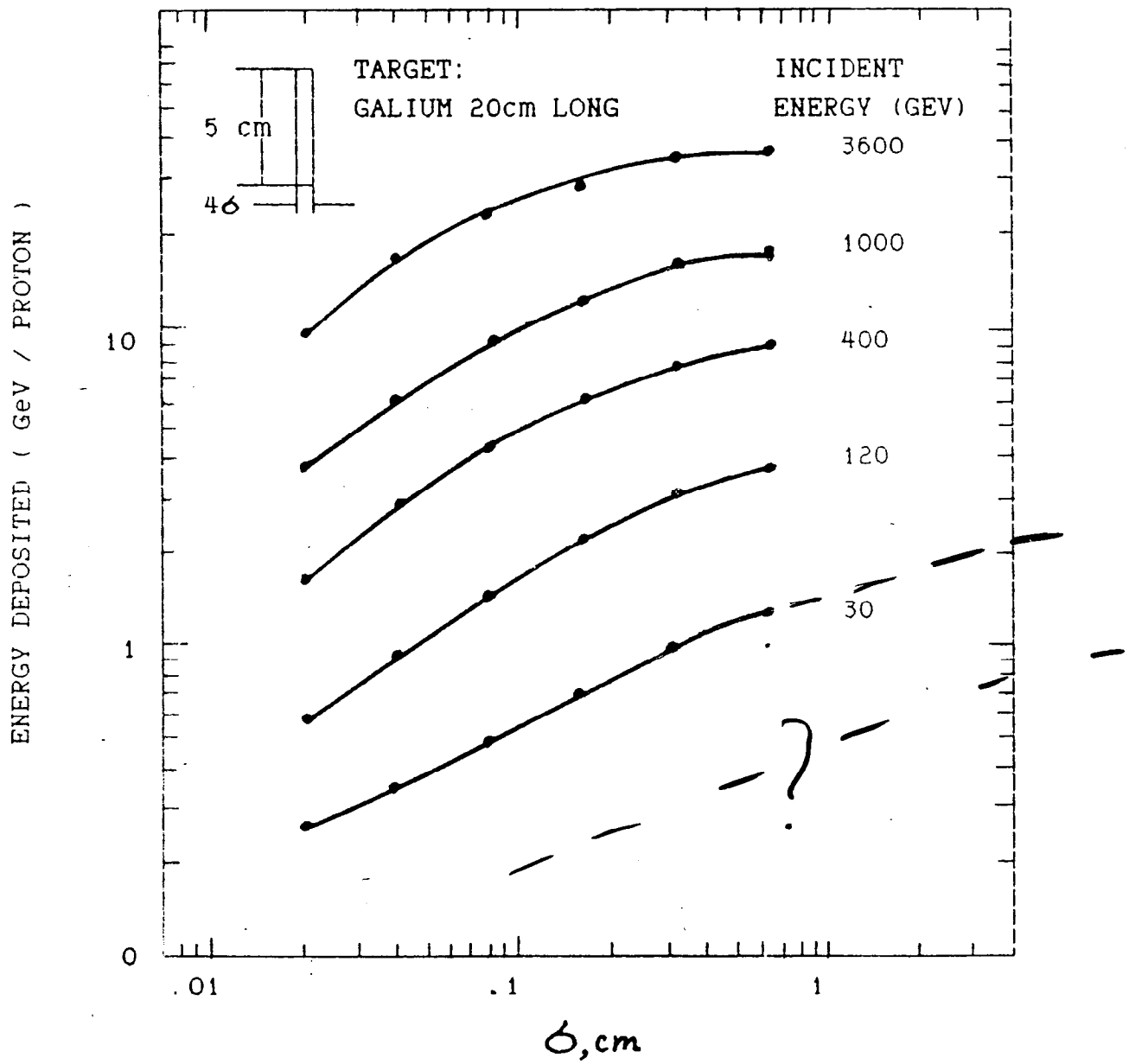
TARGET:
GALIUM 20cm LONG
INCIDENT
ENERGY (GEV)
3600
1000
400
120
30
5 cm
4σ
ENERGY DEPOSITED (GeV / PROTON)
10
1
0
.01
.1
1
σ, cm

Figure 5

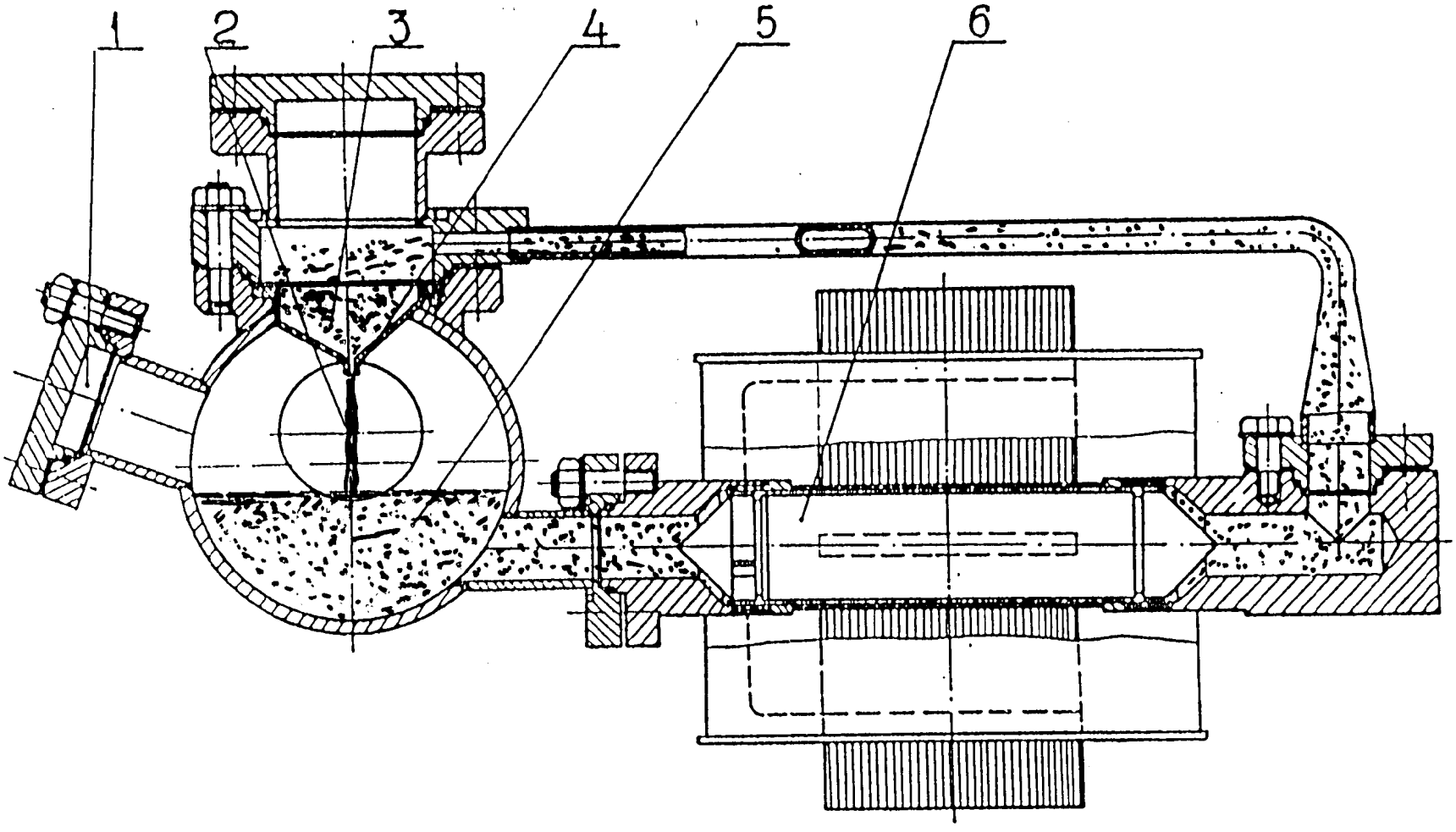

FIGURE 6 A stationary jet target:

1—observation hole; *2*—beam axis; *4*—nozzle of the drain chamber; *5*—liquid metal; *6*—pump.

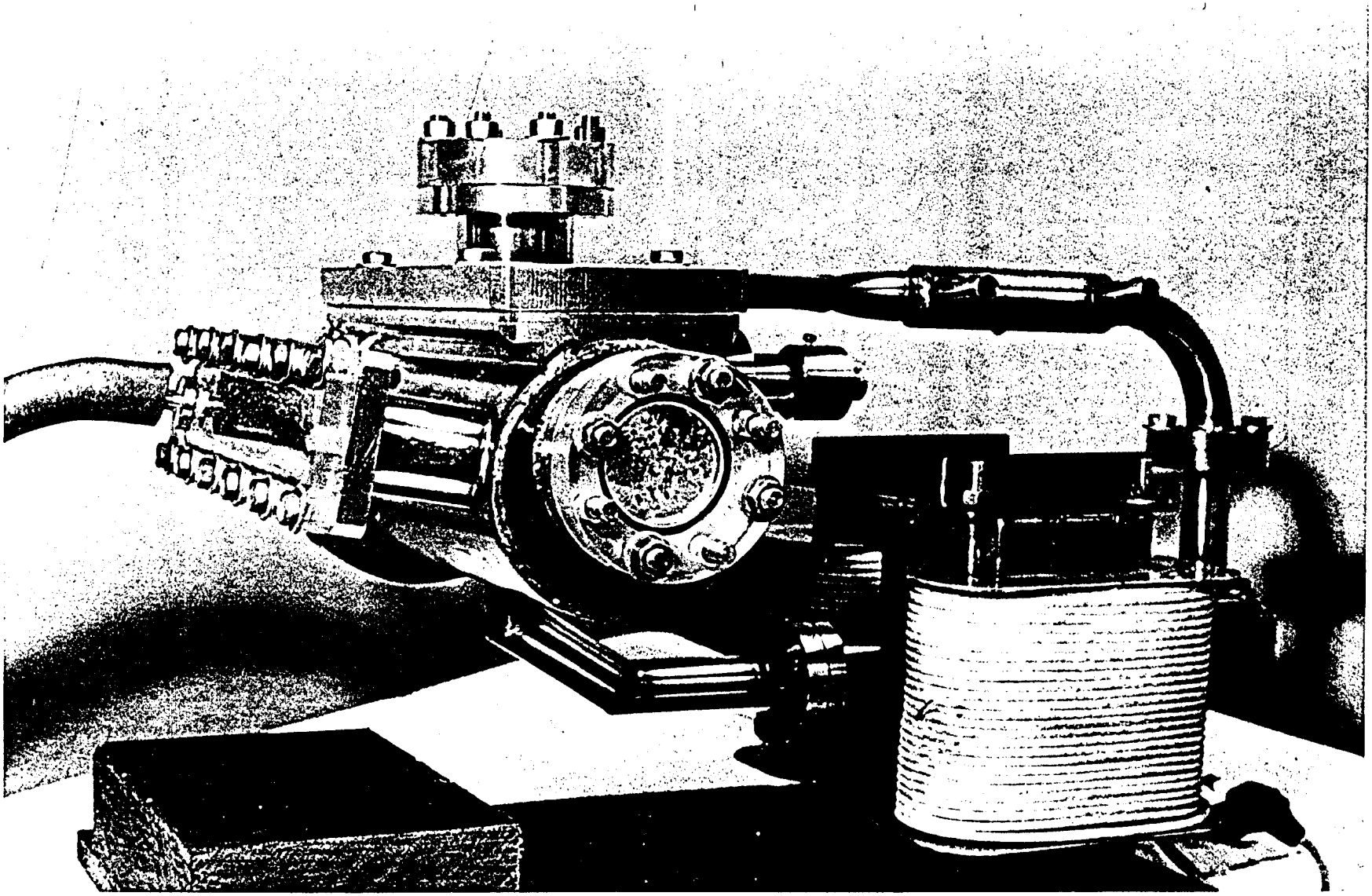

Fig. 7- Photo of a target device for the investigation of liquid metal jet formation in vacuum using a gallium-indium alloy.

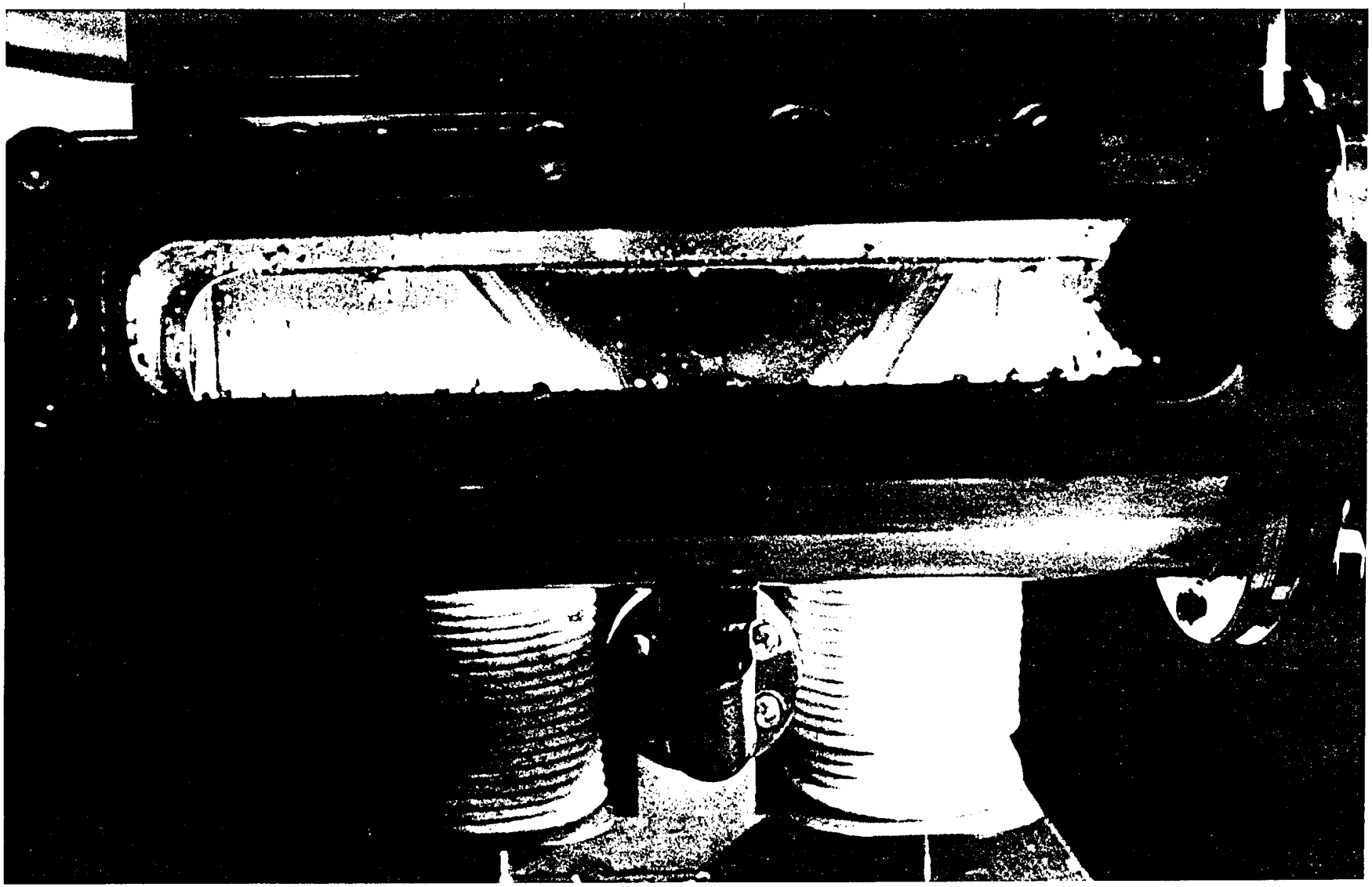

Fig. 8- Photo of a liquid metal jet in vacuum.

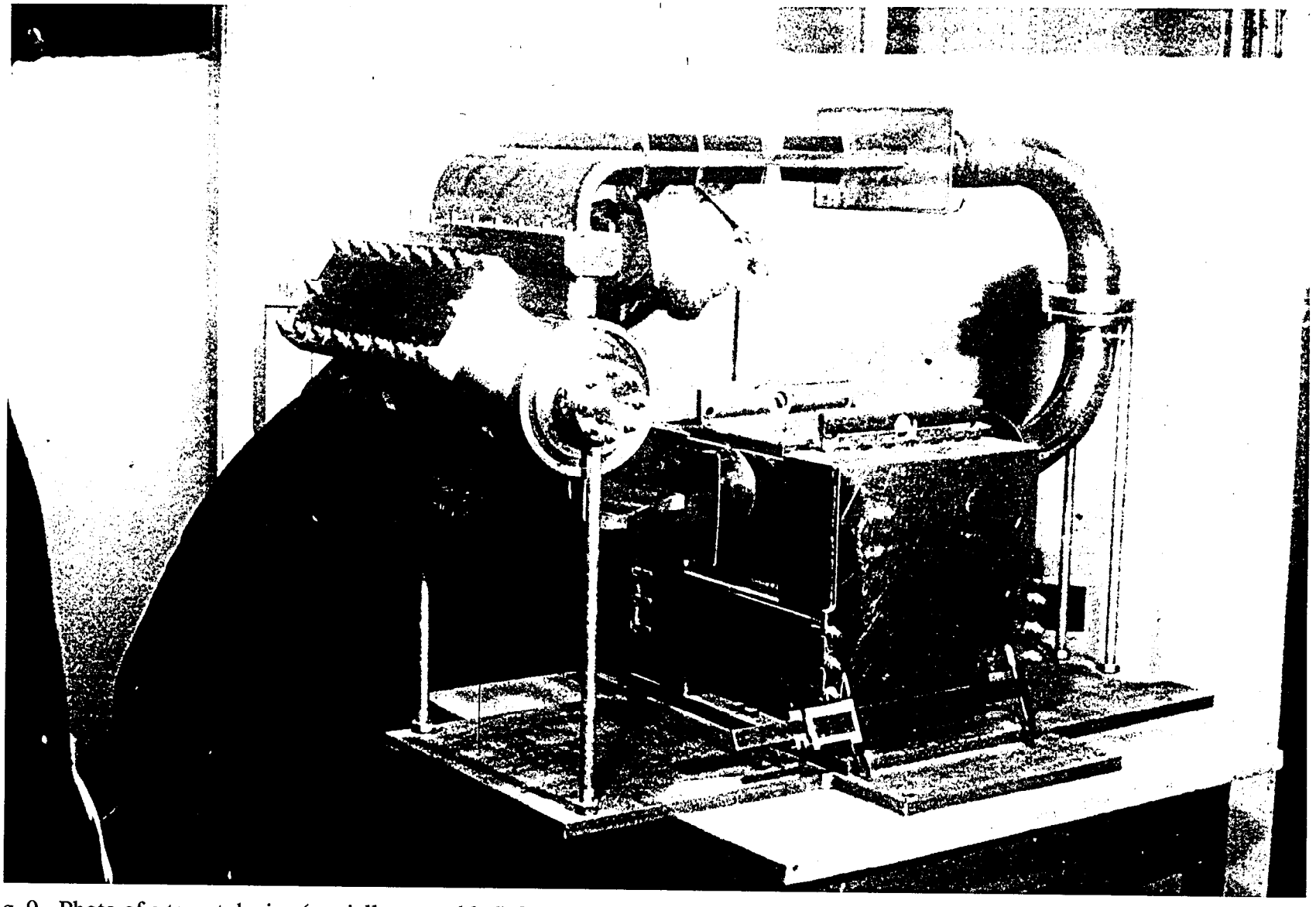

Fig. 9- Photo of a target device (partially assembled) for pumping 10 liters of liquid lead, supplying a jet of 250x2 mm2 dimension. This device is a prototype of the Mega-Watt target for the Kaon Factory.

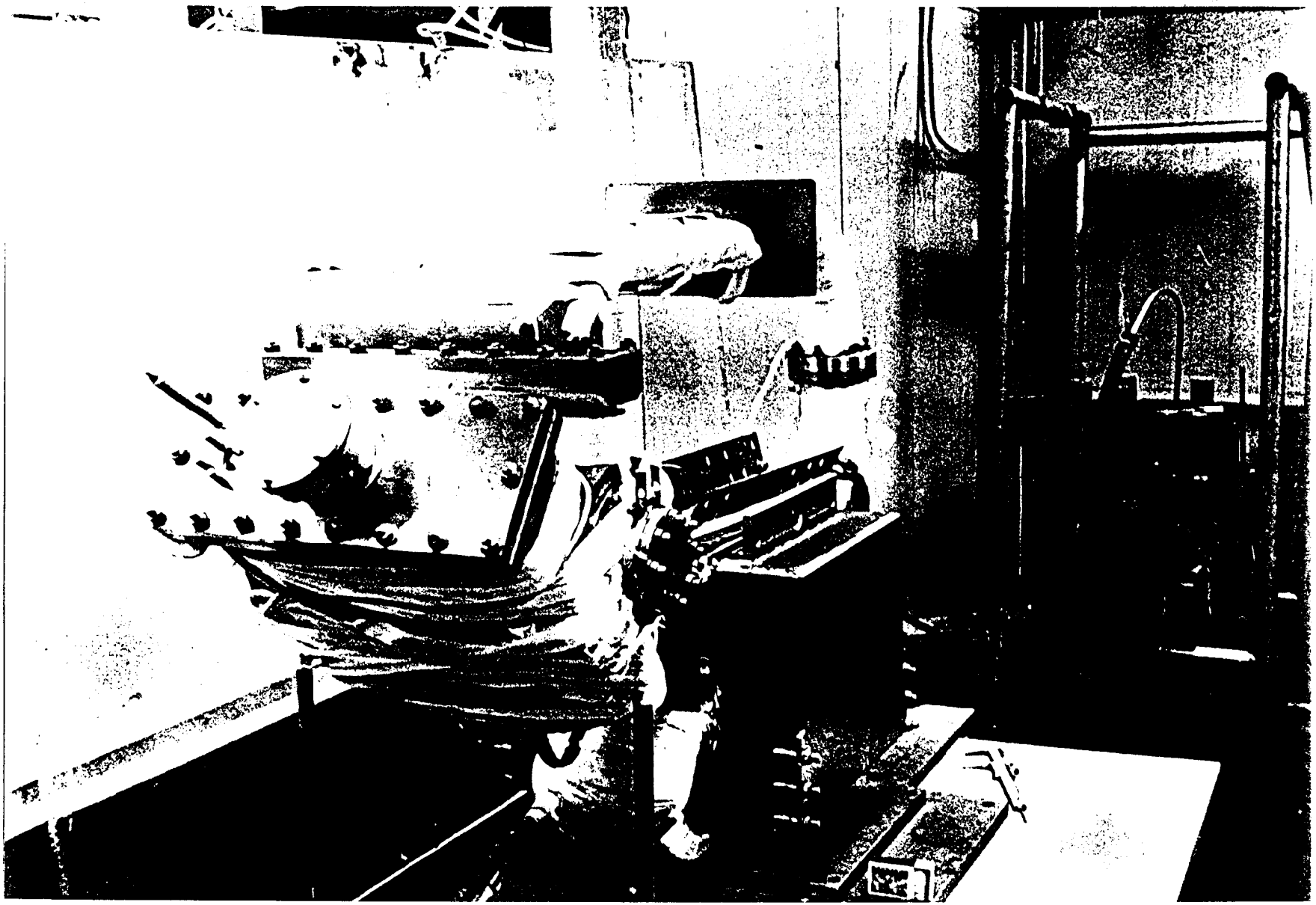

Fig. 10- Photo of a target device being used to test the pumping of 10 liters of liquid lead.

Figure 11

LIQUID GOLD JET TARGET

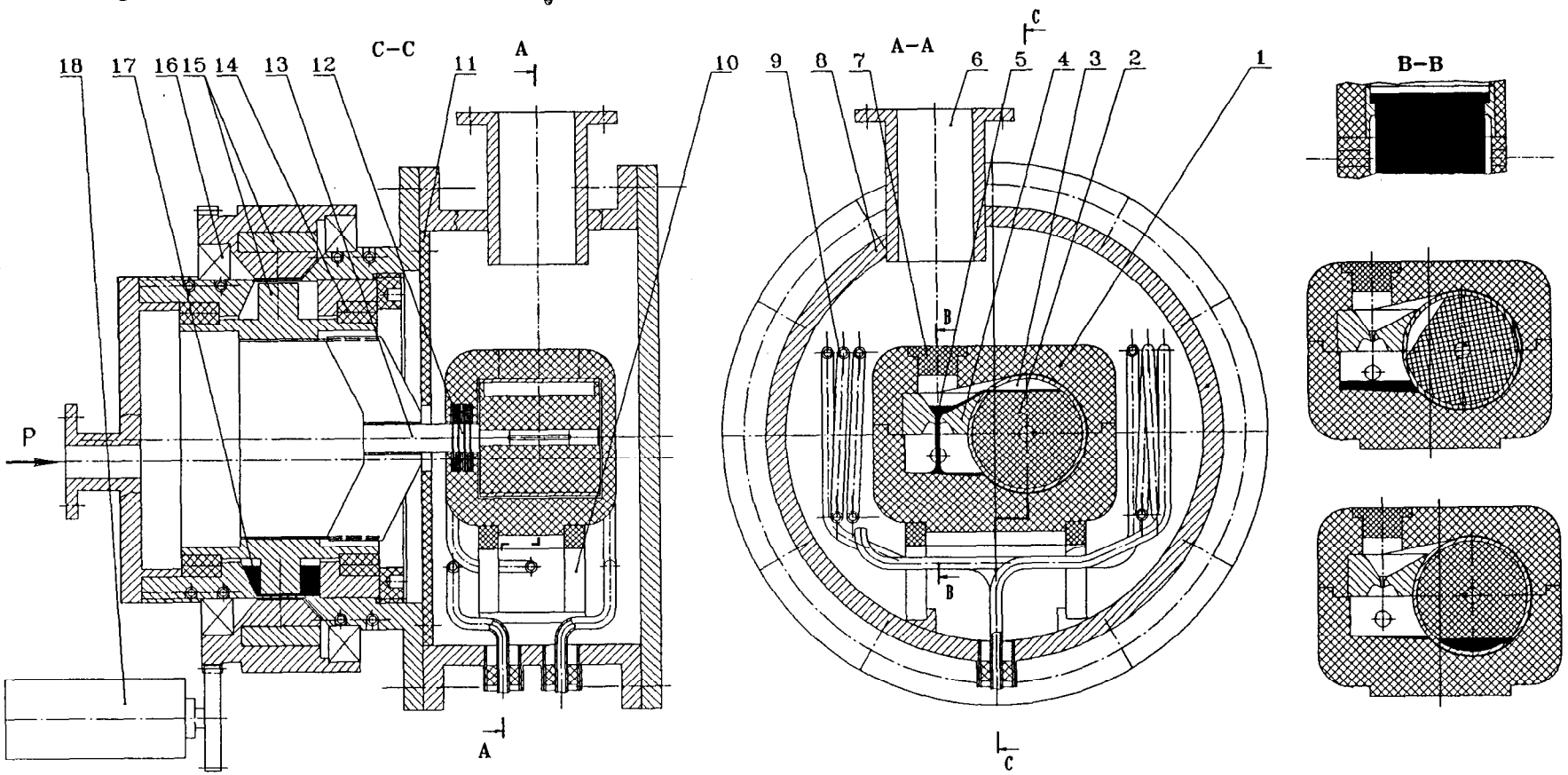

1-graphite body of pump; 2-graphite revolving cylinder with molibdenum envelope; 3-rilling cavity; 4-molibdenum drain chamber; 5-liquid metal jet and beam axis; 6-observation window; 7-closing insert; 8-vacuum chamber body; 9-RF heater; 10-ceramic support; 11-heat screen; 12-separating labyrinth; 13-revolving axle; 14-graphite bearing; 15-magnetic muff; 16-bearing; 17-gallium-indium cooler; 18-driver motor.

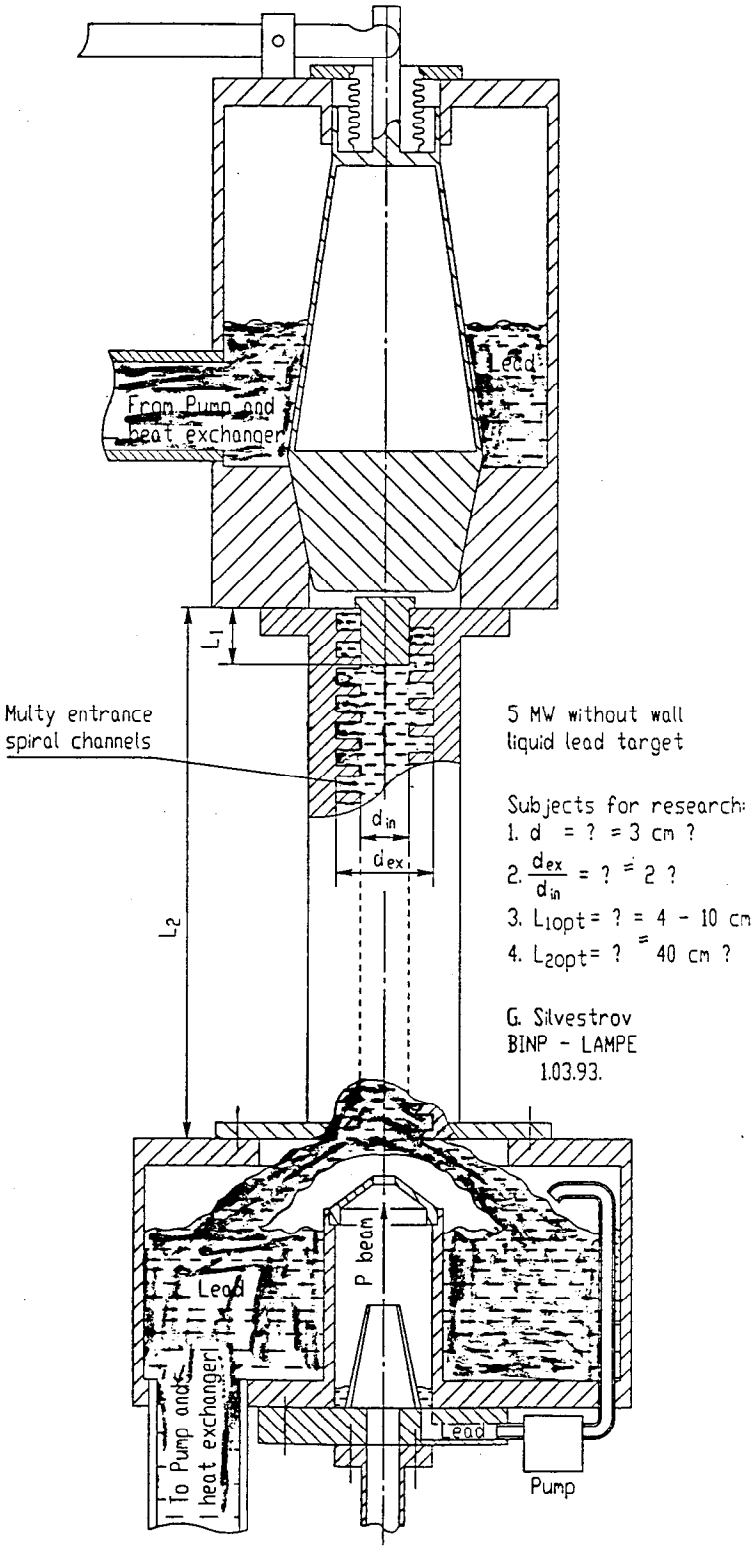

Fig. 12- Conceptual design of the Mega-Watt centrifugal-type liquid-lead target for the Neutron Spallation Source.

Positron Collection Liquid Lithium Lens

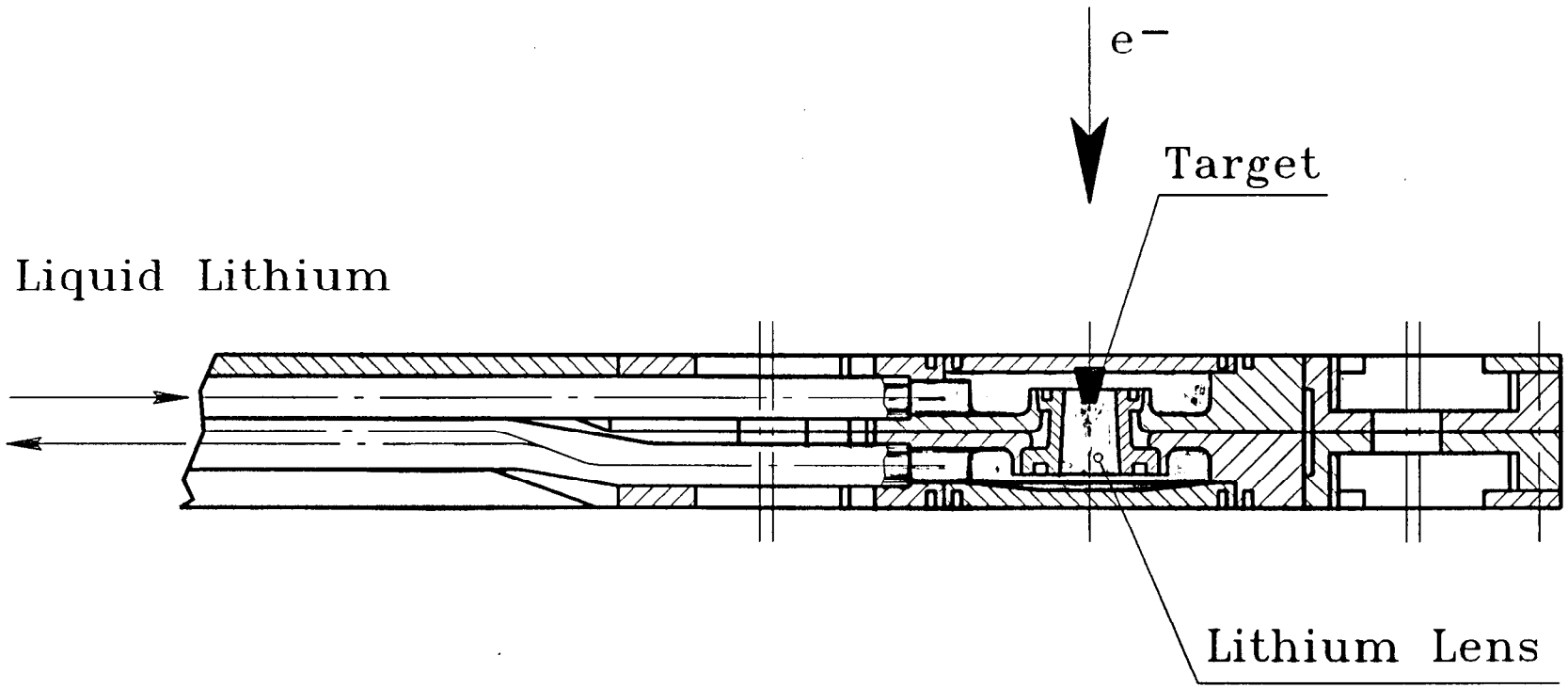

Fig. 13- The liquid lithium lens for the quarter-wave transformation of positron beam emittance. The lens length is 1 cm, field gradient G= 20 T/cm, repetition rate 150 Hz. The tungsten target is cooled by flowing liquid lithium.

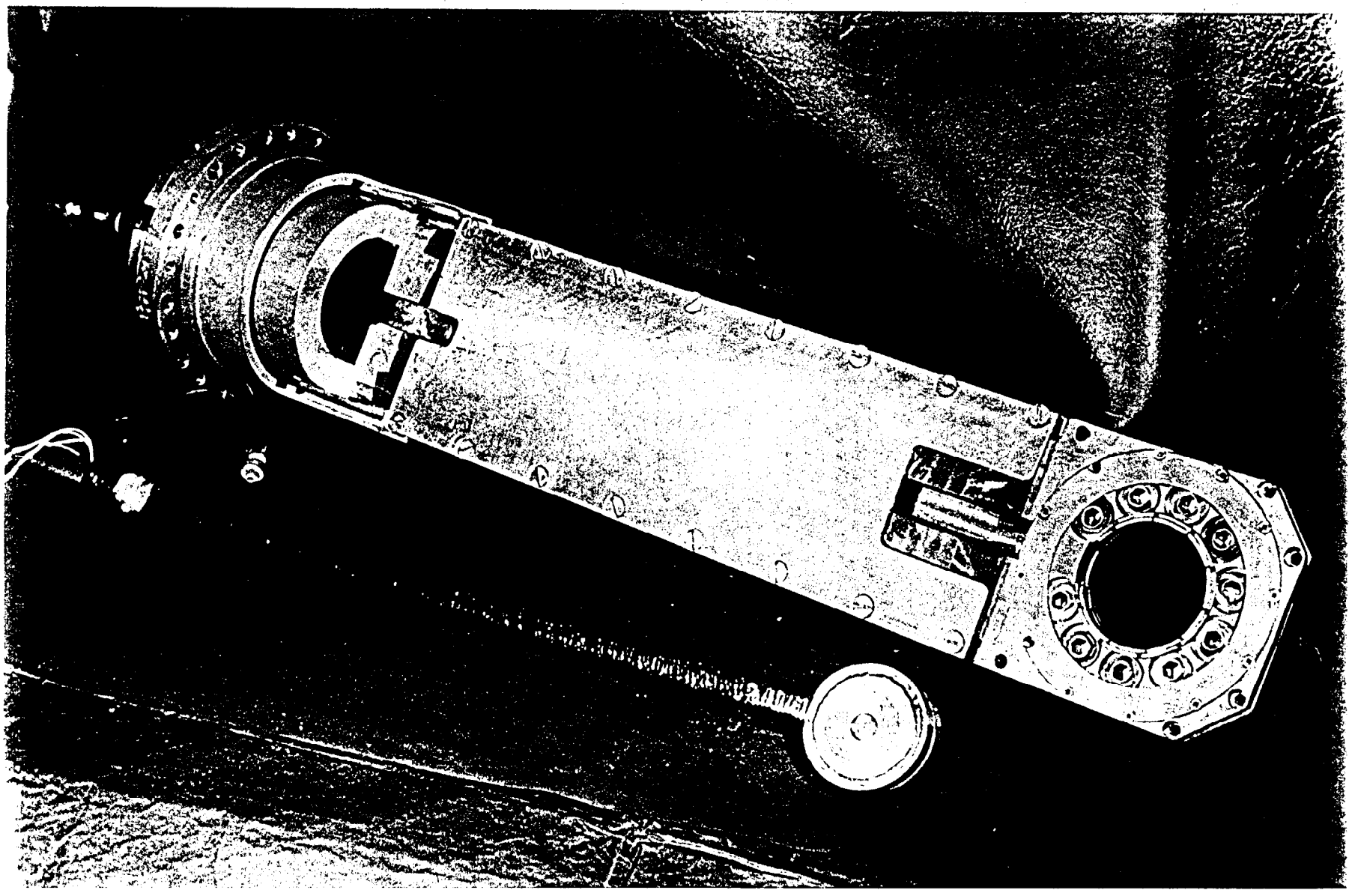

Fig. 14- Photo of liquid lithium lens with current input of strip-line type.

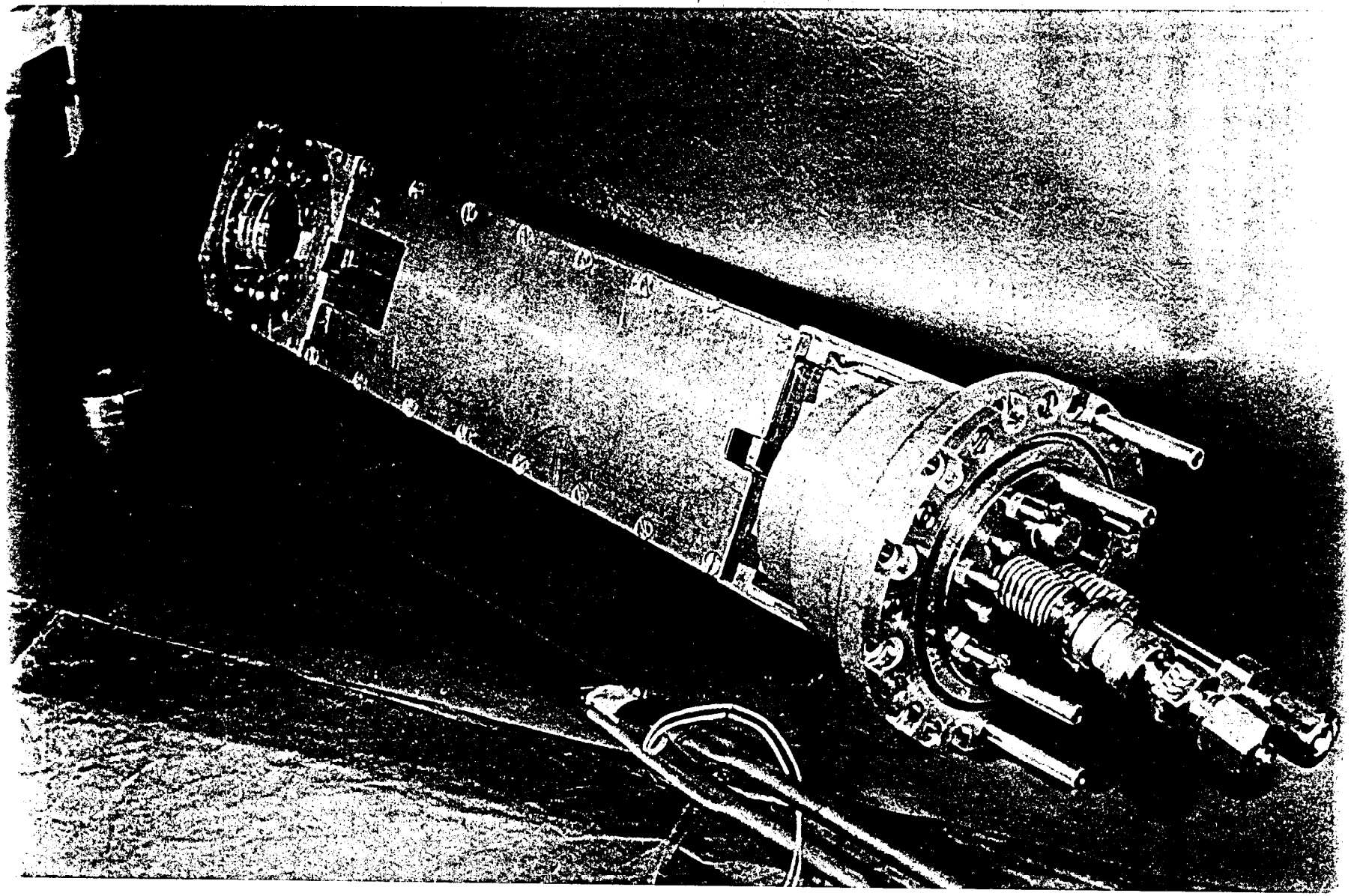

Fig. 15- Photo of liquid lithium lens with current input of strip-line type.

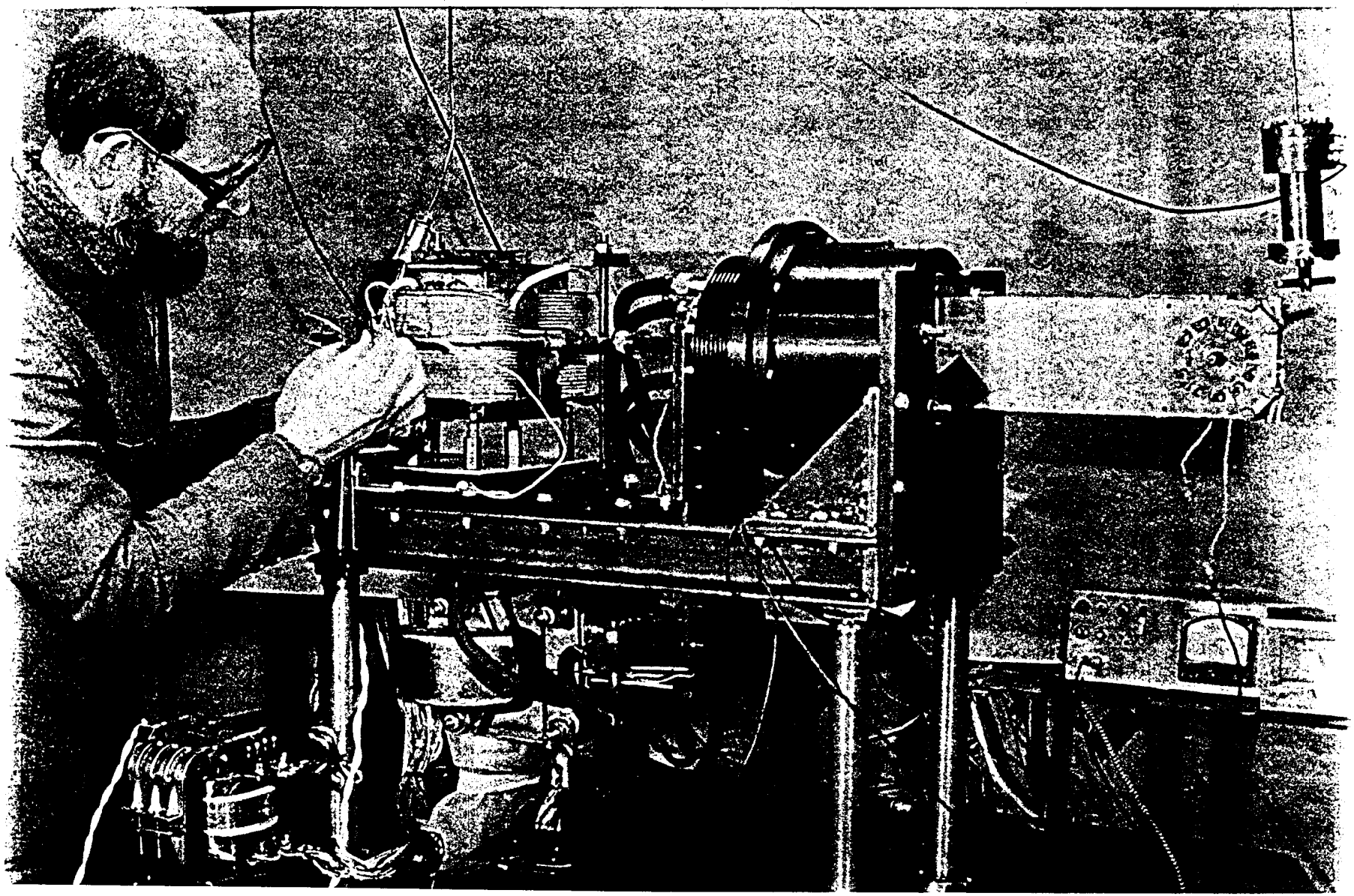

Fig. 16- Photo of a liquid lithium lens device with pump, matching transformer, and heaters.

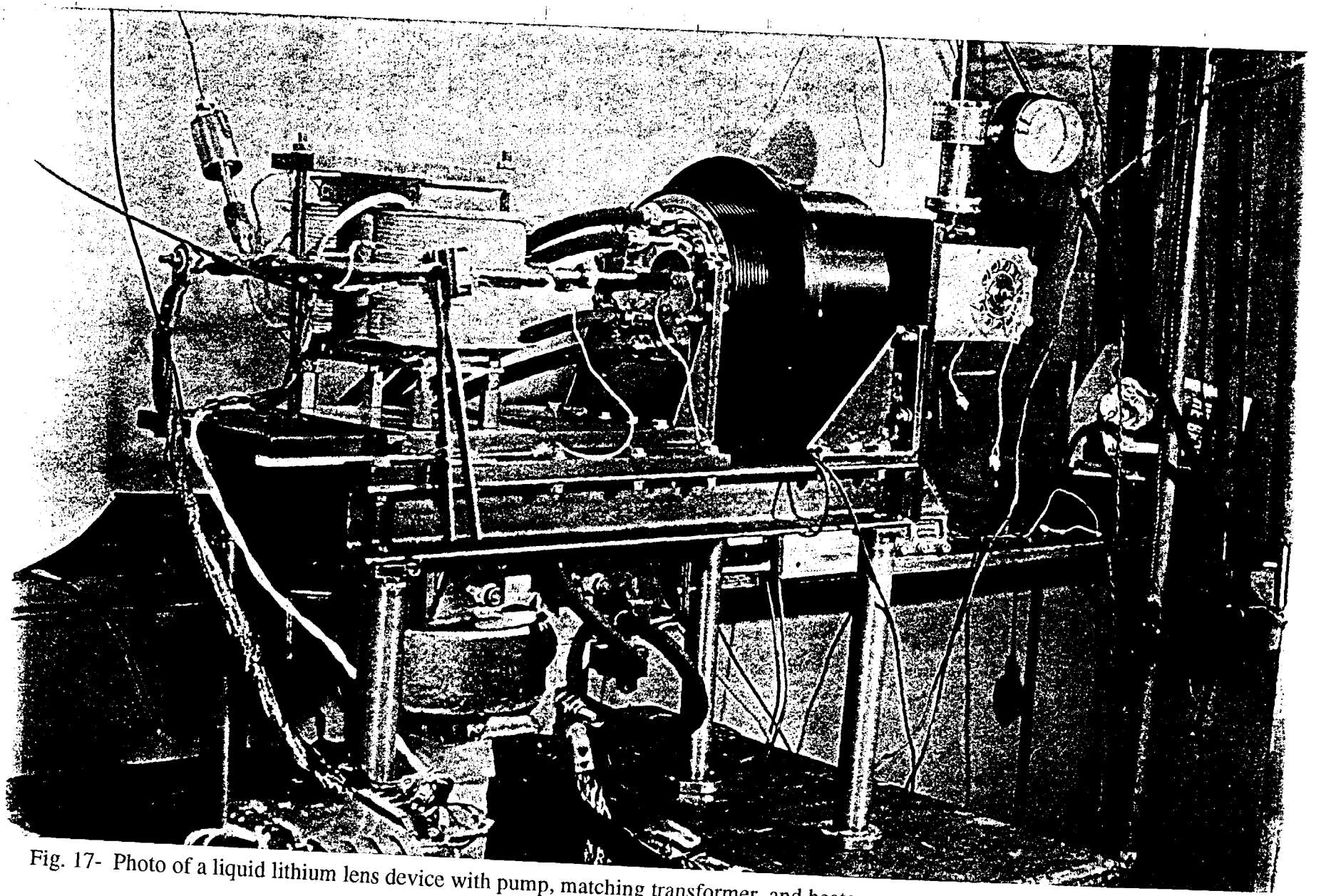

Fig. 17- Photo of a liquid lithium lens device with pump, matching transformer, and heaters.

Figure 18

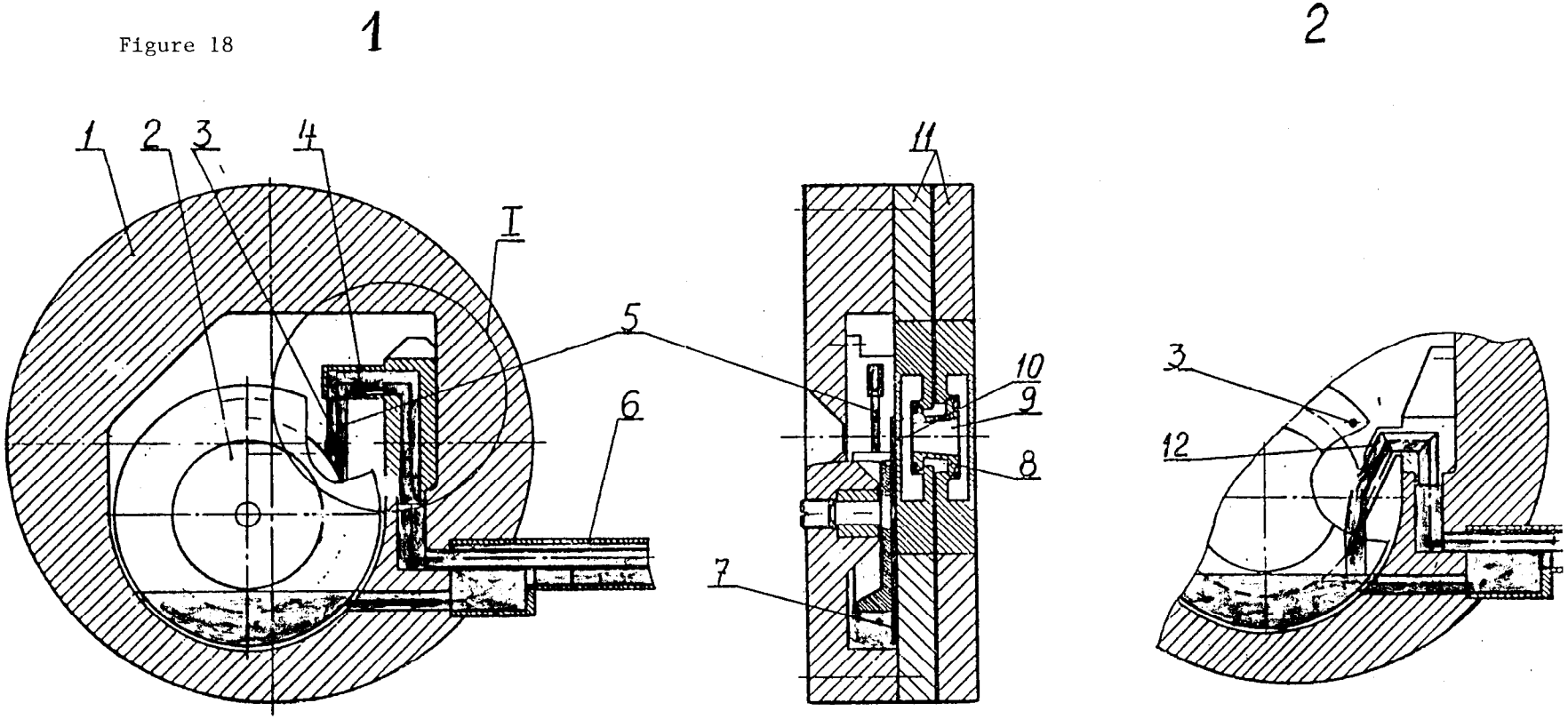

Target of the VLEPP conversion system: variant 1: mercury jet; variant 2: tungsten disk;

1—body; *2*—disk; *3*—beam axis; *4*—drain nozzle; *5*—mercury jet target; *6*—supply tubes; *7*—guard titanium disk; *8*—body of a lithium lens; *9*—operating lithium volume; *10*—entrance flange of the lens; *11*—current input; *12*—drain nozzle for the gallium jet.

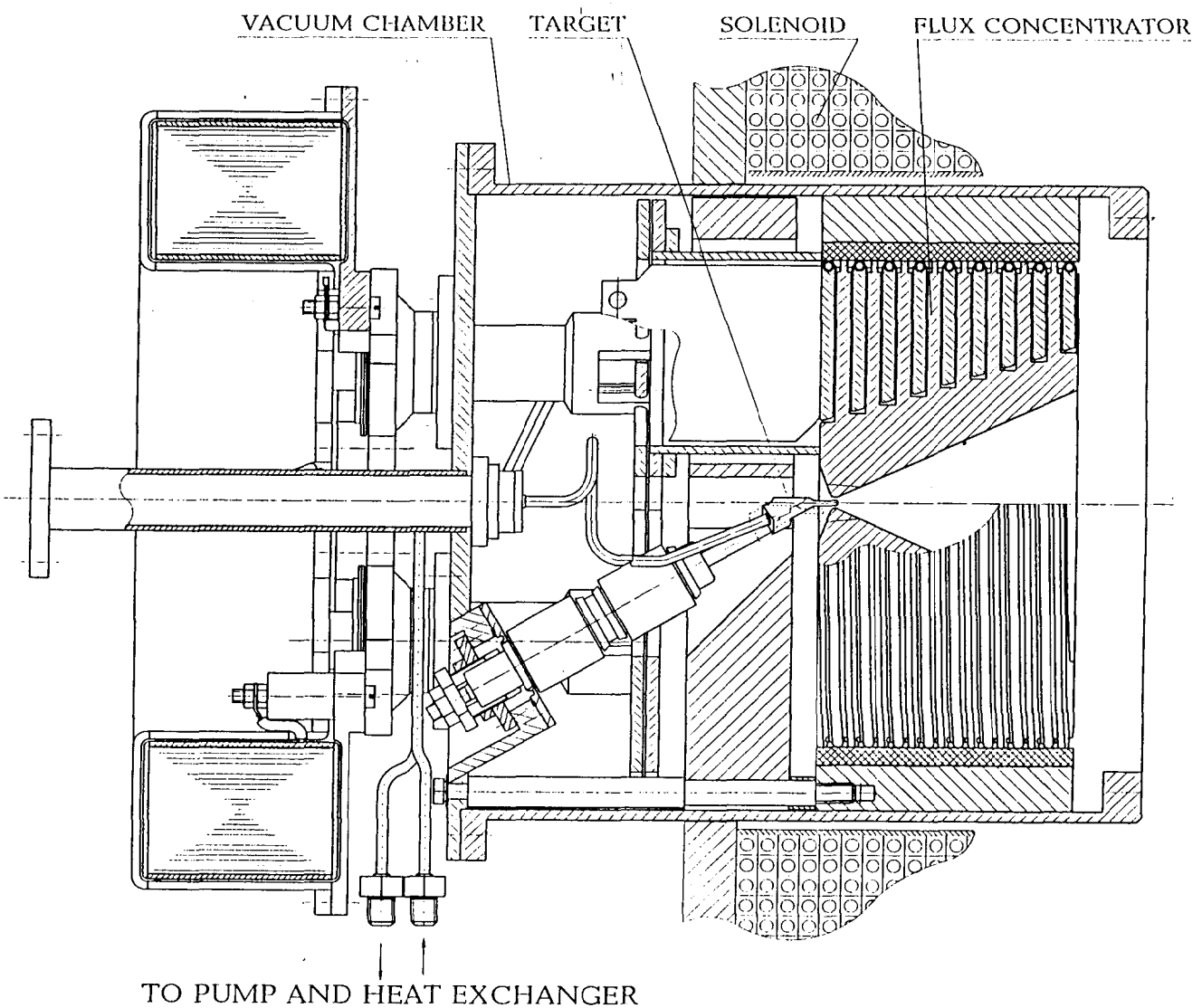

Fig. 19- Flux concentrator for positron collection with liquid lead target of the coaxial type.

Figure 20

Concentrator of Magnetic Field

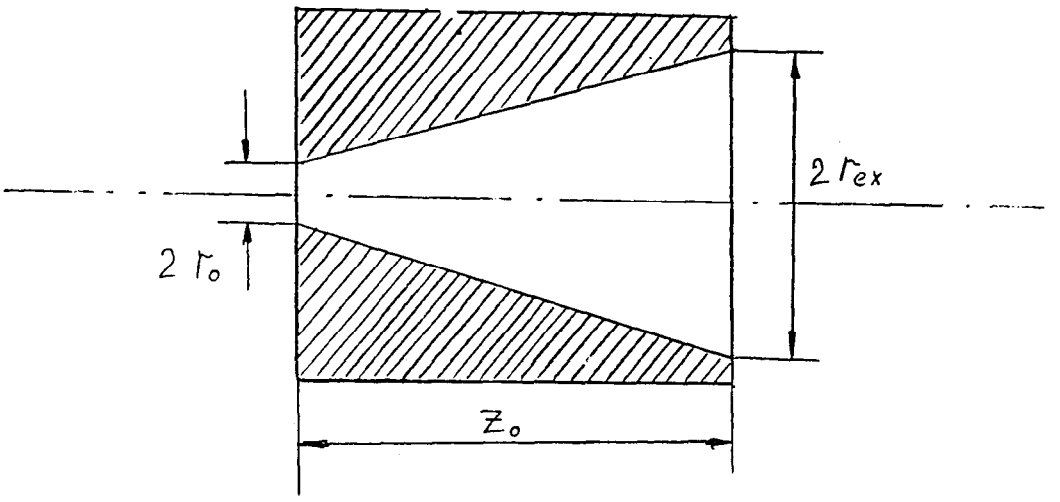

$$H(z) = \frac{H_0}{\left(1 + \frac{z}{z_0}\frac{r_{ex}}{r_0}\right)^2}$$

$\frac{r_0}{r_{ex}} \ll 1$

$\frac{\delta}{r_0} \ll 1$

$$J = \frac{H_0 z_0}{0.4\pi} \cdot \frac{r_0}{r_{ex}} \qquad L = \frac{4\pi \cdot \pi r_0 r_{ex}}{z_0}$$

$$W = \frac{H_0^2}{8\pi} \cdot \pi r_0^2 z_0 \cdot \frac{r_0}{r_{ex}}$$

$r_0 = 0.2\,cm$, $r_{ex} = 3\,cm$, $z_0 = 10\,cm$

$H_0 = 10\,T$. $J = 53\,kA$ $W = 3.2\,J$

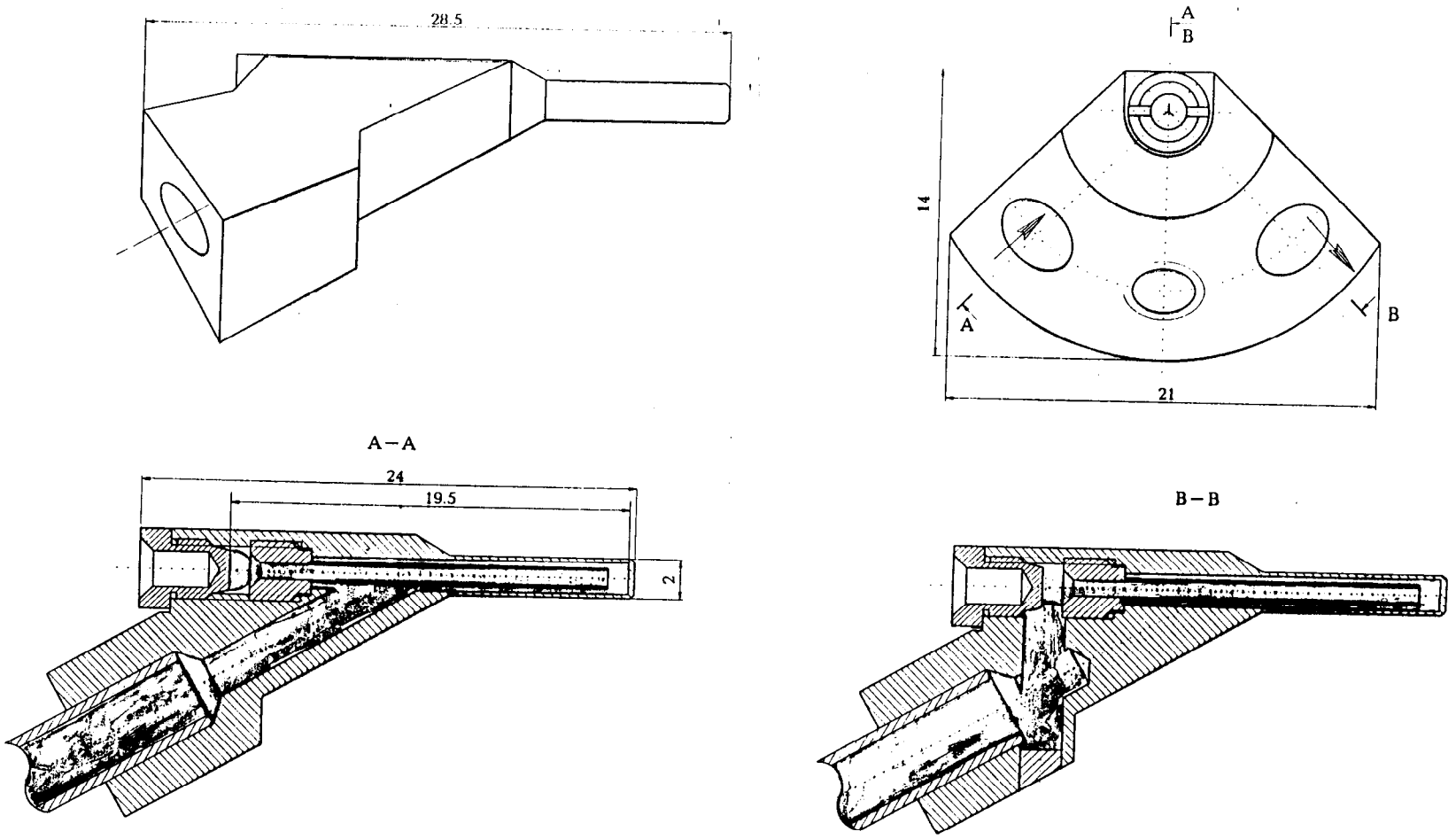

Conversion Liquid Lead Target

Fig. 21- Liquid lead target of the coaxial type.

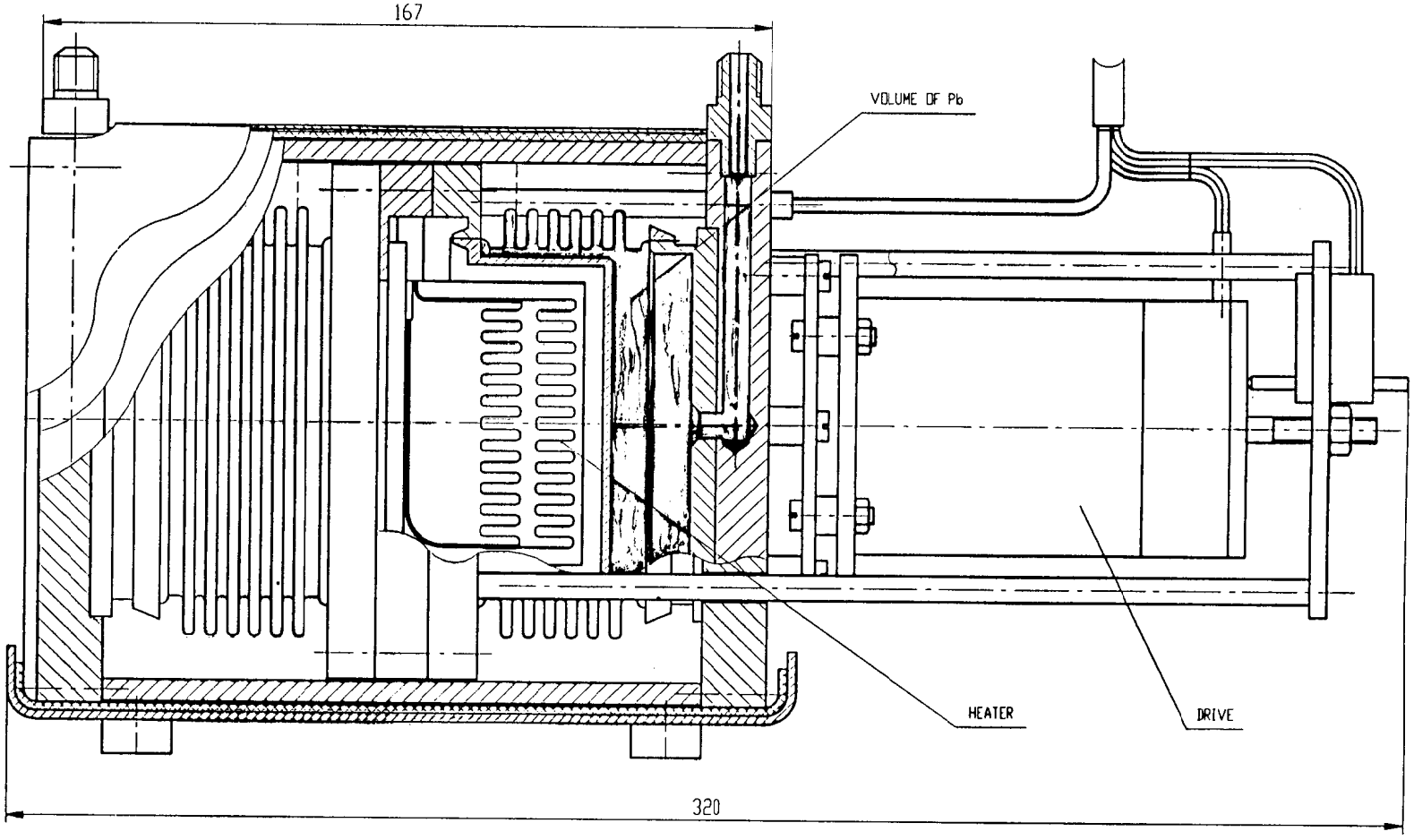

Figure 22 The Pump of melting Pb.

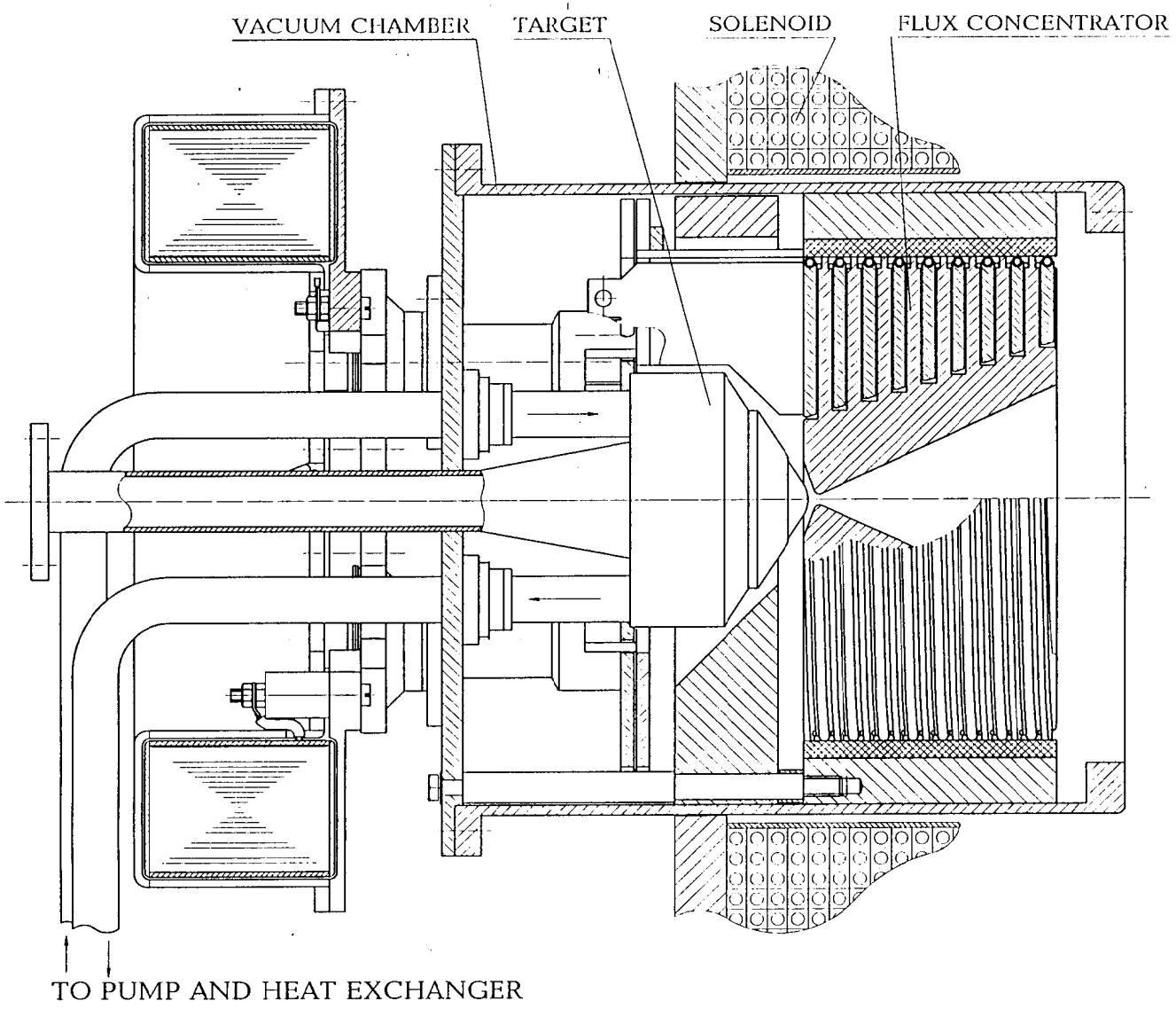

Fig. 23- Flux concentrator with liquid lead jet target.

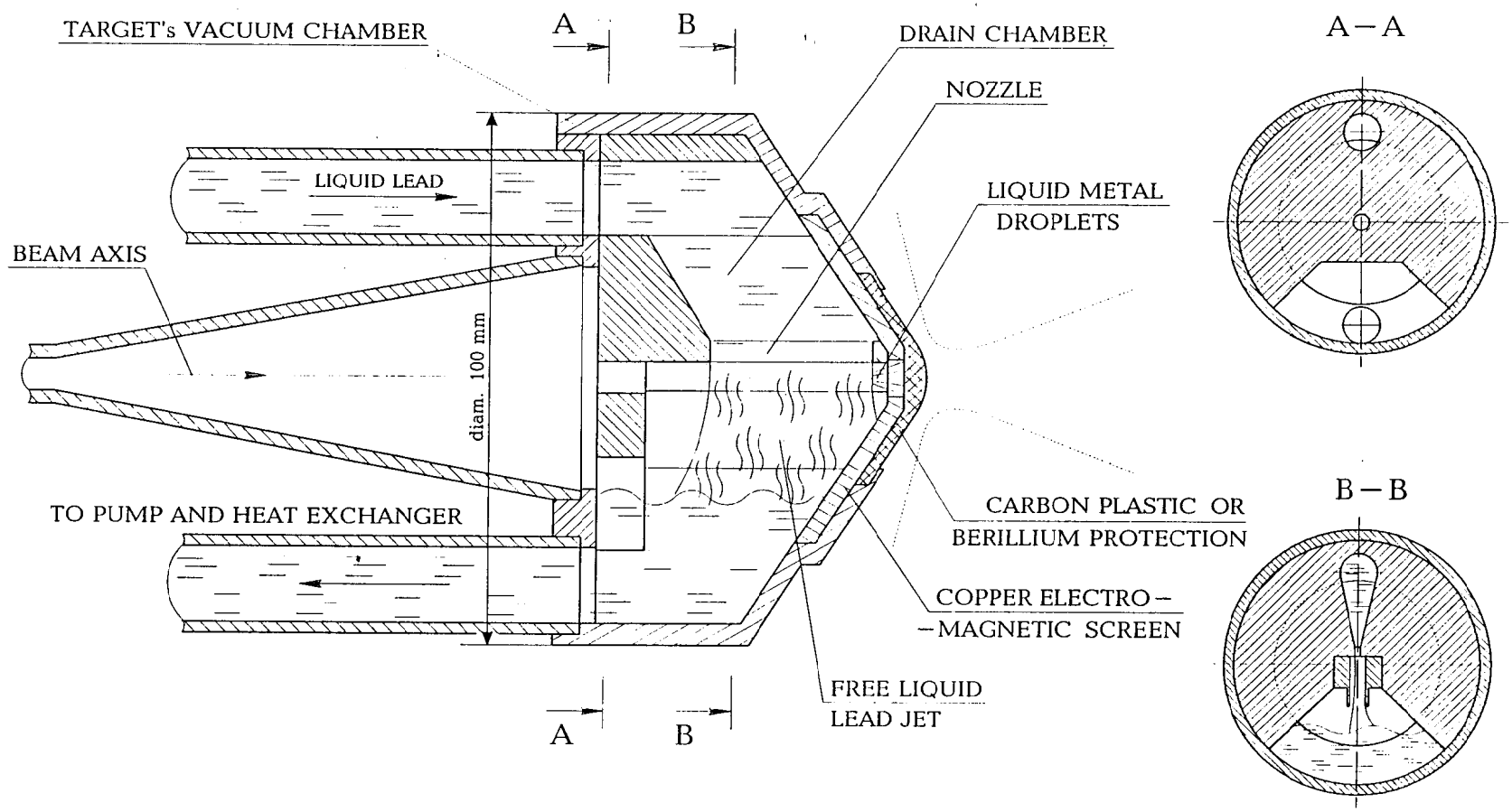

Conversion Liquid Lead Target

Fig. 24- Liquid lead jet target.

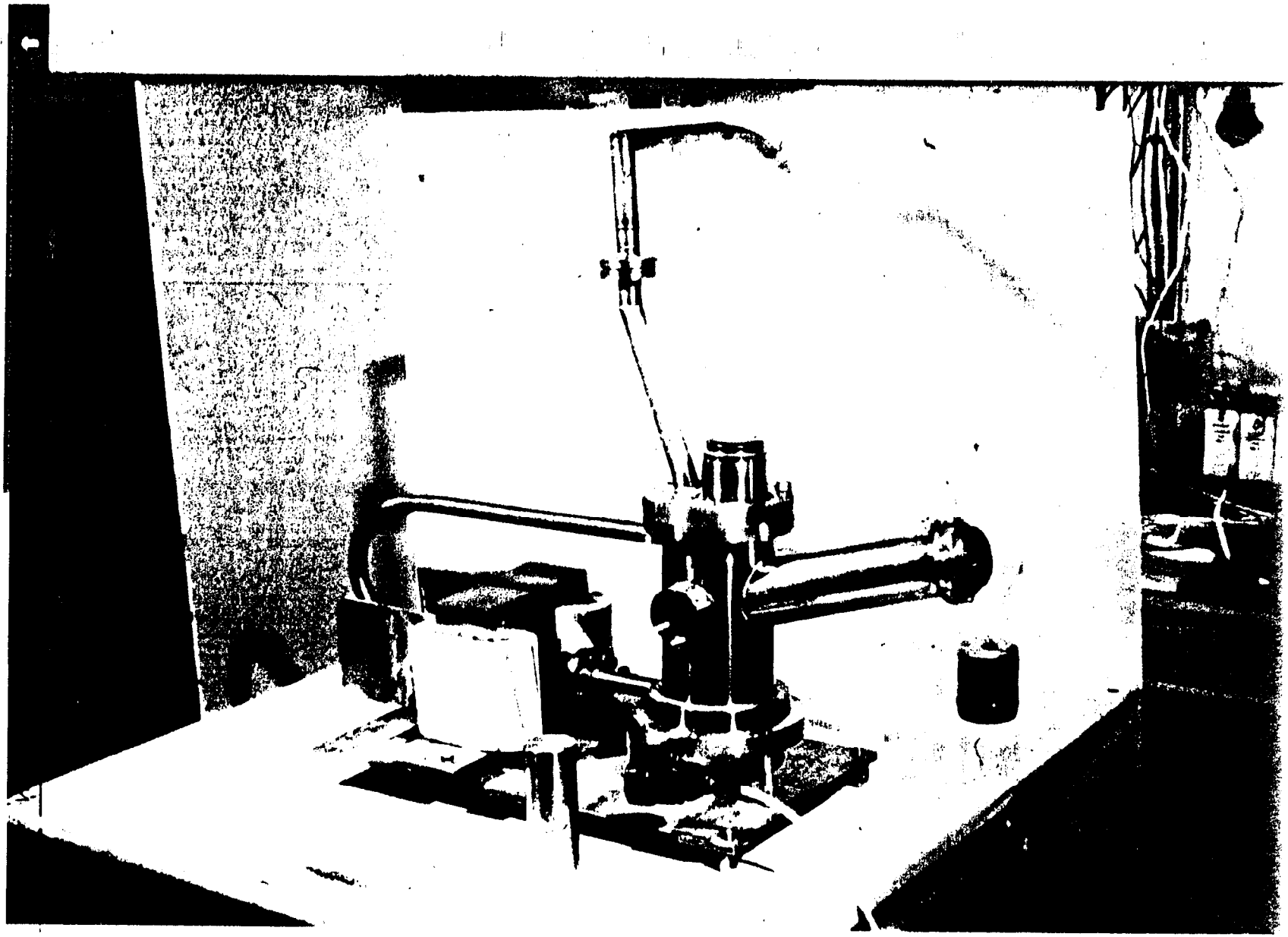

Fig. 25- Liquid lead jet target device for experiments with SLAC beam.

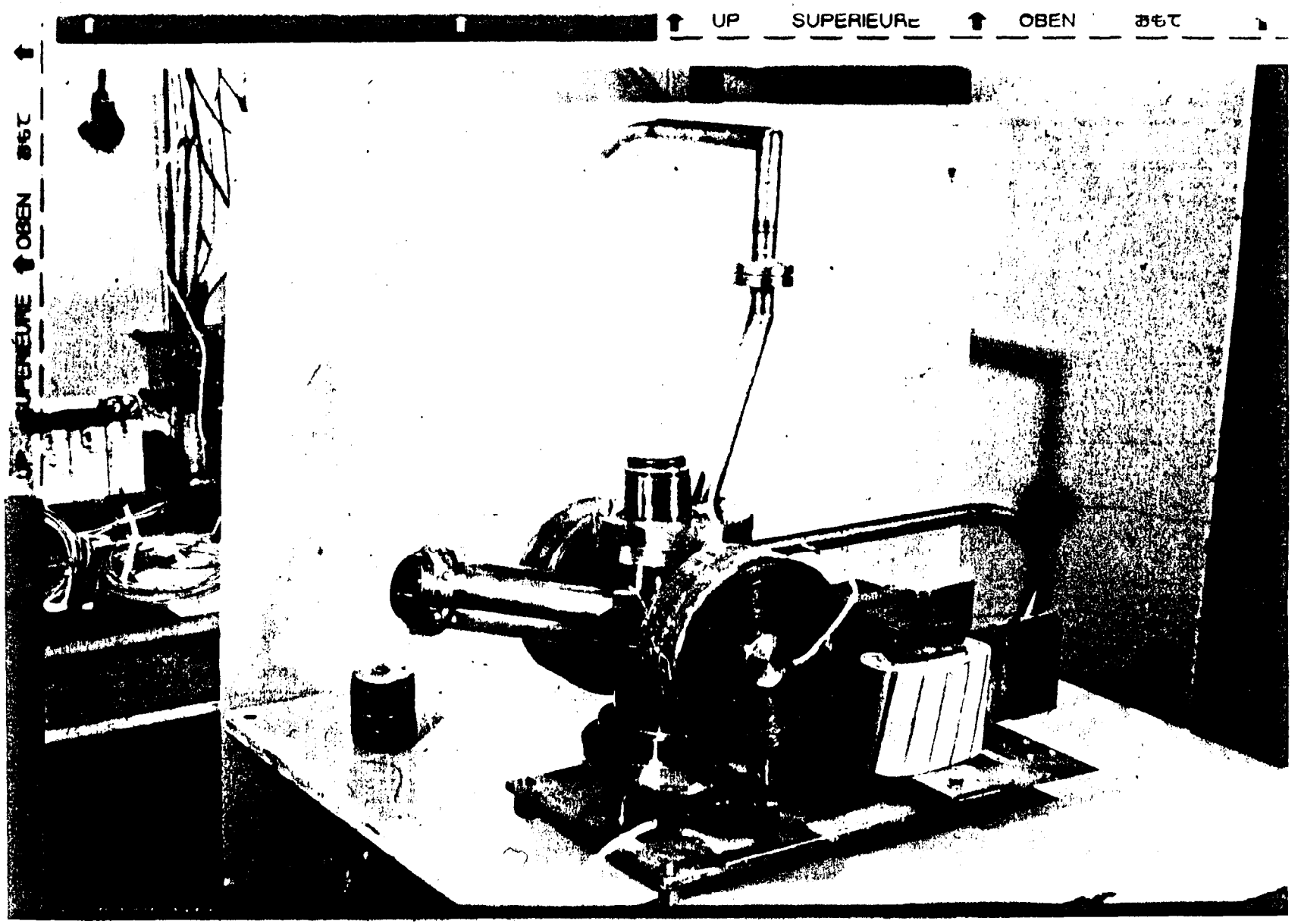

Fig. 26- Liquid lead jet target device with a longitudinal magnetic field.

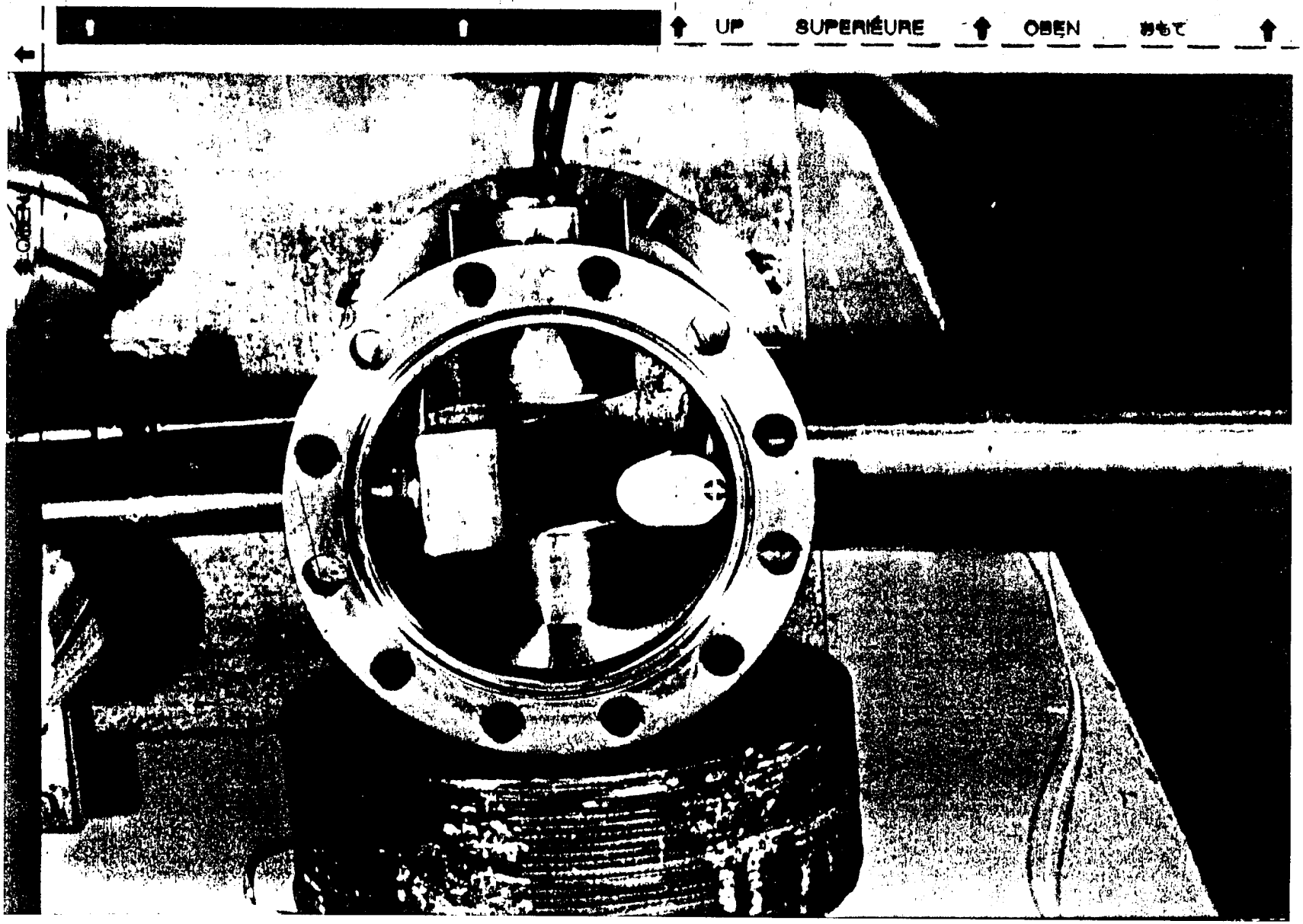

Fig. 27- Top view of the target device (Fig. 26) with open cover.

Fig. 28- For a case where the electron beam intensity does not cause the destruction of a heavy (tungsten) target during a single beam-spill but the average power dissipation in the target is high, the cooling problem could be solved using a moving target in the form of a rotating wheel. Water cooling for such a target system is difficult to provide because of the technical problem of bringing the water to the target wheel while it is rotating in vacuum.

The figure shows the design of a wheel target with transmission of rotation into the vacuum chamber by means of a magnetic muff. Heat removal is fulfilled with use of a liquid metal (gallium-indium alloy or mercury) pool through which the lower part of the wheel passes. The liquid metal contacts only with an outer radius of the wheel which is made of copper and has an extended cooling surface. The average temperature of the wheel could be several hundreds of degrees, which increases the heat flux through the liquid metal due to high temperature gradient.

The wheel is located in a separate vacuum chamber thus excluding the penetration of liquid metal vapor into the accelerator vacuum volume. At positron exit the vacuum volumes are connected through a small window of about 5-mm diameter closed by a thin (about 10-mkm) foil made of carbon plastic or beryllium. The power dissipated in the foil is removed by radiation which becomes sufficient at a temperature higher than 1000 C.

Figure 28

Flux Concentrator with Target's Wheel.

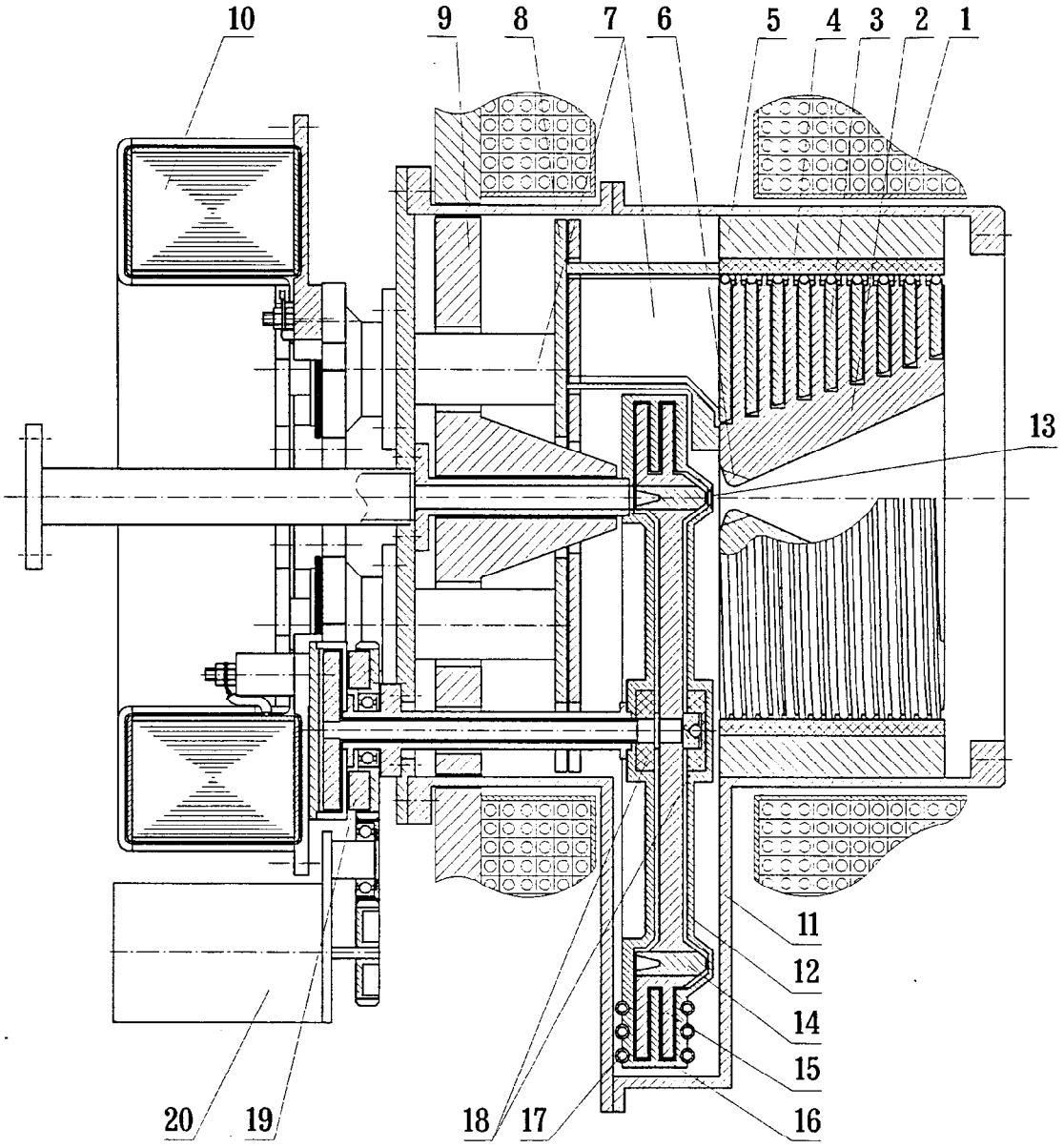

1. Soleniod. 2. Flux concentrator. 3. Well-balanced primary winding.
4. Ceramic supported cylinder. 5. Bandage. 6. Tunsten insert.
7. Current input. 8. Current collector. 9. Magnetic yoke.
10. Mutching transformer. 11. Accelerator vacuum chamber.
12. Target vacuum chamber. 13. Separating foil. 14. Tungsten target wheel.
15. Copper cooling wheel. 16. Gallium-indium or mercury pool.
17. Cooling tube of target's chamber. 18. Graphite bearings.
19. Magnetic muff. 20. Motor.

Positron Production in Single Crystals by 1.2GeV Channeling Electrons

Tohru Takahashi
Hiroshima University

We performed an experiment to observe enhancement of positron production in single crystals by 1.2 GeV electrons. The experiment was carried out at the electron synchrotron in Institute for Nuclear Study, University of Tokyo in May 1996, where electron beam of 10^6electron/s with emittance of 1mm-mr is provided.

The crystals used were, a 35 mm thick silicon and 3 tungsten crystals of 1.2 mm, 2.8 mm and 4.8 mm thick. Both positron and x ray yield in the detector downstream of the target showed clear peak when the electron beam was aligned to be on axis<100> of the target crystal. It should be noted that the width of the rocking curve was much larger than one expected from channeling condition. The enhancement factor was defined as the ratio of positron yield on axis and the one at 5 degree away from axis. For the tungsten of 1.2 mm thick, the enhancement factor was 2.56 in average. For another tungsten target, the enhancement factors were 1.63 for 2.8 mm and 1.31 for 4.8 mm thick crystals. This lower enhancement factor in thick crystals are considered to come from imperfectness of the crystals. The x-ray diffraction picture showed that the there were disorientation of crystal axis inside the crystal which was estimated to be 50 mr.

The positron yields were estimated by a simulation. The simulation of base yield of positrons agreed very well with experimental data. For the peak yields, the experimental data showed lower number than the simulation for 2.4 and 4.8 mm tungsten crystals. This can be attributed to imperfectness of the crystal as expected by x-ray diffraction picture. One interesting point is that the experimental data shows higher positron yield than the simulation. This fact is thought to be related to wider width of rocking curve. In addition to the channeling radiation, contribution for positron production from coherent bremstrahlung is not small and is estimated to be comparable with channeling radiation in our experimental condition. The estimated with in rocking curve by coherent bremstrahlung is about 20 mr(FWHM) which is consistent with experimental data.

We proposed a new experiment at KEK in October - November 1997. In the experiment, we are going to use 1 GeV electron in KEK LINAC. The LINAC is being updated for B factory and the positron capture system for the B factory has been already installed and available at time of experiment. After the extension of the LINAC, the electron beam energy will be 4 GeV at the positron target but it is not completed and 1 GeV beam can be used in next October. With the real positron capture system, it is expected to obtain data of positron yields including acceptance of the accelerator system.

Positron Production in Single Crystals by 1.2GeV Channeling Electrons

Tohru Takahashi
Hiroshima univ.

May.5 1997

- Experiment by 1.2GeV electrons with Silicon, Tangsten crystals
- Planned experiment at KEK LINAC

I. Endo, K. Goto, T. Isshiki, T. Kondo, K. Matsukado, Y. Takashima
Department of Physics Hiroshima university

K. Yoshida, H. Okuno
Institute for Nuclear Study, University of Tokyo

A. P. Potylistin, I. E. Vnukov
Tomsk Polytecnic University

Introduction

Enhancement of Positron yeild

X. Artru, V. N. Baier, R. Chehab, A. Jejcic
NIM A344 (1994) 443

→ expected 2-3 times more positrons than amorphous target
enhanse lower part to energy distribution

→ good for acceptance

↓

Experiment ?

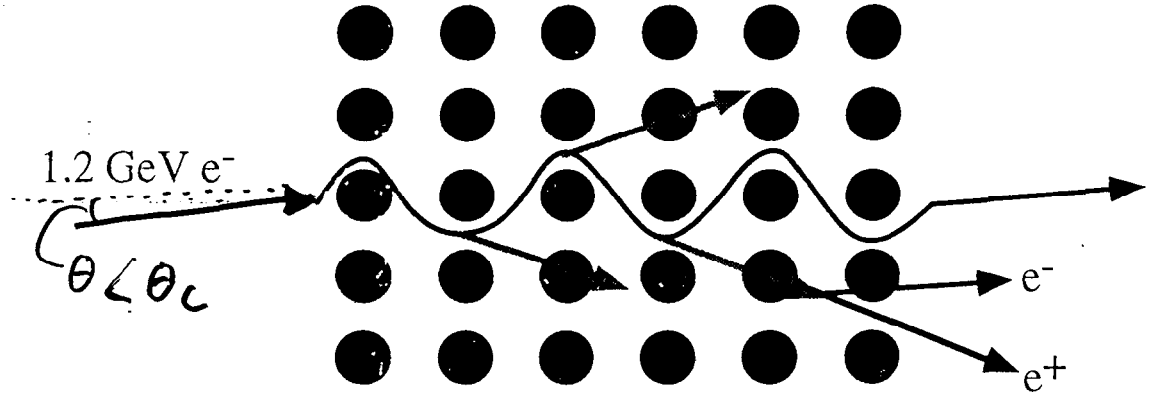

Linbard angle

Si⟨100⟩	35mm (0.34X_0)	$\theta_c = 1.17 mr$
W⟨100⟩	1.2mm (0.37X_0) 2.4mm (0.69X_0) 4.8mm (1.37X_0)	$\theta_c = 0.37 mr$

Experimental setup May 1996

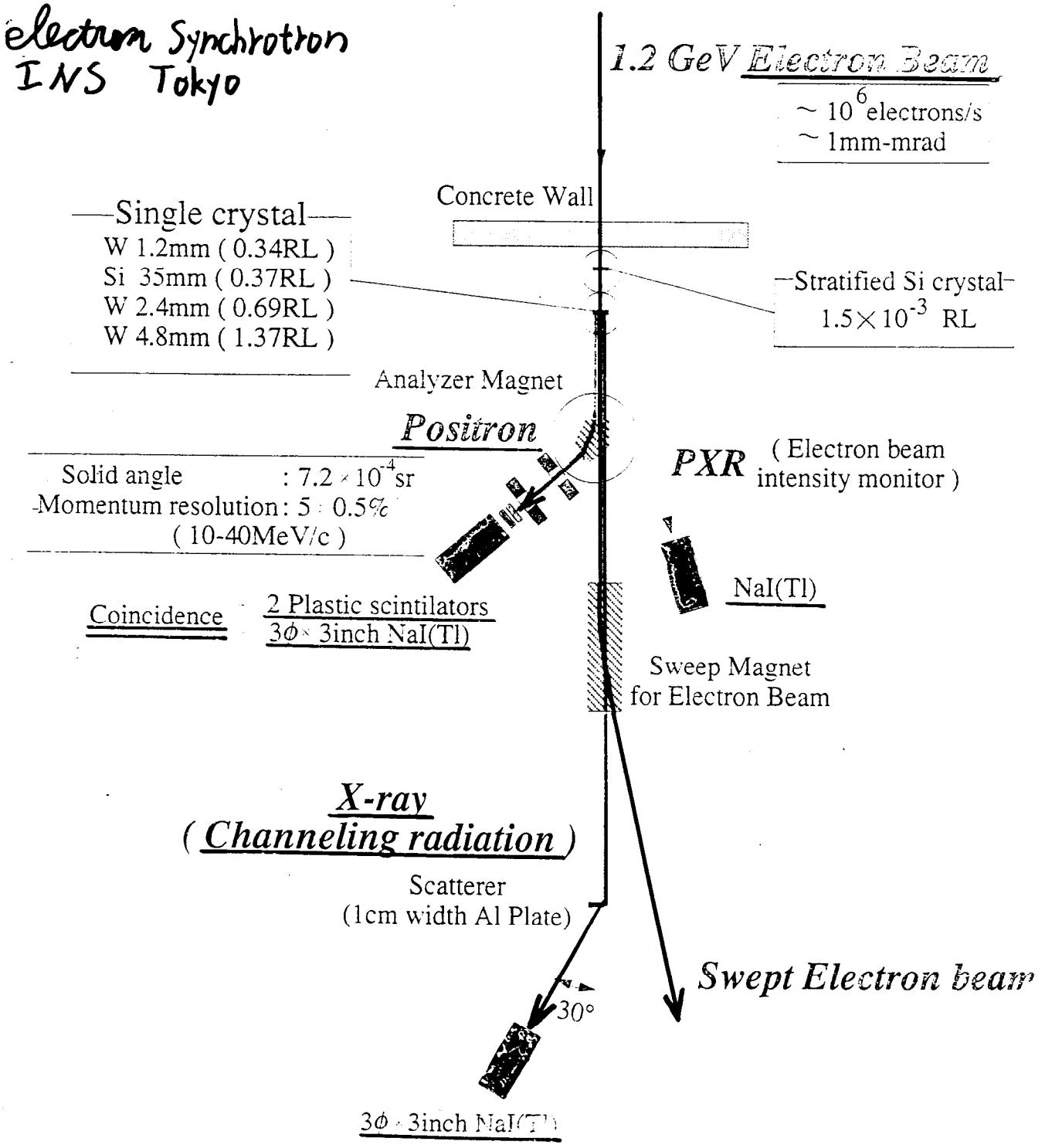

Rocking curve : W 1.2mm

@ p=20MeV/c , Emission angle=0deg.

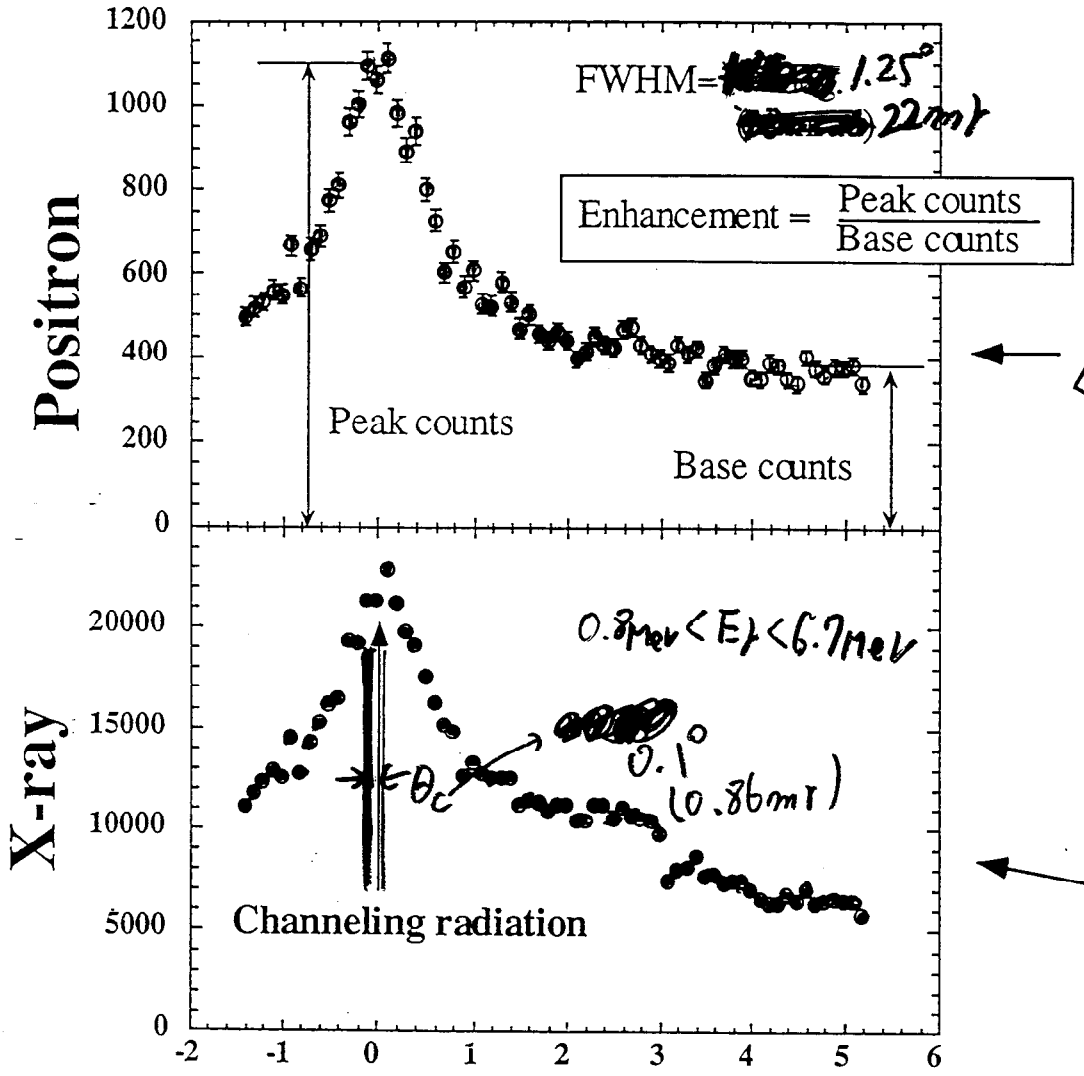

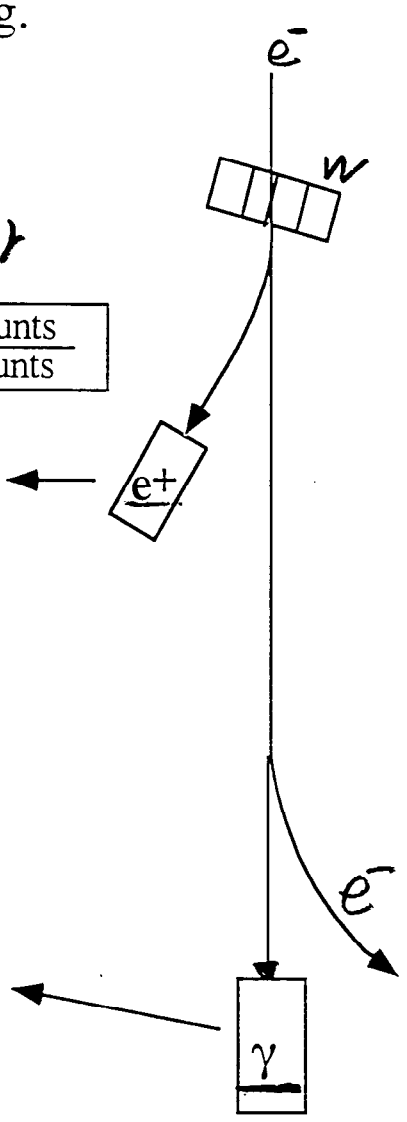

Rotation angle of the crystal target (degree)

Momentum distribution W 1.2mm
@ Emission angle = 0deg.

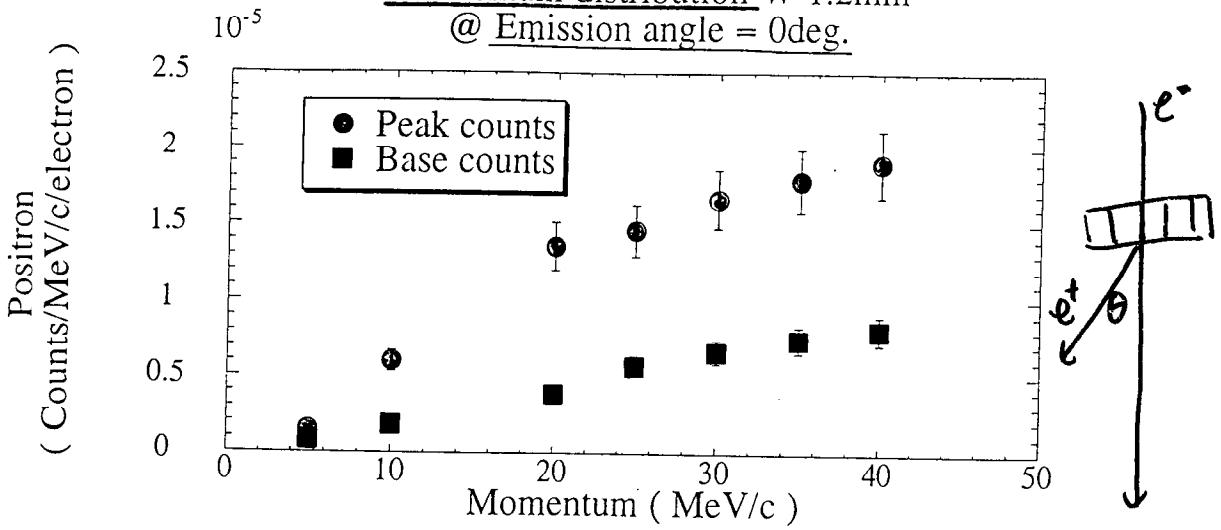

@ Emission angle = 5deg.

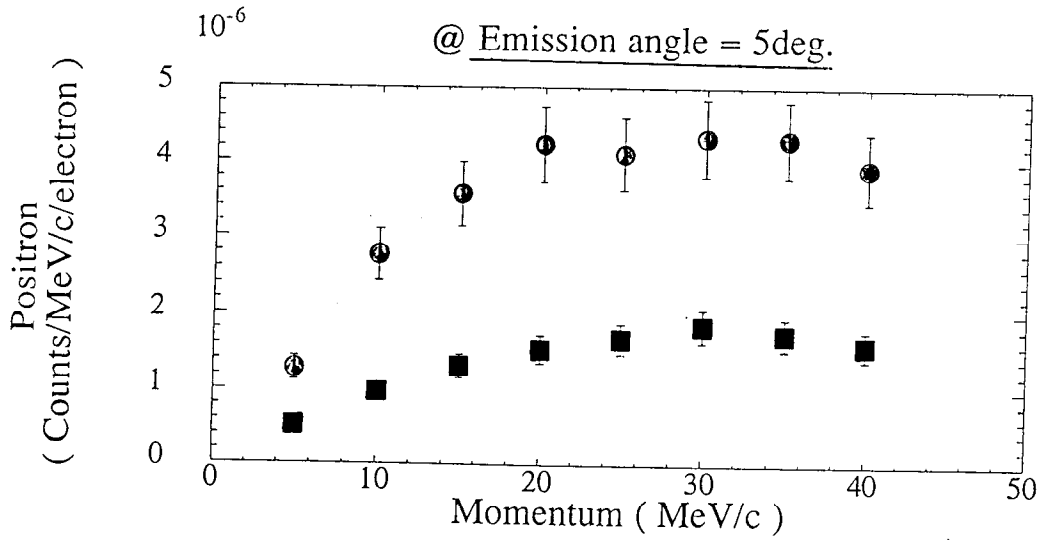

@ Emission angle =10deg.

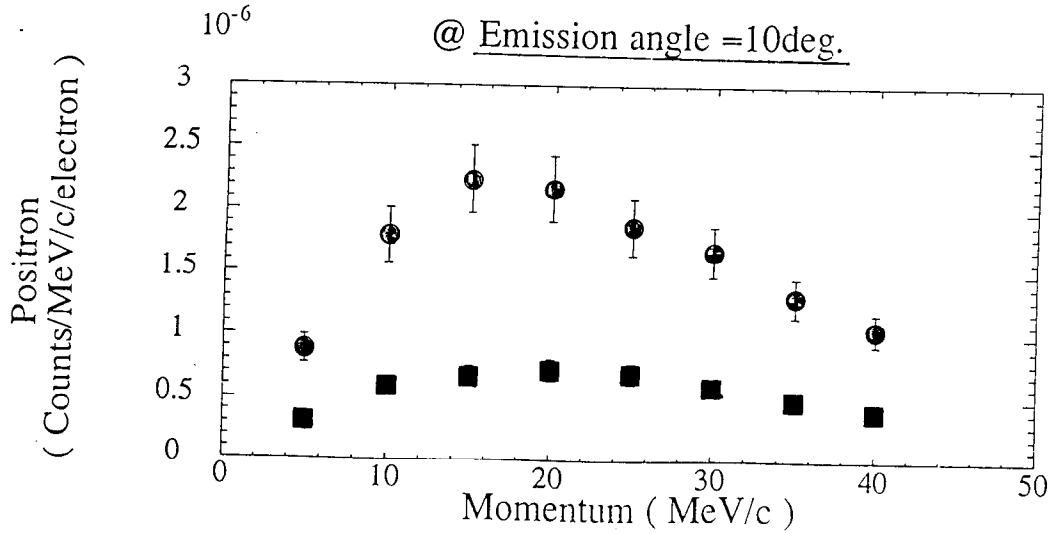

Angular dependence : 1.2mm-thick W crystal (p=20MeV/c)

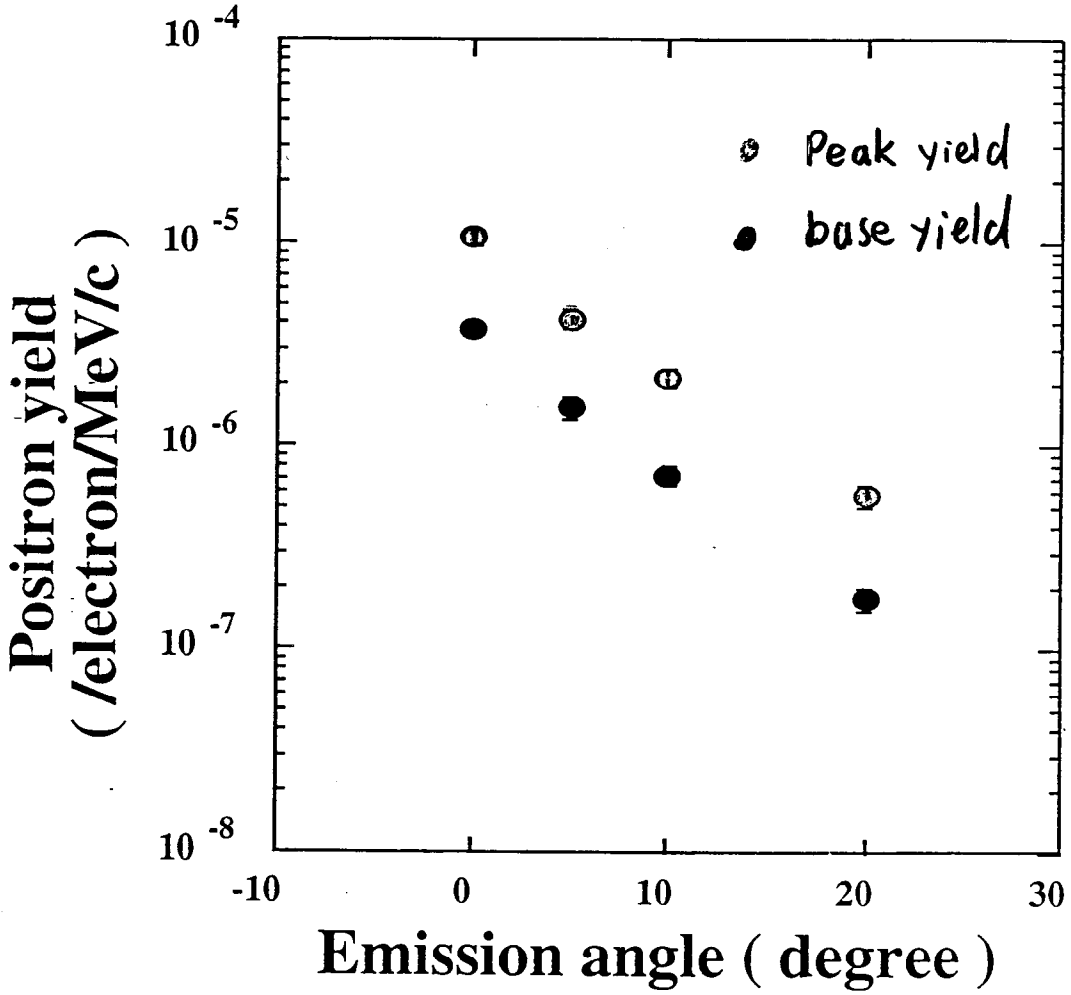

Enhancement = Peak / base

1.2mm-thick W crystal

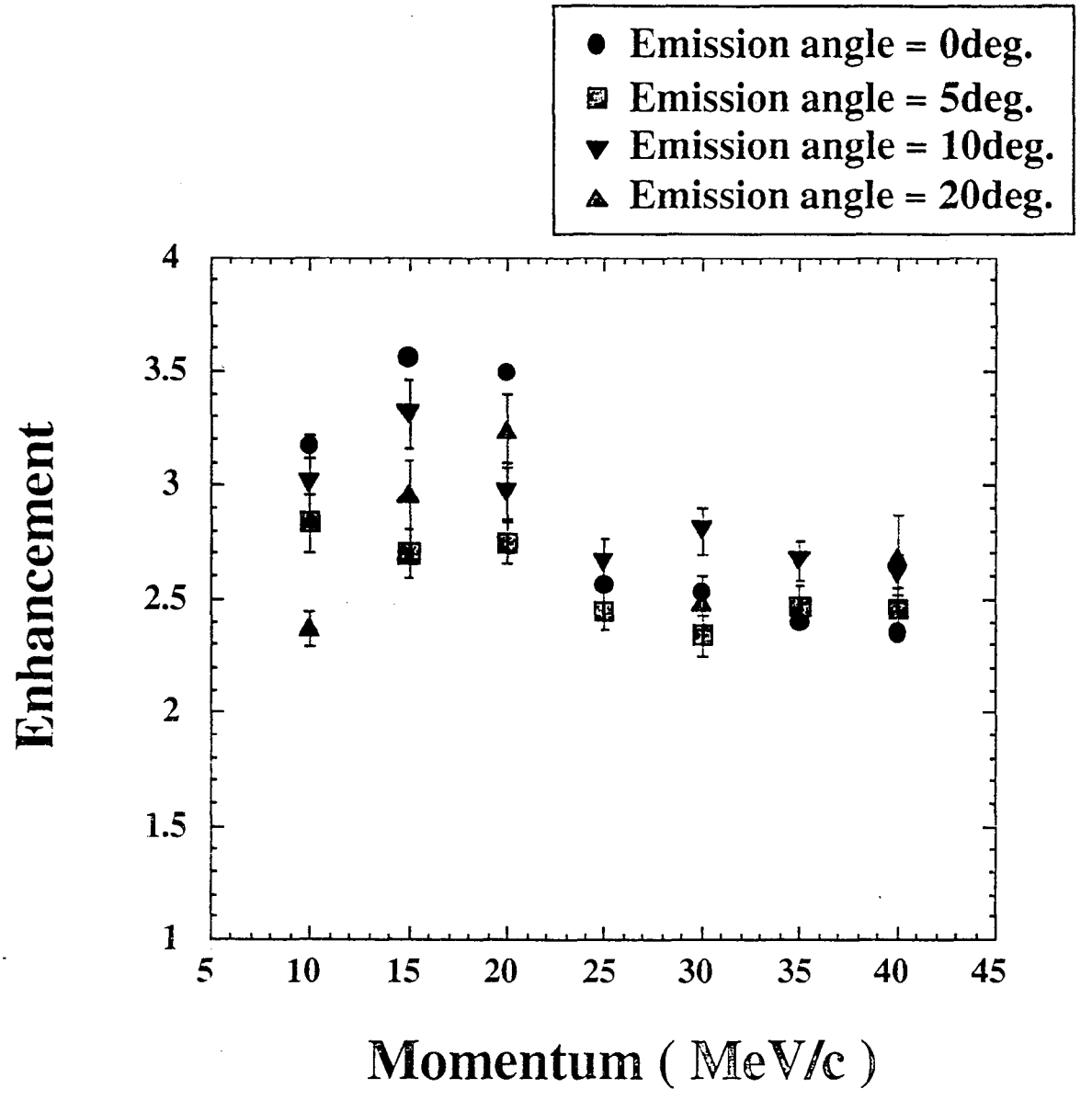

Average = 2.56 (0.01)

Experimental results

For each crystal target, we observed

the increase of the positron yield when the electron beam entered the crystal along its axis.

Crystal target (Thickness (mm))	**Enhancement** (Average)	Imperfectness (mrad)
W (1.2mm)	2.56 (0.01)	< 10
W (2.4mm)	1.63 (0.01)	~50
W (4.8mm)	1.312 (0.003)	~50

The imperfectness was measured by X-ray picture

Large imperfectness = Bad quality crystal

For 2.4mm, 4.8mm-thick W crystals, a calculation for the case of good quality crystal was necessary.

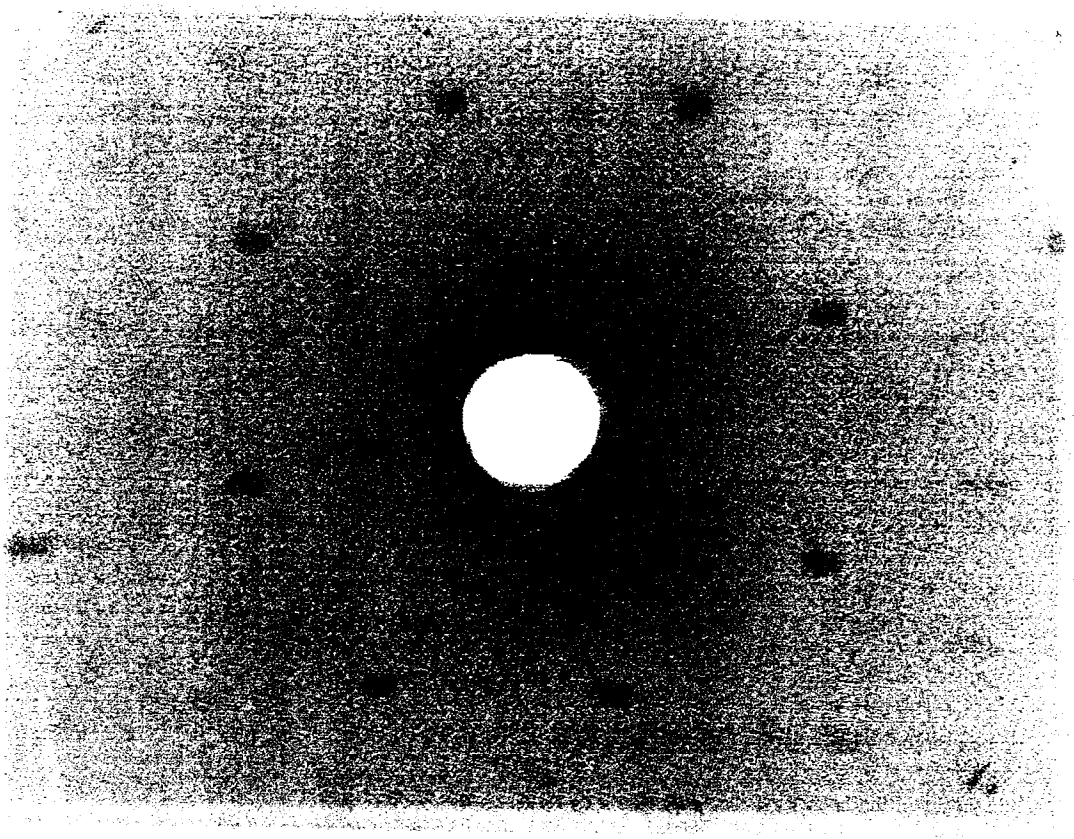

1.2mm-thick W crystal

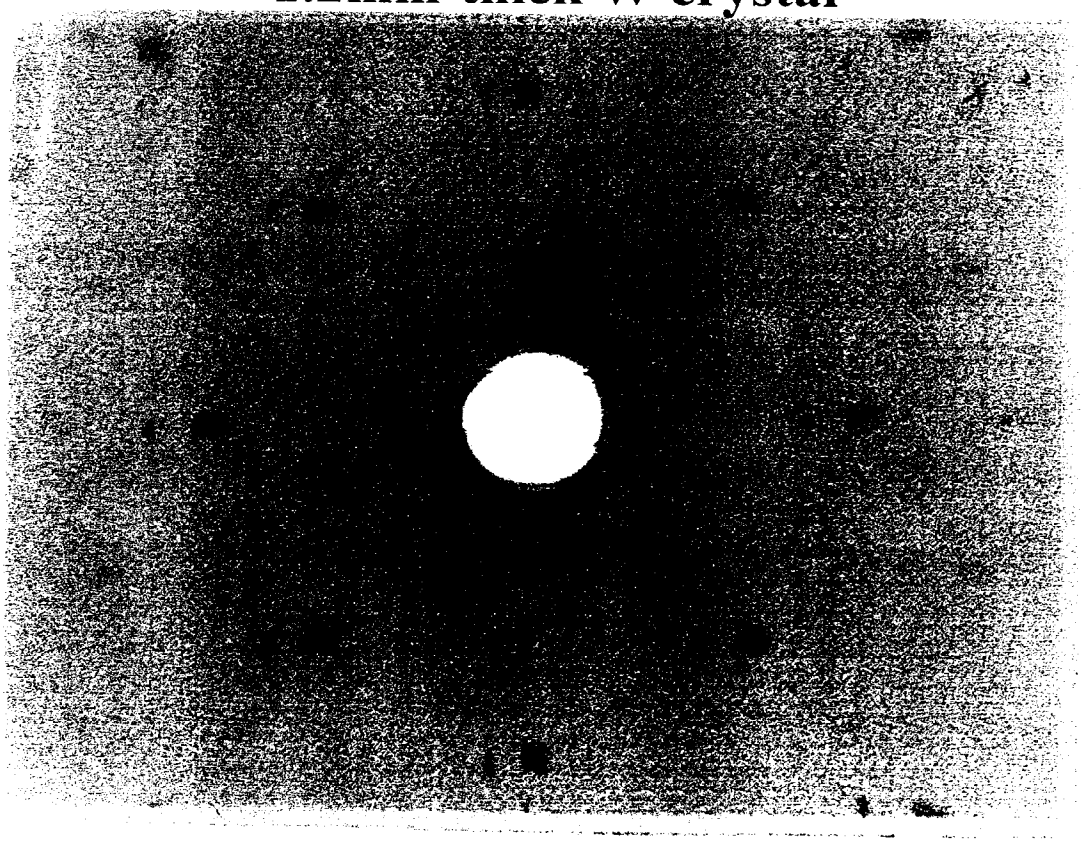

2.4mm-thick W crystal

Simulation

Assumptions

The quality of the crystal is perfect : no imperfectness

The crystal is divided to layers

(Thickness : Dechanneling length for 1GeV electrons = 100 μ m)

In each layer,

the axial channeling is considered

and the channeling radiation is generated

M. kumakhov
Ch. Trikalinos
Phys. Stat. Sol (b) 99(1980) 449

$$\frac{dI}{d\omega} = \sum_l \frac{3I_l}{\omega_l^2}\left(1 - 2\frac{\omega}{\omega_l} + 2\frac{\omega^2}{\omega_l^2}\right)\omega$$

$$I_l = \frac{8e^2 l^2 a^2 \Omega^4 \gamma^4}{3c^3}\left\{J_l(l\varepsilon)' + \left(\frac{1}{\varepsilon^2} - 1\right)J_l(l\varepsilon)^2\right\}$$

ω=Photon Energy

Electromagnetic interaction is calculated by

EGS4 Monte Carlo simulation code.

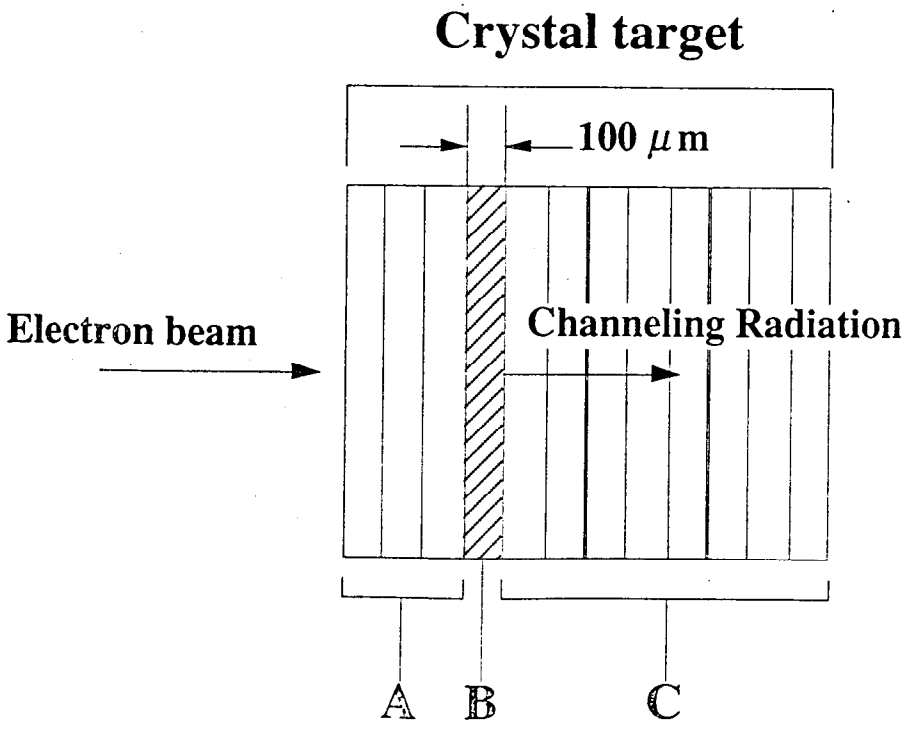

Thickness dependence of positron yield

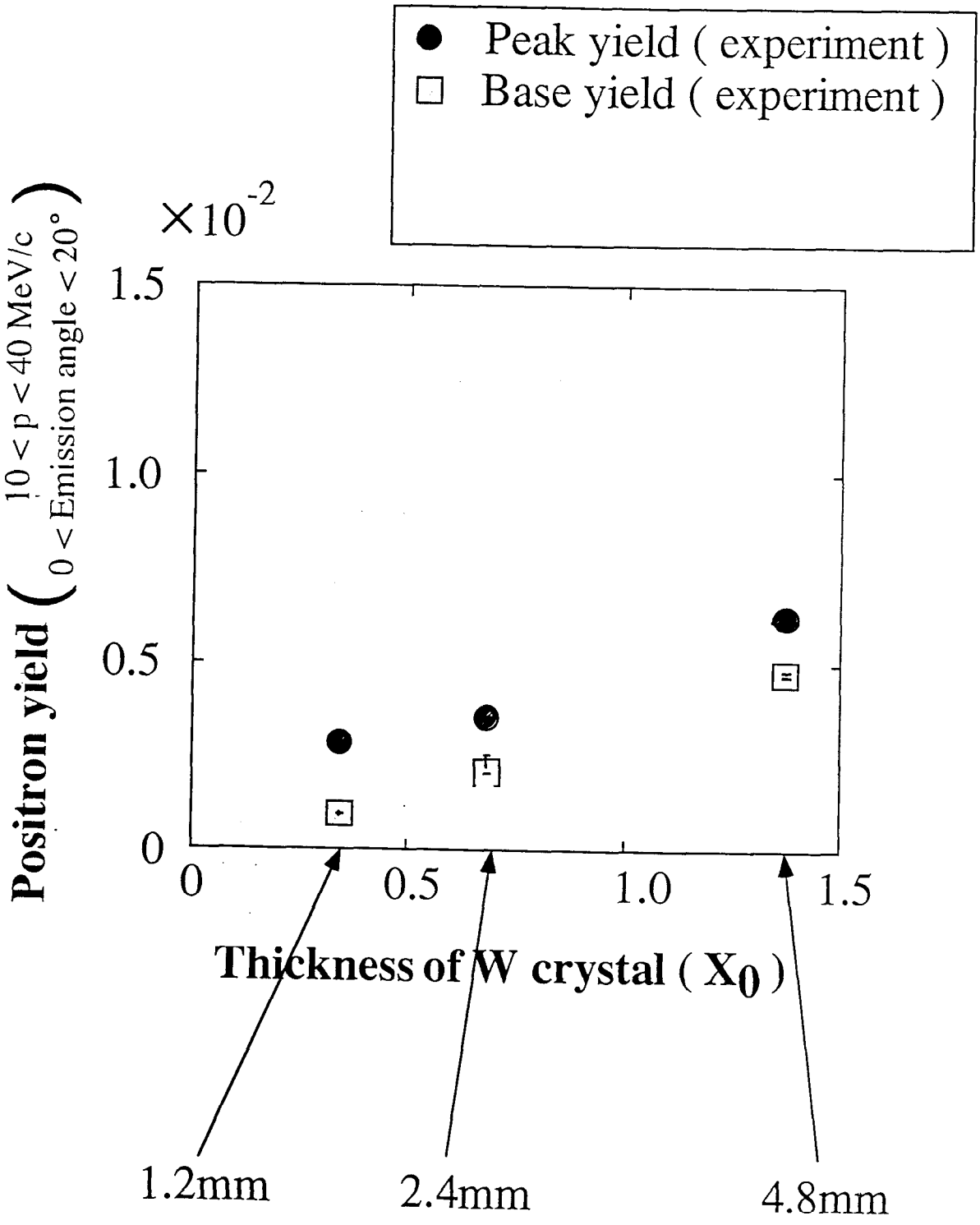

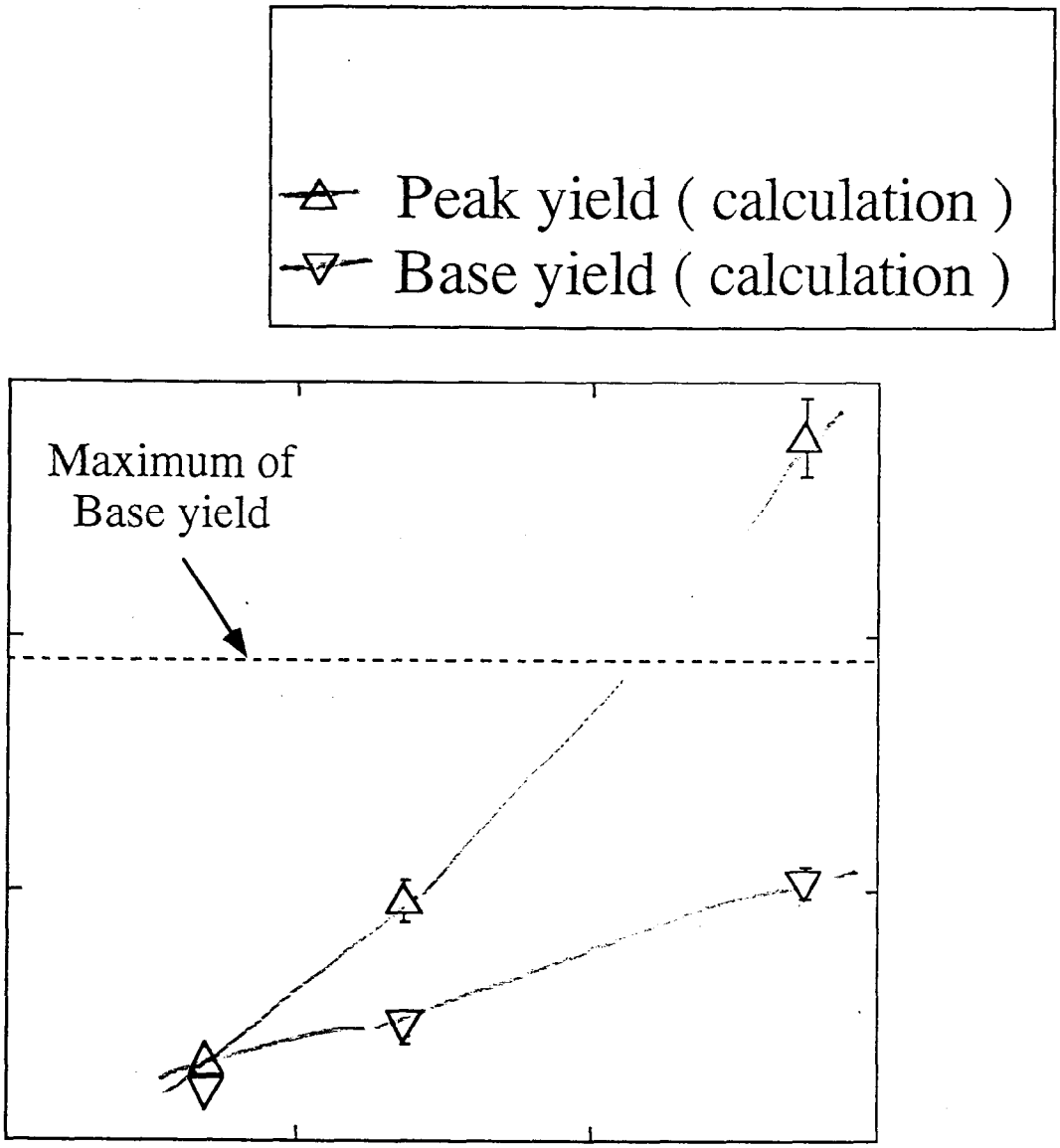
Peak yield (calculation)
Base yield (calculation)
Maximum of
Base yield

Thickness dependence of positron yield

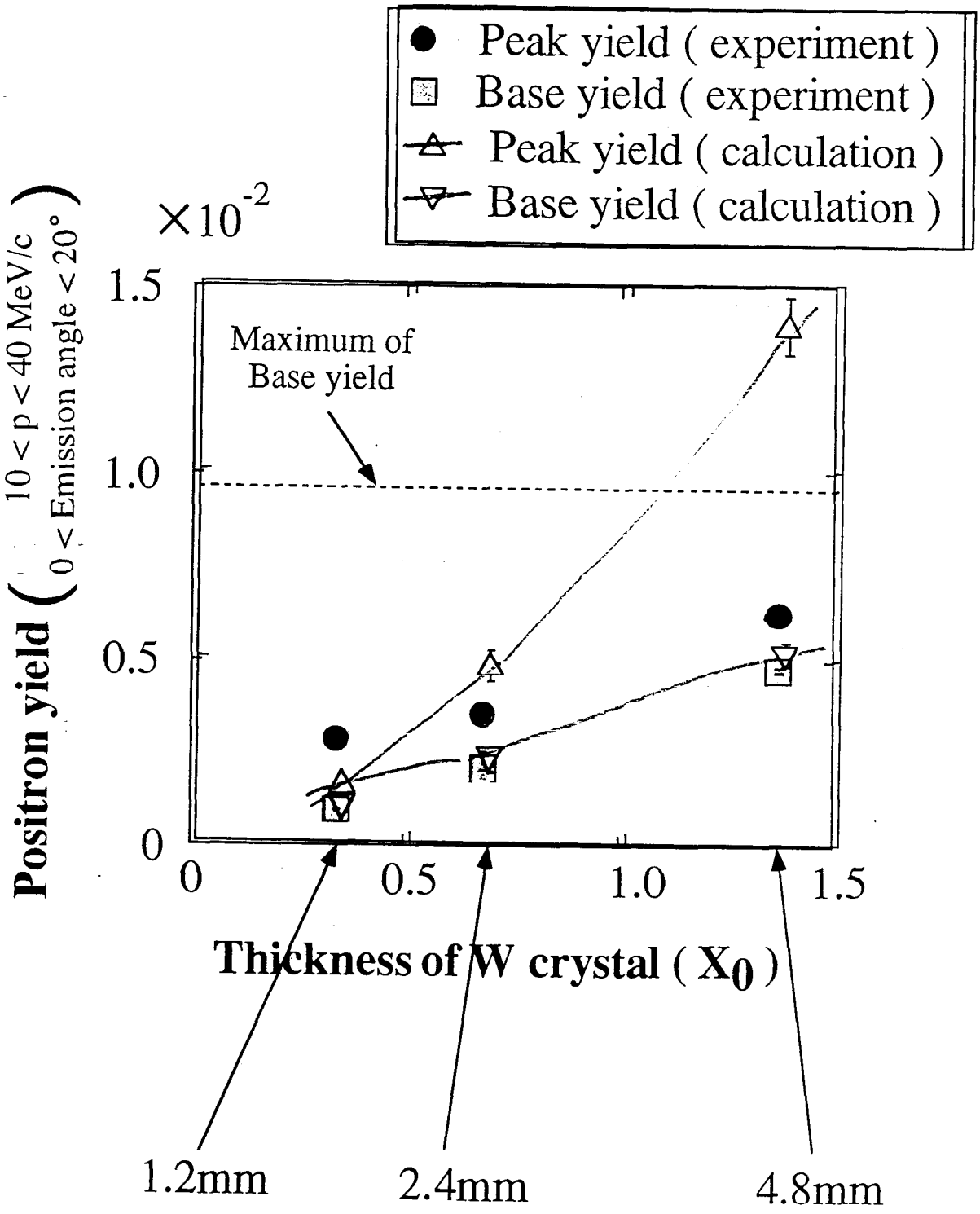

◦ Hard Photon

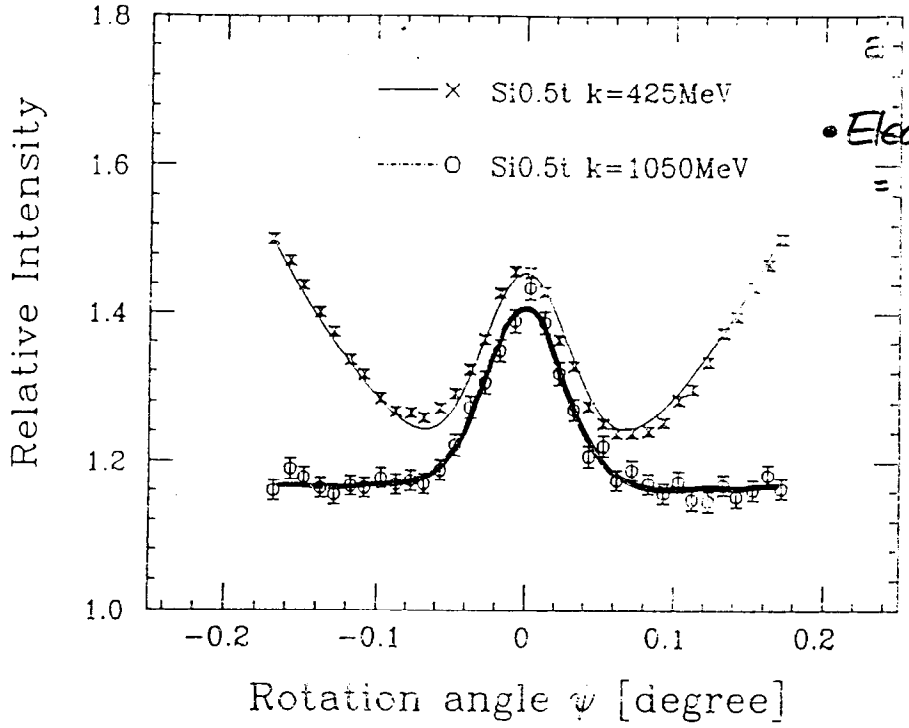

• Electron Energy = 1.2 GeV

Phys. Lett. A 146(1990)150

◦ Coherent Bremsstrahlung

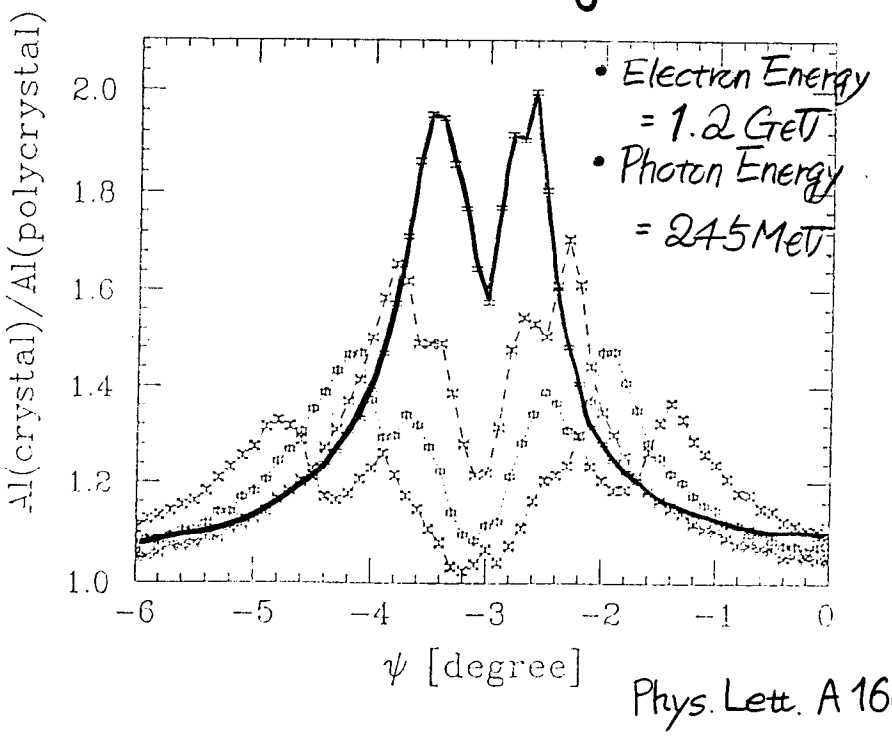

• Electron Energy = 1.2 GeV
• Photon Energy = 245MeV

Phys. Lett. A 166(1992)140

Results

In the experiment, we observed

the increase of the positron yield
when the electron beam
entered the crystal along its axis.

For the case of 1.2mm-thick W (Good quality)

Enhancement=2.6

For the cases of 2.4mm-, 4.8mm-thick W(Bad quality)

Enhancement=1.7,1.3

In the calculation considering only the axial channeling for the best quality crystals,

For the case of 1.2mm-thick W crystal

Enhancement=1.6

Experimental result > Calculated result

(The gap maybe caused by **Coherent Bremsstrahlung**)

For 2.4mm-, 4.8mm-thick W crystals,

if their qualities are good,

the calculated enhancement (= 2.2, 2.9) are expected to be observed experimentally.

New experiment at KEK LINAC

Proposed for KEK Joint R&D program

K. Yoshida (Hiroshima)

Hiroshima, KEK, INS, Tomsk, Orsay

KEK accelerator complex is now upgraded to B Factory and is going to be,,,,

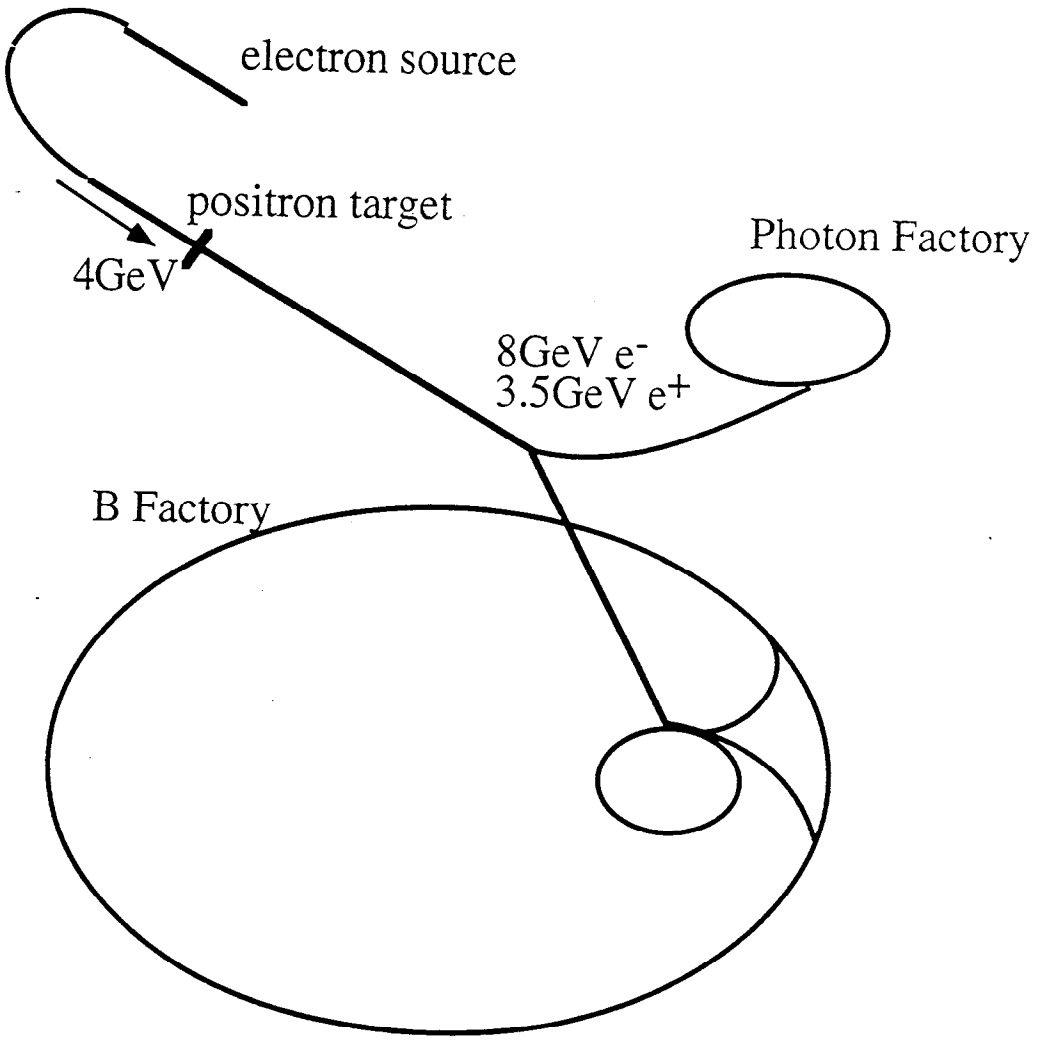

Status of LINAC now (at the time of proposed exp.)

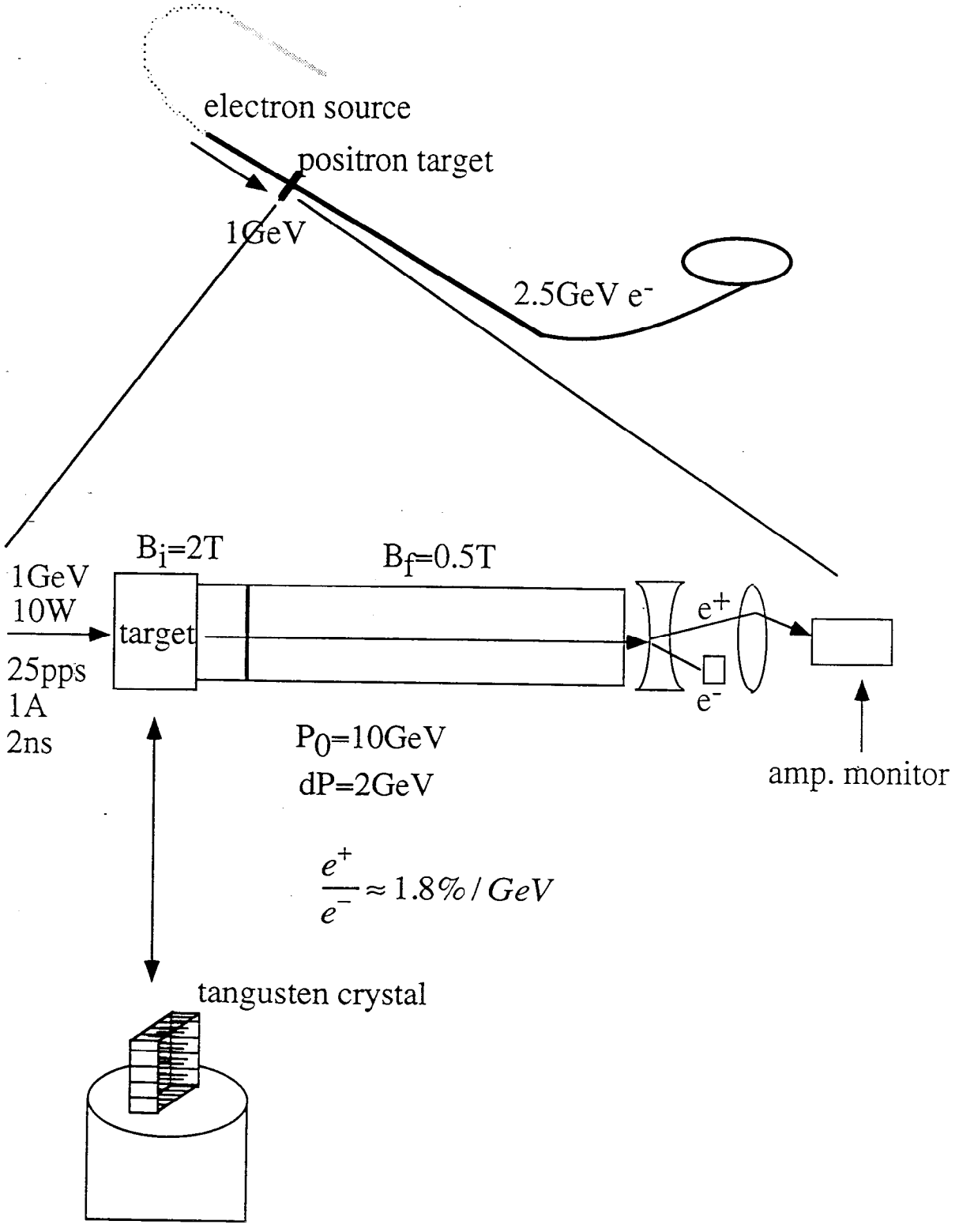

Prospect for the experiment

Replace conventional positron target with a crystal target
in
real positron system for B Factory*

*except for electron beam

See efficiency of positron yeild including acceptance

planned in Oct. - Nov. 1997

Summary

We observed enhancement of positron production by 1.2 GeV channeling electrons over amorphous target.

enhacement factor 2.5 w/ 1.2mm W

large contribution from coherent bremstrahlung

estimated to be 1:1

A expriment with with KEK LINAC is proposed

real positron caputre optics for B factory

HELICAL UNDULATOR FOR PRODUCING CIRCULARLY POLARIZED PHOTONS.

Pavel Vobly, Budker Institute of Nuclear Physics, Novosibirsk, Russia

Helical undularor consists of two planar pure permanent magnet undulators with $B_y \sin 2\pi z$ and $B_x \cos 2\pi z$ distributions of magnetic field along the longitudinal axis Z.

General view of the planar and helical undulators are shown in figures 1, 2.

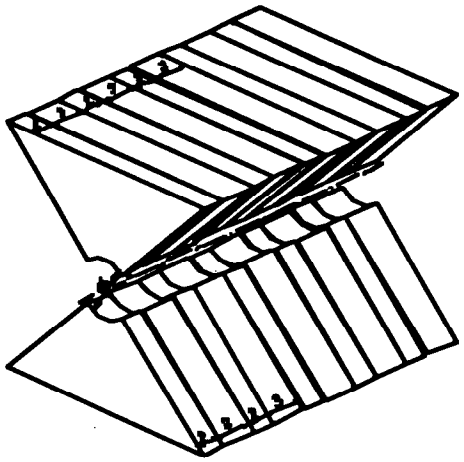

Planar undulator

Figure 1

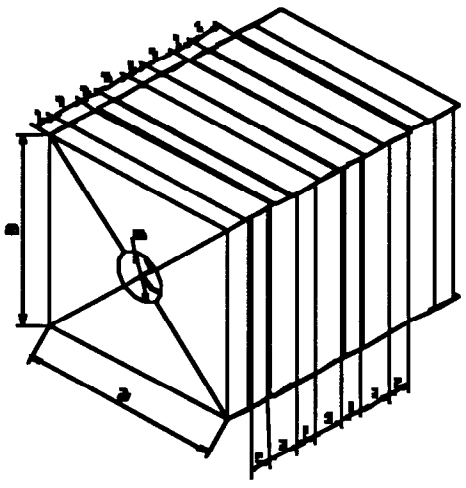

Helical undulator

Figure 2

Parameters of helical undulator.

1. Period	-	1 cm
2. Inner aperture	-	0.5 cm
3. Amplitude of magnetic field	-	5 kGs
4. Residual induction of NdFeB magnets	-	12.5 kGs
5. Overall dimensions of undulator cross-section	-	2×2 (cm)

The distributions of magnetic field along the half period of the helical undulator is shown in figure 3. (Magnetic calculations were made on Mermaid 3D magnetostatic code)

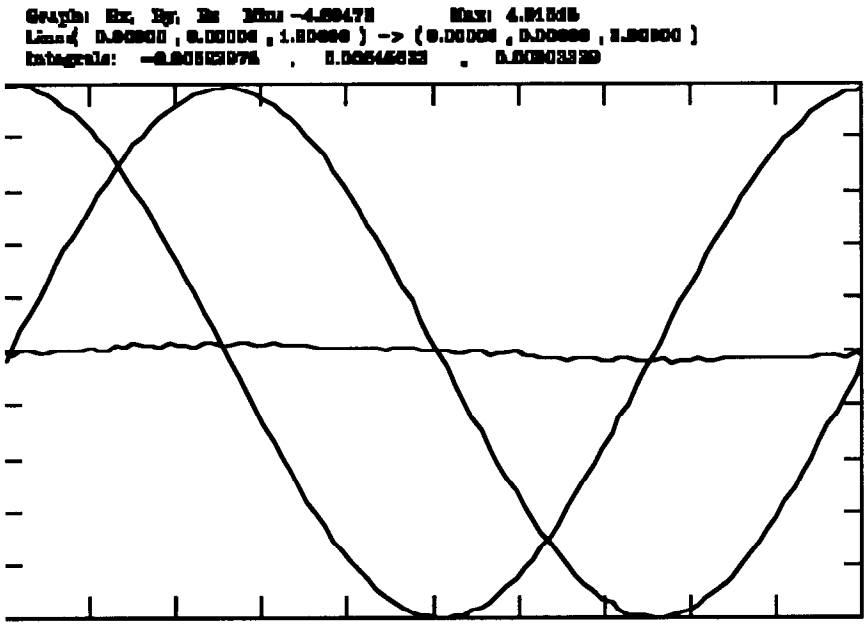

Figure 3
Distributions of B(y) and B(x) in helical undulator

List of Workshop Participants

Ray Alley
Mail Stop 66
Stanford Linear Accelerator Center
P.O. Box 4349
Stanford CA, 94309
USA
EMAIL: razar@slac.stanford.edu

Vladimir Baier
Budker Institute of Nuclear Physics
Siberian Division of Russian Academy of Sciences
Academician Lavrentiev Prospect 11
RU-630090 Novosibirsk
RUSSIA
EMAIL: baier@vxinp.inp.nsk.su

Robert Chehab
Laboratoire de l"Accelerateur Lineaire
IN2P3-CNRS et Universite de Paris-Sud
Bat. 200-91405 Orsay Cedes
FRANCE
EMAIL: chehab@lalcls.in2p3.fr

Jym Clendenin
Mail Stop 66
Stanford Linear Accelerator Center
P.O. Box 4349
Stanford CA, 94309
USA
EMAIL: clen@slac.stanford.edu

Hobey DeStaebler
Mail Stop 17
Stanford Linear Accelerator Center
P.O. Box 4349
Stanford CA, 94309
USA
EMAIL: hobey@slac.stanford.edu

Stan Ecklund
Mail Stop 17
Stanford Linear Accelerator Center
P.O. Box 4349
Stanford CA, 94309
USA
EMAIL: secklund@slac.stanford.edu

List of Workshop Participants

Klaus Flöttmann
DESY, Deutsches Elektronen-Synchrotron
Notkestrasse 85
D-22603 Hamburg
GERMANY
EMAIL: mpyflo@dsyibm.desy.de

Josef Frish
Synaptics
2698 Orchard Parkway
San Jose, CA 91534
USA
EMAIL: frisch@synaptics.com

Alain Jejcic
College de France
Lab de Physique Corpusculaire
11 Place Marcelin-Berthelot
F-75231 Paris Cedex 05
FRANCE
EMAIL: jejcic@cdf.in2p3.fr

Takuya Kamitani
KEK
National Lab for High Energy Physics
1-1 Oho, Tsukuba-shi
Ibaraki-ken 305
JAPAN
EMAIL: takuya.kamitani@kek.jp

Theo Kotseroglou
Mail Stop 66
Stanford Linear Accelerator Center
P.O. Box 4349
Stanford CA, 94309
USA
EMAIL: theo@slac.stanford.edu

Artem Kulikov
Mail Stop 66
Stanford Linear Accelerator Center
P.O. Box 4349
Stanford CA, 94309
USA
EMAIL: kart@slac.stanford.edu

List of Workshop Participants

Alexandre Mikhailichenko
Laboratory for Nuclear Studies
Wilson Laboratory
Cornell University
Ithaca, NY 14853-8001
EMAIL: mikhail@Ins62.Inx.cornell.edu

Roger Miller
Mail Stop 26
Stanford Linear Accelerator Center
P.O. Box 4349
Stanford CA, 94309
USA
EMAIL: rhm@slac.stanford.edu

Greg Mulhollan
Mail Stop 66
Stanford Linear Accelerator Center
P.O. Box 4349
Stanford CA, 94309
USA
EMAIL: mulholla@slac.stanford.edu

Al Odian
Mail Stop 65
Stanford Linear Accelerator Center
P.O. Box 4349
Stanford CA, 94309
USA
EMAIL: odian@slac.stanford.edu

Tsunehiko Omori
KEK
National Lab for High Energy Physics
1-1 Oho, Tsukuba-shi
Ibaraki-ken 305
JAPAN
EMAIL: omori@kekvax.kek.jp

Dennis Palmer
Mail Stop 26
Stanford Linear Accelerator Center
P.O. Box 4349
Stanford CA, 94309
USA
EMAIL: dtp@slac.stanford.edu

List of Workshop Participants

J.M. (Ewan) Paterson
Mail Stop 24
Stanford Linear Accelerator Center
P.O. Box 4349
Stanford CA, 94309
USA
EMAIL: jmp@slac.stanford.edu

Rainer Pitthan
Mail Stop 20
Stanford Linear Accelerator Center
P.O. Box 4349
Stanford CA, 94309
USA
EMAIL: rainer@slac.stanford.edu

John Sheppard
Mail Stop 66
Stanford Linear Accelerator Center
P.O. Box 4349
Stanford CA, 94309
USA
EMAIL: jcsrl@slac.stanford.edu

Konstantin Shmakov
Mail Stop 43
Stanford Linear Accelerator Center
P.O. Box 4349
Stanford CA, 94309
USA
EMAIL: shmakov@slac.stanford.edu

Grigory Silvestrov
Budker Institute of Nuclear Physics
Siberian Division of Russian Academy of Sciences
Academician Lavrentiev Prospect 11
RU-630090 Novosibirsk
RUSSIA
EMAIL: silvestr@inpbox.inp.nsk.su

Tohru Takahasi
Department of Physics
Hiroshima University
Higashi Hiroshima, 739
JAPAN
EMAIL: tohrut@kekux1.kek.jp

List of Workshop Participants

Huan Tang
Mail Stop 66
Stanford Linear Accelerator Center
P.O. Box 4349
Stanford CA, 94309
USA
EMAIL: tang@slac.stanford.edu

Jim Turner
Mail Stop 66
Stanford Linear Accelerator Center
P.O. Box 4349
Stanford CA, 94309
USA
EMAIL: jturner@slac.stanford.edu

Dian Yeremian
Mail Stop 26
Stanford Linear Accelerator Center
P.O. Box 4349
Stanford CA, 94309
USA
EMAIL: anahid@slac.stanford.edu